GRANULITE-FACIES METAMORPHISM, FLUID BUFFERING AND PARTIAL MELTING IN THE BUFFELS RIVER AREA OF THE NAMAQUALAND METAMORPHIC COMPLEX, SOUTH AFRICA

by Jonathan Hugh McStay

A Thesis Submitted in Fulfillment of the Requirements
for the Degree of Doctor of Philosophy
Department of Geology and Mineralogy
University of Cape Town

31 December 1991

ABSTRACT

The Buffels River area of central Namaqualand comprises a sequence of Proterozoic volcano-sedimentary gneisses intruded by granitoid orthogneisses. This study concentrates on the mechanisms of granulite-facies metamorphism in a small area of isofacial rocks. Particular emphasis is placed on the role of partial melting and the infiltration and buffering of metamorphic fluid is examined.

The Namaqualand Metamorphic Complex is a large belt of Proterozoic rocks that occurs accross the North-Western Cape Province of South Africa and southern Namibia. The Namaqua metamorphic event is dated at around 1190 Ma by Clifford et al. (1975 and 1981). The intrusion of granitoid gneisses of the Klein Namaqualand Suite is syntectonic with a period of compressional deformation that imparts a near-horizontal fabric and a well defined shallow plunging mineral lineation. Major structures produced include isoclinal folds and thrusts. This deformation is the regional D_2 of Joubert (1971). Metamorphic conditions during D_2 are difficult to quantify as growth of new minerals and recrystallisation of preexisting minerals occurred during the thermal peak (syn- to post D_2). Sillimanite was stable and limited partial melting in water saturated pelitic and semi-pelitic rocks may have occurred. Upper amphibolite-facies conditions are inferred.

The peak of granulite-facies metamorphism is syn- to post tectonic with the D_3 phase of deformation. In the Buffels River area D_3 deformation is seen as dextral shearing, particularly well developed at zones of contrasting ductility such as orthogneiss-paragneiss contacts. A strong southward dipping foliation is developed as an axial planar fabric associated with upright asymetrical folds. The thermal maximum culminates in the formation of veins and patches of partial melt in rocks of varying bulk composition. Although of local extent the veins form discordant to the D_3 structures and indicate that granulite-facies conditions outlasted the last major phase of deformation.

The pressure-temperature conditions of metamorphism were estimated using a variety of cation exchange thermobarometers and by oxygen isotopic exchange thermometry. Temperature determinations from two pyroxene, garnet-biotite, and garnet-cordierite thermometers suggests

peak temperatures around 750°C. Apparent equilibration temperatures for oxygen isotope fractionation between quartz and garnet suggest that temperatures of up to 800°C were reached. Other mineral pairs record much lower temperatures and are perceived as blocking temperatures achieved during slow cooling of the terrane. Geobarometry is limited to garnet-plagioclase-sillimanite-quartz assemblages and suggests pressures between 5 and 6.5 kb.

Field evidence and petrography from rocks in the Buffels River area demonstrates a close spatial association between hydrous and anhydrous granulite-facies mineral assemblages. Boudinaged lenses of mafic gneiss in contact with migmatitic biotite gneisses develop a cm-scale margin of anhydrous orthopyroxene-bearing granulite mantling a hornblende-rich interior. A short-range infiltration-exfiltration process activated by chemical gradients in water and silica activity and controlled by intergranular diffusion is proposed to account for cm-scale transitions of this nature. The existence of local gradients in water activity is supported by estimates of X_{H2O} from a number of hornblende-bearing mafic gneisses and from biotite-sillimanite bearing pelitic gneisses.

Oxygen isotope studies indicate that local scale variations in $\delta^{18}O$ may have been preserved during granulite-facies metamorphism. Oxygen isotope values for quartz in a number of different rock types range from 7.7 to 10.2 parts per mil. These values are low compared to many granulite-facies terranes and are thought to represent derivation from ^{18}O depleted protoliths.

Small-scale partial melting is a dominant process in the granulite-facies metamorphism of most rocks in the Buffels River area. Segregations of quartz and feldspar with anhydrous phases, such as garnet, cordierite, orthopyroxene and clinopyroxene are regarded as being the solid and liquid products of vapour-absent melting reactions. Mass balance calculations suggest that H_2O and K_2O are the only major components lost during vapour-absent melting. Evidence from mineral textures, fluid composition calculated from dehydration equilibria, oxygen isotopes and fluid inclusions are all consistent with granulite-facies metamorphism in a relatively closed system. There is no evidence to suggests an outside fluid agent acting as a mechanism for generating granulite-facies assemblages.

The retrograde history of the Buffels River area has been

determined from mineral textures and zonation patterns in mineral pairs involved in retrograde exchange re-equilibration. Experimentally derived diffusion data has been used to model cooling rates. Diffusional models indicate that cooling was moderate to slow with a maximum value of 20°C/My. The retrograde P-T-t path deduced from mineral textures and the densities of secondary fluid inclusions has an anticlockwise trajectory. Tectonothermal models that predict low-pressure granulite-facies metamorphism followed by isobaric cooling involve either magmatic accretion and/or extensional tectonic regimes. In view of the early compressional deformational history and the time span for metamorphism in Namaqualand the prefered model involves continental thickening with convective lithospheric thinning (Loosveld & Etheridge, 1990). This model provides a long-lived heat source and allows for a heating mechanism that outlasts crustal thickening. The duration of granulite-facies metamorphism is thus governed by the duration of mantle convection. The overall mechanism of low pressure granulite formation is thus linked to large scale thermal perturbations in the asthenosphere.

CONTENTS

CHAPTER 1

INTRODUCTION

1.1 REGIONAL SETTING

The Namaqualand Metamorphic Complex is a Proterozoic "mobile belt" that is well exposed over most of the north western Cape Province, South Africa. The tectonic province extends from Namibia in the north-west wrapping around the southern boundary of the Kaapvaal Craton, underneath the Karoo basin, to form the Natal Metamorphic Belt in the east (fig. 1.1) The Namaqua Province may have links to similar age Proterozoic belts in South America and Antartica. The Namaqualand Metamorphic Complex has been subdivided into a series of tectonic subprovinces (Hartnady et al., 1985) and tectonic terranes (Colliston & Praekelt, 1988). The subprovinces have distinct lithological, structural and metamorphic histories and have found widespread acceptance. Terrane subdivisions are less certain and are based on lithotectonic criteria. A discussion of the regional tectonic history is given in Chapter 2. Granulite facies rocks are exposed in various parts of the province. This study concentrates on a small area within the largest and best exposed sequence of high grade rocks in the Bushmanland Subprovince (see fig. 2.1).

In terms of this study the general geographical area is referred to as central Namaqualand following the terminology of Tankard et al. (1982). This term was chosen to differentiate between the areas to the north and east of the study area that lie within the geographical region of Bushmanland and the western coastal areas. In some studies the general area is often referred to as western Namaqualand. This term refers to the western part of the Namaqualand Metamorphic Complex and includes the whole of the Bushmanland Subprovince. The granulites of central Namaqualand are bounded to the north and south by prograde amphibolite-facies - granulite-facies transitions. The coastal areas are marked by a zone of retrograde reworking related to the late-Precambrian Pan-African orogeny (Jackson & Zelt, 1984). This study concerns a small area of granulite-facies rocks exposed in and around the upper parts of the Buffels River about 45 km south-east of the town of Springbok (see fig. 2.1). Reconnaissance sampling covered a broader area of the northern amphibolite-facies - granulite-facies

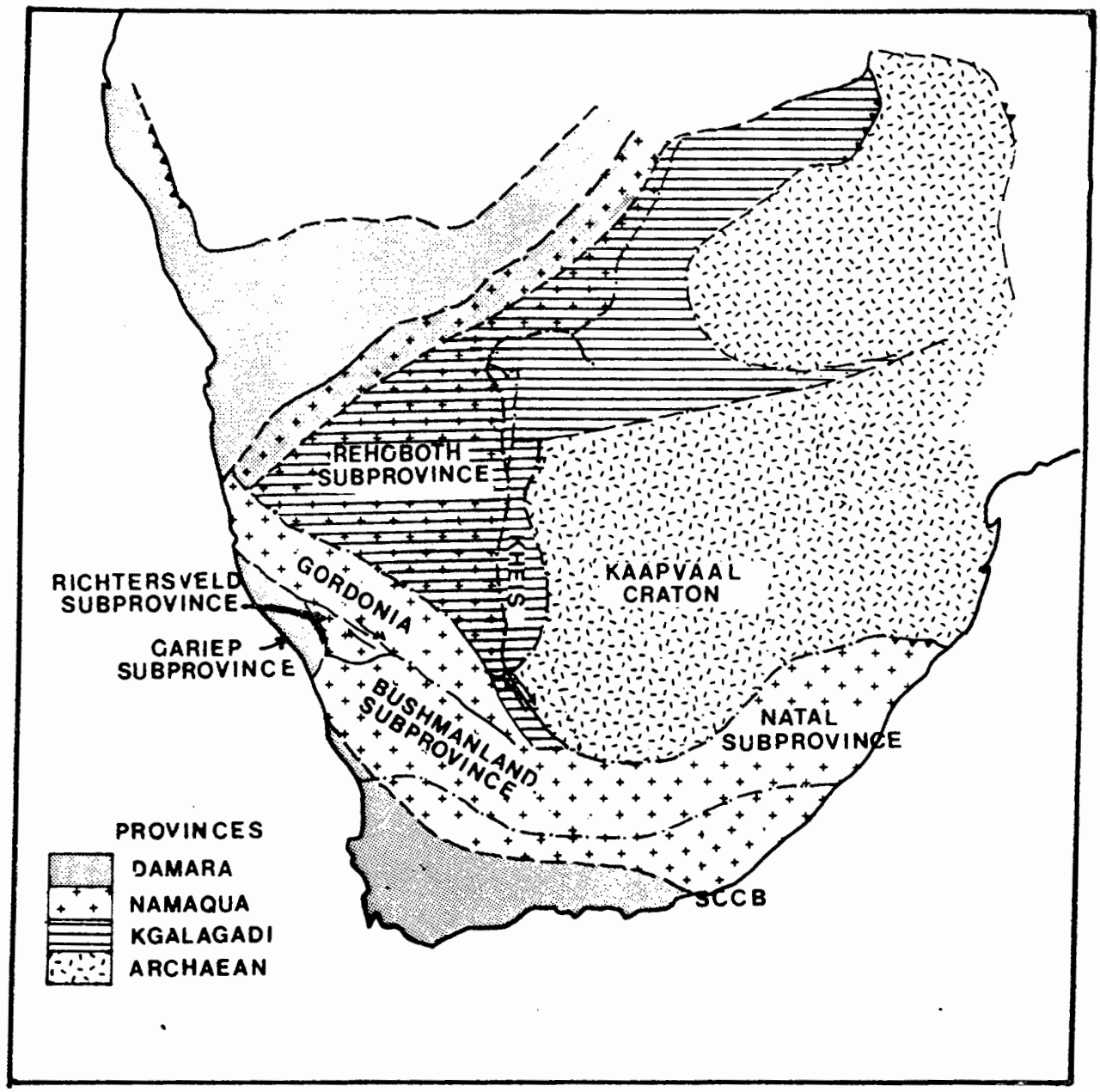

Fig. 1.1 Major tectonic subdivisions in southern Africa, after Hartnady et al. (1985)

transition. The aim of the study is to document the processes involved in granulite-facies metamorphism in central Namaqualand. A detailed description of the local geology is given in Chapter 3.

1.2 GRANULITE-FACIES METAMORPHISM

In the Buffels River area it was discovered that amphibolite-facies mineral assemblages coexisted with granulite-facies assemblages and that a prograde transition could be recognised on a cm-scale within individual rocks. This phenomena has been recognised in a variey of granulite-facies terranes throughout the world and is well documented in areas such as Sri Lanka and southern India, where in rocks of granitic and tonalitic composition, it has been described as "charnockite in the making" (Hansen et al., 1987). Within the Bushmanland Subprovince there is a very broad variation in temperature and pressure (Waters, 1986 and 1989) with little resolvable changes in pressure-temperature conditions across terrane boundaries.

There are inherent uncertainties in the application of exchange thermometers in granulite-facies terranes (Bohlen, 1987, Frost & Chacko, 1989 and Harley, 1989). Most problems are caused by retrograde exchange by diffusion during cooling and thus calculated temperatures actually represent a blocking temperature controlled by cooling rate, diffusion rate and crystal size. The advantage in examining many rocks from a small area are that the effects of pressure and temperature variation are eliminated, assuming polymetamorphism and variable overprinting has not occurred, and therefore the less obvious local factors affecting granulite-facies metamorphism can be investigated. Other advantages found in the Buffels River area are the variation in lithological types, which allow for petrological models to be tested on a variety of rocks with different bulk rock compositions and different physical properties. Rock types include mafic gneisses (metabasites), pelitic gneisses (metapelites) and charnockitic (metagranitic) gneisses. These rock types are broadly comparable in bulk composition to similar rocks in high grade terranes throughout the world and thus allow comparisons to be drawn to other terranes and permit a broad discussion of a variety of granulite-facies phenomena. In addition to the above rock types the area includes calc-silicate gneisses and magnesian gneisses. As the petrology of the magnesian gneisses was well documented prior to the commencement of this study by Waters & Moore (1985) this group of rocks was ommitted from further

detailed study.

Arguments concerning granulite-facies metamorphism have tended to concentrate on two main issues. Firstly, the role of fluids in granulite formation (Newton et al., 1980; Thompson, 1983; Powell, 1983b; Hansen et al., 1984; Lamb & Valley, 1984, Newton, 1986; Touret, 1986; Frost & Frost, 1987) and secondly, the tectonic setting of granulite formation (Wells, 1980; England & Thompson, 1984; Sandiford & Powell, 1986; Newton, 1987; Bohlen, 1987; Ellis, 1987; Harley, 1989 and Loosveld & Etheridge, 1990). In the first case there are three main proposed mechanisms that can be used to explain the low water activities that are necessary to stabilise anhydrous assemblages at temperatures below 900°C:

1. Partial Melting. Water is strongly partitioned into melt, thus anatexis and melt migration are likely to dessicate not only the source rocks but rocks adjacent to ascending melts.

2. CO_2 flushing. Water activities may be lowered if a large flux of CO_2-rich fluid passes through the lower crust. The mantle is the most likely source for the diluting fluid.

3. Metamorphism of dry rocks. The amount of fluid during metamorphism may have been negligible, especially in terranes dominantly composed of orthogneisses.

This study tests the models above by examining field relationships, petrography and textural history, mineral equilibria in the natural assemblages, fluid inclusions and oxygen isotopes. Some whole rock geochemistry is included to supplement chemical data from electron microprobe analysis of mineral assemblages.

The tectonothermal setting of the central Namaqualand granulites can be modelled by reference to the prograde and retrograde mineral textures, and the physical conditions of metamorphism as estimated from various geothermobarometers. It was not intended that this study should develop a detailed kinematic analysis of central Namaqualand. As a large part of the previous work in the Bushmanland Subprovince has been devoted to structural interpretation it was important to provide petrological contraints in order to assess the tectonic models that had been proposed for the region. In some respects the Buffels River area is atypical of the general structural trends observed

throughout the Bushmanland Subprovince. The area in this study includes the high strain zone associated with the Buffels River Shear Zone (Joubert, 1974). The shearing deformation has imparted a well developed fabric and has to a varying degree obscured the earlier fabrics. However, the mineral assemblages and fabrics associated with shearing are prograde and thus the nature of the peak metamorphism can be investigated by simple reference to the last fabric producing event. An another advantage of the Buffels River area is the absence of a pervasive retrogressive event.

1.3 PRESENT INVESTIGATION

Reconnaissance sampling covering areas from the Orange River in the north to the Kamiesberg mountains in the south was used to delineate a target area for detailed mapping and petrological study. The Buffels River area, particularly the farm Hytkoras (see fig. 2.3) provided the ideal area to study the processes acting upon a variety of lithologies. The area was well documented by Joubert (1971), Zelt (1980), and Moore (1986). Excellent outcrop is easily accessible and the old river valleys provided sections across the E-W strike. A wide range of closely interbanded paragneisses are surrounded by metaluminous granitic gneisses. Four rock types: mafic gneisses, pelitic gneisses, calc-silicate granofelses and charnockitic gneisses have been studied in detail in order to constrain the temperature, pressure and fluid activity of peak metamorphism.

Photogeological and field reconnaissance on a scale of 1:30 000 over most of the Hytkoras area was undertaken in 1984-85. A small area along the Buffels River in the central part of Hytkoras, covering the contact between orthogneisses and supracrustal gneisses was sampled by D.J.Waters in 1986 to provide material for a stable isotope study. This strip was mapped on a scale of 1:4 000 using enlargements of 1:30 000 aerial photographs and by pacing out a grid in the field. Maps and local geology are described in Chapters 2 and 3.

In order to study the nature of metamorphic banding and relate textural history to metamorphic conditions multiple thin sections and probe sections were taken from single hand specimens. Laboratory work included the petrographic description of all rock types and electron microprobe analysis of the full mineral assemblage of representative samples of the major lithological groups. The extent of chemical

heterogeneity within each probe slide was investigated, particularly the nature of mineral zonation. Mineral data was used in experimentally and thermodynamically modelled geothermometers and geobarometers to evaluate metamorphic temperatures and pressures. Fluid activity was estimated from mineral equilibria in biotite- and amphibole-bearing assemblages. Kinetic models have been applied to garnet-biotite pairs in an attempt to place limits on cooling rates.

Oxygen isotope analysis of mineral separates from a wide range of orthogneisses and paragneisses, including quartz from coarse grained veins and segregations was used to assess the extent of isotopic equilibria across a small area. Oxygen isotope values together with studies of mineral equlibria have been used to assess the role of fluid infiltration in granulite-facies metamorphism.

A fluid inclusion study was undertaken at the University of the Orange Free State in 1987. Samples from a small representative suite of gneisses with coarse well-crystallised quartz were chosen. Rocks which showed evidence of shearing or retrogression were rejected in an attempt to limit the study to those rocks which might have trapped samples of fluid in equilibrium with peak metamorphic conditions. Secondary fluid inclusions provide a means of constructing possible post-metamorphic uplift paths.

The approach adopted in this thesis allows comparison with a number of documented granulite-facies terranes. The rocks studied belong to relatively simple chemical systems and have been collected from a very small area, and thus can be considered to be isofacial. The thrust of this thesis is directed towards monitoring the role of the fluid phase in metamorphism via the progress of dehydration and melting reactions in a variety of rock types. The use of as many available geochemical techniques and conceptual models as possible is necessary to tackle the question of the causative mechanisms of granulite-facies metamorphism. The fluid evolution and post-metamorphic uplift path of gneisses from the Buffels River area have important tectonothermal implications for the Namaqualand Metamorphic Complex and for low pressure Proterozoic granulites in general.

The approach followed in the structure of this thesis has been to relate the petrography, mineral chemistry and petrological interpretation of each of the major rock types in turn. It was found that each group of rock types provided specific clues as to the nature

of granulite-facies metamorphism in the area. The investigative approach also varied in respect to each lithology. When the petrological history of the major lithologies was documented it became easier to understand the interrelationships between rock units and move towards a comprehensive model for granulite-facies metamorphism throughout the area. In order to follow this approach it was necessary to begin by outlining the physical conditions of metamorphism experienced in the area. Over this very small area the majority of the samples are assumed to be isofacial in terms of pressure and temperature. The results of exchange geothermometry reflect the "effectiveness" of the particular calibration of the thermometer used. It is appreciated that a thorough investigation of the state of equilibrium reached by mineral-pairs used in exchange thermometry is neccessary to evaluate the results obtained. As the assessment of equilibrium and disequilibrium processes has been attempted during the investigation for each of the major rock types, the approach adopted i this thesis is not at variance with the principles involved in geothermobarometry.

1.4 ACKNOWLEDGEMENTS

In a project that has changed direction and scope many times since inception it is not surprising that the number of people who have affected my thinking concerning granulite-facies metamorphism in Namaqualand have grown with time. I think the only way to justify acknowledgements is to tell the full story of the project with a chronological perspective.

In 1983 I met with Dave Waters at Cambridge University to discuss a project concerning the amphibolite-facies - granulite-facies transition across western and central Namaqualand. The aim was to build on the excellent fieldwork and lithological and geochemical investigations of John Moore, who at that time was trying to finish his PhD. The project began with a reconnaissance raid on anything that was found to outcrop between the Orange River and the Kamiesberg Mountains. I was aided by Torsten Vennemann, who several years later, acted as my "minder" during my stable isotope study. My memory of that trip centres on soaring temperatures and the hard physical labour of excavating a bakkie from the sand of the Orange River with a frying pan. On that trip I visited the farms Rietfontein and Hytkoras for the first time. Without the help and hospitality of the Roux family of Rietfontein, particularly James and his son, Albertus, this project could never have been completed. The farms around the Buffels River provided the outcrop and lithological variation that convinced me that the bulk of the fieldwork should concentrate on these areas.

I acknowledge the receipt of a study bursary from the FRD, and the research grant which financed the fieldwork and analytical costs. It was in 1983 that Prof. Arch Reid took me on to the staff of the Geology Department at the University of Cape Town. Arch Reid provided much support and advice in those early days and I thank him for his role in getting me to Cape Town. Since 1983 I have taught hundreds of undergraduate geologists and civil engineers. Not only have they provided me with a living but they have helped keep my geological perceptions as wide as possible. In the next few years a young and dedicated team of students grew up around Dave Waters. I have Dave to thank for his excellent supervision. He showed me the power of linking a thermodynamic approach to natural assemblages, and using the field as our natural laboratory. Friends and fellow students Frankie Baars and Herman Grütter and more recently Huw Humphreys provided lively

discussion in the field and back at UCT.

The project was beset with problems between 1985 and 1986. I had suffered a disc lesion in the lower back on the first field trip in 1983. I failed to complete my fieldwork objectives in 1985 and was literally rescued from the field area by my good friends Simon Milner and Chris Harris. In 1986 I had the troublesome disc removed. I thank Dr Guillaume du Toit for his skills as a surgeon and the way he dealt with my case. Special thanks go to my physiotherapist, Lindsey Maas, who never gave up and kept me moving before the operation. As fieldwork had come to a dead halt I was forced to get into the laboratory. Dave Waters collected a series of samples from a small area in the Buffels River on Hytkoras. I then went about separating minerals for an oxygen isotope study. I thank Stuart Smith and Torsten Vennemann of the Department of Geochemistry at UCT for their help and tuition in the laboratory.

In 1987 with body and mind repaired (I finally decided a fear of snakes is a healthy paranoia) I returned for an idyllic field season on Hytkoras. Later that year I began the final stage of the project by starting a fluid inclusion study at the Department of Geology at the University of the Orange Free State. I would like to thank Prof. Aylva Schoch for the use of the laboratory and Rudi Boer for his help in learning the operating procedure on the Chaixmeca stage. I also benefitted from many discussions with the structural geologists in Bloemfontein, particularly Wayne Colliston and Schalk van der Merwe, who challenged my UCT bias on matters related to the tectonic evolution of Namaqualand.

Since, 1988 I have been involved in a game of disappearing supervisors. John Moore took over from Dave Waters when Dave departed for England. I have both to thank for reviewing various chapters of this thesis. Especially John who provided pragmatic comments and helped broaden my knowledge of regional geology in Namaqualand. Thanks to my present supervisor Maarten de Wit for just letting me get on with it.

I have been involved in microprobe analysis, using the Cameca Camebax microprobe in the Department of Geochemistry at UCT, since the beginning of this project and I must thank Dick Rickard for teaching me the rudiments of probing and especially for his work in the analysis of REE-bearing minerals.

Above all I wish to express my gratitude to the staff and students at UCT for making my postgraduate studies stimulating and enjoyable.

On a personal note thanks to Mum and Dad, for their support and good humour, even though they have no idea about what I actually do. Many thanks to Simon and Chris for years of support and encouragement.

CHAPTER 2

THE NAMAQUALAND METAMORPHIC COMPLEX

2.1 INTRODUCTION

This chapter outlines the regional tectonic setting of the Namaqualand Metamorphic Complex and discusses previous work on the area. The structural and metamorphic studies which relate to the Buffels River area are discussed.

2.2 REGIONAL TECTONIC SETTING

The Namaqua tectonic province (Hartnady et al., 1985) forms part of the Kibaran (1000-1200 Ma) system of mobile belts and is thought to be part of a continuous tectonic zone which extends from Natal beneath the Karoo cover (Tankard et al., 1982). The Namaqua Province (fig. 2.1) is bounded along the west coast of South Africa by the late Precambrian Gariep fold belt, and in the south by the Southern Cape Conductive Belt, which has been interpreted as a possible buried suture (DeBeer & Meyer, 1983). This important tectonic break is covered by late Precambrian Nama sediments, rocks of the Cape Supergroup and the Karoo Supergroup.

The eastern boundary of the Namaqua Province is a complex shear system along the contact with the Kaapvaal Craton (Tankard et al., 1982). The marginal zone between the Namaqua Province and the Kaapvaal Craton is occupied by the Kheis Province (Kröner & Blignault, 1976). The Kheis belt is a fold and thrust belt comprised of early Proterozoic metamorphosed sediments and amphibolites. A

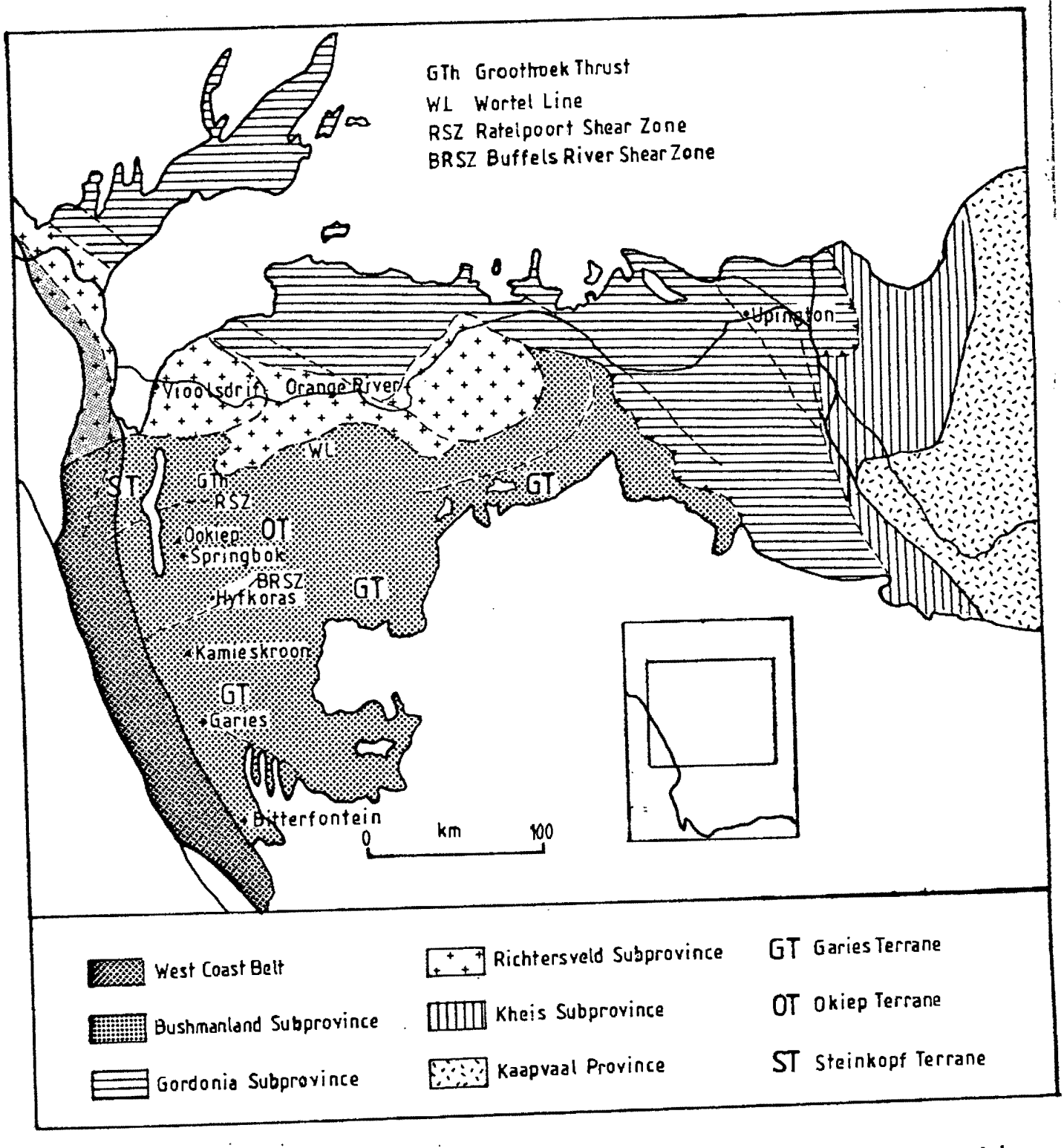

Fig. 2.1 Tectonic subdivisions of the Namaqualand Metamorphic Complex (after Hartnady et al., 1985).

basal sequence of basaltic rocks give a Rb-Sr isochron age of 2068±70 Ma (Barton & Burger, 1983). The Kheis Province is bounded to the west by the Gordonia Subprovince (Hartnady et al., 1985; Stowe, 1986). The Gordonia Subprovince consists of an older terrane consisting of 2000 Ma quartzites and pelites and a younger terrane of supracrustal gneisses interlayered with sheets of augen orthogneiss. A line of metamorphosed igneous complexes separates the Upington terrane from the high grade Kakamas terrane. This zone, termed the Jannelspan Formation (Geringer, 1979) may represent the closure of a back arc basin that initiated the Namaqua orogeny (Hartnady et al., 1985).

The western part of the Namaqua Province is divided into two subprovinces by a zone of extensive shearing. The Groothoek Thrust (Theart, 1980; Blignaut et al., 1983) a northward dipping ductile shear zone separates the 2000 to 1730 Ma Richtersveld Subprovince (Reid, 1982) and the 2000 to 1100 Ma Bushmanland Subprovince. A series of amphibolitised mafic and ultramafic bodies lying along the Groothoek Thrust are known as the Wortel Line (Joubert, 1974). The Richtersveld Subprovince consists of volcano-sedimentary rocks of the Orange River Group intruded by the Vioolsdrif Igneous Suite (Reid, 1977). The Vioolsdrif Suite is regarded as a subvolcanic root zone of a calc-alkaline volcanic pile (Reid, 1977; Blignault et al., 1980; Ritter, 1980). The volcanic rocks of the Haib Subgroup are thought to be 2000 Ma in age (Reid, 1979a) while the Vioolsdrif granitoids yield Rb-Sr and Pb-Pb isotopic data suggesting emplacement ages of 1700-1900 Ma (Reid, 1979b; Barton, 1983).

The central portion of the Namaqualand Metamorphic Complex (NMC) is termed the Bushmanland Subprovince (Hartnady et al., 1985; Joubert, 1986) and includes the area studied in this thesis. Tankard et al. (1982) refer to this broad area as the Central Zone of the Namaqualand Metamorphic Complex, with the Namaqualand highlands and the coastal plain being "its type area" (Joubert, 1971). There have been several attempts at tectonic subdivision into a series of smaller terranes. Hartnady et al. (1985) have divided the Bushmanland Subprovince into two terranes, the Okiep terrane and the Garies terrane. Colliston & Praekelt (1988) have divided up the Richtersveld and Bushmanland Subprovinces into the Pofadder terrane (Richtersveld), the Steinkopf terrane, the Aggeneys terrane and the Okiep terrane (Bushmanland), see fig. 2.2. The Garies terrane of Hartnady et al. (1985) is not recognised. Criteria for terrane

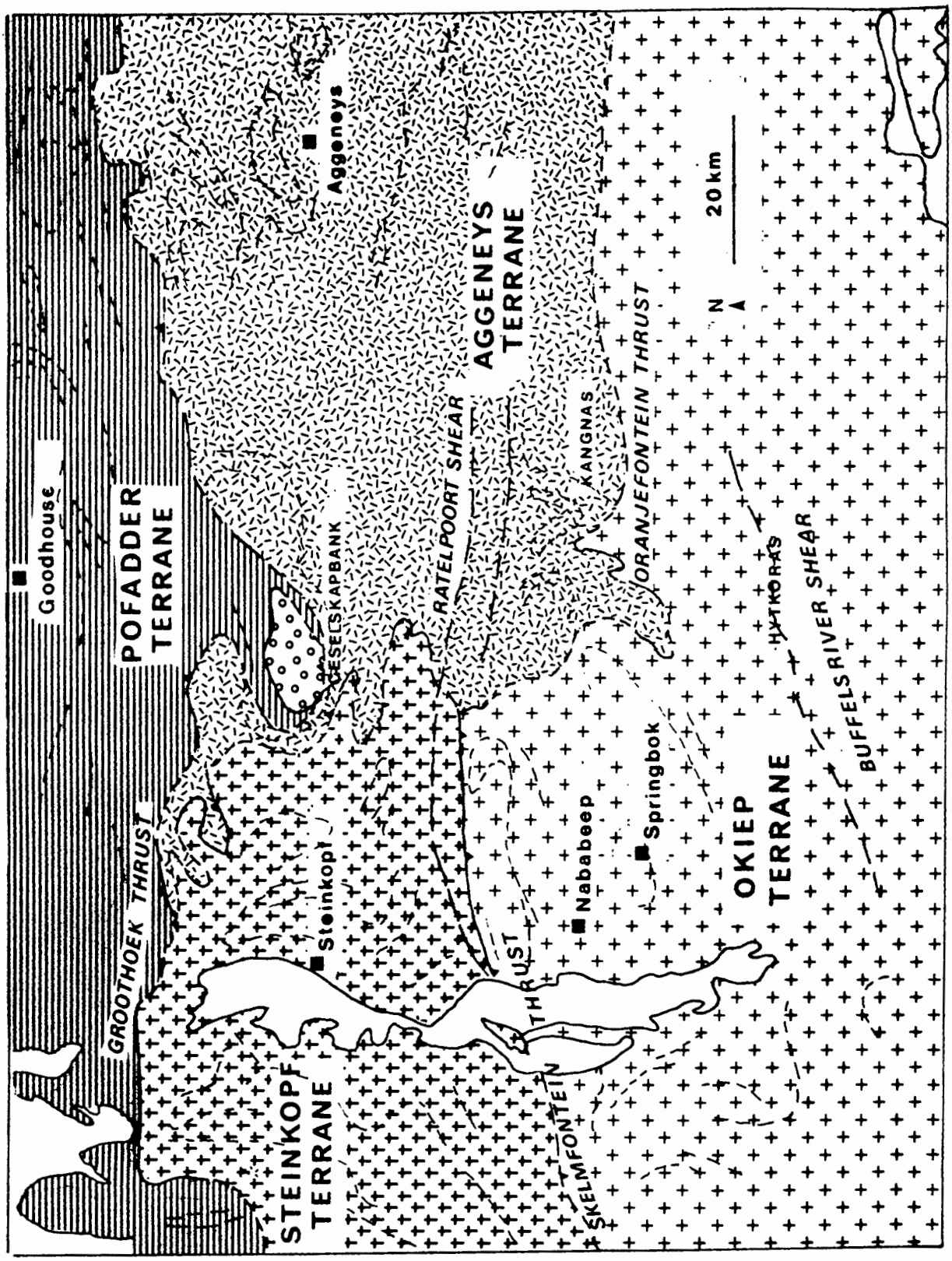

Fig. 2.2 Terrane subdivisions of the central Namaqualand Metamorphic Complex (after Colliston & Praekelt, 1988 and Colliston et al., 1989).

discrimination in the Namaqua context are dealt with by Hartnady (1987). Although the broad tectono-stratigraphic divisions have acceptance, many workers whose studies span so-called terrane boundaries find disagreement with the approach of Hartnady et al. (1985) and Colliston & Praekelt (1988). Harris (1987) gives a structural reinterpretation of a proposed subprovince boundary between the Garies terrane of the Bushmanland Subprovince and the Kakamas terrane of the Gordonia Subprovince and suggests tectonic continuity in the eastern Namaqua Province. Similar difficulties in interpretation affect the proposed boundary between the Aggeneys terrane and the Okiep terrane, termed the Oranjefontein thrust by Colliston & Praekelt (1988) and the proposed terrane boundary between the Okiep terrane and the Garies terrane of Hartnady et al. (1985) along the Buffels River Shear Zone. In this context it is important to note that late tectonic structures, in particular the late shears of Namaqualand, are not fundamental terrane boundaries, unless they form along pre-existing tectonic lines which juxtapose different lithostratigraphic units with distinct structural and metamorphic imprints.

The Steinkopf terrane (Blignault et al., 1983; Van Aswegen et al., 1987) is bounded by the Skelmfontein Thrust and the Ratelpoort Shear. The Ratelpoort Shear provides a convenient northern boundary to the rocks sampled in this study. The tectonic significance of the Ratelpoort Line is problematic. Largely inaccessible and almost entirely under thick sand cover its extension to areas east of the Steinkopf area is speculative. Moore & Reid (1988) favour lithological continuity in supracrustal sequences across the Ratelpoort Line and correlate gahnite-bearing metasediments at Oranjefontein across the Ratelpoort Line with similar metasediments at Achab near Pofadder. The Steinkopf terrane consists of granitic orthogneisses of the Gladkop Suite intruding an older series of supracrustal gneisses (Van Aswegen, 1983; 1988). Reconnaissance isotopic investigations in the Steinkopf terrane (Barton, 1983) suggest ages around 1800 Ma for the grey gneisses of the Gladkop Suite.

The Okiep terrane of Hartnady et al. (1985), which includes the Aggeneys terrane of Colliston et al. (1989), consists of lower basal units of porphyroblastic and banded biotite gneisses (Joubert, 1972; Moore, 1977; Watkeys, 1986) overlain by an extensive but relatively thin supracrustal sequence (Moore, 1986). The localites sampled in

this study lie within the Okiep terrane as defined by Hartnady et al. (1985). The various terranes in the western NMC are juxtaposed by the Groothoek thrust at Geselskapbank (see fig. 2.2). Along this zone the basement lithologies of the Richtersveld Subprovince and granulite-facies metapelites of the Grunau terrane of the Gordonia Subprovince have been thrust southwards over rocks of the Bushmanland Subprovince (Strydom & Visser, 1986; Van Aswegen et al., 1987). Detailed mapping and petrological investigation at the Slaphakskeenkop on the western margin of the Geselskapbank synform by Grütter (1986) indicate that older granulite-facies metapelites of the Geselskapbank formation were thrust over Bushmanland Group schists, and the entire package was metamorphosed to upper amphibolite-facies. The lowermost wedge of the overthrust sheet consists of biotite-hornblende schist and mafic gneiss and is considered by Grütter to belong to the Vioolsdrif Suite, however Strydom (1985) includes all these rocks in the Bushmanland Group. According to Colliston et al. (1989) the Groothoek thrust zone can be extended for more than 300 km from west to east. Ward (1989) points out that 90% of the trace of the Groothoek thrust does not outcrop. Similarities between supracrustal volcano-sedimentary rocks of the Orange River Group in the Richtersveld Subprovince and the Bushmanland Group (Reid et al., 1987) have also led to dissent as to whether the Groothoek thrust really is a major tectonic discontinuity (Ward, 1989).

The western part of Bushmanland from Geselskapbank southwards to Goinoep, has been mapped by Strydom (1985) on a scale of 1:100000 Geochemical sampling of supracrustal lithologies was undertaken by Moore (1986). The Buffels River area on the farms Rietfontein and Hytkoras was mapped by Joubert (1971), and Moore (1986) see fig. 2.3, petrological work on the mafic gneisses in this area was carried out by Zelt (1980) and geochemical sampling by Moore (1986). The area immediately to the east of the study area was mapped by Albat (1984) who compiled pressure-temperature data for granulites in that region.

The reconnaissance sampling for this study covered areas shown in fig. 2.3. The bulk of the samples come from the Buffels River area, mostly on the farm Hytkoras. The northern area of the studied strip consists of a schist-quartzite succession of the Bushmanland Group, which rests on various types of granitic gneiss. As difficulties were experienced in obtaining a diverse set of lithologies free from retrogressive alteration at these localities very few samples were

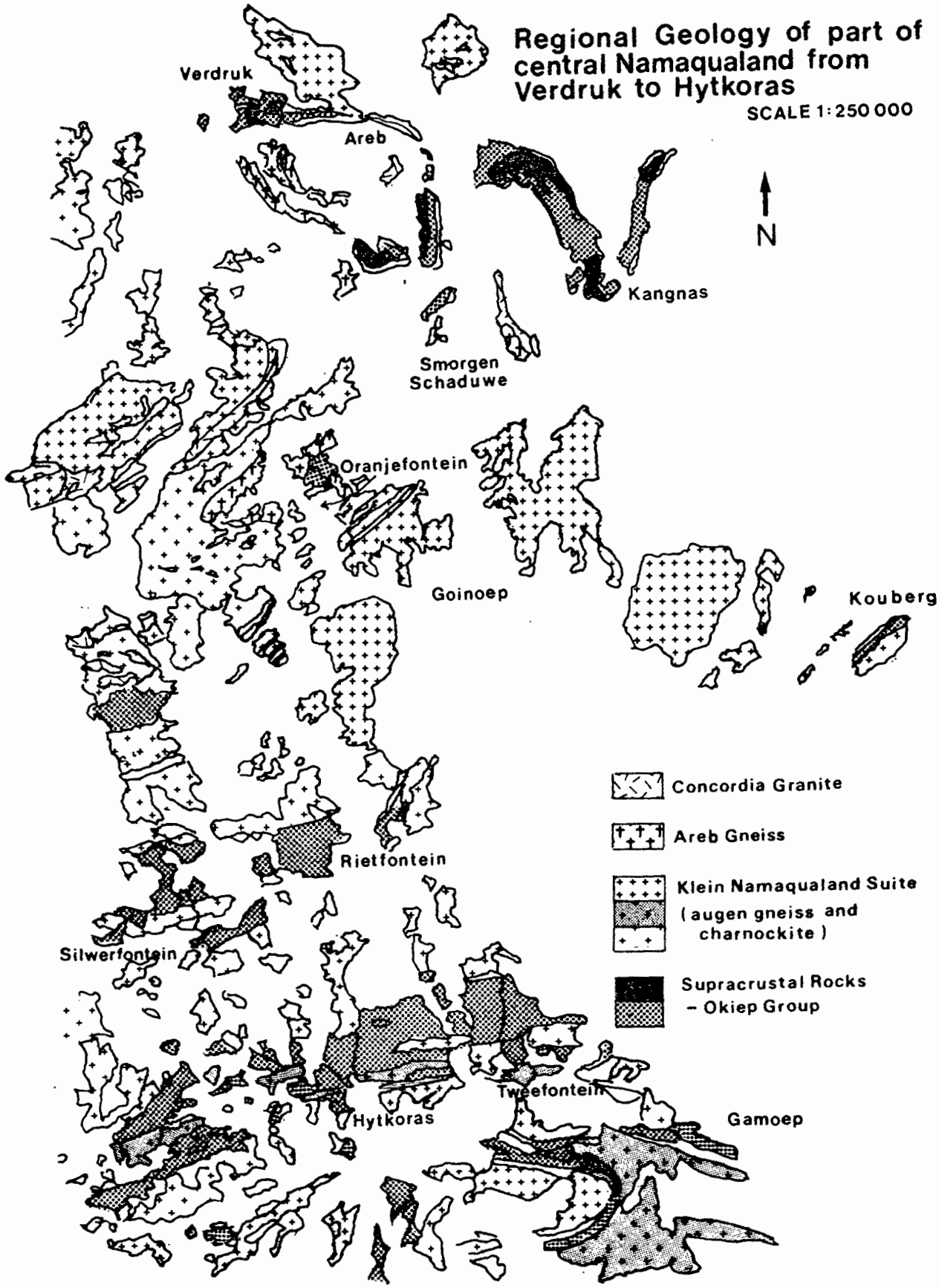

Fig. 2.3 Regional geology of part of central Namaqualand from Verdruk to Hytkoras.

examined in great detail. The following localties shown in fig. 2.3: Kouberg, Oranjefontein, Goinoep, Kangnas, Smorgen-Schaduwe, Areb, Verdruk are referred to in this study as the northern areas, or as the Kangnas mountain area. The geology of the Bushmanland Subprovince is discussed further below.

2.3 BUSHMANLAND SUBPROVINCE

2.3.1 Basement

One of the major problems involved in stratigraphic correlation in Namaqualand is the recognition of a basement to the cover sequence. No relicts of Archaean crust have yet been discovered. In the Aggeneys area the basal units comprise porphyroblastic and banded biotite gneisses (Watkeys, 1986). These include the Achab Gneiss (Moore, 1977 and Watkeys, 1985) and the rocks of the Gladkop Suite in the Steinkopf terrane. The Achab Gneiss gives Pb-Pb ages of 2020 ± 150 Ma, similar ages to gneisses of the Vioolsdrif area (Welke & Smith, 1984). Amphibolites in the overlying schist-quartzite succession give a Sm-Nd isochron age of 1649 ± 90 Ma. (Reid et al., 1987). Moore (1977) postulated that the Achab Gneiss might represent a basement to the supracrustal sequence in the Aggeneys area as it displayed more phases of deformation than the overlying units. The Achab gneiss consists of porphyroblasts comprised of feldspar-quartz aggregates, in high strain zones the porphyroblasts are flattened to produce a banded texture (Watkeys, 1986). The Achab gneiss contains a variety of xenoliths, particularly calc-silicate rocks, which point to an intrusive relationship with an older (pre-Bushmanland) sedimentary sequence. The Achab gneiss is overlain by pink quartzo-feldspathic gneisses, the contact is marked by a zone of refoliation and is interpreted by Watkeys as a footwall thrust. However, Watkeys prefers to regard the thrusting as being due to disharmonic décollement along the basement-cover interface rather than representing a major tectonic break.

In the southern areas of the Bushmanland Subprovince a basement is still more problematic. The base of the Okiep Group metasediments is generally considered to be a dark grey biotite gneiss, referred to by Joubert (1971) as Grey Gneiss. It appears to display at least one phase of deformation more than the overlying paragneisses and is itself intruded by a fine grained augen gneiss older than the

overlying metasediments (Joubert, 1971; Jack, 1980). No radiogenic isotope studies have been carried out in the Buffels River area and the age of the basal units is not known.

2.3.2 Supracrustal sequences

An extensive but relatively thin sequence of supracrustal rocks occurs throughout the Bushmanland Subprovince. In the northern areas of Bushmanland around Aggeneys the supracrustal sequence consists of a lower unit of pink quartzo-feldspathic gneisses and an upper unit of schists and quartzites. Most of the leucocratic gneisses of the lower unit are regarded as being pyroclastic deposits (Watkeys et al., 1988). The overlying units make up the Bushmanland Group (SACS, 1980). The sequence consists of quartz-biotite-sillimanite schist, quartzite, iron formations and chert, quartz-muscovite schist and conglomerate (Blignaut, et al., 1983; Moore, 1986). In the Aggeneys area the middle parts of the sequence, particularly the quartzites and iron formations are associated with Zn-Pb sulphide mineralisation (Ryan et al., 1986). Amphibolites appear at the top of the sequence and give a Sm-Nd isochron age of 1650 Ma (Reid et al., 1987), this gives a minimum age to the underlying sediments. Moore et al. (1990) regard the lower leucocratic gneisses as volcanic units that occur in the eastern part of the Richtersveld Subprovince and overlap into the Bushmanland Subprovince, and form thinner units further south in the Okiep Copper District. Moore (1986) considers the schist-quartzite successsion of the Bushmanland Group to represent reworked detritus from the same volcanic event that created the pink gneisses.

Colliston et al. (1984) and Van Aswegen et al. (1987) interpret the contact between leucocratic pink gneiss and the metasediments as a sole thrust. The thrust model has since been used to provide the basis for subdividing the northern Bushmanland Subprovince into a number of smaller terranes consisting of similar but uncorrelated cover sequences (Colliston, et al., 1989). The opposing model of Moore et al. (1990) contends that many of the formations recognised by Praekelt et al. (1983), Van Aswegen et al. (1987) and Colliston et al. (1989) can be correlated, and many of the thickness variations between formations are the result of lateral facies changes.

In the central parts of the Bushmanland Subprovince around Okiep

the supracrustal rocks form the Okiep Group (SACS, 1980). Quartzite-schist sequences occur in the northern part of the study area at Verdruk and are well exposed around Springbok, where Clifford et al. (1981) suggest that they may be correlated with similar assemblages in Bushmanland. This view is supported by Strydom (1984) and by Moore (1986) who recognises that a characteristic Ca-Na-Mg depleted chemical signature distinguishes these units from other supracrustal sequences in the western part of the Namaqualand Province. Further south in the Buffels River area there is less quartzite, and semi-pelitic and pelitic gneisses predominate. This change in lithology has been used to subdivide the supracrustal rocks in the central part of the Bushmanland Subprovince (the Okiep Group has prominent quartzites and the Garies Subgroup has fewer thinner quartzites). Joubert (1986) comments on the close similarities between the supracrustal sequences in the Steinkopf area and the Garies area. Moore (1980; 1986) suggests a series of sedimentary facies changes moving from north to south. He envisages a northern shallow marine or continental facies typified by pure quartzites and a central marine facies characterised by pelites, biotite gneiss and carbonates. In the south, around Bitterfontein feldspathic quartzites and pelites are thought to indicate a shallow marine environment.

2.3.3 Intrusive rocks

Intrusive granitoid gneisses of various ages occur throughout central Namaqualand in large east-west trending masses. A mass of enderbitic and charnockitic megacrystic intrusive rocks occurs in the Kliprand area to the south-east of the study area (Albat, 1984).

The dominant rock types in the central area of the Bushmanland Subprovince are intrusive augen gneisses of the Klein Namaqualand Suite (SACS, 1980). The dominant member of the intrusive suite in the Buffels River area is the Modderfontein Gneiss which consists of microcline-microperthite, quartz, plagioclase, biotite and minor garnet. Oval feldspar aggregates with a maximum diameter of 4 cm impart a foliation. Colour varies with biotite content and locally dark greenish patches of charnockitic gneiss occur. In the Okiep area, the Nababeep Gneiss is more common. The Nababeep Gneiss contains large composite quartz-feldspar augen surrounded by biotite. Individual augen reach the size of tennis balls in undeformed varieties. Shearing makes the distinction between the Nababeep Gneiss

and the Modderfontein Gneiss very difficult. Most of the intrusive augen orthogneisses in the study area are thought to be Modderfontein Gneiss (Prinsloo, pers comm., 1985). In the northern parts of the study area around Kangnas, Areb and Verdruk, the Areb Gneiss occurs. The Areb Gneiss is finer grained than the Modderfontein Gneiss, and consists of small composite augen. The Areb Gneiss is charaterised by a fine network of quartz-feldspar leucosome veinlets, some of which contain garnet. The Areb Gneiss has been correlated with the Brandewynsbank Gneiss of the Gladkop Suite (Strydom, 1984).

The Brandewynsbank Gneiss is thought to have an emplacement age of 1800 Ma (Barton, 1983). The early syntectonic (D_2) Klein Namaqualand Suite gives Rb-Sr ages of 1150 Ma with a relatively high initial Sr ratio of 0.725 (Reid & Barton, 1983). A poorly constrained Pb-Pb age of around 1500 Ma and the high initial Sr ratio suggest emplacement around 1500 Ma followed by metamorphic resetting between 1200 and 1150 Ma. Late tectonic (D_3) granitoids of the Spektakel Suite (SACS, 1980) give Rb-Sr ages between 1200 and 1100 Ma with low initial Sr ratios of 0.705 (Clifford et al., 1981). The emplacement age may coincide with the peak of thermal metamorphism (Clifford et al., 1981; Waters, 1988).

2.3.4 Structure

The majority of recent structural work in the Bushmanland Subprovince has concentrated on the structure and the tectonic setting of the Aggeneys/Gamsberg base metal deposits. As result of this the structural models developed in this area tend to dominate the literature.

The distribution of supracrustal sequences is strongly controlled by thrusting and isoclinal folding during an early deformational event. D_1 deformation as recognised by Moore (1977), Blignaut et al. (1983) and Jackson & Zelt (1984) is confined to the possible basement gneiss. It takes the form of intrafolial folding and fold interference patterns in the basal biotite gneisses of the Buffels River area (Jackson & Zelt, 1984). The above features could have been produced during the progressive regional deformation that Joubert (1971) terms D_2. It would seem that any earlier, D_1 fabric has been transposed and incorporated into a D_2 finite fabric. There is no indication of the metamorphic conditions accompanying the D_1 event. A

pre-Namaqua deformation is recorded in the Richtersveld Subprovince, referred to as the Orange River event by Blignaut et al. (1983). Folding with axial planar cleavage, extension lineations and a regional greenschist facies metamorphic imprint pre-date the intrusion of the Vioolsdrif Suite (Van der Merwe & Botha, 1989). It has not been possible to distinguish the Orange River event in the Bushmanland Subprovince.

The D_2 phase resulted in shortening and thickening of the crust by a series of thrust faults and recumbent isoclinal folds (Joubert, 1971; Blignaut et al, 1983; Jackson & Zelt, 1984; Strydom & Visser, 1986; Watkeys, 1986; Van Aswegen et al., 1987; Van der Merwe & Botha, 1989; Colliston et al., 1991). The planar elements associated with D_2 deformation are composite fabrics comprising foliation planes, shear and thrust planes and refoliations associated with recumbent folds. Linear elements comprise stretching lineations, composite augens and nodules, deformed clasts and xenoliths, and fold axes. Regional structural studies around the Aggeneys area (Watkeys, 1986 and Colliston et al., 1991) suggest that the general transport direction associated with the thrust faulting was chiefly from the north-east and the regional lineation pattern displays a dominant north-east trend. Colliston et al. (1991) explain the observed structural features by a process of subhorizontal progressive shear deformation. With increasing shear pre-existing linear fabric elements were rotated towards the transport direction. This event was accompanied by early syntectonic intrusions of granitic gneisses. The gneisses of the Klein Namaqualand Suite contain a D_2 planar fabric and the distinctive regional lineation (Joubert, 1971 and Blignaut et al., 1983). The D_2, Namaqua event resulted in the tectonic stacking of basement gneisses, supra-crustal sequences and intrusive orthogneisses into a series of E-W striking belts. Small scale structures such as minor isoclinal folds and mineral lineations are associated with this event. The resulting fabric is a composite flat-lying regional foliation.

The D_3 phase resulted in the development of prominent E-W striking shear zones and large scale open folds (Joubert, 1981; Blignaut et al., 1983; Jackson & Zelt, 1984). These structures post date all the major lithological units in central Namaqualand, except the intrusive rocks of the Koperberg Suite in the Okiep area, and the Orange River pegmatite belt (Tankard et al., 1982). Prominent steeply dipping shear zones, such as the Buffels River Shear Zone are

commonly associated with the limbs of large scale fold structures. In the north east part of the Bushmanland Subprovince Harris (1988) recognises that at all scales D_3 folds fold the D_2 lineation and planar fabrics. D_3 thrusts are marked by the development of cataclasites, the stretching lineation in the mylonites plunge downdip towards the north east, indicating transport towards the south west. Harris (1988) suggests that strike-slip shearing within the Bushmanland Subprovince and the Gordonia Subprovince initially took place at high temperatures, resulting in the formation of broad ductile shear zones with mylonitic fabrics. In central Namaqualand D_3 folds are open, upright structures giving rise to a dome and basin structural pattern. Strike-slip movement taking place along orthogneiss-paragneiss contacts. The Buffels River Shear Zone is a D_3 ductile shear zone which is steeply dipping to the south. A similar linear shear belt occurs in the Platbakkies area, near Garies (Baars, 1986). The shearing disrupts earlier structures and produces a spaced-refoliation. To the south of the Buffels River Shear Zone supracrustal rocks are exposed in two sheath-like, non-cylindrical, domal structures which represent the lower strain regime of D_3 deformation. The D_3 phase of deformation in central Namaqualand post-dates the intrusion of the Spektakel Suite of granitic intrusions (SACS, 1980) which do not contain D_2 structural elements. Thus, the emplacement age of the Spektakel Suite places upper and lower limits on the timing of the two deformational events. The age of the Spektakel Suite is approximately 1100 Ma (Clifford et al., 1975 and Reid & Barton, 1983). Clifford et al. (1981) and Waters (1988) speculate that this period of magmatic activity is associated with the major episode of thermal metamorphism in central Namaqualand.

N-S striking faults and minor folding occurs as part of a regional D_4 deformation and is probably uplift related.

Table 2.1 summarises the tectonic evolution of the Namaqualand Metamorphic Complex. The structural elements of the Buffels River area are described in more detail in Chapter 3.

2.3.5 Metamorphism

The regional metamorphic zonation across the Namaqualand Metamorphic Complex is shown in fig 2.4. (after Waters, 1986a; Joubert, 1986 and Waters, 1990). The general pattern is of broad areas of granulite and upper amphibolite metamorphism bounded by

patches of greenschist facies rocks.

Previous work on the metamorphic zonation in western and central Namaqualand is reviewed here. Joubert (1971) recognised that the metamorphic peak was post-F_2 in age, due to the presence of non-orientated porphyroblasts and granulite facies assemblages in intrusive sheets along F_2 foliation planes. Joubert considered that the metamorphic zonation was oriented NW-SE parallel to the Atlantic coast and proposed five zones from upper greenschist facies at the coast to garnet-granulite-facies in the Buffels River area. The recognition of a high pressure, high temperature garnet-granulite sub-facies was based on the assumption that almandine-rich garnet coexisted with clinopyroxene in certain granulose mafic rocks. These rocks have subsequently been identified as calc-silicate granofelses and the assemblage contains andradite-rich garnet coexisting with hedenbergite (Zelt, 1980). Albat (1984) showed that this association was widespread throughout central Namaqualand and also occurred in amphibolite facies areas. Albat (1984) has also recorded the assemblage garnet-orthopyroxene-clinopyroxene in one specimen. This specimen has an unusual Ca-Fe-Mn-rich bulk composition. The garnet has a significant component of both grossular and spessartine. Waters (1988) has applied the barometers of Bohlen et al., (1983a) and Powell & Holland (1988) to this assemblage yielding pressure estimates between 3.2 and 4.9 kbar.

Zelt (1980) working E-W along the Buffels River did not record any significant prograde zonation. However, Zelt did recognise a subsequent retrogressive event along the west coast. This metamorphic overprint caused replacement of pyroxene by blue-green hornblende in Namaqua age mafic gneisses, and produced amphibolite facies assemblages in the overlying Pan-African age Gariep Group (Waters et al., 1983; Jackson & Zelt, 1984).

Clifford et al., (1981) invoke very high temperatures (>800°C) in the Springbok area to explain high degrees of partial melting needed to generate certain magnesian gneisses. Clifford et al., (1975a) consider the Rb-Sr whole rock isochron age of 1187 ± 22 Ma for the Nababeep Gneiss as representing the age of the metamorphic peak and the F_2 folding in that area. Joubert (1976, 1981) regards the intrusion of Concordia Granite (Spektakel Suite) as a late syn-D_3 thermal event, dated at 1147 ± 33 Ma (Clifford et al., 1981). Joubert (1981) suggests that the metamorphic evolution involves at least two

distinct thermal events coinciding with the F_2 and F_3 fold episodes. However, Albat (1984) interprets the zonation patterns preserved in granulite-facies assemblages as being related to relatively simple single stage growth during a single metamorphic event. Waters (1988 and 1990) considers the 1187 Ma age (Clifford et al., 1975) as representing the timing of open system metamorphism associated with the imposition of the D_2 fabric, but that this was followed by further prograde mineral growth under relatively closed system conditions, resulting in low-variance peak assemblages (Waters & Whales, 1984; Waters, 1986).

Isograds and assemblage zones constructed by Waters (1986) are shown in fig 2.5. Amphibolite facies assemblages occur in the northern areas of Bushmanland. An equivalent southern amphibolite facies zone has been delineated by Waters et al. (1983) and Waters & Whales (1984) south of Bitterfontein. In central Namaqualand pelitic gneisses contain the assemblage garnet-cordierite-K feldspar, and the amphibolite-granulite facies transition in this area is defined by the reaction isograd:

Biotite + Sillimanite + Quartz = Garnet + Cordierite + K feldspar + H_2O

Waters (1986) recognises a higher grade granulite-facies zone in the Garies area, which is marked by the appearance of hercynite-rich spinel coexisting with quartz. The pelitic isograds correspond closely with the amphibole - two pyroxene transition in mafic rocks.

The granulite-amphibolite boundary as shown by Waters (1986) has a large bulge around the Springbok area and then swings southwards (see fig 2.4). This southward swing was recognised by Albat (1984), who considers that the boundary is structurally controlled by the late open folding. However, the transition in the area mapped by Albat is very poorly exposed and his orthopyroxene isograd for mafic gneisses is thus rather poorly constrained. Albat also notes outcrops of orthopyroxene-bearing mafic rocks well within his amphibolite facies zone. Altogether there seems to be considerable uncertainity in the precise location of the amphibolite-granulite facies boundary, if the Waters (1986) isograds are indeed correct a steep rise in peak metamorphic temperature moving from north to south is implied for the area covered in this study.

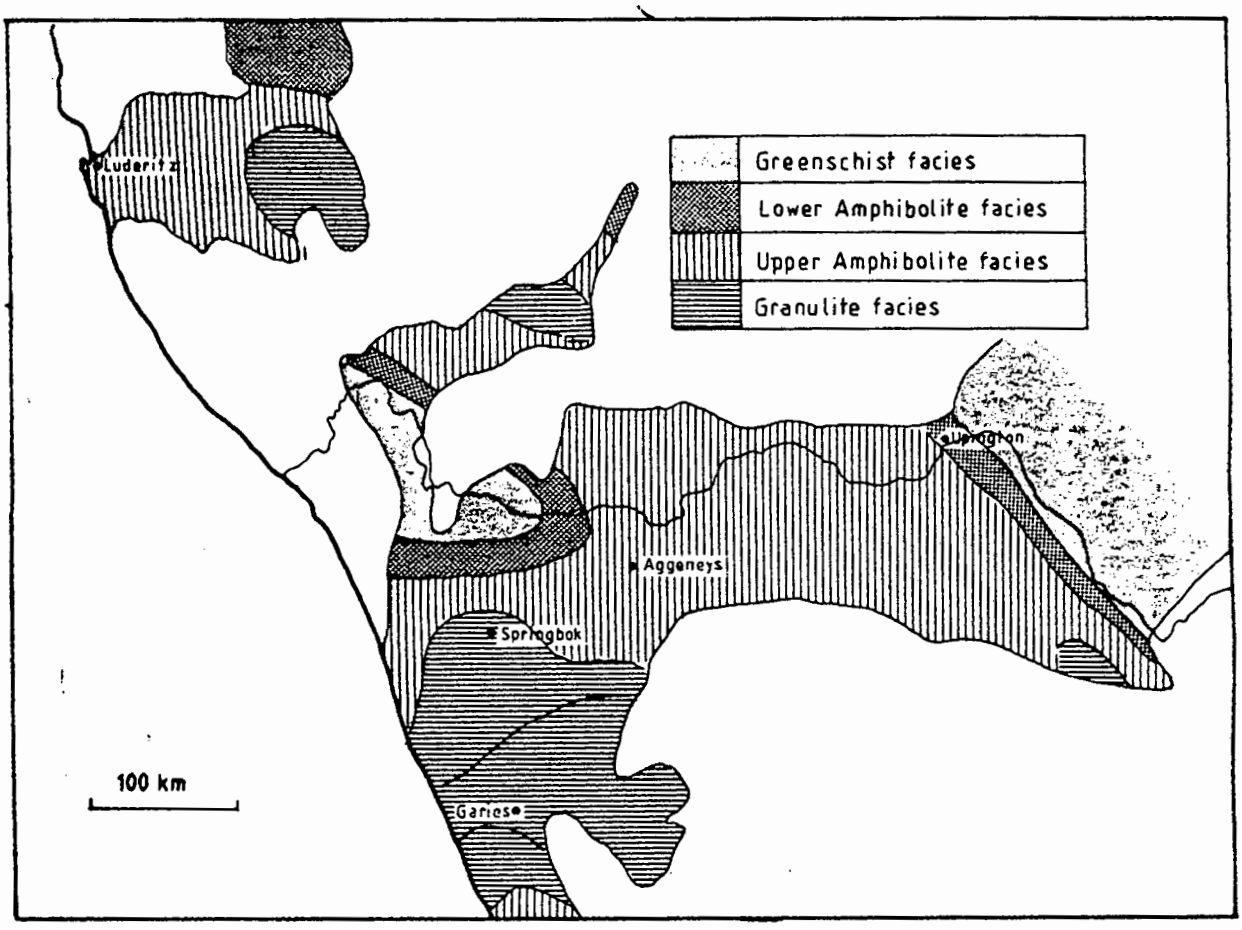

Fig. 2.4 Metamorphic zonation in the Namaqualand Metamorphic Complex.

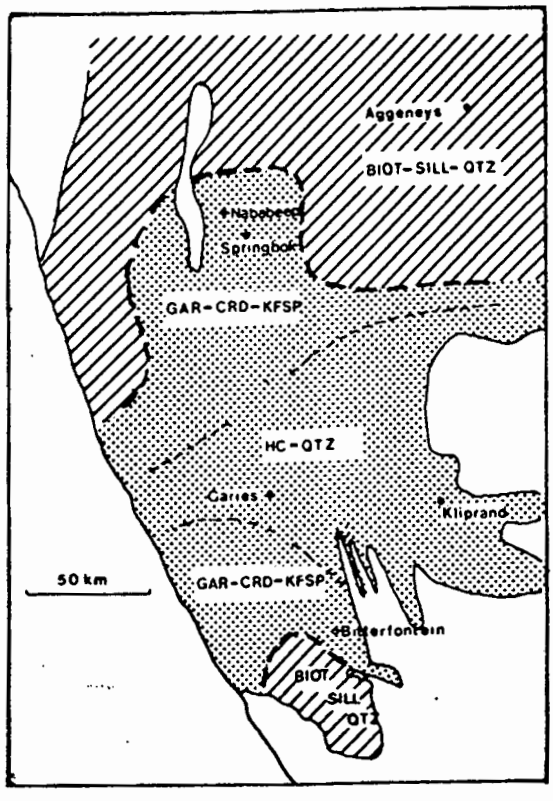

Fig. 2.5 Metamorphic zones and isograds in the Bushmanland Subprovince of the NMC (after Waters, 1986).

TABLE 2.1

TECTONIC EVOLUTION OF CENTRAL NAMAQUALAND

D_4 — S_4 locally developed, F_4 open folding,
N-S sinistral brittle shearing.
Medium P,T metamorphism, local retrogression.
Coeval with the opening of the Gariep trough.
≈ 950 Ma

D_3 — S_3 local fabric in E-W dextral ductile shear zones.
Upright, assymetric open E-trending major F_3 folds with shearing along steep limbs.
Granulite-facies metamorphism.
≈ 1100 Ma

D_2 — S_2 regional planar fabric and mineral lineation.
Shallow dipping recumbent, isoclinal folds and large-scale thrusting.
Amphibolite-facies metamorphism.
≈ 1190 Ma

Syntectonic intrusion of granitic augen gneisses, mafic sheets and dykes.

D_1 — S_1 gneissic layering, interfolial folds, transposition of original layering.
Precise nature of deformation and metamorphism unknown.

Deposition of supracrustal sequence
2000 - 1200 Ma ?
Basement ?

(Joubert, 1971 & 1986; Clifford et al., 1975 & 1981; Jack, 1980; Jackson & Zelt, 1984; Moore, 1986; Waters, 1990)

CHAPTER 3

GEOLOGY OF THE BUFFELS RIVER AREA

3.1 INTRODUCTION

This chapter aims to outline the field relationships, rock types and structures observed in the Buffels River area. Much of the detailed metamorphic work in this study was carried out within the Buffels River area on the farms Hytkoras and Rietfontein (see figs. 3.1 and 3.2). Although structurally complex, the area provides one of the few examples of a relatively diverse supracrustal sequence intimately associated with granitic orthogneisses. There has been very little retrogression, so the textures and mineralogy of peak metamorphism are well preserved. In the northern areas of central Namaqualand there is a near-pervasive greenschist-facies overprint. Particularly badly affected are pelitic rocks underlying the massive quartzites of the Bushmanland Group. All samples collected from the Kangnas mountains, Verdruk, Oranjefontein, and Goinoep in this project and by Moore (1986) and Evans (1988) show evidence of pseudomorphic retrogression similar to that described by Corbett & Phillips (1981) at Broken Hill, Australia. In some outcrops material preserving the peak metamorphic assemblage has been obtained, from Verdruk by the author and by J.M. Moore, and from Goinoep and Oranjefontein (see fig 2.3) to allow geothermometry of granulite-facies assemblages (see Chapter 4). Although there is little doubt that granulite-facies conditions prevailed throughout the area to the south of the Ratelpoort Shear, a thorough appraisal of metamorphic conditions affecting a wide variety of rock types is made difficult.

In subsequent sections of this thesis the principal rock types in

the Buffels River area are described in terms of their field relationships, mineralogy and textures. Petrological models based on well documented chemical systems are presented. Only the comparatively scarce magnesian gneisses have been omitted as they have been carefully documented already by Waters and Moore (1985), Waters (1986b) and Moore & Waters (1990).

3.2 LITHOLOGICAL DESCRIPTIONS

3.2.1 The supracrustal succession

On the basis of field evidence alone it is uncertain whether the gneisses in the basal part of the supracrustal sequence acted as the basement to a sedimentary cover sequence. Detailed isotopic work is required to resolve this problem. The stratigraphic relations of the supracrustal rocks and intrusive gneisses are described below and are shown shown schematically in fig. 3.3.

3.2.1.1 Grey biotite gneiss

Fine to medium grained biotite gneiss has a wide distribution throughout the Buffels River area and forms the basal unit of a diverse supracrustal succession. The biotite gneiss is grey in colour, with a finely banded or migmatitic texture. The gneissic foliation is highly deformed and traces of an early episode of deformation, not apparent in other gneisses, are seen as mushroom-type interference structures (see plates 3.1 & 3.2).

Dark brown biotite is an essential constituent. Plagioclase is the dominant feldspar, myrmekite is commonly observed in thin section. Magnetite is closely associated with biotite which together define the gneissic foliation. Garnet is found in some examples as xenoblastic grains in thin bands.

Patchy migmatization is common with white veins of leucosome running sub-parallel to the metamorphic banding. Mafic gneisses with discordant contacts intrude the biotite gneiss and are elongated sub-parallel to the foliation and exhibit boudinage. The surrounding biotite gneiss develops a strong foliation adjacent to the competent mafic gneiss.

Fig. 3.1 Geological map of the Buffels River area, Hytkoras.

Key

Lithologies

- Metagabbro & Pyroxenite
- Gneissic Granite
- Mafic Gneiss
- Augen Gneiss
  - Charnockite
  - Modderfontein Gneiss
  - Nababeep Gneiss
- Sillimanite Gneiss
- Quartzite
- Leucogneiss
- Magnesian Gneiss
- Pelitic Gneiss
- Grey Biotite Gneiss

RIETFONTEIN

DABEEB

N

DWN332
MCS301-06

DWN128

MCS380

DWN349
Snake Gully
MCS307
DWN353

HY8

Dreadhoek

Hans Vos se Bank

HYTKORAS

Bloubanke

TWEEFONTEIN

Buffels River

MCSH02

MCSH04-05

THE GEOLOGY OF THE HYTKORAS AREA

Scale 1:30 000

3 km

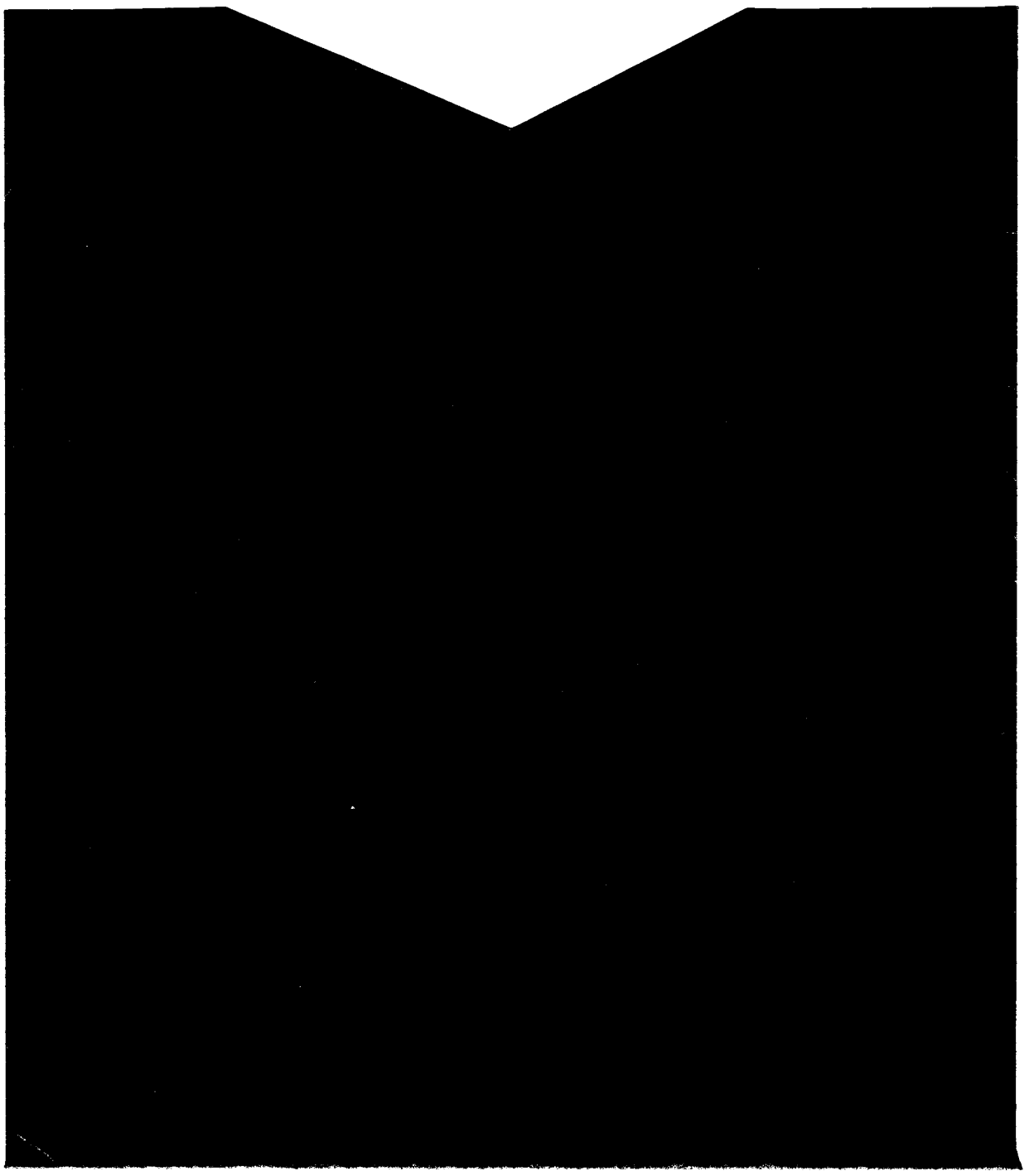

Fig. 3.2 The Geology of the Buffels River Shear Zone, Hytkoras A small area south of Draaihoek by the Buffels River. Includes outcrop localities for samples used in the oxygen isotope study (see Chapter 9).

THE GEOLOGY OF THE BUFFELS RIVER SHEAR ZONE, HYTKORAS

Key

Lithologies

- Gneissic Granite
- Augen Gneiss
- Leucogneiss
- Quartzite
- Sillimanite Gneiss
- Mafic Gneiss
- Magnesian Gneiss
- Pelitic & Quartzo-feldspathic Gneiss
- Grey Biotite Gneiss

- Farm track
- Limit of outcrop
- 60 Strike & dip of foliation
- 20 Plunge of lineation
- MCS358 Sample locality

Scale 1:4000

200 m

to Draaihoek

N

Buffels River

to Rietfontein

MCS327

MCS392

MCS390

DWN627

MCS358

DWN380-381

DWN626

MCS395

DWN625

DWN624

MCS393-394

MCS387

DWN621-623

DWN615-620

DWN613

DWN614

DWN628

DWN629-632

MCS321-322

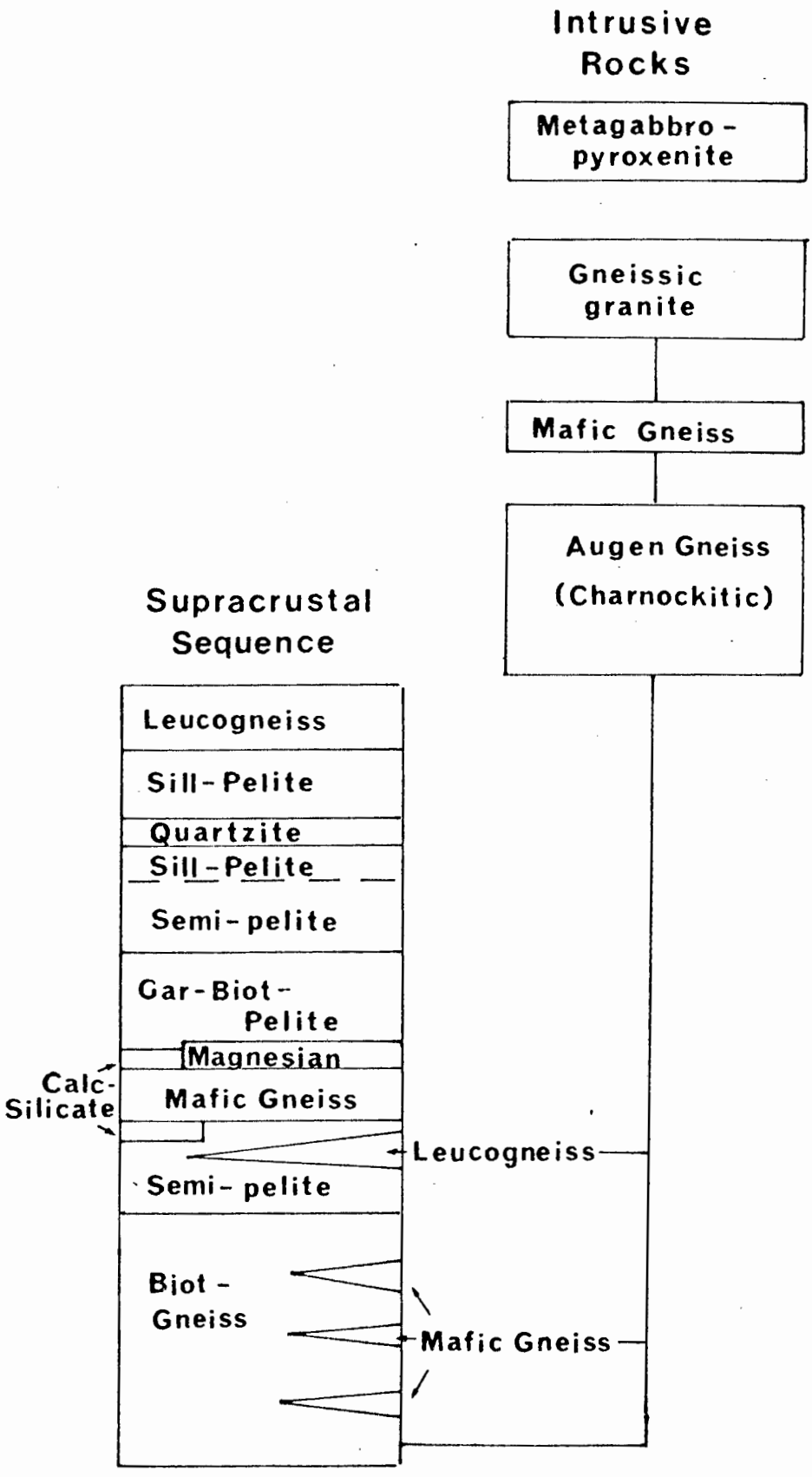

Fig. 3.3 Stratigraphic relationships in the Buffels River area

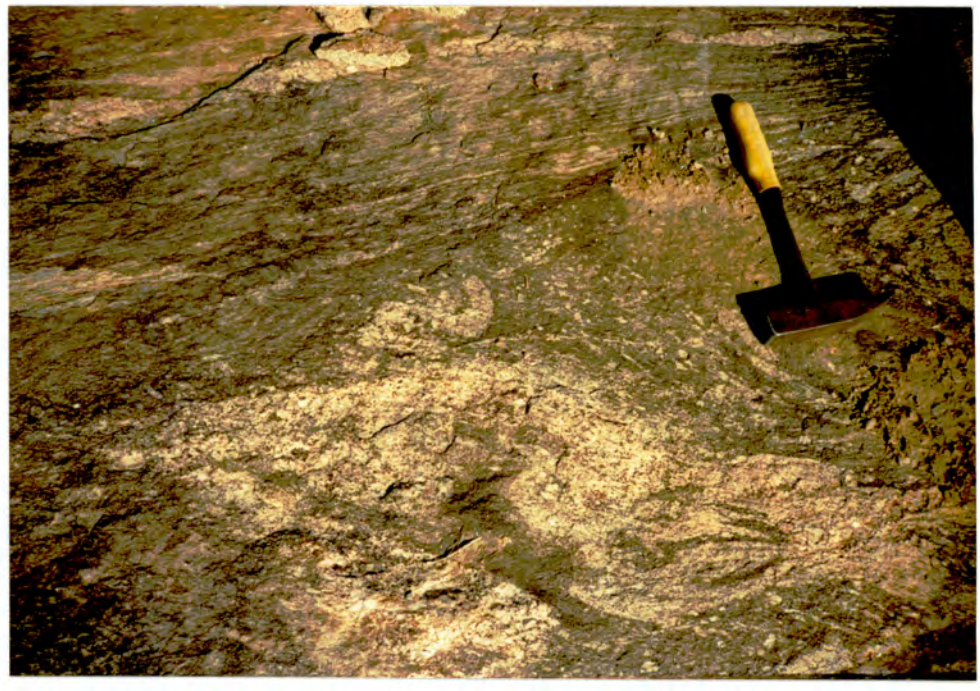

Plate 3.1 Heterogeneous grey biotite gneiss showing strongly developed S_3 fabric and nebulous leucocratic patches Hytkoras.

Plate 3.2 Disaggregated mafic band within strongly foliated grey biotite gneiss. Hytkoras.

3.2.1.2 Quartzo-feldspathic gneiss (semi-pelitic gneiss)

This group of rocks is highly variable. The term quartzo-feldspathic gneiss is used here to avoid genetic terminology and is intended to describe all types of quartz-feldspar-rich paragneiss occuring closely associated with grey biotite gneiss and pelitic gneisses. These types of gneiss are distinct from the leucogneisses described by Joubert (1971) and Moore (1986), see Section 3.2.1.3, also referred to as pink gneiss, leptynite and leptite (Joubert, 1971). Leucogneisses are thick continuous units generally poor in biotite, whereas quartzo-feldspathic gneiss normally grades into biotite-rich pelitic bands. Gradational relationships suggest a metasedimentary origin. These gneisses tend to be finer grained than adjacent biotite gneiss with a well banded flaggy appearance. Thin bands of quartz-plagioclase rocks occur and grade into diopside or andradite-bearing calc-silicate gneiss. Stringers of coarse pegmatitic quartz and K-feldspar are common.

Coarse-grained lenses of leucocratic quartzo-feldspathic rock occur throughout the supracrustal sequence. Some are noticeably discordant, but most appear to parallel the regional foliation. These rocks have the mineralogy of granitic minimum melts and are thought to be migmatitic leucosomes formed by the partial melting of pre-existing gneisses (Albat, 1984).

3.2.1.3 Leucogneiss

Quartzo-feldspathic granoblastic gneisses occur towards the base of the supracrustal sequence. The leucogneisses aare medium-grained and pink in colour, weathering to reddish brown. Banding is rare, with evenly distributed mafic minerals present in very small quantities (<5%). Microperthite is the major constituent, forming large (2mm) poikiloblasts. Rounded quartz is present as inclusions and as strained grains in the matrix. Mafic minerals are typically biotite, garnet, or magnetite. Plagioclase is a minor constituent (<10%). Joubert (1971) considers these rocks to represent metasediments. Absence of textures commonly associated with metasediments such as graded bedding or compositional variation suggest that these units could be igneous in origin, perhaps a

rhyolitic tuff.

3.2.1.4 Calc-silicate granofels

Small amounts of plagioclase-rich calc-silicate rock occur in the Buffels River area at Hytkoras. However, at Rietfontein they form thicker units and make up a significant proportion of the supracrustal package and are more widespread than pelitic and magnesian gneisses. Carbonate rocks are rare and only isolated occurrences have been noted. Moore (1986) sampled one carbonate locality at Hytkoras and a dolomitic marble to the east of Hytkoras at Velskoen in the Buffels River area. The Hytkoras example is poorly exposed and in thin section appears partly recrystallized and somewhat altered.

The calc-silicate rocks encountered in this study are carbonate-free rocks with a ferrocalcic or magnesiocalcic composition. Some show well developed compositional banding with alternating garnet-rich and clinopyroxene-rich layers. Others are more massive consisting of a polygonal mosaic of plagioclase, quartz and a variety of mafic minerals and are best described as granofelses. The detailed petrography of these rocks is discussed in Chapter 7.

There are two main groups of calc-silicate rocks: garnet-bearing granofels and banded diopside-plagioclase gneiss. Both occur towards the lower portion of the supracrustal sequence, as bands within the biotite gneiss and leucogneisses underlying the main pelitic units. Garnet-rich rocks are more massive, normally consisting of plagioclase and large dendritic poikiloblasts of andraditic garnet (up to 20 mm across). Dark green clinopyroxene occurs either in distinct bands or rimmed by garnet in a symplectic intergrowth with quartz and magnetite. Titanite is a minor constituent in most calc-silicate rocks. Scapolite- bearing rocks are less common. Some types have dark green amphibole in addition to clinopyroxene. Magnetite is present in all samples except those rich in quartz and garnet where clinopyroxene is absent. Titanite and magnetite are invariably seen in the same rocks, sometimes titanite forms fine rims around coarse magnetite grains.

Calc-silicate rocks have unusual bulk chemistry (Moore, 1986). Some of these rocks are enriched in REE, particularly Ce, La and Nd.

Allanite-rich granofelses occur at Bobbejaanpoort on the farm Rietfontein and at Smorgen-Schaduwe in the Kangnas mountain area. Their origins are discussed by Moore & McStay (1990) and their petrography is dealt with in Chapter 7.

3.2.1.5 Pelitic gneiss

Pelitic and semi-pelitic gneisses are major consitituents of the supracrustal sequences in the Buffels River area and their petrography and metamorphism is dealt with in detail in Chapter 6.

There are three main lithological groups of pelitic gneiss:

garnet-biotite gneiss
cordierite gneiss
sillimanite gneiss

Garnet-biotite gneiss is the dominant pelitic rock type consisting of very coarse grained garnet porphyroblasts (normally 5-20 mm, and in one extreme case up to 180 mm) within pale-coloured quartz-K-feldspar- rich veins and stringers. Biotite is the dominant constituent of the dark mesosome. In migmatitic varieties, quartz is present in large quantities and plagioclase is a significant component. Garnet is commonly elongated in the plane of the foliation, aligned parallel with biotite flakes. Minor cordierite occurs in fine bands or along the edges of some garnet crystals. However, large porphyroblasts of cordierite and garnet are rarely found in close contact with each other.

Cordierite gneisses tend to be dark in colour, either poorly banded, or schistose and micaeous in character. The assemblage commonly consists of: quartz-cordierite-sillimanite-biotite. Some rocks grade into magnesian gneisses, with less quartz than pelitic types and contain orthopyroxene. Large cordierite poikiloblasts with inclusions of quartz and sillimanite are distinctive and normally show well developed twinning. Sillimanite is commonly acicular and associated with biotite in the absence of garnet. Biotite is red-brown in colour and can be a very minor constituent or form 40-50% of the rock in the more micaeous (phlogopitic) magnesian pelites. Plagioclase is a minor phase. K-feldspar is either absent or present in small quantities, except in coarse-grained cordierite-bearing segregations, where large cordierite porphyroblasts are embayed by

coarse-grained quartz and K-feldspar. The assemblage cordierite-orthopyroxene-garnet-biotite-quartz is recorded in two samples and occurs in association with magnesian gneiss.

Sillimanite gneiss forms distinctive units of pink to white coloured, finely banded rock. Sillimanite-quartz-K-feldspar is the dominant assemblage with small amounts of either garnet or cordierite in some samples. Biotite is rare. Sillimanite forms discontinous bands of acicular crystals which define the foliation (see plate 3.3 and 3.4).

The lower parts of the pelitic sequence are cordierite-rich, sillimanite-poor. Sillimanite-rich units occur in the upper parts of the sequence and are closely associated with vitreous crystalline quartzites.

3.2.1.6 Magnesian gneiss

Mg-rich rocks are found in close association with pelitic gneisses and mafic gneisses. They can be subdivided into three main groups: cordierite-phlogopite gneisses, quartz-bearing cordierite gneisses with minor orthopyroxene, and quartz-free rocks with abundant ortho-pyroxene, cordierite and phlogopite. Other constituent minerals include: sapphirine, plagioclase, spinel, tourmaline, kornerupine, corundum, and garnet. Magnesian gneiss units are normally less than one metre thick but can be up to five metres in thickness. Their field relationships are fairly constant. Orthopyroxene magnesian gneiss directly overlies thick mafic gneiss bodies. Cordierite-phlogopite magnesian gneiss occurs above this and grades into cordierite-bearing pelitic gneiss.

The origin of these gneisses is discussed by Clifford et al. (1975b) and by Moore (1986). Clifford et al. interpreted orthopyroxene-sapphirine magnesian gneisses as restites after the removal of 75-80% of granitic liquid from a shale parent. This is not favoured by Moore due to their close association with pelites which have not undergone similar degrees of partial melting. Quartzo-feldspathic gneisses cannot be related to the magnesian gneisses as a simple melt extracted from a pelitic source (Moore, 1986). Cordierite-anthophyllite rocks with identical chemical compositions to the magnesian gneisses of the Nababeep region occur in the

Plate 3.3 Garnet-cordierite-sillimanite gneiss. Coarse grained garnet porphyroblasts in patchy K-feldspar-rich segregations disrupting the foliation. River bed, Hytkoras.

Plate 3.4 Pink sillimanite gneiss. Foliation is picked out by flat plates of fibrolitic sillimanite. River bed, Hytkoras.

amphibolite facies areas of Bushmanland, where peak metamorphic temperatures were too low to permit such high degrees of melting. Moore suggests a precursor rich in chlorite and illite, possibly a degraded mafic volcanic rock.

The metamorphic history of these rock types is dealt with in Water & Moore (1985) and Waters (1986a). The textural history involves the growth of fine grained prograde granulite facies mineral assemblages pseudomorphing earlier amphibolite facies minerals, Waters suggests that this occurs with increasing temperature and decreasing $a_{(H2O)}$ at constant or increasing pressure. A third generation of coarse-grained cross-cutting hydrous minerals (gedrite, kornerupine, and phlogopite) is seen. Post-peak mineral growth may result from the influence of aqueous fluids released by crystallizing partial melts as suggested fo the Willyama Complex, Broken Hill, Australia (Corbett & Phillips, 1981).

3.2.1.7 Mafic gneiss

Mafic gneisses are widespread throughout the Buffels River area. Mafic bodies range in size from thin boudinaged lenses amongst the paragneisses, to thick sheet-like bodies in the middle portions of the supracrustal sequence, and as large post-tectonic intrusions (see 3.2.2.3). Thick mafic gneiss units are concordant with the supracrustal sequence and occur above the biotite gneiss unit. They are commonly overlain by magnesian gneisses or calc-silicate rocks. This relationship has been interpreted as being due to weathering and degradation of mafic volcanics (Moore, 1986). The smaller bodies are impersistent and although shearing has drawn most into parallelism with adjacent gneisses, intrusive relationships can be demonstrated. Although not strictly paragneisses, these small sheet-like intrusives make up an integral part of supracrustal succession. Both the thicker metalavas and thin lenses are chemically similar and probably represent Fe-enriched tholeiites (Zelt, 1980).

The metalavas consist of coarse-grained hornblende-rich granulite or amphibolite with large poikiloblasts (up to 100 mm) of pyroxene, giving rise to a distinctive spotted appearance (see plate 3.5). The middle parts of thick units are often characterised by coarse grained plagioclase-quartz-pyroxene segregations and veinlets.

Plate 3.5 Coarse grained mafic gneiss consisting of large poikiloblastic pyroxenes (bleached, brown areas) and relict patches of amphibolite (dark patches). Bobejaanpoort, Rietfontein

Plate 3.6 Banded mafic intrusion in augen gneiss. Note the narrow bleached, granulite margin and darker hornblende-rich interior domain. River bed, Hytkoras

All mafic gneisses without exception show strongly developed mineralogical banding. The margins of small mafic bands are fine- to medium-grained, hornblende-absent, orthopyroxene or two-pyroxene granulites. The inner parts may be pyroxene-absent amphibolites, or hornblende granulites.

Small lenses of mafic gneiss are common within the basal biotite gneiss and also intrude the augen gneisses (see plate 3.6). They appear to predate the D2 deformation event, but are sub-concordant due to strong attenuation and refoliation in the Buffels River Shear Zone. Most are strongly boudinaged. The margins of mafic gneisses are normally strongly recrystallised to a fine-grained granoblastic orthopyroxene-plagioclase-quartz assemblage, with small orthopyroxene poikiloblasts elongated parallel to the foliation.

More Mg-rich mafic rocks occur within the lower portions of the biotite gneiss. Their mineralogy is similar to other mafic gneisses, although the hornblende has a distinctive paler green-brown colour. These may represent an earlier mafic suite or a less evolved magma type associated with the emplacement of the main tholeiitic suite (Jackson & Zelt, 1984).

The detailed petrography and metamorphic evolution of the mafic gneisses is dealt with in Chapter 5.

3.2.1.8 Quartzite

Quartzites, although dominant in the northern areas in Bushmanland (Moore, 1986) are a relatively minor component of the paragneiss sequences in the Buffels River area. Quartzites form a thin band at the top of the sequence and are closely associated with pelitic sillimanite gneiss. They are massive and coarsely crystalline, vitreous, white or bluish-grey in colour. They commonly contain a little biotite which gives the rock a slightly darker colour.

3.2.2 Intrusive rocks

3.2.2.1 Augen gneiss

Coarse grained augen gneisses are the dominant lithology throughout the central part of the Bushmanland Subprovince. They form distinctive, brown weathering gneiss domes striking E-W between low ridges of supracrustal gneisses. Their mineralogy consists of composite augen of flattened K-feldspar and quartz. The augen are commonly sheared to produce a lenticular fabric in the shear zones. Plagioclase and quartz (including myrmekite) forms the bulk of the matrix, and biotite is normally the mafic constituent (3-5 volume % biotite is typical). However, some augen gneisses are hornblende-bearing, whilst others contain orthopyroxene or garnet (see Chapter 8). Xenoliths of aluminous rocks are common and occasionally large rafts of grey gneiss are seen.

Incipient metamorphic charnockitisation occurs at contacts with the supracrustal gneisses. Dark green patches and veins contain coarse- grained K-feldspar, quartz and equant pseudomorphs of dark green biotite, chlorite and iron oxides after orthopyroxene. Away from the contact zone the augen gneiss is finer grained, paler coloured, without charnockitic veins and patches. Small amounts of orthopyroxene occur throughout.

Within the augen gneisses are sheets of charnockitic gneiss (plate 3.7). They are very strongly weathered, with a characteristic dark brown colour. Their mineralogy is similar to the main suite but with a higher content of orthopyroxene and hornblende.

The augen gneisses exposed in the Buffels River area are members of the Klein Namaqualand Suite (SACS, 1980) thought to represent the intrusive products of the partial melting of a 2000-1900 Ma crustal protolith (Reid & Barton, 1983). On a regional scale the augen gneisses occur as large, tabular bodies, associated with D_2 thrusting and overfolding. The augen gneisses contain a shallow-dipping planar fabric and the augen define a regional L_2 mineral lineation (Joubert, 1971; Blignaut *et al.*, 1983; Jackson & Zelt, 1984). Joubert (1971) considered the gneisses of the Klein Namaqualand Suite to be the basement to the supracrustal succession in the Buffels River area,

3.2.2 Intrusive rocks

3.2.2.1 Augen gneiss

Coarse grained augen gneisses are the dominant lithology throughout the central part of the Bushmanland Subprovince. They form distinctive, brown weathering gneiss domes striking E-W between low ridges of supracrustal gneisses. Their mineralogy consists of composite augen of flattened K-feldspar and quartz. The augen are commomly sheared to produce a lenticular fabric in the shear zones. Plagioclase and quartz (including myrmekite) forms the bulk of the matrix, and biotite is normally the mafic constituent (3-5 volume % biotite is typical). However, some augen gneisses are hornblende-bearing, whilst others contain orthopyroxene or garnet (see Chapter 8). Xenoliths of aluminous rocks are common and occasionally large rafts of grey gneiss are seen.

Incipient metamorphic charnockitisation occurs at contacts with the supracrustal gneisses. Dark green patches and veins contain coarse- grained K-feldspar, quartz and equant pseudomorphs of dark green biotite, chlorite and iron oxides after orthopyroxene. Away from the contact zone the augen gneiss is finer grained, paler coloured, without charnockitic veins and patches. Small amounts of orthopyroxene occur throughout.

Within the augen gneisses are sheets of charnockitic gneiss (plate 3.7). They are very strongly weathered, with a characteristic dark brown colour. Their mineralogy is similar to the main suite but with a higher content of orthopyroxene and hornblende.

The augen gneisses exposed in the Buffels River area are members of the Klein Namaqualand Suite (SACS, 1980) thought to represent the intrusive products of the partial melting of a 2000-1900 Ma crustal protolith (Reid & Barton, 1983). On a regional scale the augen gneisses occur as large, tabular bodies, associated with D_2 thrusting and overfolding. The augen gneisses contain a shallow-dipping planar fabric and the augen define a regional L_2 mineral lineation (Joubert, 1971; Blignaut *et al.*, 1983; Jackson & Zelt, 1984). Joubert (1971) considered the gneisses of the Klein Namaqualand Suite to be the basement to the supracrustal succession in the Buffels River area,

Plate 3.7 Intrusive sheet of dark brown charnockitic gneiss in augen gneiss. Hytkoras.

Plate 3.8 Intrusive contact between gneissic granite (foreground) and grey biotite gneiss (background). The gneissic granite has a pegmatitic margin. River bed, Hytkoras.

but this is not supported by field evidence in the area mapped at Hytkoras. The abundance of xenoliths and heterogeneous nature of the augen gneisses suggests an intrusive relationship. The augen gneiss-paragneiss contact in the area mapped is strongly deformed by the D_3 shearing and a basement-cover relationship cannot be recognised.

3.2.2.2 Gneissic granite

A small outcrop of late syntectonic foliated granite occurs in the area mapped on Hytkoras. Joubert (1971) mapped it as Concordia-type Granite (Spektakel Suite, SACS, 1980). It intrudes as a sheet-like body into the supracrustal gneisses. Tongue-like granite dykes penetrate the surrounding gneisses. The contact zone is marked by the presence of coarse leucocratic garnet-quartz-K-feldspar veins (see plate 3.8).

The granite is poorly foliated, biotite-bearing and K-feldspar mega-crystic. Garnet occurs as coarse spots and is common in the migmatitic banding which parallels the contacts. The K-feldspar megacrysts are poorly defined and are easily distinguished from the characteristic feldspar augen observed in other orthogneisses. Typically, it has a dark orange-brown weathering skin.

3.2.2.3 Metagabbro and pyroxenite

Pre-D2 layered intrusions that retain igneous sructures such as cumulus crystals, layering and grading are recorded by Jackson & Zelt (1984) from an area to the west of Hytkoras along the Buffels River Shear Zone. A small circular intrusion of pyroxenite and noritic gabbro occurs in the southern part of Hytkoras. The country rock is augen gneiss although no contacts are visible.

Mineralogy within the intrusion varies between areas of coarse megacrystic plagioclase with inclusions of granular pyroxene and hornblende to coarse pyroxenite with ophitic texture. Pale green hornblende replaces pyroxene and small amounts of cross-cutting orange-brown phlogopite are seen in thin section. The matrix generally consists of annealed pyroxene showing a granoblastic, equidimensional texture, no foliation is present. Orthopyroxene makes up most of the pyroxene content (the ratio of orthopyroxene to

clinopyroxene is about 4:1). The rocks are thus noritic in character.

In the northern part of Hytkoras a mafic dyke cross-cuts the supracrustal gneisses. It is similar to the larger body to the south except for its finer grain size and texture. Euhedral laths of plagioclase are poikilitically enclosed by plates of orthopyroxene partially replaced by hornblende. The presence of this undoubtably igneous texture suggests little in the way of metamorphic recrystallisation, except for an annealing of pyroxenes and hornblende. Apatite is a conspicuous accessory mineral in these intrusive mafic rocks.

3.3 STRUCTURE

The aim of the thesis is a detailed study of the metamorphic processes responsible for the amphibolite facies - granulite facies transition, so no attempt has been made to produce a detailed kinematic interpretation of structural events. However, the timing of peak metamorphism in relation to the structural evolution of the area, the general style of deformation and its tectonic setting are important in understanding the nature of granulite metamorphism in central Namaqualand.

3.3.1 D_1 structures

There is no unequivocal evidence of a D_1 (sensu Joubert, 1971) structural event as such. The well developed compositional banding in pelitic, quartzo-feldspathic, calc-silicate and biotite gneiss seems to represent original sedimentary bedding. The presence of intrafolial folds, strongly developed in the grey biotite gneiss, suggests that this fabric has been produced by transposition. It is unclear whether refolding of D_1 structures in F_2 folds has taken place, or whether intrafolial structures developed during a single progressive event. Due to the intense shearing accompanying D_3 deformation the relationship between D_1 and D_2 in this area is difficult to resolve.

3.3.2 D_2 structures

F_2 folds are isoclinal with round to sharp hinge zones and limbs lying within the plane of the gneissic foliation. A penetrative flat-lying axial-planar foliation is developed, coplanar with the S_1 compositional banding, giving a finite S_2 foliation. In the Buffels River area the foliation dips steeply to the south. Shortening and thickening in a N-S direction took place. Moore (1986) regards D_2 deformation as thrust related. Basement augen gneisses are thrust over the footwall supracrustal sequence.

A well developed mineral lineation, particularly well defined in pelitic rocks by garnet and sillimanite, plunges parallel to the axes of minor F_2 folds in a general southerly direction. This mineral lineation could possibly be a composite D_2-D_3 fabric, further growth of porphyroblasts during D_3 being mimetic and hence coaxial with F_2-L_2. Due to the paucity of open structures of D_3 age at Hytkoras it is not possible to observe a swing in the plunge of L_2 lineations due to refolding of F_2 folds.

3.3.3 D_3 structures

The dominant structural pattern in many areas of the Bushmanland Subprovince of the NMC consists of large basin-shaped structures separated by narrow steeply dipping zones of paragneiss. The Buffels River Shear Zone is a steeply south dipping E-W striking zone. It is bounded to the north by a tight synformal structure and to the south by prominent shallow-plunging sheath-like domal structures (Joubert, 1971 and Moore, 1986).

F_3 folds have E-W trending near-vertical axial planes and moderate plunges (plate 3.9). Minor folds are strongly asymmetrical, long limbs dipping steeply to the south. Their form is dependant on lithology. Dextral shearing is observed in mesoscale S and C structures, and in rotational boudinage in homogeneous, semi-brittle lithologies, such as mafic gneiss and augen gneiss. In the very ductile pelitic rocks flexural-flow seems to be the dominant fold mechanism. Mafic gneiss bands at low angles to the limbs of folds have undergone extreme thinning. Cusps are formed by shortening in

Plate 3.9 F_3 folds in pelitic gneiss. Note the growth of coars garnet in leucocratic layers parallel to S_2 layering Garnet growth controlled by existing compositional layering. River bed, Hytkoras.

Plate 3.10 Strong L_2 mineral lineation defined by garnet and clinopyroxene in calc-silicate gneiss. Hytkoras.

the foliation plane. Dynamic recrystallisation in ductile materials causes reduction in grain size. In the core of large mafic sheets coarse grain size is preserved and strain-shadowed pyroxenes are found. A spaced refoliation occurs within the augen gneiss at the contact with the supracrustal gneisses. There is no evidence of mylonite accompanying this event in the area mapped.

Most of the fabric elements in the Bushmanland Subprovince of the NMC are northward dipping, the southward dipping Buffels Shear Zone is thus somewhat unique in this regard. The Buffels River Shear Zone dies out about 10 km to the east of Hytkoras in the Gamoep area. The scale of the zone is thus not comparable with that of the megashears i the Namaqualand Metamorphic Complex. The Pofadder lineament has an 85 km displacement and forms a linear feature that extends at least 200 k (Joubert, 1974 and Maclaren, 1988). The Buffels River Shear Zone is thus a relatively minor feature with displacements limited to 10 or 20 km. In view of the lithological similarities in rock types to the nort and south of the zone it is unlikely that this zone represents a major tectonic discontinuity or terrane boundary.

The large basin structures bounding the Buffels Shear Zone have curvilinear fold axes and rotation of earlier planar fabrics and lineations has been recorded (Moore, 1986).

3.3.4 D_4 structures

D_4 structures are not well developed in the Buffels River area. Albat (1984) mapped NE plunging folds with steep NW dipping surfaces. Dextral shearing accompanies D_4 folding. The nature of the shearing is more brittle than D_3 deformation and extensional zones are filled with pegmatite. The absence of F_4 folds is probably due to the accomodation of D_4 strain by reactivation along the pre-existing Buffels River Shear Zone.

Vertical movements along N-S striking faults are observed to the south in the Witwater area (Baars, pers.comm.). Breccia zones along N-S fractures occur at Hytkoras. Chlorite and epidote mineralization are associated with these zones suggesting low temperature conditions accompanying brittle deformation. Strike slip displacement along the prominent N-S water course of the Buffels River in the western part of Hytkoras is less than one metre.

3.3.5 Interpretation

In arriving at a kinematic interpretation of the Buffels River Shear Zone the following should be borne in mind: the geometric characteristics, the style of deformation, and whether sporadic shear criteria can be extrapolated to a larger scale.

D_2 deformation is characterised by E-W striking shallow dipping planar fabrics and a prominent L_2 mineral lineation (see plate 3.10). If stretching lineations track the shearing direction, then D_2 deformation is consistent with N-S shear along a flat-lying plane. This is in agreement with thrust tectonic models developed for Bushmanland (Van Aswegen et al., 1987). The position of the thrust plane and the recognition of footwall and hanging wall in the Buffels River area is problematic. Moore (1986) interprets the repetition of orthogneiss and paragneiss units as a thrust related imbricate structure. The shear zone in the central part of the farm Hytkoras is thus regarded as the D_2 thrust plane. Augen gneisses either represent basement or syntectonic intrusive sheets along a tectonic discontinuity. The intrusive features observed in the augen gneisses favours the latter. The absence of a recognisable mylonite zone and the lack of a major lithological contrast to the north or south of the thrust are not consistent with the style of deformation and scale of displacement envisaged for Bushmanland (Van Aswegen et al., 1987; Colliston et al., 1991).

D_3 deformation results in asymmetric structures. Dextral shearing is recognised from sigmoidal foliation, asymmetric C planes and asymmetric boudinage. Curved fold axes result from the imposition of D_3 strain on D_2 folds.

CHAPTER 4

GEOTHERMOBAROMETRY

4.1 INTRODUCTION

The aim of this chapter is to evaluate the peak pressure-temperature conditions experienced in the Buffels River area during the granulite facies event.

Most of the samples collected come from a very small area (a few km^2) on the farm Hytkoras, hence the prevailing P,T conditions should be relatively constant across such a small area. The application of a variety of well calibrated geothermometers can be examined and compared. The precision of individual techniques is highlighted.

A paucity of fresh pelitic rocks and the absence of mafic gneisses in the Kangnas mountain area makes P,T determinations difficult. Two pyroxene temperature determinations are available for one sample, MCS207, and coexisting garnet-cordierite occur in two samples, MCS273 and VD3. These rocks represent the most northerly outcrops of granulite-facies assemblages in this study.

Values quoted here are for mineral core compositions, see Appendix for mineral analyses. Mineral zonation patterns and possible P-T-time paths are presented in Chapters 5 and 6.

The following geothermometers were applied :

Mafic rocks :

Coexisting orthopyroxene and clinopyroxene (Wood & Banno, 1973; Wells, 1977 Lindsley, 1983)

Pelitic rocks :

Coexisting garnet and cordierite (Thompson, 1976; Holdaway & Lee, 1977; Perchuk & Lavrent'eva, 1983 Bhattacharya et al., 1988)

Coexisting garnet and biotite (Thompson, 1976;
Holdaway & Lee, 1977;
Ferry & Spear, 1978;
Perchuk, 1983)

Coexisting garnet and orthopyroxene (Harley, 1984).

Most barometric determinations in granulite-facies terranes are based on garnet bearing assemblages (Newton & Perkins, 1982). Garnet is stable over a wide range of P,T conditions in a variety of rock types. Garnet-bearing reaction equilibria frequently have relatively large changes in ΔV, making them appropriate for geobarometry (Essene, 1982; Bohlen et al., 1983).

Low pressure granulite-facies terranes (Newton & Perkins, 1982; Newton, 1983) are characterised by the absence of garnet from mafic gneisses and the presence of cordierite and garnet in pelitic rocks. The absence of the well calibrated metaluminous garnet geobarometers in low pressure granulites restricts barometric determinations to peraluminous pelitic and semi-pelitic rocks, using equilibria such as plagioclase-garnet-Al_2SiO_5-quartz, and garnet-cordierite-sillimanite-quartz. However, isolated occurences of garnet-pyroxene-bearing assemblages have been used to produce pressure estimates, see Albat (1984) and Waters (1988). The rocks used in these determinations have Fe or Mn-rich bulk rock compositions and seem to be closely akin to calc-silicate lithologies, rather than typical metabasic rocks. In general, pressure estimates are lower than expected because of difficulties encountered in assessing the effects of components such as Mn and Fe^{3+}, and low grossular contents in garnet. The equilibria:

ferrosilite + anorthite = garnet + quartz

gives a pressure estimate of 4.9 kb (at 770°C) for a single sample. In this study mineralogical barometry is limited to pelitic rocks.

4.2 GEOTHERMOMETRY

4.2.1 Pyroxene thermometry

The enstatite-diopside solvus has been investigated experimentally and empirically by many workers (Boyd & Schairer, 1964; Davis & Boyd, 1966; Lindsley & Dixon, 1976; Kretz, 1982) and much thermodynamic

modelling has been undertaken (Lindsley, 1980; Saxena, 1981; 1983).

At high temperatures the diopside limb of the solvus is temperature dependant, making this an ideal thermometer for igneous rocks, particularly those undergoing rapid cooling. At temperatures below 850°C it is relatively insensitive to temperature (Bohlen & Essene, 1976; Lindsley & Anderson, 1982).

The relationship between ortho- and clinopyroxene can be simply described as:

$$Mg_2Si_2O_6\ (Opx) = Mg_2Si_2O_6\ (Cpx) \qquad (4.1)$$

where

$$K = \frac{a_{Cpx,en}}{a_{Opx,en}} \qquad (4.2)$$

according to Wood & Banno (1973)

$$T = \frac{-10202}{\ln\left(\frac{a\ Cpx,Enst}{a\ Opx,Enst}\right) - 7.65\ X_{Opx,Fe} + 3.88\ X_{Opx,Fe}^{2} - 4.6} \qquad (4.3)$$

where $X_{Opx,Fe} = \frac{Fe^{2+}}{(Fe^{2+} + Mg)}$ (4.4)

Wells (1977) revised the Wood & Banno (1973) geothermometer and produced the expression :

$$T = \frac{7341}{3.355 + 2.44\ X_{Opx,Fe} - \ln K} \qquad (4.5)$$

The Wells (1977) thermometer works consistently for ultramafic systems at temperatures above 900°C (Wells, 1977; Ernst, 1981), but gives scattered and high values for iron-rich pyroxenes from granulites (Bohlen & Essene, 1979).

Results for Wood & Banno (1973) and Wells (1977) calibrations are given in Table 4.1. All temperature estimates are calculated assuming a pressure of 5 kb (Albat, 1984; Waters, 1986).

Although discredited by many authors (Essene, 1982; Fonarev & Graphichikov, 1982) the values for the Wood & Banno (1973) and Wells (1977) thermometers are given here for comparison with other data

sets for mafic gneisses which have not been re-calculated using Lindsley's graphical quadrilateral method (1983). In general the two methods over -estimate by 70-100°C compared with the Lindsley (1983) method and other mineralogical thermometers.

The method of Lindsley (Lindsley & Anderson, 1982 and Lindsley, 1983) attempts to account for the presence of other components and gives isotherms for coexisting pyroxenes in the system $CaMgSi_2O_6$ - $CaFeSi_2O_6$ - $Mg_2Si_2O_6$ - $Fe_2Si_2O_6$.

The effect of Lindsley's correction procedures are to maximise the Wo value : where Wo = Ca + Na (M2) - Ca in Tschermakitic molecules with Fe, Al, Cr.

Difficulties involve the estimation of Fe^{3+} from microprobe data, and the effect of Mn partitioning between M1 and M2 sites.

The method gives lower temperatures than the Wood & Banno (1973) and Wells (1977) calibrations, and good correlation with other mineralogical geothermometers. The method is not very suitable for very low Ca orthopyroxene, giving a wide scatter. Fig. 4.1 shows the composition of coexisting pyroxenes on a Lindsley (1983) quadrilateral contoured for temperature at a pressure of 5 kb.

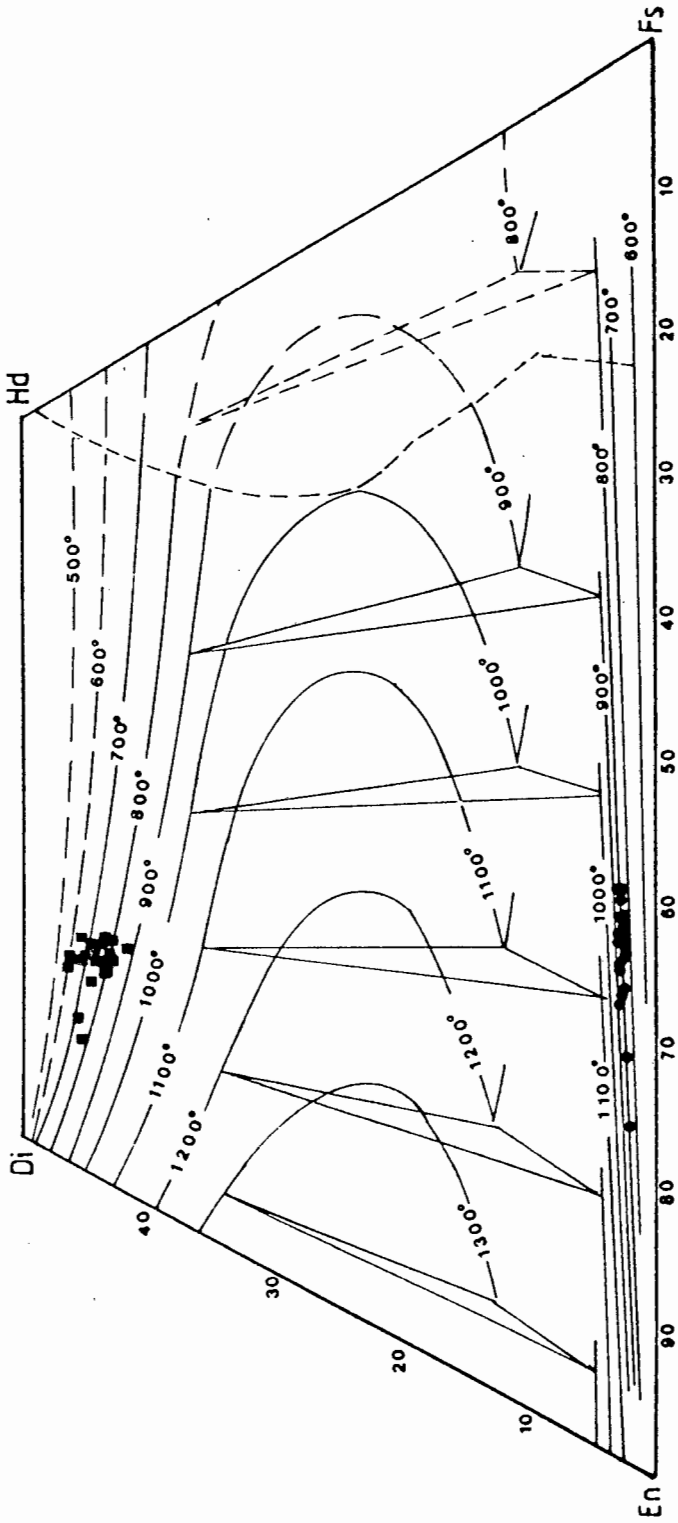

Fig. 4.1 Pyroxene quadrilateral contoured for temperature at a pressure of 5 kb (Lindsley, 1983)

TABLE 4.1

Pyroxene thermometry based on the calibrations of Wells (1977) and Wood & Banno (1973)

Sample	$X_{opx,Fe}$	$a_{cpx,enst}$	$a_{opx,enst}$	K	Temperature°C	
					Wells	Wood & Banno
DWN129	0.3551	0.0382	0.3870	0.0848	850	843
DWN129A	0.3380	0.0263	0.4081	0.0644	788	803
DWN332B	0.3615	0.0458	0.3656	0.1253	890	869
DWN3322	0.3611	0.0465	0.3664	0.1269	892	871
DWN3473	0.3381	0.0444	0.4190	0.1059	870	862
DWN348	0.3295	0.0414	0.4115	0.1006	864	861
DWN349	0.3459	0.0343	0.3950	0.0868	832	833
DWN353	0.3576	0.0280	0.3753	0.0746	803	808
DWN353S	0.3517	0.0315	0.3760	0.0838	824	825
DWN380	0.3659	0.0494	0.3495	0.1413	910	882
DWN381	0.3678	0.0463	0.3698	0.1252	887	865
DWN625	0.3797	0.0321	0.3665	0.0876	820	815
HY8	0.3525	0.0405	0.3800	0.1066	864	854
HY23	0.3621	0.0339	0.3782	0.0896	831	827
MCSH04	0.2824	0.0375	0.5045	0.0743	832	854
MCSH05	0.2423	0.0392	0.5429	0.0722	844	879
MCSS04	0.4030	0.0303	0.3197	0.0948	824	811
MCSS05	0.3966	0.0330	0.3343	0.0987	833	819
MCS301	0.3594	0.0272	0.3729	0.0729	799	805
MCS301A	0.3496	0.0256	0.3875	0.0661	787	799
MCS302C	0.3652	0.0419	0.3598	0.1165	875	857
MCS303	0.3744	0.0302	0.3538	0.0854	815	813
MCS304	0.3717	0.0422	0.3775	0.1118	865	848
MCS304M	0.3928	0.0441	0.3402	0.1296	882	854
MCS305I	0.3663	0.0284	0.3718	0.0764	803	806
MCS317	0.3518	0.0410	0.3770	0.1088	868	857
MCS327	0.3790	0.0463	0.3437	0.1377	895	867
MCS327T	0.3795	0.0434	0.3496	0.1241	880	857
MCS384B	0.3595	0.0381	0.3866	0.0986	848	840
MCS207	0.4130	0.0414	0.3256	0.1271	869	841
				Mean	848	840
				σ_{n-1}	34	25

TABLE 4.2

Pyroxene thermometry based on the graphical method of Lindsley (1983)

Temperatures for Clinopyroxene

Sample	Wo	En	Fs	Estimated Temperature°C
DWN129 A	0.446	0.409	0.145	710
DWN129 B	0.443	0.422	0.135	760
DWN332 2	0.425	0.414	0.161	820
DWN332 3	0.427	0.412	0.161	830
DWN347	0.432	0.422	0.146	810
DWN348	0.431	0.422	0.147	820
DWN349	0.437	0.407	0.156	770
DWN353	0.448	0.403	0.149	710
DWN353 S	0.445	0.394	0.161	710
DWN380	0.413	0.387	0.200	830
DWN381	0.432	0.414	0.154	800
DWN625	0.453	0.390	0.157	670
HY8	0.436	0.413	0.151	790
HY23	0.455	0.397	0.148	690
MCSH04	0.451	0.442	0.107	750
MCSH05	0.451	0.458	0.091	750
MCSS04	0.451	0.388	0.161	660
MCSS05	0.430	0.403	0.167	800
MCS301	0.450	0.400	0.150	630
MCS301 A	0.461	0.395	0.144	600
MCS302 C	0.417	0.412	0.171	860
MCS303	0.462	0.401	0.137	620
MCS304	0.431	0.410	0.159	810
MCS304 M	0.426	0.423	0.151	840
MCS305 I	0.447	0.399	0.154	700
MCS317	0.432	0.414	0.154	800
MCS327	0.415	0.414	0.171	860
MCS327 T	0.441	0.402	0.157	750
MCS327 M	0.435	0.398	0.168	770
MCS384 B	0.444	0.407	0.149	740
MCS207	0.433	0.392	0.175	790
			Mean	756
			σ_{n-1}	71

TABLE 4.3

Pyroxene thermometry based on the graphical method of Lindsley (1983)

Temperatures for orthopyroxene

Sample	Wo	En	Fs	Estimated Temperature°C
DWN129	0.021	0.623	0.356	750
DWN129^{A}	0.022	0.640	0.338	750
DWN332^{B}	0.021	0.613	0.366	700
DWN332^{2}	0.022	0.613	0.366	725
DWN347^{3}	0.019	0.606	0.375	700
DWN348	0.022	0.646	0.332	775
DWN349	0.024	0.629	0.347	850
DWN353	0.020	0.619	0.361	725
DWN353^{S}	0.024	0.620	0.356	800
DWN380	0.025	0.602	0.373	800
DWN381	0.023	0.609	0.368	775
DWN625	0.024	0.605	0.371	750
HY8	0.023	0.651	0.326	700
HY23	0.025	0.614	0.361	750
MCSH04	0.018	0.708	0.274	675
MCSH05	0.016	0.741	0.243	775
MCSS04	0.027	0.568	0.405	800
MCSS05	0.024	0.579	0.397	750
MCS301	0.023	0.608	0.369	775
MCS301^{A}	0.023	0.612	0.365	750
MCS302^{C}	0.022	0.614	0.364	800
MCS303	0.021	0.594	0.385	750
MCS304	0.022	0.622	0.356	725
MCS304^{M}	0.023	0.643	0.334	800
MCS305^{I}	0.021	0.620	0.359	700
MCS317	0.024	0.592	0.384	775
MCS317	0.021	0.596	0.383	725
MCS327^{S}	0.025	0.650	0.325	850
MCS327^{B}	0.023	0.573	0.404	775
MCS384^{S}	0.025	0.625	0.350	800
MCS207	0.022	0.574	0.404	700
			Mean	756
			σ_{n-1}	45

TABLE 4.4

Mean temperature determinations for coexisting orthopyroxene and clinopyroxene based on the graphical method of Lindsley (1983), using data from Tables 4.2 & 4.3

Sample	Mean temperature °C	Sample	Mean temperature °C
DWN129	730	MCSH05	762.5
DWN129^{A}	755	MCSS04	730
DWN332^{B}	760	MCSS05	775
DWN332^{2}	777.5	MCS301	702.5
DWN347^{3}	755	MCS301^{A}	675
DWN348	797.5	MCS302^{C}	830
DWN349	810	MCS303	685
DWN353	717.5	MCS304	805
DWN353^{M}	755	MCS304^{M}	795
DWN380^{S}	815	MCS305^{I}	700
DWN381	787.5	MCS317	787.5
DWN625	712.5	MCS327	762.5
HY8	745	MCS327^{M}	810
HY23	720	MCS384^{B}	770
MCSH04	712.5	MCS207	745
		Mean	756
		σ_{n-1}	41

4.2.2 Garnet-biotite thermometry

Garnet-biotite Fe-Mg exchange thermometry has been calibrated from natural mineral assemblages (Thompson, 1976; and Perchuk, 1977) and by experimentation (Ferry & Spear, 1978 and Perchuk & Lavrent'eva, 1983).

The exchange reaction is :

$$Biot_{Fe} + Gar_{Mg} = Gar_{Fe} + Biot_{Mg} \qquad (4.6)$$

where

$$K_D = (Fe/Mg)^{Biot} / (Fe/Mg)^{Gar} \qquad (4.7)$$

The equilibrium above can be described by the following expression :

$$\Delta G^0 = \Delta H^0 - T\Delta S^0 + P\Delta V^0 + 3RT \ln K_D = 0 \qquad (4.8)$$

Perchuk (1977) corrects for the effect of Mn on the exchange equilbria :

$$T = (3650/\ln K_D + 2.57) + 252.25(X_{Mn,Gar} - 0.035) \qquad (4.9)$$

where $X_{Mn,Gar} = Mn/(Mn + Fe + Mg)$

Ferry & Spear (1978) limit the model to compositions which closely approximate the binary Mg - Fe^{2+} system, where :

$(Ca + Mn)/(Ca + Mn + Fe + Mg)$ in garnet < 0.2 and

$(Al^{VI} + Ti)/(Al^{VI} + Ti + Fe + Mg)$ in biotite < 0.15

The effects of garnet zonation on temperature estimates are discussed in Chapter 6. Many workers have commented on the selection of garnet-biotite pairs used for temperature determinations and have attempted to evaluate local equilibria criteria (Tracy et al., 1976; Ghent et al., 1979; Loomis, 1983; Indares & Martignole, 1985). In most cases matrix biotite surrounded by quartz or feldspar paired with garnet cores give the highest temperature estimates, the assumption being that a pervasive state of equilibrium is reached during mineral growth accompanying peak metamorphism. Retrograde reequilibration during cooling is likely between adjacent Fe-Mg phases, thus giving lower calculated peak temperatures. Contact pairs may be useful in understanding post-peak thermal history if a suitable model for retrograde exchange and chemical zonation can be developed (see Chapter 6).

TABLE 4.5

Garnet-Biotite Fe-Mg exchange thermometry, based on Thompson (1976)[1], Holdaway & Lee (1977)[2], Ferry & Spear (1978)[3] and Perchuk & Lavrent'eva (1983)[4].

Sample	core compositions $X_{Mg,Gar}$	matrix compositions $X_{Mg,Biot}$	K_D	Temperature°C 1	2	3	4	
DWN617	0.302	0.596	3.410	752	712	787	688	
DWN618	0.386	0.684	3.443	749	709	782	686	
DWN620	0.371	0.594	2.840	884	821	986	769	Crd
DWN622	0.294	0.637	4.214	680	651	686	641	Opx
DWN623	0.294	0.734	6.626	555	543	523	554	Opx
DWN624	0.343	0.618	3.099	789	742	840	711	Crd
DWN627	0.319	0.571	2.841	824	772	893	733	
MCSH02	0.196	0.446	3.302	764	722	804	696	
MCS322	0.261	0.555	3.531	740	701	769	680	
MCS332	0.261	0.545	3.391	754	714	790	689	
MCS343	0.208	0.483	3.557	737	699	765	678	
MCS393	0.307	0.571	3.005	801	753	858	719	Crd
MCS394	0.284	0.531	2.840	824	772	893	733	Crd
MCS395	0.276	0.511	2.741	839	784	916	742	Crd
MCS273	0.286	0.567	3.269	768	725	810	698	Crd
VD3	0.189	0.441	3.385	754	714	791	690	Crd
			Mean	763	721	806	694	
			σ_{n-1}	74	62	104	48	
Cordierite-absent assemblages			Mean	760	718	799	693	
			σ_{n-1}	30	25	44	19	
Cordierite-bearing assemblages			Mean	808	759	871	723	
			σ_{n-1}	44	37	67	27	

Mean temperatures in Table 4.5 are given for cordierite-absent and cordierite-bearing assemblages. The widely used Ferry & Spear (1978) calibration gives the highest temperature determinations. The highest mean value, 871°C, would appear to be an overestimate of 100°C compared with the two-pyroxene estimates presented in Table 4.4. The error claimed by the authors is ± 50°C. The calibrations of Holdaway & Lee (1977) and Perchuk & Lavrent'eva (1983) are broadly in agreement. Perchuk & Lavrent'eva (1983) model yields temperatures about 25°C lower than Holdaway & Lee (1977). Thompson (1975) calibration based on natural assemblages gives temperatures similar to two-pyroxene estimates (Table 4.4).

Assemblages containing cordierite give the highest temperature estimates. Samples containing four coexisting Fe-Mg silicates, garnet-biotite-cordierite-orthopyroxene, yield anomalously low values. The simple equilibrium in Equation 4.6 may be invalid in more complex pelitic systems, thus those rocks containing garnet-biotite only are thought to give the best estimates of peak metamorphic temperature. The nature of exchange equilibria in the pelitic system is discussed in Chapter 6.

4.2.3 Garnet-cordierite thermometry

The garnet-cordierite geothermometer is based on Fe-Mg partitioning between coexisting garnet and cordierite.

The equilibrium conditions for the reaction :

$$1/3\ Fe_3Al_2Si_3O_{12} + 1/2\ Mg_2Al_4Si_5O_{18} = 1/3\ Mg_3Al_2Si_3O_{12} + 1/2\ Fe_2Al_4Si_5O_{18} \quad (4.9)$$

can be expressed as :

$$0 = \Delta G_{1,T} + P\Delta V + RT \ln K_D \quad (4.10)$$

where $K_D = \dfrac{(X_{Fe,Gar} \cdot X_{Mg,Crd})}{(X_{Mg,Gar} \cdot X_{Fe,Crd})}$ (Thompson, 1976) (4.11)

for other calibrations (Holdaway & Lee, 1977; Perchuk & Lavrent'eva, 1983 and Bhattacharya et al., 1988) the K_D for Fe-Mg exchange between garnet and cordierite is the inverse of equation 4.11.

Experimental studies show a wide discrepancy concerning the

relationship between K_D and temperature (Currie, 1971; Hensen & Green, 1973; Perchuk, 1977; Perchuk *et al.*, 1980). Studies based on natural assemblages show that ln K_D, as defined in equation 4.11, decreases with increasing temperature (Thompson, 1976; Holdaway & Lee, 1977).

The above calibrations assume ideal mixing in both phases. For multicomponent garnets Ganguly & Saxena (1984) propose the formulation

$$RT \ln (Mg/Fe)^{Gar} = 2500(X_{Fe} - X_{Mg}) + 3000(X_{Ca} + X_{Mn}) \qquad (4.12)$$

Bhattacharya *et al.* (1988) used non-ideal mixing models on a wide sample of published data and produce higher precision than the formulations of Thompson (1976) and Holdaway & Lee (1977).

TABLE 4.6

Values used in Garnet-cordierite thermometric calibrations

Calibration	H/R	S/R	V/R
Thompson (1976)	2725	0.896	0.0155
Holdaway & Lee (1977)	3095	1.354	0.01525
Perchuk & Lavrent'eva (1983)	3020	1.287	0.018
Bhattacharya *et al.* (1988)	1814	1.028	0.0152

The Bhattacharya *et al.* (1988) calibration yields the highest mean temperature determination and gives the lowest standard deviation. The Thompson (1976) calibration gives a wide spread of values as no attempt is made to estimate the effects of minor components on Fe-Mg mixing in garnet. Holdaway & Lee (1977) and Perchuk & Lavrent'eva (1983) calibrations are in close agreement but appear to underestimate temperature by about 50°C compared with two-pyroxene thermometry.

TABLE 4.7

Garnet-Cordierite Fe-Mg exchange thermometry based on Thompson (1976)[1], Holdaway & Lee (1975)[2], Perchuk & Lav'renteva (1983)[3].

					Temperature°C		
	X Crd,Fe	X Crd,Mg	X Gar,Fe	X Gar,Mg	1	2	3
Sample							
DWN620	0.2348	0.7652	0.5818	0.3627	826	781	784
DWN622	0.2172	0.7828	0.6459	0.3016	680	660	661
DWN623	0.2161	0.7849	0.6460	0.2921	668	650	650
DWN624	0.2511	0.7489	0.6124	0.3360	810	768	771
MCS393	0.2482	0.7518	0.6580	0.2953	726	699	700
MCS394	0.2448	0.7552	0.6684	0.2834	729	677	678
MCS395	0.2350	0.7650	0.6570	0.2757	730	678	659
MCS273	0.2302	0.7698	0.6879	0.2822	663	646	646
VD3	0.3324	0.6676	0.7377	0.2528	779	743	745
				Mean	726	698	699
				σ_{n-1}	64	53	54

TABLE 4.8

Garnet-cordierite Fe-Mg exchange thermometry based on Bhattacharya et al. (1988).

	K_D from data above	X Gar,Mn	X Gar,Ca	Temperature°C
Sample				
DWN620	0.1913	0.0256	0.0299	788
DWN622	0.1296	0.0328	0.0198	716
DWN623	0.1245	0.0371	0.0248	713
DWN624	0.1840	0.0221	0.0323	785
MCS393	0.1482	0.0185	0.0282	742
MCS394	0.1374	0.0216	0.0266	729
MCS395	0.1289	0.0575	0.0297	730
MCS273	0.1227	0.0141	0.0158	703
VD3	0.1706	0.0049	0.0046	761
			Mean	741
			σ_{n-1}	31

$$*K_D = \frac{(X_{Mg,Gar} \cdot X_{Fe,Gar})}{(X_{Fe,Gar} \cdot X_{Mg,Crd})}$$

4.2.4 Garnet-orthopyroxene thermometry

Only two samples from the study area contain coexisting garnet and orthopyroxene. Fe-Mg exchange between garnet and orthopyroxene has been investigated experimentally by Harley (1984). The equilibrium can be represented as follows :

$$1/3\ Mg_3Al_2Si_3O_{12} + 1/2\ Fe_2Si_2O_6 = 1/3\ Fe_3Al_2Si_3O_{12} + 1/2\ Mg_2Si_2O_6 \qquad (4.13)$$

yielding the expression :

$$T = \frac{3740 + 1400\ X_{Gar,Gros} + 22.86\ P(kb)}{R \ln K_D + 1.96} \qquad (4.14)$$

where $K_D = \frac{(X_{Fe,Gar} \cdot X_{Mg,Opx})}{(X_{Mg,Gar} \cdot X_{Fe,Opx})}$ (4.15)

The effect of Fe^{3+} in garnet is not considered, if an Fe^{3+} estimate is made K_D will be reduced thus increasing the estimated temperature. If Mn in garnet is ignored then the temperature estimate is too low. $X_{Gar,Gros}$ may be estimated from the expression :

$$X_{Gar,Gros} = (Ca+Mn)/(Ca+Mn+Mg+Fe) \qquad (4.16)$$

TABLE 4.9

Garnet-orthopyroxene Fe-Mg exchange thermometry based on Harley (1984)

Sample	$X_{Gar,Fe}$	$X_{Gar,Mg}$	$X_{Gar,Gros}$	$X_{Opx,Fe}$	$X_{Opx,Mg}$	K_D	T°C
DWN622	0.6993	0.3007	0.0525	0.4455	0.5545	2.8946	692
DWN623	0.6460	0.2921	0.0619	0.4279	0.5721	2.9569	685

4.3 GEOBAROMETRY

4.3.1 Garnet-plagioclase-sillimanite-quartz barometry

The equilibrium between plagioclase, garnet, Al_2SiO_5 and quartz provides a barometer for use in peraluminous rocks (Ghent, 1976; Newton & Haselton, 1981). The equilibrium can be described by :

$$3\ CaAl_2Si_2O_8 = Ca_3Al_2Si_3O_{12} + 2\ Al_2SiO_5 + SiO_2 \qquad (4.17)$$

Pressure can be determined using the following expression :

$$P = 1/\ V\ [P^0\ .\ \Delta V - 5.962\ T\ \ln a_{Gar,Ca}/a_{Plag,Ca}] \qquad (4.18)$$

where P^0 is -1.17 + 0.0238 T (Froese, 1988)

This assemblage is multivariant as the result of solid solution in plagioclase and garnet. This gives a wide temperature and pressure stability range. Difficulties concerning the equilibrium anorthite-grossular-sillimanite-quartz include: the temperature dependance of the reaction (thus accurate independant temperature determinations are necessary for reliable pressure estimates), uncertainties in the value of ΔV from experimental studies, and the very low activity of grossular in garnets coexisting with plagioclase. The scarcity of the full assemblage amongst pelitic rocks not only in Namaqualand but in most other high-grade terranes has prevented thorough testing of the barometer across a granulite- or amphibolite-facies terrane.

TABLE 4.10

Values used in garnet-plagioclase-sillimanite-quartz barometric calibrations

Calibration	H	S	V
Ghent (1976)	11673.33	32.80969	1.300290
Newton & Haselton (1981)	10179.40	31.83174	1.304465
Powell & Holland (1988)	5726.00	26.83000	1.234000

Assuming from section 4.2 peak metamorphic temperature of 750°C the following pressures were determined :

TABLE 4.11

Garnet-plagioclase-sillimanite-quartz barometry based on Ghent (1976)[1] Newton & Haselton (1981)[2] and Powell & Holland (1988)[3].

Sample	$a_{gar,gros}$	$a_{plag,an}$	K_D	Pressure (kb)		
				1	2	3
MCS322	0.049	0.449	1080.254	5.9	6.3	6.1
MCS387	0.046	0.442	900.537	6.2	6.6	6.4
MCS393	0.037	0.441	1670.628	5.2	5.6	5.4

4.4 DISCUSSION

In the absence of well calibrated geobarometers the regional pressure estimate of 5 kb (Albat, 1984 and Waters, 1986) has been used in temperature determinations. Only three samples were suitable for barometry using the garnet-plagioclase-sillimanite-quartz method (Ghent, 1976; Newton & Haselton, 1981; Powell & Holland, 1988) values are in agreement with previous work, suggesting pressures of 5-6 kb.

Pyroxene geothermometry on 30 samples using the graphical method of Lindsley (1982) yields a mean temperature of 756°C with good agreement between values for clinopyroxene and orthopyroxene, indicating a good approach to equilibrium. It is interesting to note that analyses from different textural domains in the same rock can yield widely varying temperature estimates. Thus a large data base seems necessary to overcome local scale chemical variation. This observation is important when considering sample MCS207, the most northerly recorded mafic granulite from Goinoep. MCS207 gives a temperature estimate of 745°C which is consistent with values from mafic gneisses in the Buffels River. However, individual samples can depart from the mean by as much as 80°C, the standard deviation of 41°C is in agreement with the error of ± 50°C associated with the method (Lindsley, 1982). Without a similar size data base for the Kangnas mountain area close comparison of peak metamorphic temperature from two-pyroxene thermometry is clearly misleading.

Garnet-biotite thermometry on 16 samples gave a mean temperature estimate of 763°C using the calibration of Thompson (1976). Other methods gave values either anomalously high (806°C for Ferry & Spear, 1978) or too low (721°C using Holdaway & Lee, 1977; and 694°C for Perchuk & Lavrent'eva, 1983). It has been noted that assemblages containing cordierite in addition to garnet and biotite give higher temperature estimates. Samples from Verdruk in the Kangnas mountain area, MCS273 and VD3, gave estimates in agreement with those from the Buffels River, although the number of samples is too small to draw any conclusions from this, particularly as both rocks are cordierite-bearing.

Garnet-cordierite thermometry on 9 samples yielded slightly lower temperatures than garnet-biotite thermometry using Thompson's calibration. Thompson (1976) garnet-cordierite thermometry gave a

mean value of 726°C. Perchuk & Lavrent'eva (1983) garnet-cordierite and garnet-biotite methods are in very good agreement, but both gave temperatures below 700°C. The recalibration of Bhattacharya et al. (1988) produces higher temperatures and the mean value of 741°C is consistent with two-pyroxene thermometry. Questions concerning whether peak metamorphic temperatures can be determined from pelitic geothermometers have to be examined in the light of garnet zonation, and possible retrograde reequilibration of cordierite and biotite during cooling (see Chapter 6).

Garnet-orthopyroxene thermometry (Harley, 1984) on samples DWN622 and DWN623 yielded low values around 690°C. This is in agreement with estimates from the same samples using garnet-biotite and garnet-cordierite methods. It is unlikely that the assemblage garnet-orthopyroxene-cordierite-biotite was in equilibrium. Since, texturally biotite seems to represent secondary growth.

Other techniques that are applicable to the gneisses described in this study were thought to be unreliable. These include two-feldspar thermometry (Stormer, 1975) the main difficulties being the integration of analyses of perthitic and antiperthitic feldspar, commonly seen in augen gneisses. Most studies indicate that two-feldspar thermometers underestimate temperature in slowly cooled igneous and metamorphic rocks, and are best suited to volcanics (Essene, 1982). Two-oxide thermometry is well calibrated and has been applied to many granulite terranes (Buddington & Lindsley, 1964; Bohlen & Essene, 1977). Oxides are plentiful in the mafic gneisses and are described in detail in Chapter 5. On examination they proved to be coexisting pure end member magnetite and grains of pure hematite with exsolved ilmenite. This complete exsolution is indicative of very slow cooling rates, and records temperatures below 400°C.

The assemblage garnet-cordierite-sillimanite-quartz provides a potential geobarometer (Martignole & Sisi, 1981; Lonker, 1981 and Aronovich & Podlesskii, 1983). Sources of error include the slope and P-T location of end-member reactions, activity models assumed for the solid solutions involved, and the unknown fluid content of cordierite, its H_2O-CO_2 ratio and its effect on the equilibrium. Pelitic samples with the full assemblage above are comparatively scarce and coincide with those used in garnet-plagioclase-sillimanite-quartz barometry, which in light of the above problems

provides a better geobarometer.

Oxygen isotope thermometry is discussed in Chapter 9 and P-T estimates from fluid inclusion densities are dealt with in Chapter 10.

The peak metamorphic conditions experienced in the Buffels River are approximately 750°C at pressures below 6 kb. It is at present difficult to discriminate a regional pressure-temperature gradient across the study strip. It appears likely that metamorphic conditions south of the Ratelpoort line were relatively constant with granulite-facies prevailing throughout. Such a wide belt of low pressure-high temperature metamorphism represents a major thermal anomaly in the Upper Proterozoic crust.

CHAPTER 5

PETROLOGY OF THE MAFIC GNEISSES

5.1 INTRODUCTION

The classical definition of the amphibolite-granulite facies transition involves the first appearance of orthopyroxene at the expense of hornblende (Eskola, 1939). The numerous well exposed mafic lenses in the Buffels River area allow a detailed study of the breakdown of hornblende and the development of pyroxene. Most of the mafic rocks in this area are hornblende granulites with a well developed banded structure that consists of pyroxene granulite margins mantling hornblende-rich interiors.

The banded structure is finely developed on the thin section scale and is thus ideally suited to a detailed electron microprobe study. The mafic gneisses of the Buffels River area can be regarded as transitional granulites as many show the development of small pyroxene granules along the rims and in the cores of coarse hornblende crystals. The physical and chemical processes affecting hornblende breakdown on the small scale may be applicable to the regional facies transition.

In conjunction with the forty probe samples, two whole rock close pairs (margin and interior) were analysed for major elements by XRF spectrometry. Samples from mafic gneisses were also included in the stable isotope study and the fluid inclusion study.

Full mineral analyses are available for the complete assemblage in virtually all samples studied. The mineral chemistry of each phase is discussed, particularly the nature of chemical zonation. Two-pyroxene thermometry (Wood & Banno, 1975; Wells, 1977 and Lindsley, 1982) is presented in Chapter 4. The relationship of solid solution behaviour in plagioclase and hornblende is discussed. Existing methods of estimating water activity from amphibole compositional relationships (Spear, 1981 and Phillips, 1980) are evaluated and alternatives are suggested.

The breakdown of hornblende in granulite facies is given by the

reaction:

Hornblende + Quartz = Orthopyroxene + Clinopyroxene + Plagioclase + H_2O

Textural evidence illustrating the progress of the reaction are outlined, and the role of water activity and silica mobility is discussed. A mechanism to explain the ubiquitous banded texture observed is proposed.

Thicker mafic units develop anhydrous pyroxene-rich, plagioclase-quartz segregations in the form of coarse grained veins and patches. This texture is consistent with in-situ partial melting. The breakdown of hornblende via partial melting reactions in mafic gneiss places important constraints on fluid behaviour.

The textural history of mafic gneisses from the Buffels River illustrates the importance of hydrous minerals in buffering fluid composition.

5.2 PETROGRAPHY

5.2.1 Introduction

In terms of field relations there are three main types of mafic gneiss occuring in the Buffels River area at Hytkoras (see 3.2.1.7). Mafic sheets associated with the supracrustal sequence are divided into two groups on the basis of petrography. The dominant group termed the Buffels River dykes by Jackson & Zelt (1984) consist of poikiloblastic, strongly pleochroic pyroxene, replacing coarse grained granoblastic, brown coloured hornblende. Other than a change in grain size there is no petrographic difference between the thick concordant mafic sheets and the small discordant lenses. A minor group of mafic gneisses intruding grey biotite gneiss have medium grained, poikiloblastic, green hornblende. The post-tectonic intrusions of noritic metagabbro and pyroxenite are much coarser grained, have no foliation and are characterised by relict igneous textures. Green hornblende is found replacing pyroxene.

Table 5.1 lists the estimated modal proportions and general textural features of all mafic rocks sampled for thin section examination and for microprobe, whole rock, stable isotope, and fluid inclusion studies. Petrography is in note form and refers to the

textural relations of pyroxene, plagioclase zonation, type of fabric and nature of quartz content. Localites of samples chosen for geochemical studies are shown in figs 2.3, 3.1 and 3.2.

TABLE 5.1

Modal proportions and petrographic characteristics of mafic gneisses

Sample	Opx	Cpx	Hbl	Plag	Biot	Qtz	Oxides
*DWN129$_A$	20	20	5	55	-	-	tr
coarse poikiloblastic, slightly zoned plag, patchy hbl							
*DWN129$_B$	25	25	1 inc	48	-	-	1
coarse poikiloblastic, zoned plag							
*DWN288	7	5	40	43	-	-	5
medium foliated, coarse hbl, abundant oxides							
*DWN332$_1$	18	7	-	50	16	8	1
medium granular, foliated, strongly zoned plag, matrix qtz							
*DWN332$_2$	15	20	8	46	-	12 vein	1
medium poikiloblastic, fine granular plag, matrix and vein qtz							
*DWN332$_3$	7	12	35	34	1	12	1
coarse granular, foliated, slightly zoned plag, matrix and vein qtz							
*DWN347	15	10	15	58	2	-	1
coarse poikiloblastic, zoned plag							
*DWN348	8	22	1 inc	57	tr	10	2
coarse poikiloblastic, strongly zoned plag, matrix qtz							
*DWN349	8	24	4 inc	59	tr	2	3
coarse poikiloblastic, opx strained, zoned plag, matrix qtz							
	-	20	-	57	tr	20	2
segregation							
*DWN353$_A$	6	3	40	46	3	-	2
medium granoblastic, zoned plag							
	29	7	1 inc	56	2	-	5
segregation							
*DWN353$_B$	3	2	48	44	tr	-	3
medium granoblastic, zoned plag							
	10	35	tr inc	53	tr	-	3
segregation							
*DWN354	30	-	-	48	6	15	1
fine granular, slightly zoned plag, matrix qtz							
*DWN380	23	12	6	42	4	10	3
poikiloblastic, foliated, patchy hbl, fine granular plag, matrix qtz							
*DWN381	16	7	5	40	22	10	tr
fine poikiloblastic, biot foliated, slightly zoned plag, matrix qtz							
O*DWN615	28	-	-	61	5	3	3
medium poikiloblastic, slightly zoned plag, matrix qtz							
O*DWN625	20	10	-	60	2	7	1
coarse poikiloblastic, strongly zoned plag with qtz inc, matrix qtz							
*HY8	15	15	10	52	1	5	2
granoblastic hbl, coarse poikiloblastic pyx, slightly zoned plag							
*HY23	20	30	2 inc	46	tr	-	2
coarse poikiloblastic, hbl as inclusions only							
*VK7	-	10	45	45	tr	-	tr
coarse granoblastic amphibolite							
*MCSH04	10	15	15	60	-	-	tr
coarse, partly granoblastic, relict cumulate, coarse plag with px inc							
*MCSH05	15	35	30	19	1	-	tr
coarse, polygonal pyx replaced by large plates of hbl							
*MCSS04	15	3	25	55	2	-	tr
coarse poikiloblastic, biot foliated, zoned plag							
*MCSS05	5	2	48	44	tr	-	1
matrix, coarse granoblastic, incipient pyx growth, zoned plag							
	35	7	-	47	tr	10	1
segregation							

	Opx	Cpx	Hbl	Plag	Biot	Qtz	Oxides
*MCSS08	-	-	55	45	-	-	tr
granoblastic amphibolite, zoned plag with slight altn							
*MCST02	3	1	55	41	-	-	-
granoblastic, slightly zoned plag, incipient pyx growth							
*MCST03	-	-	40	60	-	-	-
granoblastic amphibolite, plag altd to ser + cc							
MCSBV08	-	5	50	43	1	-	1
granoblastic amphibolite, small cpx granules, strongly zoned plag							
MCSBV09	35	-	5	47	7	5	1
coarse poikiloblastic opx, zoned plag, matrix qtz							
MCS300	16	4	25	55	-	-	-
granoblastic, slightly zoned plag							
*MCS301$_A$	23	2	55	20	-	-	tr
coarse hbl patch replaced by opx poikiloblast, strongly zoned plag							
*MCS301$_B$	-	20	-	59	-	20	1
medium granoblastic, foliated, matrix and vein qtz, zoned plag							
*MCS301$_C$	10	10	20	49	2	8	1
coarse granoblastic, strongly zoned plag, matrix qtz							
*MCS302	13	8	17	39	16	3	4
medium poikiloblastic, coarse biot patch, zoned plag, matrix qtz							
MCS303	8	4	45	40	-	2	tr
coarse granoblastic, core replacement of hbl by pyx, zoned plag							
*MCS303	6	4	45	43	-	2	tr
coarse granoblastic, incipient pyx growth, zoned plag							
W*MCS304$_M$	16	4	38	40	tr	1	1
medium foliated, coarser and poikiloblastic away from the margin							
W*MCS304$_I$	8	3	46	40	tr	2	1
coarse granoblastic, incipient pyx growth, strongly zoned plag							
*MCS305	18	8	7	57	3	5	2
coarse poikiloblastic, zoned plag, matrix qtz							
MCS306	20	-	tr	50	10	18	2
margin, fine granoblastic biot-qtz on contact and opx-plag interior							
MCS312	20	-	-	55	1	23	2
margin, fine granoblastic, zoned plag, qtz-rich matrix							
MCS313	16	4	1	45	tr	30	3
margin, medium granoblastic, zoned plag, qtz in veins and matrix							
MCS314	25	5	5	64	-	tr	1
margin, medium granoblastic,							
MCS315	30	10	1 inc	55	3	tr	1
coarse poikiloblastic, slightly zoned plag							
MCS316	20	15	-	49	4	10	2
coarse poikiloblastic, slightly zoned plag, matrix qtz							
*MCS317	25	-	-	57	-	15	3
matrix halo							
	5	28	2 inc	60	2	-	3
segregation							
MCS318	25	5	-	62	1	5	2
coarse granoblastic							
MCS320	20	5	10	41	18	5	1
pale green hbl, strongly foliated, matrix qtz							
*MCS327$_T$	15	18	8	48	-	10	1
medium poikiloblastic, foliated, slightly zoned plag, matrix qtz,							
*MCS327$_I$	4	8	45	38	-	2	3
medium poikiloblastic							
	40	-	-	10	-	49	1
segregation, exsolution lamellae in opx							
*MCS327$_B$	25	12	-	52	-	10	1
fine granoblastic, foliated, matrix qtz							
MCS335$_M$	33	-	1	56	7	tr	3
coarse poikiloblastic							

	Opx	Cpx	Hbl	Plag	Biot	Qtz	Oxides
MCS335$_I$	18	-	20	51	4	5	2
coarse poikiloblastic, slightly zoned plag, matrix qtz							
MCS353	84	-	-	-	15	-	1
margin, coarse polygonal, pale green hbl, phlogopite, spinel							
MCS354	10	-	65	25	-	-	tr
interior, coarse polygonal hbl replacing opx, plag euhedral, apat acc							
MCS355	10	-	-	64	15	10	1
coarse poikiloblastic, biot foliated, strongly zoned plag, matrix qtz							
W*MCS358$_M$	33	-	-	56	-	8	3
fine granoblastic, strongly zoned plag, matrix qtz							
W*MCS358$_I$	-	-	47	42	-	8	3
medium poikiloblastic amphibolite, vermicular plag inc, matrix qtz							
MCS362	26	4	5 inc	55	10	-	tr
coarse granoblastic, pale green hbl, phlogopite, slightly zoned plag							
MCS363	4	6	45	45	-	tr	tr
medium granoblastic, incipient pyx growth, zoned plag assoc with pyx							
MCS365	10	2	60	28	tr	-	-
coarse polygonal hbl, fine grained zoned plag, incipient pyx growth							
MCS368	10	10	30	45	3	tr	tr
coarse poikiloblastic pyx, granoblastic hbl, zoned plag							
MCS369	15	-	25	54	-	5	tr
coarse poikiloblastic, slightly zoned plag, matrix qtz							
MCS374	3	-	50	47	-	-	tr
coarse polygonal pale green hbl replacing opx							
MCS375	15	15	15	55	-	-	tr
coarse poikiloblastic							
MCS376	10	10	35	45	-	-	-
medium poikiloblastic pyx replacing coarse granoblastic hbl							
MCS379	10	3	20	60	-	5	2
medium granoblastic, foliated, zoned plag, matrix qtz							
*MCS380	-	8	25	53	-	10	4
coarse poikiloblastic hbl, titanite as accessory, calc-silicate ?							
*MCS383	22	-	-	55	15	4	4
margin, fine granular to coarse biot-rich poikiloblastic							
*MCS384	20	10	-	49	5	15	1
highly altered, medium poikiloblastic, secondary qtz							
*MCS385	20	-	13	47	10	10	tr
margin, fine, strongly foliated, matrix qtz, altered plag							
*MCS386	17	8	-	64	7	2	2
medium poikiloblastic, foliated, zoned plag, matrix qtz							
	9	-	-	61	5	22	3
segregation							
MCS396	16	4	-	59	8	10	3
medium poikiloblastic, foliated, matrix qtz							
MCS401	15	20	1 inc	42	1	20 vein	2
coarse poikiloblastic, vein and matrix qtz,							
MCS404	10	2	30	58	-	-	tr
coarse polygonal plag with deformation lamellae, granular pyx							
MCS405	38	27	20	15	-	-	-
coarse polygonal							

Northern Areas

	Opx	Cpx	Hbl	Plag	Biot	Qtz	Oxides
*MCS207	25	20	tr inc	47	1	5	2
fine poikiloblastic, slightly altered							
MCS217	-	30	1 inc	49	-	15	5
coarse sieve textured cpx, matrix qtz, calc-silicate ?							
MCS218	-	40	-	43	-	15	2
coarse poikiloblastic, sieve textured cpx							
*MCS220	-	9	20	54	-	15	2
medium sieve textured cpx, matrix qtz							
MCS221	-	35	-	45	-	20	2
coarse sieve textured cpx and plag, calc-silicate ?							
*MCS235	-	10	89	-	-	1	tr
very coarse, polygonal granoblastic, hbl-rich pod							

* Mineral analysis by microprobe
W Whole rock geochemical analysis of major elements
O Oxygen isotope determinations for quartz, biotite and magnetite
I Fluid inclusion study

5.2.2 Textural history

From the table 5.1, above it can be seen that there is tremendous variation in the mode amongst mafic gneisses . The following petrographic groups can be recognised: amphibolites, hornblende granulites, two-pyroxene granulites, orthopyroxene granulites and coarse grained pyroxene-bearing segregations. It is important to note that a single mafic lens may consist of all the above groups. It is rare to find that a single thin section is representative of the texture or mineral assemblage of any single mafic gneiss body. However, there is abundant textural evidence that the petrographic groups can be related to each other through a simple textural history that may provide important contraints on the mechanisms of granulite-facies metamorphism in mafic gneisses. Thus in this section petrography is presented as a textural evolution from hornblende-rich mafic gneisses to pyroxene granulites.

Amphibolites: Very few rocks are amphibolites throughout. Most develop orthopyroxene along their margins or in internal banding. Hornblende and plagioclase are present in equal amounts. The texture is generally coarse granoblastic, see plate 5.1, some samples e.g. MCS358$_I$ have poikiloblastic hornblende with vermicular plagioclase inclusions. Hornblende is green-brown in colour and grain size is 3-4 mm. Plagioclase occurs as xenoblastic, polygonal grains, smaller than hornblende, about 2 mm across. Plagioclase is unzoned except for those sections that contain clinopyroxene.

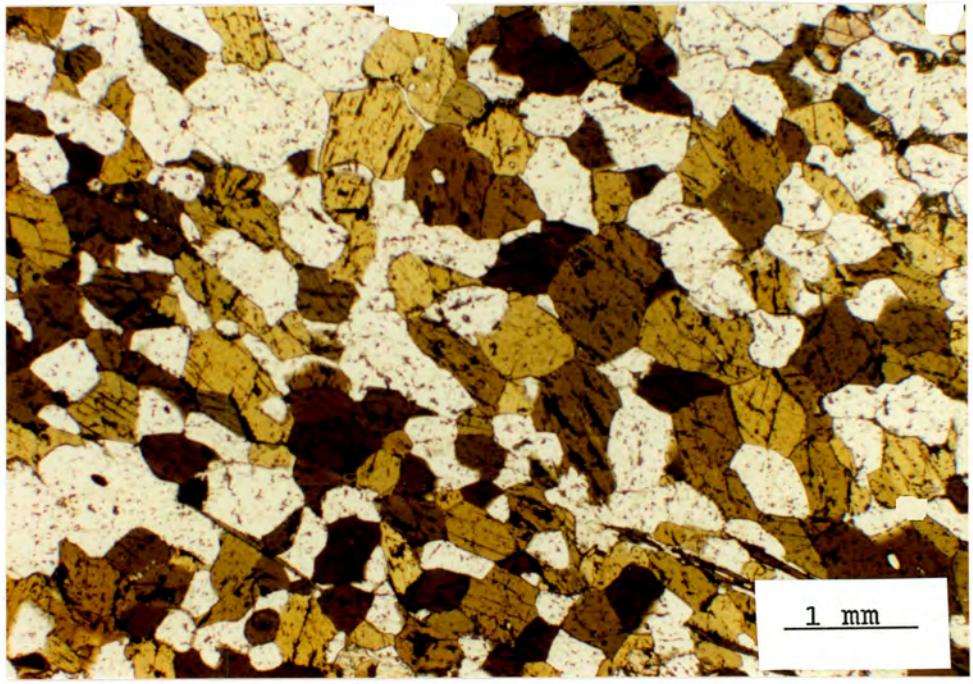

Plate 5.1 Granoblastic amphibolite domain in mafic gneiss. Green-brown hornblende, plagioclase and minor biotite. PPL. Sample MCSS05 (Silwerfontein).

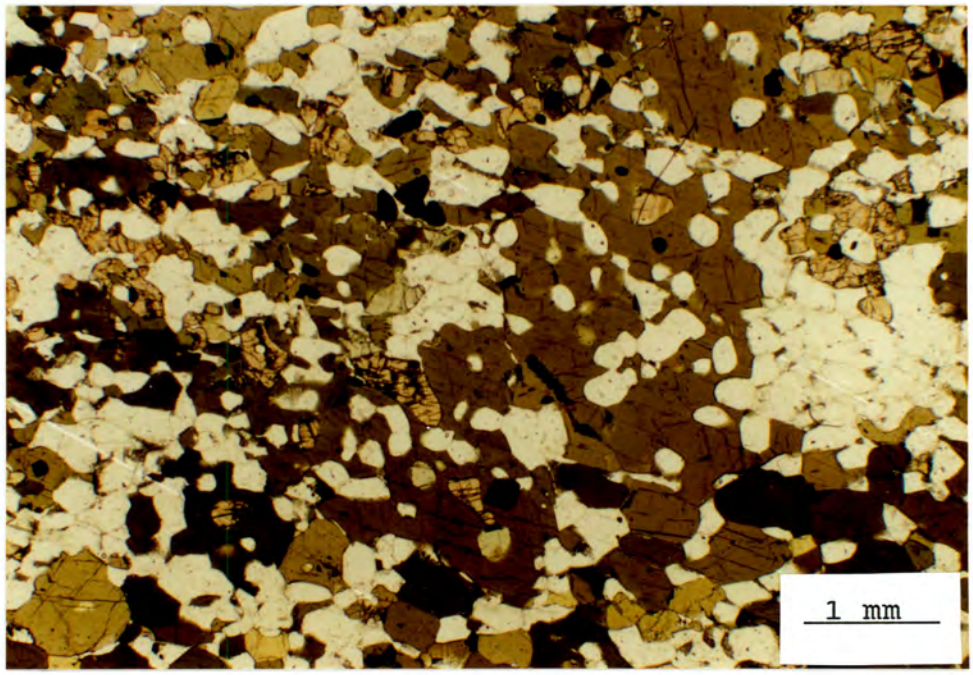

Plate 5.2 Hornblende-granulite showing incipient pyroxene growth at grain boundaries of poikiloblastic hornblende. PPL. Sample MCS304 (Hytkoras).

In the Buffels River area clinopyroxene-bearing amphibolites are rare. Sample VK7 provides an example (VK7 comes from Velskoen a locality a few km east of Tweefontein). In VK7 clinopyroxene forms polygonal grains in a similar fashion to hornblende. In mafic gneisses collected from the northern areas clinopyroxene is present as large, 10 mm rounded, sieve textured poikiloblasts. Accessory minerals such as titanite and apatite suggest a similarity with calc-silicate gneisses observed throughout central Namaqualand. These types of "mafic gneiss" contain more than 10% quartz. Quartz is absent or present only in very small amounts in amphibolites from the Buffels River area.

Hornblende granulites: Most of the mafic gneisses observed in Buffels River area can be descibed as hornblende granulites, i.e. assemblages consisting of two pyroxenes + hornblende. The amount of hornblende varies from trace amounts as inclusions in pyroxenes to over 50% of the mode. In some cases hornblende is in textural equilibrium with pyroxene and are found in contact evenly distributed throughout the rock. Others show mm scale banding of hornblende-rich domains and pyroxene-rich bands.

Incipient pyroxene development can be seen in a number of samples, see plates 5.2 & 5.3. Small, 0.2 mm granules of pyroxene occur at the contacts between hornblende and plagioclase and along hornblende cleavage planes. Core replacement of hornblende by pyroxene produces an atoll-type texture. It appears that ortho- and clinopyroxene grow in the same fashion. Plagioclase at sites of incipient pyroxene growth is strongly zoned.

Optical zonation in plagioclase takes the form of a concentric shadowy extinction. In some crystals small rounded spots with sharply defined extinction positions occur in the centre of the grain. No other minerals show optical zonation. Pyroxene and hornblende are unzoned except for slight chemical variations on the outermost rims.

Hornblende develops tiny laths of ilmenite along cleavages and grain boundaries (see plate 5.4). The ilmenite is partially pseudomorphed by hematite and rutile.

When pyroxene content is in excess of 5% a network of poikiloblasts replaces hornblende. Pyroxene encloses rounded

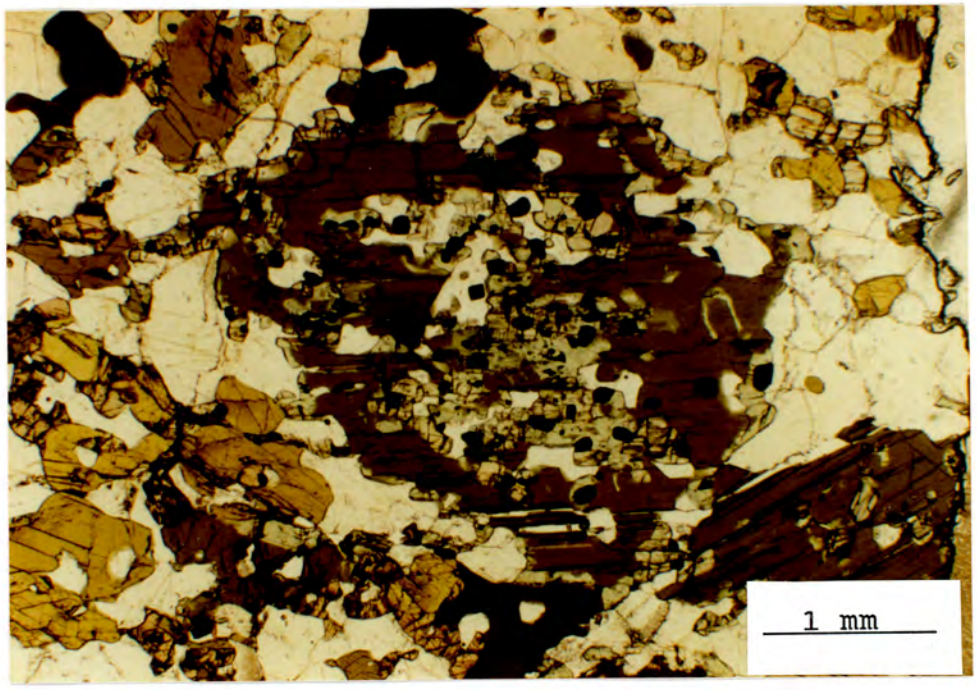

Plate 5.3 Hornblende-granulite showing clinopyroxene replacing the core of a large poikiloblastic hornblende. PPL. Sample MCS305 (Hytkoras).

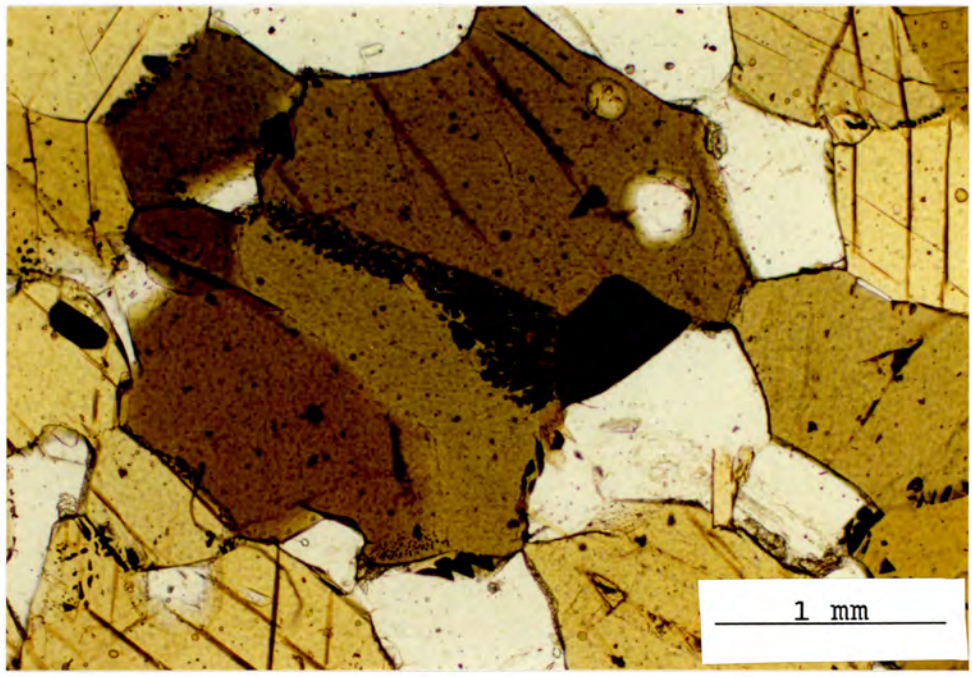

Plate 5.4 Development of ilmenite laths along hornblende grain boundaries. Amphibolite domain of mafic gneiss. PPL. Sample MCS304 (Hytkoras).

plagioclase crystals and islands of granoblastic hornblende. When pyroxene content exceeds that of hornblende in the mode the granoblastic texture is lost and hornblende occurs as isolated patches or as small rounded inclusions in clinopyroxene.

Pyroxene granulites: Coarse grained larger bodies of mafic gneiss often develop very large 5 cm poikiloblasts of pyroxene. Although in plane polarised light the texture has a granoblastic appearance, the pyroxene grains are in optical continuity. Plagioclase undergoes a reduction in grain size and is usually well rounded (see plates 5.5 & 5.6). Clinopyroxene contains small hornblende inclusions, rarely seen in orthopyroxene. Pleochroism in pyroxene is marked: orthopyroxene is pinkish-brown to greenish to pale yellow pleochroic; clinopyroxene is bluish-green to pale green to pale yellow pleochroic.

Nineteen of the samples studied are hornblende-absent granulites, most of which have a coarse poikiloblastic texture. Plagioclase is optically zoned. Quartz is present in the matrix or in the form of thin veins.

Towards the margin of strongly boudinaged mafic bands recrystallization of pyroxene occurs, resulting in a medium grained granular texture. Intermediate steps are seen as undulose extinction and sub-grain development in large poikiloblasts, and sub-grain rotation. The marginal refoliation is the S_3 fabric produced during shearing.

Orthopyroxene granulites: Ten of the samples studied contain orthopyroxene without clinopyroxene or hornblende. All of these are from the margins of mafic lenses. Generally finer grained (1-2 mm grain size) than the interior domains, they contain poikiloblastic orthopyroxene with a strong foliation. Some of margins are granular without optical continuity between pyroxene grains.

Margins often contain 5-15% modal biotite, strongly concentrated on the contact itself, but sometimes evenly distributed about the marginal zone. The biotites have strong prefered orientation, in some samples e.g. in DWN615 this fabric is oblique to the foliation defined by orthopyroxene and plagioclase. Biotite is dark brown to pale yellow-brown pleochroic and occurs as individual flakes (1-2 mm) or as clusters, up to 2 cm in size. Oxide minerals are seen as inclusions in reflected light.

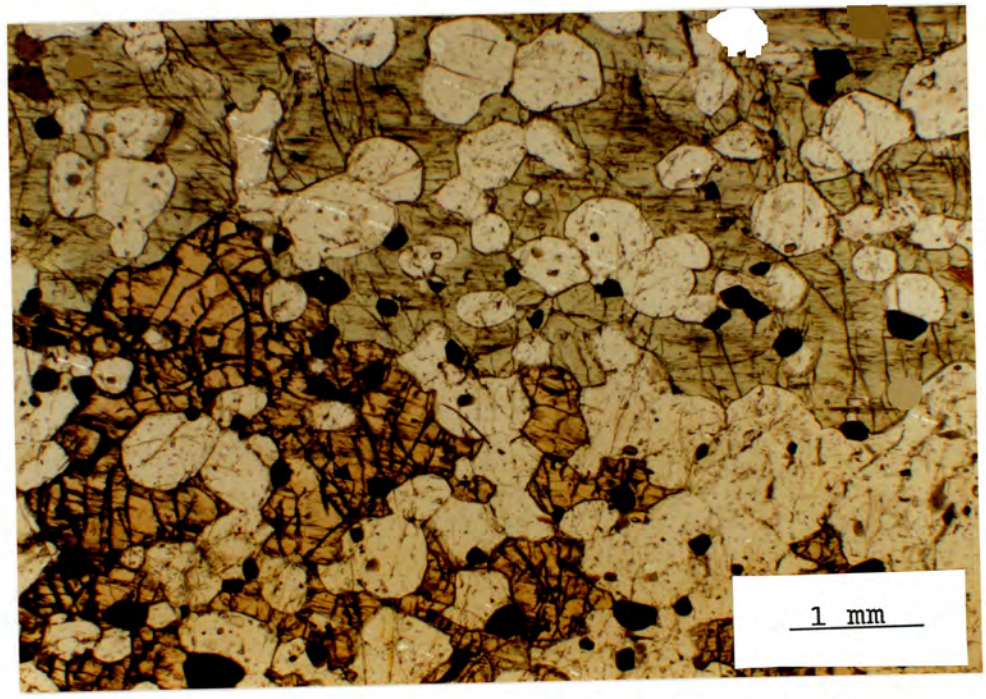

Plate 5.5 Pyroxene-granulite showing poikiloblasts of clinopyroxene (above) and orthopyroxene (below). Note the rounded form of plagioclase inclusions. PPL. Sample HY8 (Hytkoras).

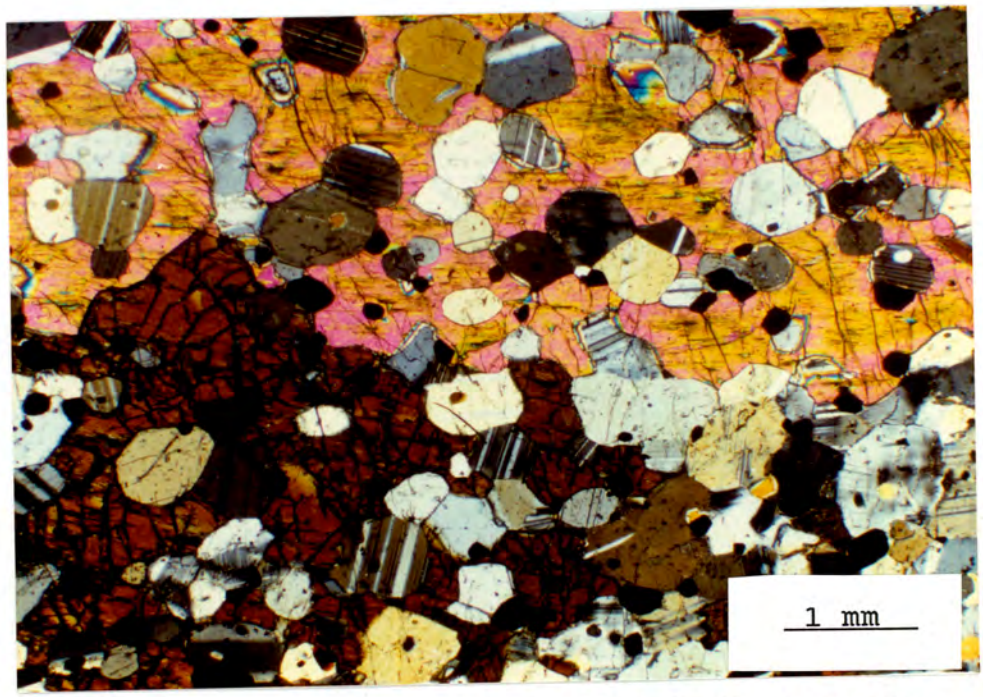

Plate 5.6 As above, cross polars. Note that both pyroxene poikiloblasts are in optical continuity.

Segregations: Mafic bodies over 2-3 m in width contain coarse grained, structureless, pyroxene-bearing segregations. Modal proportions are difficult to assess as segregation boundaries are not always sharply defined. It is better to integrate entire veins and patches in outcrop because a normal thin section does not give a representative sample. The minerals are coarse and appear to be randomly distributed in three dimensions. The approximate modal proportions of mafic segregations are given below:

TABLE 5.2

Modal proportions for veins and segregations in mafic gneisses

Sample	Opx	Cpx	Hbl	Plag	Biot	Qtz	Oxides
DWN349	-	20	-	57	tr	20	2
DWN353	29	7	1 inc	56	2	-	5
DWN353[A]	10	35	tr inc	53	tr	-	3
MCSS05[B]	35	7	-	47	tr	10	1
MCS317	5	28	2 inc	60	2	-	3
MCS327	40	-	-	10	-	49	1
MCS386[I]	9	-	-	61	5	22	3

Segregations take the form of small 5 cm clots of coarse pyroxene surrounded by a halo of coarse grained pyroxene, plagioclase and quartz (plate 5.9), or vein-like segregations that form an inter-connecting network superimposed over the existing foliation (plate 5.10). Pyroxene content is high, greater than in the matrix. Hornblende is found in small amounts as inclusions in clinopyroxene within segregations. Very coarse grained hornblende (10 cm) is observed in segregations from some of the thicker, quartz-rich mafic lenses. Hornblende-bearing segregations do not contain pyroxene. Plagioclase is common to all types of segregation and is coarse grained, equant and unzoned. In some cases quartz far exceeds plagioclase in the segregations, others are quartz-free. Segregations are limited to the centre of mafic units and do not trangress into surrounding lithologies.

Plate 5.9 Large patch-like segregation of coarse grained pyroxene, plagioclase and quartz, hosted by medium grained pyroxene-granulite. Hytkoras.

Plate 5.10 Network of pyroxene-rich veinlets in a thick lens of quartz-rich pyroxene-granulite. River bed, Hytkoras.

5.3 MINERALOGY AND MINERAL CHEMISTRY

5.3.1 Hornblende

Amphibole structure consists of a double chain of silica tetrahedra with octahedrally co-ordinated cations in M1, M2, M3 and M4 sites. The M4 site is occupied by larger cations, an additional site may be occupied by large cations, principally Na and K. The overall formula has the form:

$$A_{(0-1)}\ M4_{(2)}\ M1,3_{(2)}\ M2_{(2)}\ T_{(8)}\ O_{22}\ (OH,F,Cl)$$

End members in a pure Mg system can be represented as follows:

	A	M4	M1,3	M2	T		V
Tremolite	[]	Ca_2	Mg_3	Mg_2	Si_8	O_{22}	OH
Tschermakite	[]	Ca_2	Mg_3	Al_2	Al_2Si_8	O_{22}	OH
Edenite	Na	Ca_2	Mg_3	Mg_2	$AlSi_7$	O_{22}	OH
Cummingtonite	[]	Mg_2	Mg_3	Mg_2	Si_8	O_{22}	OH
Gedrite	[]	Mg_2	Mg_3	Al_2	Al_2Si_6	O_{22}	OH

(Powell, 1975 and Spear, 1981)

Subsitutions can occur on all sites:
K or Ca for Na in the A site
Mg, Na, Mn for Ca in the M4 site
Fe, Mn for Mg in M1,3
Al^{VI}, Fe^{III}, Ti, Cr, and Mg can occupy the M2 site
Si and Al^{IV} occupy the tetrahedral site
F and Cl can substitute for OH.

Fig. 5.1 shows amphibole classification according to Leake (1978). This system considers Si, Ca+Na, Na+K and Mg/(Mg+Fe). Sodic amphiboles have a full A site and Na in the M4 site. The amphiboles in this study are calcic amphiboles with Na+K > 0.5, except for MCS358 which has a very low K content and is classified as a tschermakitic hornblende. There is a restricted range of chemical compositions, most samples fall within the fields of ferroan pargasitic hornblende and edenitic hornblende. The classification of Miyashiro (1973), (fig.5.2) plots Al^{IV} against K+Na, the amphiboles in this study plot in the field of green-brown hornblende clustering almost equidistant from the end-members edenite and tschermakite.

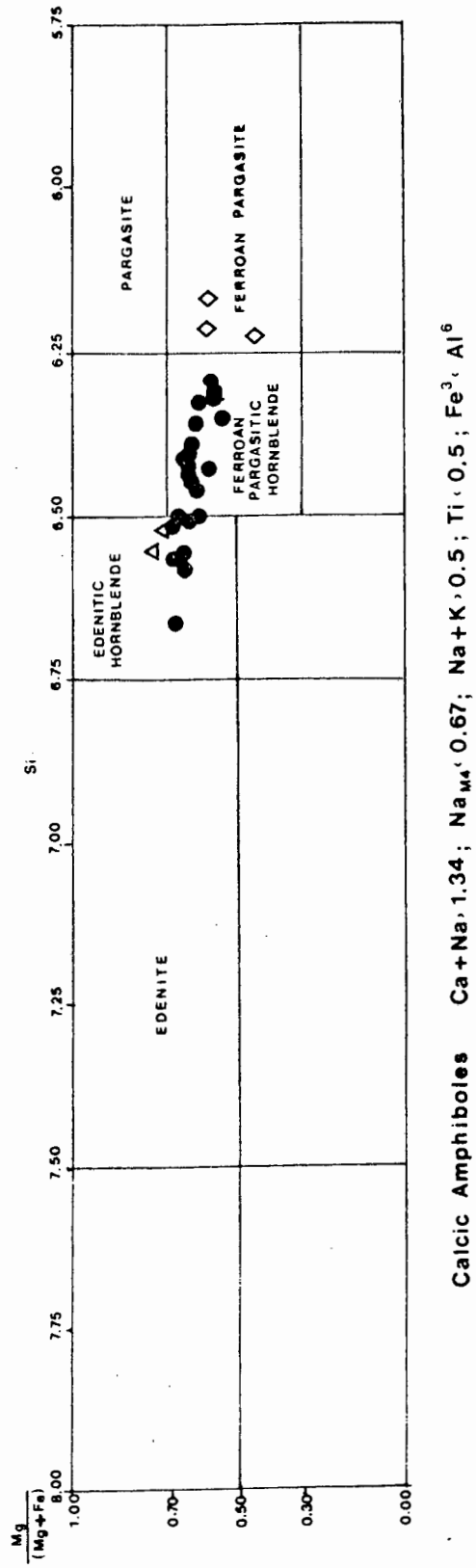

Fig. 5.1 Classification of hornblendes from mafic gneisses according to Leake (1978). Cation proportions based on 23 oxygens.

● Hornblende-granulites
◇ Amphibolites
△ Metagabbros

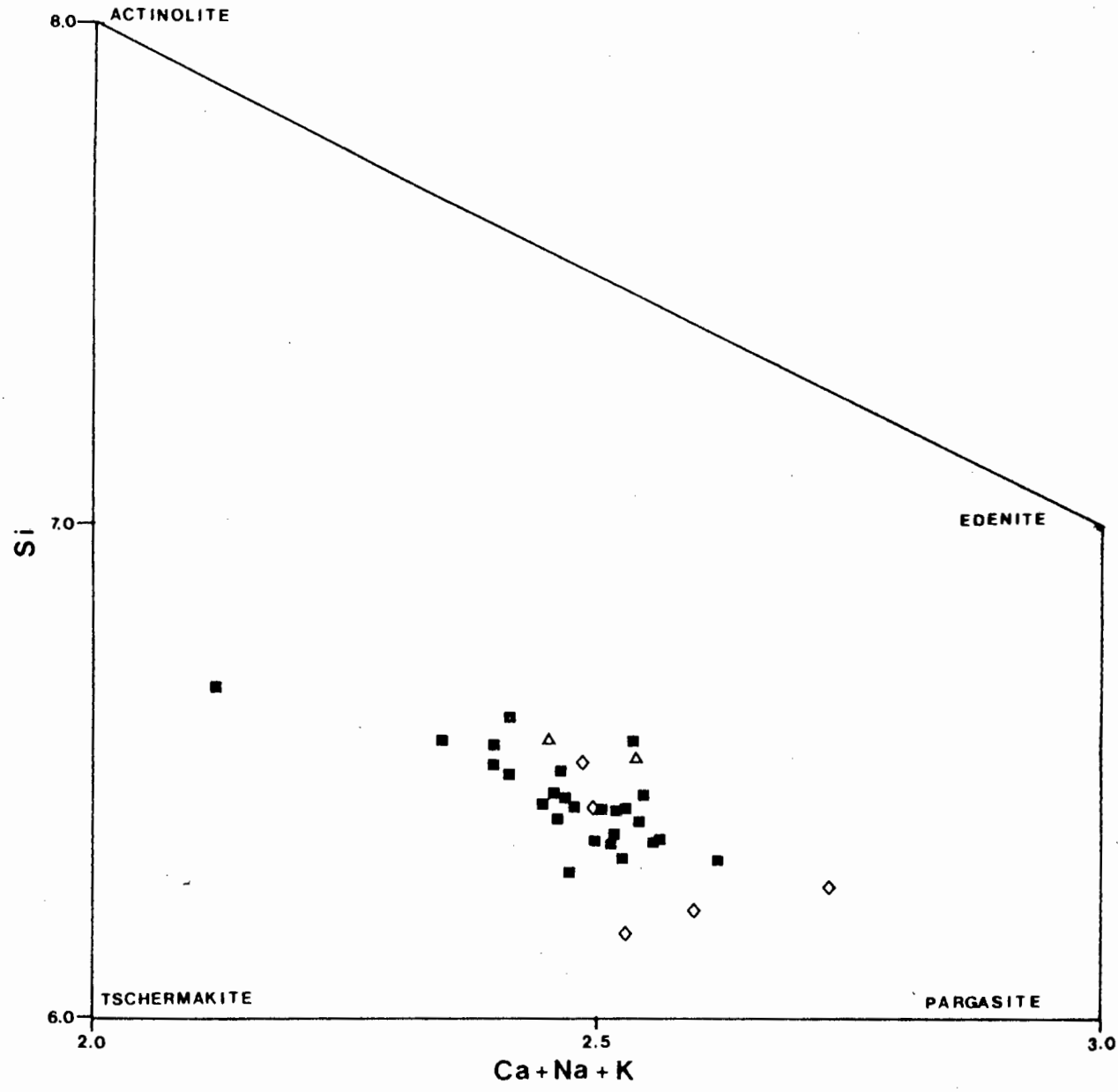

Fig. 5.2 Classification of hornblendes from mafic gneisses after Miyashiro (1973). Cation proportions based on 23 cations.

■ Hornblende granulites
◇ Amphibolite
△ Metagabbros

Blue-green hornblendes are recorded in the northern amphibolite-facies zone (Albat, 1984). The colour change to green-brown hornblende in granulite-facies has been recorded in several localities: Broken Hill (Binns, 1965), the Adirondacks (Engel & Engel, 1962) and Aracena (Bard, 1969). The colour change is attributed to increasing Ti and Fe^{3+} contents with increasing temperature. Hornblende grains show the development of ilmenite granules along cleavages and grain boundaries (plate 5.4) this suggests the M2 site is fully saturated in respect to Ti. Ti content is normally 0.2 cation units per 23 oxygens. Sen & Ray (1971) regard the presence of opaque granules as evidence for the continuous prograde nature of hornblende breakdown.

Slight variations in Mg/(Mg+Fe) ratio occur and reflect differences in bulk rock composition.

Most hornblendes in this study show remarkably similar compositions suggesting that we are dealing with equilibrium compositions at peak or near peak conditions in rocks of similar bulk composition. The mean hornblende composition and standard deviation is given below:

	mean weight %	σ_{n-1}
SiO_2	43.31	(1.14)
TiO_2	1.82	(0.43)
Al_2O_3	11.23	(0.62)
FeO	13.88	(1.76)
MnO	0.30	(0.30)
MgO	12.75	(1.30)
CaO	11.70	(0.31)
Na_2O	1.39	(0.27)
K_2O	1.24	(0.26)

Slight zonation is present along thin rims (20-50 μm) adjacent to plagioclase. Increase in Na with an equivalent decrease in Ca is observed. Reequilibration along grain boundaries during cooling is probably responsible for these minor changes (Loomis, 1983). Otherwise grains can be regarded as homogeneous.

A few hornblende samples were analysed for fluorine. In all cases fluorine was below detection limit.

By comparison with amphibolite facies hornblendes from Namaqualand (Albat, 1984) and other terranes, e.g. the Willyama Complex, Broken Hill (Binns, 1965 and Corbett & Phillips, 1981) the transition to granulite facies is marked by increases in Al, Na, K and Ti with decreases in Si. Edenitic substitutions are typical of high pressure terranes (Raase, 1974 and Laird & Albee, 1981). Hornblendes from the Buffels River area plot in the low pressure field of Laird & Albee and occupy the same range as amphiboles from the Abukuma terrane, Japan, see fig 5.3.

Fig. 5.4 shows the variation in "edenitic alkalis" with Al^{iv} for hornblendes in this study, hornblendes from the amphibolite-facies zone of central Namaqualand and the amphibole compositions from the three prograde zones at Broken Hill (Binns, 1965) and the composition of retrograde amphiboles from the same area (Corbett & Phillips, 1981). Hornblendes from the amphibolite-facies zone of Albat (1984) and from the Buffels River area, this study, plot in the same field as hornblendes from Zone C (granulite-facies) of the Broken Hill area (Binns, 1965). Hornblendes from amphibolites in the Tweefontein area (MCST02, MCST03, and VK7) plot outside the range of compositions recorded from Broken Hill, and are characterised by very high alkali contents.

5.3.2. Pyroxenes

Two-pyroxene assemblages occur in the interiors of most mafic gneiss bands. The development of a very coarse poikiloblastic crystal network is typical.

There is no optical zonation. The only systematic chemical zonation is a slight increase in Mg and decrease in Fe along thin rims. Two-pyroxene thermometry (Lindsley, 1983), see Section 4.2.1 gives temperatures around 750°C which suggests that core compositions represent equilibrium values at peak metamorphism.

The composition of pyroxenes in different textural domains is almost identical. Orthopyroxenes from biotite-bearing, hornblende-absent margins have the same Mg/(Mg+Fe) ratios as small granules forming along hornblende cleavages and large equant orthopyroxene in segregations.

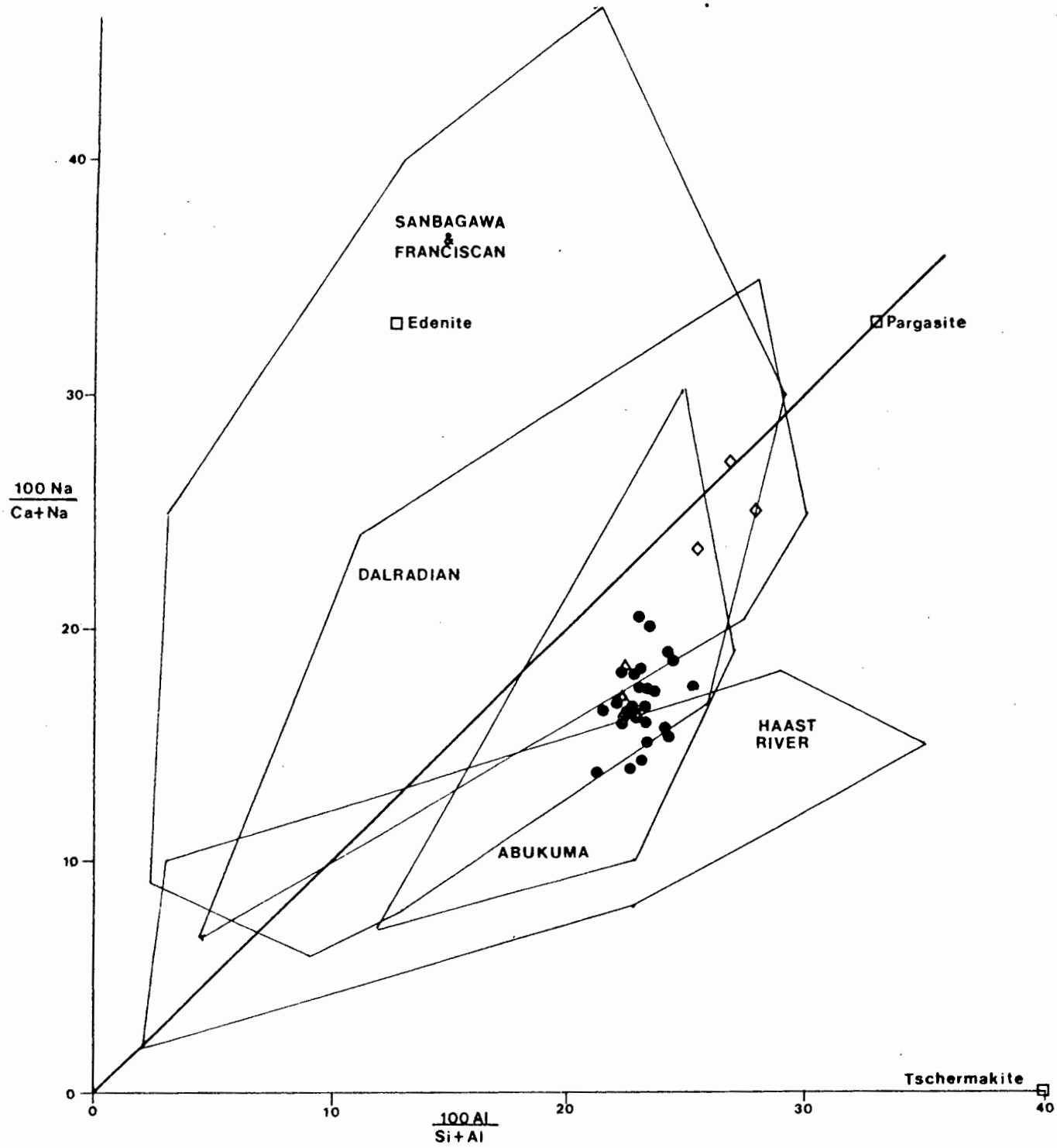

Fig. 5.3 Comparison of hornblende compositions from the Buffels River and other high grade terranes. Increasing Na in the A-site at the expense of Ca in the M4 site is a feature of high pressure terranes. Based on the data in Laird & Albee (1981).

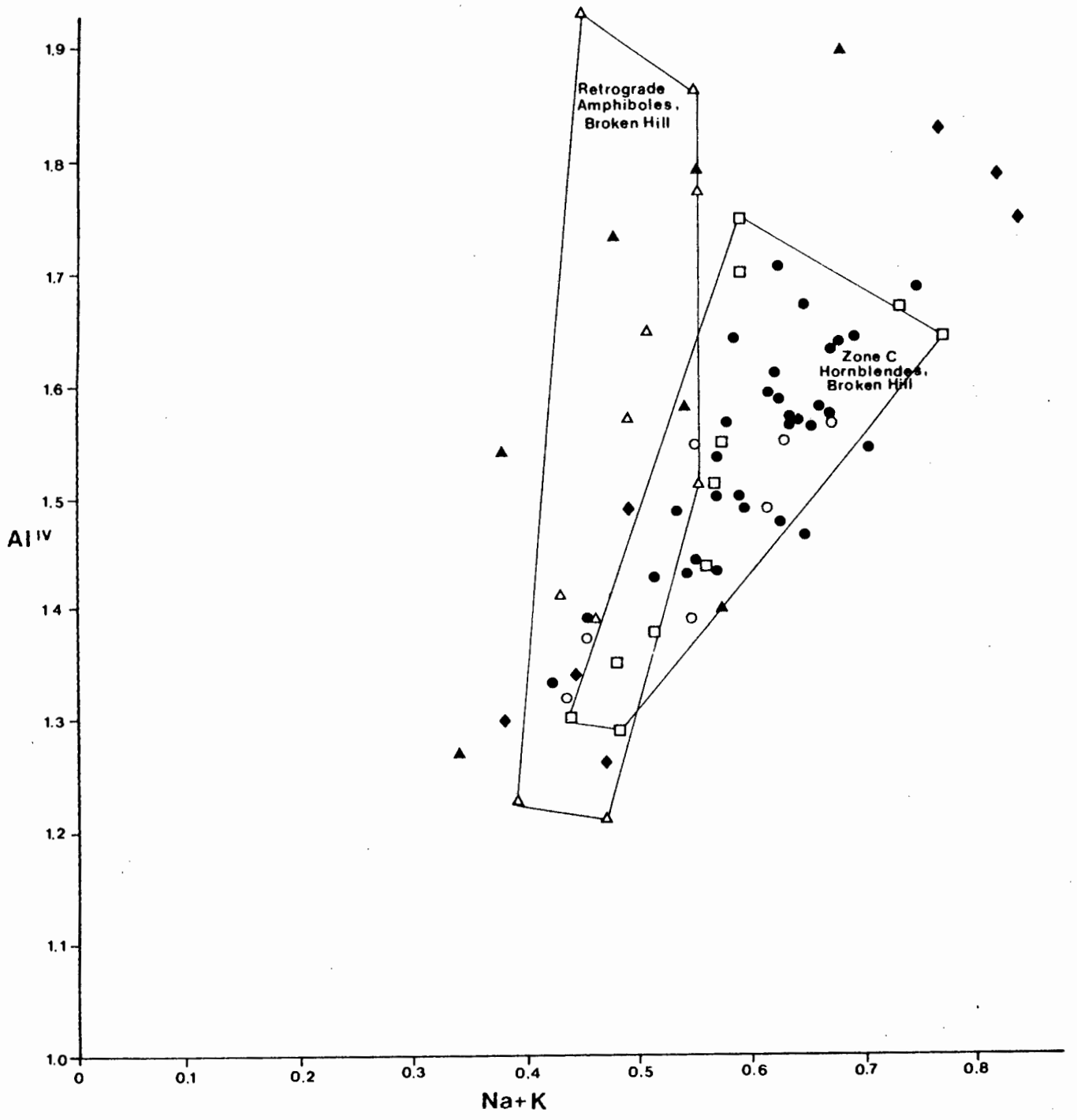

Fig. 5.4 Variation in edenitic alkalis with Al^{IV}. Cation proportions based on 23 oxygens. Comparison of amphibole compositions from central Namaqualand and Broken Hill, Australia.

●Hornblende-granulites, Buffels River
◆Amphibolites, Buffels River
▲Amphibolites, central Namaqualand (Albat, 1984)

□Prograde amphiboles, (granulite-facies) Broken Hill (Binns, 1965)
○Prograde amphiboles, Broken Hill (Corbett & Phillips, 1981)
△Retrograde amphiboles, Broken Hill (Corbett & Phillips, 1981)

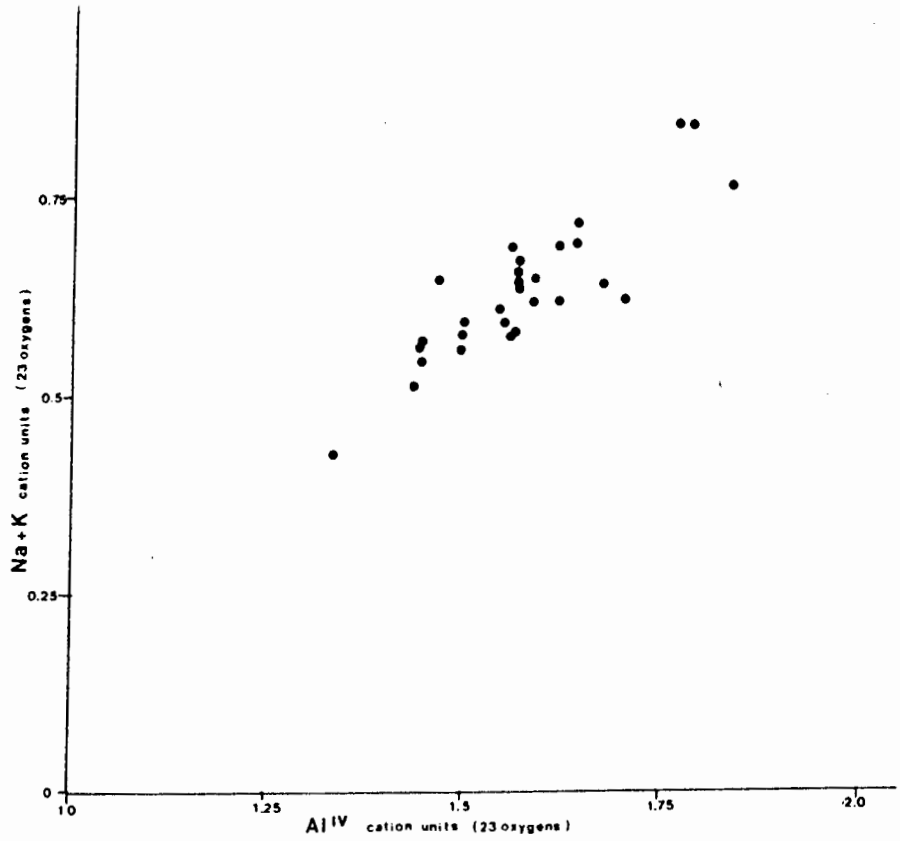

Fig. 5.5 Plot of Na+K against Al^{IV} for hornblendes from the Buffels River area. Note A-site occupancy increases with increasing Al^{IV} substitution in the tetrahedral site.

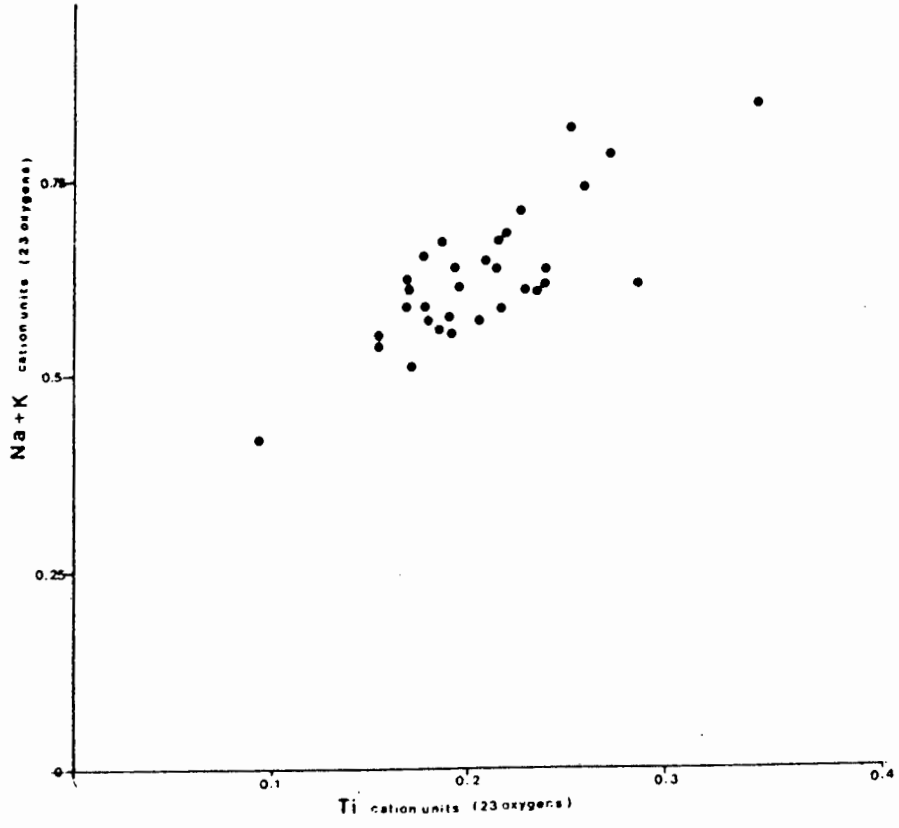

Fig. 5.6 Plot of Na+K against Ti. Ti increases with edenitic substitution.

The compositions of coexisting pyroxenes following the classification scheme of Morimoto et al. (1988) are given in fig. 5.7. All orthopyroxenes are enstatites with very low Wo contents, maximum Wo is 1.36. En varies between En 55-66 in mafic gneisses within the supracrustal sequence, increasing to En 71-75 in the metagabbros. Mean value is En 62.

Most clinopyroxenes plot in the field of diopside, but there are a few compositions falling into the augite field. Clinopyroxene from the intrusive metagabbros are more magnesian and have slightly higher Wo contents. En values range from 38-41, with clinopyroxenes from meta-gabbros yielding En 43-45. Mean value is En 40.

The lack of crossing tie-lines is consistent with the compositions representing equilibrium compositions.

The mean contents of minor constituents in ortho- and clinopyroxene are given below:

	Orthopyroxene		Clinopyroxene	
	mean	σ_{n-1}	mean	σ_{n-1}
TiO_2	0.07	(0.03)	0.24	(0.04)
Al_2O_3	1.43	(0.32)	2.33	(0.23)
MnO	0.90	(0.28)	0.48	(0.34)
Na_2O			0.41	(0.07)

Ti and Al are strongly partitioned into clinopyroxene and Mn is partitioned into orthopyroxene. Generally, the minor element contents are very constant.

5.3.3 Plagioclase

Plagioclase shows considerable chemical variation, both internally and throughout the sample. Core and rim analyses were carried out on single grains and as many as twelve grains in different textural domains in the same thin section were analysed.

Most hornblende-bearing mafic gneisses have plagioclase with core compositions of An_{50-60}, and rim compositions of An_{60-75}. Some

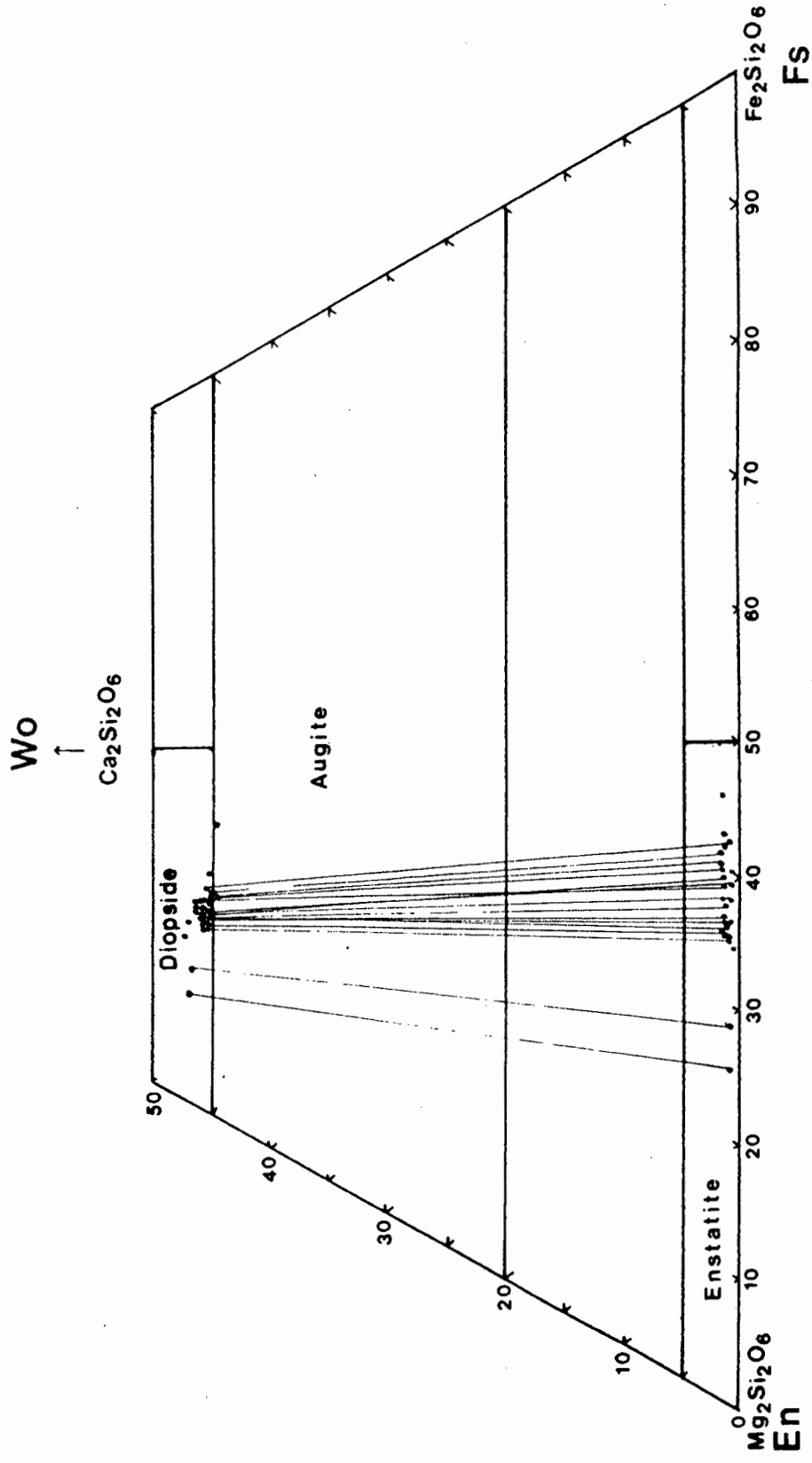

Fig. 5.7 Composition of coexisting pyroxenes, following the classification of Morimoto et al. (1988).

samples show a range of compositions on the thin section scale. The spread can be large, from An_{55} to An_{78}, depending on grain size and adjacent minerals. There is no simple relationship between plagioclase composition and the modal mineral assemblage. Fig. 5.8 shows core and rim compositions for plagioclase plotted against a ratio of modal hornblende/total Fe-Mg minerals expressed as a percentage, so that amphibolites will have a value of 100% and hornblende-absent granulites a value of 0%. There is a slight trend towards increasing Ca contents in rocks with low hornblende contents. However there are examples of hornblende-rich rocks with highly anorthitic, and unzoned, plagioclase. A series of samples were collected in order to monitor the chemical nature of the mineralogical banding which is so prominent in these gneisses. Table 5.2 lists the sample name and its lithological type together with the An content of plagioclase and the Ca/(Ca+Na) ratio of coexisting hornblende.

TABLE 5.2

Ca-Na equilibria in plagioclase and hornblende from mafic gneisses

		Plag XAn	Hbl Ca/(Ca+Na)
$DWN129_A$	Hbl granulite	0.59-0.74	0.84
$DWN129_B$	Opx-Cpx (Hbl incs only)	0.74	0.80
$DWN332_3$	Hbl granulite	0.83	0.84
$DWN332_2$	" "	0.83	0.85
$DWN332_1$	Opx granulite	0.54-0.78	----
DWN349	Hbl granulite	0.67-0.72	0.84
DWN349	Cpx segregation	0.59-0.69	----
DWN353	Hbl granulite	0.50-0.76	0.84
DWN353	Opx-Cpx granulite (modified matrix)	0.56-0.66	----
DWN353	Opx-Cpx segregation	0.54	----
MCSS05	Hbl granulite	0.48	0.81
MCSS05	Opx-Cpx segregation	0.49	----
$MCS301_A$	Hbl granulite	0.56-0.75	0.82
$MCS301_C$	" "	0.56-0.71	0.83
$MCS301_B$	Cpx (Hbl-absent) band	0.71-0.80	----
$MCS327_T$	Hbl granulite	0.86	0.84
$MCS327_B$	" "	0.86	0.84
$MCS327_I$	Opx segregation	0.87	----
$MCS358_I$	Amphibolite	0.83	0.83
$MCS358_M$	Opx granulite	0.61-0.51	----

There is a tendency for strong zonation in hornblende-granulites,

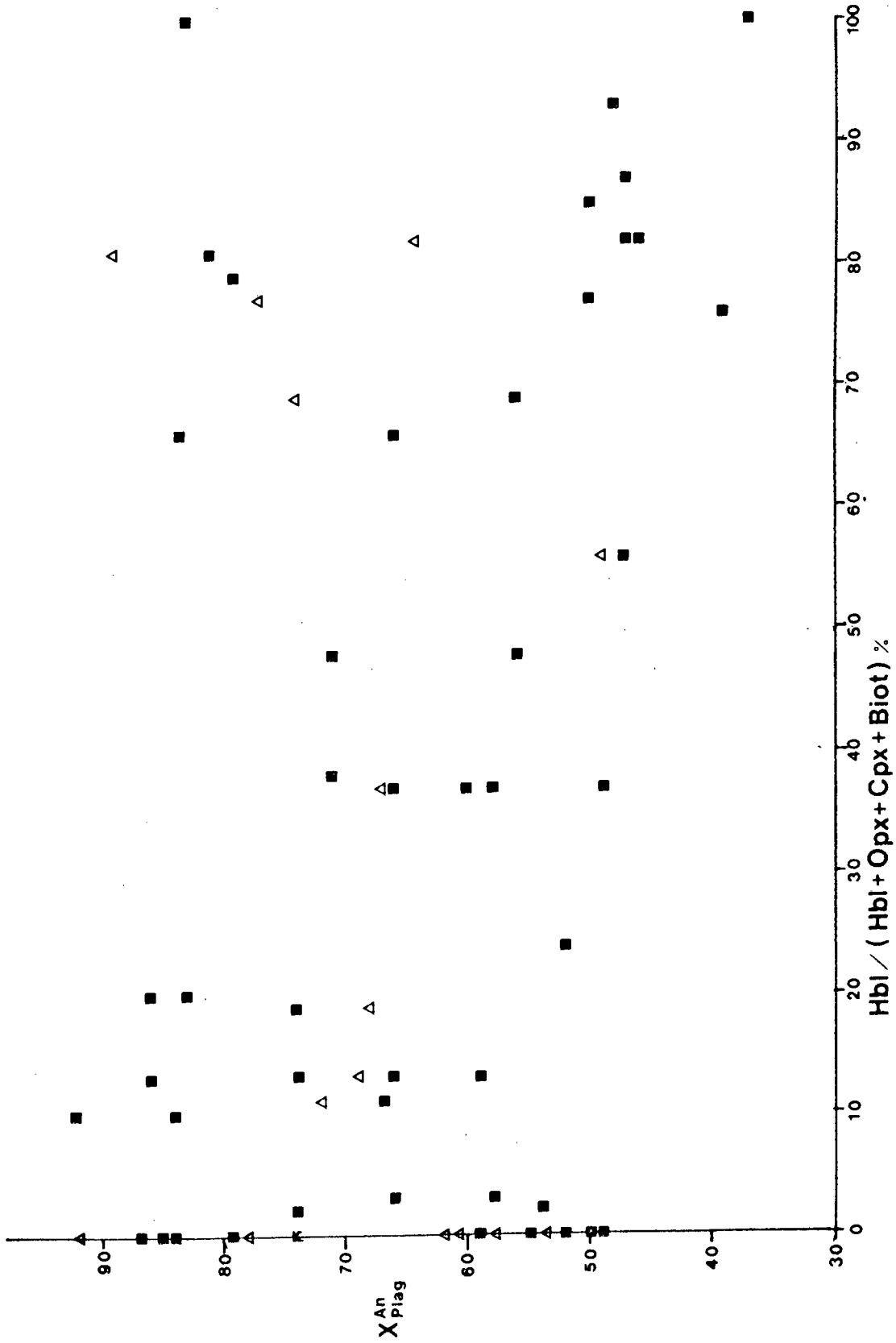

Fig. 5.8 Plot of plagioclase composition (X_{an}) against modal mineralogy (hornblende/total Fe-Mg phases).
■cores △rims.

with a broad core of intermediate composition and narrow rims with increasing An content, see fig. 5.9. However in orthopyroxene-granulites plagioclase have broad rims of intermediate composition, showing increasing Na and small rounded cores of high An content. In hornblende-granulites unzoned plagioclase with high An content occurs, presumably the unzoned nature of these grains is an indication of the attainment of equilibrium which is in some way inhibited in other rocks. The same range of compositions is recorded from the anhydrous, orthopyroxene-bearing margins.

Plagioclase from segregations has intermediate An contents. Generally, unzoned or with a restricted range of composition.

Fe is detected in most plagioclases in this study. Fe increases with Ca content. The most likely substitution is Fe^{3+} for Al^{3+} in the anorthite molecule.

5.3.4 Biotite

Biotites occur in small amounts in about half the samples in this study, only 10 samples collected contain more than 10% in the mode. Distinct layers and clusters of biotite are found at the margins of mafic bands. Single biotites form coarse (1-2 cm) flakes with random orientations. In refoliated (S_3) margins small biotites have strong prefered orientation. Pleochroism is from dark red-brown or chocolate-brown to straw yellow.

Ti is high, with a mean value of 0.54 cation units per 22 oxygens. X_{Mg} is also high, ranging between 0.6-0.75 with a mean value of 0.67. Cr, Mn and Na are sometimes present in small quantities. Fluorine was found in all biotites that were analysed for halogens. Chlorine was below detection limit in all cases. F content is usually below 1 weight %. MCS385 contains 10 modal % biotite coexisting with hornblende, the biotite contains 1.5 weight % F. Other samples containing trace amounts of biotite can have high F contents. Biotite coexisting with orthopyroxene in marginal bands has lower F contents, around 0.4 weight %. This can be explained in part by the greater abundance of biotite along the margins of mafic gneisses. F is strongly partitioned into biotite over hornblende, as in all cases F was below detection limits in hornblende.

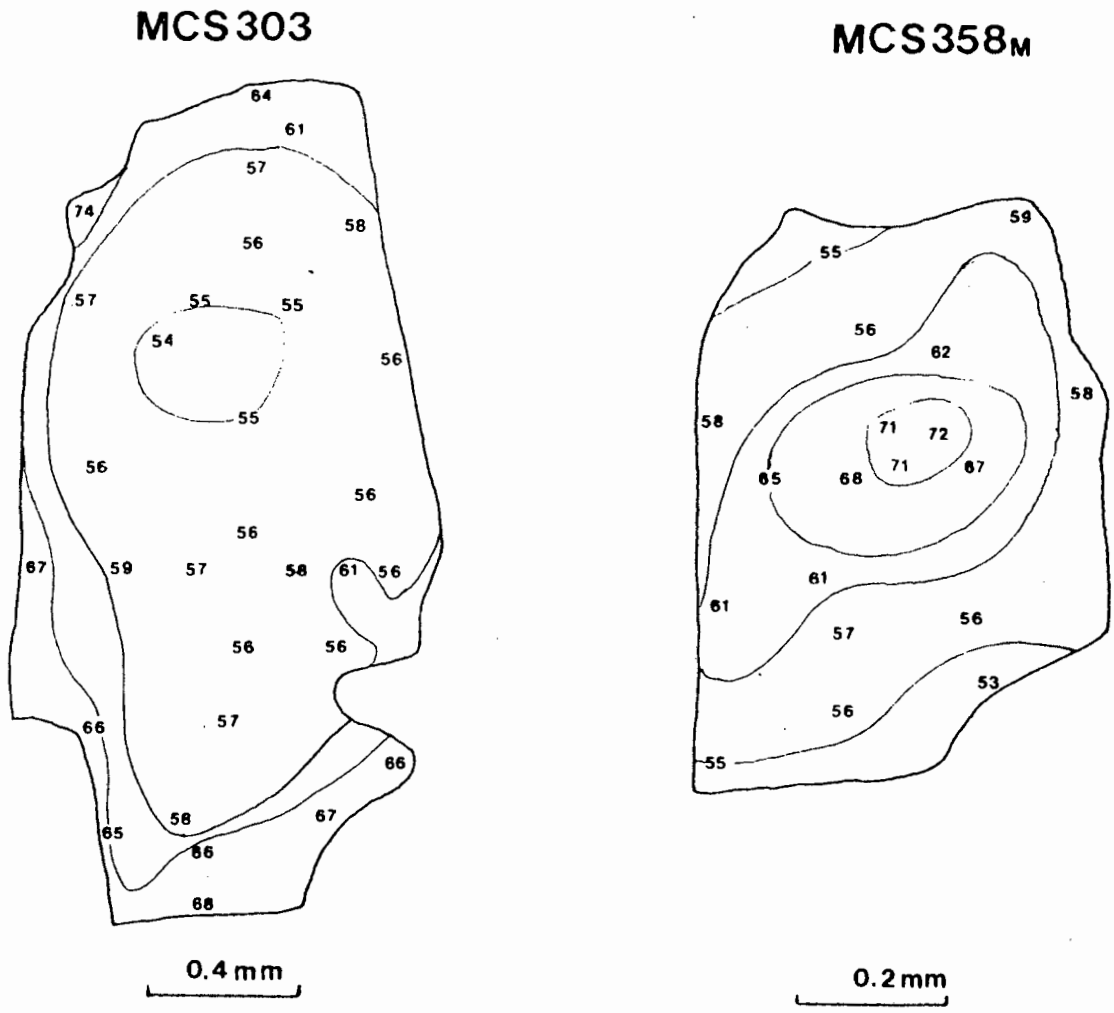

Fig. 5.9 Compositional zonation in plagioclase. MCS303 is an example of the commonly observed reverse-zonation. Increasing Ca along the rims. Note the large uniform core area. $MCS358_M$ is an example of normal-zonation. Increasing Na towards the rims. This type of zonation is observed in plagioclase from in the marginal domains of some mafic gneisses. Small "eyes" of calcic plagioclase are surrounded by more Na-rich zones.

5.3.5 Oxides and Sulphides

Oxide minerals have been well documented in mafic igneous and metamorphic rocks (Haggerty, 1976 and Rumble, 1976) and have applications in geothermometry and in the estimation of oxygen fugacities (see Buddington & Lindsley, 1964). Important solid solution series include Fe_2TiO_4 - Fe_3O_4 (ulvöspinel-magnetite), and $FeTiO_3$-Fe_2O_3 (ilmenite-hematite).

A common oxide assemblage is found in all samples studied. The assemblage consists of discrete magnetite grains and composite grains of ilmenite and titanohematite (see plates 5.11 and 5.12). In the ilmenite$_{ss}$ series individual Ti-bearing hematites are referred to as titano-hematites. Grains composed of fine scale lamellae of ilmenite in host of hematite$_{ss}$ are termed ilmeno-hematites (Buddington et al., 1963). The mixed grains in this study have ilmenite lamellae within hematite$_{ss}$ and hematite lamellae within ilmenite.

Individual grains are xenoblastic, rounded and sometimes embayed. No zoning or rimming textures are observed. No magnetite occurs within ilmenite-hematite grains. There are no internal lamellae observed in magnetite grains. In some of the more weathered mafic rocks the magnetite shows small white spots, probably hematite, a texture typical of oxidation during weathering (Haggerty, 1976). Ilmenite undergoes alteration to hematite and rutile.

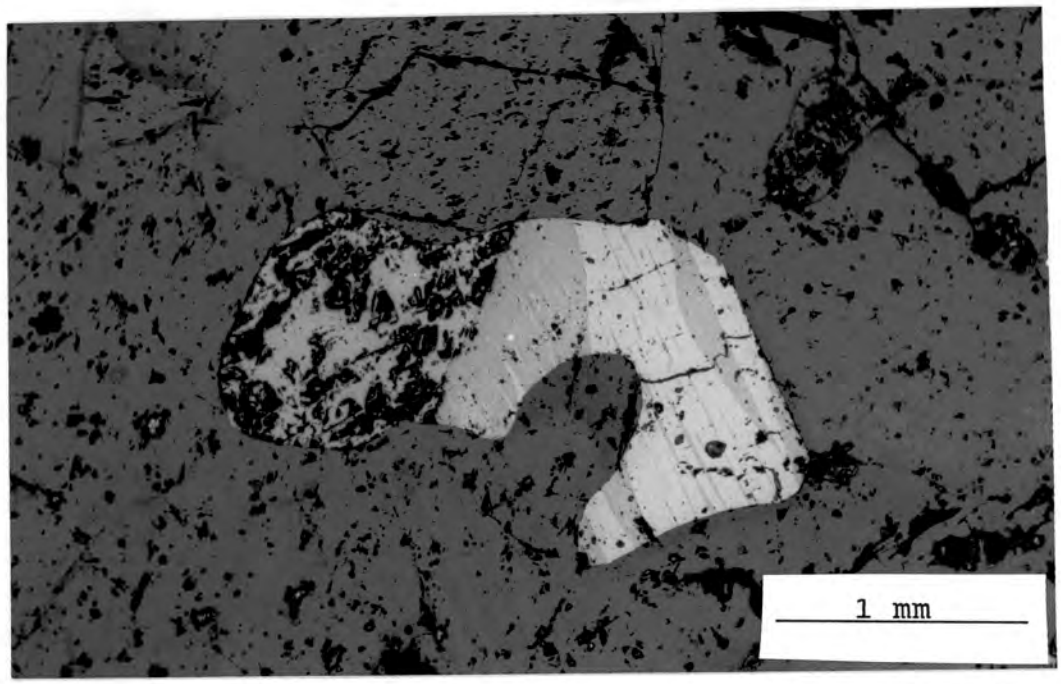

Plate 5.11 Oxide assemblage in pyroxene-granulite. Darker coloured and heavily pitted magnetite (left). Ilmeno-hematite (right), light coloured lamellae are titanohematite, darker lamellae are ilmenite. Reflected light. $MCS358_M$. River bed, Hytkoras.

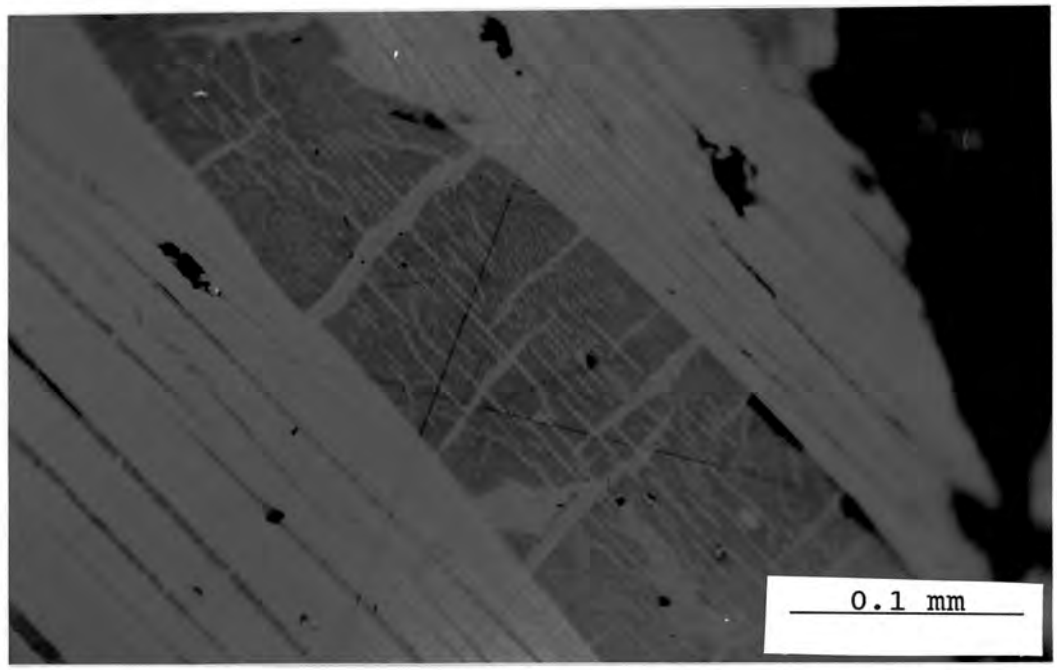

Plate 5.12 Detail of complex lamellae in ilmeno-hematite above. Central darker ilmenite band contains parallel blebs of hematite and lamellae of hematite and rutile at right angles. Reflected light.

TABLE 5.3

Composition of coexisting oxide phases from orthopyroxene-granulite MCS358$_M$

	Magnetite	Ilmenite	Titanohematite
TiO_2	----	48.45	14.00
Al_2O_3	0.07	----	----
Cr_2O_3	0.37	0.10	0.29
Fe_2O_3	68.49	7.85	73.19
FeO	31.00	40.36	12.27
MnO	----	2.70	0.28
MgO	----	0.15	----
Total	99.93	99.61	100.03
	4 oxygens	3 oxygens	
Ti	-----	0.926	0.276
Al	0.003	-----	-----
Cr_{III}	0.011	0.002	0.006
Fe	1.986	0.150	1.443
Fe	0.999	0.857	0.269
Mn	-----	0.059	0.006
Mg	-----	0.006	-----
Sum	2.999	2.000	2.000

Oxide percentages recalculated on the basis of stoichiometry (see Droop, 1987)

The composition of coexisting oxides are close to pure-end members, a significant Mn content is found in ilmenite and small amounts of Cr are recorded in magnetite. It was possible to analyse the titano-hematite lamellae, but the corresponding ferrianilmenite lamellae in hematite hosts are replaced by a very fine intergrowth of rutile and hematite too fine grained to resolve the composition of individual grains. Fig. 5.10 shows the composition of coexisting Fe-Ti oxides. Fig. 5.11 shows the compositions of coexisting Fe-Ti oxides plotted as functions of T and f_{O2} (Buddington & Lindsley, 1964). It can be seen from figs. 5.10 and 5.11 that compositions retained by oxide minerals in the mafic gneisses of the Buffels River area represent equilibration at low temperatures (>500°C), outside the experimentally calibrated region of Buddington & Lindsley. The oxide mineralogy in this study is very similar to that described for the diorites of the Koperberg Suite (Conradie & Schoch, 1986), and has been suggested as evidence for very slow cooling after the metamorphic peak.

Sulphides are rare, but pyrite with minor chalcopyrite is found

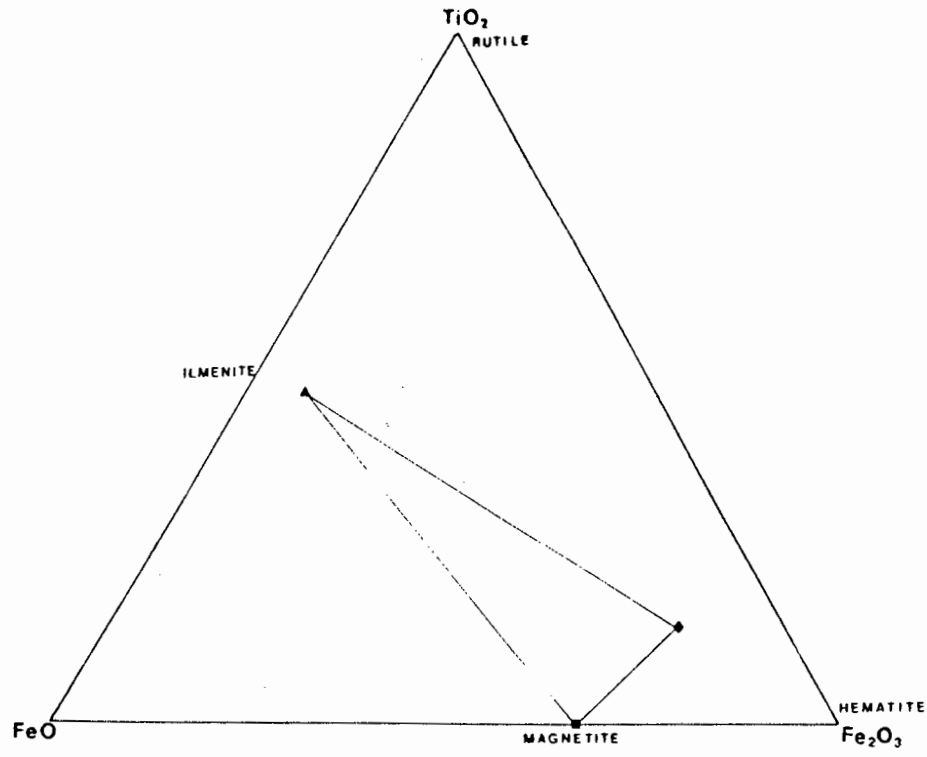

Fig. 5.10 Compositions of coexisting oxides from mafic gneiss $MCS358_M$

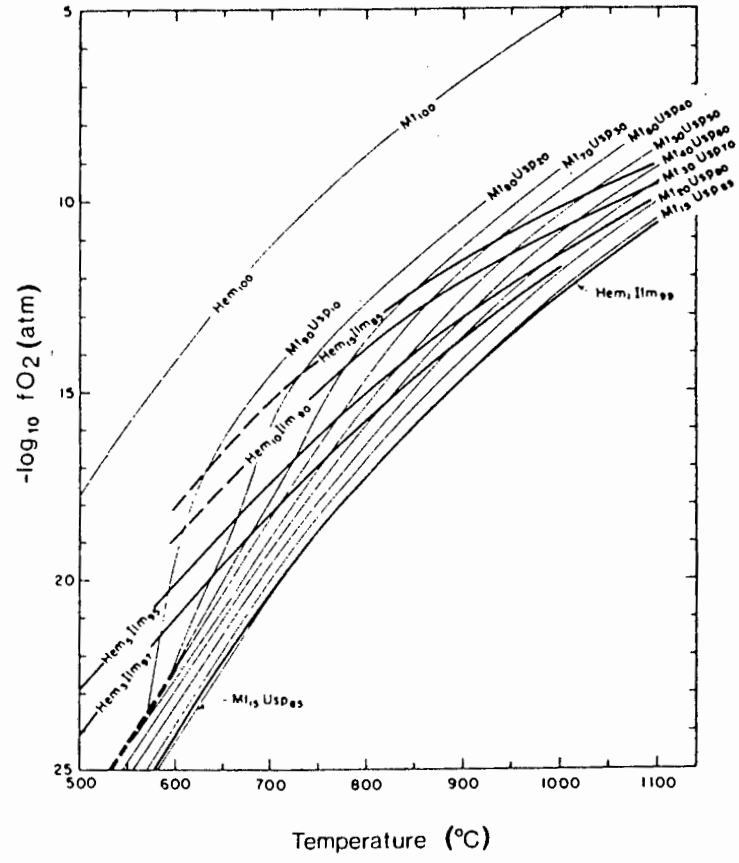

Fig. 5.11 Compositions of coexisting Fe-Ti oxides plotted as function of T and f_{O_2} (Buddington & Lindsley, 1964) Note that any $(Ilm\text{-}Hem)_{ss}$ composition coexisting with pure end-member magnetite is outside the scale of the calibration and indicate equilibrium at temperatures below 500°C.

in DWN380 and MCSS05.

5.3.6 Discussion

All Fe-Mg silicates have restricted and uniform compositions. Minerals are in Fe-Mg exchange equilibrium, with the possible exception of biotite with X_{Mg} for coexisting phases: Cpx > Biot > Opx = Hbl, the degree of retrograde exchange is limited to narrow rim zones. X_{Mg} for coexisting phases is shown in figs. 5.12 and 5.13. Plagioclase is the only mineral showing large variation and strong zonation in individual grains.

Progressive amphibole breakdown produces an increasingly calcic plagioclase (Sen & Ray, 1971; Spear, 1980; Robinson et al., 1982; Stoddard, 1985 and Raase et al., 1986). Hornblende compositions from the mafic gneisses in this study indicate that edenitic and tschermakitic substitutions play an increasingly important role in high grade amphiboles. The breakdown of these components in a pure Mg system is as follows:

$$Ca_2Mg_3Al_4Si_6O_{22}(OH)_2 + SiO_2 = 1.5\ Mg_2Si_2O_6 + 2\ CaAl_2Si_2O_8 + H_2O$$

tschermakite quartz enstatite anorthite

and

$$NaCa_2Mg_5AlSi_7O_{22}(OH)_2 + 3\ SiO_2 =$$

edenite quartz

$$2\ CaMgSi_2O_6 + 1.5\ Mg_2Si_2O_6 + NaAlSi_2O_8 + H_2O$$

diopside enstatite albite

a coupled breakdown of tschermakitic and edenitic components produces a plagioclase of intermediate composition. The bulk of plagioclase cores are typically around An_{55}. Reverse zonation, that is, increasing Ca towards the rims results in the plagioclase having a Ca/(Ca+Na) ratio equal to that of the coexisting hornblende, around An_{85}. The existance of isolated spots of albitic plagioclase in the cores of larger crystals suggests the preservation of a relict

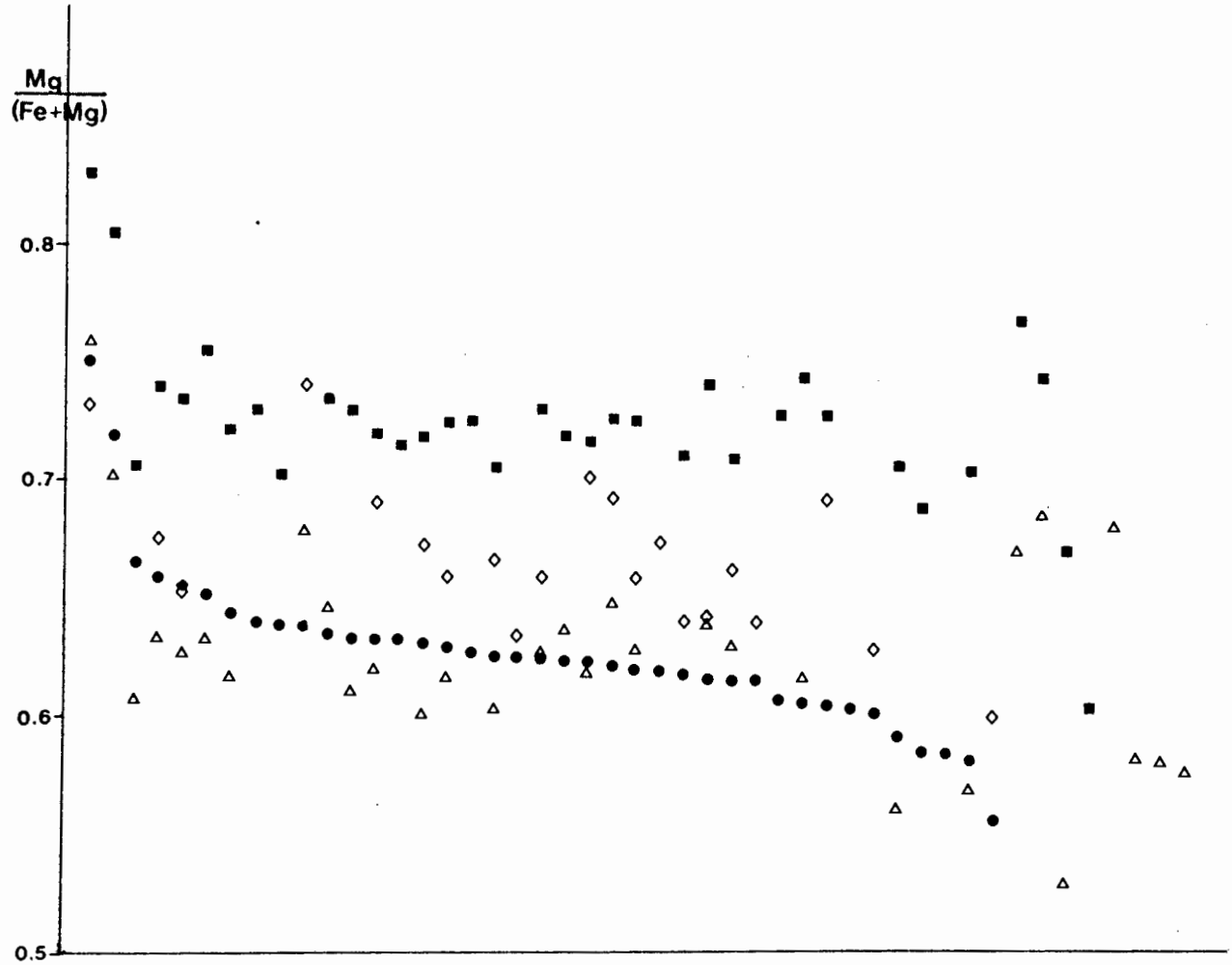

Fig. 5.12 X_{Mg} for coexisting phases in mafic gneisses from the Buffels River area. The general relationship is Cpx>Biot>Opx=Hbl.

■ clinopyroxene
◇ biotite
● orthopyroxene
△ hornblende

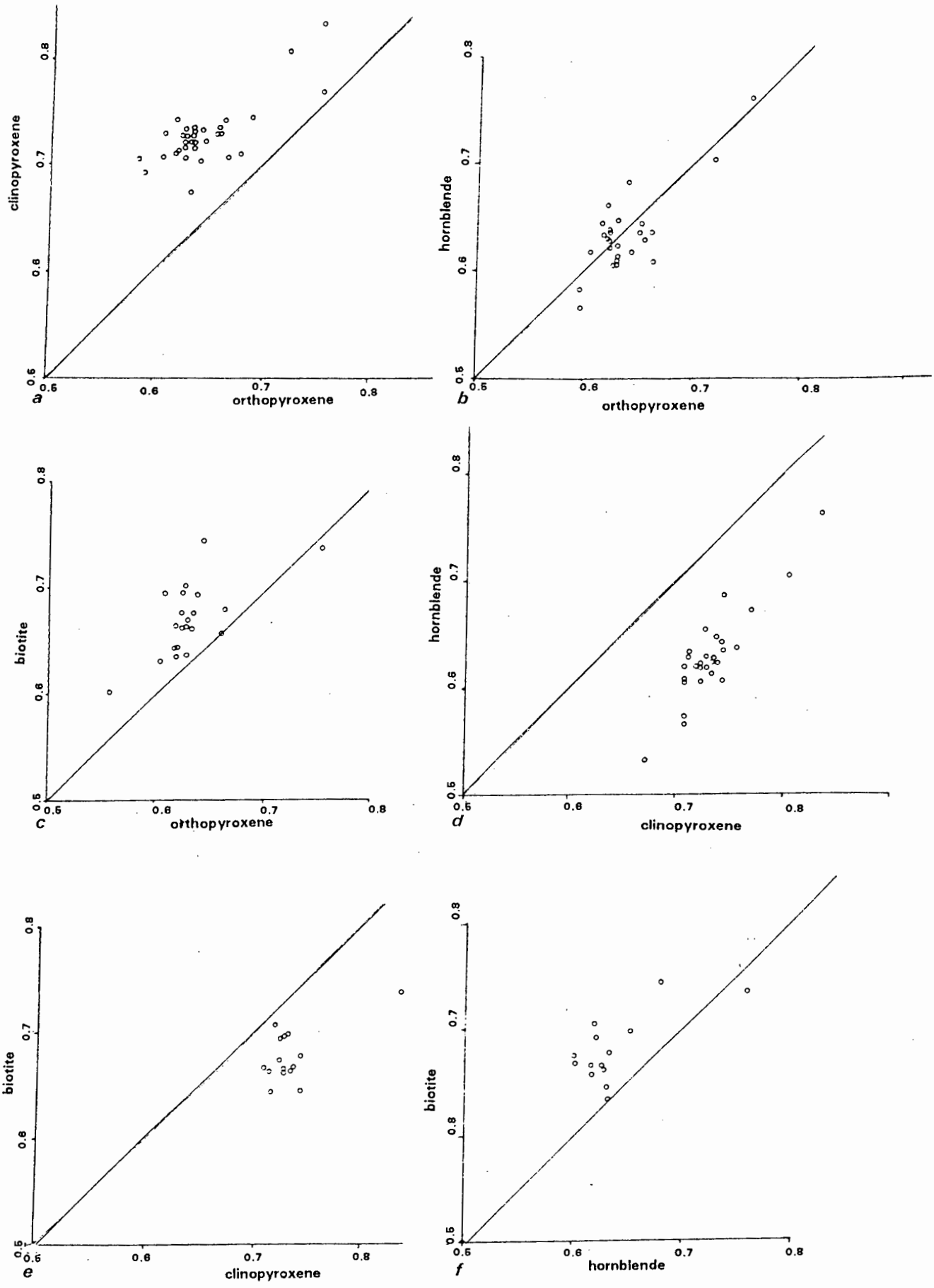

Fig. 5.13 X_{Mg} for coexisting phases
a. Clinopyroxene/Orthopyroxene
b. Hornblende/Orthopyroxene
c. Biotite/Orthopyroxene
d. Hornblende/Clinopyroxene
e. Biotite/Clinopyroxene
f. Biotite/Hornblende

composition no longer in equilibrium with a new growth of plagioclase produced by continuous hornblende breakdown.

Raase et al., (1986) attribute the presence of biotite in mafic gneisses to K saturation of coexisting hornblende. This may be the case as K-poor hornblende is not found coexisting with biotite in the Buffels River mafic gneisses. The association of biotite with orthopyroxene in the margins of mafic gneisses indicate that biotite is formed as a direct result of hornblende breakdown following a reaction of the type:

$$KCa_2Mg_5AlSi_7O_{22}(OH)_2 = KMg_3AlSi_3O_{10}(OH)_2$$

K-edenite phlogopite

$$+ Mg_2Si_2O_6 + 2\ SiO_2 + 2\ Ca^{2+} + O^{2-}$$

enstatite quartz

However, this reaction requires removal of Ca or a change in plagioclase composition to higher An contents, not compatible with the normal (increasing Na) zonation seen in some marginal domains.

Other possibilities include:

$$KCa_2Mg_5AlSi_7O_{22}(OH)_2 = KMg_3AlSi_3O_{10}(OH)_2 + 2\ CaMgSi_2O_6$$

K-edenite phlogopite diopside

The assemblage biotite-clinopyroxene is rarely seen, this reaction may form part of a coupled breakdown with edenite and tschermakite components.

It is possible that the biotite along margins of mafic gneisses is secondary in origin, caused by the short range infiltration of K-rich fluids from the surrounding granitic and pelitic migmatites, perhaps migrating partial melts, giving rise to the breakdown of orthopyroxene to produce biotite rinds via a reaction such as:

$$1.5\ Mg_2Si_2O_6 + KAlSi_3O_8 + H_2O = KMg_3AlSi_3O_{10}(OH)_2 + 3\ SiO_2$$

enstatite K-feldspar phlogopite quartz

5.4. WHOLE ROCK CHEMISTRY OF A BANDED MAFIC GNEISS

A single mafic lens was chosen for whole rock geochemical analysis by XRF spectrometry. The lens has a maximum width of 70 cm, consisting of an interior amphibolite domain with narrow margins of orthopyroxene -granulite (maximum width 8 cm). The surrounding rock is a biotite gneiss, containing small amounts of garnet. The mafic band can be traced for 15 m and is medium to fine grained and well foliated throughout.

The preparation of the close pairs for analysis involved careful cutting along the sinuous amphibolite-granulite boundaries often down to single grain width. However, without resort to a microscopic technique it is impossible to exclude all hornblende from marginal samples, in any case isolated patches and inclusions of hornblende are frequently record in granulite bands. The results are given in table 5.4.

TABLE 5.4

Whole Rock Geochemistry of banded mafic gneiss MCS358 - major elements

				Normalised		
	Top	Interior	Base	Top	Interior	Base
SiO_2	54.60	52.02	56.17	54.80	52.48	56.31
TiO_2	1.52	1.54	1.46	1.53	1.56	1.46
Al_2O_3	14.28	13.75	14.16	14.33	13.87	14.19
Fe_2O_3	13.80	13.82	13.01	13.85	13.94	13.05
MnO	0.30	0.24	0.26	0.30	0.24	0.26
MgO	6.02	6.39	5.67	6.04	6.45	5.68
CaO	7.30	9.48	7.27	7.32	9.56	7.29
Na_2O	1.20	0.87	1.22	1.21	0.88	1.22
K_2O	0.44	0.87	0.38	0.44	0.88	0.38
P_2O_5	0.17	0.16	0.16	0.17	0.16	0.16
H_2O-	0.14	0.36	0.08			
LOI	0.71	1.02	0.51			
Total	100.48	100.50	100.34	100.00	100.00	100.00

The major changes from interior amphibolite to marginal granulite are an increase in SiO_2 and Na_2O and a decrease in CaO, K_2O and L.O.I.. The changes in Na_2O and CaO are reflected in the plagioclase composition which changes within the space of a few cm from An_{82} in amphibolite domains to normal-zoned crystals with wide rims of composition An_{51} and small patchy cores of An_{71} in granulite margins, see fig 5.9. The increase in SiO_2 may not be so easy to characterise, it may be in part due to influx of SiO_2 from the adjacent leucogneiss, or may be a feature of sample preparation as the margin with adjacent biotite gneiss is a mm scale gradation from a quartz-bearing, orthopyroxene-rich rock to a thin rind of biotite bounded by quartz. It is thus open to interpretation as to whether the biotite rind is part of the mafic gneiss or the surrounding gneiss. Biotite compositions tend to favour the former. In this study the biotite-quartz rind is included as part of the marginal domain.

Fig 5.14 shows a graphical representation of mass balance relationships in sample MCS358.

K_2O is reduced by a factor of two, despite the presence of biotite in the marginal domains. Together with H_2O this represents the only clear major element loss from the mafic band. K released during hornblende breakdown may be strongly partitioned in to the fluid phase produced by devolatilisation reactions.

The transition from amphibolite to granulite in small mafic bands appears to be a relatively closed system, except for the most volatile components H_2O, K_2O, and to a limited extent the addition of SiO_2.

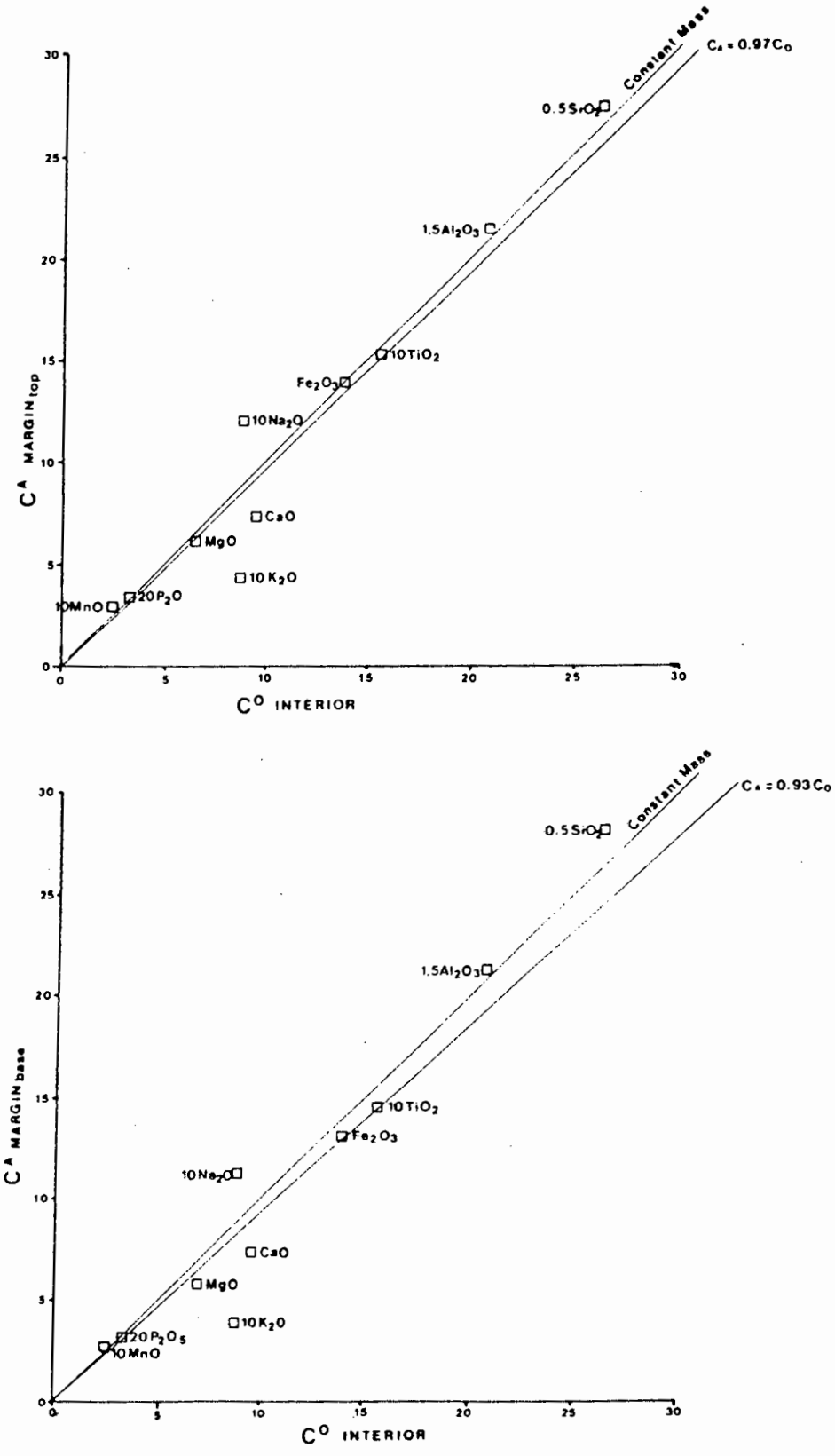

Fig. 5.14 Isocon diagram (Grant, 1986) to illustrate mass balance relations in the banded mafic gneiss $MCS358_M$. Scaled concentrations of major major element oxides in the margins of the mafic lens (C^A) are plotted against scaled concentrations of major element oxides from the interior (C^O). The slope of the isocon defines the mass change in dehydration of the marginal domains. Details for construction are given in Grant (1986).

5.5 HORNBLENDE BREAKDOWN

The breakdown of hornblende and first appearance of orthopyroxene has been the subject of many studies in high grade terranes. The Madras granulites show numerous thin mafic bands surrounded by migmatites and granitic gneisses, it is considered by Sen & Ray (1971a and 1971b) that a major control is exerted by a_{SiO2}. Externally derived silica, introduced by anatectic melts is necessary to drive hornblende breakdown to completion. A simultaneous control is applied by a_{H2O}, thin bands of hornblende-rich rocks are attributed to local gradients in a_{H2O}. Hornblende-free granulites are rare due to a paucity of available silica. The presence of K-feldspar, antiperthite and secondary biotite in mafic gneisses were cited to support a metasomatic control exerted by K-rich, high silica partial melts.

Banded mafic gneisses in the Agto area of West Greenland were the subject of a detailed whole-rock and mineral chemistry study by Glassley & Sorensen (1980). The banded nature of these dykes is the opposite to that observed in the Buffels River in this study. Two-pyroxene granulites occur at the centre of the mafic unit with amphibolites forming the margins. Glassley & Sorensen consider the role of a_{H2O} and a_{SiO2} in hornblende breakdown equilibria. Differences in a_{H2O} are thought to be inherited from earlier metamorphic history. The stoichiometry of breakdown equilibria are controlled by bulk rock composition. At Agto the breakdown of hornblende involves the extraction of edenitic and tschermakitic components in a 2:1 ratio.

Experimental work on amphibole phase relationships in amphibolite and granulite facies is summarised by Spear (1980, 1981a and 1981b). Spear indicates that at high a_{SiO2} there is a tendency for hornblendes to shift from pargasitic compositions towards tschermakite. Calculations of a_{H2O} from the breakdown of the tremolite component gave values ranging from 0.38 at 700°C for the first appearance of ortho- and clinopyroxene to 0.1 at 910°C for complete dehydration.

Phillips (1980) followed a similar approach in calculating water activity for mafic gneisses from Broken Hill, Australia. Local control of a_{H2O} due to external buffering by partial melting in

adjacent pelites was thought to be responsible for the uniform K_D obtained for tremolite breakdown equilibria.

The effects of hornblende breakdown on the compositional zoning exhibited by plagioclase in Adirondack granulites is discussed by Stoddard (1985). Two types of mafic gneiss occur, one is high in Ca and Al and comparatively lower in Fe and Ti, and is characterised by a trend towards reversely zoned plagioclase with rims approaching An_{80}. Very similar to the zonation pattern observed in many of the mafic gneisses from the Buffels River area. Raase et al. (1986) show similar relationships for coexisting plagioclase in mafic rocks of the Dharwar craton in India.

Robinson et al. (1982) describe a model mafic system. The factors which play the largest part in the breakdown of hornblende include: the Fe/Mg ratio of the ferromagnesian silicates, Na/Ca in coexisting plagioclase, together with the effects of a_{H2O} and a_{SiO2}. Robinson et al. indicate that there is no particular hornblende composition for any given pressure and temperature.

5.5.1 Amphibole breakdown equilibria

There have been several efforts to estimate water activity in granulite-facies terranes using amphibole breakdown equilibria (Phillips, 1980 and Spear, 1981). The following breakdown equation is used:

$$Ca_2Mg_5Si_8O_{22}(OH)_2 = 2\ CaMgSi_2O_6 + 3\ MgSiO_3 + SiO_2 + H_2O$$

tremolite diopside enstatite quartz

Although simple breakdown of tremolite is easy to model and adequate experimental thermodynamic data is available, the very low activity of the tremolite component in granulite-facies hornblendes tends to give an underestimation of a_{H2O}. All determinations following these methods yield extremely low values, implying a constant water activity throughout all hornblende-granulites or a lack of sensitivity in the method.

Use of equilibria relating to the breakdown of the edenitic or tschermakitic components are preferable but difficulties concerning the complexity of amphibole solid solution and a lack of experimental

data allow only qualitative modelling.

In modelling X_{H2O} values for mafic gneisses in the Buffels River area, it is necessary to use an amphibole breakdown expression that is independant of a_{SiO2}, as not all mafic gneisses have quartz in excess. Holland & Powell (1985) define an "end-member hornblende" component, the activity of which is given by the following expression:

$$X_{Amphibole,hornblende} = F.[X_{[],A}].[X_{Ca,M4}]^2.[X_{Mg,M13}]^3.[X_{Mg,M2}].[X_{Al,M2}].[X_{Al,T1}].[X_{Si,T1}]^3.[X_{Si,T2}]^4.[X_{OH,V}]^2$$

where F is a constant (F = 37.93), so that the above expression equals unity for pure end-member compositions.

Activity calculations (see table 5.6) indicate that this component has the highest activity values of all amphibole end-members for amphiboles in the Buffels River area.

The breakdown of hornblende (hb) is given by the expression:

$$2\ \text{hornblende} = 2\ \text{diopside} + 3\ \text{enstatite} + 2\ \text{anorthite} + 2\ H_2O$$

The K_D for the reaction above can be expressed as:

$$\frac{(XCpx,Diop)^2 \cdot X(Opx,En)^3 \cdot X(Plag,An)^2 \cdot X(H2O)^2}{X(Amph,Hb)^2}$$

The stability of the above reaction in the pure Mg-system was calculated using the internally consistent data-base of Powell & Holland (1988), the P-T-X relationships are given in fig. 5.15.

Fig. 5.16 relates ln K_D for the breakdown of hornblende (hb) to X_{H2O} at temperatures, 600, 700, 750 and 800°C at 5 kb.

Table 5.5 gives the values for the activities of the amphibole components, tremolite, hornblende and edenite, and the activites of diopside in clinopyroxene, and enstatite in orthopyroxene, and the core composition of coexisting plagioclase. Sample DWN545 is from the high temperature granulite zone of central Namaqualand (Baars, 1986).

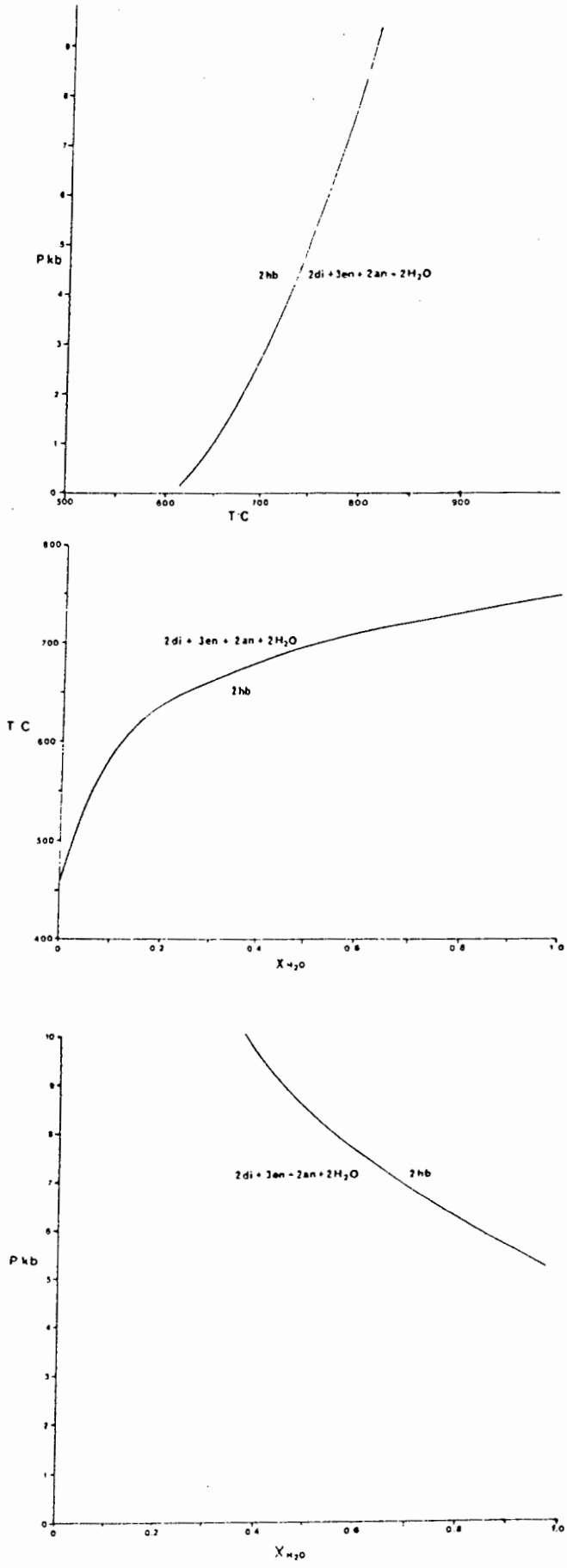

Fig. 5.15 P-T-X_{H2O} relations of the hornblende breakdown reaction: 2hb = 2 di + 3 en + 2 an + 2 H_2O derived from the thermodynamic data-base of Powell & Holland (1988)

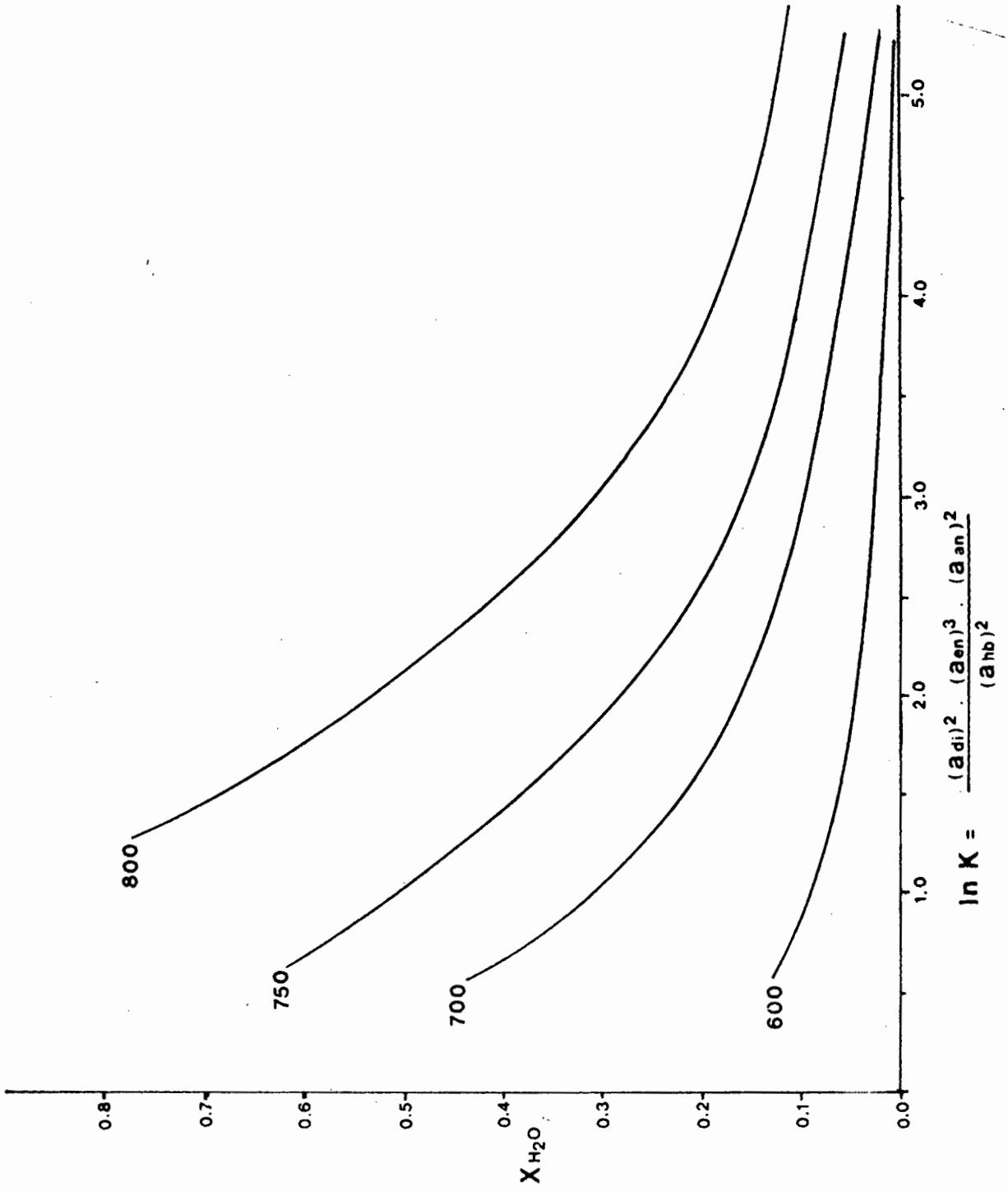

Fig. 5.16 Graphical estimation of X_{H_2O} in hornblende-granulite at 5 kb, for temperatures 600, 700, 750 and 800°C.

Samples HA1025, HA1050, HA306 are hornblende granulites, and HA1110, HA1091, HA1129, are diopside-bearing amphibolites, from areas to the east of this study, taken from Albat (1984).

TABLE 5.5

Activities of end-member components for mafic gneisses

Sample	X_{Tr}	X_{Hb}	X_{Ed}	X_{Di}	X_{En}	X_{An}	X_{Ab}
DWN129	0.00179	0.0188	0.0145	0.632	0.391	0.596	0.404
DWN129A	0.00225	0.0231	0.0143	0.656	0.412	0.744	0.256
DWN332B	0.00186	0.0221	0.0104	0.609	0.370	0.834	0.166
DWN3473	0.00227	0.0244	0.0111	0.614	0.426	0.604	0.396
DWN348	0.00259	0.0268	0.00985	0.611	0.417	0.665	0.335
DWN349	0.00270	0.0251	0.0111	0.609	0.401	0.670	0.330
DWN353	0.00225	0.0224	0.00913	0.607	0.378	0.665	0.335
DWN380	0.00311	0.0320	0.0102	0.568	0.355	0.864	0.136
DWN381	0.00447	0.0315	0.0139	0.611	0.375	0.852	0.148
HY8	0.00209	0.0175	0.0102	0.619	0.384	0.528	0.472
MCSH04	0.00495	0.0499	0.0197	0.700	0.523	0.712	0.288
MCSH05	0.00826	0.0754	0.00629	0.729	0.548	0.584	0.416
MCSS04	0.000867	0.0137	0.00457	0.617	0.323	0.480	0.520
MCSS05	0.000843	0.0101	0.00594	0.607	0.338	0.487	0.513
MCS301	0.00217	0.0222	0.0245	0.629	0.378	0.681	0.319
MCS301A	0.00226	0.0214	0.0126	0.637	0.393	0.709	0.291
MCS302C	0.00212	0.0286	0.00681	0.570	0.365	0.495	0.505
MCS303	0.00201	0.0185	0.0115	0.651	0.378	0.563	0.437
MCS304	0.00183	0.0165	0.0135	0.606	0.383	0.845	0.155
MCS305M	0.00144	0.0142	0.00989	0.619	0.374	0.748	0.252
DWN545	0.00174	0.0141	0.00859	0.575	0.329	0.511	0.489
HA1025	0.00259	0.0272	0.0145	0.655	0.427	0.679	0.321
HA1050	0.000325	0.00391	0.00423	0.506	0.221	0.526	0.474
HA306	0.000435	0.00693	0.00389	0.546	0.260	0.584	0.416
HA1110	0.000559	0.00943	0.00237	0.579	-----	0.863	0.137
HA1091	0.00166	0.0207	0.00755	0.645	-----	0.732	0.268
HA1129	0.00179	0.0232	0.00759	0.623	-----	0.742	0.258

5.5.2 Estimation of equilibrium plagioclase composition

One of the notable petrological characteristics of the mafic gneisses in the Buffels River area is the strongly zoned nature of plagioclase. As the activity of anorthite is an important factor in the equation used to estimate water activity it is important to test whether the plagioclase compositions as analysed from cores and rims represent equilibrium compositions or not.

The interdependence of amphibole and plagioclase composition is best illustrated by using an equilibrium relationship which is independant of SiO_2 and H_2O:

3 Tremolite + Edenite + 4 Anorthite = 4 Hornblende + 4 Diopside + Albite

The equilibrium constant for the above equation is:

$$K = \frac{(XAmph,Tr)^3 \cdot (XAmph,Ed) \cdot (XPlag,An)^4}{(XAmph,Hb)^4 \cdot (XCpx,Di)^4 \cdot (XAb)}$$

$$\text{or} \quad \ln K = \ln \{(XAmph,Tr)^3 \cdot (XAmph,Ed) \cdot (XPlag,An)^4\} - \ln \{(XAmph,Hb)^4 \cdot (XCpx,Di)^4 \cdot (XAb)\}$$

Fig 5.17 shows a plot of the these two ln terms against each other. The Buffels River samples can be considered to be isofacial. One would expect that equilibrium between amphibole and plagioclase would result in a straight line of slope = 1, and an intercept at x=0 of ln K. It can be seen that there is no strong correlation.

Data from mafic gneisses sampled by Albat (1984) were added for comparison. These samples are taken from the northern granulite-facies amphibolite-facies transitional zone to the east of the Buffels River and are considered to be isofacial with the mafic gneisses in this study. In fig. 5.17 it can be seen that these samples, that show no sign of plagioclase zonation, give a good 1:1 positive correlation. A best-fit line for these samples ($r^2 = 0.91$) defines the equilibrium ln K of 6.53 ± 0.19. A number of samples from the Buffels River with unzoned plagioclase plot close to this line, and samples with zoned plagioclase have core to rim values which cut-

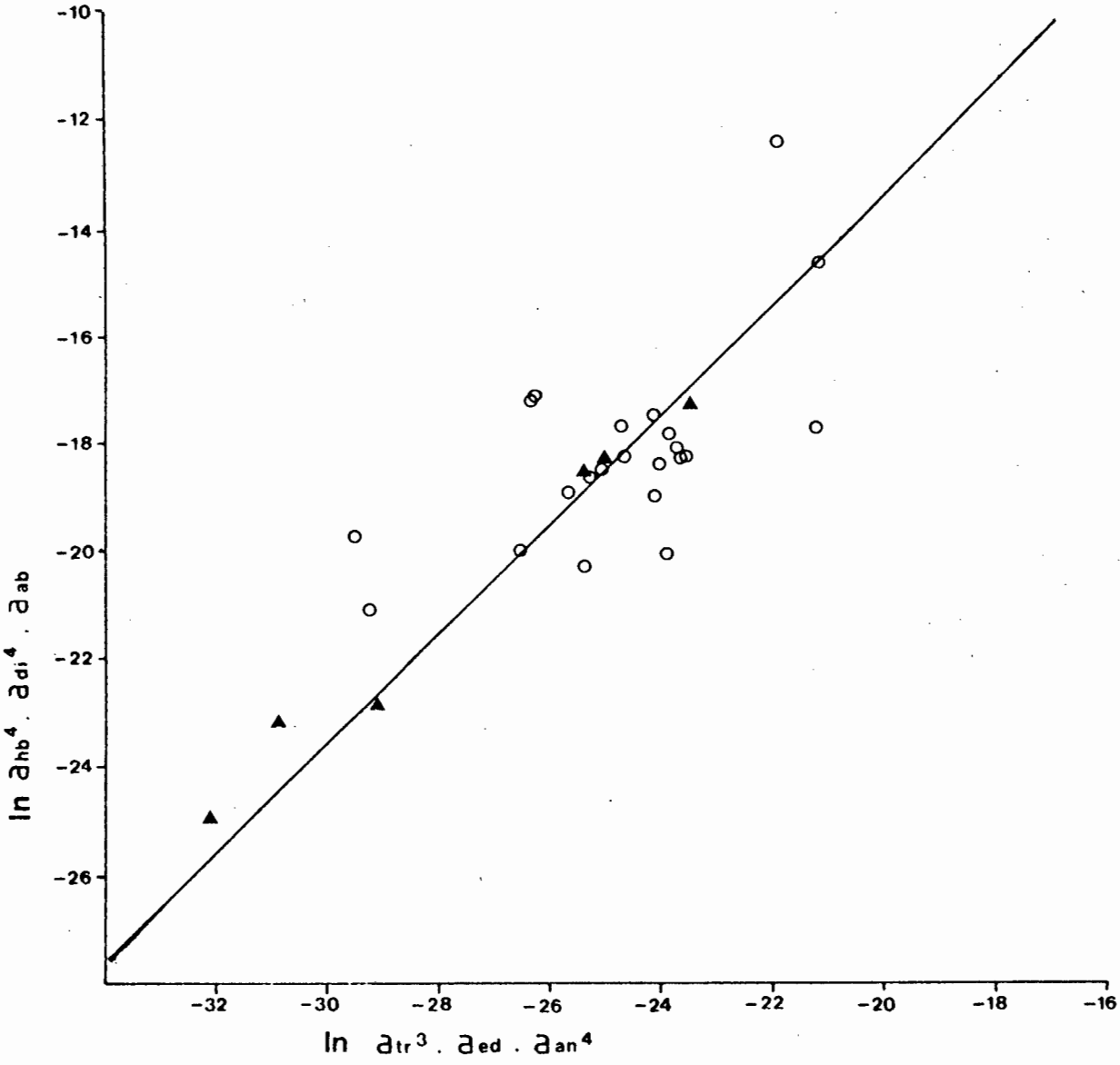

Fig. 5.17 Graphical representation of the equilibrium:
3 tr + ed + 4 an = 4 hb + 4 di + ab

Best fit line (r^2 = 0.91) defines equilibrium ln K = 6.53 ± 0.19. Departures from best-fit line indicate disequilibrium between amphibole and plagioclase.
○ Buffels River
▲ Central Namaqualand (Albat, 1984)

across this line. Table 5.6 shows a comparison between observed and model plagioclase composition. In zoned samples a median core composition is given. Fig. 5.18 shows the variation of observed and model plagioclase compositions.

TABLE 5.6

Comparison of observed and model X_{An} for plagioclase in mafic gneisses

Sample	$X_{An,obs}$	$X_{An,model}$	Sample	$X_{An,obs}$	$X_{An,model}$
DWN129	0.596	0.608	MCSH04	0.712	0.714
DWN129[A]	0.744	0.641	MCSH05	0.584	0.857
DWN332[B]	0.834	0.795	MCSS04	0.480	0.820
DWN347[3]	0.604	0.662	MCSS05	0.487	0.664
DWN348	0.665	0.657	MCS301	0.681	0.624
DWN349	0.670	0.613	MCS301[A]	0.709	0.610
DWN353	0.665	0.609	MCS302[C]	0.495	0.774
DWN380	0.864	0.652	MCS303	0.563	0.601
DWN381	0.852	0.526	MCS304	0.845	0.535
HY8	0.528	0.556	MCS305[M]	0.748	0.595

5.5.3 Water activity

Water activities for two-pyroxene-bearing hornblende granulites have been calculated from the breakdown of end-member hornblende (Powell & Holland, 1988) using the model plagioclase compositions above and the activity relationships listed in table 5.5. Values for X_{H2O} are given in table 5.7.

The values for X_{H2O} are fairly constant, although small amounts of variation occur even within samples that have close spatial relationships, e.g. samples MCS301, 302, 303, 304 and 305. Most estimates are between 0.1 and 0.2, with two samples DWN380 and 381 giving X_{H2O} of 0.31 and 0.33. These samples together with MCSH05 are thought to contain a high temperature retrograde amphibole. This is supported by textural evidence. From table 5.6 and fig. 5.18 it can be seen that there is a large discrepancy between observed and model plagioclase composition indicating disequilibrium. Sample DWN545 from the high temperature granulite zone, south of the study area, gives a higher value of X_{H2O} = 0.35. This would be expected as higher water

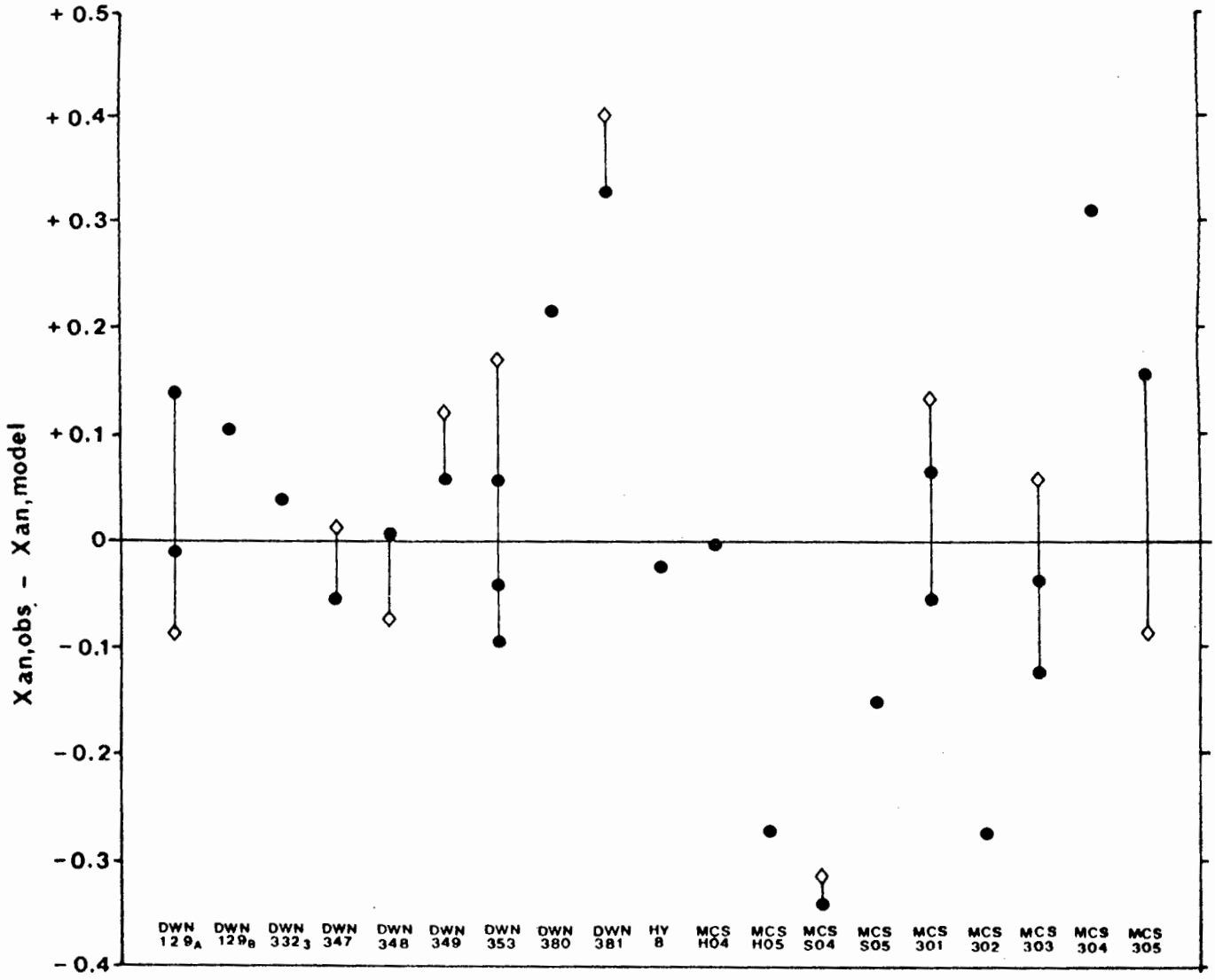

Fig. 5.18 Variation of observed and calculated model plagioclase compositions, see table 5.7.

activities are required to stabilise hornblende at temperatures of 800°C. However, this amphibole contains 1.07 weight % fluorine. Fluorine contents were not taken into account in the calibration of the hornblende breakdown equilibria, as the amphiboles in the Buffels River samples are essentially fluorine-free. It is thought that reduced activity of the hydrous end-member hornblende due to the presence of fluoro-hornblende would reduce the X_{H2O} estimate to around 0.2. This would be consistent with estimates of water activity for the Buffels River area.

It can be seen from table 5.7 that the presence or absence of quartz does not greatly affect X_{H2O} estimates. Although it is worth noting that the samples giving the lowest values for X_{H2O} are from quartz-free mafic gneisses, where X_{SiO2} <1.

TABLE 5.7

X_{H2O} estimates from the equation 2 hb = 2 di + 3 en + 2 an + 2 H_2O
Mafic gneisses from the Buffels River calculated at 750°C and 5 kb

Sample	ln K	X_{H2O}	Qtz	Sample	ln K	X_{H2O}	Qtz
DWN129	3.218	0.13	-	MCSH04	2.664	0.18	-
DWN129A	3.143	0.14	-	MCSH05	2.425	0.21	-
DWN332B	3.191	0.14	+	MCSS04	3.828	0.11	-
DWN3473	3.066	0.14	-	MCSS05	4.119	0.09	-
DWN348	2.789	0.17	+	MCS301	2.826	0.17	-
DWN349	2.658	0.18	+	MCS301A	2.996	0.15	+
DWN353	2.688	0.18	-	MCS302C	2.449	0.20	+
DWN380	1.790	0.31	+	MCS303	3.185	0.14	+
DWN381	1.703	0.33	+	MCS304	3.077	0.14	+
HY8	3.086	0.14	+	MCS305M	3.561	0.12	+

Mafic gneisses from other areas in Namaqualand

Sample	ln K	X_{H2O}	Qtz	
DWN545	2.739	0.35	+	at 800°C, 5 kb
HA1025	3.000	0.15	-	at 750°C, 5 kb
HA1050	3.893	0.10	-	at 750°C, 5 kb
HA306	4.027	0.09	+	at 800°C, 5 kb

5.6 MELTING IN MAFIC GNEISSES

The abundance of coarse grained segregations in mafic gneisses is consistent with local partial melting. Melting in a H_2O-saturated system would generate a liquid of approximately tonalitic composition. At any given temperature it would require higher a_{H2O} to initiate melting in a mafic assemblage than to produce the first granitic melts in a typical pelitic assemblage seen in the Buffels River area (Qtz-Kfsp-Plag-Biot-Sill).

The production of water-saturated melts in surrounding granitic, semi-pelitic and pelitic gneisses would have the affect of reducing a_{H2O} in the host rocks to the mafic bands. Melting would then only proceed via vapour-absent reactions. In mafic bodies the vapour-absent reaction would take the form:

Hornblende + Quartz = Orthopyroxene + Clinopyroxene + Plagioclase + Liquid

Equilibria in a simple mafic system (CMAS) are shown in fig. 5.19. Initial melting in quartz-bearing hornblende-granulites occurs at curve (Cpx) or at curve (Opx) for a quartz-bearing amphibolite in the presence of a small amount of a high a_{H2O} vapour. At low a_{H2O} melting will commence at the invariant point after the buffered progress of hornblende breakdown has driven a_{H2O} to higher values along the curve (L). Continued melting of hornblende-bearing assemblages under vapour-absent conditions should produce clinopyroxene and orthopyroxene as solid products. Observed segregations are characterised by the presence of one or both pyroxenes as coarse equant crystals.

5.6.1 Mass balance of melting reaction

The simplest model for vapour-absent melting is given here. Fe and Mg are treated together, and the reaction above is regarded as discontinuous. The phase compositions are taken from the sample DWN353 and are listed in table 5.8. It is assumed that the first melt will have an approximately tonalitic composition (Johannes, 1985).

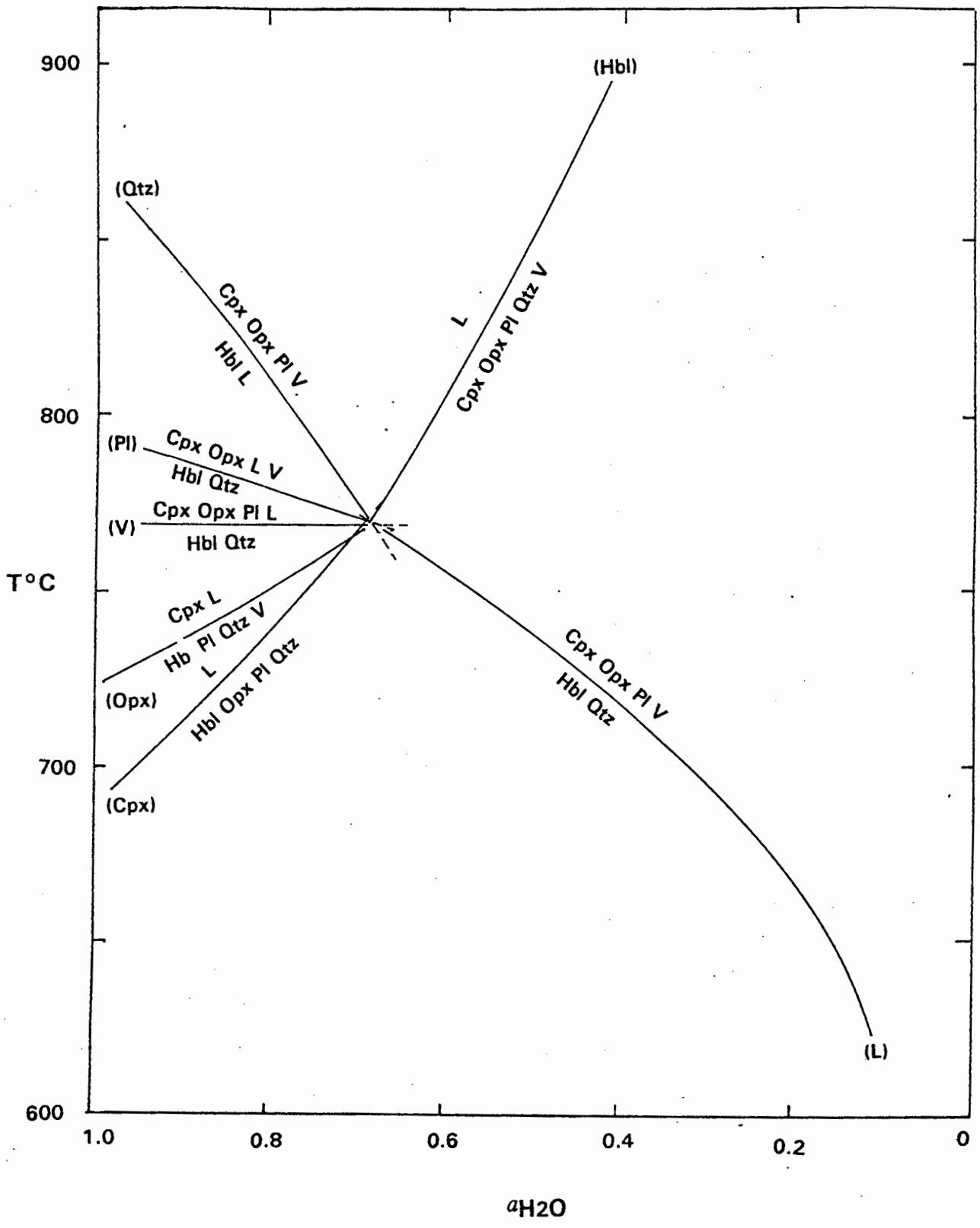

Fig. 5.19 T-X_{H2O} relations for dehydration and melting equilibria in a simple mafic system (CMAS). Calculated using the Holland & Powell data thermodynamic data-set (Holland & Powell, 1988).

TABLE 5.8

Composition and volumes of phases used for mass balance of vapour-absent melting reaction, expressed as cations per formula unit.

	Hbl	Qtz	Opx	Cpx	Plag (An)	Liq*	
Si	6.5	1.0	2.0	1.9	2.0	3.59	
Al	1.9			0.1	2.0	1.12	
Fe + Mg	4.6		2.0	1.0		0.46	
Ca	1.9			1.0	1.0	0.34	
Na	0.36					0.40	
K	0.25					0.15	
H	2.0					variable	
Molar volume (cm^3)	273	23	64	66	100	150	
	Mass balance factors						**R**
	1.0	2.79	1.50	1.20	0.39	0.90	
Si	6.5	2.79	3.00	2.28	0.78	3.23	----
Al	1.9			0.12	0.78	1.00	----
Fe + Mg	4.6		3.00	1.20		0.41	- 0.01
Ca	1.9			1.20	0.39	0.31	----
Na	0.36					0.36	----
K	0.25					0.14	0.11
H	2.00					?	?
	Volume balance						
	21.25	5.00	7.50	6.25	3.03	10.5	

* Liquid composition

	Weight %
SiO_2	61.0
Al_2O_3	17.0
FeO + MgO	8.0
CaO	5.4
Na_2O	3.6
K_2O	2.0

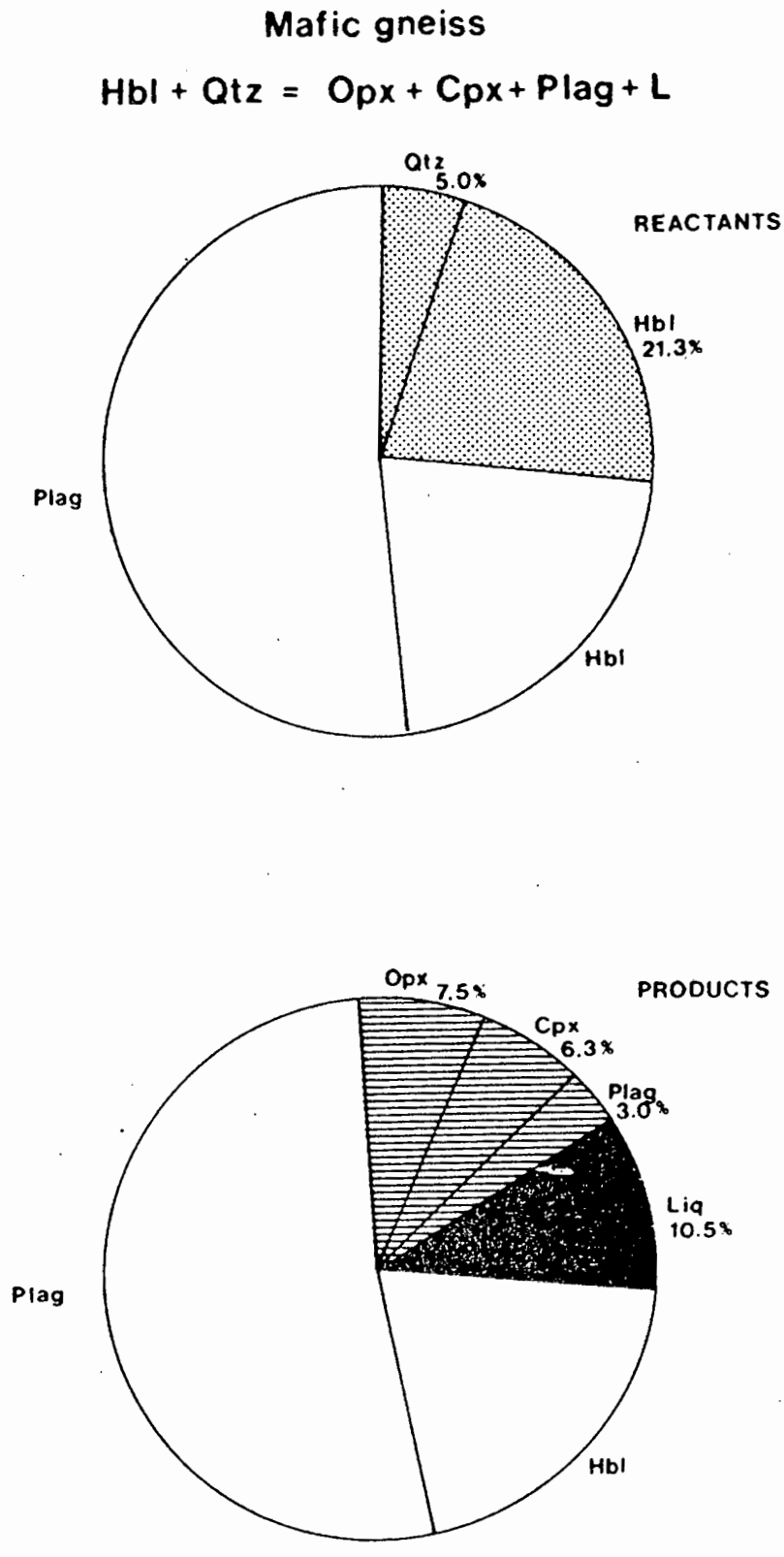

Fig. 5.20 Pie charts illustrating the mass balance relations for vapour-absent melting reaction:
Hornblende + Quartz = Orthopyroxene + Clinopyroxene + Plagioclase + Liquid
using phase compositions in table 5.9.

Fig. 5.20 shows the mass balance for a model mafic gneiss containing 52.25% Plag, 42.75% Hbl, 5.00% Qtz, using the compositions above. It can be seen from fig. 5.20 that a large proportion of the rock is not directly involved in the melting reaction, thus the liquid and solid products of the melting reaction coexist with excess plagioclase and hornblende. The amount of melt produced is controlled by the temperature and the initial quartz content. It is likely that the excess K is partitioned strongly into the vapour released on crystallisation of the melt.

5.7 DISCUSSION

Almost all mafic bands in the Buffels River area consist of hornblende-bearing two pyroxene granulites. Such assemblages are able to buffer a_{H2O} via the reaction Hbl + Qtz = Opx + Cpx + Plag + H_2O. All mafic gneiss bands have, without exception, a dehydrated outer margin of pyroxene granulite. Thicker mafic bands contain coarse-grained, structureless segregations devoid of hydrous minerals.

Fig. 5.19 shows a simple T-a_{H2O} model for dehydration and melting reactions at 5 kbar. With increasing temperature a_{H2O} is buffered along the curve Hbl + Qtz = Opx + Cpx + Plag + V to the isobaric invariant point. In an externally buffered system the infiltration of a low a_{H2O} fluid will produce an unbuffered anhydrous assemblage when the buffering capacity of the hornblende-bearing assemblage is exhausted. The rocks surrounding mafic gneiss bands are migmatitic pelitic and biotite gneisses. Partial melting in the migmatitic host rocks has the tendency to drive H_2O into the leucosomes and lower a_{H2O} in the resulting mesosome. Thus, mafic gneisses are bounded by rocks which buffer a_{H2O} at lower values than hornblende-bearing assemblages. The scale of the dehydrated margins are consistent with mass transfer of H_2O out of the mafic gneiss in response to an externally imposed gradient in a_{H2O}, see fig. 5.21.

Fig. 5.22 illustrates the relationship between a_{H2O} and a_{SiO2} for simple dehydration and melting reactions in the CMAS system. A local increase in a_{SiO2} at a fixed value of a_{H2O} favours hornblende breakdown. Quartz-absent mafic bands should contain hornblende, as the a_{H2O} gradient could continue smoothly across such bands. Quartz

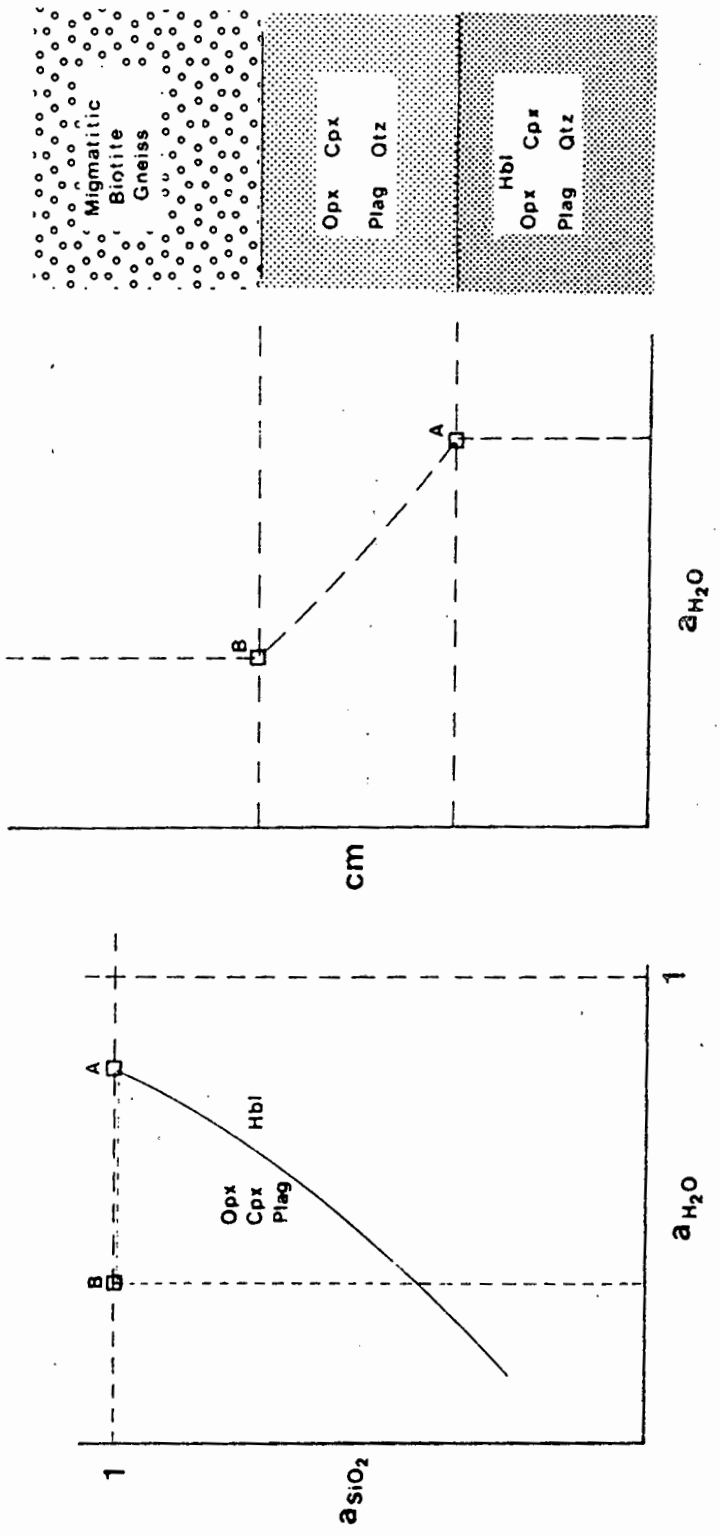

Fig. 5.21a Simple dehydration equilibria for mafic gneiss as a function of a_{SiO2} and a_{H2O}. The buffer assemblage Hbl-Opx-Cpx-Plag-Qtz defines a_{H2O} at point A. At point B a_{H2O} is defined at a (new) lower value in migmatitic biotite gneiss hosting the mafic band.

Fig. 5.21b The a_{H2O} gradient between points A and B results in the development of a dehydrated margin consisting of Opx-Cpx-Plag-Qtz. The scale in the diagram is consistent with field observations.

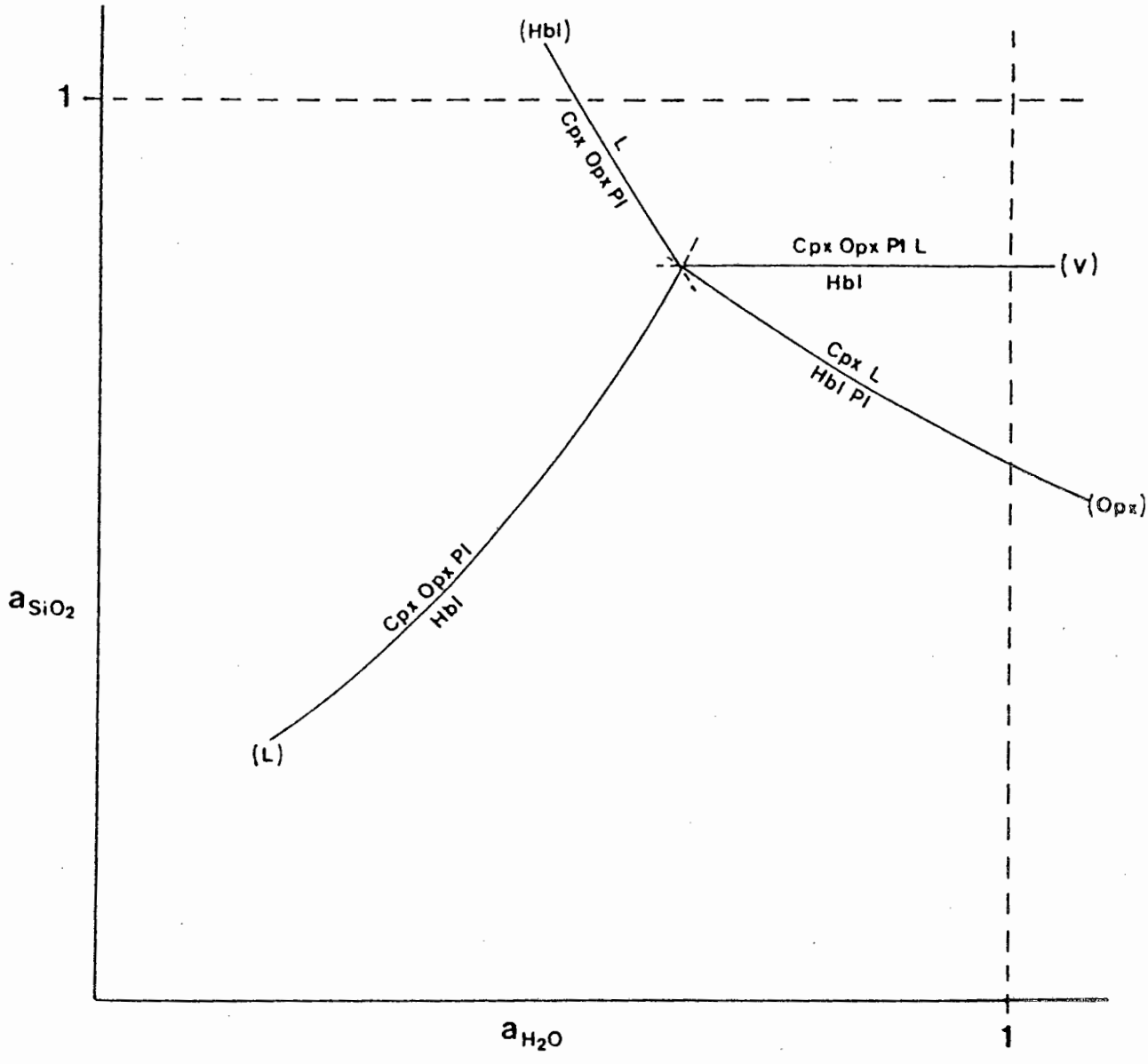

Fig. 5.22 a_{SiO2} - a_{H2O} relations in the simple mafic system CMAS. Calculated using the thermodynamic data set of Holland & Powell (1988).

veins will cause an increase in a_{SiO2} and could cause a thin halo of hornblende-absent granulite. Shearing and reduction in grain-size may aid the expulsion of volatiles from the rock aiding the external buffering process.

Slight changes in Fe:Mg will have an effect on the development of mafic banding. As a band of Fe-rich mafic rock in a more Mg-rich host would be expected to lose its hornblende. Fe-rich hornblende would breakdown at higher a_{H2O} and lower a_{SiO2} than Mg-rich hornblende. It is also likely that the protoliths of Mg-rich mafic gneisses would be undersaturated with respect to quartz and thus preserve hornblende even at very low a_{H2O}. In a similar fashion the Na:Ca ratio will effect the dehydration of hornblende. Increasing Na in hornblende would favour hornblende stability.

The stoichiometric breakdown of hornblende upsets the buffered equilibrium controlling plagioclase composition. The plagioclase generated by hornblende breakdown will have Ca:Na ratios similar to that of the reactant hornblende. Plagioclase being relatively refractory is unable to reequilibrate to the newly imposed equilibrium composition. Therefore plagioclase develops strong reverse zonation from An_{55} in the cores to An_{85} on the rims. The complete stoichiometric breakdown of hornblende will occur when a_{H2O} is lowered by external buffering. Thus, outer margins will contain unzoned plagioclase with high An contents, and towards the hornblende-bearing domains strongly reverse-zoned plagioclase will occur. The centre of mafic bands will have plagioclase of intermediate composition coexisting with hornblende.

Model plagioclase compositions indicate that in some rocks the observed plagioclase compositions are not in equilibrium with the coexisting hornblende and pyroxene. If all reactions are externally controlled then all crystals will be in equilibrium with one another at each stage of development. If growth is limited by diffusion then small domains within the rock will be in equilibrium. Disequilibrium is promoted by rapid changes in physical conditions. It is unlikely that the disequilibrium plagioclase compositions are a result of sudden fluctuations in regional pressure and temperature. It is more likely that rapid changes in X_{H2O} are responsible. Possible mechanisms include the channeling of low a_{H2O} fluids along the margins of mafic gneiss units, or the sudden lowering of local X_{H2O} values by in-situ partial melting of the mafic gneiss or adjacent

lithologies. Either process might be capable of inducing overstepping in a continuous dehydration reaction. Disequilibrium conditions may be followed by long periods of thermal stability with resultant annealing producing textural equilibrium, but the interiors of plagioclase would retain their disequilibrium characteristics.

Segregations have been attributed to vapour-absent partial melting as their textures are very similar to segregations in pelitic rocks described by Tracy & Robinson (1983) from central Massachusetts, and mafic gneisses from Antartica (Tait & Harley, 1988), which are thought to be formed by the same process, see Waters (1988). These segregations probably represent the solid and liquid products of vapour-absent melting. Segregations always have a halo of dehydrated poikiloblastic pyroxene and plagioclase around them. It is suggested that the formation of anhydrous melt segregations sets up a gradient in a_{H2O} and thus, is able to dehydrate its own hornblende-rich matrix. The amount of partial melting is limited by low quartz contents, less than 10% melt is typical, such small amounts of partial melt are unlikely to leave the host rock (McKenzie, 1985).

The textures and mineral compositions are consistent with local control of a_{H2O}. Fluid activity is largely internally buffered with limited external buffering causing cm-scale dehydration. Large scale flux of a low a_{H2O} fluid would favour wholescale conversion of hornblende-bearing assemblages to granulites depending on local permeability constraints. The regular width of the dehydrated margins is likely to result from a long sustained a_{H2O} gradient imposed by adjacent lithologies.

5.8 SUMMARY

Mafic gneisses have a regular banded structure consisting of hornblende-rich interiors and margins of hornblende-absent pyroxene granulite. Thicker mafic bands develop coarse grained anhydrous segregations that truncate earlier fabrics.

Hornblende is green-brown, with high Ti and relatively enriched in edenitic alkalis. All minerals have remarkably constant compositions except plagioclase, which shows strong reverse zonation (increasing Ca towards the rim). Plagioclase varies in composition from An_{45} to An_{90}. Pyroxene-granulite margins and especially the transitional domain with hornblende-bearing granulite is characterised by highly calcic plagioclase. Plagioclase coexisting with hornblende, orthopyroxene and clinopyroxene is generally intermediate in composition. Model plagioclase compositions expected to be in equilibrium with hornblende of observed composition indicate that the observed plagioclase composition may be a disequilibrium one. Fe-Ti oxide assemblages consist of pure end-member magnetite, and composite grains of the hematite-ilmenite solid solution series. This assemblage is common to all mafic gneisses and is thought to be the result of oxidation on slow cooling.

X_{H2O} estimates from the breakdown of end-member hornblende give values between 0.09 - 0.20 for most assemblages with prograde hornblende. Those rocks with coarse patchy hornblende, possibly of retrograde origin define higher value of 0.31 - 0.33.

Mass balance relationships for hornblende dehydration indicate a loss of K_2O in addition to the expected loss of H_2O from the margins of mafic bands. Segregations are best modelled as the liquid and solid products of vapour-absent melting reactions. There is no evidence of rehydration of the segregation assemblages, loss of H_2O is accompanied by loss of K_2O. Otherwise, in-situ partial melting is a closed system process which produces small amounts of liquid (>10%), without melt extraction.

The imposition of local gradients in a_{H2O} and a_{SiO2} account for the observed marginal banding. Surrounding migmatitic biotite gneisses define a_{H2O} at lower levels than in hornblende-bearing mafic gneiss, with SiO_2 in excess. Mass transfer of H_2O out of mafic bands

produces a thin rim of pyroxene-granulite. Partial melting within mafic rocks draws H_2O into segregations and sets up and maintains a gradient in a_{H2O} which results in the formation of a halo of anhydrous minerals between the melt segregation and its hornblende-rich matrix.

The preferred model to explain the petrographic and chemical features present in the mafic gneisses of the Buffels River area involves strong local control of fluid composition by internal and external buffering of a_{H2O}. Partial melting within mafic gneisses and in surrounding lithologies provides a suitable mechanism.

CHAPTER 6

THE PETROLOGY OF PELITIC GNEISSES

6.1 INTRODUCTION

A wide variety of pelitic bulk compositions have been sampled and emphasis has been placed on the coexisting Fe-Mg silicate phases, particularly the nature of chemical zonation in porphyroblasts. A kinetic approach to cation-exchange in garnet and biotite can provide useful constraints on cooling rates and the temperature estimates from conventional geothermometry, discussed in Chapter 4. Migmatites form an important part of the supracrustal sequence. Their field relationships are outlined and the role of partial melting in pelitic gneisses is discussed.

6.2 FIELD RELATIONSHIPS

Pelitic and semi-pelitic gneisses form a large part of the supracrustal sequence in the Buffels River area. Pelitic gneisses can be divided into three main groups: 1. garnet-biotite gneiss, which is the most common, grading with increasing cordierite content into 2. cordierite gneiss, which may contain orthopyroxene and grades into magnesian gneiss, and 3. sillimanite gneiss, quartz-rich rocks containing some garnet or cordierite, but very little biotite. Most pelitic gneisses are coarse grained with conspicuous porphyroblasts of garnet and cordierite. Strong gneissose banding of quartz-feldspar-rich layers and Fe-Mg-rich layers occurs. Migmatitic banding occurs on cm and macroscale. Leucosome material varies between thin quartz-feldspar-garnet veinlets to massive coarse grained discordant sheets containing large porphyroblasts of garnet and cordierite mantled by K-feldspar and quartz.

High grade pelitic mineral assemblages define the S_2 foliation. A strong mineral lineation developed in garnet porphyroblasts and in coarse sillimanite laths is interpreted as L_2. However, coarse grained structureless segregations cross-cut early fabrics and suggest a high temperature metamorphic event accompanying and

continuing after F_3 deformation.

6.2.1 Pelitic migmatites

Most pelitic rocks in the Buffels River area have undergone some form of partial melting. Their field relationships are briefly described here.

The term leucosome describes a body of pale-coloured, quartzo-feldspathic rock (Mehnert, 1968 and Ashworth, 1985). Sheets of leucosome containing large porphyroblasts of garnet or cordierite form a striking and volumetrically significant part of the supracrustal package at Hytkoras. The degree of separation of leucosome from the palaeosome (parent rock) is in some cases complete. Large dykes of coarse leucosome cross-cut other rock types and represent either remobilised quartzo-feldspathic gneisses or leucosome derived from a pelitic or semi-pelitic protolith. Since the mineralogy of many gneisses in the Buffels River area is close to that of a granite minimum melt correlating leucosomes with parent rocks is impossible.

Pelitic gneisses have a well defined layered structure with concordant layers of k-feldspar, quartz and plagioclase alternating with layers rich in biotite, sillimanite and garnet or cordierite. The layering is folded by F2 folds and refolded by F3 (see plate 6.1). The resultant fabric is truncated by coarse grained veins containing large garnets with haloes of quartz and feldspar. This may represent two distinct periods of melt generation, a syn-F2, water-saturated melting generating well-banded, biotite-bearing migmatites and a post-F3 vapour -absent melting producing anhydrous discordant veins.

The southern contact between pelitic gneisses of the supracrustal sequence with the augen orthogneiss is occupied by a diatexite (Ashworth, 1985, p3.). Extensive partial melting has produced a leucosome with large numbers of garnet porphyroblasts and rafts of darker biotite-cordierite-garnet bearing melanosome (plate 6.1). Small intrusive bodies of gneissic granite, as observed in the Draaihoek area of Hytkoras, may represent the products of diatexis in the rocks directly underlying the supracrustal sequence.

Plate 6.1 F_2 and F_3 folds in migmatitic garnet-cordierite-biotite gneiss. Note coarse grained garnets grow across the folded compositional banding. River bed, Hytkoras.

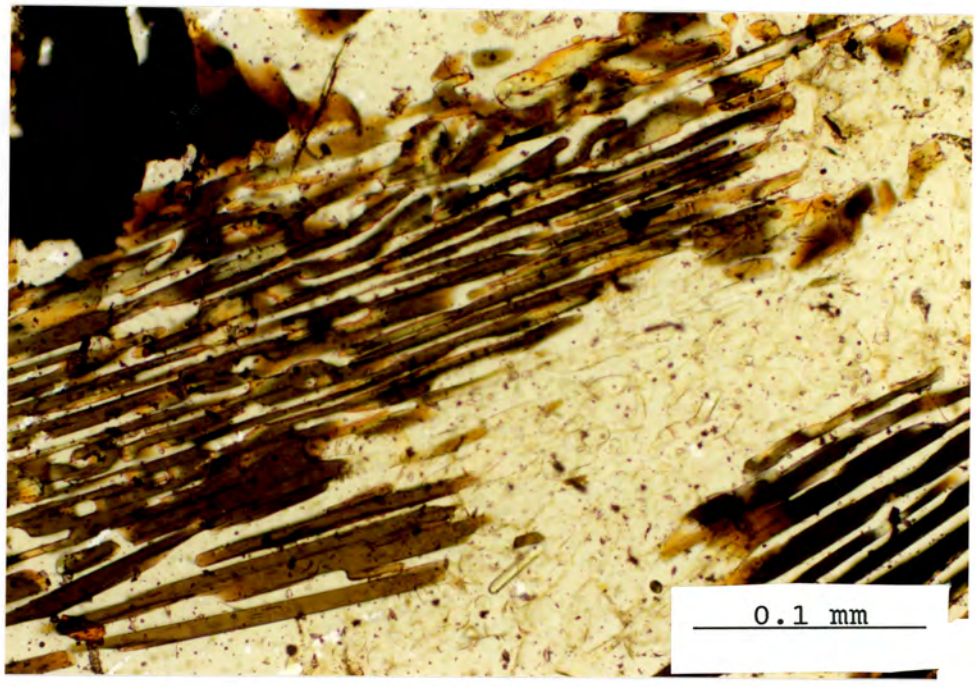

Plate 6.2 Skeletal biotite with vermicular intergrowth of quartz and cordierite in magnesian pelitic gneiss. Cross Polars. $DWN622_A$. Hytkoras

Pelitic gneisses are often characterised by a texture of mafic clots surrounded by pale-coloured haloes of quartz and K-feldspar set in a host mesosome. The mesosome consists of any combination of biotite-sillimanite-cordierite-plagioclase-quartz. The clots consist of garnet or cordierite, often with some biotite along their rims, or as a selvedge outside the quartz-feldspar halo. Garnet is heavily embayed by quartz and has a sieve texture with quartz inclusions, that strongly indicates that the mafic clot develops as a garnet-quartz intergrowth. Such garnets are ameboid or dendritic in outline. The largest garnet observed in the area is over 18 cm in diameter. The segregations and veins in most pelitic rocks generally do not have compositions close to minimum melts, however the abundance of quartz and feldspars makes it unlikely that they represent a restite after melt extraction. Segregations of this type are most likely to be the products of vapour-absent melting reactions (Tracy & Robinson, 1983 and Waters, 1988).

6.3 PETROGRAPHY

In this section the general petrographic characteristics of the constituent phases are briefly discussed.

Garnet - Porphyroblasts are common and have a variety of growth textures. Most garnets are irregular in shape, showing lobate crystal boundaries with quartz and containing numerous inclusions. They are generally elongated parallel to the gneissic banding. In quartz-absent and quartz-poor biotite gneisses garnets form coarse idioblastic porphyroblasts. There is no evidence of rotation recorded in the inclusion trails of any garnet. Corona textures and cordierite haloes are absent. Generally, garnet and cordierite do not share crystal boundaries, in the few cystals that do the contact is always straight. Cordierite is not seen rimming garnet or invading along cracks. In some examples cordierite is mantled by garnet. Biotite is seen as rounded inclusions and forms on garnet rims and along fractures. Quartz forms the dominant type of inclusion, others include sillimanite and oxide minerals. Plagioclase is not recorded. Garnets in segregations are often rimmed by a very fine rind of quartz, mantling garnet from hydrous minerals in the matrix.

Cordierite - Occurs as a dominant matrix mineral or as coarse irregular porphyroblasts, up to 5 cm across in some segregations.

Twinning is common. Porphyroblasts are relatively fresh with pinite alteration limited to grain boundaries and cracks. Pleochroism is very weak with pale mauve being the maximum absorption colour. Quartz and sillimanite are common inclusions, zircons with accompanying pleochroic haloes are conspicuous. Cordierite in association with orthopyroxene occurs as a vermicular intergrowth with skeletal biotite and quartz. In the Buffels River spinels are absent from pelitic gneisses so the corona textures observed between cordierite and spinel (Albat, 1984 and Baars, 1986) are not seen. Some cordierite poikiloblasts contain complex internal trails of sillimanite needles which may indicate the inclusion of a folded fabric or some degree of rotation during growth.

Orthopyroxene - A common constituent in magnesian gneisses also occurs in Mg-rich pelitic gneisses. Orthopyroxene forms very coarse equant porphyroblasts. Strong pleochroism is from pinkish-brown to yellowish-brown. Orthopyroxene is rimmed by a intergrowth of cordierite, biotite and quartz. Inclusions of biotite and plagioclase occur.

Biotite - Occurs in virtually all pelitic gneisses varying in abundance from accessory amounts in sillimanite-rich gneisses to melanocratic bands consisting wholly of biotite. Pleochroism is from red-brown to straw yellow, some examples are a darker chocolate-brown in colour. Biotite has strong preferred orientation in the plane of the gneissose foliation. Biotite can form in coarse grained random clusters or as individual flakes rimming garnet. Skeletal biotite occurs in some garnet-rich segregations and intergrown with cordierite and quartz in orthopyroxene-bearing pelitic gneisses (plate 6.2).

Sillimanite - Occurs as coarse prismatic crystals in the matrix or as fibrolitic inclusion trails in poikilobastic cordierite or garnet or as fine grained bands within well foliated quartz-rich gneisses. Fine scale compositional banding of idioblastic sillimanite is a feature of the pink coloured, K-feldspar-rich, sillimanite gneisses. No other Al_2O_5 polymorphs are recorded and there is no textural evidence of sillimanite pseudomorphing earlier andalusite or kyanite in pelitic rocks.

K-feldspar - Size varies from less than 1 mm to 3 mm. Most crystal are fresh, mesoperthitic, equant grains.

Plagioclase - Occurs in the more semi-pelitic and magnesian types of gneisses. Tends to be xenoblastic and fine grained. Optical zonation is absent, most grains are fresh and albite twin lamellae are visible. Myrmekite is common at K-feldspar-quartz contacts, particularly in pelitic segregations.

Quartz - Commonly forms coarse lobate grains embaying large porphyroblasts. Most grains show undulose extinction, however sub-grain development and fine grained neoblasts are not recorded. Quartz is the dominant inclusion type in garnet and cordierite poikiloblasts. Quartz is also found as fine rinds along the rims of garnets in segregations.

Oxides - In nearly all samples the oxide phase is ilmenite. Textures are similar to those recorded in mafic gneisses (see section 5.3.5). Fine lamellae of titano-hematite occur in host ilmenite. Some pelitic samples contain trace amounts of magnetite in addition to ilmenite. In sample MCS395 the major oxide phase is magnetite. In this sample magnetite contains fine scale trellis ilmenite with only limited development of coarser "sandwich-type " lamellae (Haggerty, 1976). Oxidation "exsolution" (Haggerty, 1976) results in the formation of ilmenite lamellae along {111} planes in the magnetite from the initial ulvospinel component contained in the phase. This texture is normally found in basalts that have undergone oxidation at temperatures above 600°C (Haggerty, 1976). The oxide phases in the mafic gneisses showed monotonous regularity in texture and composition and were best explained by exsolution on cooling to low temperatures (<500°C). It seems that this pelitic sample may have experienced a localised high temperature oxidation event.

Pelitic samples and estimated modal proportions

	Opx	Gar	Crd	Biot	Sill	Kfsp	Plag	Qtz	Oxide	Spn
O*DWN617	-	7	-	10	-	-	29	53	1	-
O*DWN618$_A$	-	-	2	98	-	-	-	-	-	-
O*DWN618$_B$	-	29	-	70	-	-	-	-	-	-
O*DWN619$_A$	69	-	22	29	-	-	-	-	-	-
O*DWN619$_B$	37	-	20	42	tr	-	-	-	-	-
O*DWN620$_A$	-	13	10	8	-	-	9	60	-	-
O*DWN620$_B$	-	-	16	3	-	-	10	71	-	-
O*DWN622$_A$	16	-	39	19	-	-	-	24	2	-
O*DWN622$_B$	4	7	40	27	-	-	-	32	-	-
O*DWN623	13	7	25	24	-	-	-	28	3	-
O*DWN624$_A$	-	46	5	8	-	-	16	25	-	-
O*DWN624$_B$	-	29	19	12	-	-	-	34	-	-
MCSS01	-	8	-	4	-	-	24	63	1	tr
I*MCSH02	-	30	-	15	-	19	6	30	-	-
*MCS321$_A$	-	-	26	6	5	4	-	59	1	-
*MCS321$_B$	-	-	26	4	10	35	3	20	2	-
*MCS322	-	8	-	tr	15	5	tr	69	3	-
MCS324	-	-	25	2	10	26	-	35	2	-
MCS329	-	-	-	1	6	46	-	46	1	-
MCS330	-	-	30	2	4	27	-	35	2	-
*MCS331	-	-	12	25	20	-	-	39	4	-
*MCS332	-	20	-	50	-	2	-	11	7	-
*MCS343	-	12	-	5	-	28	12	40	3	-
*MCS387	-	12	-	-	4	20	1	60	3	-
MCS389	-	-	36	-	-	19	9	36	tr	-
*MCS390	-	-	29	1	8	25	35	-	2	-
*MCS391	-	-	-	3	16	6	-	72	3	-
*MCS393	-	28	5	4	12	14	2	32	3	-
*MCS394$_A$	-	6	6	10	-	-	29	49	tr	-
MCS394$_B$	-	18	14	9	-	4	20	35	-	-
*MCS395	-	10	13	6	-	16	13	38	4	-
MCS399	-	-	6	tr	5	16	-	79	tr	-
MCS403	-	5	-	9	tr	17	23	44	2	-
Northern Areas										
*VD3	-	4	16	8	5	20	-	47	tr	-
*MCS212	-	25	-	-	11	-	-	64	-	-
*MCS273	-	17	36	7	-	-	-	40	-	-

* Mineral analysis by electron microprobe
O Oxygen isotope study
I Fluid inclusion study

6.4 MINERAL CHEMISTRY

Analyses are listed in the Appendix. Values listed are mean core compositions based on three or more spot analyses unless otherwise stated. In all samples the full assemblage with the exception of the oxide phases was analysed. Fig. 6.1 shows AFM diagrams for pelitic assemblages.

6.4.1 Garnet

Garnet zonation profiles for all samples in this study are shown in fig. 6.2. Most garnets are surrounded by quartz, biotite is the most frequently observed Fe-Mg-bearing phase in contact with garnet, some garnets are in contact with cordierite. Analytical traverses were selected to determine the extent of chemical zoning between adjacent Fe-Mg-phases and provide data for geothermometry.

All garnets analysed have core regions that are largely homogeneous. Garnets are iron-rich with end-member proportions ranging from Alm 56-83, Py 15-39, Sp 11-0.4, Gr-7-0.2. There are marked compositional gradients at the rims. Garnets in contact with biotite have narrow (200μm) rims which show rapidly increasing Fe with an accompanying equal decrease in Mg. It is uncommon to find garnets in contact with cordierite, in the few examples studied there is no pronounced zonation, in one case (MCS273) there is a slight increase in Fe, with a decrease in Mg. Garnets in contact with quartz show no compositional variation from core to rim. Ca and Mn concentrat are low and no show significant variation between core and rim. In grains containing biotite inclusions there are extremely narrow compositional haloes (20μm) around the inclusions with higher Fe and lower Mg than the mean core composition. In all cases compositional gradients appear to be relatively smooth and there is no trace of shar compositional discontinuites.

6.4.2 Cordierite

Cordierite was analysed from fourteen samples. Compositions occupy a very restricted range. Mg/(Mg+Fe) ratio falls in a narrow

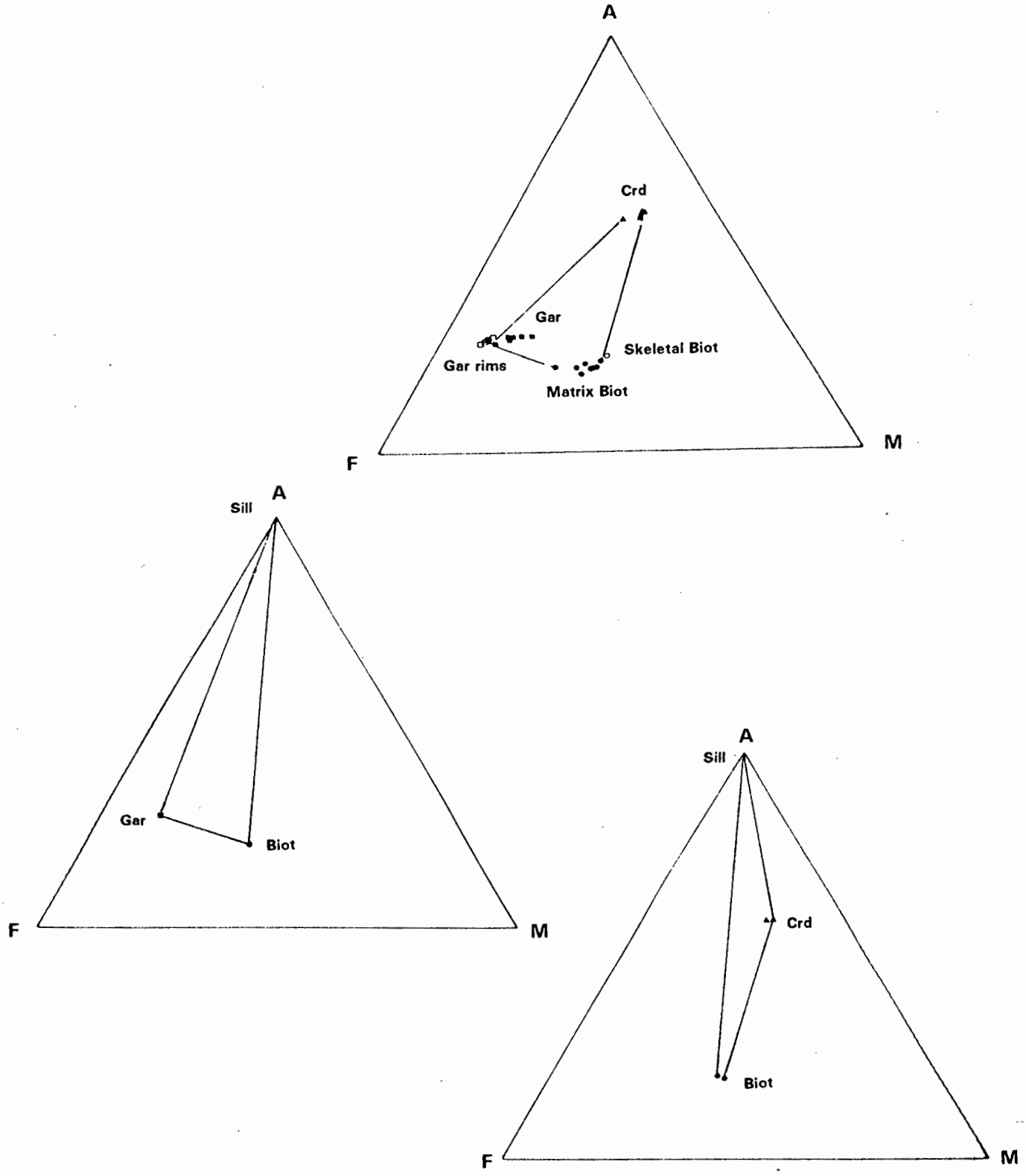

Fig. 6.1 AFM diagrams for coexisting phases in pelitic gneisses.
a. gar-crd-biot
b. gar-sill-biot
c. crd-sill-biot

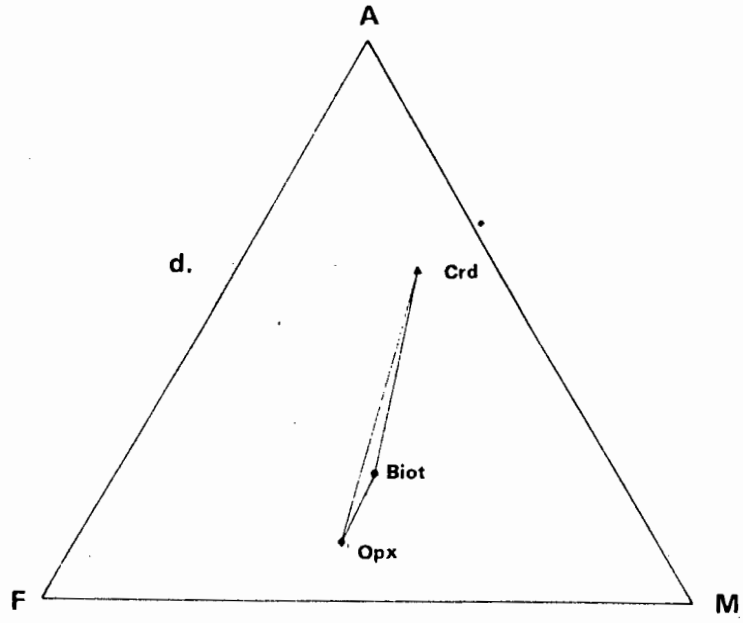

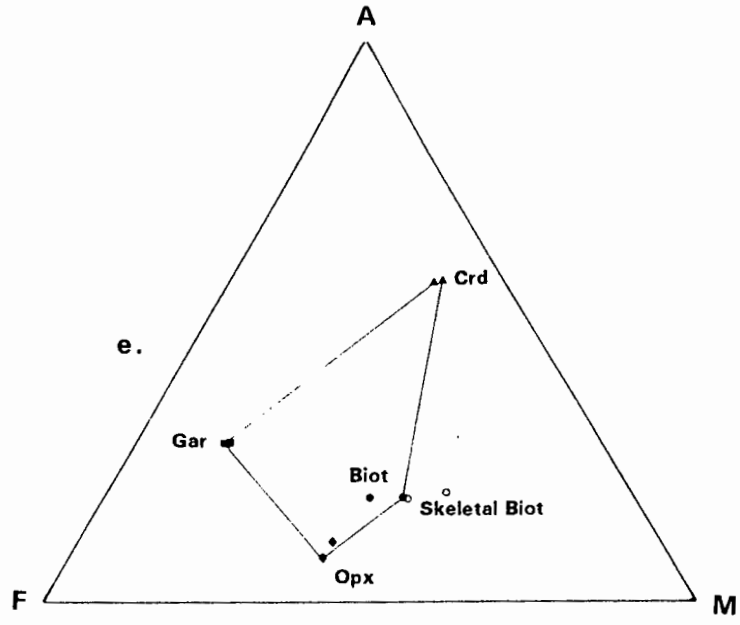

Fig. 6.1 AFM diagrams for coexisting phases in Mg-rich pelitic gneisses.
d. crd-biot-opx
e. gar-crd-biot-opx

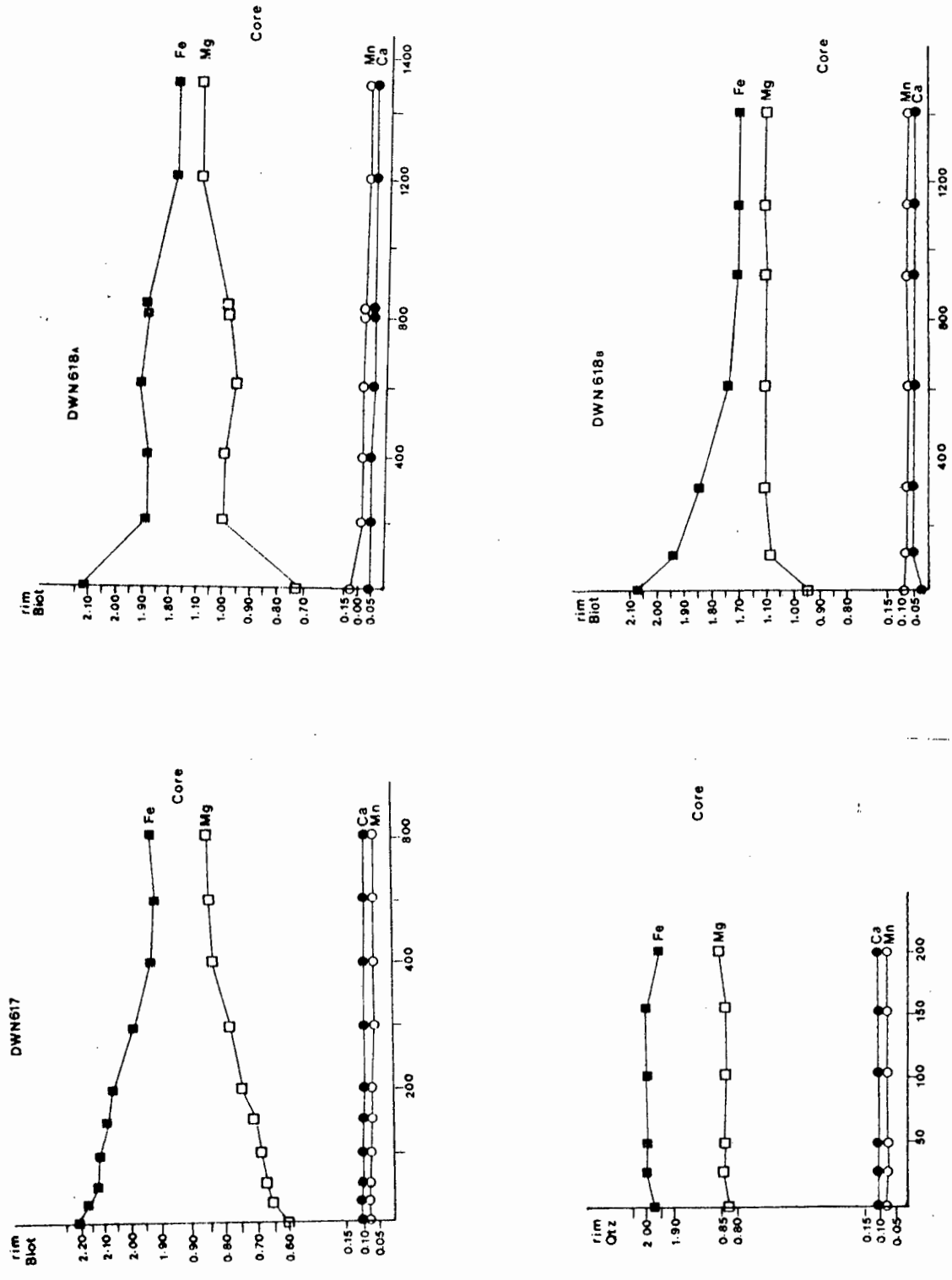

Fig. 6.2 Garnet zonation profiles. Rim to core, contact phase listed on the vetical axis.
Cation units per 12 oxygens.

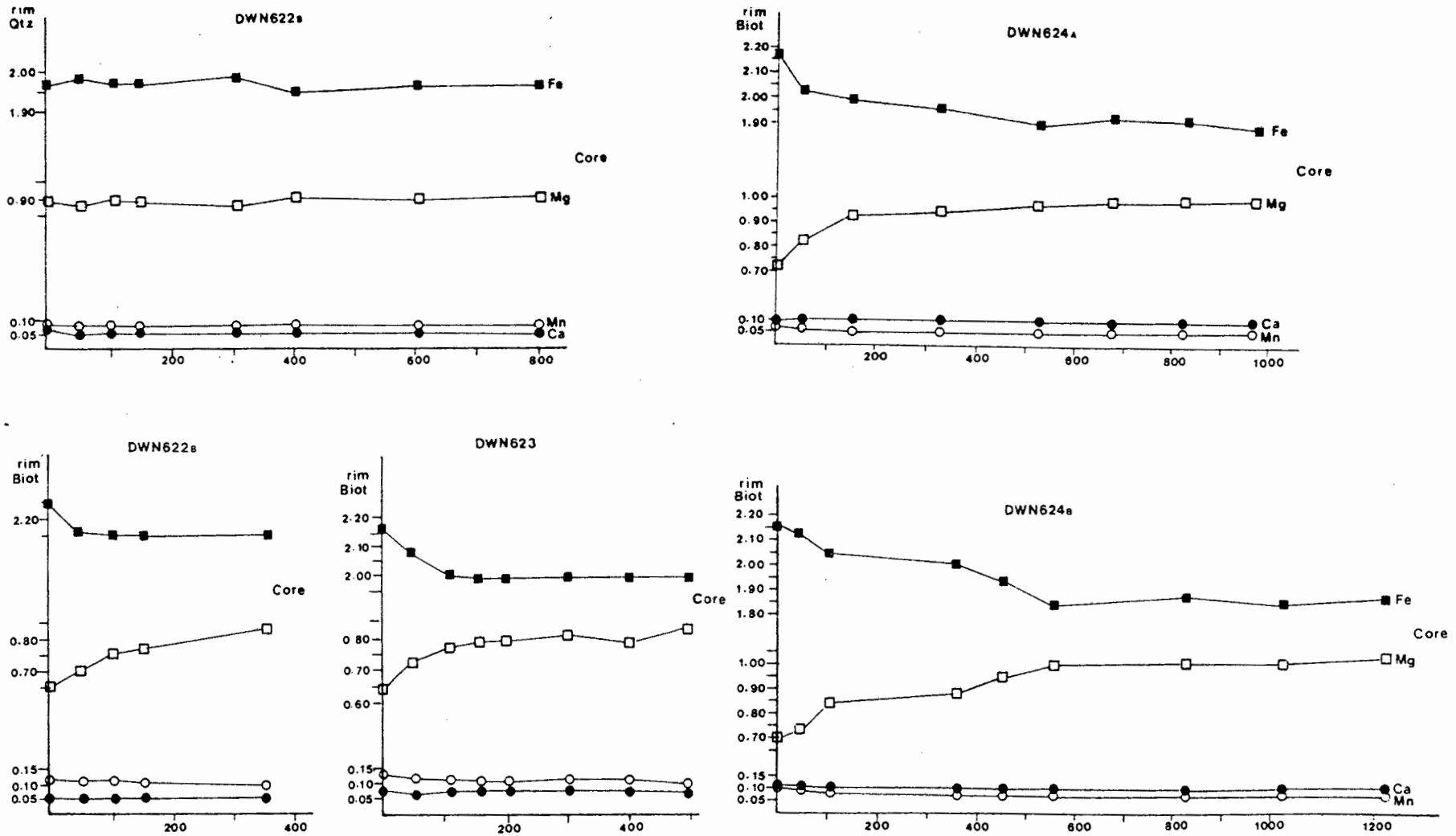
DWN622s
rim
Qtz
Core
Fe
Mg
Mn
Ca
DWN624A
rim
Biot
Core
Fe
Mg
Ca
Mn
DWN622s
rim
Biot
Core
DWN623
rim
Biot
Core
DWN624s
rim
Biot
Core
Fe
Mg
Ca
Mn

Fig. 6.2 cont.

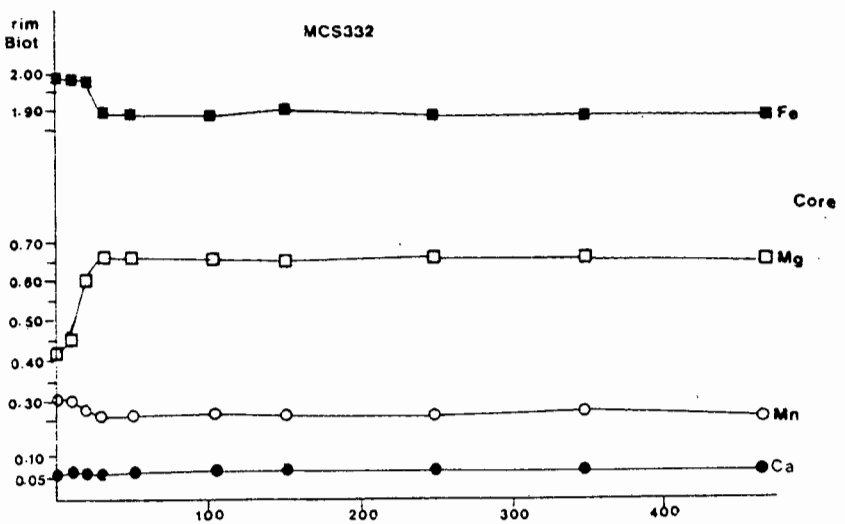
MCS332
rim
Biot
2.00
1.90
Fe
Core
0.70
0.60
0.50
0.40
Mg
0.30
Mn
0.10
0.05
Ca
100
200
300
400

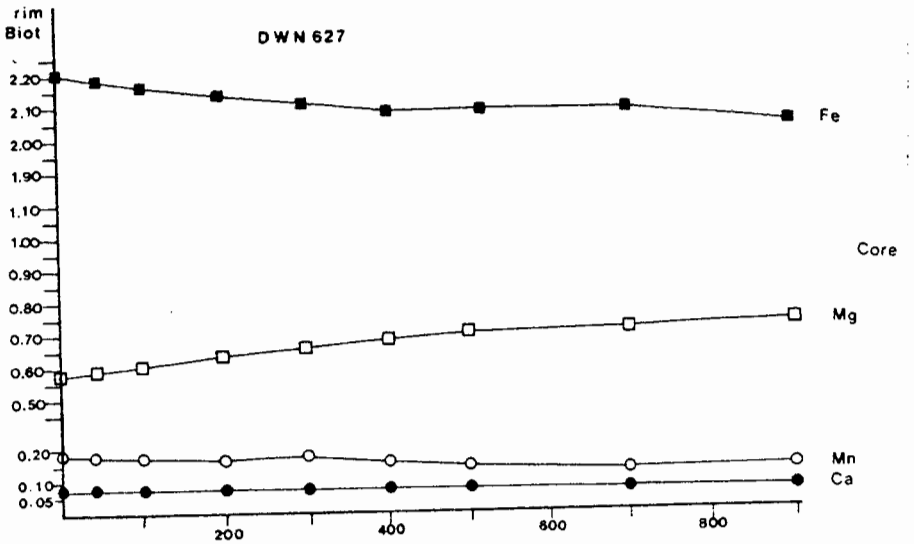
DWN 627
rim
Biot
2.20
2.10
2.00
1.90
1.10
1.00
0.90
0.80
0.70
0.60
0.50
Fe
Core
Mg
0.20
0.10
0.05
Mn
Ca
200
400
600
800

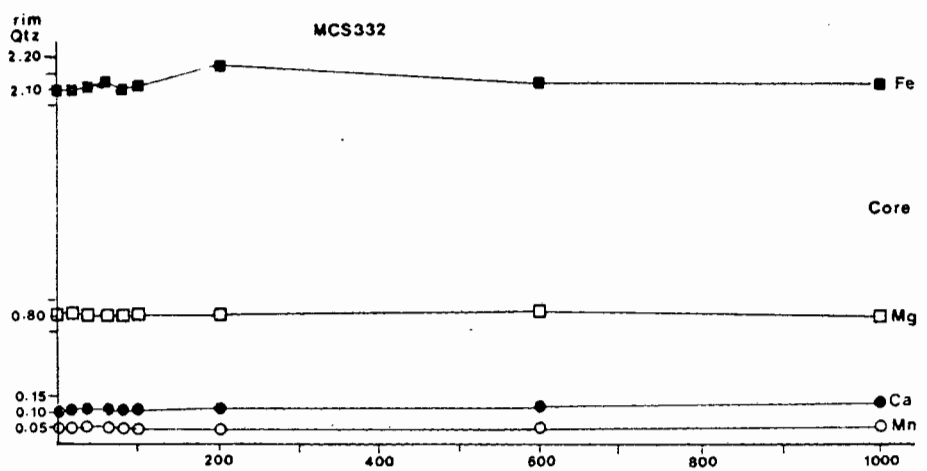
MCS332
rim
Qtz
2.20
2.10
Fe
Core
0.80
Mg
0.15
0.10
0.05
Ca
Mn
200
400
600
800
1000

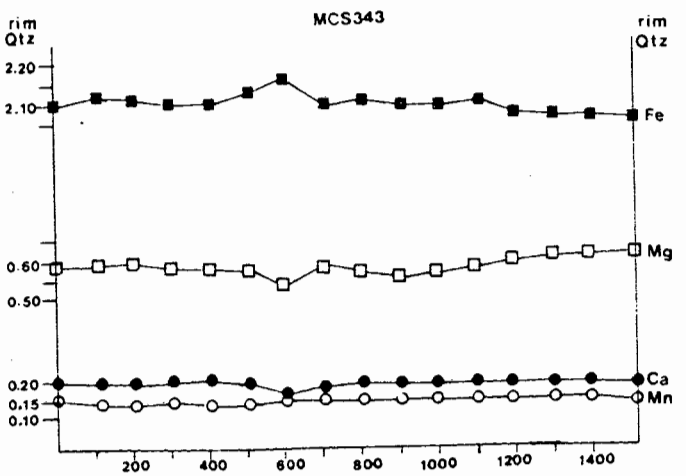
MCS343
rim
Qtz
rim
Qtz
2.20
2.10
Fe
0.60
0.50
Mg
0.20
0.15
0.10
Ca
Mn
200
400
600
800
1000
1200
1400

Fig. 6.2 cont.

Fig. 6.2 cont.

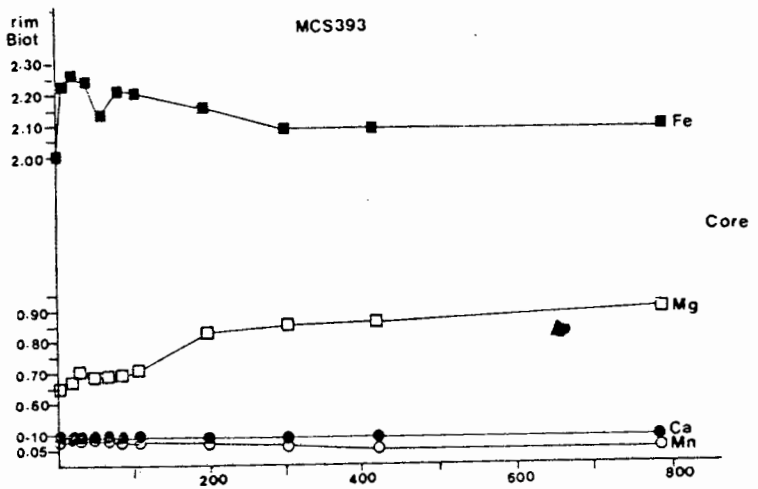
MCS393
rim
Biot
2·30
2.20
2.10
2.00
Fe
Core
Mg
0.90
0.80
0.70
0.60
0·10
0.05
Ca
Mn
200
400
600
800

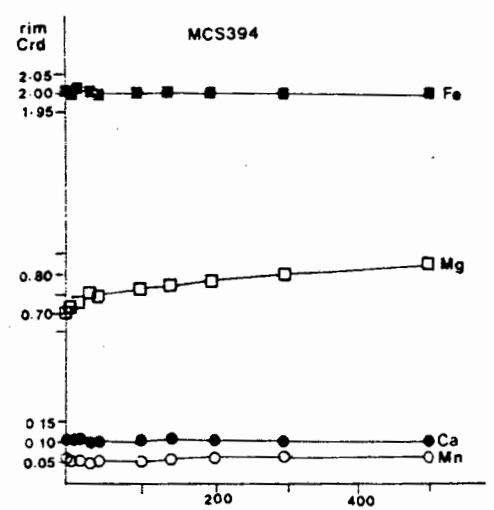
MCS394
rim
Crd
2·05
2·00
1·95
Fe
0.80
0.70
Mg
0 15
0 10
0.05
Ca
Mn
200
400

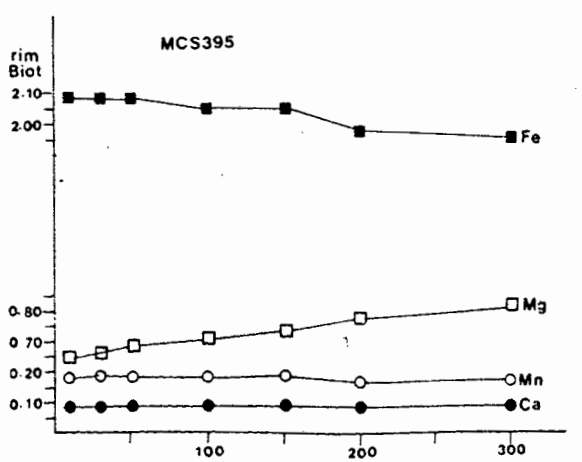
MCS395
rim
Biot
2·10
2·00
Fe
Mg
0·80
0 70
0·20
0.10
Mn
Ca
100
200
300

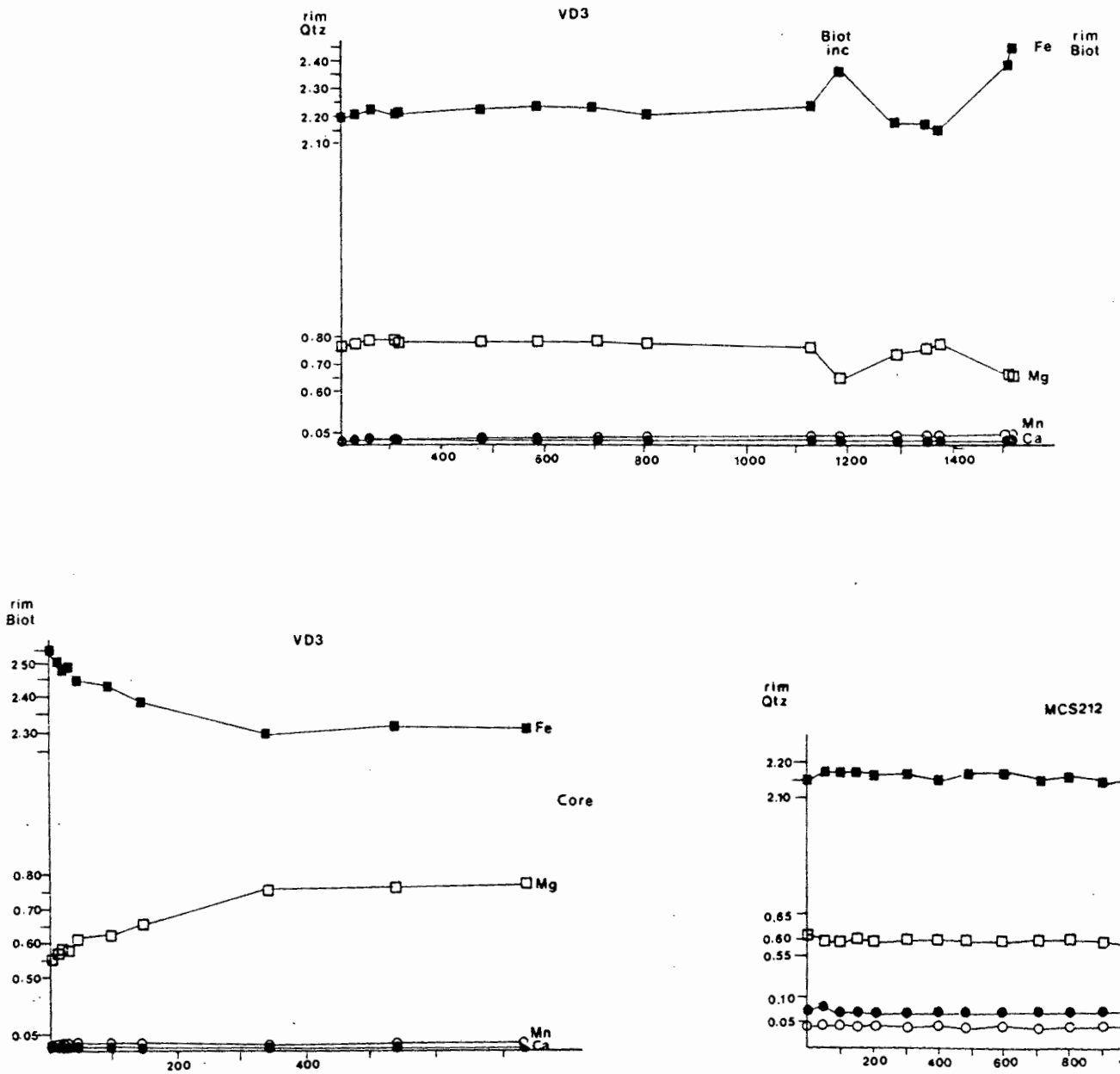
VD3
rim Qtz
Biot inc
Fe
rim Biot
2.40
2.30
2.20
2.10
0.80
0.70
0.60
0.05
Mg
Mn
Ca
400
600
800
1000
1200
1400
rim Biot
VD3
2.50
2.40
2.30
Fe
Core
0.80
0.70
0.60
0.50
0.05
Mg
Mn
Ca
200
400
rim Qtz
MCS212
rim Qtz
2.20
2.10
Fe
0.65
0.60
0.55
Mg
0.10
0.05
Ca
Mn
200
400
600
800
1000
1200
1400

Fig. 6.2 cont.

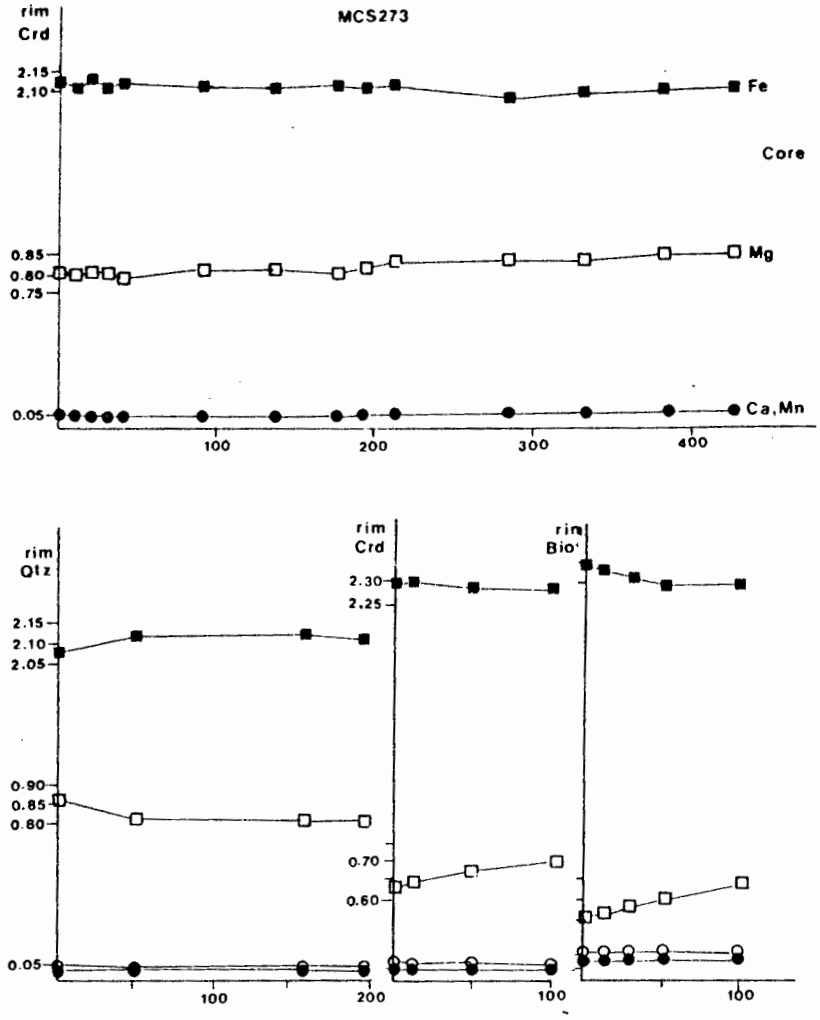
rim
Crd
MCS273
2.15
2.10
Fe
Core
0.85
0.80
0.75
Mg
0.05
Ca,Mn
100
200
300
400
rim
Qtz
rim
Crd
rim
Bio
2.30
2.25
2.15
2.10
2.05
0.90
0.85
0.80
0.70
0.60
0.05
100
200
100
100

Fig. 6.2 cont.

range between 0.80 and 0.74 for pelitic gneisses from the Buffels River area, mean X_{Mg} 0.76 ± 0.03, but is slightly lower for VD3 (0.68) a northern sample from Verdruk. Mg content increases towards the rim for cordierite coexisting with garnet. This is accompanied by a corresponding decrease in Fe. The cores are wide compositional plateaus with strong compositional gradients developed within 30 μm of adjacent Fe-Mg phases. Minor components include small, variable amounts of Mn, restricted to the cores, up to 0.43% MnO. Na is present and shows an increase on the rims, up to 0.43% Na_2O. Fresh cordierite gives analytical totals of 97-98% suggesting 2% volatiles.

6.4.3 Orthopyroxene

Orthopyroxene occurs in Mg-rich pelites. X_{Mg} varies between 0.57 and 0.61 for cores, and shows a slight increase towards the rims. Ti content is fairly low (<0.1% TiO_2). Al content is high, Al_2O_3 reaches up to 7.5%. Mn shows a very strong enrichment from core to rim. The range of MnO values varies between 0.45 and 1.03 %.

6.4.4 Biotite

Biotite was analysed from nineteen samples. Different textural varieties were treated separately. Matrix biotite is the term used to describe grains making up the foliated matrix of a pelitic gneiss that are free from contact with other Fe-Mg minerals (including oxides). Matrix biotite is usually interbanded with quartz or in some samples sillimanite. The term rim biotite is used for biotites in contact with garnet. Grains which form small, somewhat rounded inclusions in garnet are treated separately and are termed inclusions. Skeletal biotites have been analysed from three rocks. This textural form is part of a fine vermicular intergrowth with cordierite and quartz.

Fig. 6.3 shows the composition of biotites in the ideal plane annite-phlogopite-siderophyllite-eastonite (Guidotti, 1984). There is a tendency for matrix biotite to show increasing Al^{VI} with increasing Mg/(Mg+Fe). Ti increases with decreasing Al^{VI}, see fig. 6.4. Negative correlation between Ti and X_{Mg} is weak (fig. 6.5). Fluorine has been analysed in about half the samples. Most biotites contain less than

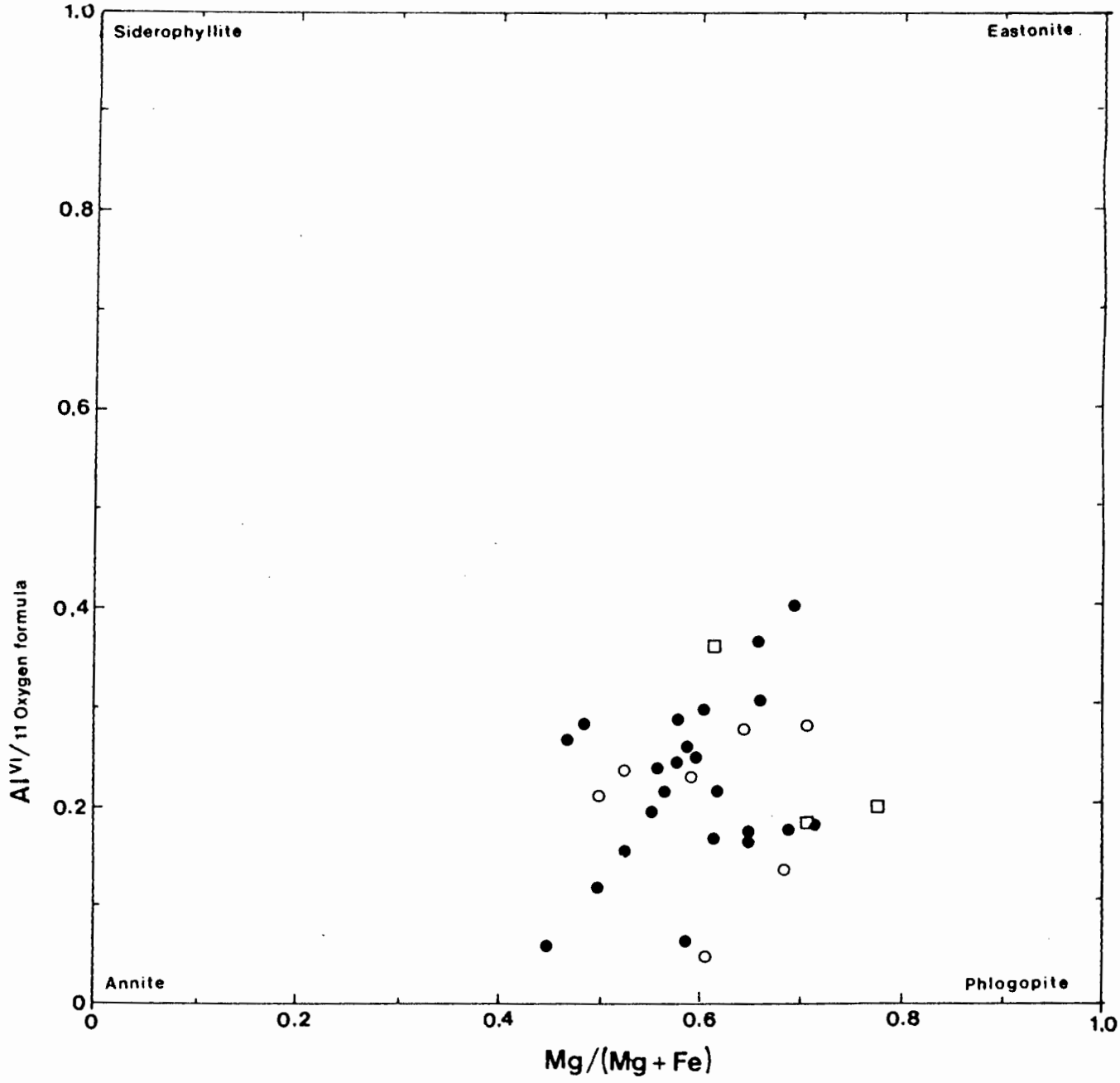

Fig. 6.3 Biotite compositions in the ideal plane annite-phlogopite-siderophyllite-eastonite.
● Matrix biotite
○ Rim and inclusion biotite
□ Skeletal biotite

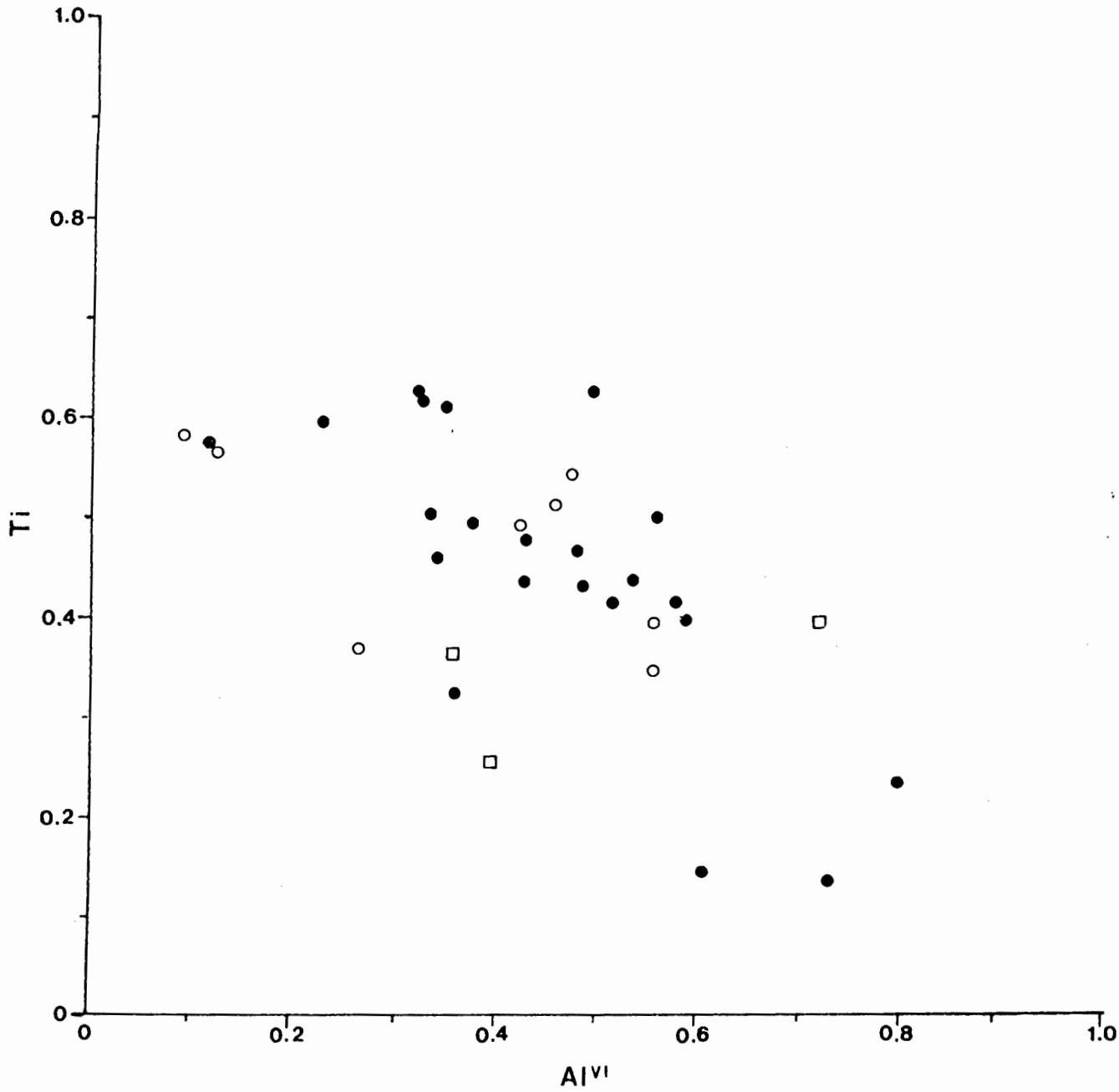

Fig. 6.4 Plot of Ti against Al^{VI} for biotite. Cation units based on 22 oxygens.
● Matrix biotite
○ Rim and inclusion biotite
□ Skeletal biotite

1 wt% F. There is a tendency for increasing X_F with increasing X_{Mg}, see fig. 6.6. Skeletal biotite in three samples are characterised by higher Mg contents, lower Ti and higher F than matrix biotite. Rim biotite in contact with garnet have higher X_{Mg} than matrix biotite. Biotite in contact with cordierite have lower X_{Mg} than matrix biotite. Ti is slightly lower for biotites in contact with garnet and higher for biotite on cordierite rims, compared to matrix biotite. Compositional variation in biotite is shown in a plot of octahedral cation site occupancy (Kretz, 1990). Mg and Fe^{2+} filling 70-75% of the octahedral site with Fe^{3+}, Al and Ti with occupying the remainder. Skeletal biotite has a lower Fe-Mg site occupancy, see fig. 6.7.

In comparison with biotites from other low pressure granulite-facies terranes samples from the Buffels River show compositonal similarities with biotites from the McCullough Range Gneisses, Nevada (Young et al., 1989), the Otter Lake terrane, Quebec (Kretz, 1990) and the West Uusimaa Complex, Finland (Schreurs, 1985). However, samples from Broken Hill, Australia (Phillips, 1980) have higher Al^{VI} contents, with low Ti and lower Mg, see fig. 6.8. and 6.9. The relationship between Al^{IV} and X_{Mg} in samples from Broken Hill is opposite to that seen in the Buffels River with Al^{IV} decreasing with higher X_{Mg} values. Biotites from other terranes show a similar broad distribution to the Buffels River area at lower values of X_{Mg}. Important substitutions in pelitic biotites are thus:

$$Mg\ Fe_{-1}$$

$$Ti^{VI}\ Al^{IV}\ Al^{VI}_{-1}\ Si_{-2}$$

$Ti[]Mg_{-2}$ has been cited as an important substitution in biotite from granulite facies pelitic gneisses (Dymek, 1983; Guidotti, 1984 and Indares & Martignole, 1985). In this study there is little strong evidence to suggest that this exchange mechanism has any great significance.

X_{Mg} for biotite and coexisting Fe-Mg exchange partners garnet and cordierite are shown in fig. 6.10. Orthopyroxene-bearing assemblages from relatively Mg-rich bulk compositions have the highest Mg content. Otherwise, there is no systematic variation in X_{Mg} between different assemblages. Kretz (1990) reports higher X_{Mg} in sillimanite-bearing pelitic gneisses from the Otter Lake terrane,

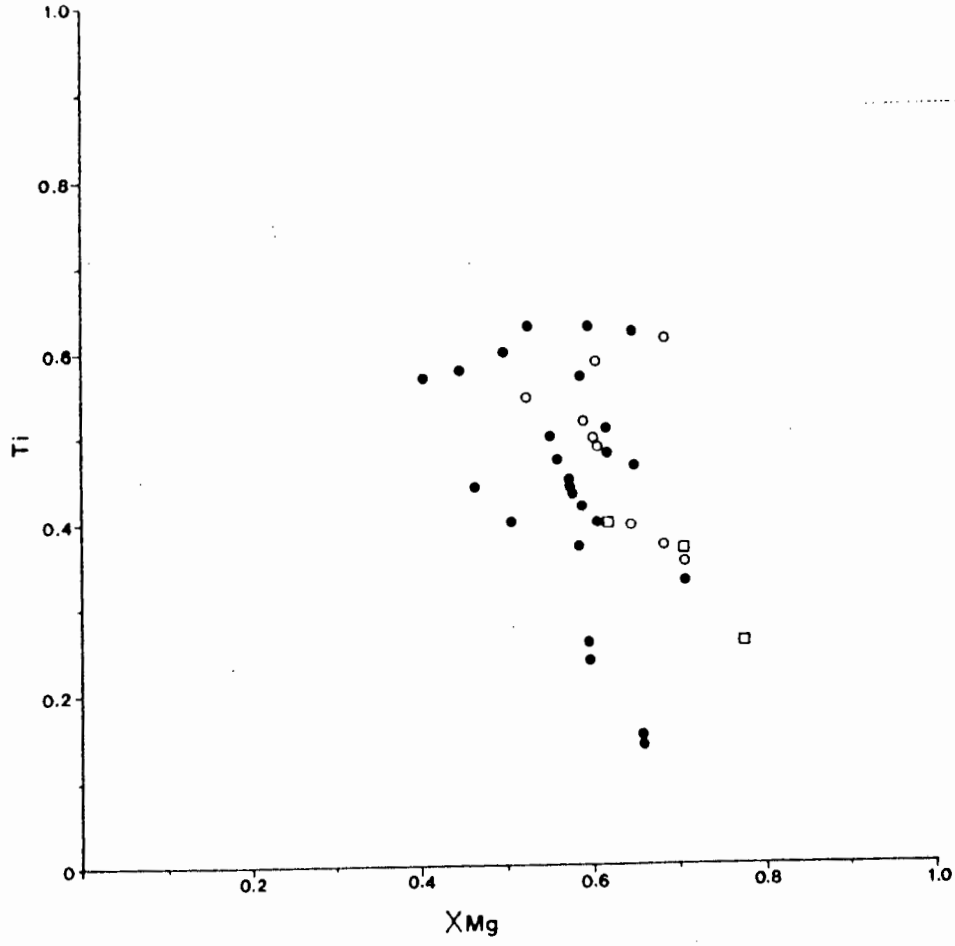

Fig. 6.5 Plot of Ti against X_{Mg} for biotite. Cation units based on 22 oxygens.
●matrix biotite
○rim and inclusion biotite
□skeletal biotite

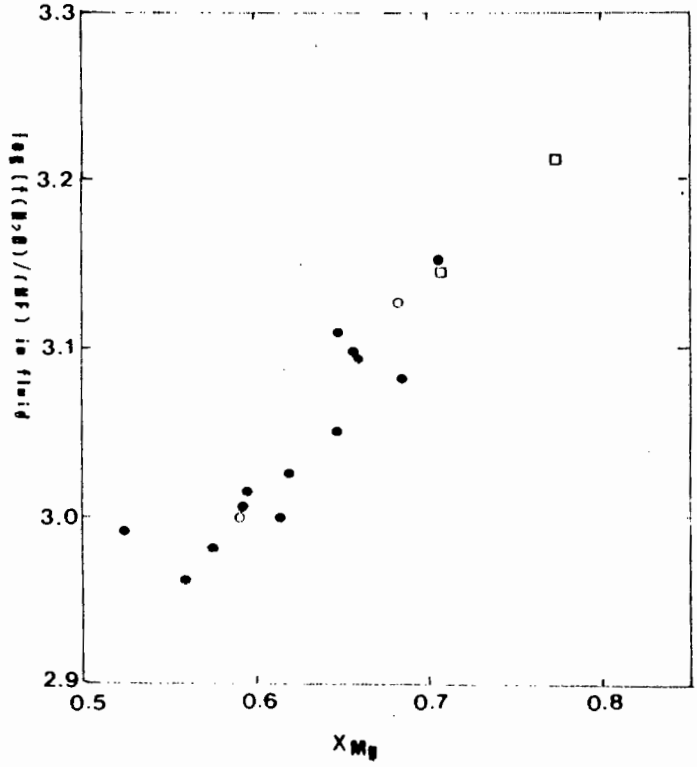

Fig. 6.6 log f $(H_2O)/(HF)$ in fluid versus X_{Mg} for biotites at 750°C. Calculated following the method of Munoz (1978). ●matrix biotite
○rim biotite
□skeletal biotite

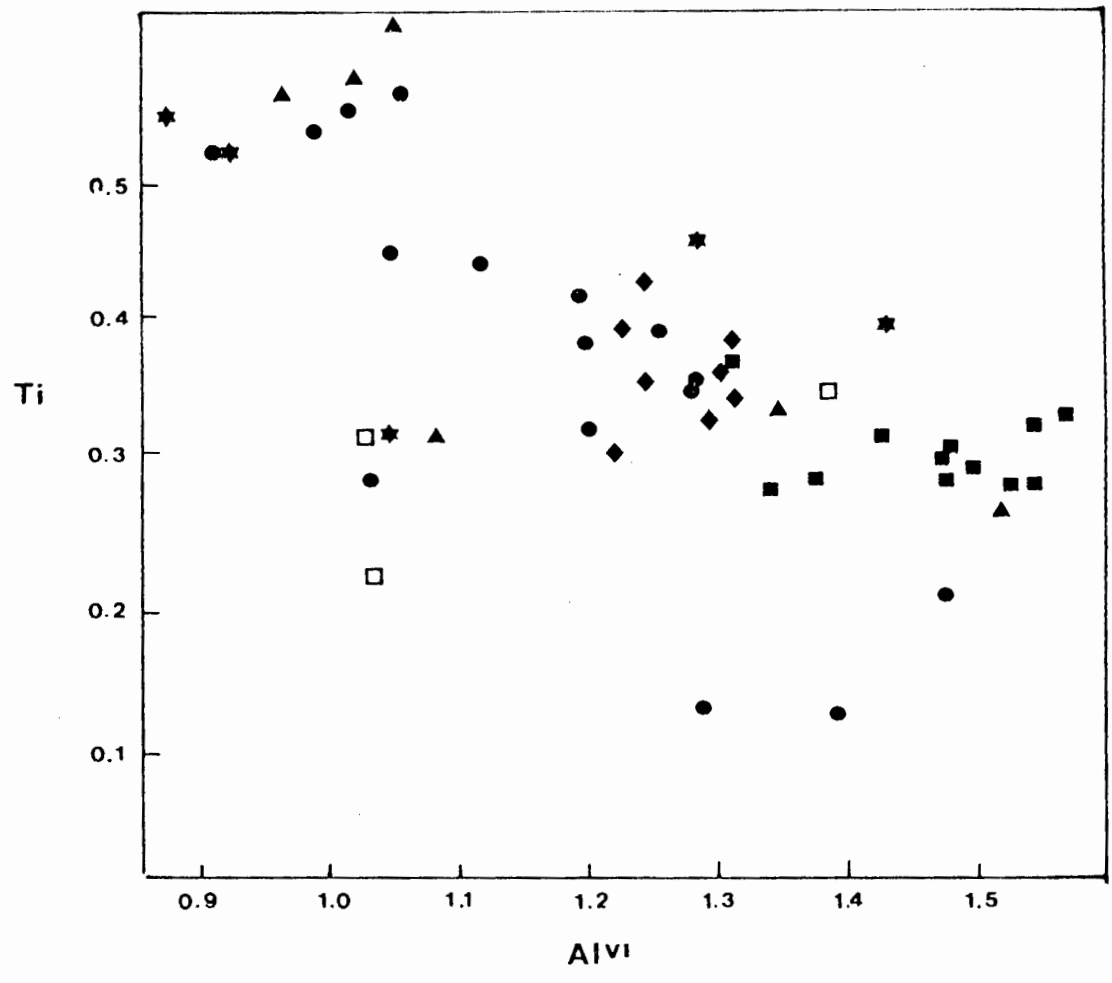

Fig. 6.7 Comparison of high grade biotites. Ti against Al^{VI}. Cation units based on 22 oxygens.
- ●Matrix biotite Buffels River
- □Skeletal biotite Buffels River
- ■Broken Hill, Australia (Phillips, 1980)
- ◆McCullough Range, Nevada (Young et al., 1989)
- ▲Otter Lake, Quebec (Kretz, 1990)
- ✸West Uusimaa, Finland (Schreurs, 1985)

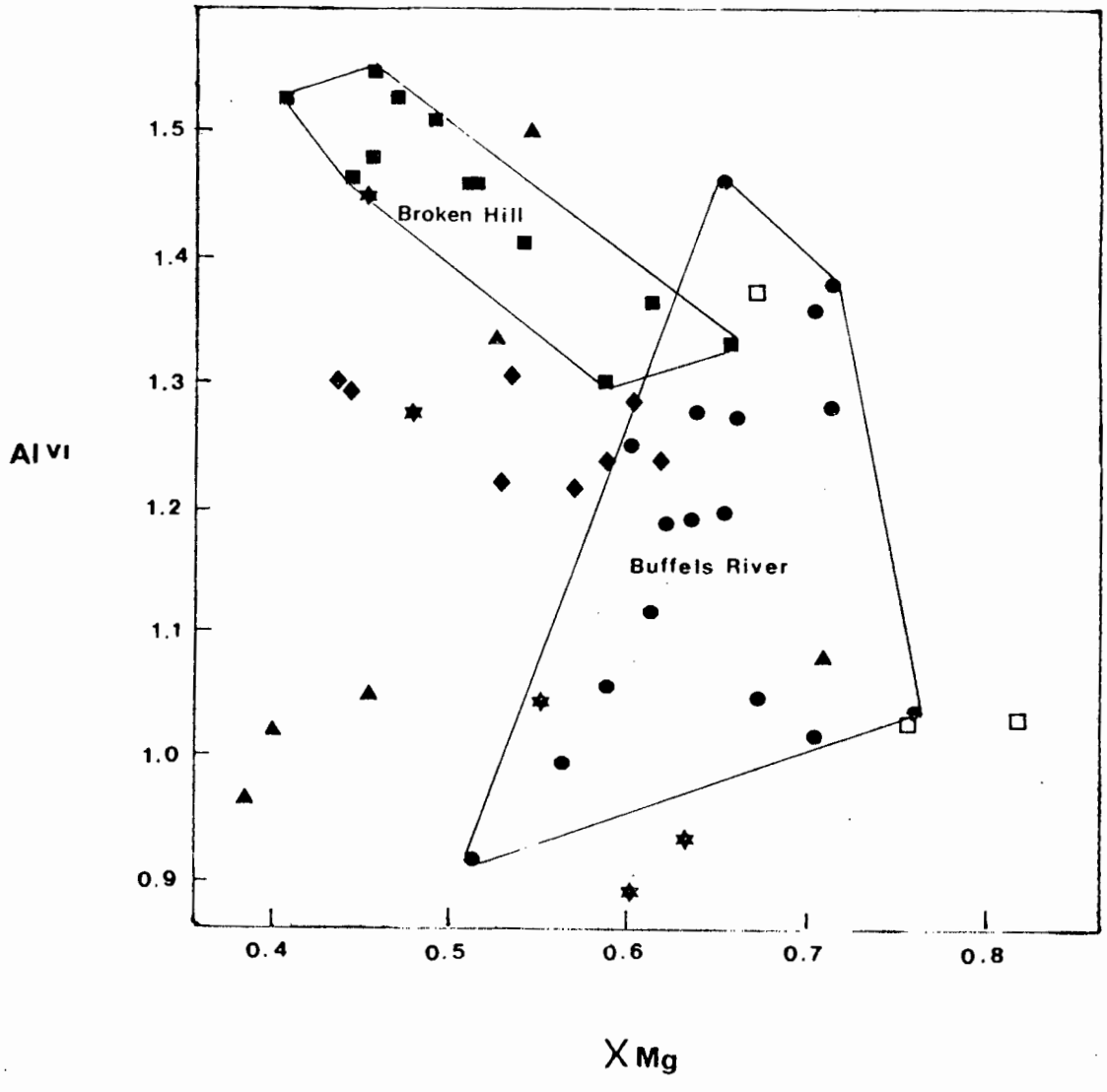

Fig. 6.8 Comparison of high grade biotites. Al^{IV} against X_{Mg}. Cation units based on 22 oxygens. Fields for Buffels River and Broken Hill, Australia.
- ●Matrix biotite Buffels River
- □Skeletal biotite Buffels River
- ■Broken Hill, Australia (Phillips, 1980)
- ◆McCullough Range, Nevada (Young et al., 1989)
- ▲Otter Lake, Quebec (Kretz, 1990)
- ★West Uusimaa, Finland (Schreurs, 1985)

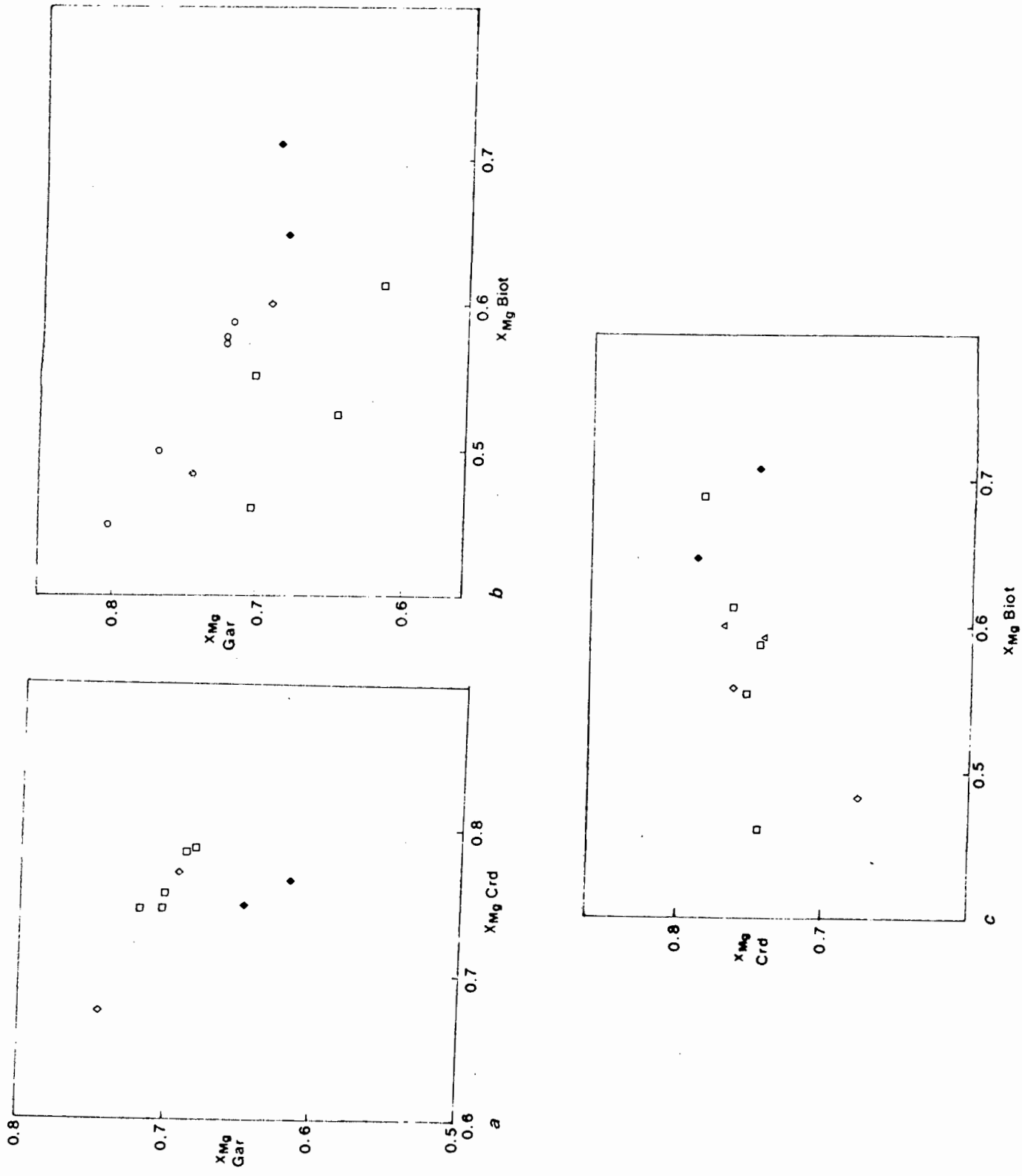

Fig. 6.10 X_{Mg} distribution between coexisting Fe-Mg phases for different assemblages from pelitic gneisses.
a. garnet-cordierite
b. biotite-garnet
c. biotite-cordierite
Assemblages:

◆ Gar-Crd-Biot-Opx
○ Gar-Biot
□ Gar-Crd-Biot
◇ Gar-Crd-Sill
△ Crd-Biot-Sill

Quebec. Kretz relates increase in X_{Mg} in rocks of similar bulk chemistry to increasing temperature or lower a_{H2O}, the latter is more likely in samples from the Buffels River area, which are isofacial. Increasing X_{Mg} is accompanied with by a decrease in Al, Fe3+, Ti (see fig. 6.7).

6.4.5 Plagioclase

No optical zonation was noted and little significant chemical variation is recorded in this study. Albat (1984) records core to rim variations for plagioclase in contact with garnet, both normal and reverse zonation occurs, changes were up to 17% of the anorthite molecule, but no systematic trends were found. Plagioclase from eleven samples in this study have rather uniform compositions, ranging from oligoclase to andesine, varying from An_{25} to An_{42}.

6.4.6 K-feldspar

Difficulty was found in integrating the compositions of coarsely perthitic alkali feldspar. However, most alkali feldspar in pelitic gneisses are meso- to microperthitic in character and easily analysed with a broadened electron beam (10-20μm). Albite content varies between Ab_{10} and Ab_{20}. The coarse bleby perthites have up to 33% of the albite molecule. Barium was analysed in a few feldspars from pelitic and augen gneisses. BaO is less than 0.5% for alkali feldspar from pelitic samples.

6.5 GARNET ZONATION

Garnets are largely unzoned with low Mn and Ca contents. When in contact with biotite Fe is strongly enriched on the rims with a matching depletion in Mg, this profile is less steep or absent at contacts with quartz and feldspar.

Reduction in the Mn content on garnet rims has been attributed to reaction induced zonation (Loomis, 1983). In garnets from this study there is no strong decrease in Mn along the rims. High or constant Mn suggests late-stage continuous reactions producing cordierite or biotite (Tracy & Robinson, 1976 and St-Onge, 1984).

Fig. 6.2 shows the zonation profiles from all garnets in the study. All garnets have large compositional plateaus defining a broad core region. The extent of any zoning is strongly dictated by the adjacent phase. Biotite contacts give rise to marked enrichment in Fe and depletion in Mg. Without significant change in Mn or Ca. It can be assumed that as the same pattern is developed to roughly the same extent in each case the process responsible is essentially the same.

6.5.1 Induced diffusion zonation

The profiles observed in garnets are best attributed to retrograde reequilibration with adjacent biotite on cooling (Tracy et al., 1976). The critical assumptions in the analysis of garnet zonation are that the mineral assemblages maintain local equilibrium during the initial stages of retrogression and do so by a process of solid-solid diffusion.

Elphick et al. (1981, 1982) indicate that for temperatures above 550°C diffusion controlled zoning of Mg-Fe and Mn-Fe should be significant. The closure temperature for garnet is the temperature at which mass transfer through the rock matrix becomes so slow that the garnet is effectively isolated from its exchange partner, or the temperature at which cation diffusion within the garnet is so slow as to reduce the rate of flux to the exchange partner to zero. In either case the garnet will become a closed chemical system. Diffusion data is listed by Lasaga et al. (1979), Freer (1981), Cygan & Lasaga (1985), and Elphick et al. (1985). The actual closure temperature for Fe-Mg exchange in natural garnets is thought to lie in a range between 550-650°C, depending on cooling rates.

Diffusion controls zoning in two ways; it tends to eliminate growth history. Thus, at high temperatures garnets equilibrate to produce large homogeneous crystals with all previous growth history overprinted by rapid internal diffusion. On cooling diffusion will promote inward compositional change from the edge of a crystal. In some cases this may homogenise the crystal, while in others a compositional gradient will be preserved in the form of a narrow rim at the contact with another Fe-Mg phase (Loomis, 1983).

In the case of Fe-Mg exchange between garnet and biotite on

cooling biotite shifts to more Mg-rich compositions. Rapid intracrystalline diffusion causes biotite to remain homogeneous, but a great deal of mass transfer is required to change the composition of all biotites in the immediate domain. Thus, matrix biotites away from garnets isolated by inert grains of quartz, retain their peak equilibrium composition. In garnet slow diffusion rates isolate the edges from the interior. If Fe-Mg exchange is simply controlled by thermally activated diffusion then the relationship between garnet and included biotite should be the same as that observed at the edge of garnets. Garnet-biotite inclusion pairs should give the same temperatures as rim-contact pairs. However, since most inclusions are relatively small (30-50μm), the diffusion shell produced in the surrounding garnet would be about 5μm or less at temperatures around 600°C, (Loomis, 1983). This very narrow shell would be too small to resolve with the microprobe. Hence, garnet-biotite inclusion pairs should yield temperature estimates higher than rim-contact pairs, but less than the assumed peak temperature. However, the Mg content of inclusion biotites should be the same as biotites in contact with the garnet rims. Sample MCS343 provides an example of this X_{Mg} for inclusion biotite is 0.586, compared to 0.603 for rim biotite and 0.499 in matrix biotite.

6.5.2 Geospeedometry

Assuming that there has been no leakage of components, the composition of each crystal surface will depend on changing K_D and the rate of diffusion of each crystal. Lasaga (1983) describes an approach to calculating approximate cooling rates of rocks from the diffusion controlled exchange of components in mineral pairs. His general approach is followed here.

Changes in K_D due to cooling produce diffusive fluxes in each mineral, laws related to diffusion can be applied to the exchanging mineral pair to yield the following relationship:

$$\frac{\delta C_{Mg,A}}{\delta t} = D_A(t) \cdot \frac{\delta^2 C_{Mg,A}}{\delta x^2} \quad (1)$$

$$\frac{\delta C_{Mg,B}}{\delta t} = D_B(t) \cdot \frac{\delta^2 C_{Mg,B}}{\delta x^2} \quad (2)$$

where $C_{Mg,A}$ equals the concentration of Mg, in mole %, in phase A. x equals the distance from the exchange interface. D_A and D_B are binary interdiffusion coefficients in each phase. t equals the time.

The ratio of cation exchange in a mineral is controlled by stoichiometry, hence it is only necessary to consider one component of the exchange couple, biotite has a positive flux of Mg, whilst garnet has a negative flux of Mg. In this study phase A represents garnet and phase B biotite.

The thermal history is quantified through the time dependancy of the diffusion coefficient and the K_D of the exchange reaction. So that:

$$D(t) = A\, e^{-(Ea/RT)} \tag{3}$$

where A is a pre-exponential factor and Ea is the diffusion activation energy.

D has a strong time dependancy so Lasaga (1983) advocates the use of a compressed time-scale, so that time, t', cannot keep on increasing but reaches a finite value.

$$dt' = d(t)\, dt \tag{4}$$

Changes in composition will occur as t' varies. High values of t' will destroy evidence of previous thermal history. For small values of t, t and t' are essentially the same. If t' is small then there will be little time available to modify the composition of the mineral phase and original high temperature compositons will be preserved.

It is assumed that the only boundary changes occur at x=0, and that no material was exchanged along the other side of the mineral, a equals the crystal length in the x-direction.

Lasaga relates the thermal history of the system, Y, with following expression:

$$Y \equiv \frac{Ea\ S}{R\ T_o^2} \tag{5}$$

where S is the initial cooling rate, and T_o is the initial

temperature (peak conditions). The maximum value of t' will determine the net effect of the thermal history on the mineral assemblage as:

$$t' = \frac{1}{Y}\left[1 - e^{-Yt}\right] \tag{6}$$

so that, $t' < 1/Y$.

The diffusion exchange properties of the components and the mineral pair are related by the term ß in the following expression:

$$ß = \frac{H^0_s \, D^0_{B/D^0_A}}{RT^2 \{ D^0_{B/D^0_A} [1+(C^I_{1,A}/C^I_{2,A})]+[(C^I_{1,A}/C^I_{1,B})+(C^I_{1,A}/C^I_{2,B})]\}} \tag{7}$$

where C refers to concentration of component 1, in phase A and B, at the initial temperature.

The rate of change of the boundary concentrations depends not only on the cooling rate S, and the enthalpy of change H^0, but also on the ratio of the diffusion coefficients and the initial composition of the two minerals. The thermal history can be related to the size of the exchanging crystal and its diffusion coefficient by the following expression:

$$Y' = \frac{a^2}{D_0} \cdot Y \tag{8}$$

As cooling progresses the kinetics of diffusion become extremely slow, therefore, t' attains a maximum value. Low values for Y' yield higher t' values hence more complete re-equilibration, resulting in flat homogeneous profiles without preserving the peak metamorphic temperature.

If D^0_B/D^0_A is very small then ß is small. Therefore, garnet may be the mineral with the rapidly varying boundary concentration if other minerals with much faster diffusion coefficients are exchanging with it, as is the case with biotite.

If $D^0_B >> D^0_A$ and $C_{2,A} > C_{1A}$ then:

$$ß/Y \approx \frac{H^0}{Ea} \tag{9}$$

this would be typical of slow diffusion. If D^0_B/D^0_A is very large as is the case with fast diffusion in mineral A then:

$$ß/Y \approx \frac{H^0}{Ea} \cdot \sqrt{D^0_B/D^0_A} \qquad (10)$$

ß/Y is not dependant on the rate of change of temperature, but relates to diffusion exchange characteristics of the mineral pair. Y' is strongly governed by thermal history, so that:

$$Y' \equiv \frac{Ea\ s\ a^2}{D^0\ RT_0^2} \qquad (11)$$

where a is the crystal size.

Enthalpy for Fe-Mg exchange in garnet-biotite is given by Ferry & Spear (1976) as 4.2 Kcal/mol. Diffusion data for garnet are taken from the experimental work of Cygan & Lasaga (1987), as shown in fig. 6.11.

Figs 6.12 show model curves for the kinetic response of a mineral with slow diffusion, typical of Mg in garnet, and a mineral with fast diffusion, typical of Fe in biotite, at different cooling rates, after Lasaga (1983). Fig 6.13 shows the natural compositional profiles of garnet and biotite in contact from the pelitic gneiss $DWN624_A$.

The diffusion rates for garnets are assumed to be much slower than biotites, hence ß/Y approximates 0.15. Y' can be calculated for a variety of crystal sizes (a) and cooling rates (s) from equation (11), where:

$Ea = 239$ kj/mole

$D^0 = 9.8 \times 10^{-9}\ m^2/sec$

$T_0 = 1023$ K

Y'is strongly dependant on cooling rate, at low values for s, extensive homogenization of garnet can be expected, thus results from garnet-biotite thermometry would underestimate peak temperature. High values for s, indicative of fast cooling, would be expected to produce cystals with unzoned rims. If Y is large (100-1000) then the

entire compositional profile would be close to the original compositio at t_o. If Y is small (<10) then zoning around the edge would be pronounced and calculated temperature (T_{calc}) would be less than T_o. For large garnets used in this study, for example, DWN624, a = 5mm, Y ' = 10.0, which suggests cooling rates around 20°C/m.y. Sample DWN62 gives a maximum temperature estimate of 840°C using the Ferry & Spear (1978) calibration (see Chapter 4). Suggesting that T_{calc} is roughly equal to T_o. Cooling rates lower than 5°C/m.y. would produce T_{calc} much lower than T_o (<700 C). Crystal size is important, if small garnets (a = 0.1 mm) were used at an assumed cooling rate around 20°C/m.y. T_{calc} would be reduced by over 100°C compared to T_o. No very fine-grained pelitic gneisses occur to test this hypothesis.

The effect of temperature on diffusion controlled zonation can be seen from measuring the penetration rate for Mg diffusion in garnet using the diffusion data of Cygan & Lasaga (1987) and the expression:

$$x = \sqrt{4Dt} \quad \text{(Crank, 1975)} \qquad (12)$$

TABLE 6.2

Effects of temperature and time on diffusion rates and extent of internal equilibration in garnets

Diffusion rate	Temperature °C	Time (m.y.)	Penetration distance (mm)
9.75×10^{-21}	750	50	7.8
9.75×10^{-21}	750	10	3.7
9.75×10^{-21}	750	1	1.1
11×10^{-22}	650	50	2.6
11×10^{-22}	650	10	1.18
11×10^{-22}	650	1	0.30
12×10^{-24}	550	50	0.275
12×10^{-24}	550	10	0.123
12×10^{-24}	550	1	0.039

It can be seen from the data in Table 6.2 that at high temperatures crystals would reequilibrate internally in relatively short geological time-spans. Together with the empirical values for Y' the above data indicates that the cooling episode for the Namaqua metamorphic event must have lasted between 10-20 m.y. It is unlikely

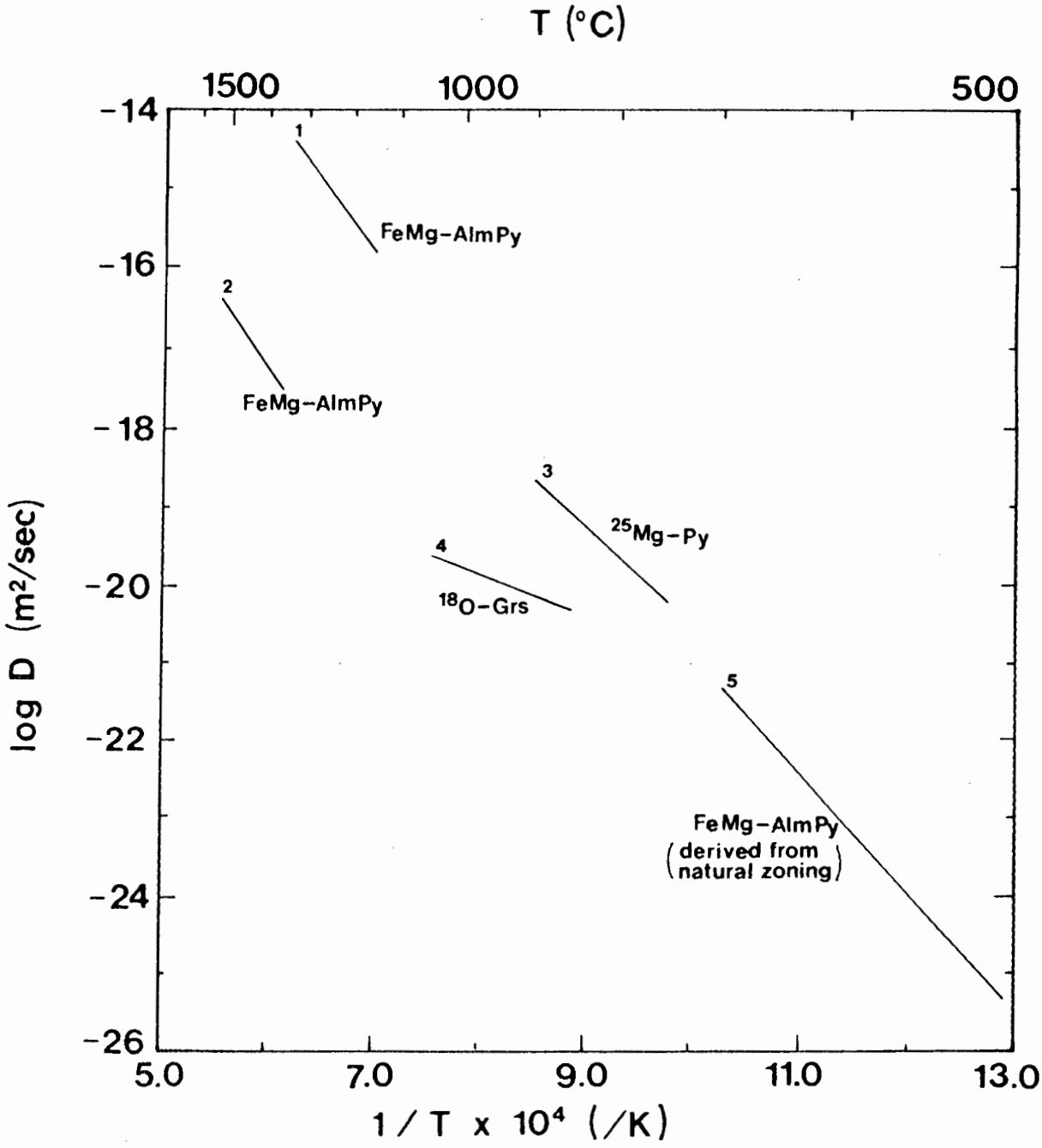

Fig. 6.11 Experimental diffusion data for garnet (after Cygan & Lasaga, 1987).
1. Duckworth & Freer (1981)
2. Elphick et al. (1981)
3. Cygan & Lasaga (1987)
4. Freer & Dennis (1982)
5. Lasaga et al. (1977)

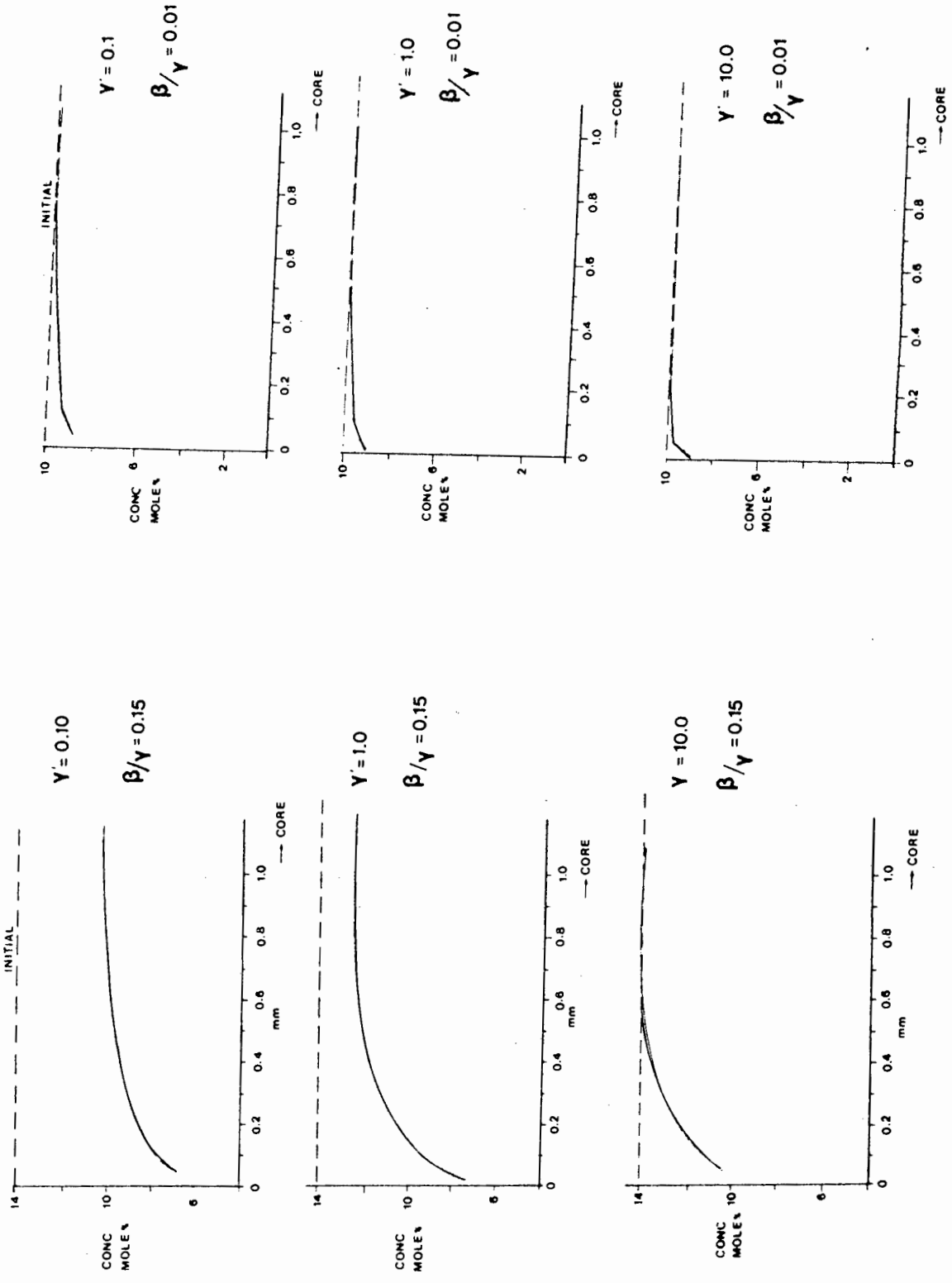

Fig. 6.12a Modelled kinetic response of a mineral with slow diffusion, $\beta/\gamma = 0.15$ at different cooling rates (γ' values 0.1 to 10.0) after Lasaga, 1983.

b Modelled kinetic response of a mineral with rapid diffusion, $\beta/\gamma = 0.01$ at different cooling rates (γ' values 0.1 to 10.0) after Lasaga, 1983.

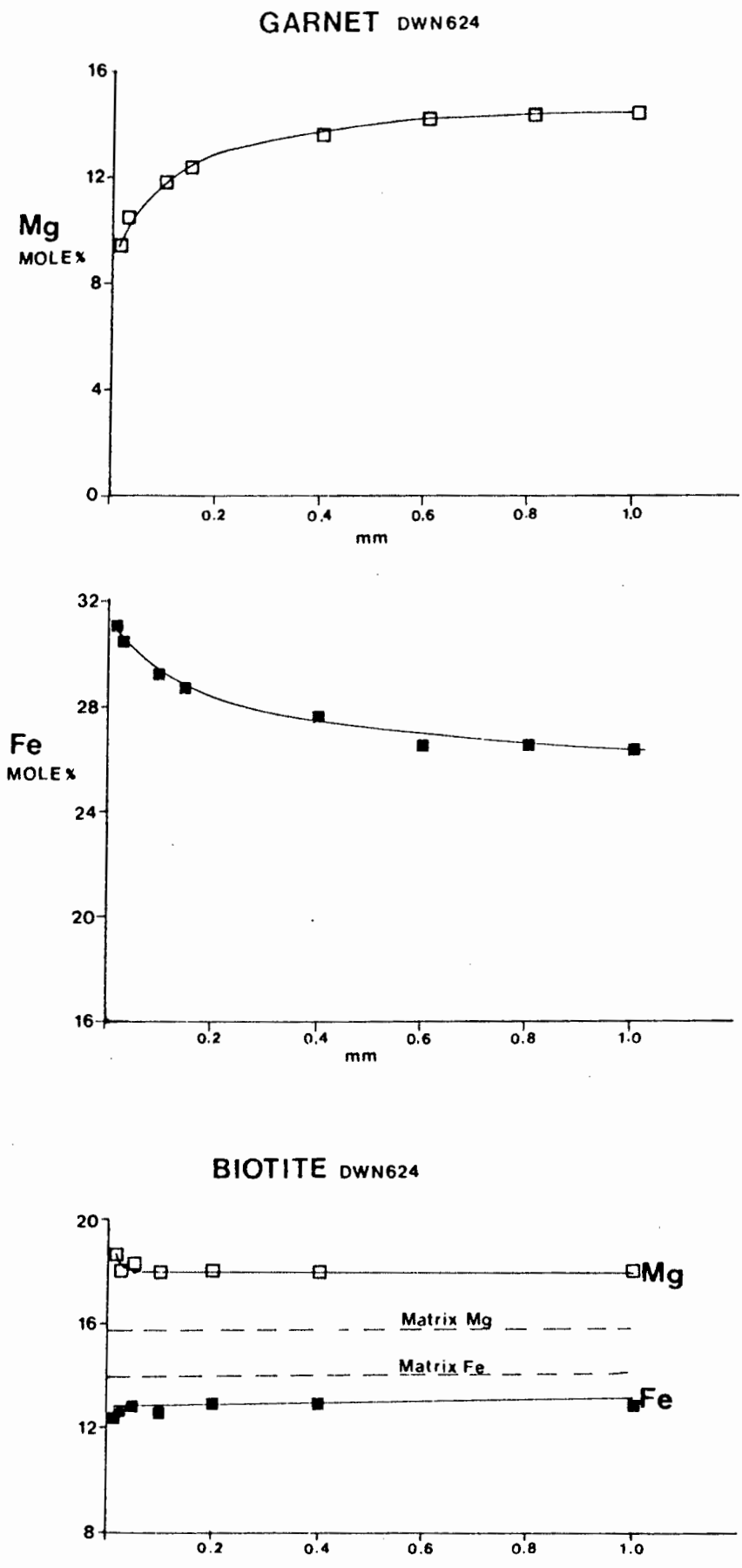

Fig. 6.13 Natural zonation profiles of garnet-biotite pair DWN624.

that elevated temperatures could have been maintained for a longer period (Waters, 1989). The preserved zonation profiles preclude very rapid cooling. The limits on cooling given here span most of the range of other Proterozoic terranes and hence are not diagnostic of an particular setting or mechanism.

6.6 DEHYDRATION EQUILIBRIA AND PARTIAL MELTING

The breakdown of biotite occurs to produce garnet-cordierite gneisses. The migmatitic nature of most of these rocks suggests that biotite breakdown proceeds via melting reactions. Melting in pelitic gneisses in Namaqualand is covered in some detail by Waters (1988) and by Baars (1990). The important equilibria are briefly summarised below. On increasing temperature during prograde metamorphism the first melting reactions experienced are those involving free H_2O. Melting in a simple pelitic system, as shown in fig. 6.14 will follow the curve:

$$\text{Biot} + \text{Sill} + \text{Qtz} + \text{Plag} + H_2O = \text{L}$$

Melting will commence in more Fe-rich bulk compositions. The amount of melt produced will depend on the amount of H_2O available, this may already be very low in amphibolite-facies rocks. The melt produced will be a granite minimum, quartz, k-feldspar.

The most significant melt generating breakdown reactions will be those which are vapour absent:

$$\text{Biot} + \text{Sill} + \text{Qtz} + \text{Plag} = \text{Kfsp} + \text{Gar/Crd} + \text{L}$$

The vapour-absent reactions occur at the isobaric-invariant intersections between subsolidus dehydration reactions and the water-undersaturated solidus. In a vapour-absent pelitic gneiss biotite is stable up to temperatures at which the above reaction takes place. The vapour-absent reaction will proceed until one of the reactant phases is used up. For pelitic gneisses with large biotite contents (>25%) the amount of liquid produced may exceed 40% by volume (Clemens & Vielzeuf, 1987). Most pelitic gneisses in this study contain quartz in greater abundance than biotite, therefore biotite is usually the first of the reactant phases to be exhausted, but quartz content may be critical in very silica-poor, magnesian pelitic

bulk compositions. In the case of some semi-pelitic gneisses sillimanite may be a limiting factor on the amount of melt generated. Melting in pelitic system will occur in the presence or absence of plagioclase.

Dehydration and melting equilibria in the pelitic system have to be considered as continuous reactions involving Fe-Mg. The important dehydration reaction:

$$\text{Biot} + \text{Sill} + \text{Qtz} = \text{Gar} + \text{Kfsp} + H_2O$$

begins in Fe-rich compositons and shifts to Mg-rich compositions on increasing temperature (figs. 6.14 and 6.15). However, the cordierite producing reactions act in the opposite sense, shifting to Fe-rich compositions with increasing temperature. The garnet and cordierite producing reactions converge at the isobaric-invariant point, the vapour-absent reaction:

$$\text{Biot} + \text{Sill} + \text{Qtz} + \text{Plag} = \text{Gar} + \text{Crd} + \text{Kfsp} + \text{L}$$

At temperatures above this point vapour-absent melting may continue via the reaction:

$$\text{Biot} + \text{Crd} + \text{Qtz} + \text{Plag} = \text{Gar} + \text{Kfsp} + \text{L}$$

The nature of exchange substitutions in biotite, particularly the role of Ti, F and Al (eastonite) are poorly understood, but it is likely that the above reactions are displaced over a wider spread of $T\text{-}X_{H2O}$ conditions.

Published estimates of rheologically critical melt percentages are in the range 20-35 vol% melt (Arzi, 1978). Field evidence from this area indicates that some of the melt produced has remained in-situ. However, the large sheet-like leucosomes indicate that larger scale mobilisation has taken place. Unless melting is fluid-present and accompanied by very high a_{H2O} it is unlikely that quartzo-feldspathic gneisses can generate large amounts of melt (Clemens & Vielzeuf, 1987). The existence of a number of quartzo-feldspathic gneisses showing well developed compositional banding and gradational contacts with other metasediments indicates that the biotite-absent, quartzo-feldspathic lithologies have not been extensively mobilised. It is believed that the sheeted leucosomes may represent water-

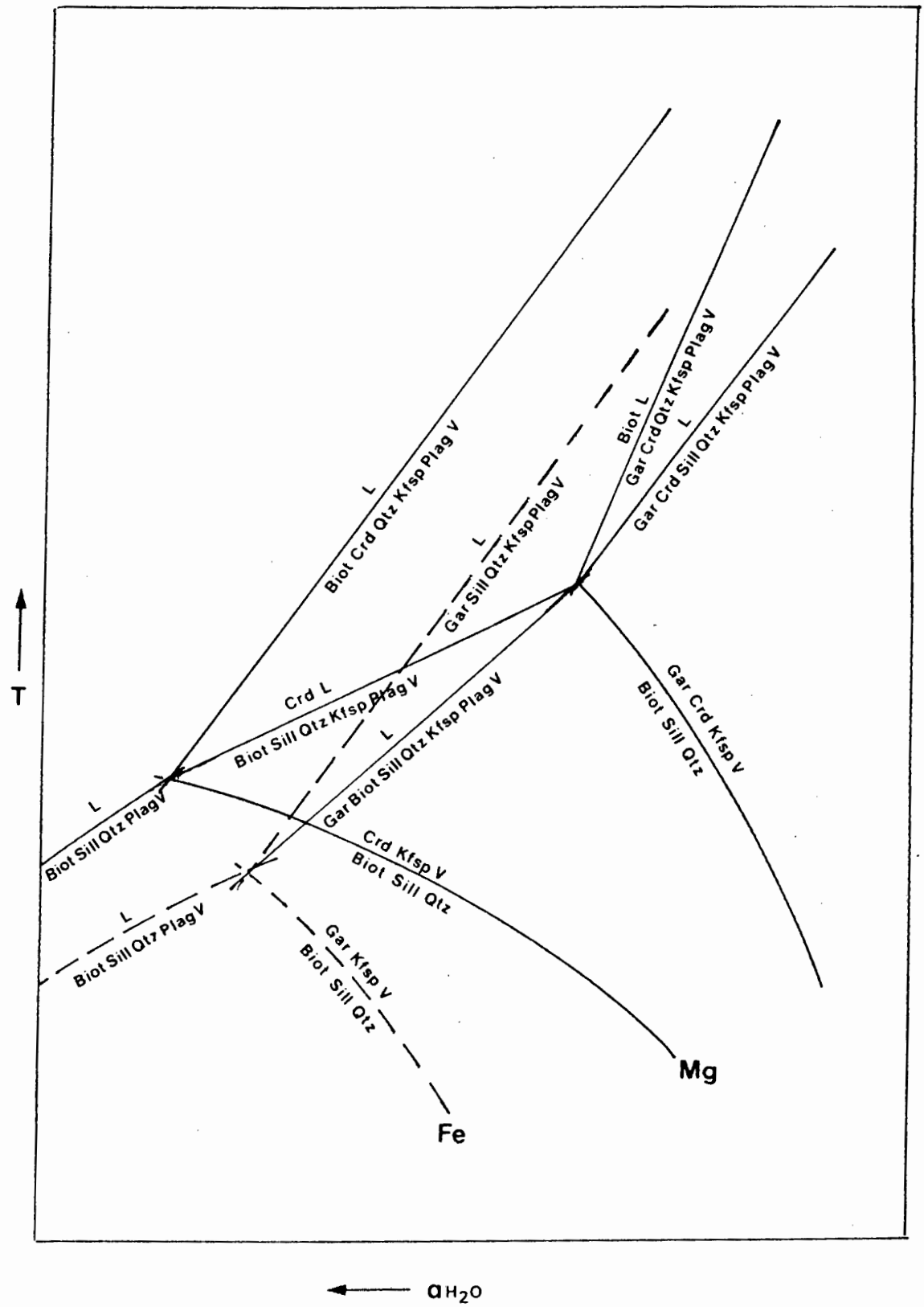

Fig. 6.14 Dehydration and melting curves for pelitic gneisses in the system K_2O-Na_2O-FeO-MgO-Al_2O_3-Si_2O-H_2O at 5 kb. Curves for Fe and Mg end-members after Waters (1988).

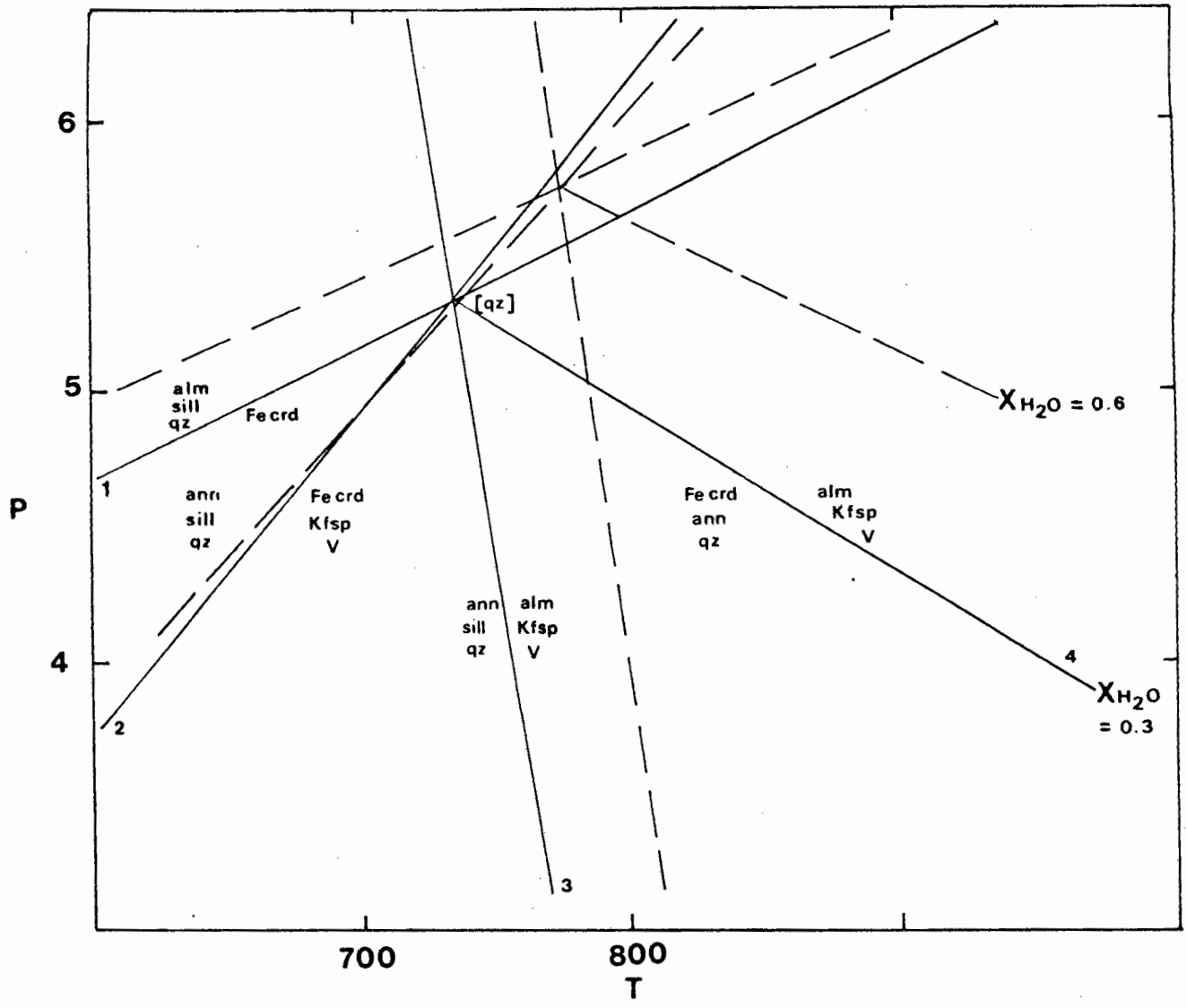

Fig. 6.15 Dehydration equilibria in the system K_2O-FeO-Al_2O-SiO_2-H_2O (KFASH).

saturated melting of a pelitic source. Due to the high viscosity of these melts (Wickham, 1987) their migration may be of limited extent.

6.6.1 Water activity

The pressure-temperature relations of important dehydration-reactions in the simple pelitic system KFASH, calculated from the the thermodynamic data base of Holland & Powell (1987) using the program THERMOCALC (Powell & Holland, 1990) are shown in fig. 6.15. Reactions such as:

annite + sillimanite + quartz = almandine + K-feldspar + vapour

are displaced by decreasing water activity to lower temperatures and are insensitive to pressure changes.

Water activity can be calculated in pelitic gneisses using equilibrium amongst biotite, sillimanite, quartz, garnet and K-feldspar, following the method of Phillips (1980).

$$KFe_3AlSi_3O_{10}(OH)_2 + Al_2SiO_5 + 2SiO_2 = KAlSi_3O_8 + Fe_3Al_2Si_3O_{12} + H_2O$$

Annite + Sillimanite + Quartz = Almandine + K-Feldspar + Water

Where, $a_{ann,biot} = X_K.(X_{Fe})^3.X_{Al}.(X_{Si})^3.(X_{OH})^2$

and $a_{alm,gar} = (X_{Fe})^3$

Thermodynamic data for the reaction was taken from the data base of Holland & Powell (1990). In all cases the activity of K-feldspar, quartz and sillimanite are considered to equal unity. A maximum estimate of X_{H2O} can be made from pelitic gneisses that contain the above assemblage minus sillimanite, sillimanite being used up during the progress of biotite dehydration. Values for X_{H2O} were modelled using the computer program THERMOCALC (Holland & Powell, 1990). Table 6.3 gives the K_D for the reaction above :

TABLE 6.3

X_{H2O} estimates for pelitic gneisses containing the assemblage biotite- quartz- garnet- K-feldspar ± sillimanite

Sample	X_{ann}	X_{alm}	lnK_D	Temperature 750°C X_{H2O}	Temperature 800°C X_{H2O}
MCS322	0.0185	0.326	2.869	0.25	0.35
MCS393	0.0145	0.284	2.975	0.22	0.31
VD3	0.0270	0.396	2.686	0.31	0.43
Sillimanite-absent samples					
MCS332	0.0172	0.248	2.669	0.31	0.44
MCS343	0.0318	0.377	2.473	0.40	0.57
MCS394	0.0229	0.296	2.559	0.35	0.49
MCS395	0.0221	0.267	2.492	0.39	0.56

Water activities calculated for pelitic gneisses with the water-buffering assemblage biotite-garnet-sillimanite-quartz-K-feldspar yield values for X_{H2O} between 0.22 and 0.43, depending on the assumed peak temperature. However, most pelites show evidence of having undergone vapour-absent melting and thus were able to define X_{H2O} at higher values. It is only when the melt crystallizes and H_2O is released that X_{H2O} drops to zero, as a_{H2O} in a system undergoing vapour-absent partial melting is buffered as long as the melt coexists with biotite.

The lack of retrograde biotite is probably a feature of the paucity of water in the fluid phase that accompanied retrograde cooling. Presumably most of the available fluid must have been taken-up by evolving partial melts. Water must then be released upon melt crystallisation. The presence of small amounts of biotite in some segregations probably represents a partial back-reaction. Ashworth & McLellan (1985) interpreted similar textures as being formed by retrograde reaction with crystallizing melt. However, the amount of retrograde biotite is too small to account for all the water in the melt. Waters (1988) discusses mechanisms which may prevent back-reaction between the crystallising melt and the anhydrous minerals of

the segregations. Waters favours the shielding of anhydrous minerals by the solid products of melt, there is textural evidence for this in the presence of quartz rinds around garnet. Waters also suggests kinetic inhibition of back-reactions by analogy with experiments on vapour-absent melting (Bohlen et al., 1983). Peterson & Newton (1989) indicate that reaction reversal in the vapour-absent melting of biotite -quartz takes place in a comparatively short time. This suggests that water would have to be rapidly channelised out of segregations in order to limit access to the anhydrous phases. Powell (1983) suggests diffusive loss of H_2O from the segregation back into the surrounding matrix, the process driven by water activity gradients set up by different internal buffering paths for the segregation and its host. More unlikely is that partial melting is followed by infiltration of CO_2, in effect reversing any rehydration reactions (Janardhan et al., 1982). The total removal of any melt generated is an obvious method of producing a dry restite (Fyfe, 1973) but is not consistent with the field or petrographic relationships given here or cited by Waters (1988).

The virtual absence of any back-reactions has important contraints on the form of the retrograde P-T-t path. As can be seen from fig. 6.15 the equilibria between garnet and cordierite (curves 1 and 4) are sensitive not only to changing temperature but also to changing pressure. A retrograde path that experiences high temperature decompression will intersect equilibria of the form:

$$Gar + Sill + Qtz = Crd$$

This would tend to produce corona-type textures of cordierite rimming garnet as recorded from other granulite terranes (Schenk, 1984 and Harley, 1989). The absence of decompression haloes around garnet favours an initial isobaric cooling episode for Namaqua granulites, see also Waters (1986a, 1986b).

6.7 SUMMARY

Field relationships in pelitic gneisses indicate local partial melting plays an important role in the amphibolite-granulite facies transition. Partial melting occurred in steps. Firstly, water-saturated partial melts formed layered migmatites during D_2 deformation. Secondly, at higher temperatures, vapour-absent partial-melting produced coarse-grained garnet or cordierite-bearing segregations, formed syn- to post-tectonic in relation to D_3 deformation.

The textures observed suggest that the growth of garnet and cordierite was a single step process, and that prexisting fabric has been largely overgrown by granulite-facies porphyroblasts, some following compositional heterogeneties in mimetic fashion.

Values for X_{H2O} amongst pelitic gneisses are calculated from the water buffering equilibria:

annite + sillimanite + quartz = almandine + K-feldspar + H_2O

Values are around 0.3. Pelites having undergone partial melting define values for $X_{H2O} \approx 0$ after devolatilisation upon melt crystallisation.

Garnet zonation patterns indicate local reequilibration with adjacent biotite. The model of Lasaga (1983) has been applied to diffusion exchange of Fe-Mg between garnet and biotite. The results of this approach indicate slow to moderate cooling rates of around 5-20°C/m.y. The absence of decompression haloes of cordierite around garnet are taken as evidence for isobaric cooling. From the diffusion data available it appears that temperatures deduced from equilibria involving garnet (see Chapter 4) probably give good estimates of the actual peak thermal conditions.

CHAPTER 7

THE PETROLOGY OF CALC-SILICATE ROCKS

7.1 INTRODUCTION

Calc-Silicate gneisses and granofelses occur as small lenses and bands in most of the supracrustal sequences across Namaqualand (Moore, 1988; Albat, 1984 and Jackson, 1976). In the Buffels River area they occur towards the base of the sequence commonly associated with mafic and quartzo-feldspathic gneisses. On the basis of whole-rock geochemistry, Moore (1988) interprets plagioclase-garnet and plagioclase-clinopyroxene-bearing calc-silicate rocks as being derived from carbonate-alumino-silicate protoliths (marls) possibly derived from degraded mafic volcanics. The best developed thicknesses of calc-silicate rocks are on the farm Rietfontein, at a locality known as Bobbejaanpoort. In these rocks are local concentrations of REE-bearing granofelses, containing the mineral allanite. Another locality at Smorgen-Schaduwe in the Kangnas mountains area is also described. In this chapter the petrography, mineral chemistry and progressive metamorphism of calc-silicate assemblages is described. The formation of allanite-rich granofelses is discussed.

7.2 PETROGRAPHY

Calc-silicate granofelses are coarse to medium grained granoblastic rocks composed of plagioclase and dark coloured ferro-calcic silicates, the most important of which are garnet, clinopyroxene, amphibole, and local concentrations of REE-rich allanite. Calc-silicate granofelses have variable quartz contents, with quartz-absent lithologies and quartz-rich rocks (quartz forming >30% of the mode). Many of these rocks have granoblastic textures without well developed compositional or gneissose banding thus the term granofels is used, some varieties show strongly banded textures and are termed gneisses. Rock types considered to be part of the calc-silicate group have the following petrographic features in common: the absence of K-feldspar, high oxide content, and the conspicuous presence of titanite. These features can be used to

distinguish calc-silicate rocks from quartz-rich mafic gneisses and plagioclase-rich quartzo-feldspathic rocks. Table 7.1 lists the modal proportions for calc-silicate rocks from this study. Clinopyroxene is given as either hedenbergite (Hed) or diopside (Di) on the basis of colour, hedenbergite is recognised by a dark green colour.

Plagioclase is the major constituent of these calc-silicate rocks and usually occurs as granoblastic mosaics of equidimensional grains. It is mostly unzoned and generally contains numerous inclusions of quartz, apatite, and in some samples, allanite and zircon.

Clinopyroxene occurs as pale green diopside in well banded, pale coloured plagioclase-rich gneisses, and as dark green hedenbergite in dark coloured granofelses. In most samples it occurs as polygonal grains. Large crystals occur in sample MCS350 and contain hundreds of tiny rutile inclusions. In sample MCS351 clinopyroxene is rimmed by garnet and in places totally replaced by a symplectite of andradite, magnetite and quartz (see plates 7.1, 7.2). The symplectite is best developed adjacent to quartz veins.

Garnet is dark brown in hand specimen, orange in thin section. It is associated with clinopyroxene as either thin rims or vermicular intergrowths. In pyroxene-free rocks it forms large (up to 20 mm) dendritic poikiloblasts enclosing plagioclase and allanite (see plate 7.3).

Amphibole occurs in small amounts in a few calc-silcate rocks. It tends to be restricted to more Mg-rich bulk compositions, found in association with diopside and absent from garnet-bearing samples. Only in sample SS18 is amphibole found together with hedenbergite. This amphibole has a very strong pleochroism from dark-green to green to yellow-green and is thought to be an Fe-rich pargasite. Amphibole in SS18 forms idioblastic poikiloblasts with small rounded grains of plagioclase and quartz as inclusions. Most amphibole is sub-idioblastic, inclusion free and is in textural equilibrium with diopside.

Titanite occurs in most calc-silicate rocks and varies in abundance from a few small xenoblastic inclusions to large aggregates of grains forming up to 8% of the mode. Most grains are non-metamict and range in colour from pale-cinnamon brown to bright orange. Metamict crystal of titanite composition are bright golden in colour

and surrounded by radiating cracks. Titanite is also found forming fine rims aroung magnetite.

Quartz is present in calc-silicate rocks either as a disseminated xenoblastic matrix mineral together with plagioclase, or as coarse veinlets.

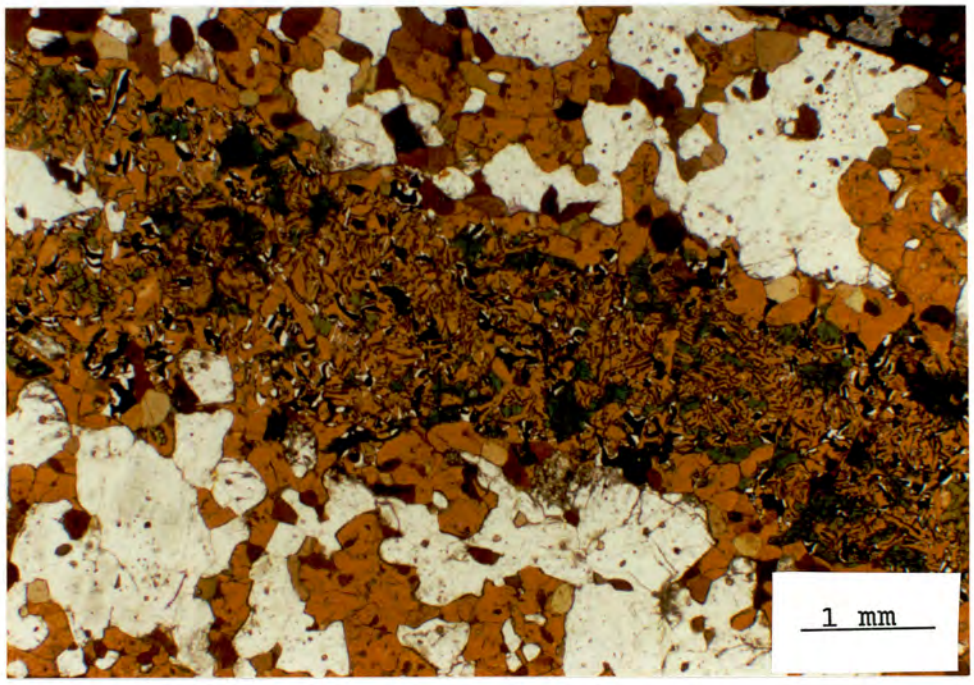

Plate 7.1 Vein-like symplectite of garnet, quartz and magnetite replacing clinopyroxene (green) in calc-silicate granofels. PPL. MCS350. Bobejaanpoort, Reitfontein.

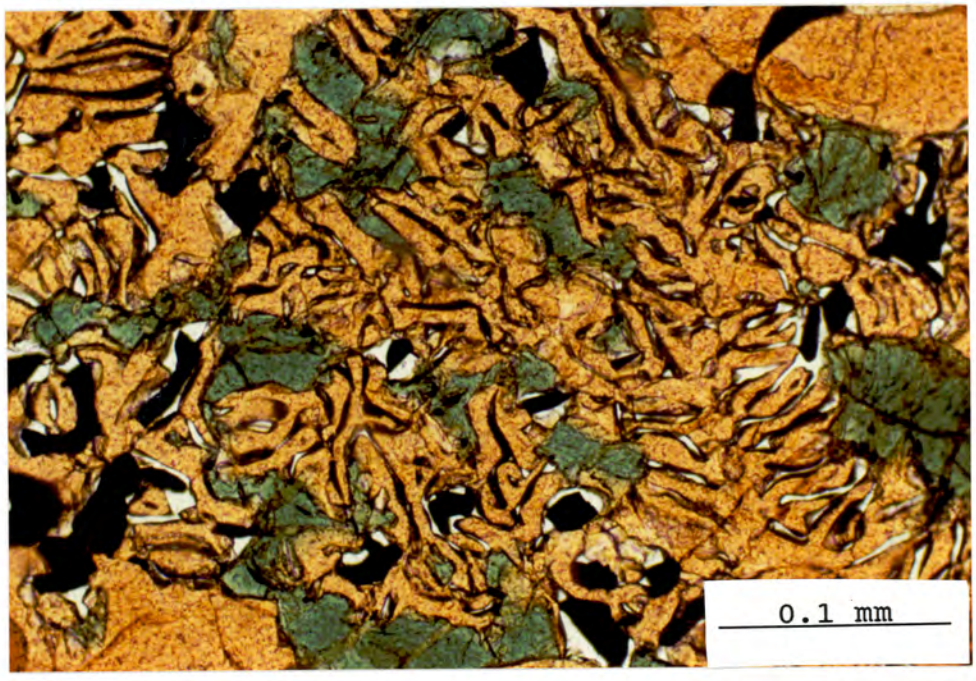

Plate 7.2 Detail of symplectite showing vermicular intergrowth of garnet, quartz and magnetite replacing clinopyroxene (green, relic grains). PPL. MCS350. Bobejaanpoort, Rietfontein.

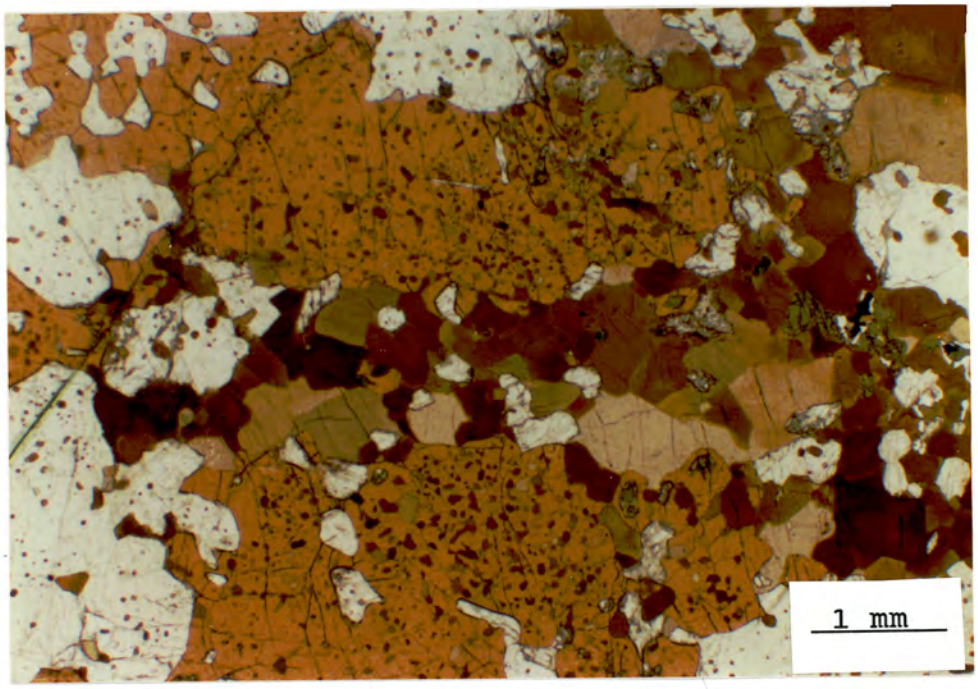

Plate 7.3 Poikiloblastic garnet with rounded inclusions of allanite (brown). Centre occupied by granoblastic allanite and plagioclase. PPL.
SS4. Smorgen Schaduwe.

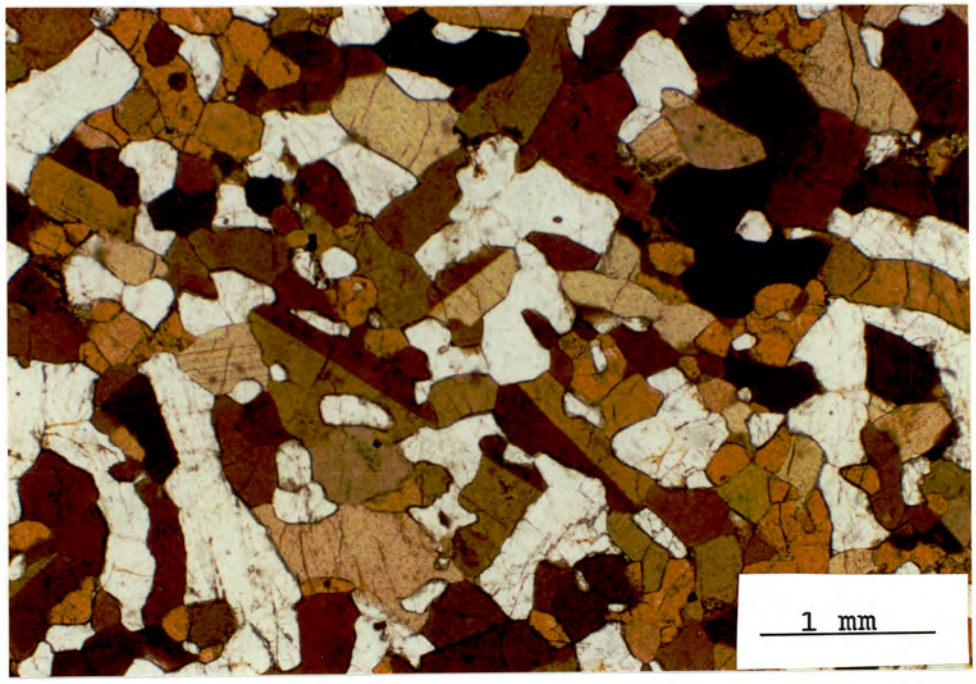

Plate 7.4 Granoblastic allanite (brown with simple twinning) and plagioclase in allanite-rich calc-silicate granofels. PPL.
MCS350. Bobejaanpoort, Rietfontein.

TABLE 7.1

Modal proportions for Calc-silicate assemblages

Sample	Cpx	Gar	Plag	Qtz	Ttn	Amph	Oxide	Other
*MCSR01	25 Hed	20	47	-	5	-	3	-
*MCSR02	9 Di	-	78	-	6	-	7	-
MCSR03	10 Di	-	49	35	tr	1	5	-
MCS310	35 Hed	-	52	-	8	-	tr	Apat 5% Zir
*MCS319	35 Di	-	9	50	2	-	1	Scheelite 3%
MCS319	18 Di	-	34	45	tr	-	1	Scheelite 2%
*MCS338	7 Di	-	83	-	6	-	4	Apat
MCS338	8 Di	-	83	-	6	tr	3	Apat
MCS339	-	-	95	-	1	-	2	Apat
MCS340$_A$	4 Di	-	58	36	-	-	2	Apat
MCS340$_B$	23 Hed	3	60	10	tr	-	4	Apat Rut
MCS340$_C$	19 Hed	8	59	10	-	-	4	Apat Rut
MCS341	4 Hed	26	55	15	-	-	tr	Zir
MCS342	-	38	58	-	4	-	-	-
MCS346	6 Di	-	34	55	2	-	3	Apat
MCS347	5 Di	-	52	40	1	-	2	Apat
MCS348	-	-	55	33	-	10	2	Apat Zir
MCS349	-	-	50	45	tr	3	2	Apat
*MCS350	13 Hed	2	43	19	1	-	2	Alln 20% Rut
MCS350	9 Hed	19	43	4 vein	1	-	1	Alln 22% Rut
*MCS351	4 Hed	22	55	1	1	-	3	Alln 14% Rut
MCS351	12 Hed	1	30	35 vein	1	-	5	Alln 16% Rut
MCS352	4 Di	-	88	5	1	-	2	-
MCS367	14 Hed	tr	31	45	2	-	3	2nd Zois 5%
MCS371	1 Hed	19	59	15	3	-	3	-
MCS378	7 Hed	10	57 altd	-	1	-	tr	2nd Epid 25%
MCS381	2 Hed	14	44	40	tr	-	-	Zir
MCS402	-	-	65	30	1	-	3	Apat Zir
MCS407	3 Di	-	41	45	2	8	1	Apat Zir
MCS408	11 Di	-	77	-	1	8	3	Apat Zir

Northern areas

	Cpx	Gar	Plag	Qtz	Ttn	Amph	Oxide	Other
SS3	28 Di	-	57	12	-	3	-	Apat
*SS4	5 Hed	16	40	4	tr	-	tr	Alln 33% Scap2%
SS4	1 Hed	32	50	4	tr	-	tr	Alln 13%
*SS18	2 Hed	-	73	12	1	-	2	Alln 10% Apat
*SS18$_A$	4 Hed	-	70	15	2	7	tr	Alln 2% Apat
*SS18$_B$	15 Hed	-	68	8	2	-	1	Alln 6% Apat
MCS216	30 Di	-	55 altd	10	tr	-	5	Apat
MCS218	33 Di	-	47	15	-	-	5	-
MCS222$_A$	26 Hed	8	56	7	-	-	1	2nd Musc 2%
MCS222$_B$	10 Hed	2	53	35	tr	-	tr	2nd Musc
MCS223	36 Di/Hed	2	50 altd	10	tr	-	2	2nd Musc
MCS224	7 Hed	13	73	5	tr	-	2	-
MCS232$_A$	10 Di	4	38	48	tr	-	-	-
MCS232$_B$	12 Di	-	38	50	tr	-	-	-
MCS233	14 Di	-	69	26	tr	-	1	-
MCS234	8 Di	-	11	80	tr	-	1	-
MCS236	32 Hed	38	30	-	-	-	tr	-

Compositional banding is evident in the samples from Smorgen Schaduwe, SS18 is a feldspathic granofels with over 70% plagioclase, allanite is the dominant ferro-calcic constituent. Bands rich in allanite, titanite, garnet or clinopyroxene occur interspersed with feldspathic layers. SS4 from the same locality is more massive and much darker in colour, allanite is evenly distributed throughout comprising over 30% of the mode. Samples from Rietfontein, MCS350 and MCS351 also contain large amounts of granoblastic allanite in boudinaged pods, which are cut by abundant sigmoidal quartz veins.

Allanite shows several textural variations in calc-silicate rocks. In the allanite-rich pods, it occurs as medium grained (up to 1mm) brown to red-brown, tabular sub-idioblastic crystals showing simple twinning (see plate 7.4). In most samples the allanite is non-metamict and grains show mutual 120° contacts. One sample shows evidence of metamictisation, in this case allanite forms a partial rim and vermicular intergrowth with titanite. Observations of rounded metamict inclusions within plagioclase in calc-silicate rocks from Namaqualand tentatively described as allanite by Albat (1984) are identified as being thorium-bearing titanites.

Pleochroism in allanite is from light brown, X to brown, Y to dark reddish brown, Z. Metamict grains are very dark brown and are almost isotropic. Optical zonation occurs with most grains having darker cores with distinct narrow (50 μm) pale coloured rims. In the allanite-rich pods the zoning is more complex with large grains having light coloured cores that grade progressively into darker mantles with fine impersistent light coloured rims.

Numerous small rounded inclusions in plagioclase and garnet produce a remarkable sieve texture in the host poikiloblast (see plate 7.5).

Scapolite occurs as a minor constituent of sample SS4 in small aggregates associated with garnet-rich domains.

Magnetite is the common oxide phase observed in most calc-silicate rocks. It occurs as rounded xenoblastic grains. Some grains are up to 3 mm in size and often show fine rims of titanite. In symplectitic intergrowths the magnetite forms small arcuate plates.

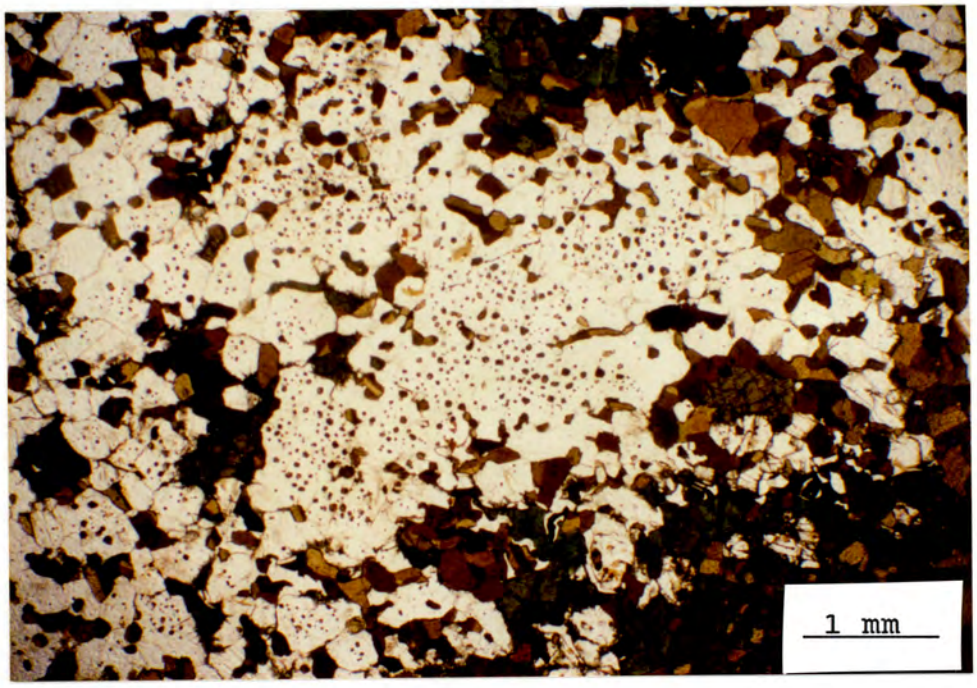

Plate 7.5 Sieve textured plagioclase with many tiny inclusions of rounded allanite. In calc-silicate granofels. PPL.
MCS351. Bobejaanpoort, Rietfontein.

Apatite and zircon are conspicuous accessory phases in the rocks from Smorgen-Scaduwe. Scheelite is found forming a thin continuous band in one sample, MCS319 from Hytkoras.

7.3 MINERAL CHEMISTRY

7.3.1 Clinopyroxene

All clinopyroxenes analysed in this study come from Fe-rich calc-silicate rocks and plot in the hedenbergite field of the pyroxene quadrilateral (Morimoto et al., 1988), see fig. 7.1. All clinopyroxenes show marked substitution of Fe^{3+} and Al^{3+} for Fe^{2+} and Si^{4+}. Fe^{3+} is greater than 0.1 cation units per 6 oxygens. Zonation is weak, but Mg and Al increases towards the rims with Fe and Si decreasing.

7.3.2 Garnet

Garnets are andradite-rich (>60% andradite molecule) with varying proportions of the grossular and almandine molecules, with low spessartine content and a virtual absence of the pyrope component. Fig. 7.2 gives the composition of garnet plotted on the ideal plane andradite-grossular-pyralspite. Zonation is limited, although MCS351 shows a decrease in Al and an increase in Fe^{3+} towards the rim where the garnet is in contact with clinopyroxene. There are no major compositional differences between large garnet poikiloblasts and fine grained garnet present as rims around clinopyroxene or symplectite garnet.

7.3.3 Plagioclase

More Fe-rich calc-silicate rocks with significant amounts of clinopyroxene and garnet present have highly calcic bytownite as the dominant matrix mineral. In the highly feldspathic banded rock SS18 the plagioclase is a sodic andesine. There is little zonation present in any of the samples analysed.

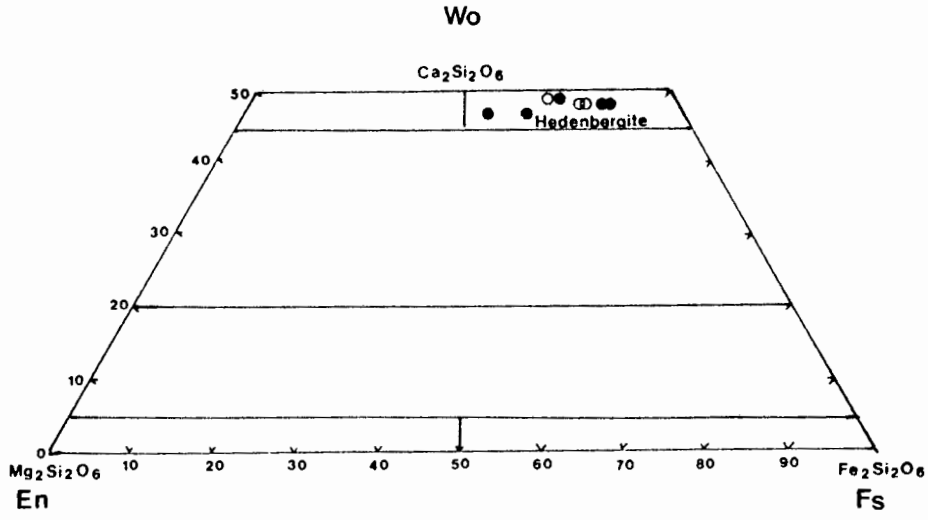

Fig. 7.1 Composition of clinopyroxene in calc-silicate rocks

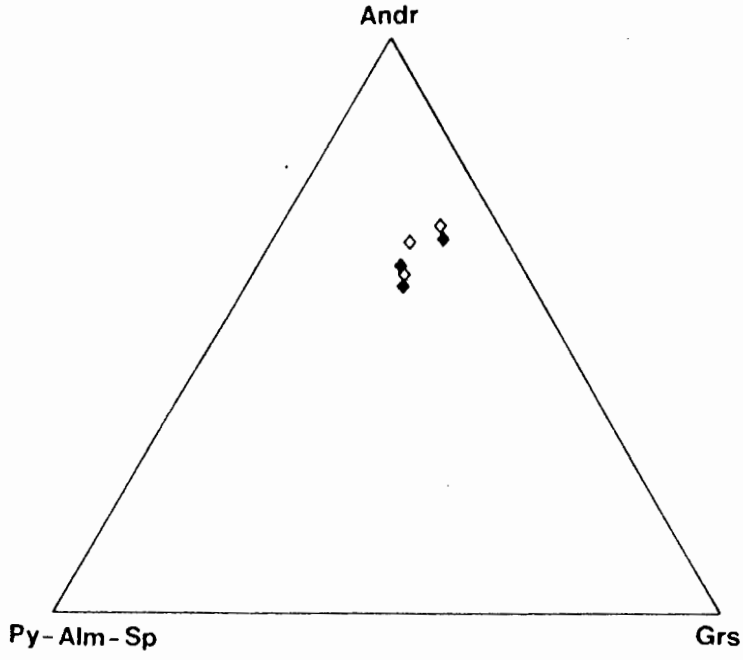

Fig. 7.2 Composition of garnet in calc-silicate rocks.

7.3.4 Scapolite

Scapolite is found in a single sample SS4. It is dominantly meionite. It is impossible to determine the role of CO_3, SO_4 and OH in the formula, but from stoichiometric considerations (see Appendix) there is insufficient Ca for CO_3 to be the only volatile component in the scapolite.

7.3.5 Allanite-(Ce)

Analyses of allanite, see table 7.2, indicate relatively low REE contents compared to published analyses from a variety of lithologies (Cech et al., 1972; Rao et al. , 1979; Harding et al., 1982; Andersen, 1986). The absence of thorium and uranium accounts for the non-metamict nature of most of the allanite. It is suggested that metamict allanite found intergrown with titanite in sample SS18c has gained thorium from the parent titanite.

Allanite is enriched in light REE particularly Ce, with La and Nd present in appreciable amounts. Ce content ranges from 12.71 to 8.85 weight %. La content ranges from 7.40 to 5.01 weight %, and Nd content ranges from 1.88 to 1.49 weight % . The Ce-La ratio is slightly less than 2:1 and does not vary from core to rim, although overall REE content decreases by between 2 and 4 weight %.

Fe is probably present as both ferrous and ferric forms. All analyses are given with Fe_2O_3 calculated on the basis of stoichiometry as outlined by Droop (1987).

Zonation is present in all samples, normally limited to narrow rims characterised by a decrease in REE with a corresponding increase in Ca. Increasing Al at the rims is accompanied by a decrease in Fe^{2+}. In SS4 the optical zonation pattern is more complex. Microprobe analysis indicates a wide REE-rich mantle around a slightly REE depleted core with the usual narrow Ca-Al-rich rim at the contact with adjacent plagioclase, see fig.7.3. Exley (1980) finds similar zoning in allanites from granites to that seen in the Namaqualand samples, particularly the marked Al enrichment on the rims. Fig. 7.4 shows the relationship between Ca + Al and REE + Fe. Much of the

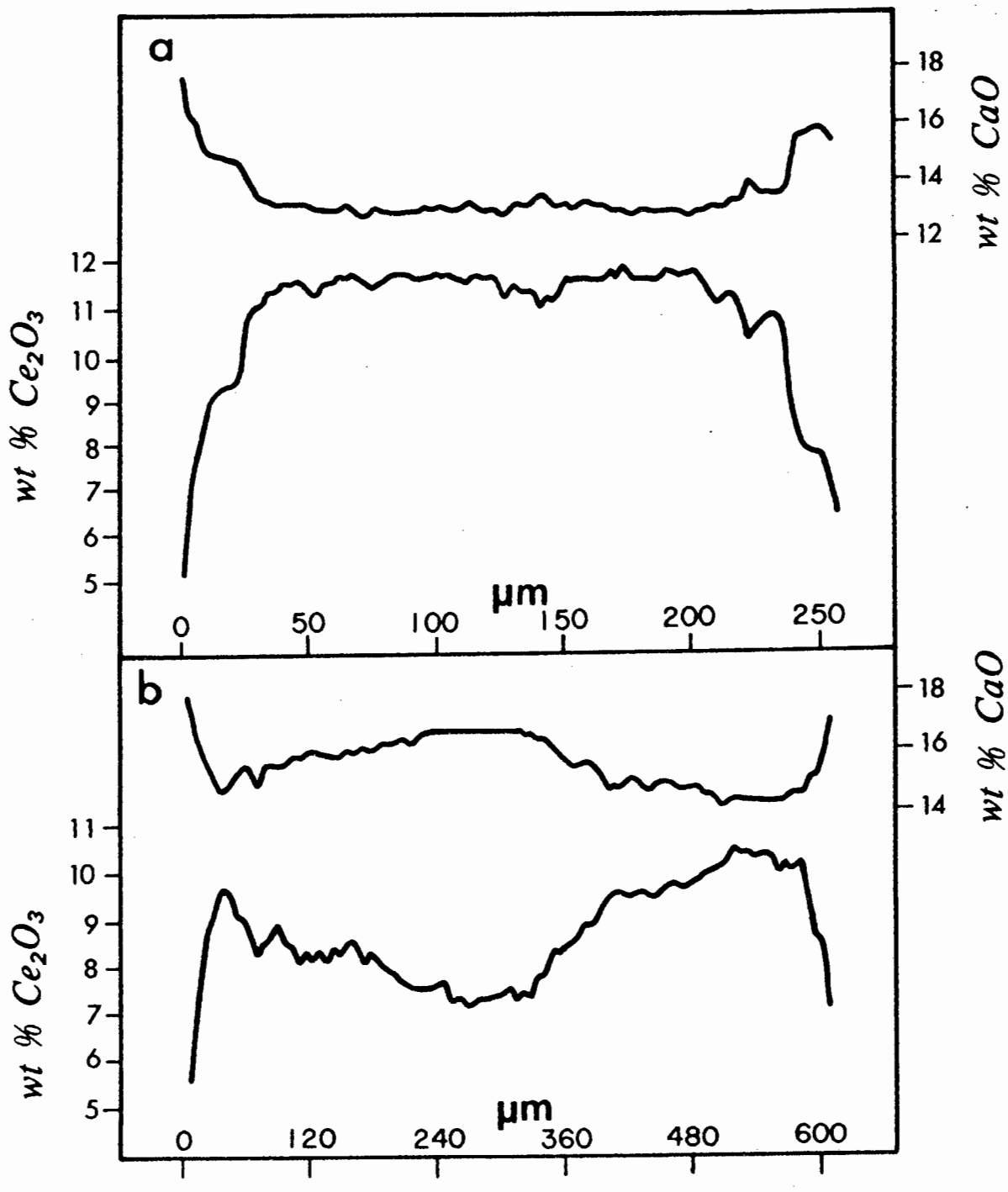

Fig. 7.3 Zonation in allanite from sample SS4. Adjacent crystals are plagioclase in both a and b.
a. the most common profile with low Ce_2O_3 and high CaO at the rims with a wide core region of constant composition.
b. the above profile with a more complex core region of lower Ce_2O_3.

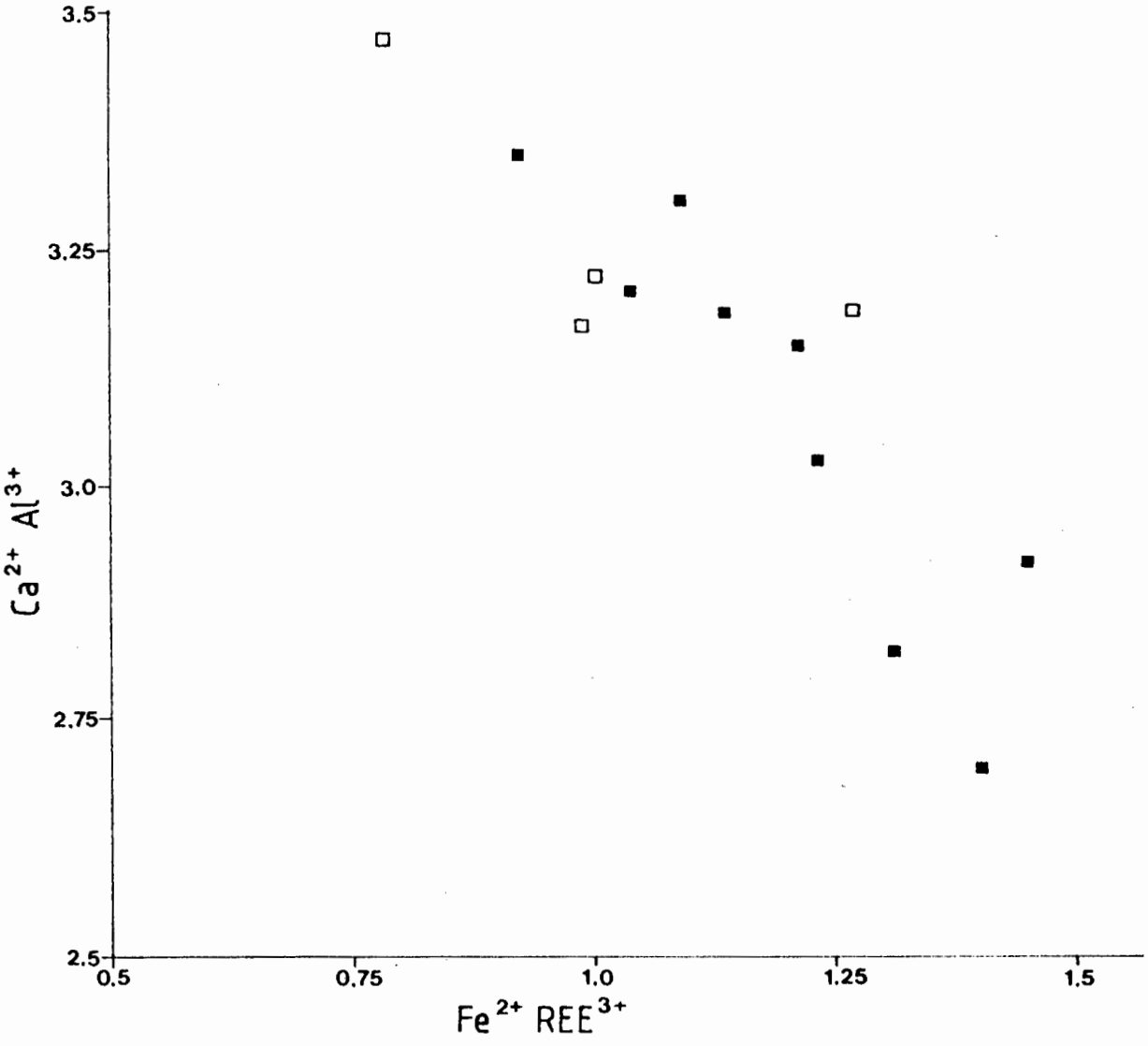

Fig. 7.4 Plot of Ca^{2+} Al^{3+} against Fe^{2+} REE^{3+} in allanite.
■Cores
□Rims

zonation observed follows the substitution mechanism:

$$Ca^{2+} \; Al^{3+}_{-1} = REE^{3+} \; Fe^{2+}_{-1}$$

Other substitution mechanisms involving Mg, Mn and Fe^{3+} may also have a role.

Metamictisation results in a dramatic reduction in Ca together with slight decreases in Ce and Fe. Low totals may indicate that H_2O has been introduced into the structure.

No fluorine was detected, in sharp contrast with the fluorian allanites from calc-silicate granulites described by Rao et al. (1979). It is therefore assumed that the Namaqualand allanite is hydrous and contains about 2 weight% H_2O.

Most of the samples have very similar composition with the individual bands in SS18 showing the highest REE contents, perhaps related to residual REE concentrations in the protolith.

7.3.6 Titanite

Coexisting titanites have relatively low concentrations of REE, commonly < 2 wt %. However, some allanite-free samples contain titanites with up to 3.5 wt % REE. The ratio of Ce:La:Nd is very different to that in allanites and shows a much greater spread of values, La is in much lower abundance, Ce is the dominant REE (Ce_2O_3 up to 2 wt %) see fig. 7.5. In rocks where allanite and titanite share mutual grain boundaries the titanites tend to have low REE contents. In sample SS18 the rocks show fine banding with single crystal layers of both allanite and titanite. Within such gneisses titanite shows considerable compositional variation from band to band. All titanites show wide departure from pure end-member titanite. The most important substitution is:

$$Al^{3+}_{-1} \; Ca^{2+}_{-1} = REE^{3+} \; Fe^{2+}$$

Thorium was detected in titanites from allanite-free rocks, and reaches 0.2 wt % in bright yellow metamict grains. No fluorine was dectected. Low totals and poor stoichiometry suggest the presence of small amounts of other elements. Nb and Y are likely, the low totals

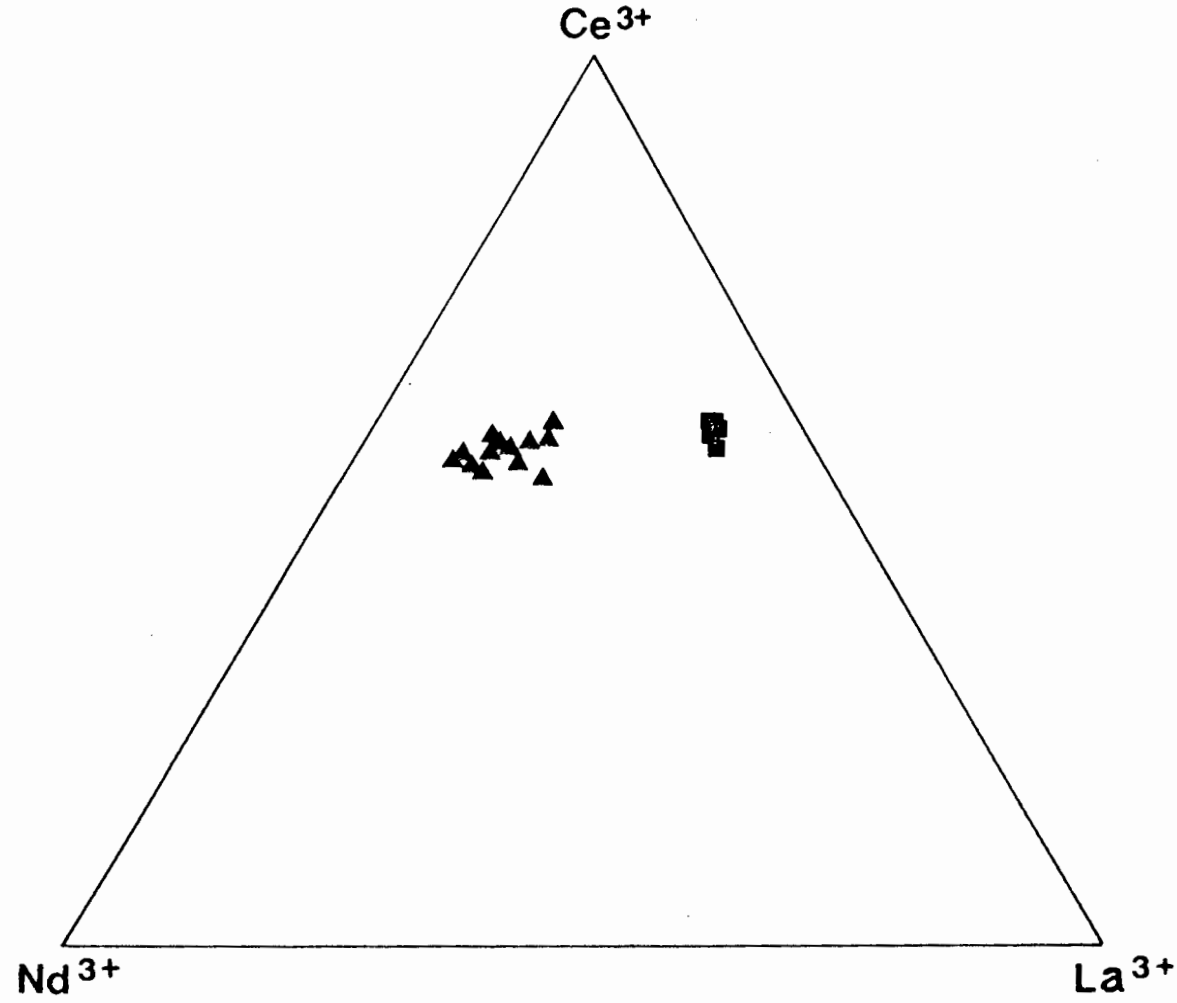

Fig. 7.5 Comparison of REE content of allanite and titanite.
■allanite
▲titanite

probably indicate extensive substitution of OH for O. Sample MCS356 provides a good illustration of the chemical variation in titanites from a single rock. Matrix grains, metamict grains and titanites rimming magnetite can be distinguished by variations in Al, Fe, Ca, REE and Th, see Appendix.

The chemistry of titanites suggest that most of the REE in these rocks is strongly partitioned into allanite when present. No other REE-bearing phases have been identified in these samples.

TABLE 7.2

CHEMICAL COMPOSITION OF ALLANITE FROM SMORGEN SCHADUWE

	SS4 core	SS4 mantle	SS4 rim	SS18 core	SS18 rim
SiO_2	32.73	32.09	33.31	31.60	32.81
TiO_2	0.33	0.30	0.26	0.43	0.27
Al_2O_3	16.96	16.15	17.56	14.59	16.40
Fe_2O_3	10.21	9.30	10.83	7.76	10.36
FeO	5.39	6.59	4.58	9.46	6.20
MnO	n.d.	n.d.	n.d.	0.28	0.29
MgO	0.30	0.34	0.23	0.51	0.38
CaO	15.77	14.35	16.93	13.03	15.04
La_2O_3	4.82	5.89	4.19	6.59	5.10
Ce_2O_3	8.86	10.27	7.38	11.36	8.89
Nd_2O_3	1.45	1.58	1.16	1.90	1.60
Pr_2O_3	0.65	0.76	0.53	0.85	0.69
F	n.d.	n.d.	n.d.	n.d.	n.d.
Total	97.47	97.62	96.96	98.36	98.03
	Stoichiometry based on 25 Oxygens				
Si	5.951	5.942	5.953	5.920	5.967
Ti	0.022	0.021	0.035	0.061	0.037
Al_{3+}	3.635	3.526	3.700	3.223	3.516
Fe^{3+}	1.397	1.294	1.457	1.094	1.391
Fe^{2+}	0.820	1.020	0.685	1.482	0.925
Mn	-----	-----	-----	0.044	0.045
Mg	0.081	0.093	0.061	0.142	0.103
Ca	3.072	2.847	3.242	2.615	2.931
La	0.323	0.402	0.276	0.456	0.342
Ce	0.590	0.697	0.483	0.779	0.592
Nd	0.094	0.105	0.074	0.127	0.104
Pr	0.015	0.051	0.034	0.058	0.046
F	-----	-----	-----	-----	-----
Sum	16.000	16.000	16.000	16.000	16.000

Fe^{3+} estimated after Droop (1987). n.d. below detection limit. See Appendix for analytical conditions. Analyses of allanites from other localities are given in the Appendix.

7.4 METAMORPHISM OF CALC-SILICATE ROCKS

There is a noticeable absence of carbonate-bearing assemblages in the Buffels River area. A single lens of marble occurring on the western edge of the farm Hytkoras was found to be highly altered, and the carbonate minerals present may have been secondary. The absence of carbonate is also a feature of most Fe-rich calc-silicate rocks in the amphibolite-facies zone of central Namaqualand (Albat, 1984). Thus, any major decarbonation reactions must have reached completion during the lower amphibolite-facies segment of the prograde metamorphic path. In view of the unusual bulk chemical composition of some of the calc-silicate rocks in this study it is possible that the precursor assemblages were dominated by epidote and iron oxides, rather than carbonate.

Field evidence for amphibolite-facies reactions in calc-silicate rocks comes from the Aus area of Namibia (Jackson, 1976). Plagioclase-quartz-epidote-titanite assemblages are stable at lower amphibolite-facies conditions in the north-western part of the Namaqualand Metamorphic Complex exposed in Namibia. Breakdown of epidote-group minerals occurs with increasing temperature to form garnet-plagioclase-quartz assemblages. Jackson (1976) records the presence of epidote grains as inclusions in poikiloblastic garnet.

Important reactions in the system $CaO-Fe_2O_3-FeO-Al_2O_3-TiO_2-SiO_2-H_2O-CO_2-O_2$ were modelled for a range of temperatures and pressures (fluid conditions taken as $x_{H2O} = 0.5$, $x_{CO2} = 0.5$, appropriate for upper amphibolite-facies conditions) using the thermodynamic database of Holland & Powell (1988). Useful equilibria are shown in fig. 7.6. Epidote breakdown commences at temperatures around 600°C following reactions such as:

4 Epidote + 3 Ilmenite + Quartz = 2 Hedenbergite + 4 Anorthite + 3 Titanite + 2 Magnetite + H_2O (1)

and

4 Epidote + 5 Ilmenite + 2 Quartz = Almandine + 3 Anorthite + 5 Titanite + 2 Magnetite + 2 H_2O (3)

Depending on the activity of H_2O, and CO_2 in carbonate-bearing rocks

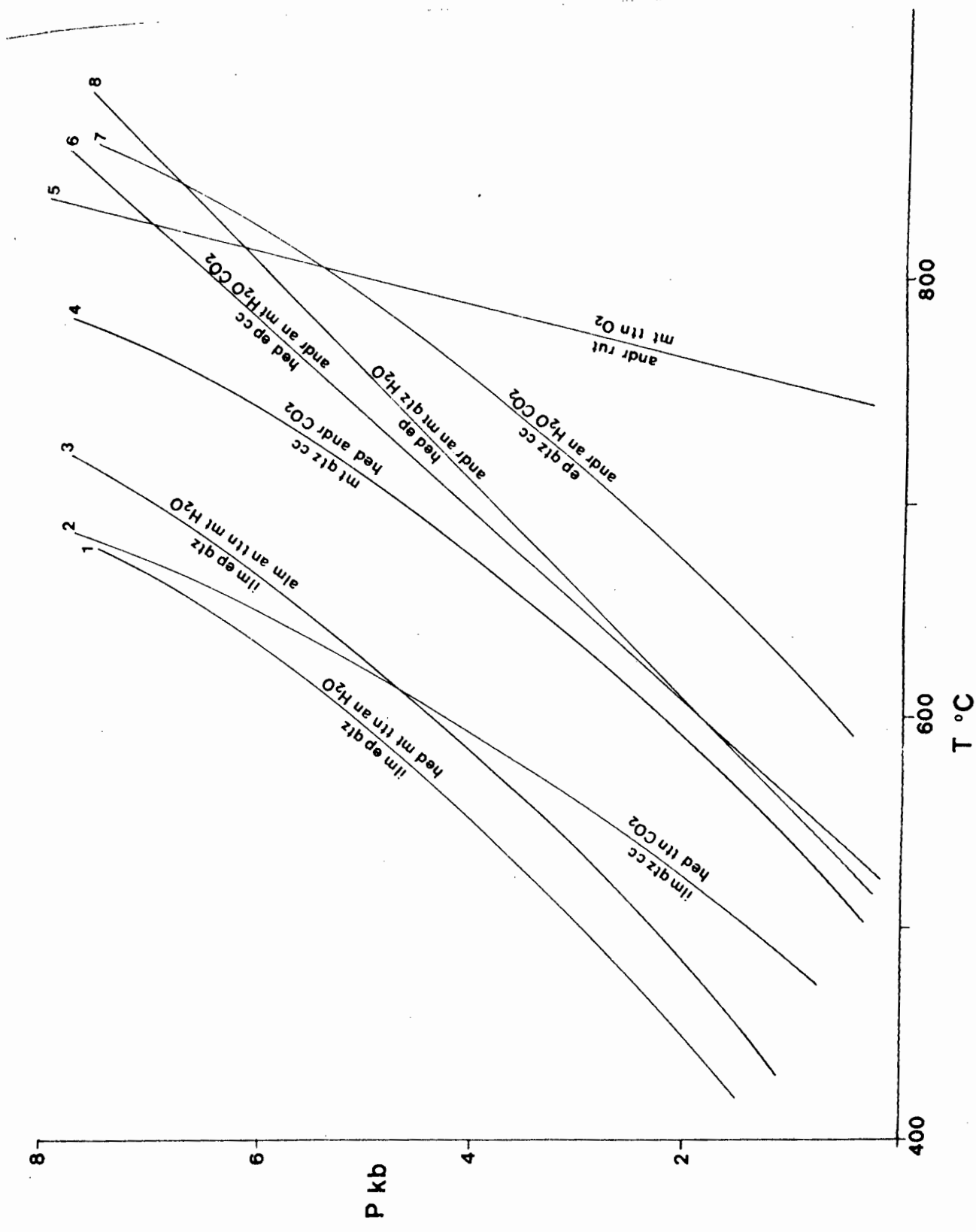

Fig. 7.6 P-T relations of reactions in the system: $CaO-Fe_2O_3-FeO-TiO_2-SiO_2-H_2O-CO_2-O_2$. $X_{H2O}=0.5$, $X_{CO2}=0.5$.

and oxygen fugacity the assemblage hedenbergite-titanite-plagioclase will develop at expense of epidote with increasing temperature. At higher temperatures epidote will react with hedenbergite to produce the assemblage andradite-plagioclase-magnetite-quartz via the reaction:

$$8\ \text{Epidote} + \text{Hedenbergite} = 3\ \text{Andradite} + 8\ \text{Anorthite} + \text{Quartz} + \text{Magnetite} + 4\ H_2O \quad (8)$$

There is no evidence of epidote as inclusions within garnet poikiloblasts to suggest that the above reaction is responsible for producing the characteristic garnet-clinopyroxene-bearing granofelses seen in this study. However, retrograde coronas of epidote around garnet observed by Albat (1984) suggest a reversal of reaction 8 with hydration on cooling.

Textural observations suggests that the assemblage hedenbergite-andradite is a prograde feature possibly formed by the breakdown of calcite-magnetite-quartz at upper amphibolite facies conditions:

$$\text{Magnetite} + 5\ \text{Quartz} + 4\ \text{Calcite} = \text{Hedenbergite} + \text{Andradite} + 4\ CO_2 \quad (4)$$

The reactions above and in fig. 7.6 indicate that calcite and epidote would be largely eliminated from Fe-rich calc-silicate rocks during progressive prograde metamorphism under amphibolite-facies conditions.

Textural evidence points to the importance of garnet growth at the expense of clinopyroxene at granulite-facies conditions. From the mineral compositions given in the Appendix (discussed in section 7.3) it can be seen that any reaction producing andradite-rich garnet from hedenbergite-rich clinopyroxene involves the oxidation of Fe^{2+} to Fe^{3+}. High temperature reactions in the system $CaO-FeO-Fe_2O_3-Al_2O_3-SiO_2-O_2$ were modelled using the computer program THERMOCALC (Powell & Holland, 1988). The P-T curves of important reactions are given in fig. 7.7, it can be seen that andradite-producing reactions (1,2,3 and 4) have steep P-T gradients, thus andradite is likely to be formed under conditions of increasing temperature with increasing oxygen fugacity. The T-f_{O2} relations of some of the reactions in fig. 7.7 have been calculated from the Holland & Powell data-base (1989) using the activities of solid-phases recorded in sample MCS350 and

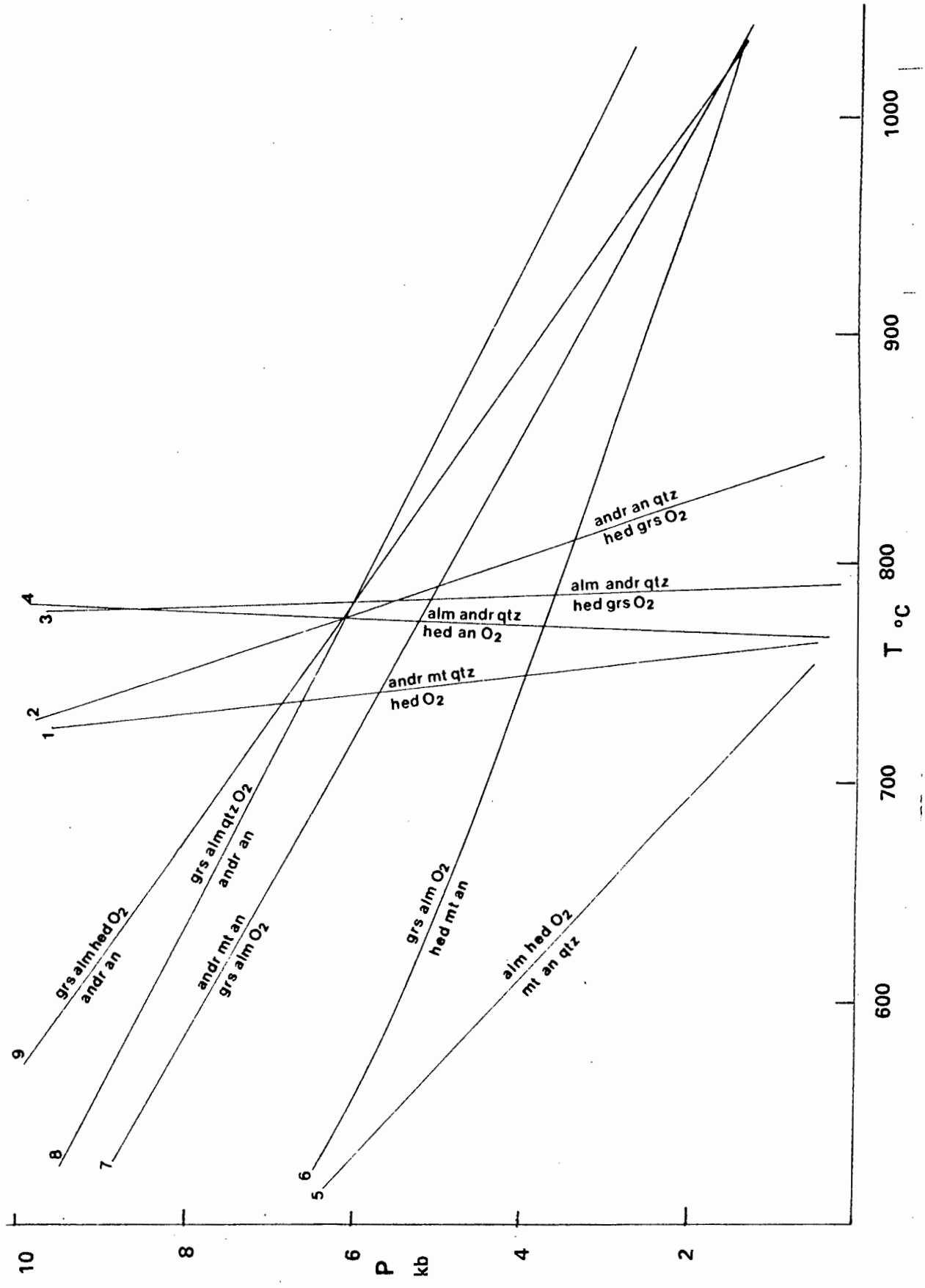

Fig. 7.7 P-T relations for reactions in the system: CaO-FeO-Fe_2O_3-Al_2O_3-SiO_2-O_2. Calculated from the thermodynamic data-base of Holland & Powell (1988).

extrapolated to lower temperatures, see fig. 7.8. All define moderate to high oxidation states at granulite-facies temperatures.

The breakdown of hedenbergite to form an andradite-magnetite-quartz assemblage as seen in the symplectites (see, plate 7.2) can be described by the reaction:

$$9\ \text{Hedenbergite} + 2O_2 = 3\ \text{Andradite} + 9\ \text{Quartz} + \text{Magnetite} \qquad (1)$$

Fig.7.8 shows the T-f_{O2} curve for hedenbergite-andradite-magnetite-quartz calculated from the Holland & Powell data-base. The modelled curve suggests a moderately oxidising environment at the peak metamorphic temperature of 750°C (log f_{O2} = -12). This is consistent with the preserved oxide assemblage which indicates f_{O2} to be below the HM buffer curve. Work on hedenbergite-titanite-magnetite-bearing igneous assemblages by Wones (1989) also confirms stability under relatively high f_{O2}. A possible mechanism for the oxidation of hedenbergite involves introduction of water-rich fluid producing reactions such as:

$$9\ \text{Hedenbergite} + 4\ H_2O = 3\ \text{Andradite} + 9\ \text{Quartz} + \text{Magnetite} + 4\ H_2$$

this is supported by the occurrence of garnet-magnetite-quartz symplectites after clinopyroxene adjacent to quartz veins. The fluid which deposited the quartz must have been of a highly oxidising nature. Water, rather than CO_2 would be most effective in the oxidation process. The presence of hydrous silicates in these rocks (allanite, titanite and amphibole) suggests a high water activity accompanied the breakdown of clinopyroxene.

A number of reactions involving garnet, clinopyroxene and plagioclase have shallow P-T slopes and are potential geobarometers (reactions 6, 7, 8 and 9 in figs. 7.6-7). Accurate pressure determinations cannot be made due to the low activities of the grossular component in garnet, uncertainity in the thermodynamic properties of many of the calc-silicate end-members, particularly andradite, and the need for independant estimates of f_{O2}.

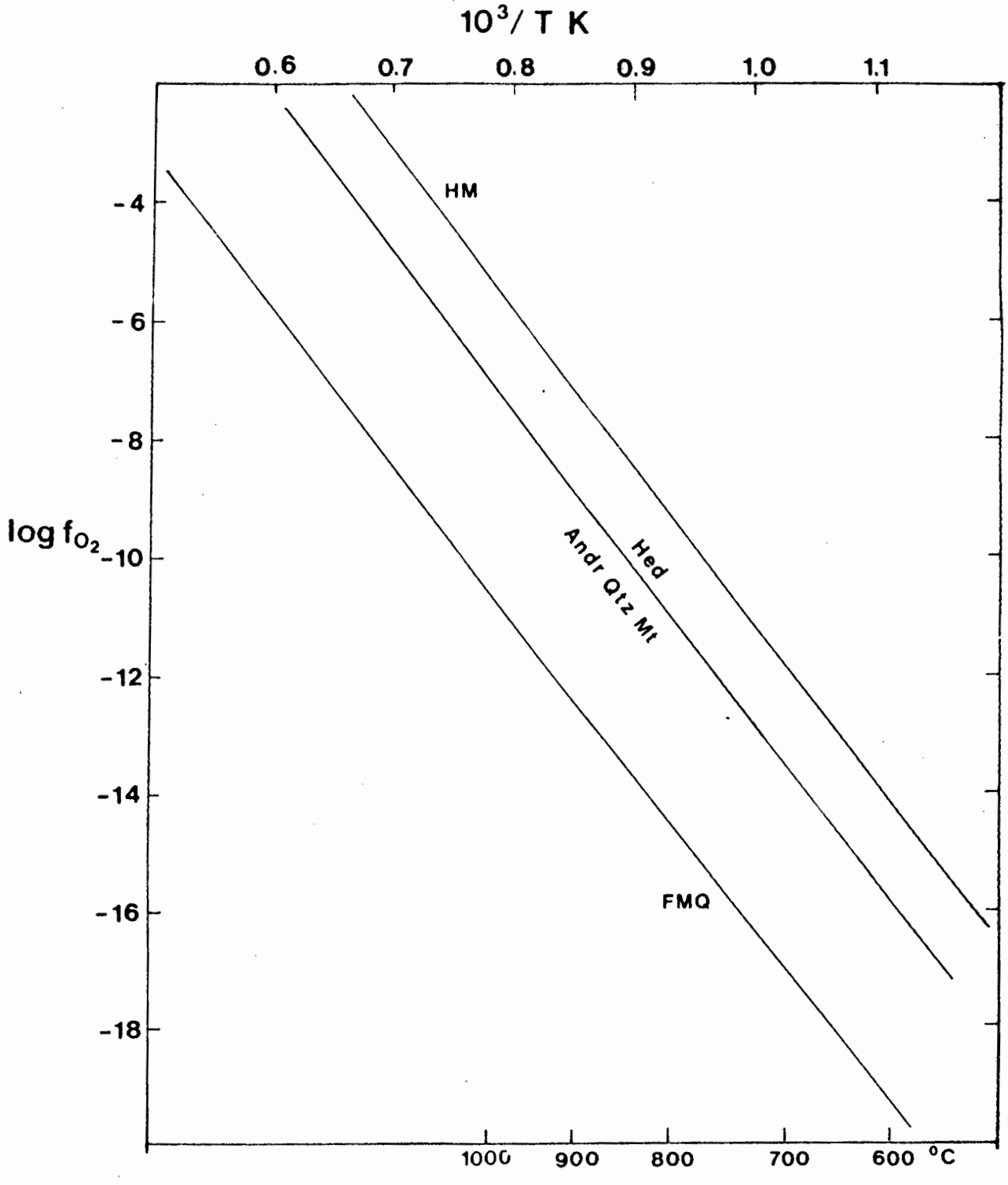

Fig. 7.8 T-f_{O2} relations for the assemblage Hedenbergite-Andradite-Quartz-Magnetite calculated from the thermodynamic data-base of Holland & Powell (1988).
HM = Hematite-Magnetite buffer
FMQ = Fayalite-Magnetite-Quartz buffer

7.5 DISCUSSION - THE FORMATION OF ALLANITE

Based on their bulk chemistry and local association with marble lenses, calc-silicate granofelses are believed to represent thin impure Fe-, Al-rich carbonate sedimentary layers associated with rhyolitic volcanics and volcaniclastic deposits (Moore, 1986; Watkeys et al., 1988 and Moore & McStay, 1990). In some cases calc-silicate rocks are intimately related with mafic gneisses, suggesting that the more Fe-rich varieties may represent hydrothermally altered mafic volcanics that were heavily epidotised at low metamorphic grades. Prior to metamorphism these rocks may have consisted mainly of quartz, calcite, kaolinite, chlorite, smectites and iron oxides/hydroxides (Moore, 1986).

Epidote breakdown will occur at temperatures between 600 and 700°C, forming grandite garnet and anorthite (Liou, 1973) by the general reaction:

epidote = garnet + anorthite + iron oxide + quartz + H_2O

in the same temperature range, epidote will react with ilmenite to form titanite in reactions such as:

epidote + ilmenite = anorthite + clinopyroxene + garnet + iron oxide + titanite + H_2O

In contrast to epidote, allanite is stable at granulite facies conditions. Assuming that the calc-silicate rocks originally comprised REE-bearing epidote, then on the commencement of epidote breakdown during prograde metamorphism, the REE could not be accomodated in the mineral products formed by the continuous breakdown of epidote. Instead REE become progressively concentrated in residual epidote-allanite enclaves.

Significant REE concentrations (at least 2 weight % REE oxides) must have been present in epidote to account for the large amount of allanite formed. The small scale local concentration of allanite can be observed on the thin section scale. Coarse clusters of allanite are surrounded by progressively finer and more disseminated allanite, mostly as inclusions in sieve-textured plagioclase and garnet.

The narrow Ca-, Al-rich rims (see fig 7.3) displayed by virtually all allanite grains are probably the result of slow cooling, resulting in the formation of more epidote-rich rims (see Section 6.5). The more complex pattern seen in large grains from the allanite-rich pods at Smorgen Schaduwe, however, is interpreted as a combination of the above process superimposed on an earlier prograde zonation pattern. The latter zonation to pale-coloured, more Ca-, Al-rich cores can be attributed to the diffusion of REE into residual allanite enclaves during continuous epidote breakdown, and the creation of local chemical gradients in REE concentrations in individual grains. Black (1970) reports similar zoning in allanites from biotite-plagioclase-quartz hornfelses.

The primary, but localised, concentration of REE in calc-silicate rocks from Namaqualand is somewhat enigmatic. Allanite-bearing granofelses generally show a thousand fold increase in LREE contents compared to similar calc-silicate rocks in western and central Namaqualand (Moore, 1986) and to adjacent rocks. The following enrichment processes can be considered:

1. Detrital concentrations of REE-bearing minerals.
The banded nature of the basal plagioclase-quartz gneiss at Smorgen Schaduwe suggests that sedimentary heavy mineral layers are preserved. However, if these layers represent heavy mineral sands, they must have been of an unusual composition as modern-day REE placer deposits are dominated by ilmenite, rutile and zircon, with monazite forming the principal REE ore (Neary & Highley, 1984). Moore (1986) reports localised concentrations of magnetite, ilmenite and zircon in quartzites and quartzo-feldspathic gneisses in the N.M.C. as heavy mineral layers. The allanite in sample SS18c is rounded and xenoblastic and occurs in thin layers the width of a single grain. Titanite occurs in similar fashion in distinct layers separate from allanite in the same rock. In these samples both allanite and titanite record their highest concentration of REE. Allanite-(Ce) commonly occurs as a minor constituent of acid to intermediate igneous rocks, it is possible that leucogneisses of volcanic origin provided the initial source of REE-rich detritus.

2. Chemical precipitation of REE-bearing minerals.
The largest ore reserves of REE occur in carbonate and iron formations in China (Neary & Highley, 1984). Their origin is thought to be related to the chemical precipitation of REE, Fe, Mn, and P

caused by a reduction of CO_2 in the Proterozoic atmosphere. The localised nature of the Namaqualand occurrences and the absence of notable chemical anomalies in P and Mn contents precludes this model.

3. Metamorphic mobilization of REE.

The mobility of REE is largely dependant on the nature of the original mineral phases containing the REE, the composition of the fluid phase, and the ability of new minerals formed to accomodate REE (Humphris, 1984). During the initial low temperature phase of the prograde Namaqua metamorphic event it is possible that REE were mobilised from accessory minerals present in metavolcanics and deposited on increasing temperature by fluids channelised along shear zones. Fluorine-bearing metamorphic fluids have been cited as important mineralising fluids in other parts of Namaqualand (Moore, 1986; Moore & Reid, 1988 and Watkeys et al., 1988). However, most of the minerals present in these rocks, including the allanite are hydrous, non-fluorine bearing phases.

4. CO_2-associated REE concentrations.

The Namaqua metamorphic event is accompanied by the intrusion of suites of charnockites and anorthositic/noritic rocks (McIver et al., 1983; Albat, 1984; Andreoli & Hart, 1987). Fractional crystallisation of the noritic suite led to residual concentrations of silica-poor melts enriched in oxides, sulphides and phosphates (Andreoli & Hart, 1987). REE enrichment is apparent in these rocks and may be a result of the partitioning of REE into late-stage melts and an associated CO_2-rich vapour phase (Wendlandt & Harrison, 1979). The interaction of such a vapour phase with a calc-silicate rock might lead to the deposition of REE from the evolving fluid phase. The allanite-bearing rocks do not contain the full complement of large-ion lithophile elements anticipated, with K, Th and P being noticeably absent.

In view of the chemical and textural relationships listed above, a model involving initial detrital concentration followed by localised low temperature remobilisation is favoured (Moore & McStay, 1990).

7.6 SUMMARY

Fe-rich calc-silicate granofelses make up an important part of the supracrustal sequence, especially on the farm Rietfontein. The most commonly observed assemblage consists of andradite-hedenbergite-plagioclase-quartz-magnetite. In addition some rocks are rich in REE-bearing phases, titanite and allanite.

Allanites are Ce-rich with a total REE content up to 20 weight %. Individual crystals are zoned with REE-rich cores and Ca-Al-rich rims. Some have a complex optical zonation that includes a REE-rich mantle around the core and an outer REE depleted rim. Coexisting titanites have low REE contents, rarely more than 2 weight %. Titanite has higher Nd than La in contrast to allanite. Titanites in the same sample often show a wide compositional range. In allanites compositional variation in a single zoned crystal is greater than the range of core compositions from an entire rock.

Andradite-hedenbergite calc-silicate rocks developed from the breakdown of epidote-rich rocks which may have had relatively low carbonate contents. Much of the prograde history is lost as important devolatilisation reactions probably occurred under amphibolite-facies conditions. The formation of a symplectite of andradite, magnetite and quartz at the expense of hedenbergite is interpreted as a high temperature oxidation reaction, probably due to an influx of water-rich fluid. Thermodynamic modelling suggests the relatively high log f_{O2} value of -12 at a temperature of 750°C.

The formation of allanite-rich rocks in general may be attributed to four main processes: 1. The detrital concentration of REE-bearing minerals. 2. The chemical precipitation of REE-bearing minerals during diagenesis. 3. Metamorphic remobilization of REE. 4. Metasomatism by a REE-enriched CO_2 flux. Chemical and textural evidence favours initial detrital concentration of REE-bearing minerals and subsequent early prograde metamorphic remobilisation.

CHAPTER 8

THE PETROLOGY OF CHARNOCKITIC GNEISSES

8.1 INTRODUCTION

Granitic gneisses of various types make up the largest portion of exposed Proterozoic crust in the Namaqualand Metamorphic Complex (Joubert, 1986). The distribution of granitoid gneisses in central Namaqualand is shown in fig. 2.3. In the Buffels River area many of these rocks are orthopyroxene- or garnet-bearing orthogneisses and show textural and petrographic features that can be compared to well documented charnockitic gneisses in southern India and other parts of the world (Janardhan et al., 1982; Friend, 1983; Park & Dash, 1984; Hansen et al., 1987; Stähle et al., 1987; McLelland et al., 1988). In this chapter the field relationships and petrography of charnockitic gneisses in the Buffels River area are described and models for charnockite formation are discussed.

8.2 CHARNOCKITE OCCURRENCES IN THE NAMAQUALAND METAMORPHIC COMPLEX

In this study charnockitic gneisses can be defined as orthopyroxene -bearing rocks of granitic composition. In the Kliprand area Albat (1984) recognised two main types: an earlier group of gneissic rocks (pre-F_2 folding) and a later suite of megacrystic intrusives (syn-to post F_3). The latter probably represent H_2O-undersaturated magmatic rocks. The earlier charnockites may be the foliated derivatives of similar magmatic rocks, or may be of metamorphic origin. Joubert (1971) refers to homogeneneous dark-weathering charnockitic gneisses in central Namaqualand as hornblende-hypersthene gneiss. Jackson (1976 and 1979) summarises the occurrences of Namaqua age charnockitic intrusives in Namibia. In the Aus area, mapped by Jackson (1976), orthopyroxene-bearing metaluminous orthogneisses are mainly megacrystic enderbites and charno-enderbites (Jackson also includes orthopyroxene-bearing megacrystic mafic rocks amongst his charnockitic suite). These rocks are broadly similar to th Kliprand suite described by Albat (1984) and intermediate members of the Koperberg suite in the Okiep area described by Conradie & Schoch (1986). In all cases the absence of chilled contacts and the abundance

of xenoliths is taken as evidence for emplacement into heated country rocks. Many of these intrusive rocks preserve igneous textures such as lath-shaped feldspars, poikilitic textures, and carlsbad twinning in feldspar. Others show annealed polygonal crystal outlines.

Intrusive charnockites of Namaqua age are also reported from Natal. The Nicholson's Point Granite is dated 1011 þ 14 Ma (Eglinton et al., 1989). Ages for the Mgeni Complex (Kerr & Milne, 1988) range from 1127-1030 Ma. Similar aged granites and charnockites occur in Sverdrupfjella, Heimefrontfjella and Kirwannveggan in Antarctica (Groenewald et al. 1988) and are thought to represent a continuation of the Namaqua-Natal Mobile Belt.

In the Buffels River area two further types of orthopyroxene-bearing rocks are recognised, 1. gneisses with disseminated orthopyroxene and 2. gneisses with charnockitic veins and patches. Both types are most abundant among paragneisses and die out gradually away from paragneiss contacts. Original rocks probably represent syntectonic granitoids. The occurrence of these and other charnockitic gneisses is widely distributed in the granulite-facies zone of Central Namaqualand.

8.3 FIELD RELATIONSHIPS AND PETROGRAPHY

The well exposed pavements and gneiss domes that border the Buffels River at Hytkoras provide abundant field evidence of charnockitisation. The regional S_3 fabric takes the form of a spaced refoliation that corresponds to steep asymmetric folding in adjacent paragneisses. Granitic veinlets containing biotite or hornblende or garnet (see plate 8.1), pegmatitic stringers of quartz and K-feldspar, and dark charnockitic veins form sub-parallel with the steep fabric (plates 8.2 and 8.3) and obliterate earlier foliation. Hornblende-bearing granitic veins are more common than charnockitic veins away from the contact zone with the paragneisses. Hornblende segregations normally consist of an extremely coarse (5-10 cm) single crystal surrounded by a quartz-rich halo (see plate 8.4).

Gneisses with small amounts of disseminated orthopyroxene have a light coloured matrix of quartz and feldspar with small (1 cm) dark flecks consisting of orthopyroxene. The full assemblage consists of quartz-K-feldspar-plagioclase-biotite-orthopyroxene þ hornblende.

Plate 8.1 Garnet-bearing granitic vein in strongly foliated biotite-bearing augen gneiss. River bed, Hytkoras

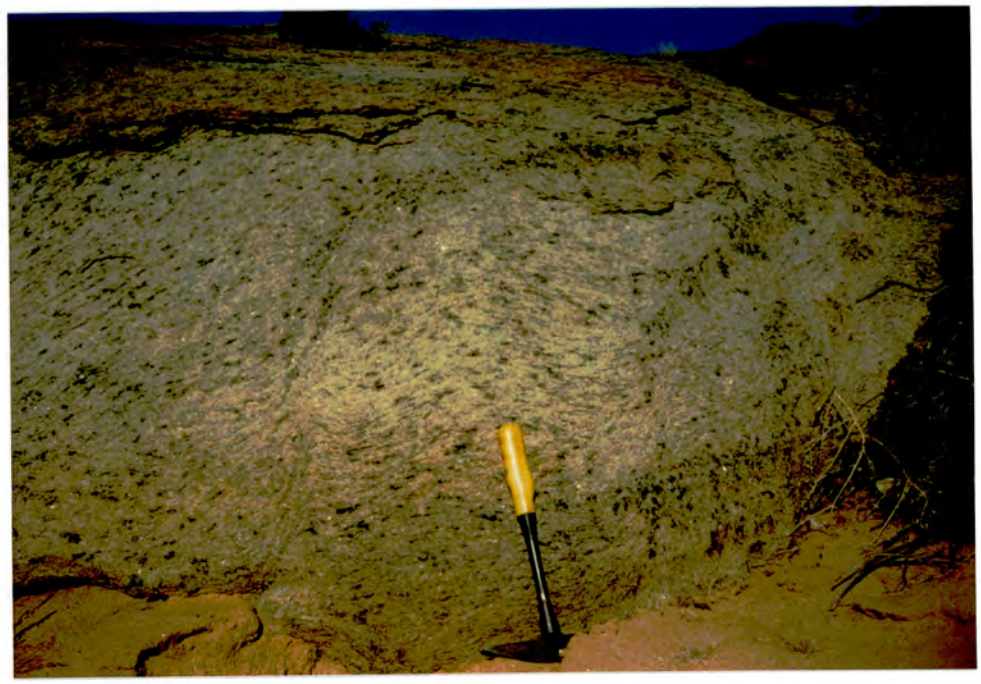

Plate 8.2 Flecky charnockitic gneiss. Patches of charnockite form sub-parallel to steep S_3 foliation. Folded S_2 foliation defined by disseminated orthopyroxene partially replacing biotite. River bed, Hytkoras.

Plate 8.3 Pavement outcrops of charnockitic gneiss. Coarse patches of charnockite, charnockitic veins and quartz-veins can be seen. River bed, Hytkoras.

Plate 8.4 Coarse hornblende segregation surrounded by a halo of recrystallised quartz and feldspar in strongly foliated biotite-bearing augen gneiss. River bed, Hytkoras.

Orthopyroxene occurs as small xenoblastic grains or as elongate poikiloblasts formed roughly along quartz-feldspar grain boundaries overgrowing the S_2 biotite foliation.

In the charnockitic veins all minerals are coarser grained than in the host gneiss. Veins and patches have no foliation and consist of equidimendimensional, subidioblastic orthopyroxene (3-5 modal %) together with coarse (1-2 cm) K-feldspar and quartz. Margins are not sharp in character. Biotite and hornblende are sometimes present in small amounts. A late growth of coarse red-brown biotite can be seen in some patches cross-cutting early minerals and fabrics. Orthopyroxene is present in greater amounts in the veins than in the surrounding gneiss which may contain disseminated orthopyroxene, but is often a biotite gneiss. Vein and patch charnockite has a conspicuous dark green colour and a greasy lustre. The colour is due to extensive alteration of orthopyroxene to a fine growth of green biotite, chlorite and iron oxide which also veins neighbouring feldspar. Weathered outcrops of charnockitic gneiss are a distinctive orange-brown colour.

Charnockitisation is most marked at the contact between the augen orthogneisses and the supracrustal sequence at Hytkoras away from this zone the gneisses preserve the shallow lying S_2 foliation defined by orientated flakes of dark brown biotite.

No fresh orthopyroxene is preserved in the charnockitic veins and patches seen in the Buffels River outcrops at Hytkoras. The compositions of biotite, K-feldspar and plagioclase in biotite gneisses are given in the Appendix . Intrusive leucocratic gneisses which occur within the supracrustal sequence (see Section 3.2.1.3.) tend to have more Mg-rich biotites. In addition leucogneiss sample DWN621 has Ba-enriched K-feldspar (0.75 wt % BaO). In most samples feldspar compositions are fairly uniform. K-feldspar is microperthitic with 10-15% albite molecule. Plagioclase is usually unzoned sodic andesine. Biotite in the biotite gneiss DWN613 has higher Mg and Al, and lower Ti and Fe than biotite in the charnockitic vein sample DWN629 and its host biotite gneiss DWN628. High Ti is a feature of biotite in charnockitic gneisses (DWN629 has 0.68 cations per 24 oxygens). Fluorine content is around 0.7 wt %, this is low compared to fluorine content in biotite from charnockitic and granitic gneisses from the high temperature granulite-facies zone around Garies (Baars, 1986) and examples from southern India (Hansen

et al., 1987) in which fluorine contents may exceed 3 wt %.

Biotite gneisses often contain large amounts of accessory phases, apatite, zircon, allanite and monazite. Sample DWN628 has conspicuous apatite and zircon closely associated with orientated biotite flakes and oxide grains. Individual zircons show strong optical zonation and evidence of complex growth history. In contrast accessory phases are noticeably fewer in coarse grained charnockitic veins and patches. Similar observations are recorded by Barbey et al. (1989) from the Telhot Migmatites, Algeria. In these rocks mesosomes and melanosomes are typified by high contents of accessory minerals, leading to enriched REE contents.

TABLE 8.1

Modal Proportions in Biotite and Charnockitic Gneisses

Sample	Qtz	Kfsp	Plag	Myrm	Biot	Hbl	Opx	Gar	Oxides	Acc
DWN613	43	30	18	1	5	-	-	-	3	
DWN621	43	34	16	tr	5	-	-	-	2	
DWN626	42	26	26	1	4	-	-	-	1	
DWN628	34	32	24	1	9	-	-	-	1	Zir, Apat
DWN629$_A$	34	40	13	2	10_{2nd}	-	-	-	1	
DWN629$_B$	38	47	7	1	1_{2nd}	-	5_{psd}	-	1	
MCSGM01	33	37	21	1	1	4	2	-	1	
MCSGM02	30	43	20	3	4	-	-	-	tr	
MCSH01	30	23	39	1	3	-	3_{psd}	-	1	Chl, Carb
MCSH08	34	33	25	2	1	2	3	-	1	
MCSR06	31	45	15	5	4	-	-	-	tr	
MCS310	42	36	18	1	tr	-	2_{psd}	-	1	
MCS344	39	29	22	tr	8	-	1	-	1	Apat
MCS345	45	21	25	-	8	-	-	-	1	Zir, Apat
MCS348	40	-	50	-	-	9	-	-	1	Apat
MCS357	24	44	26	5	1	-	-	-	1	
MCS359	30	48	12	4	5	-	2_{psd}	-	1	Zir, Apat
MCS360	21	58	14	1	4	-	2_{psd}	-	1	Zir
MCS361$_A$	35	41	18	2	-	3	-	-	1	Chl
MCS361$_B$	36	49	10	1	tr	2	-	-	tr	Chl
MCS373	42	49	5	tr	1	-	1_{psd}	-	2	Zir, Apat
MCS377	45	30	22	tr	1	-	2	-	tr	
				Northern areas (Areb Gneiss)						
MCS272	30	40	24	-	1	-	-	4	tr	Zir, Apat
MCS281	34	30	28	1	2	-	-	5	tr	
MCS282	40	23	29	tr	-	-	-	8	tr	Zir, Apat
MCS283	34	34	26	2	tr	-	-	4	tr	

2nd Secondary
psd Pseudomorphs after orthopyroxene

8.4 WHOLE ROCK GEOCHEMISTRY OF VEIN-TYPE CHARNOCKITE

Large blocks of charnockitic gneiss containing vein-type charnockite and host biotite gneiss were sampled by D.J. Waters for oxygen isotope studies in 1986. The coarser grained, dark-stained charnockitic patches were separated from the lighter coloured biotite-bearing rock by cutting on a rock-saw. A portion of the fresh material was analysed by XRF in the Department of Geochemistry at the University of Cape Town for major elements. The results of this close-pair analysis are given in table 8.2.

TABLE 8.2

Major Element Analysis of host matrix Biotite Gneiss and Charnockitic Patch, DWN629

	DWN629 A Matrix	DWN629 B Patch
SiO_2	72.42	71.14
TiO_2	0.32	0.53
Al_2O_3	13.48	14.01
Fe_2O_3	3.07	3.32
MnO	0.05	0.05
MgO	0.48	0.63
CaO	1.23	1.68
Na_2O	2.22	2.68
K_2O	6.25	5.69
P_2O_5	0.07	0.12
L.O.I.	0.42	0.24
Total	100.01	100.09

A chemical comparison between the close-pair DWN629 is given in fig. 8.1 which shows an isocon diagram (based on the approach outlined by Grant, 1986). Although there is no dramatic change in chemistry a number of subtle differences occur. Charnockite shows small increases in Al_2O_3, CaO, Na_2O that are reflected by increasing plagioclase content. Increasing Fe_2O_3 and TiO_2 are correlated with the higher oxide content of vein-charnockite. Increases in Al_2O_3, TiO_2, Fe_2O_3, CaO, Na_2O are balanced by decreasing Si and K. The vein

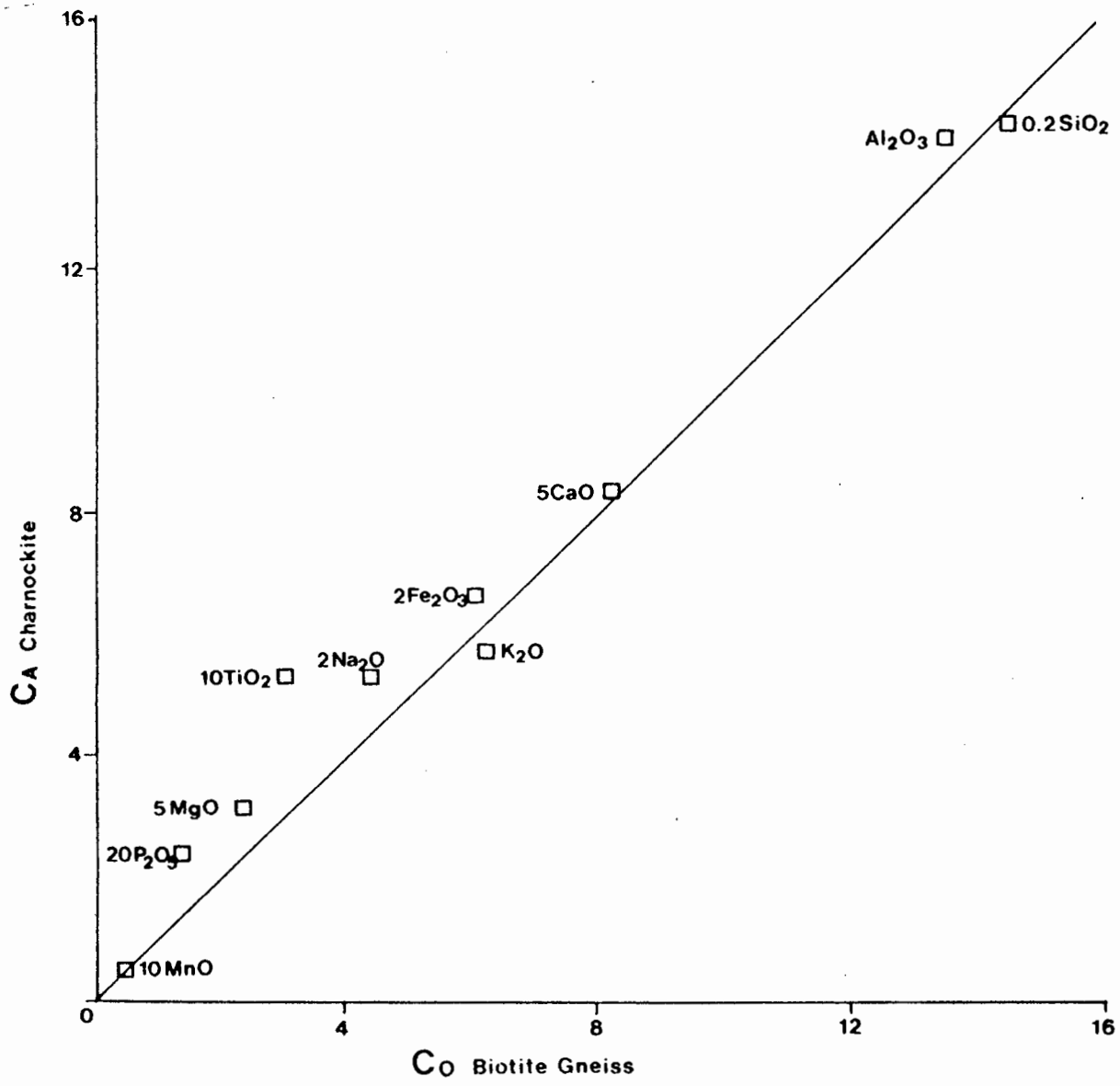

Fig. 8.1 Isocon diagram (Grant, 1986) illustrating the chemical variation between charnockitic patch (C_A) and matrix biotite gneiss (C_O). DWN629. Hytkoras.

material shows the typical chloritic and micaeous alteration phenomena seen in all Buffels River charnockites. The role of this alteration on major element chemistry is difficult to assess. The fresh, unaltered nature of feldspar and low L.O.I. suggests that retrograde hydration of orthopyroxene does not require large volumes of fluid and that changes in major element chemistry are likely to be relatively small. However, it may be difficult to distinguish prograde from retrograde chemical changes.

Similar geochemical studies of charnockites from southern India (Allen et al., 1982; Weaver & Tarney, 1983 and Hansen et al, 1987) show a variety of chemical changes. Problems concerning the purely geochemical approach are the selection of appropriate samples and the definition of terms such as: host gneiss, close-pair, and amphibolite- facies equivalent. Another difficulty is assessing changes in chemistry due to retrograde alteration of orthopyroxene. As most authors claim that charnockite patches are recognised by their dark green-colour and greasy lustre one would assume some degree of chloritic alteration is present.

A geochemical comparison can be made between the conversion of biotite gneiss to charnockite in the Buffels River area to incipient charnockitisation in other areas of the world. Most of the analysed samples from southern India tend to have granodioritic or tonalitic compositions. The charnockitic gneisses commonly contain garnet as reactants or products of charnockitisation so precise analogues are not available for comparison. In the Adirondacks local-scale charnockitisation of alaskitic gneisses is recorded (McLelland et al., 1988). The comparative features of both are briefly described.

The locality of Arni, South Arcot, Tamil Nadu, India is described by Hansen et al. (1987). This area is close to the orthopyroxene-in isograd of the South Indian Shield. Charnockitisation takes the form of dark ovoid patches in strings parallel to the pre-existing foliation. The area is steeply dipping and tightly folded. The dark charnockititic patches consist of orthopyroxene poikiloblasts surrounded by coarse quartz and feldspar. Some skeletal retrograde biotite occurs replacing orthopyroxene, and chlorite veinlets are present. Hansen et al. attributed the charnockitisation to be the result of a biotite-quartz reaction (termed the Ponmudi-facies by Hansen et al.). Charnockitisation does not appear to be due to

channelised fluid movements along shears. Hansen et al. prefer pervasive percolation of CO_2-rich fluid along foliation planes resulting in the breakdown of biotite. This type of texture is not dissimilar to prograde textures observed in Namaqualand, the difference being that most charnockititic veins tend to be discordant. The metamorphic grade at Arni is identical to that experienced in the Buffels River area. Table 8.3 gives the whole rock chemical analysis for the close-pair of biotite gneiss and charnockite from Arni, taken from Hansen et al.(1987). Fig. 8.2 shows an isocon plot for the Arni samples.

In the Adirondacks McLelland et al. (1988) observe biotite- and hornblende-bearing granitic gneiss coexisting with charnockitic gneiss. Charnockitisation occurs adjacent to marbles and is locally controlled by the evolving fluid-composition on devolatilisation of the marbles (McLelland et al., 1988). Table 8.3 gives the whole rock chemical composition of massive granitic gneiss and layered charnockite from McLelland et al.. Fig. 8.3 shows an isocon plot for these samples.

TABLE 8.3

Whole Rock Geochemical analysis of host matrix Biotite Gneiss and Charnockite, from the Arni area, India and the Adirondacks.

	T6-30 (Hansen et al., 1987)		(McLelland et al., 1988)	
	Biotite Gneiss	Charnockite	Biotite Gneiss	Charnockite
SiO_2	71.1	71.4	67.7	69.0
TiO_2	0.34	0.13	0.88	0.68
Al_2O_3	15.3	14.6	15.0	14.00
Fe_2O_3	2.21	3.13	3.16	4.15
MgO	0.65	0.86	1.04	0.74
CaO	3.23	2.95	2.16	2.06
Na_2O	5.25	4.88	3.72	3.78
K_2O	1.35	1.66	4.34	4.58
P_2O_5	0.09	0.08	----	----
L.O.I.	0.39	0.23	0.85	0.31
Total	99.91	99.92	98.85	99.30

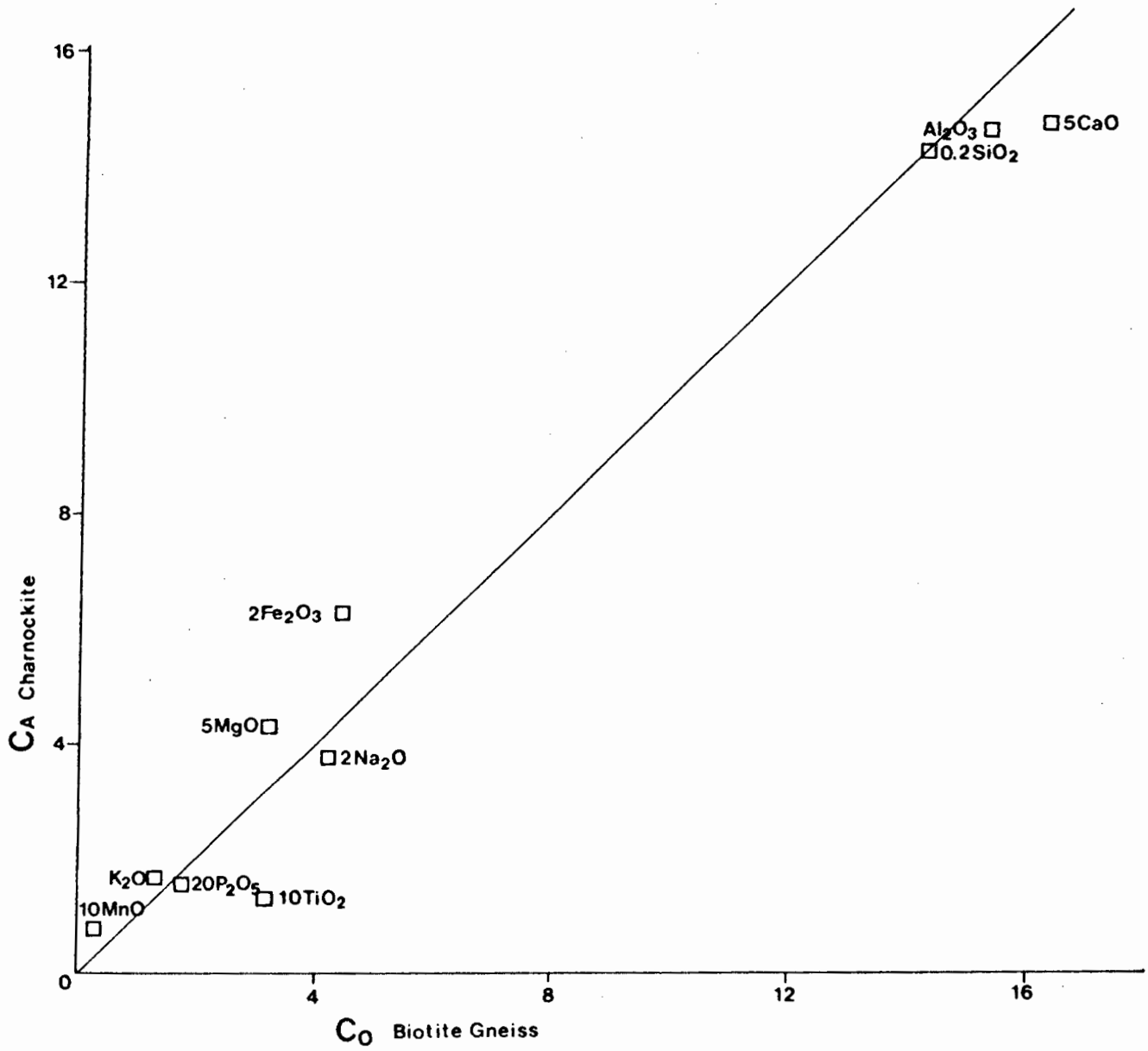

Fig. 8.2 Isocon diagram (Grant, 1986) illustrating the chemical variation between charnockitic patch (C_A) and matrix biotite gneiss (C_O). Arni, S.India, data from Hansen *et al.* (1987).

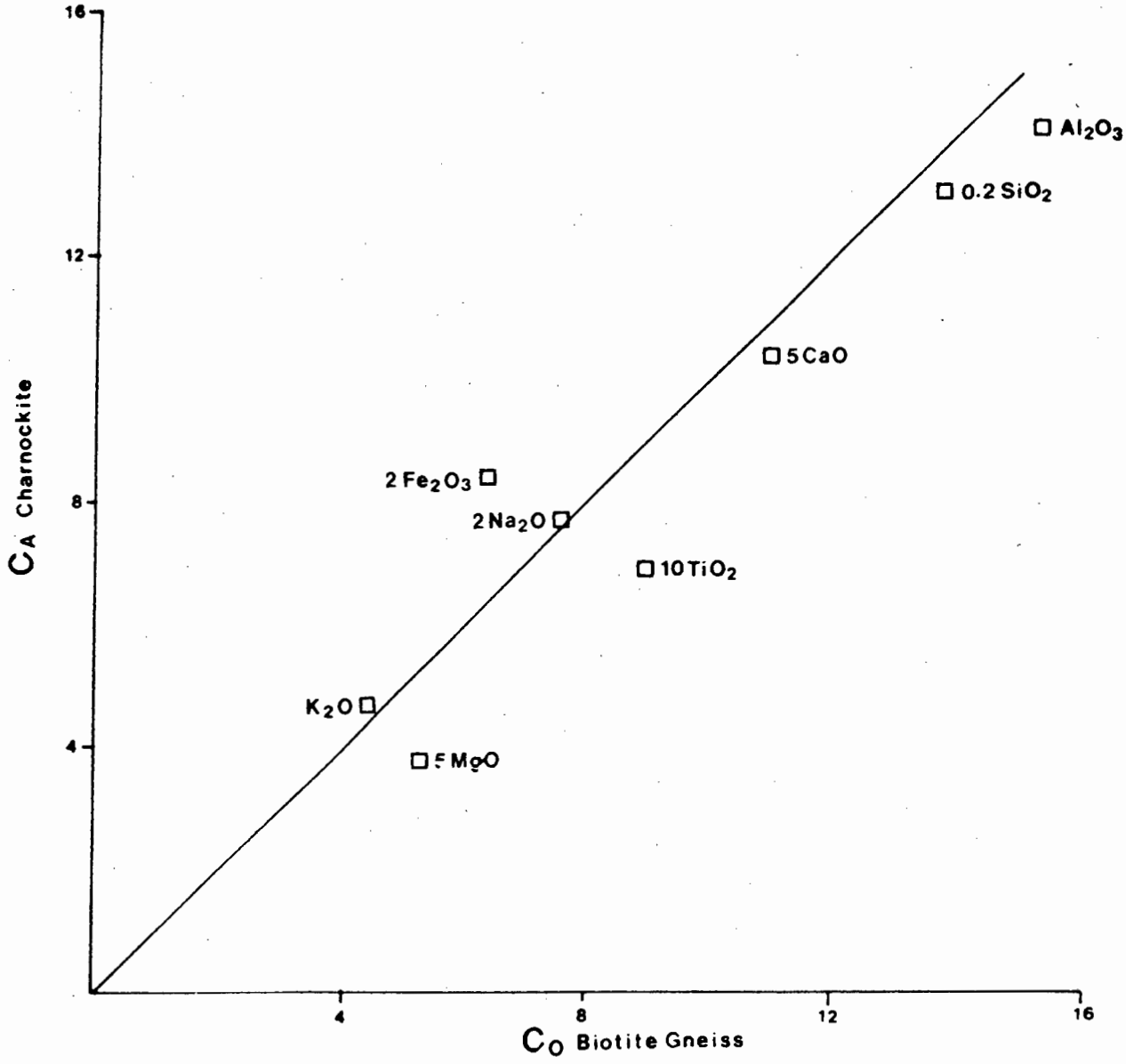

Fig. 8.3 Isocon diagram (Grant, 1986) illustrating the chemical variation between charnockite (C_A) and matrix biotite gneiss (C_O). Adirondacks, data from McLelland et al. (1988).

The changes in whole rock chemistry can be summarised as follows: In all examples Al_2O_3 and SiO_2 are fairly constant. The rocks from Arni are more Ca-rich and are considered by Hansen et al. (1987) to represent paragneisses. In the Hytkoras example the loss of elements is minor, only small depletions in SiO_2, K_2O and H_2O (assumed from L.O.I. measurements) are recorded. Ti is concentrated in the charnockite. At Arni Fe_2O_3 increases in the charnockite and TiO_2 is depleted. CaO and Na_2O are also depleted in the charnockite suggesting that plagioclase is more abundant in the biotite gneiss. In the Adirondacks charnockite there are slight depletions in Al_2O_3, TiO_2 and MgO. In similar fashion to Arni the charnockite is richer in Fe_2O_3 and K_2O. The high L.O.I. in the biotite gneiss from the Adirondaks is mostly due to the hydrous nature of its mineral assemblage (8% biotite and 7% hornblende).

In all examples host biotite gneiss and charnockite are chemically very similar. Some mass transfer accompanies biotite breakdown and the formation of oxides as reaction products, ilmenite in the Hytkoras rocks and magnetite in the Arni rocks accounts for the apparent mobility of Ti and Fe. The lack of depletion in K, particularly at Arni is not wholly consistent with pervasive fluid fluxing, Hansen et al. imply that retrograde influx of K-enriched fluid took place.

8.5 DEHYDRATION AND MELTING EQUILIBRIA IN BIOTITE GNEISSES

Equilibria for biotite and charnockitic gneisses can be modelled in the simple system K_2O-Na_2O-FeO-MgO-Al_2O_3-SiO_2-H_2O following the relations given by Grant (1985) and Waters (1988). Liquid composition is assumed to an Al-poor minimum melt, similar to the S-type composition of White & Chappell (1977). Fig. 8.4 shows the melting and dehydration equilibria for a simple metaaluminous granitic system. At low water activities the first reaction encountered during the prograde evolution of such a system is the dehydration of biotite to form orthopyroxene:

Biotite + Quartz = Orthopyroxene + K-feldspar + H_2O

The coexistence of biotite-orthopyroxene-k-feldspar-quartz will buffer water activity to the equilibrium curve, see fig. 8.4. Under

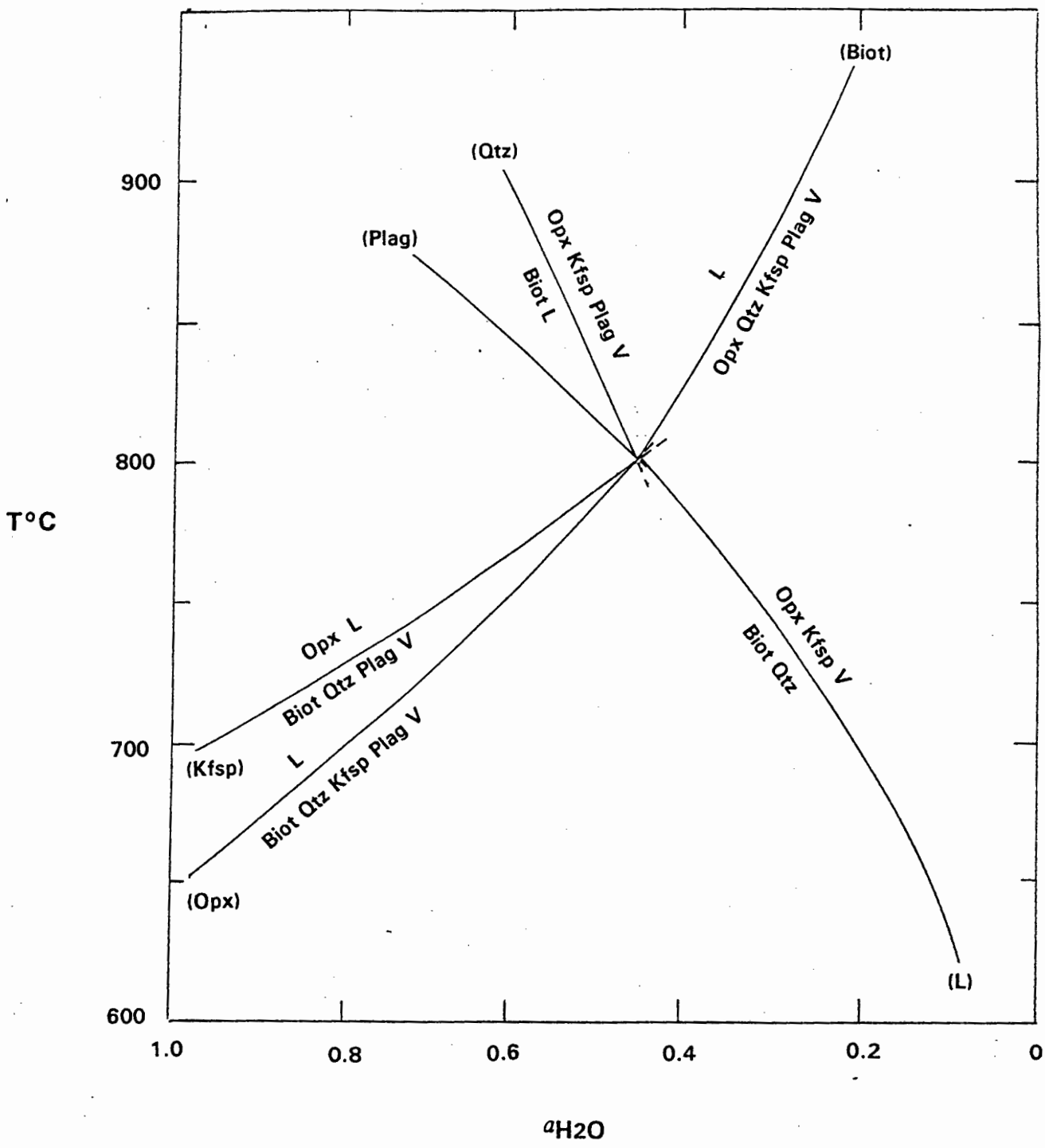

Fig. 8.4 Dehydration and melting equilibria for a simple metaluminous granitic system, after Waters (1988).

vapour-absent conditions biotite is stable up to the temperature at which the vapour-absent melting occurs via the reaction:

Biotite + Plagioclase + Quartz = Orthopyroxene + K-feldspar + Liquid

This reaction will proceed until biotite is exhausted, the water activity is then buffered by the coexistence of melt and the anhydrous solid phases.

In the presence of an aqueous vapour melting will occur following the reaction:

Biotite + Quartz + K-feldspar + Plagioclase + H_2O = Liquid

Coexisting melt and solid residues will buffer small amounts of vapour. Water will be strongly partitioned into the silicate liquid and as a result a_{H2O} becomes progressively lowered in the vapour phase. If the vapour phase is pure water then all the vapour will be used up when the prograde P-T-t path intersects the vapour-present melting reaction.

If the fluid is CO_2-rich then buffered fluid evolution follows the dehydration curve:

Biotite + Quartz = Orthopyroxene + K-feldspar + H_2O

With increasing temperature the fluid evolves to the isobaric invariant point where vapour-absent melting occurs.

If infiltration of externally derived fluids occurs the buffering capability of the rock may be exceeded. Influx of H_2O will cause melting to produce a granitic liquid without the formation of orthopyroxene. Influx of CO_2 will lower a_{H2O} in the vapour phase and promote dehydration of biotite.

Waters (1988) presents modelled mass balance relationships for dehydration and melting of biotite gneisses from the high T granulite-facies zone of the central Namaqualand, his conclusions are: 1. For internally buffered systems where vapour is ≤1% by volume the vapour-absent melting reaction is the melt producing step. 2. The amount of melt produced is proportional to the amount of biotite consumed. 3. A large proportion of the rock is not directly involved

in the production of melt, solid phases quartz, K-feldspar and plagioclase are available in excess.

The vapour-absent melting of biotite has been modelled for the mineral composition recorded for DWN629. The melt composition is based on the granite solidus in H_2O-CO_2 mixtures according to Keppler (1989). Water activity for melt of given water content is estimated from the data of Burnham (1981).

TABLE 8.4

Composition and volumes of phases used for mass balance of vapour-absent melting reaction, expressed as cations per formula unit.

	Biot	Kfsp	Plag Ab	Plag An	Qtz	Opx	Liquid*	
Si	5.55	3.0	3.0	2.0	1.0	1.95	3.79	
Al	2.44	1.0	1.0	2.0		0.10	0.76	
Fe + Mg	5.10					1.95	0.08	
Ca				1.0			0.06	
Na			1.0				0.30	
K	1.80	1.0					0.31	
H	4.00						1.66	
Molar volume (cm^3)	300	109	100	100	23	64	141.74	
Mass balance factors								
	0.42	0.45	0.30	0.06	3.86	1.06	1.0	
								R
Si	2.33	1.35	0.90	0.12	3.86	2.07	3.79	---
Al	1.03	0.45	0.30	0.06		0.11	0.76	0.07
Fe + Mg	2.14					2.07	0.08	0.01
Ca				0.06			0.06	---
Na			0.30				0.30	---
K	0.76	0.45					0.31	---
H	1.68						1.66	0.02
Volume balance								
	10.00	3.89	2.38	0.48	7.05	5.38	11.25	

* Liquid Composition

	Weight %
SiO_2	70.0
Al_2O_3	15.0
FeO + MgO	4.3
CaO	2.0
Na_2O	3.5
K_2O	4.2

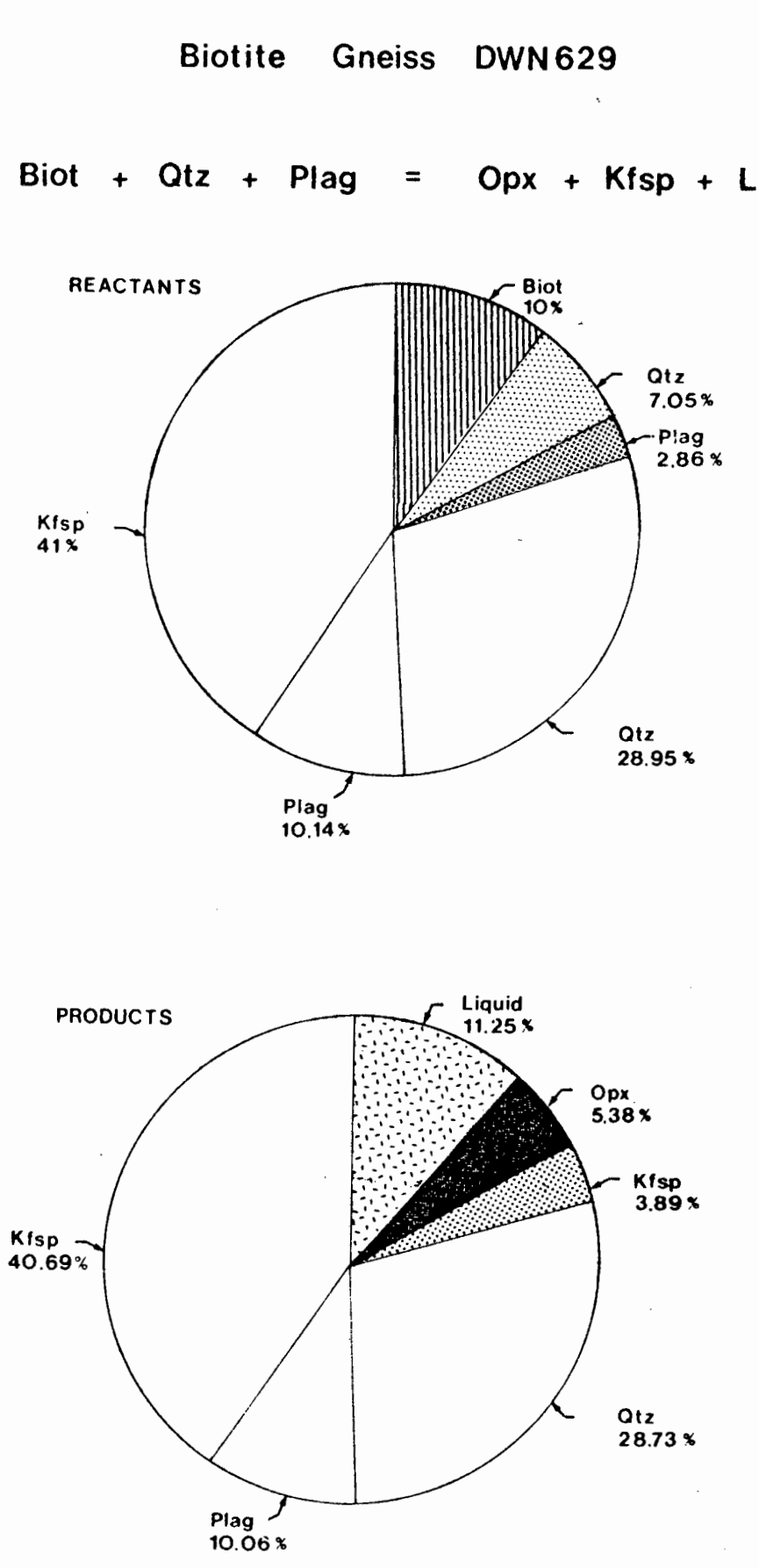

Fig. 8.5 Pie-chart illustrating the mass balance relations for the vapour-absent melting of biotite in biotite gneiss. From the data in table 8.4.

The results of the mass balance calculation for sample DWN629 are shown in fig. 8.5. The results support the conclusions of Waters (1988). The volume of liquid generated is roughly equal to the amount of biotite present. Comparison of the modelled reaction products and the observed modal proportions in $DWN629_B$ (see table 8.1) show a wide variance. Calculated orthopyroxene percentages match the observed proportion of orthopyroxene pseudomorphs, but phases that occur in both the matrix and the segregation show poor correlation. The proportion of observed modal K-feldspar and quartz in the charnockitic segregation exceeds that predicted in fig. 8.5, while plagioclase content is noticeably lower. Geochemical analysis (see table 8.2) indicates increasing CaO in the segregation and hence the observed modal plagioclase content in the two thin sections used for point-counting does not reflect the true abundance of plagioclase in the segregation. Difficulties in conventional point-counting from standard size thin-sections of coarse grained rocks and the uneven distribution of phases within segregations negate critical comparison of observed proportions and calculated results. Work in progress by Baars and Waters (unpublished data) on techniques of assessing the modal volumes of phases in coarse grained veins and patches may improve the interpretation of modal mass balance equations on natural assemblages. Hence, the results in fig. 8.6 are generally consistent with the natural assemblages observed in charnockitic segregations at Hytkoras, and strongly suggests that such segregations are the liquid and solid products of the vapour-absent melting of biotite.

8.6 DISCUSSION - MODELS FOR CHARNOCKITISATION

It is important to make a distinction between the terms charnockite and charnockitisation as used in this study. The term charnockite is used to decribe any orthopyroxene-bearing granitoid gneiss. All the charnockites sampled in this study are thought to have developed their orthopyroxene as a result of granulite-facies metamorphism. Hence the term charnockitisation is used to describe the metamorphic processes that result in the conversion of biotite gneiss to orthopyroxene-bearing gneiss. Magmatic charnockites are common in other parts of Namaqualand (Jackson, 1979 and Albat, 1984). Massive, megacrystic intrusive rocks with xenoliths, and the partial preservation of igneous textures are best interpreted as having crystallised from H_2O-undersaturated melts. Subsolidus

recrystallization may result in polygonal crystal boundaries. Magmatic charnockites could originate in a number of ways: 1. through the partial melting of a 'dry' source rock; 2. within large stratified magma chambers, strongly H_2O-undersaturated melts could develop at the base of large convecting magma chambers in thick crust (Ridley & Kramers, 1990); 3. partial melting of a granitic source in the presence of CO_2-rich fluid at granulite facies temperatures (Wendlandt, 1981). Otherwise crystallisation of hydrous assemblages must be inhibited by influx of CO_2-rich fluid.

Vein-like charnockite in amphibolite-facies gneisses was first recorded by Pichamuthu (1960) from Kabbaldurga, southern India. Many workers have described the geochemical characteristics and structural aspects of such veins. In most cases the charnockitic veins have higher Si and Na, and lower Ca, Mg and Fe than their host rock, usually a grey biotite gneiss. Structural control is commonly observed in many examples. This, together with observed minor element variations between vein and host, has led to the conceptual model of charnockitisation via channelised metasomatic fluids (Friend, 1983).

Calculations based on high temperature C-O-H fluid systems (Hansen et al., 1987) indicate that fluids in equilibrium with biotite-bearing charnockite have $X_{H2O} \leq 0.35$. These figures are close to those proposed for mafic and pelitic gneisses from the Buffels River area in Chapters 5 and 6. The presence of Ti and F are likely to stabilise biotite to even lower water activities. Under high temperature conditions the speciation of C-O-H fluids is strongly dependant on f_{O2} (Lamb et al., 1987 and Hansen et al., 1987). CO_2-rich fluids require highly oxidising conditions, H_2O-rich fluids are favoured by intermediate f_{O2}, and H_2O-CH_4 mixtures occur at low f_{O2} conditions. The assemblage orthopyroxene-magnetite-ilmenite-quartz can be used to infere f_{O2} conditions, see fig. 8.6. The absence of graphite suggests log $f_{O2} > -16$. More precise estimates are negated by the absence of fresh orthopyroxene and the slow cooling history experienced by the terrane, as indicated from garnet zonation profiles from pelitic gneisses (Section 6.5) and oxide assemblages in mafic gneisses (Section 5.3.5).

In-situ charnockitisation in southern India may be an open-system process, as concluded by Hansen et al. (1987) and Stähle et al. (1987). Geochemical evidence of minor element depletions have been found in many granulite-facies terranes (Greenland: Wells, 1979;

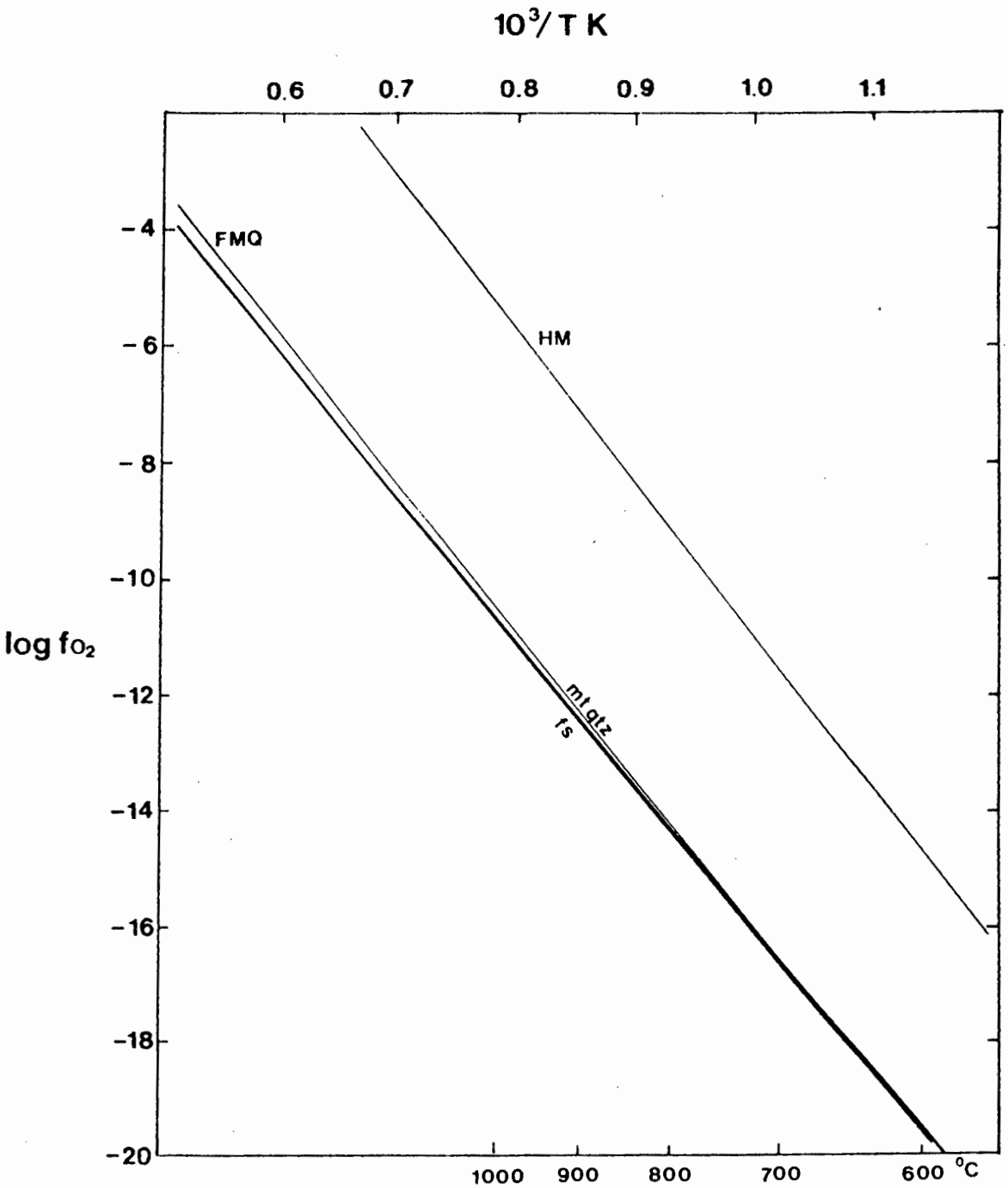

Fig. 8.6 T-f_{O2} relations for the assemblage magnetite-quartz-ferrosilite at 5 kb. Calculated from the data-base of Holland & Powell (1988).
HM = Hematite-Magnetite buffer, FMQ = Fayalite-Magnetite-Quartz buffer.

southern India: Weaver & Tarney, 1983; and southern Norway: Lamb et al., 1986). The depletion of L.I.L. (large ion lithophile) elements has been ascribed to removal by pervasive movement of low-a_{H2O} fluids. The CO_2 streaming hypothesis (Newton et al., 1980) is supported by the low X_{H2O} nature of fluids coexisting with orthopyroxene-bearing assemblages, apparent open-system conditions indicated by close-pair geochemical analysis, the abundance of high density CO_2-rich fluid inclusions in charnockites (Hansen et al., 1984 and Touret, 1986) and field relationships indicating a close spatial association between shear zones and charnockitisation.

A spatial relationship between charnockite and garnet-bearing leucogneiss (leptynite) is common throughout southern India. In the Eastern Ghats terrane Park & Dash (1984) recognise veins and micro-veins of charnockitic neosomes. Both charnockite and leucogneiss post-date the dominant regional foliation and are controlled by small-scale brittle-shears and asymmetrical open folds. Mesoscopic orientation of charnockitic patches is recorded, but the microscopic texture is equigranular. Park and Dash attribute early formed granitic veins to in-situ partial melting. Charnockitic veins form later and could be related to a retrogressive fluid-flux associated with late tectonic intrusions of alkaline magmas.

In examples of charnockitisation in southern India (Stähle et. al, 1987) rock fabric undergoes a considerable coarsening of mineral grain size up to double the size of surrounding biotite gneiss. Modal mineralogy shows increasing K-feldspar and quartz and reduced plagioclase content. Hornblende, biotite and magnetite occur in both charnockitic- and biotite gneiss. Myrmekite is commonly recorded in charnockites from Kabbaldurga (Janardhan et al., 1982 and Stähle et al., 1987) and is also conspicuous in the Nicholson's Point charnockitic granite in southern Natal (Grantham, 1988). Modal changes of this nature must be accompanied by significant mass transfer. Charnockitic rocks have a high concentration of fluid inclusions which may indicate the presence and influx of pore fluids during the process of charnockitisation. Areas of high permeability such as small-scale shears are affected by charnockitisation. Close-pair whole-rock geochemistry by Stähle et al. (1987) reveals depletion in Fe_2O_3, MgO, CaO and increases in K_2O and SiO_2 accompanied charnockitisation. There is an increase in trace elements such as Rb and Ba. REE are depleted in the charnockitic rocks, especially the HREE which suggests dissolution of zircon. This

process depends on the influx of CO_2-rich fluids enabling transport and removal of REE in the form $[REE(CO_3)_3]^{3-}$ complexes. Depletions of this sort also occur in portions of the biotite gneiss in direct contact with charnockitic rocks that show no obvious change in mineralogy or texture. There are no significant changes in $\delta^{18}O$ and values of 6.9 to 8.0 per mille are consistent with a deep crustal or upper mantle source for infiltrating fluids (Oxygen isotope data for Buffels River charnockitic gneisses are presented in Chapter 9).

Stähle et al. indicate that the process is tectonically controlled. Dehydration of biotite gneisses started in ductile shears and then proceeded along foliation planes. Absence of partial melting in the closely associated grey gneisses suggest that these rocks were fluid-poor at the onset of charnockitisation. Influx of fluids could result in heat-transfer and cause local heating and hence dehydration of biotite. Such small-scale thermal gradients would be impossible to detect with conventional geothermometry if they did occur. Increases in K_2O could be due to the strong partitioning of Na into the fluid phase with K partitioned into the feldspar. Most workers favour a two stage process (Janardhan et al., 1982; Condie et al., 1982; Friend 1983 and 1985) involving potassium metasomatism by ascending water-rich fluids followed by near-isochemical conversion to charnockite by CO_2-rich fluids lagging behind the aqueous metasomatic front. Stähle et al. (1987) regard the process of charnockitisation at Kabbaldurga as being a local process restricted to the zone of amphibolite-facies to granulite-facies transition which involved the release of CO_2-rich fluids, possibly from leaked fluid inclusions, during shear deformation during or after the main granulite forming event.

Frost & Frost (1987) consider that charnockite formation can occur via CO_2-streaming, partial melting, or recrystallisation of originally dry rocks. These processes need not be independant and may all be related to the passage of melts through the crust. Frost & Frost (1987) suggest that melts saturated with respect to CO_2 crystallise at higher temperatures and pressures than H_2O-saturated melts. If vapour is progressively removed from the melt as the melt rises the exsolved fluid should become progressively enriched in H_2O. Deep crustal melts produced by the thermal effect of basaltic underplating are likely to be vapour-undersaturated, or may coexist with CO_2-rich fluid evolved from the basaltic magma. Passage of such melts through the crust is likely to absorb H_2O from surrounding rocks or exsolve CO_2. The model of Frost & Frost (1987) implies that

granulite-facies events are ultimately tied to magmatic events.

Field evidence from Namaqualand (Andreoli & Hart, 1987) points to a close-spatial relationship between intrusive rocks of the Koperberg Suite and narrow transgressive zones of charnockite. Andreoli et al. (1988) reports that granitic gneiss hosting a monazite vein deposit at Steenkampskraal, near Garies, is in places converted to charnockite. This contact consists of coarsely recrystallised orthopyroxene-bearing granite (charnockite) along an intrusive contact with later enderbite. Andreoli & Hart (1987) invoke CO_2-saturated KREEP basalts as a parental magma for the REE-enriched intrusives of the Koperberg suite (Conradie & Schoch, 1988). REE-enrichment in certain crustal rocks, anorthositic intrusions, release of metasomatic CO_2-rich fluids and charnockitisation are regarded as part of a complex igneous and metamorphic cycle (Andreoli et al., 1990). As yet these ideas have not been tested in terms of age and geochemical relations. Field evidence needs careful re-examination.

By analogy with models presented for the behaviour of mafic and pelitic gneisses in the Buffels River area the common coexistence of anhydrous and hydrous minerals in low variance assemblages may indicate local control of water activities.

The mineralogy and textures of granitic gneisses with disseminated granoblastic or poikiloblastic orthopyroxene are consistent with the prograde dehydration of biotite via the reaction:

Biotite + Quartz + Plagioclase = Orthopyroxene + K-feldspar + H_2O

Production of around 3 % volume of orthopyroxene implies fluid rock ratios of approximately 1:100. This would be the case in a closed system with < 1% pore space. The breakdown of biotite may be assisted by minor infiltration of CO_2-rich fluid and equally by the removal of buffered fluid into a nearby low X_{H2O} sink, such as the strongly H_2O-undersaturated leucosomes found in pelitic and quartzo-feldspathic gneisses.

Charnockitic veins most probably result from the vapour-absent melting reaction:

Biotite + Quartz + Plagioclase = Orthopyroxene + K-feldspar + Liquid

Mass balance calculations, see Waters (1988), indicate that the reaction above can generate 3 % volume of orthopyroxene from a rock containing 5% volume biotite with the production of < 10% liquid. Experimental work by Jurewicz & Watson (1985) indicates that small amounts of melt are insufficient to separate and removal of the liquid does not occur (Wickham, 1987).

There is little evidence of high temperature back-reactions to form retrograde biotite or hornblende. Arguments outlining the preservation of anhydrous assemblages in melt segregations are discussed in Section 6.6. In charnockitic veins orthopyroxene is pseudomorphed by a very fine grained micaeous and chloritic product, it is unlikely that this material formed at high temperatures. Thus, hydration is most likely a late-stage, low temperature process caused by interaction with groundwater aided by the development of fracture porosity during tectonic unloading accompanying uplift.

Structural controls on charnockitisation may be important. Veins are localised around strongly refoliated zones and occur sub-parallel to the S_3 refoliation planes. There are several possible explanations for this relationship. The zones occupied by charnockitic veins represent areas of dilation caused by volume changes accompanying melt generation. Heat-flow anisotropy provided by steeply dipping, strongly folded rocks in a terrane of flat-lying granitic gneisses may be responsible for slightly higher temperatures in the Buffels River Shear Zone. It is also likely that they represent channelways for fluid migration. Infiltration of CO_2-rich fluid could promote the dehydration of biotite but does not account for the difference in grain size and textures between vein and surrounding matrix gneiss. If the infiltrating fluid is H_2O-rich then it will tend to promote the vapour-present melting reaction:

Biotite + Quartz + K-feldspar + Plagioclase + H_2O = Liquid

The result would be the formation of a granitic veinlet along the fluid channelway. There is abundant field evidence of such veinlets in non-charnockitic gneisses in the study area. If the liquid composition is more Al-rich then hornblende is likely to be the solid Fe-Mg phase associated with the melt generated (Abbott & Clarke, 1979). This perhaps accounts for the coarse grained idioblastic hornblende seen in some veinlets.

If buffering operates together with infiltration, coexisting fluid composition evolves towards more CO_2-rich compositions, and reaches the isobaric invariant point [V] as shown in fig. 8.4. Thus a charnockitic segregation ultimately forms along a zone of limited H_2O introduction. The occurrence of charnockitic veins therefore depends on the supply of aqueous fluid, and on the extent to which fluid composition is controlled by the melting process or by the adjacent mineral assemblages. Aqueous fluid may be locally derived from dehydration reactions in progress in mafic gneisses, or from fluids released by the crystallisation of late-tectonic granitoids.

Some of the processes discussed above require local infiltration of fluids. At the low porosities expected for high-grade gneisses grain boundary diffusion is likely to result in activity gradients being maintained on a 10 cm scale. This is consistent with field evidence and the calculation of water activities from mafic gneisses in Buffels River area (Section 5.5.3) which indicates the existence of X_{H2O} gradients on a cm scale.

8.7 SUMMARY

Charnockitic gneisses are widely distributed within the granulite facies zone of the Namaqualand Metamorphic Complex. Some of these rocks are late syn- to post-tectonic megacrystic intrusions of H_2O undersaturated magma. In the Buffels River area charnockitic gneisses appear to be metamorphic in origin.

Two types of charnockitisation are recognised, one has small amounts of granular orthopyroxene disseminated throughout, the other consists of coarse veins and patches of charnockite within a host of biotite gneiss. Veinlets form sub-parallel to the local S_3 spaced refoliation

Whole rock geochemistry of a charnockite patch and its host biotite gneiss show a slight decrease in K_2O, Si_2O and H_2O in the charnockite, all other elements show a slight increase. Incipient charnockitisation in granitoid rocks of similar metamorphic grade in southern India and the Adirondacks show similar textural features to charnockites in the Buffels River area. However, close-pair geochemistry gives a different pattern to that observed in the Hytkoras sample. Samples from Arni, Tamil Nadu, India, analysed by Hansen et al. (1987) and the Adirondacks, analysed by McLelland et al. (1988) show increasing K_2O in the charnockitic patch. They are similar to the Hytkoras sample in that chemical changes are very minor. From the chemical evidence it is difficult to relate such small scale changes to massive scale fluid fluxing, but it is equally clear that the process of charnockitisation observed in the Buffels River area is not a simple closed system. The presence of chloritic veinlets replacing orthopyroxene and invading along feldspar cleavages indicate that retrograde chemical changes must also be considered when comparing close-pair samples. At best the chemical changes accompanying incipient charnockitisation are ambiguous.

On textural grounds it is thought that charnockites with disseminated orthopyroxene formed by the simple dehydration of biotite on increasing temperature. Coarse grained discordant charnockitic veins and patches are thought to represent the solid products and part of the liquid products of the vapour-absent melting of biotite.

CHAPTER 9

OXYGEN ISOTOPE STUDY

9.1 INTRODUCTION

This study is a small-scale pilot study undertaken to supplement mineral equilibria studies of the dominant rock types of the Buffels River area. The contact between supracrustal gneisses and augen orthogneisses exposed in the dry river bed of the Buffels River near Draaihoek provides the ideal locality in which to sample a wide range of lithologies on various scales, from cm to 100 m scales. Good, fresh outcrop and the general absence of retrograde alteration were added advantages. The area was first sampled by D.J. Waters in 1986 and further sampling and mapping were undertaken in 1987.

The aim of this study is to record the isotopic character of a series of closely interlayered gneisses. No data for oxygen exists for ortho- and paragneisses in central Namaqualand and very little oxygen isotope data is available for the metamorphic complex as a whole. The limitations of this study prevented the analysis of entire assemblages and the analysis of whole-rock samples.

The oxygen isotope composition of metamorphic rocks is controlled by four factors: 1. the composition of the pre-metamorphic protolith, 2. the effect of devolatilisation reactions, 3. isotopic exchange with infiltrating fluids, and 4. the temperature of exchange among minerals and fluids. The extent of oxygen isotopic equilibrium can be evaluated by assessing the fractionation of ^{18}O between mineral pairs and triplets in different rocks. The study concentrates on quartz (common to all but one of the samples), biotite, and garnet, particularly in pelitic gneisses. The fractionation of ^{18}O between minerals can be used for geothermometry, and, with a knowledge of oxygen diffusion, geospeedometry. Quartz values can be used to suggest possible protolith types for metasediments. Quartz was sampled from segregations with granulite-facies assemblages for comparison with the matrix quartz of the host gneisses. Quartz was also sampled from quartz veins. The veins are discordant with S_3 foliation and are closely associated with charnockitic veins in augen

gneiss. The presence of equilibrium or lack of it may be used to assess the extent of fluid infiltration in the formation of granulites.

9.2 SAMPLES AND MINERAL SEPARATION

The samples collected for the oxygen isotope study reflect the variation of rock types within the augen gneisses and the supracrustal sequence as seen in the dry river bed of the Buffels River, a few kilometres south of Draaihoek, on the farm Hytkoras. The sample localities are shown in fig. 3.2. Sample rock types, their general field relationships and their modal mineralogy are given in table 9.1. Samples selected are of three types: 1. Rock types common to the general area and lithologically homogeneous on a metre scale. These include augen gneiss DWN628, pelitic gneiss DWN624, mafic gneiss DWN625, leucogneiss DWN626 and peraluminous leucogneiss DWN627. 2. Closely interbanded supracrustal rocks. Samples were collected from thin bands within a few metres of each other. Examples are DWN615-618, see fig 9.1, and nearby DWN619-620, and DWN621-623. The aim of this sampling was to examine the variation in $\delta^{18}O$ values in closely related paragneisses. 3. Heterogeneous rocks with xenoliths, veins and segregations were sampled to determine the isotopic nature of their component parts. These samples include augen gneiss DWN613 and its xenolith DWN614. Augen gneiss DWN629 includes a charnockitic patch together with quartz veins and a quartz-feldspar pegmatite (DWN630-632). Detailed descriptions of rock types can be found in previous chapters.

Each sample assemblage was fully investigated by electron microprobe. Mineral compositions are given in the Appendix. On the basis of mineral composition none of the minerals chosen appears to be affected by secondary alteration. Garnets have thin rims of biotite. Some biotites may contain small amounts of chlorite. All veins and coarse grained, discordant segregations were carefully removed by cutting with a rock-saw and were treated separately from their host gneiss. To obtain mineral separates, the rocks were crushed and sieved. The grain sizes used for hand-picking were between 40 and 120 mesh. The sieved rock was washed and magnetite-bearing particles were removed with a hand-magnet.

Magnetite separates were prepared by hand grinding the magnetic

particles to extremely fine powder (<300 mesh) followed by repeated washing with acetone in a beaker below which a small magnet was placed. The beaker was shaken continously and the non-magnetic fraction was washed out. Each separate was then examined optically under high magnification and any silicate-containing composite grains removed. The technique produced separates of very high purity, believed to be better than 98%.

The silicate grains were separated by use of a Franz isodynamic separator. Garnet and biotite were then hand-picked. The remaining, non-magnetised fraction was etched with hydrofluoric acid fumes for 30 seconds and rinsed with distilled water immediately. Quartz grains remain clear and could be hand-picked from feldspar. As all garnets are poikiloblastic it was necessary to optically examine each grain. A number of biotite-bearing composite grains were discarded. However, composite grains containing small colourless inclusions of quartz were difficult to detect and may have been included in the final sample. Thus $\delta^{18}O$ values for garnet may be slightly too heavy.

9.3 ANALYTICAL PROCEDURE

The routine technique used for oxygen extraction from silicates and oxides in the Geochemistry Department, University of Cape Town is described in detail in Vennemann (1989) and in Vennemann & Smith (1990). A short summary is given here.

10 mg of finely crushed mineral sample (15 mg for magnetite) is loaded into nickel reaction vessels which are overpressurised by 150-200 mbar above atmospheric pressure by dry nitrogen. Once loaded with sample, the reaction vessels are evacuated at 200°C to around 10^{-5} mbar for a minimum of two hours. The vessels are then charged with an excess of ClF_3 reagent, after a short period of evacuation at liquid nitrogen temperatures, the vessels are isolated and heated to the appropriate reaction temperature. Reaction temperatures used in this study are: 550°C for quartz and plagioclase, 600°C for biotite and magnetite, and 625°C for garnet. Reaction times vary but most were reacted overnight for 8 to 12 hours. During the course of this study it was discovered that quartz would yield satisfactory results with much shorter reaction times (see Vennemann & Smith, 1990) so later quartz analyses had reaction times of between 2 and 4 hours.

The extracted oxygen is converted to CO_2 by passing it over a hot platinised carbon rod. The yield of CO_2 produced is measured in a mercury-filled manometer. Yields are used to assess the quality of the sample, its reaction and transfer. A number of poor yields <97% were experienced with garnet, while other minerals gave yields closer to 100%. Minerals showing yields between 96 and 103% gave $\delta^{18}O$ values that were indistinguishable between duplicate samples, with an analytical uncertainity of ± 0.2‰. After extraction the residual gases are passed over heated KBr crystals and then frozen into a waste trap. Vessels are examined and residual solids are dumped.

The CO_2 extracted was analysed for its oxygen isotope composition using a VG Micromass 602E, double collector ratio mass spectrometer in the Department of Archaeology, University of Cape Town.

9.4 RESULTS

All values are reported as δ notation in units per mil relative to V-SMOW. Where:

$$\delta^{18}O/^{16}O,sample = 1000\ (R^{sample}/R^{standard} - 1)$$

The isotopic values for most minerals are reproducible to 0.1-0.2 ‰. The value obtained for NBS-28 quartz standard is 9.65‰ ± 0.14 (24 samples).

The relationship between temperature and the fractionation of oxygen isotopes between two coexisting minerals is given by the equation:

$$^{18}O_{x-y} = A + (B \times 10^6)/T^2$$

$^{18}O_{x-y}$ is defined as 1000 ln α_{x-y} and for relatively small fractionations, can be approximated by $\delta^{18}O_x - \delta^{18}O_y$, where x and y are the two coexisting minerals, α is the fractionation factor between the two minerals, and A and B are coefficients derived empirically from natural samples (Bottinga & Javoy, 1975), see table 9.3. and T is temperature in Kelvins.

The fractionation factor α is defined as:

$$\alpha_{x-y} = \frac{(^{18}O/^{16}O)x}{(^{18}O/^{16}O)y} = \frac{1 + \delta^{18}Ox/1000}{1 + \delta^{18}Oy/1000}$$

where x and y are the mineral phases considered.

TABLE 9.1

Sample description and modal proportions

Sample and Lithology	Modal Proportions						Estimated WR $\delta^{18}O$
	Opx	Biot	Qtz	Plag	Kfsp	Oxide	
Samples from the augen gneiss body							
DWN613 Augen gneiss	-	5	44	18	30	3	6.8
DWN614 Quartzo-feldspathic paragneiss. Xenolith in DWN613	-	6	40	25	25	4	7.8
DWN626 Leucogneiss. Possibly intrusive into augen gneiss	-	4	43	26	26	1	8.4
DWN628 Augen gneiss. Homogeneous flecky biotite gneiss	-	9	34	24	32	1	8.4
DWN629 Augen gneiss with charnockitic segregation	2	9	35	13	40	1	6.6
DWN630 Pegmatite vein in charnockitic gneiss DWN629	-	-	65	35	-	-	7.7
DWN631 Lenticular quartz vein in charnockitic gneiss DWN629	-	-	100	-	-	-	6.1
DWN632 Lenticular quartz vein in charnockitic gneiss DWN629	-	-	100	-	-	-	6.6

TABLE 9.1 cont.

Sample and Lithology	Modal Proportions									Estimated WR $\delta^{18}O$
	Opx	Cpx	Gar	Crd	Biot	Qtz	Plag	Kfsp	Oxide	
Close sampling of supracrustal gneisses										
DWN615	28	-	-	-	5	3	61	-	3	6.6
Mafic gneiss. Adjacent to DWN616. See fig 9.1										
DWN616	30	-	-	20	43	-	7	-	-	6.5
Magnesian gneiss. Adjacent to DWN615. See fig 9.1										
DWN617	-	-	7	-	10	53	29	-	1	7.5
Semi-pelitic gneiss. Dominant rock type in the supracrustal sequence										
DWN618	-	-	30	-	70	-	-	-	-	6.8
Coarse grained biotite segregation from magnesian gneiss. See fig 9.1										
DWN619	49	-	-	15	35	1	-	-	-	7.8
Magnesian gneiss. Adjacent to DWN620. 20 m from DWN617.										
DWN620	-	-	10	10	5	65	10	-	-	8.4
Pelitic gneiss. Adjacent to DWN619. 20 m from DWN617.										
DWN621	-	-	-	-	5	43	16	34	2	8.2
Leucogneiss. Close to DWN622-623, probably intrusive.										
DWN622	10	-	7	38	20	25	-	-	-	7.0
Magnesian-pelitic gneiss. 1 m from DWN623.										
DWN623	13	-	7	25	24	28	-	-	3	7.3
Magnesian-pelitic gneiss. 1 m from DWN622.										

TABLE 9.1 cont.

Sample and Lithology	Modal Proportions									Estimated WR $\delta^{18}O$
	Opx	Cpx	Gar	Crd	Biot	Qtz	Plag	Kfsp	Oxide	
Samples from individual units										
DWN624 Pelitic gneiss with garnet-bearing segregation	-	-	35	14	10	25	16	-	-	8.3
DWN625 Mafic gneiss	20	10	-	-	2	7	60	-	1	6.3
DWN627 Garnet-biotite (peraluminous) gneiss	-	-	8	-	3	47	10	31	1	9.4
MCS392 Quartzite	-	-	-	-	tr	100	-	-	-	10.2

Whole rock $\delta^{18}O$ estimates are based on modal mineralogy assuming a closure temperatures of 650°C for all minerals assumed to be in equilibrium with quartz. Values for quartz, biotite, garnet and magnetite are from table 9.2. The fractionation factors used are: quartz-K-feldspar 1.0, quartz-plagioclase 1.5, quartz-pyroxene 2.2, quartz-cordierite 2.3, quartz-oxide 7.3.

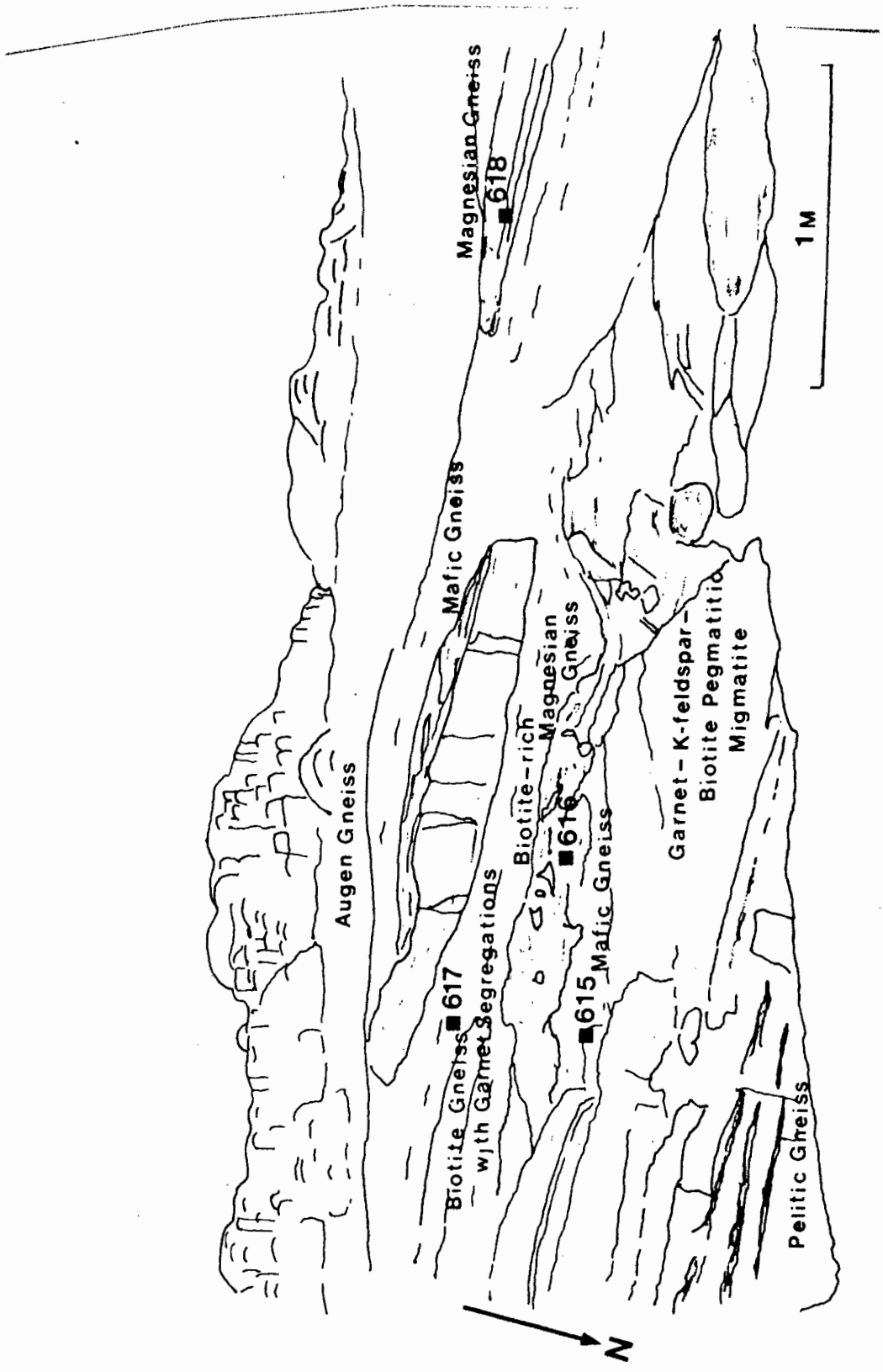

Fig. 9.1 Sketch of field relationships at the sampling site of DWN615-618. River bed, Hytkoras. See fig. 3.2.

TABLE 9.2
Mineral $\delta^{18}O$ for gneisses from the Buffels River

Sample	Qtz	Biot	Gar	Mt	Plag
DWN613	8.01, 7.75 7.88	3.39	----	-0.85, -0.92 -0.89	----
DWN614	9.07, 8.92 9.00	4.04	----	1.77	----
DWN615 (matrix)	9.12, 9.08 9.10	5.28	----	0.82, 0.96 0.89	----
(segregation)	8.63, 8.53 8.58	----	----	----	----
DWN616	----	5.32	----	----	----
DWN617	8.74, 8.68 8.71	5.55, 5.39 5.47	7.09, 7.02 7.06	----	----
DWN618	----	6.84	6.84, 6.83 6.84	----	----
DWN619	----	6.77	----	----	----
(vein)	9.15, 9.11 9.13				
DWN620	9.35, 9.11 9.23	5.08	6.78, 6.71 6.75	----	----
DWN621	9.43, 8.95 9.19	3.79	----	----	----
DWN622	8.84, 8.74 8.79	5.00	6.61	----	----
DWN623	9.64, 9.58 9.61	5.29	6.81, 6.59 6.70	----	----
DWN624 (matrix)	10.21, 9.88 10.05	5.88	7.92, 7.77 7.85	----	----
(segregation)	10.12,10.04 10.08				
DWN625 (matrix)	8.50, 8.43 8.47	4.21, 3.95 4.08	----	1.49, 1.30 1.40	----
(segregation)	7.21, 7.02 7.12				
DWN626	9.94, 9.64 9.79	5.12	----	----	----
DWN627	10.13,10.08 10.11	----	7.37, 7.15 7.26	----	----
DWN628	9.63, 9.60 9.62	4.14	----	----	----
DWN629 (matrix)	7.71, 7.67 7.69	2.97	----	----	----
(segregation)	7.34, 7.28 7.31				
MCS392	10.21,10.19 10.20	----	----	----	----
DWN630 (pegmatite)	8.25, 8.20 8.23	----	----	----	6.78, 6.62 6.70
DWN631 (vein)	6.11, 6.10	----	----	----	----
DWN632 (vein)	6.67, 6.55 6.61	----	----	----	----

TABLE 9.3

A and B coefficients for mineral-pair fractionation (Bottinga & Javoy, 1975)

Mineral pair	A	B
quartz-garnet	----	2.88
quartz-biotite	-0.6	3.69
quartz-magnetite	----	5.57
quartz-plagioclase*	----	1.28

*for plagioclase an_{30}

TABLE 9.4.

Apparent equilibration temperatures of mineral pairs

Sample	Qtz-Biot	T°C	Qtz-Gar	T°C	Qtz-Mt	T°C	Qtz-Plag	T°C
DWN613	4.49	581			8.77	525		
DWN614	4.96	544			7.23	607		
DWN615	3.82	644			8.21	553		
DWN617	3.24	710	1.65	1053				
DWN620	4.15	611	2.48	809				
DWN621	5.40	514						
DWN622	3.79	647	2.18	881				
DWN623	4.32	596	2.91	726				
DWN624	4.17	610	2.20	876				
DWN625	4.39	589			7.07	617		
DWN626	4.67	567						
DWN627			2.85	737				
DWN628	5.48	508						
DWN629	4.72	562						
DWN630							1.53	645

9.5 INTERPRETATION

9.5.1 Quartz values

Values for quartz are shown in fig. 9.2. The range of values is fairly restricted and towards the low end of the reported range for high-grade metamorphic rocks (Shieh & Schwarz, 1974; Wilson & Baksi, 1983; Huebner et al., 1986 and Jiang et al., 1988; Vennemann, 1989). Fig. 9.3 shows a comparison of $\delta^{18}O$, quartz from the Buffels River area and other high grade terranes. It can be seen that the gneisses from the Buffels River area are somewhat depleted in ^{18}O compared to similar granulite-facies rocks in other terranes.

The lowest values come from mafic gneisses and augen orthogneisses, rocks which are thought to have igneous precursors. Quartz from charnockitic gneisses has values between 7-8‰ for matrix quartz and is similar in isotopic composition to quartz in southern Indian charnockites recorded by Stähle et al. (1987) and Jiang et al. (1988). Quartz from paragneisses is typically 1-2‰ higher than that from orthogneisses. Some samples do not follow this simple pattern. Sample DWN628, an augen gneiss, very similar in mineralogy to orthogneisses DWN613 and DWN629 has a $\delta^{18}O$ value for quartz of 9.6 ‰, which is typical of paragneisses from the Buffels River. Field relationships indicate that the augen gneiss in this area is rather heterogeneous, although obvious xenoliths are scarce. Augen gneiss DWN613 and its xenolith preserve mineral differences of around 1‰ in $\delta^{18}O$. It is possible that intrusive augen gneisses, such as DWN628 may be locally derived partial melts from supracrustal rocks very similar in composition to those sampled here.

Quartz values from mafic gneisses are more difficult to interpret as quartz makes up only a small proportion of the mode. It is possible that quartz could be introduced into these rocks at any stage of their metamorphic history. Matrix quartz from the mafic gneiss DWN615 has a composition that would be consistent with being derived from the adjacent pelitic rocks. The quartz from segregations in mafic gneisses has a much higher modal proportion (often greater than 20%) and probably gives a more realistic assessment of the isotopic character of the quartz in these rocks.

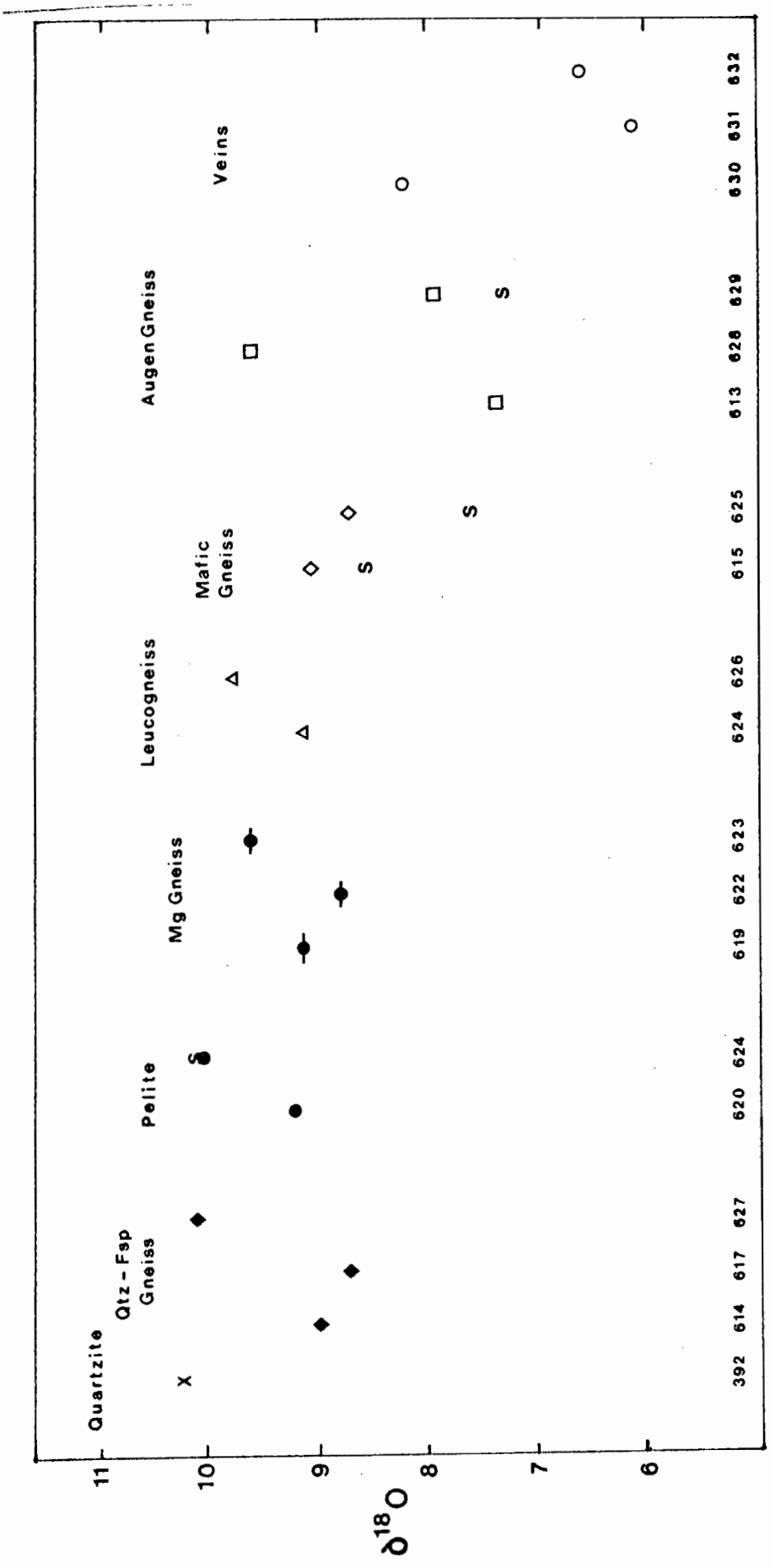

Fig. 9.2 $\delta^{18}O_{quartz}$ for rocks from the Buffels River.

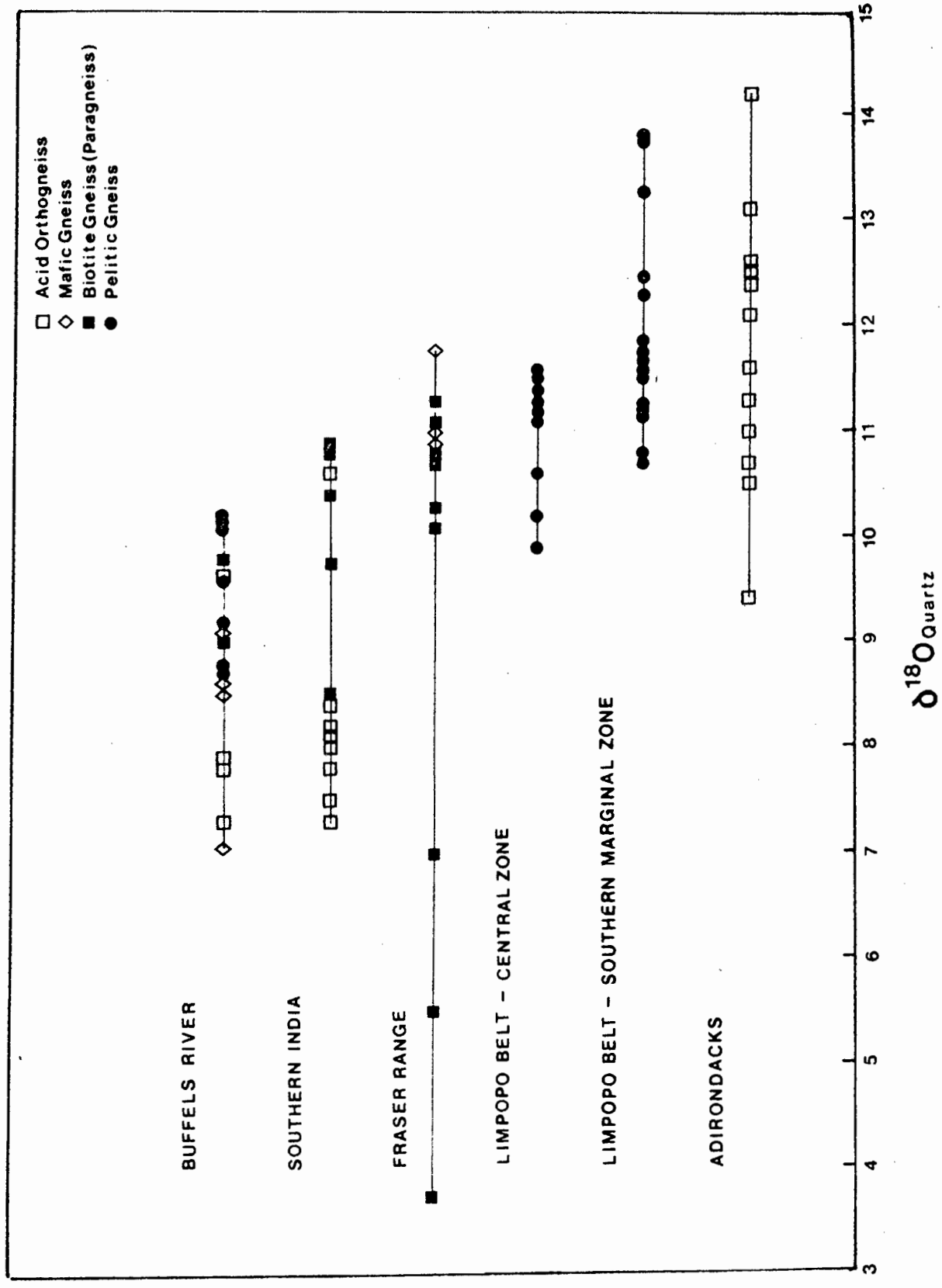

Fig. 9.3 $\delta^{18}O_{quartz}$ for high grade metamorphic terranes. See text for sources of data.

The pelitic gneisses also show low values, average 9.5, compared to other terranes (metapelites, Central Zone, Limpopo Belt, average 11.2, Huebner et al., 1986 and paracharnockites(?) southern India, average 10.1, Jiang et al., 1988). In close sampled supracrustal gneisses there are small differences in $\delta^{18}O$ with magnesian gneisses being similiar to mafic gneisses and pelitic gneisses are somewhat heavier. Larger units of Mg-poor, quartz-rich pelitic gneiss, such as DWN624 give heavy values for quartz of 10.1 ‰. It would appear that small differences in oxygen isotopes between adjacent rocks are the norm in this area and that the protolith signature of different metasediments can be recognised.

The possible parent rocks of different members of the supracrustal sequence in the Buffels River area are discussed in detail by Moore (1986), summarised here with reference to the oxygen isotopic evidence of this study.

Moore models possible parent rock types on the basis of major and trace element geochemistry. Pelitic rocks have bulk compositions similiar to unmetamorphosed Proterozoic platform shales. High values for Al_2O_3, Na_2O, K_2O support a shale-protolith, rather than a greywacke protolith. Moore (1986) recognises two groups of pelitic rocks, a northern group with higher Al_2O_3 and K_2O, and a southern group with higher CaO, FeO, MgO, Na_2O. There is overlap between the two groups in the Buffels River area. In terms of the petrographic variation observed in this study the northern group is typified by sillimanite-rich, K-feldspar-bearing gneisses, the southern group by plagioclase-bearing gneisses containing biotite, garnet and/or cordierite. Moore favours different source areas for each group. The southern group representing a mature shale composed of illite, chlorite and quartz, with a significant plagioclase component. The detritus being derived from either a mixed "granite-basalt" terrane or a granodiorite dominated source region. La/Th ratios suggest a post-Archaean granitic source. The northern group is less mature and has a strong kaolinitic component and is probably derived from a granitic source area. Samples DWN620 and DWN624 are typical of Moore's southern pelitic group and both have high $\delta^{18}O$ of >9‰ for quartz.

The protoliths of quartzo-feldspathic gneisses, biotite gneisses and leucogneisses are more difficult to assess. There is some controversy as to whether these rocks represents arkosic sediments or

igneous rocks. The extremely uniform chemical composition, with a narrow range of SiO_2/Al_2O_3 ratios is typical of extrusive acidic rocks. The K_2O/Na_2O ratio is too high for a greywacke protolith (Moore, 1986). Moore considers these rocks to represent distal ignimbrites, air-fall tuffs and mud-flows of rhyolitic to rhyodacitic composition. Moore suggests that some degree of diagenetic alteration may have taken place to explain the relatvely high K_2O and low Na_2O and CaO of some samples. The $\delta^{18}O$ of quartz from leucogneisses is between 9 and 10 ‰ and is very similiar to that of pelitic rocks. If the protolith was volcanic in origin it could also represent a suitable source rock for sediments in the area. Alternatively, the leucogneisses may be interpreted as metasediments sharing a common source of detritus with the pelitic gneisses.

The major and minor element geochemistry of metabasic rocks from the Buffels River area have been studied by Zelt (1980) and by Moore (1986). The mafic gneisses are typified by relatively high Al_2O_3 and fairly low K_2O. They represent silica-saturated tholeiitic rocks possibly of continental derivation. Moore recognises anomalously high SiO_2-rich granulites and suggests that they may have been partly silicified prior to metamorphism. Due to the low modal abundance of quartz in the mafic gneisses it is not possible to assess whether the $\delta^{18}O$ of quartz in these rocks reflects the original composition of the protolith. The low value of 7.12 ‰ for quartz from the segregation in DWN625 is consistent with a basaltic protolith.

Moore (1986) describes two groups of magnesian gneiss. One is Al-rich and strongly depleted in CaO and Na_2O. This group is represented by sillimanite-bearing, phlogopite-rich magnesian gneisses in the Buffels River area. The second group has a more mafic component with higher FeO, MgO and CaO. This group includes orthopyroxene-cordierite gneisses. The field relationships of these rocks with other members of the supracrustal sequence is consistent with the trends in bulk compositions. Those magnesian gneisses with a mafic component are found overlying mafic gneisses, and those with an Al-rich, pelitic component are closely associated with pelitic gneisses. Moore suggests that the high MgO contents of these rocks represent a high chlorite content in the protolith, perhaps derived from the weathering of mafic rocks, possibly mafic ash bands. Some magnesian gneisses contain abundant boron-rich phases such as tourmaline and kornerupine. Moore suggests that the high boron contents could be related to deposition under hypersaline conditions. A number of

pelitic, mafic and magnesian gneisses with close or gradational contacts were sampled in this study. Magnesian gneiss, DWN616 lies above the mafic gneiss, DWN615 and shows a close similarity in the $\delta^{18}O$ values for biotite. Pelitic gneiss, DWN617 has lower $\delta^{18}O$ values (<9‰) than other metasediments. This may indicate the presence of a mafic component in the protolith, similar to that proposed by Moore for magnesian gneisses.

Moore (1986) argues for a chemogenic origin for many of the quartzites in the northern areas of Kangnas and Oranjefontein. Feldspathic quartzites are common to the south of the Buffels River area and are regarded as clastic sandstones. The quartzite sampled in this study has a $\delta^{18}O$ value of 10.2 ‰. This is the highest recorded in the area and is similiar to that recorded in pelitic gneisses and quartzo-feldspathic gneiss this suggests a detrital origin for the quartzite.

Quartz values from segregations are equal to, or slightly lower than values for quartz in the host matrix. In previous chapters the textures and mineral assemblages observed in segregations have been attributed to partial melting. The process of partial melting at peak metamorphic temperatures in excess of 700°C is unlikely to result in large fractionations of oxygen between residual solids and liquid products. The mass balance modelling of vapour-absent melting in these rocks (see Sections 5.6.1 and 8.5) indicates that the proportion of liquid generated is usually less than 25%. Assuming that all of this liquid escapes from the remaining restite rock (which seems unlikely in the case of the assemblages observed in the preserved segregation) the effect on the restite will be to reduce the modal proportions of reactant phases, particularly quartz. This will cause a redistribution of oxygen amongst restite phases in the remaining rock, without causing a significant loss of ^{18}O. In the case of 25% partial melting in a pelitic gneiss, the depletion of ^{18}O in the restite rock will be around 0.2‰ The effect of partial melting on quartz values observed in the restite matrix will be to increase the $\delta^{18}O$ value as a smaller volume of quartz is left to reequilibrate with other remaining phases in the matrix. This model assumes that melt is removed from the matrix and accumulates in the segregations, and that the segregations reequilibrate internally without exchanging oxygen with the matrix to any great extent. In quartz-rich rocks such as pelitic gneisses these differences should be very minor as the modal balance between quartz and feldspar (which

make up greater than 80% of the mode in fairly equal proportions) is virtually unaffected by partial melting. Hence, in sample DWN624 quartz in the segregation and the matrix have near identical $\delta^{18}O$ values. The greatest variation should be seen in mafic gneisses where segregations are strongly enriched in quartz relative to the matrix. Thus, matrix quartz should give much higher $\delta^{18}O$ values. DWN625 shows a 1.35‰ increase in the matrix quartz value and DWN615 shows a 0.52‰ shift.

Vein occurrences of quartz in pegmatites and monomineralic quartz veins have rather low values (DWN631, 6.11 and DWN632, 6.61). The vein quartz samples were chosen from veins that on the basis of structural criteria were believed to be related to peak-metamorphism, i.e. spatially associated with D_3 shears. The relationship of DWN632 to the surrounding charnockitic gneiss can be seen in plate 8.3. Assuming these veins are high temperature in origin, a fair assumption considering the lack of retrograde fluid alteration in this area, the veins can be used to model possible fluid compositions.

For mineral-fluid calculations the following equations can be used (Friedman & O'Neil, 1977):

At T = 500-750°C

1. $1000 \ln \alpha \text{ qtz-}H_2O = 2.51(10^6/T^2) - 1.46$

2. $1000 \ln \alpha \text{ qtz-}CO_2 = -1.533(10^6/T^2) + 10.611(10^3/T) - 4.2$

For a pure H_2O fluid the isotopic composition of the fluid in equilibrium with quartz veins DWN631 and DWN632 at 750°C equals 7.04 or 7.54. The calculation above gives CO_2 isotopic values of 11.31 and 10.81 for equilibrium with quartz at 750°C. Although, the low solubility of quartz in CO_2 makes it unlikely that quartz was deposited from a pure-CO_2 fluid. These values are not consistent with mantle-derived CO_2, which would have values closer to 7.5‰, the value for Laacher See carbonatites by Taylor et al. (1967). However deposition from a H_2O-rich fluid derived from the host augen gneiss (estimated whole rock $\delta^{18}O$ value of 6.3) is more probable.

The somewhat low values recorded by quartz and other minerals from the Buffels River area could be attributed to a number of

possible factors: 1. Protoliths underwent hydrothermal alteration with meteoric water. Lithostratigraphic and geochemical relationships between certain rock types suggest that they may be weathering or alteration products of felsic and mafic volcanic rocks, see Moore (1986). 2. Protoliths of metasediments were composed of detritus with low $\delta^{18}O$ values. This would be consistent with a source region composed of volcanic or plutonic igneous rocks (Fourcade & Javoy, 1973). 3. The gneisses have had their $\delta^{18}O$ values lowered by exchange with an external fluid reservoir depleted in ^{18}O. Shieh & Schwarz (1974) attribute low $\delta^{18}O$ values to isotopic exchange with H_2O-rich fluid from a deep-seated mafic reservoir. Fourcade & Javoy (1973) invoke mantle-derived CO_2 to explain low $\delta^{18}O$ values from high grade rocks in the Saharan Archaean. 4. ^{18}O was depleted during prograde devolatilisation. Dehydration reactions progressively lower $\delta^{18}O$ values as clay minerals, chlorites, micas and amphiboles breakdown on increasing temperature. However, the preceeding diagenetic and greenschist-facies processes, which may involve reaction with hydrothermal fluids at lower tempertures may cause large changes in the rocks $\delta^{18}O$ depending on the $\delta^{18}O$ of the fluid, the fluid-rock ratio and the temperature of exchange. Amphibolite-facies rocks generally have slightly higher $\delta^{18}O$ values than granulite-facies rocks (Valley, 1986). Amphibolite-facies pelitic rocks normally have 10 to 20% modal biotite, containing 4% H_2O. On the basis of the estimated fractionation factor for biotite and water (Bottinga & Javoy, 1975), the breakdown of biotite and subsequent loss of water at temperatures around 700°C will cause a depletion of 0.1‰ in the whole rock value. 5. Partial melting was cited by Wilson & Baksi (1983) as an effective method of depleting $\delta^{18}O$ in the restite. This method is most likely to reduce $\delta^{18}O$ values if large amounts of partial melt can be generated via vapour-present melting reactions at the lower temperatures of amphibolite-facies. Petrological evidence suggests that segregations sampled in this study were produced by partial melting at peak-metamorphic temperatures of 750°C or higher. This would produce negligible shifts in whole rock values, although mineral values could be effectively reset.

9.5.2 Oxygen isotope thermometry

Table 9.4 shows the apparent equilibration temperatures for the mineral pairs quartz-garnet, quartz-biotite and quartz-magnetite based on the empirical calibrations of Bottinga & Javoy (1975) see

table 9.3 shown graphically in fig. 9.4. There is considerable scatter amongst all apparent temperature values and poor agreement with temperature estimates based on mineralogical cation exchange geothermometers which give values around 750°C (see Chapter 4).

Fig. 9.5 shows a plot of $\delta^{18}O$ values for garnet, biotite and magnetite against $\delta^{18}O$ for quartz. The trends follow poorly constrained isotherms with each mineral-pair defining a broad temperature range. If rocks were subjected to identical temperature conditions, then the same mineral pairs in different rock samples should show the same oxygen isotopic fractionation and hence should fall on the same isotherm. The position of minerals along this isotherm is controlled by the whole rock $\delta^{18}O$ and by the modal proportions of the minerals in the rock. Deviations from the isothermal lines favour open system behaviour (Gregory & Criss, 1986 and Gregory, 1986). The deviations from parallelism in fig. 9.5 in quartz-garnet and quartz-magnetite pairs are difficult to assess as in both cases the sample populations are small. In a open system the slope of the trend lines on a δ-δ plot is a function of the mineral-fluid exchange rates, the isotopic composition of the fluid, the fluid-rock ratio and the temperature of exchange. Two possible closed system mechanisms could account for the observed isotopic disequilibrium. The recorded oxygen isotope fractionation is a result of intercrystal diffusion of oxygen during cooling. Thus the recorded mineral fractionation is a function of relative oxygen isotopic closure between phases, which will be influenced by cooling rate, modal abundance and crystal size. The other possibility is that recrystallisation occured during cooling, and the isotopic fractionation between minerals records the final crystallisation temperature. This mechanism may be important in crystallising melt segregations.

Quartz-garnet pairs give the highest values. Three samples give tempertures which are anomalously high (>850°C). Oxygen isotopic fractionation between quartz and garnet becomes very small at high temperatures and any errors during the preparation of mineral separates or during extraction or analysis will have a large effect on the temperature estimates. It has been noted already that highly poikiloblastic garnet with minute quartz inclusions caused problems during sample preparation. The presence of quartz in garnet would tend to increase the observed $\delta^{18}O$ values for garnet and reduce the observed fractionation between the natural mineral pair leading to an

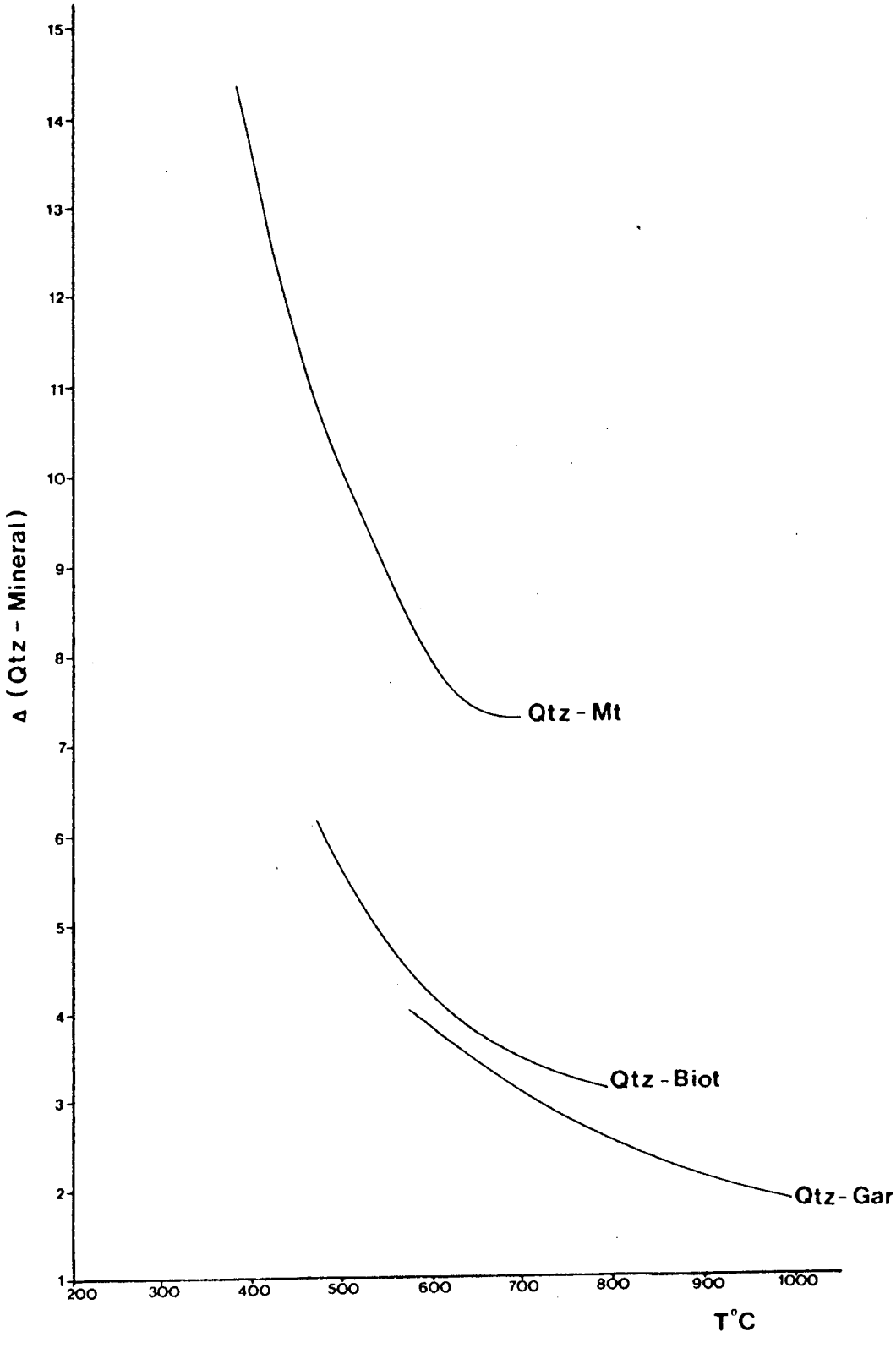

Fig. 9.4 ^{18}O fractionation curves for exchange between mineral pairs quartz-garnet, quartz-biotite, and quartz-magnetite. Based on the empirical calibrations of Bottinga & Javoy (1975) for temperatures applicable in metamorphic rocks.

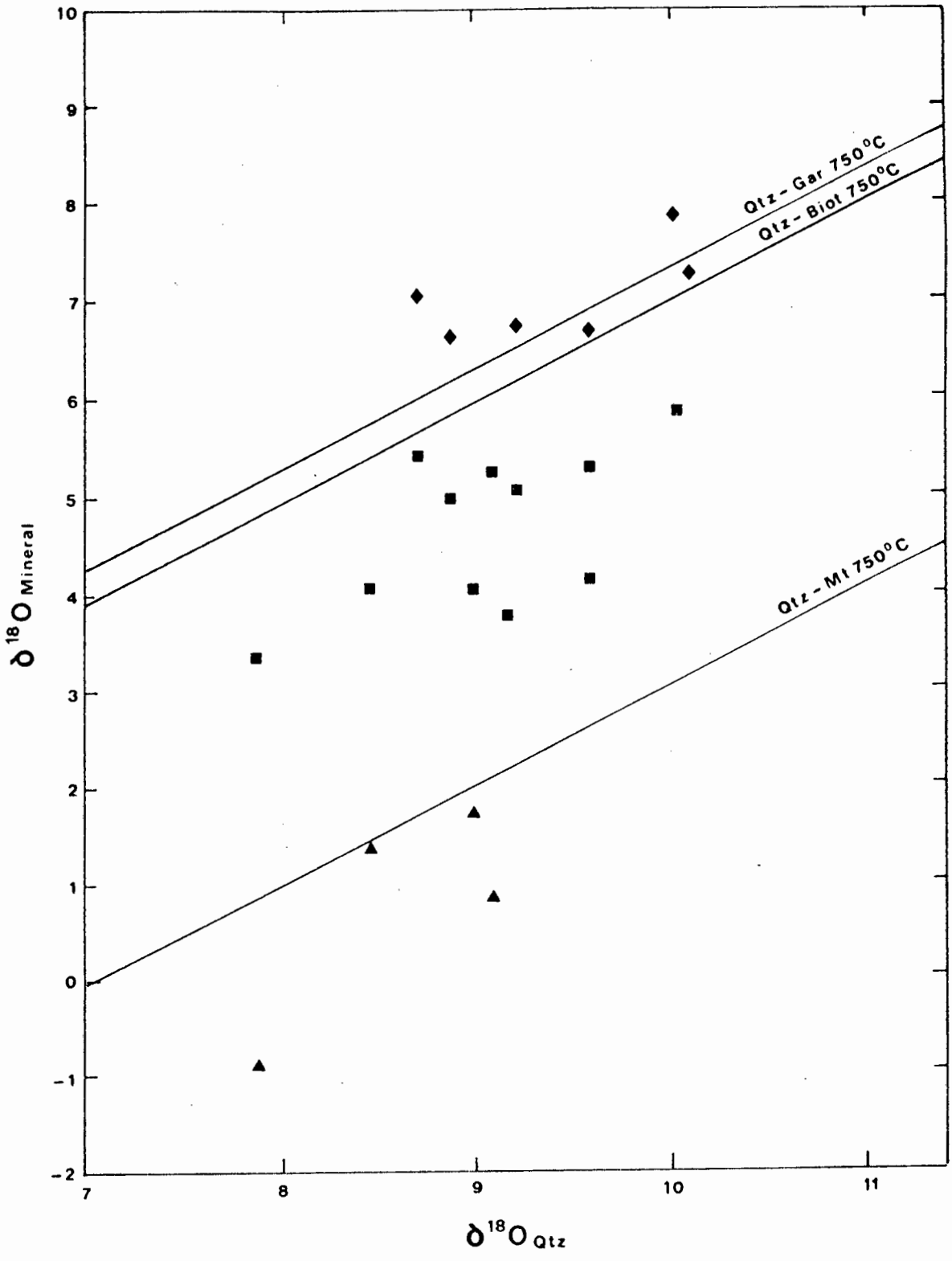

Fig. 9.5 δ-δ plot for δ^{18} garnet(◆), biotite(■) and magnetite(▲) against $\delta^{18}O$ quartz.

overestimate of the equilibration temperature. The effect of 10% quartz contamination would increase garnet values by about 0.3-0.4‰. Assuming this level of contamination the temperature estimates could be up to 100°C too high.

Quartz-biotite temperature estimates are considerably lower than quartz-garnet values, the average temperature from this method is 591°C and there is a fairly wide scatter (508-710°C). Similar values are recorded by different workers in other terranes (Huebner et al., 1986; Jiang et al., 1988 and Vennemann, 1989). Quartz-magnetite temperature estimates are also below assumed peak conditions and show wide variation. Rocks with coarse grained magnetite, such as DWN614 give higher temperature estimates than those with finer, disseminated grains. It is likely that quartz-biotite and quartz-magnetite equilibration temperatures are a form of diffusion-controlled blocking temperature. This argument has been cited by the authors above and may have potentially useful applications in geospeedometry.

9.5.3 Diffusion effects on oxygen isotopic exchange

During cooling the isotopic composition of a mineral becomes fixed when a temperature is reached when diffusion becomes too slow to allow isotopic exchange with adjacent minerals, or, perhaps more importantly, with the surrounding grain boundary fluid. Table 9.5 shows the relevant experimental data available for the minerals used in this study. Fig. 9.6 shows the diffusion rate for ^{18}O in various minerals as a function of temperature for grain sizes of 1 mm.

The available diffusion data has been obtained mainly by using secondary ion mass spectroscopy under hydrous conditions, except that for phlogopite which was measured using the bulk isotope method (Gilletti & Anderson, 1977). The data suggests that quartz, biotite and magnetite continue to exchange oxygen to lower temperatures than garnet (assuming grossular and almandine behave in similar fashion). Oxygen isotope thermometry is based on equilibrium exchange of oxygen between a pair of minerals. If one phase ceases oxygen exchange because internal or external diffusion rates have become too sluggish while the other phase continues to exchange oxygen with the metamorphic fluid, the temperature determined from the mineral pair will not represent equilibrium fractionation. At low fluid-rock ratios the oxygen isotopic composition of the fluid is buffered by

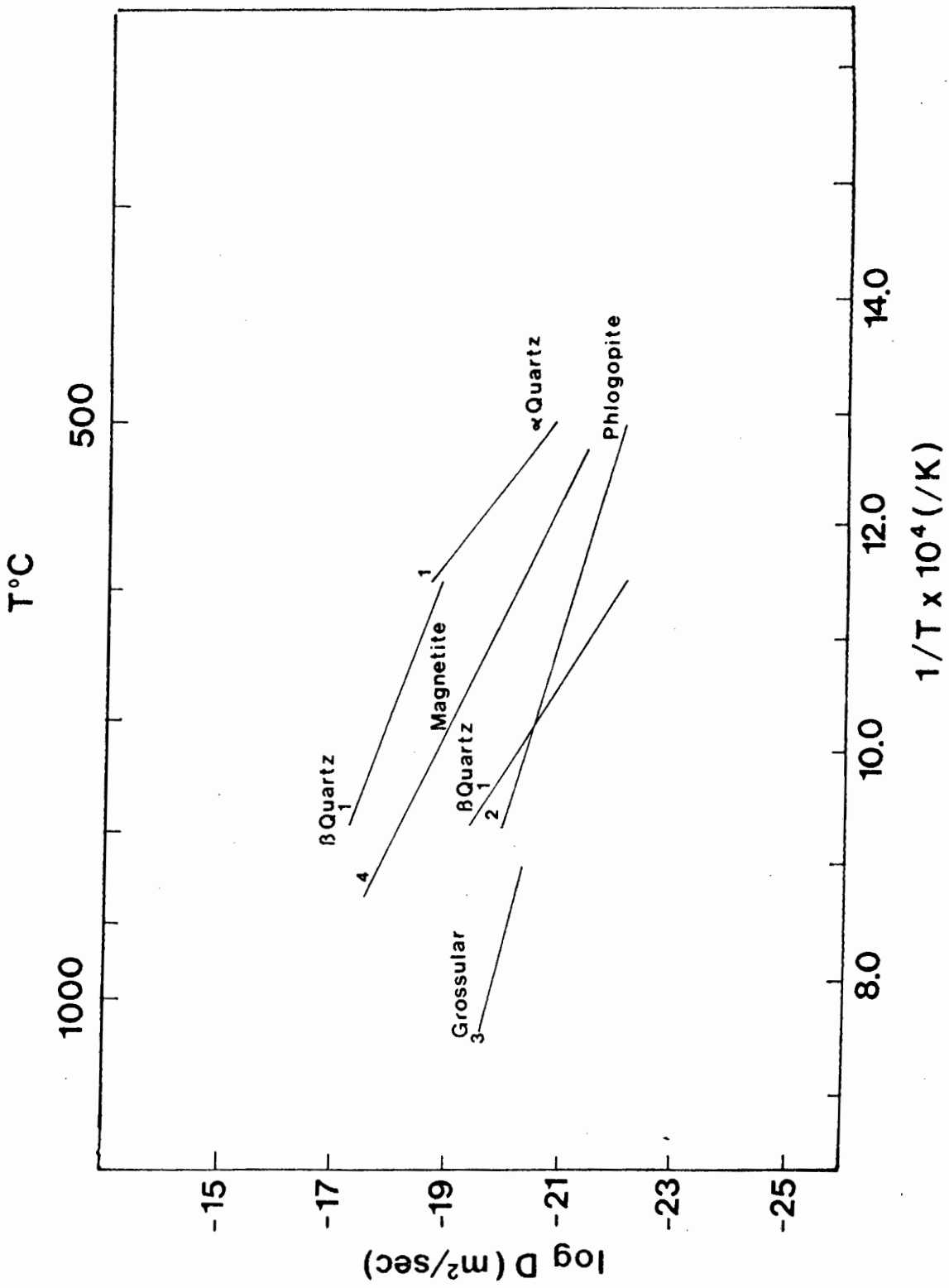

Fig. 9.6 Experimentally determined diffusion rates for oxygen in minerals used in the study, for grain sizes of 1 mm.
1. Gilletti & Yund (1984)
2. Gilletti & Anderson (1977)
3. Freer & Dennis (1982)
4. Gilletti & Hess (1988)

the rock. Therefore if a phase continues oxygen exchange with the grain-boundary fluid its isotopic composition will remain constant, as the mineral will tend to buffer the fluid composition.

TABLE 9.5

Experimental diffusion data for ^{18}O in various minerals

Mineral	T (K)	D_0 (cm^2/s)	Q (kJ/mol)	Ref
Quartz	1073-873	1.0×10^{-4}	234	1
Quartz	1073-873	4.0×10^{-7}	142	1
Quartz	873-773	1.9×10^{2}	284	1
Phlogopite	1073-773	1.03×10^{-14}	122	2
Grossular	1323-1123	2.67×10^{-16}	102	3
Magnetite	1073-773	3.75×10^{-6}	188	4

References: 1. Gilletti & Yund (1984), 2. Gilletti & Anderson (1977), 3. Freer & Dennis (1982), 4. Gilletti & Hess (1988)

Quartz-biotite pairs provide low temperature estimates. From the available experimental data it appears that quartz has a lower blocking temperature, although this is by no means certain, as data for biotite have not been determined using the same method. The role of feldspar in this process cannot be ignored, as most rocks in this study consist dominantly of feldspar and quartz. Diffusion data from Gilletti et al. (1978) and Freer & Dennis (1982) together with evidence from high-grade rocks (Huebner et al., 1986 and Vennemann, 1989) suggests that the closure temperature for oxygen exchange in feldspars is similar to or slightly higher than that for quartz. In rocks with a low fluid-rock ratio the isotopic composition of the fastest diffusing mineral will be controlled somewhat by the closure temperature of the second fastest diffusing mineral. In most of these samples feldspar will exert a close control on the isotopic composition of the quartz. Biotite and magnetite will play a minor role due to their much lower modal abundance. However, their finer grain size, particularly of magnetite, will enable diffusion-controlled exchange to be effective even at temperatures below 550°C. The effect of retrograde reequilibration between different groups of minerals during a prolonged cooling episode will result in apparent

disequilibrium temperature estimates as shown in fig. 9.5. The preservation of equilibrium oxygen isotope fractionation at the high temperature of granulite-facies would only occur if cooling was extremely rapid or the rocks were devoid of grain-boundary fluid.

A simplistic form of geospeedometry can be attempted using the diffusion data listed in table 9.4. As a first step the closure temperatures of the phases involved can be calculated using the expression (Dodson, 1973):

$$\frac{E}{RT_c} = \ln \frac{(ARTc^2 DO)}{(r^2 E\, dT/dt)}$$

Where T_c is the closure temperature, dT/dt is the cooling rate, r equa the radius of the grains, E is the activation energy, and A is a geometrical coefficient (55 for a sphere, 27 for a cylinder, and 8.7 for a plane sheet) and D is the diffusion coefficient.

Table 9.6 lists the closure temperatures of minerals in this study calculated for different cooling rates.

TABLE 9.6

Calculated closure temperatures for minerals for given radius at different cooling rates

Mineral	Radius (r)	A	Cooling rate (dT/dt) °C/my		
			1	10	100
Quartz	1.0 mm	27	470	500	550
Magnetite	0.1 mm	55	380	420	470
Garnet	5.0 mm	55	720	800	900

Closure temperatures calculated for a cooling rates of 10°C/my seem to give the best correlation with the observed data in table 9.2. This is also supported from cation closure temperatures postulated for garnets (see Section 6.5.2).

Available evidence (see review by Cole & Ohmoto, 1986) suggests that diffusion rates for mineral-fluid exchange are considerably higher in the presence of hydrous fluid compared to CO_2-rich fluids

(Muehlenbach & Kushiro, 1974) and that measurement of solid-solid diffusion under dry conditions is virtually impossible. Evidence based on mineral equilibria studies presented in earlier chapters indicates equilibrium was achieved under conditions of low and variable X_{H2O}. It seems possible that many rocks were effectively "dry". The concept of fluid-absent metamorphism (Thompson, 1983) does not exclude the presence of a grain-boundary fluid that may be only one or two molecules thick. Such low volumes of fluid may be chemically inert but still able to participate as a diffusion enhancing medium on a grain-size scale. Evidence on the character of the metamorphic fluid preserved in these rocks is examined in the fluid inclusion study (see chapter 10).

9.6 SUMMARY

Values for all minerals vary on a cm scale, suggesting that finely interbanded gneisses retained differences in isotopic signatures through the granulite-facies metamorphic event. $\delta^{18}O$ values for quartz vary between 7.7-10.2 ‰ and are low compared to other granulite-facies terranes. The depletion of ^{18}O in these metasediments is thought to be related to protolith composition, low values indicating detritus derived from a volcanic or plutonic terrane. High temperature devolatilisation and partial melting reactions can only account for depletions of no more than 0.3-0.4 ‰.

Quartz from segregations gives lower values than quartz from the host rock matrix. This is thought to result from a shift in the modal proportions of quartz inside and outside the segregation. A reduction in matrix quartz caused by small amounts of local partial melting increases the $\delta^{18}O$ value for remaining matrix quartz as the smaller volume of quartz is buffered to higher values by exchange with adjacent matrix minerals. It appears that matrix and segregation equilibrated as separate "closed" systems.

Quartz veins assumed to have a high temperature origin have values between 6.1-6.6 ‰. If the quartz was deposited from a pure H_2O fluid or a mixed fluid dominated by H_2O, the modelled fluid compositions are consistent with a fluid derived from the host gneisses. The small-scale isotopic variations recorded in these gneisses suggests that fluid infiltration was very minor, and the isotopic composition of the fluid was buffered by the rocks.

Oxygen isotope thermometry gives poor correlation with cation mineral thermometry. Quartz-garnet pairs give anomalously high equilibration temperatures (probably due to quartz contamination in the garnet samples). Quartz-biotite and quartz-magnetite pairs give equilibration temperatures well below the estimated metamorphic peak. Diffusion data can be used to produce theoretical closure temperatures for oxygen exchange. Observed equilibration temperatures are consistent with slow cooling rates around 10°C/My.

CHAPTER 10

FLUID INCLUSION STUDY

10.1 INTRODUCTION

In previous chapters the importance of low water activity in the fluid phase has been cited as an important factor in the formation of granulite facies mineral assemblages. Fluid inclusions trapped in quartz may provide direct samples of the metamorphic fluid at the time of granulite metamorphism. This chapter outlines a small scale study aimed to assess the character of fluid inclusions within a variety of lithologies. Textural relationships and inclusion petrography are used to infer a relative chronology of fluid populations. The fluid evolution and retrograde uplift path can then be modelled using the composition and density of inclusions determined by microthermometry.

Many granulite-facies terranes are marked by the presence of high density CO_2-rich fluids (Touret, 1971; Hollister & Burruss, 1976; Touret & Dietvorst, 1983; Hansen et al., 1984; Rudnik et al., 1984; Schreurs, 1985). The presence of these fluids has been used to argue for CO_2 infiltration as a mechanism for lowering water activity in granulites (see Hansen et al., 1984 and 1987). Other workers regard CO_2-rich inclusions as residual fluid left behind after the partitioning of H_2O into silicate liquid produced by partial melting (Olsen, 1987). Lamb et al. (1987) have demonstrated that "primary-appearing" high density CO_2-rich inclusions may occur in rocks which equilibrated under conditions of low CO_2 fugacity, and hence probably represent post-metamorphic entrapment. The lack of certainity in the interpretation of early fluid inclusion populations suggests that the technique is best applied to the study of cooling and uplift history from the "mapping" and analysis of the many secondary inclusion trails.

10.2 ANALYTICAL METHOD

All microthermometric measurements were conducted on a Chaixmeca heating-freezing stage in the Department of Geology at the University

of the Orange Free State. Daily standardisation against a natural CO_2 inclusion was performed for the triple-point of CO_2 (-56.6°C). At temperatures between -60°C and 30°C the reproducibility was always within ±0.2°C for duplicate measurements. At higher temperatures >200°C the error on measurements was about ±3°C. Initial inclusion petrography was carried out on 1 mm thick doubly polished wafers prepared at room temperature using "Super-Glue" as a mounting medium. This proved excellent for "mapping-out" inclusion trails and observation of a large number of inclusions in a single sample. However, to reduce thermal lag between stage and inclusion and to improve optical resolution when using the heating-freezing stage microthermometry was carried out on 100μm wafers prepared from the original thick-wafers. With the Chaixmeca stage only small mineral chips can be observed, so the prepared wafers were broken up into a series of numbered chips. The position of each chip in the wafer was recorded.

10.3 FLUID INCLUSION PETROGRAPHY

Six samples were chosen for the study. The aim was to examine a representative range of inclusion-types in a number of common lithologies. All measurements were carried out on inclusions within quartz crystals. Quartz is an ideal host mineral as it is presumed that the quartz will not react with the trapped fluid and therefore is more likely to preserve the original composition of the fluid provided the inclusion has not leaked. Quartz has the advantage of good optical properties which allowed small 1μm-size inclusions to be measured. None of the samples selected showed obvious evidence of recrystallisation or strain-shadowing. Quartz recrystallises readily especially after it has been strained, this may result in changes in volume and redistribution of preexisting inclusions (Kerrich, 1976). It was hoped that "primary" inclusions would be preserved in the samples selected.

The samples were as follows:

MCS327 - quartz from a pyroxene-bearing segregation in a mafic gneiss
MCSHO2 - quartz from the matrix of a garnet-biotite pelitic gneiss
MCS311 - quartz from the matrix of a leucogneiss
DWN628 - quartz from the matrix of a biotite-bearing augen gneiss
DWN629 - quartz from a charnockitic segregation
DWN632 - vein quartz within augen gneiss DWN628

All samples are taken from Hytkoras, except MCS311 which occurs on the farm Rietfontein. Sample mineralogy can be found in previous chapters, samples DWN629, DWN629 and DWN632 were also part of the oxygen isotope study described in Chapter 9.

Inclusions can be grouped into categories on the basis of texture, together with the inclusion composition and density this can be used to assess a relative chronology. The identification of metamorphic fluid inclusions from textural evidence was made following the approach of Hollister & Burruss (1976). Inclusions were grouped into three categories or generations: 1. Solitary inclusions, inclusions in small clusters, inclusions with negative crystal shapes. 2. Inclusions along well healed fracture planes that do not cross grain boundaries. 3. Inclusions along open, immature fractures that cross grain boundaries. Roedder (1971 and 1984) suggests that annealing and recrystallisation of quartz results in the transposition and in some cases the obliteration of older inclusion trails such that the earliest formed inclusions are those which no longer lie along recognisable planes. Hence the categories above may be interpreted as a poorly constrained trapping sequence. The ease of transposition and reentrapment of fluids suggests that it would be unwise to designate any inclusion in a metamorphic rock as primary (using the classification of Ermakov, 1965). In most studies of granulite-facies rocks the earliest inclusions often have higher densities than inclusions in later trails (Hollister & Burruss, 1976; Touret & Dietvorst, 1983). Some workers believe that inclusions with a negative crystal shape indicate older entrapment ages than irregular or ellipitical inclusions, because this shape requires time for diffusion and recrystallisation of the host mineral (Olsen, 1987). Natural decrepitation of early inclusions is observed as a series of satellite inclusions around a single larger inclusion, which may have a stellate texture or may exhibit a definite tail marked by a miriad of tiny inclusions. The relative ages of fractures may be determined by cross-cutting relationships. In the case of fluid aided retrogression inclusion trails may parallel veinlets of the alteration mineral assemblage. This is observed in sample DWN629, where fractures in quartz are filled with tiny fluid inclusions (too small for microthermometry) which develop into chloritic veinlets in adjacent K-feldspar. It is impossible to determine whether this represents fluid entering or leaving the rock. Immature fractures consist of a clearly visible fracture lined with small, closely

spaced, irregular shaped inclusions. Preliminary inclusion petrography produced the following inclusion types (see plate 10.1):

1. Type I ("primary")
   Ia. Dense, monophase CO_2 clusters and solitary inclusions.
   Ib. Rare, dark coloured, monophase inclusions, presumed to be CH_4 or N_2.
   Ic. Rare, solitary H_2O inclusions.

2. Type II ("secondary")
   IIa. Low density CO_2 (vapour bubble commonly visible at room temperature) along healed fractures. Decrepitation clusters around Type Ia inclusions.
   IIb. H_2O inclusions in trails along well healed fractures.
   IIc. Mixed CO_2-H_2O inclusions, often located at the intersection of single fluid H_2O and CO_2 trails.
   As a general rule fratures containing H_2O tend to be older than fractures containing CO_2. However there are many exceptions.

3. Type III
   Late open fractures filled with many small H_2O inclusions.

10.4 MICROTHERMOMETRY - RESULTS

Measurement of critical phase changes in this study followed the routine observational techniques outlined by Roedder (1984) and Shepherd et al. (1985). T_m represents the temperature of final melting of solid phases formed on cooling. T_h represents the temperature of homogenisation of liquid and vapour phases. T_m measurements are used to determine the composition of the inclusion and T_h measurements are used to determine the density of the fluid. At any known temperature the density of liquid coexisting with vapour in a one-component system is uniquely defined. If the volume of the cavity has remained constant, the density is that of the fluid at the time of entrapment. Isochores are lines of equal density extending from T_h on the liquids boiling curve in P,T space. The representative isochores can be used to determine pressure if the temperature of entrapment can be estimated.

Melting temperatures for CO_2-rich inclusions are presented in fig. 10.1. Melting temperatures range from -56.6 to -60.2°C. The

a. Type Ia solitary, monophase CO_2-rich inclusion.
MCS327
T_m -56.1, T_H -1.5

b. Natural decrepitation of Type Ia CO_2 inclusion.
$DWN629_b$

c. Type Ib solitary mononphase N_2-CH_4-rich inclusion.
MCS327

d. Type Ic solitary H_2O inclusion with daughter crystal
MCS327
T_m -0.9, T_H 321

e. Type Ia cluster of monophase CO_2-rich inclusions
$DWN629_b$
T_m -55.6, T_H -1.4, -1.1, -0.2, -0.8, -0.8, -0.7, -0.6

f. Type IIa trail of moderate density CO_2-rich inclusions.
DWN632
T_m -56.0, T_H 5.5, 5.7, 5.4, 7.3, 9.3

g. Type IIb trail of H_2O inclusions.
DWN632
T_m -0.7,-0.6,-0.5,-0.4,-0.4, T_H 222, 222, 228, 229, 244

h. Type IIc mixed H_2O-CO_2 inclusion.
DWN632
CO_2 T_m -56.2, T_H 29.7

Plate 10.1 Fluid inclusion types from gneisses in the Buffels River area. Photographed at 20°C.

Plate 10.1

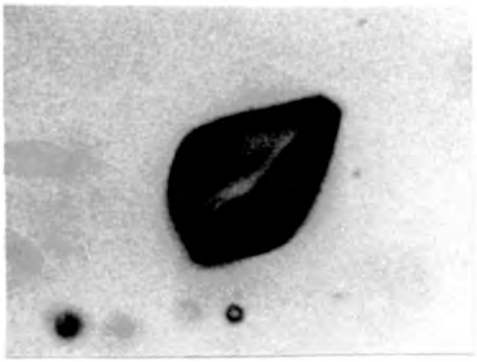

a

5 μm

b

5 μm

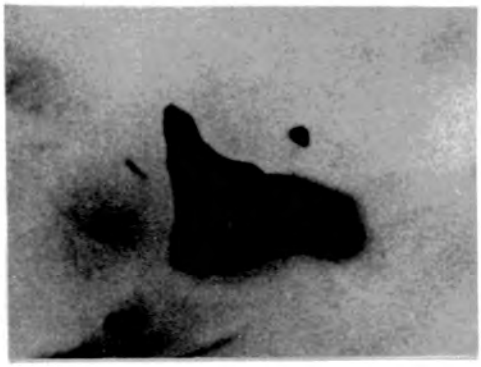

c

10 μm

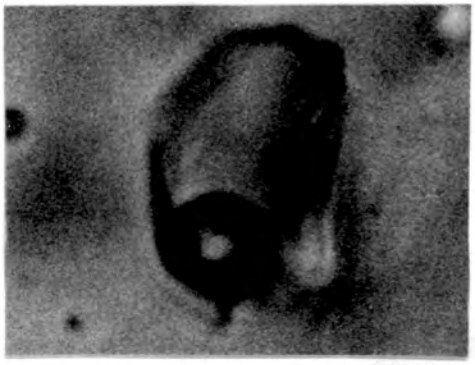

d

2 μm

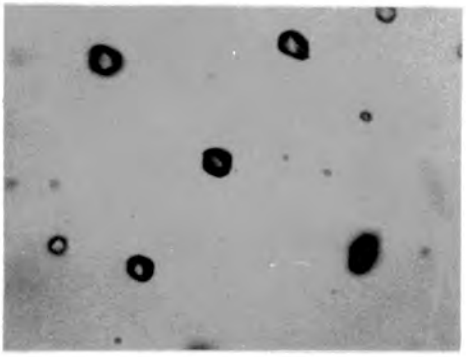

e

10 μm

f

10 μm

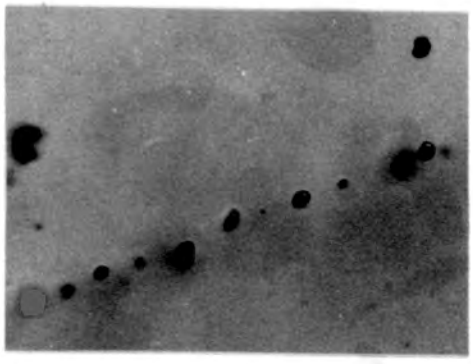

g

10 μm

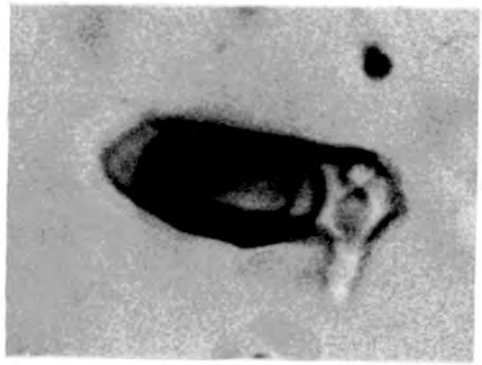

h

2 μm

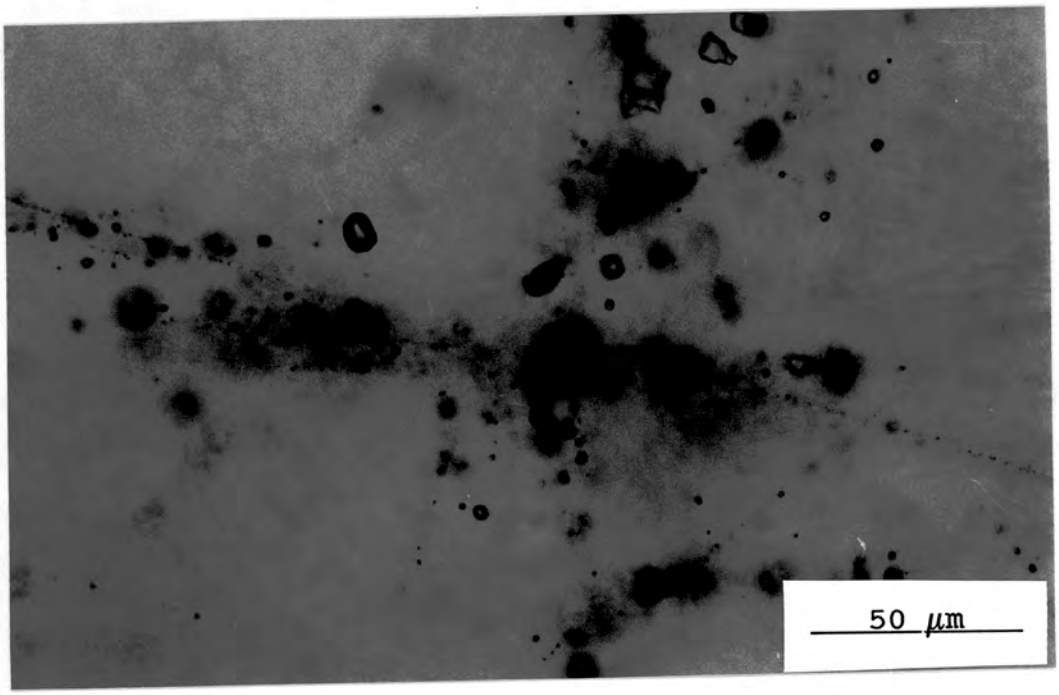

Plate 10.2 Intersecting trails of separate CO_2 and H_2O fluids. At the crossover point fluid mixing occurs and mixed CO_2-H_2O inclusions are observed. DWN632.

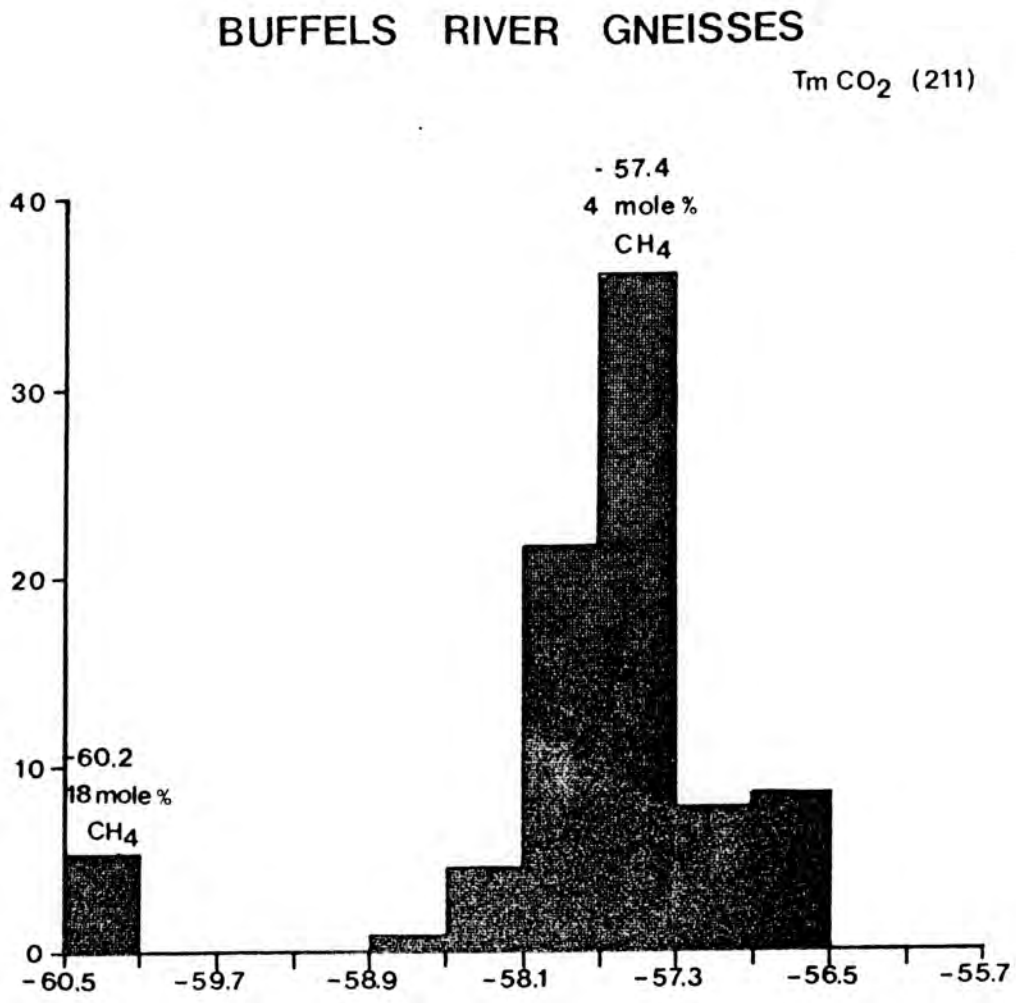

Fig. 10.1 T_m for CO_2-rich inclusions

depression of the melting point from that for pure CO_2 at -56.6°C is attributed to the presence of additional components. Most Type Ia CO_2 inclusions melt at -57.4°C. Type IIa inclusions in sample DWN628 show a greater depression of the melting point to -60.2°C (T_h ranges from 4.2 to 17.7°C). Hall & Bodnar (1990) review data from seven studies on CO_2-rich inclusions in granulite-facies rocks and show that T_m varies between -55.5 to 62.5°C. As accuracy in most studies are generally ± 0.1° at these temperatures on a variety of microthermometric equipment such variations can be regarded as significant. Methane, Nitrogen and Water are the most probable extra components in the fluid. It was not possible to undertake Raman spectroscopy on the samples in this study so the nature of additional components is speculative. T_m of -57.4°C corresponds to approximately 4 mol% CH_4, if a negligible volume of vapour is present (Van den Kerkoff, 1988). T_m of -60.2°C corresponds to 18 mol% CH_4. The above compositions assume that CH_4 is the only extra component. N_2 has the effect of lowering the melting temperture more drastically due to its lower critical point (-147°C for N_2 compared to -83°C for CH_4). H_2O would have little effect. However, if H_2O is present, due to its wetting characteristics, it would form a rim on the walls of the inclusion cavity, so that up to 20 mol% H_2O may be optically undetectable (Burruss, 1981 and Shepherd et al., 1985). The nature and importance of the additional component(s) will be discussed later.

Type Ia CO_2-rich inclusions are common in quartz from segregations (MCS327 and DWN629) and homogenise at temperatures between -5 and 2°C, see fig. 10.2, with a well defined group at 0°C. Homogenisation of all CO_2 inclusions is from liquid plus vapour into the liquid state.

A rare group of dark monophase inclusions do not form a solid on cooling to temperatures of -180°C. A vapour bubble forms at -155°C. On heating homogenisation occurs to the liquid phase at around -140°C. This is termed type H1 homogenisation by Van den Kerkoff (1988) and is characteristic of almost pure CH_4-N_2 fluids. All Type Ib inclusions show sudden dissappearance of the interphase boundary without relative liquid-vapour volume change, this is typical of near critical homogenisation (Touret & Dietvorst, 1983). As calibration of the stage is poorly constrained at such low temperatures these inclusions could consist of pure N_2 as the critical point for N_2 is at -147°C. However, two large (20 μm) inclusions in sample MCS327

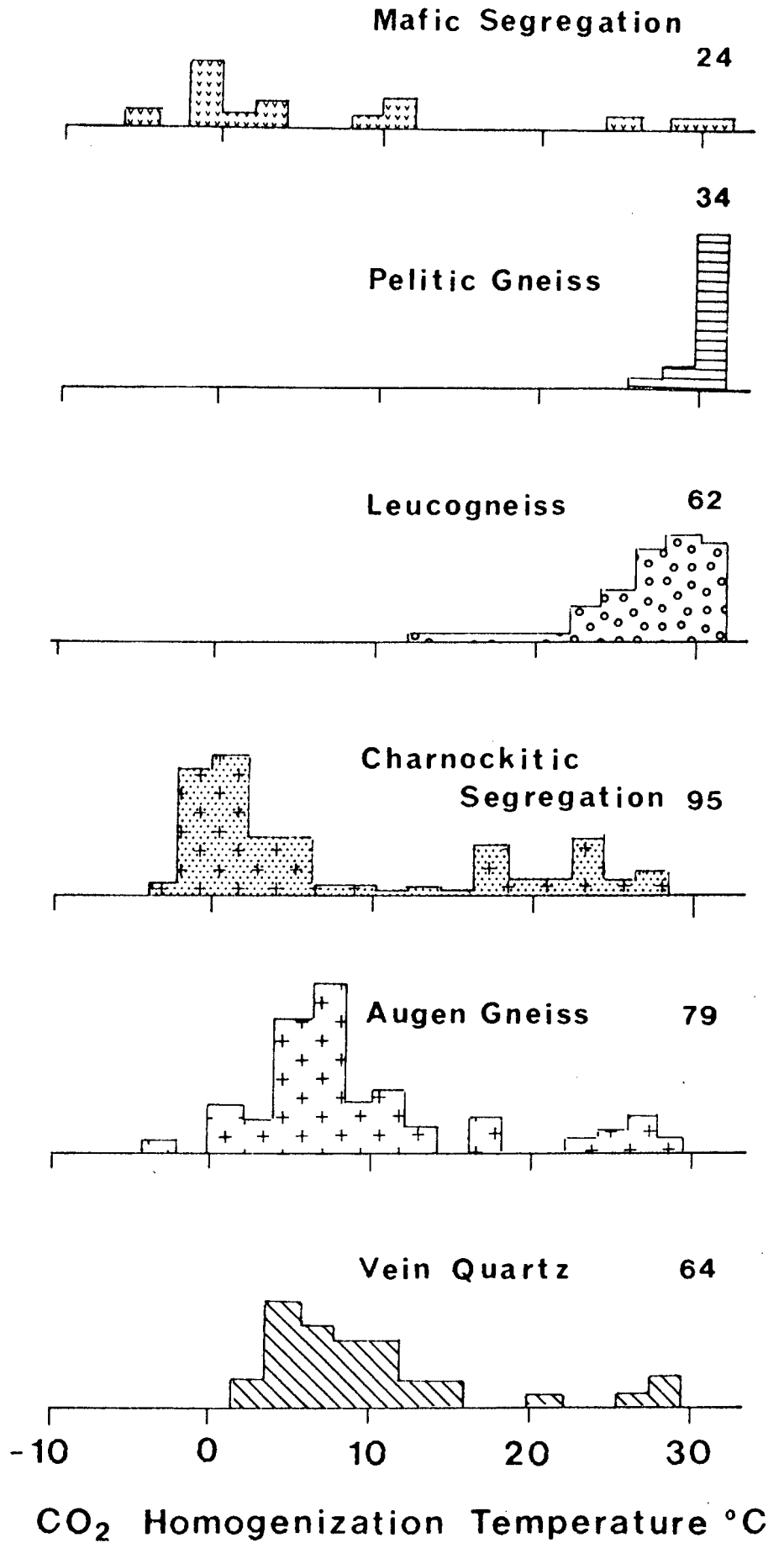

Fig. 10.2 T_h for CO_2-rich inclusions

show the formation of solid particles on repeated heating and cooling between -30 and 0°C. This behaviour seems to resemble the formation of clathrates in the CO_2-H_2O system, and suggests a multi-component fluid, which may include some H_2O. No behaviour of this type has been reported in the literature for CH_4-N_2 inclusions.

Type Ic inclusions have melting temperatures between -3.8 and -0.5°C (see fig. 10.3). Salinity varies between 6 and 1.3 weight % NaCl, assuming that NaCl is the only dissolved salt present. Eutectic points were difficult to observe in all except the largest inclusions (>10μm). Small cubic crystals are seen in the more saline inclusions. These are assumed to be NaCl. Under high power magnification (x1000) other daughter crystals can be observed (plate 10.1 c and g). Identification is impossible. Homogenisation temperatures vary between 225-325°C, see fig. 10.4.

Type II inclusions occur in secondary trails. They comprise CO_2-rich inclusions, aqueous inclusions and mixed CO_2-H_2O inclusions. Type IIa inclusions give homogenisation temperatures between 6 and 31°C. Larger inclusions (>2μm) along well-healed fractures homogenize at lower temperatures (<23°C) than smaller inclusions along visible fractures. These inclusions commonly show homogenisation close to the critical temperature for CO_2 (as recorded in sample MCSH02). Clusters of secondary inclusions often surround earlier Type Ia inclusions, this is interpreted as reentrapment after the natural decrepitation of large CO_2 inclusions (Roedder, 1984 and Crawford & Hollister, 1986). Most Type IIb aqueous inclusions have melting temperatures close to 0°C and are thus of low salinity. Daughter crystals are not normally observed. In some cases salinity is much higher with T_m as low as -11.5°C indicating 16 weight % NaCl, assuming a simple H_2O-NaCl system. Homogenisation temperatures vary between 160 and 325°C. The histograms in fig. 10.4 indicate that a large number of secondary, near-pure H_2O inclusions homogenise between 235 and 265°C. It is clear that no single generation of aqueous inclusions can be picked out from the histograms in fig. 10.4.

Type IIc mixed CO_2-H_2O are very rare. They often occur at the intersection of separate CO_2 and H_2O trails (see Plate 10.2). No distinct trails of mixed CO_2-H_2O were observed, although it is impossible to distinguish a double miniscus in very small (1μm) inclusions. For mixed CO_2-H_2O inclusions in plate 10.2 $T_{m,CO2}$ = -56.8°C, $T_{m,H2O}$ = -1.3°C, $T_{m,Clath}$ = 8.8 $T_{h,CO2}$ = 29°C and

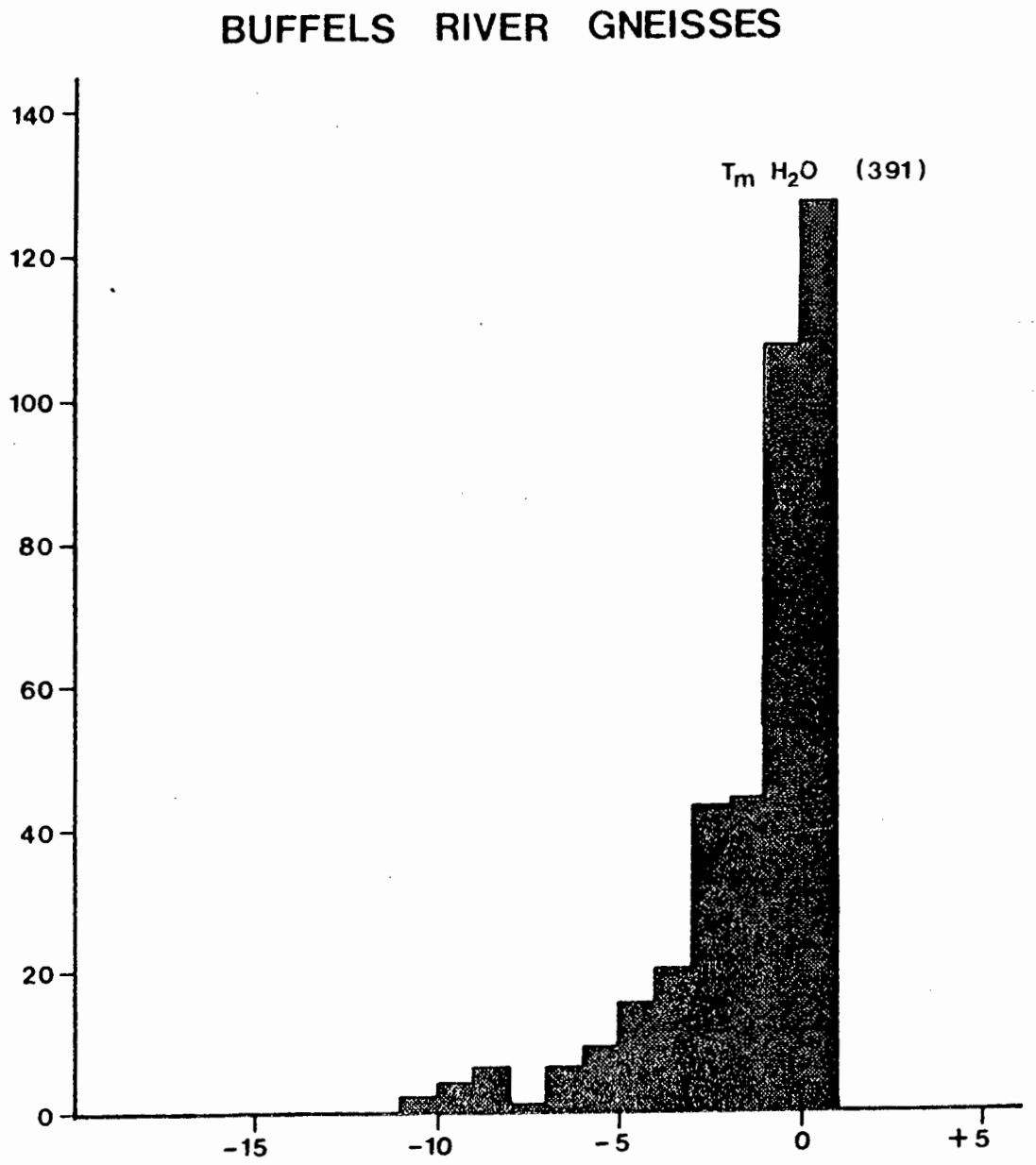

Fig. 10.3 T_m for H_2O inclusions

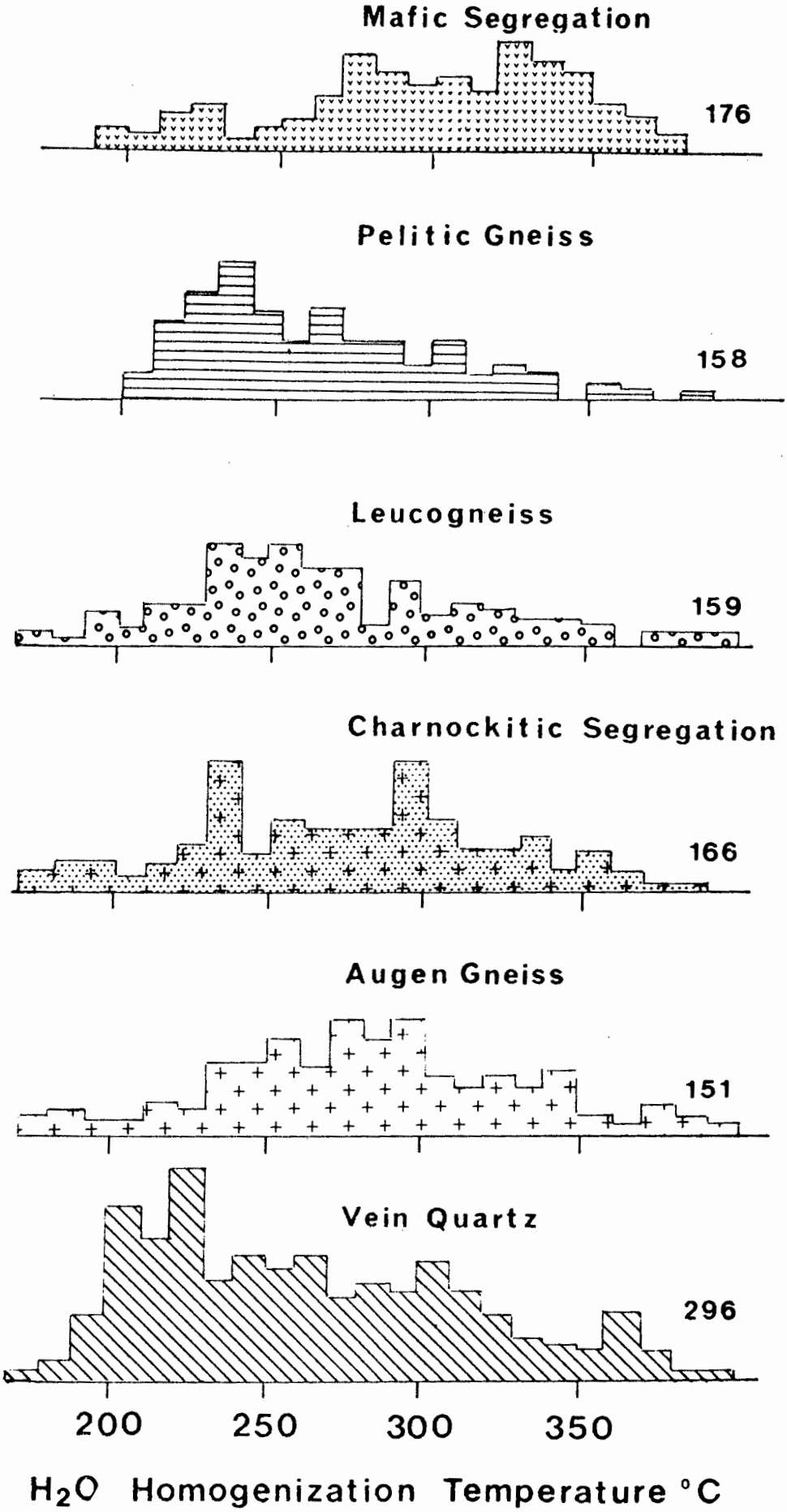

Fig. 10.4 T_h for H_2O inclusions

$T_{h,Total}$ = 275°C. This would indicate a CO_2-H_2O fluid of low salinity and low to moderate density.

Type III inclusions are pure H_2O with melting temperatures close to 0°C. Homogenisation temperatures vary between 160 and 390°C and may represent the temperature of entrapment.

The results of microthermometry combined with inclusion petrography are given in table 10.1. There is wide variation between samples and multiple inclusion populations occur within individual samples. Only the charnockitic segregation (DWN629), spatially associated vein quartz (DWN632) and their host, biotite-bearing augen gneiss show prominent secondary trails that cut crystal boundaries and suggest some form of fluid infiltration.

TABLE 10.1

Fluid inclusion compositions and densities

Inclusion type	Composition	Density
Type Ia	CO_2 ($\pm H_2O$-CH_4-N_2)	high 0.93 gcm^{-3}
Type Ib	N_2-CH_4	unknown presumed to be low <0.3 gcm^{-3}
Type Ic	H_2O-NaCl	moderate 0.75 gcm^{-3}
Type IIa	CO_2 CO_2 ($\pm CH_4$-N_2)	moderate to low
Type IIb	H_2O	moderate 0.85 gcm^{-3}
Type IIc	CO_2-H_2O	low
Type III	H_2O	variable

10.5 INTERPRETATION - FLUID EVOLUTION AND UPLIFT HISTORY

Isochores for the dominant inclusion populations are shown in fig. 10.5. Fluid densities were calculated using the computer program of Nicholls & Crawford (1985). The density of early Type Ia CO_2-rich inclusions together with temperature estimates from mineralogical geothermometers (see Chapter 4) give pressure estimates between 4 and 5 kbar. This is slightly lower than pressure estimates determined from garnet-sillimanite-plagioclase-quartz equilibria in Chapter 4. An isochore constructed from the small number of Type Ic aqueous inclusions bisects the isochore for Type Ia CO_2 inclusions at temperatures and pressures close to maximum PT estimates. It is possible that both sets of inclusions were trapped close to the peak of metamorphism. As both sets of fluid would be perfectly miscible at granulite-facies temperatures (Bowers & Helgeson, 1983) it is necessary to invoke the passage of two distinct fluids through the rock. Otherwise, textural criteria may be unreliable and the fluids were trapped at much lower temperatures and pressures (<500°C). The presence of separate CO_2 and H_2O fluids in early generation inclusions in granulites has been noted by Hollister & Burruss (1976).

Secondary inclusions define a series of isochores. A possible uplift path can be constructed to intersect the appropriate isochores in a chronological order consistent with the inclusion petrography. Most of the isochores for secondary inclusions are likely to be intersected at temperatures below 400°C at low pressures (<2 kb) in order to explain the abundance of single component inclusion trails. To prevent decrepitation of the higher density CO_2 inclusions it must be assumed that the PT path never dropped more than 2 kbar below the pressure indicated by the early, high density inclusions on cooling (Naumov et al., 1966 and Crawford & Hollister, 1986). There is some evidence in this study to suggest that some degree of natural decrepitation has taken place. Some large CO_2 inclusions (>10μm) have an irregular star-shaped appearance and are surrounded by tiny inclusions in radial trails (see plate 10.1 b). Such features are also recorded by Swanenberg (1980), Kreulen (1980) and Hollister (1982). Smaller inclusions (<10μm) are able to contain much a higher overpressure. Swanenberg (1980) reports an excess pressure of 6 kb for a 1μm inclusion in quartz. The range of densities for Type IIa

CO_2 inclusions in this study is best explained by selective leakage of larger early inclusions when uplift led to the formation of an overpressure sufficient to fracture the early generation of inclusions. As the resultant secondary inclusions are nearly pure CO_2, leakage and reentrapment must have occurred below the solvus for H_2O-CO_2 mixing. Assuming early inclusions were trapped close to peak metamorphic temperatures and pressures (750-800°C at 4-6 kb) the later secondary inclusions probably formed at conditions below 3 kb at temperatures below 400°C.

A number of studies modelling uplift paths for granulite-facies terranes have been based solely on CO_2-rich inclusions (for example, Schreurs, 1985). The association of high density CO_2 with successive trails of lower density CO_2 has been considered to be the result of rapid isothermal uplift (Hollister, 1982; Touret & Dietvorst, 1983 and Selverstone et al., 1984). The slope of isochores for H_2O inclusions provides important constraints on the uplift path. The numerous Type IIb H_2O inclusion trails in this study suggest successive trapping of H_2O-rich fluid during cooling. Hence, the uplift path must intersect the representative isochores for secondary H_2O inclusions. If the final uplift trajectory follows the slope of an isochore for H_2O then a large number of unrelated secondary H_2O inclusions would have the same density. Thus, the well defined population of secondary aqueous inclusions with densities around 0.85 gcm^{-3} may represent entrapment of relatively small volumes of transient metamorphic fluid rather than a significant fluid event. The only textural evidence of fluid aided retrogression occurs in the charnockitic segregation, DWN629. In this case inclusion trails cut across grain boundaries and run into vein and patches of chloritic alteration. Unfortunately the inclusions in these trails are extremely small (<0.5μm) and cannot be measured by microthermometry. They are tentatively identified as aqueous inclusions on the grounds that some appear to have vapour bubbles at temperatures above the CO_2 critical point.

On conventional PT diagrams, such as fig. 10.5, uplift paths for granulites can follow three main trajectories. They can be strongly convex towards the temperature axis (Hollister et al., 1979; Hollister, 1982; Schreurs, 1984; and Santosh, 1987) or uplift can follow a T-concave path (Swanenberg, 1980, and Olsen, 1987). Rudnik et al. (1984) propose a path for the Kapuskasing granulites of Ontario that closely parallels an isochore for dense, primary CO_2-

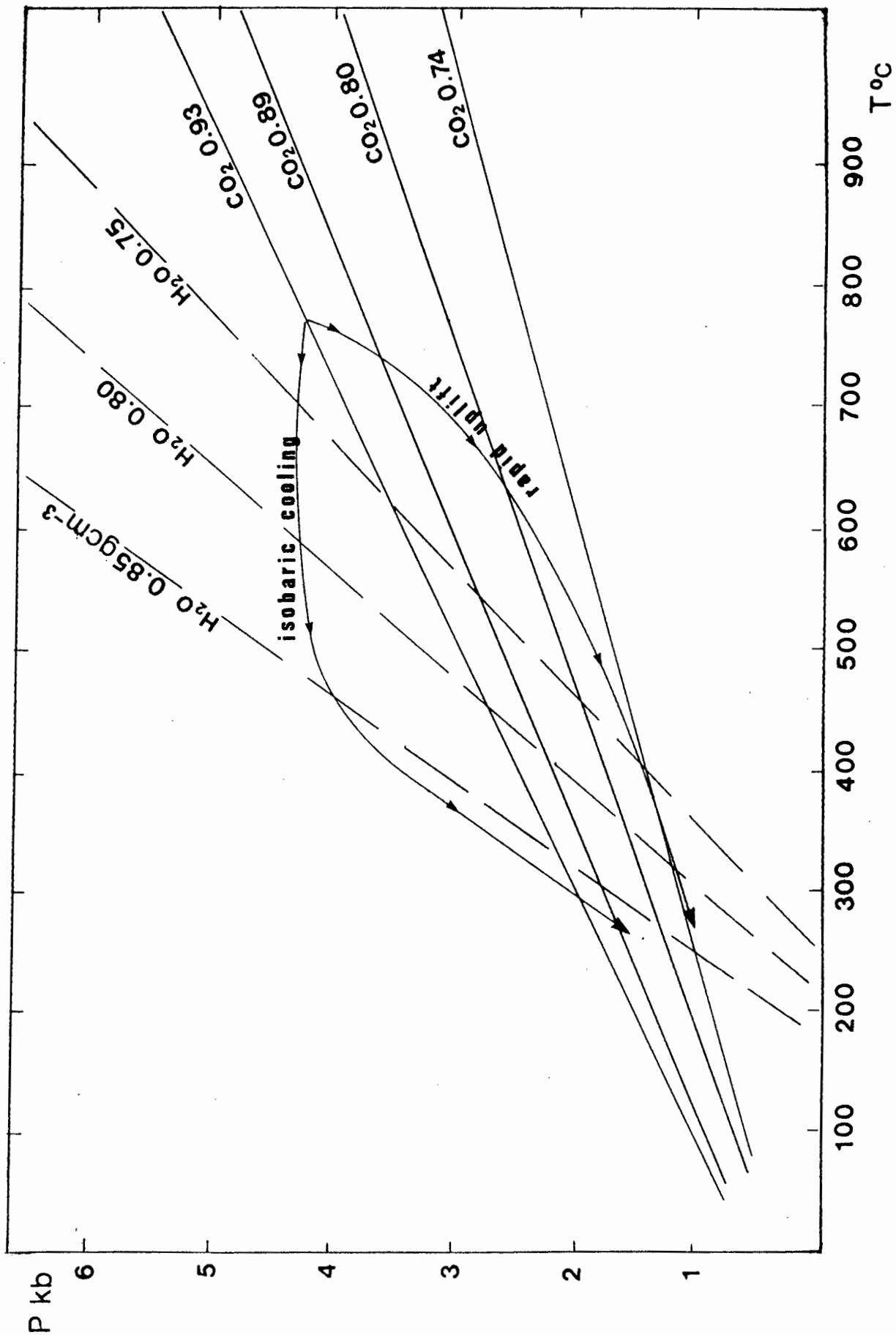

Fig. 10.5 Isochores for dominant fluid populations from table 10.1 (calculated from the computer program of Nicholls & Crawford (1985). Uplift paths can be either T-concave or T-convex.

rich fluid. This implies almost simultaneous decrease in pressure and temperature. The difficulty in interpretation of uplift paths and fluid evolution history from inclusion studies is highlighted in Touret & Olsen (1985) who describe the uplift path of the Bamble granulites, Norway, as being T-concave, reversing the deductions of Touret & Dietvorst (1983) who interpreted the same inclusion data in terms of a T-convex uplift trajectory.

Mineral textures and equilibria presented in earlier chapters support an isobaric cooling path. Evidence from fluid inclusions can be modelled to produce either a T-concave (isobaric cooling path) or a T-convex (isothermal decompression) path. In either case inferences concerning the nature of secondary inclusions are used to support the model.

In fig. 10.5 a T-convex path assumes entrapment of high density CO_2-rich fluid close to the peak of metamorphism. This would be followed by the entrapment of secondary CO_2 inclusions of decreasing density with age of entrapment. T-convex paths are also consistent with decrepitation of early high density inclusions (see Hollister, 1979). The isochores for secondary H_2O inclusions are met at low temperatures and pressures as the path flattens.

A T-concave path also assumes entrapment of early high density CO_2. Then successive batches of H_2O-rich fluid are trapped. This fits textural observations of isolated, Type Ic, early aqueous inclusions. The commencement of uplift follows along the isochore for H_2O of density 0.85 gcm^{-3}. All pure H_2O fluids trapped during the major uplift phase of the cooling history will have approximately the same density. This path intersects a series of CO_2 isochores of decreasing density on continued uplift, starting with fluids which have equal densities to those thought to represent primary fluids. Leakage of larger early inclusions will occur during the uplift phase at temperatures consistent with the entrapment of single component fluids. This results in the formation of secondary trails of low density CO_2. The presence of CO_2-rich inclusions with anomalous high densities is often cited as evidence for a T-concave uplift path (Swanenberg, 1980 and Olsen, 1985). Only a few individual CO_2 inclusions with densities above 0.93 gcm^{-3} are recorded in this study. This could simply be due to the lack of an infiltrating fluid of a CO_2-rich composition during the isobaric cooling phase of the PT path. Hall & Bodnar (1990) argue that T-concave uplift paths are

conducive to generating high overpressures in matrix fluid which may result in the diffusion of other components (H_2 or H_2O) into CO_2 inclusions. This may explain the presence of other components in CO_2-rich inclusions indicated by the depression of the final melting temperature below the CO_2 triple point of -56.6°C. The presence of mixed H_2O-CO_2 inclusions at the junction of early secondary CO_2 inclusion trails and later secondary trails of H_2O inclusions (see plate 10.2) supports the diffusion of H_2O into the older inclusions. As these inclusions have clearly not retained a constant density, they cannot be used to constrain possible uplift paths.

The latter model of T-concave uplift is preferred for this study, as it is in agreement with mineral textures and equilibria. It requires only minor influx of H_2O rich-fluids following the peak of metamorphism. The infiltration of aqueous fluids may be responsible for the minor retrogression seen in some rock-types and could be related to the release of H_2O-rich fluids from crystallising granitic melts. All other inclusions can be accounted for by selective leakage and reentrapment of small amounts of early fluids.

10.6 DISCUSSION - GRANULITE-FACIES FLUIDS

Touret (1971) first reported the presence of dense CO_2 inclusions in granulite-facies rocks. It has since been argued that these fluids are representative of the peak-metamorphic fluid and that such fluids are the causative mechanism of granulite-facies metamorphism (Newton *et al.*, 1980; Hansen *et al.*, 1984; Schreurs, 1985 and Newton, 1986). Crawford & Hollister (1986) list the problems that are not addressed by the proposers of the CO_2-streaming model. They are as follows: 1. The equilibria of fluid with graphite at high temperatures (Hollister & Burruss, 1976; Lamb & Valley, 1984; Lamb *et al.*, 1987 and Hall & Bodnar, 1990). Oxide and silicate equilibria indicate that oxygen fugacities in most granulites are buffered to values that are to low to be in equilibrium with pure CO_2 at peak temperatures. 2. Dense, CO_2-rich inclusions also occur in low and medium grades of metamorphism (Crawford *et al.*, 1979; Sisson *et al.*, 1981). 3. The occurrence of early mixed H_2O-CO_2 inclusions in granulites from the Khtada Lake area, British Columbia, studied by Hollister & Burruss (1976). 4. The role of partial melts in the preferential extraction of H_2O from granulites (Fyfe, 1973; Nesbitt, 1980 and Powell, 1983).

To support the CO_2-streaming model the increase in the abundance of CO_2 inclusions is noted in areas where sharp transitions between amphibolite- and granulte-facies are reported (Touret, 1971; Schreurs, 1985 and Vry & Brown, 1986) and on a local scale in examples of vein-like charnockitisation (Hansen et al., 1984 and Jackson et al., 1988). The presence of calcite along grain boundaries is cited as evidence of CO_2-influx (Janardhan et al., 1979; and Morrison & Valley, 1988). Jackson et al. (1988) demonstrated differences in the isotopic character of carbon from CO_2 inclusions in charnockitic veins compared with that from host biotite gneiss. An external source for CO_2 is suggested but it is unclear from the isotopic evidence in their study whether the infiltrating CO_2 was derived from the Mantle.

In this study high density, early Type Ia inclusions occur in segregations. These segregations have been modelled as being the products of vapour-absent melting. The values of H_2O and CO_2 fugacities were effectively buffered only by solid phases or silicate liquids (see Chapters 5, 6 and 8). Thus, early fluid inclusions might represent small amounts of residual grain-boundary fluid that have infiltrated the segregations. If early fluid inclusions are samples of grain boundary fluid, then some H_2O would be expected in the inclusions. This may be the case as less than 20% H_2O would be impossible to observe in such small inclusions (Shepherd et al., 1985). Type Ic inclusions also have textures and densities that would favour entrapment at peak metamorphic conditions. This implies that two distinct fluids accompanied granulite-facies metamorphism. This is proposed for charnockitisation phenomena in southern India, where a metasomatic aqueous fluid front was followed by a dehydrating flux of CO_2 (Newton et al., 1980; Janardhan et al., 1982; Friend, 1983; and Newton, 1985). It seems unlikely that some form of fluid mixing could be avoided in such a system at granulite-facies temperatures. The movement of large volumes of fluid through a terrane should be reflected in uniform inclusion populations in all types of granulite-facies rocks. This study indicates a great deal of heterogeneity in the early fluid content of individual gneisses. Differences that appear to be on a cm-scale. The alternatives require that both CO_2 and H_2O were present as a single fluid phase and were later separated, either before or after entrapment, or, that the rocks were totally fluid-absent, and inclusions represent distinct pulses of later post-metamorphic fluids.

Crawford & Hollister (1986) and Olsen (1987) consider possible mechanisms for the separation of CO_2 and H_2O. The generation of silicate melts is likely to preferentially partition H_2O into the melt leaving CO_2 enriched in the coexisting vapour (Powell, 1983b). It is possible that large-scale leucosome dykes and veins acted as sinks for H_2O-rich fluid, leaving a residual CO_2-rich fluid in the surrounding granulites. In this case it is not neccessary to remove all the melt generated from the terrane. The presence of secondary aqueous inclusion trails may represent the release and re-infiltration H_2O-rich fluids from crystallising melts. In some cases there appears to be direct evidence of infiltration of H_2O being linked to the alteration of orthopyroxene in charnockitic segregations.

A number of mechanisms have been proposed to account for possible post-entrapment separation of CO_2 and H_2O. Spear & Selverstone (1983) propose leakage of H_2O by diffusion into the quartz lattice. Roedder (1984) suggests diffusion through the quartz lattice with escape along grain boundaries. Also possible is escape via minute fractures with H_2O wetting the walls and escaping preferentially (Crawford *et al.*, 1979). Other workers propose internal reactions that generate H_2 which is subsequently lost by diffusion. Examples are:

$$C + 2H_2O = CO_2 + 2H_2 \qquad \text{(Kreulen \& Schuiling, 1982)} \qquad (1)$$

and

$$CH_4 + 2H_2O = CO_2 + 4H_2 \qquad \text{(Hollister, 1981)} \qquad (2)$$

Olsen (1987) rules out the above processes because they alter inclusion density. Reaction (2) would produce super-dense inclusions (recorded by a number of workers, including Swanenberg, 1980; Lamb *et al.*, 1987 and Olsen, 1988). Other processes produce lower densities. Hall & Bodnar (1990) indicate that depending on the presence and composition of matrix fluids it is more likely that components such as H_2 and H_2O diffuse into inclusions rather than out of them.

The presence of N_2-rich inclusions in the rocks in this study also needs to be addressed. In low grade metamorphic rocks it is reasonable to suggest that N_2 is released from the thermal decomposition of organic compounds (Paxton, 1984). However, this is impossible in this study (the mafic segregation, MCS327, has several N_2-rich inclusions). It has been noted that micas, particularly

biotite can contain ammonium ions (NH_4^+) replacing K^+ (Duit et al., 1986). Crawford & Hollister (1986) suggest the breakdown of ammonium-bearing biotite during anatexis as the origin of N_2-rich inclusions in migmatites. N_2-rich inclusions are problematic because conventional microthermometry cannot give accurate compositional data. The presence of additional components such as CH_4, CO_2 and H_2O is indicated in this study and other components, such as H_2 and He cannot be discounted. The rarity of N_2-rich inclusions and their close association with melt segregations discounts any influx of N_2-rich fluids, as in the model proposed by Kreulen & Schuiling (1982).

Lamb et al. (1987) prefer to regard dense, texturally "primary", CO_2-rich fluid inclusions in Adirondack granulites as being secondary in origin. As mineral equilibria studies indicate peak metamorphism in the Adirondacks took place under conditions of low CO_2 fugacity. In this study calculations of oxygen fugacity (see Chapters 7 and 8) are consistent with a more oxidised environment than that demonstrated for the Adirondacks by Lamb et al.. The coexisting fluid would have to have a mixed CO_2-H_2O composition. Morrison & Valley (1988) found a close spatial association of minute grains of secondary calcite with high density CO_2-rich inclusions in Adirondack anorthosites and support the view of Lamb and his co-workers that these fluids are retrograde in origin.

In this small study of inclusions in quartz from six different rock types the following observations can be stressed: 1. Dense CO_2-rich inclusions are associated with rocks that have undergone partial melting. 2. H_2O and N_2-rich inclusions have similar spatial relationships to that observed in dense CO_2-rich inclusions. 3. Fluid inclusions have a much lower abundance in the matrix quartz of other gneisses (MCS311 and MCSH02) and in the matrix minerals around segregations. Most of the inclusions observed are obviously secondary in origin. 4. A wide scatter of T_h values is recorded for all inclusion types in all samples. Textural observations and microthermometric data are consistent with the leakage of some early formed inclusions, and with post-entrapment modification of inclusion composition and density.

Thus, the importance of early generation Type I inclusions is somewhat enigmatic. It is suggested in Chapter 9 that the re-equilibration of oxygen isotopes amongst coexisting silicates on cooling, by diffusion in a closed system, is favoured by the presence

of a grain-boundary fluid film. Perhaps early generation fluid inclusions are samples of these early post-peak fluids trapped during cooling.

10.7 SUMMARY

A small scale study of fluid inclusions in quartz from six different rock types shows the following petrographic features: Dense CO_2 inclusion are found in quartz from segregations. Early generation H_2O and N_2-rich inclusions occur in the same material as separate inclusions. Fluid inclusions are less abundant in matrix quartz from all rocks and are normally found in secondary trails. Evidence for natural decrepitation is observed in some larger inclusions. Post-entrapment processes are thought to play an important role in modifying fluid composition and densities during uplift.

The variety of inclusion-types are best explained by a model for fluid evolution and uplift history that includes the following steps: 1. Entrapment of residual metamorphic fluids at peak or near peak metamorphic conditions. 2. Sampling of transient H_2O possibly released from crystallising granitic melts. 3. The initial cooling path was isobaric. Decompression after cooling may follow a dominant H_2O isochore. 4. After a pressure release equivalent to 2 kb leakage of early CO_2 inclusions took place, resulting in secondary entrapment of CO_2-rich fluids.

The origin of early generation inclusions is enigmatic. Inclusion petrography provides no strong support for a major fluid infiltration event accompanying peak-metamorphism.

CHAPTER 11

SYNTHESIS AND CONCLUSIONS

11.1 INTRODUCTION

The aim of this chapter is to draw together the petrological information outlined in previous chapters and produce a coherrent model for the granulite-facies metamorphism experienced in the Buffels River area of central Namaqualand. In any granulite-facies terrane a number of key questions must be addressed: 1. The timing of metamorphism. No age determinations are available for the Buffels River area, so deductions are based on the data of Clifford and co-workers from the Okiep area (Clifford et al., 1990). 2. The structural style of the terrane. The relationship between granulite-facies metamorphism and deformation provides clues to the tectonic setting of the terrane. 3. The pressure-temperature conditions of metamorphism can be quantitatively assessed by applying mineral-exchange geothermometers and barometers. The results are governed by the closure temperatures for the exchange reactions. These can be modelled using diffusion kinetics to produce an estimate of cooling-rate. Phase equilibria for coexisting mineral assemblages provide important constraints on the P-T conditions calculated from geothermobarometry. 4. The P-T path can be modelled by using mineral reaction textures to deduce the direction and progress of reactions. The conditions of peak -metamorphism and the subsequent cooling history are the important parameters in the modelling of the tectono-thermal evolution of the terrane. 5. The role of fluids in granulite formation can be assessed by calculating fluid activites from mineral-fluid equilibria and by oxygen isotope studies. Samples of the fluid at the time of granulite-facies metamorphism may be preserved as fluid inclusions.

11.2 AGE OF GRANULITE-FACIES METAMORPHISM

The age of regional metamorphism for central Namaqualand is normally quoted as 1190 Ma, based on the Rb/Sr isochron of 1187 ± 23 Ma determined by Clifford et al. (1975 and 1981). This isochron was constructed from both orthogneisses (Nababeep Gneiss)

and from supracrustal rocks from the Okiep area, and includes samples from Smorgen Schaduwe (see fig. 2.3). Barton (1983) gives an Rb/Sr isochron age of 1179 ± 28 Ma for Nababeep Gneiss. Waters (1990) interprets these dates as a record of open-system isotopic equilibration accompanying penetrative fabric development during D_2 deformation. Many authors regard D_2 deformation as being coeval with peak-metamorphism in the northern areas of Bushmanland (Blignaut et al., 1983 and Moore, 1986) and in the central part of Namaqualand (Joubert, 1986). However, in this study the reactions that define the highest PT conditions of metamorphism are syn-to-post D_3 in age (see Chapter 3). The presence of numerous discordant, un-foliated, granulite-facies segregations indicates that peak-metamorphism outlasted the major penetrative phase of deformation. The formation of a localised D_3 fabric characterised by granulite-facies mineral assemblages places the peak of metamorphism in the Buffels River area as synchronous with shearing along the Buffels River Shear Zone (D_3). It is not clear whether the D_3 ductile shearing recognised in this area is related to the regional D_3 open folding recorded by Joubert and others (Joubert, 1971; Jackson & Zelt, 1984; Albat, 1984; and Moore, 1986). Waters (1990) believes the metamorphic climax is closely associated with and may slightly post-date the intrusion of the late-tectonic Spektakel Suite granitoids. Clifford et al. (1981) give a Rb/Sr whole-rock isochron of 1147 ± 33 Ma for rocks from the Spektakel Suite and regard this as an emplacement age. Armstrong et al. (1988) produce single zircon ages of around 1130 Ma for late syntectonic granites in Bushmanland. Clifford et al. (1990) review age determinations for the Koperberg Suite. U-Pb ages indicate intrusion at 1075 ± 49 Ma, Nd model ages suggest protolith ages between 1627 and 2050 Ma. Field evidence and mineral textures indicate intrusion into hot crust with subsequent annealing and slow re-equilibration. It is not clear whether the intrusion of the Koperberg Suite represents a thermal event distinct from the peak of metamorphism as recorded in the surrounding country rocks. New isotopic data from central Namaqualand is needed to resolve the problem. No textural evidence exists in the Buffels River area to suggest a polymetamorphic history. A single prograde event with increasing heat flow at near constant pressure is the prefered model for metamorphism in the Buffels River area.

11.3 STRUCTURAL STYLE AND METAMORPHISM

The structural style of the terrane places important constraints on the tectonic setting of granulites. In central Namaqualand the earliest observed structures that affect the supracrustal gneisses, orthogneisses and possible basement gneisses are associated with regional horizontal tectonics. Large scale F_2 structures take the form of recumbent isoclinal folds. Large thrusts are recognised in the Aggeneys area of Bushmanland (Blignaut et al., 1983; Strydom & Visser, 1986 and Van der Merwe & Botha, 1989). The Groothoek Thrust Belt strikes east-west and dips to the north; it separates 2000-1730 Ma age rocks of the Richtersveld Subprovince from the younger Bushmanland Subprovince. Ductile conditions prevailed during thrusting and movement was accomodated throughout the lower portions of the thrust sheet. A penetrative fabric was imposed on supracrustal rocks and the intrusive gneisses of the Klein Namaqualand Suite. This phase of deformation is sometimes referred to as the Namaqua deformation (Blignaut et al., 1983 and Van der Merwe & Botha, 1989). Little can be determined from pre-Namaqua fabrics preserved in rocks south of the Groothoek Trust. In the Buffels River area the basal grey biotite-gneisses show complex intrafolial fold patterns that suggests a preexisting fabric prior to the regional isoclinal folding. The pre-Namaqua deformation in the Richtersveld Subprovince occurs as macroscopic fold structures with axial planar foliations, extension lineations and a greenschist grade of metamorphism, which all predate the intrusion of the Vioolsdrif Suite. This deformation is referred to as the Orange River event by Blignaut et al. (1983).

The Groothoek Thrust Belt is regarded as a ramp structure by Van der Merwe & Botha (1989) who recognise a progressive increase in homogeneous simple shear from north to south. Folding formed by differential movement between layers during the development of the thrust, possibly by a process of layer-parallel shortening along the thrust. Subsequent thrusting undercuts the Groothoek Trust Belt and is syntectonic with the intrusion of the Spektakel Suite granitoids. This event is associated with the growth of large retrograde muscovite flakes, notably in pelitic schists. The general tectonic model for the Namaqua Orogeny was developed in Bushmanland as the majority of workers were involved in studies which concerned the regional setting of the Aggeneys/Gamsberg base metal deposits. The

model proposed by Blignaut et al. (1983) involves large scale movement of thick, ductile, crustal sheets towards the south-west. Blignaut et al. (1983) regard the thrusting episode as being protracted with thrusts cutting up-section and deforming the D_2 fabric. Blignaut et al. regard the Skelmfontein thrust as a terrane boundary that carries the Bushmanland thrust sheet over the Steinkopf terrane and re-activates the Groothoek thrust. Penetrative re-foliation associated with the Skelmfontein thrust is associated with granulite-facies metamorphism. Pyroxene-bearing melt segregations are undeformed.

Early studies in the central parts of Namaqualand were focused on the large scale F_3 structures that control the present outcrop pattern (Joubert, 1971 and 1974). Moore (1986) applies the model of thrust tectonics to the Buffels River area and places thrust contacts between supracrustal sequences and the augen gneisses. The style of deformation associated with F_2 in the Buffels River area is very similar to that in Bushmanland. The presence of isoclinal, non-cylindrical folds with a flat-lying axial planar foliation and a strongly developed elongation mineral lineation is ubiquitous. The D_3 structural event is characterised by large-scale open folds with near-vertical fold axes, and by east-west trending shear zones. The Buffels River Shear Zone (Kameelboomberg Shear Zone) is regarded as an example of an F_3 high strain zone (Joubert, 1971; Jackson & Zelt, 1984 and Moore, 1986). The folding is coaxial with F_2 and also appears to be non-cylindrical in nature (Albat, 1984; Moore, 1986). A shear fabric develops in high strain zones, particularly in competent lithologies. Most of the later deformation in the Namaqua Complex is limited to wrench tectonics along linear belts. The Pofadder Megashear (Toogood, 1976 and McLaren, 1985) is the largest of these later structures with a dextral displacement of at least 85 km (Toogood, 1976).

Key questions arise from the application of the Namaqua tectonic model (Blignaut et al., 1983; Van Aswegen et al., 1987; Van der Merwe & Botha, 1989; Colliston et al., 1991) for areas in central and southern Namaqualand. Can large scale thrust belts be recognised and can the area be divided into a series of distinct terranes? What is the relationship between the various granitoid intrusives and this phase of deformation? How is granulite-facies metamorphism related to this tectonic event?

Firstly, the presence of major displacements along tectonic structures associated with D_2 deformation in central Namaqualand has not been conclusively demonstrated. Colliston et al. (1989) propose a terrane boundary along the Oranjefontein thrust. The contact lies between the Areb Gneiss, which is correlated with the 1800 Ma Gladkop Suite of the Steinkopf terrane (Van Aswegen et al., 1987) and the 1200 Ma Nababeep Gneiss of the Okiep terrane. The Areb Gneiss lies at the base of a schist-quartzite succession. In the Oranjefontein area it is not clear whether the Areb gneiss is intrusive or represents a local "basement". There is abundant evidence of the younger Nababeep Gneiss being intrusive into older supracrustal rocks and orthogneisses. Strydom (1984) mapped the area and gives no indication of a thrusted contact. The basis for terrane divisions is mainly lithotectonic and assumes a broad correlation amongst various types of granitic gneisses over wide areas. Without detailed chemical and isotopic investigation, such correlations are tenuous and it is unreasonable to assume a tectonic contact without direct field evidence.

The second problem surrounds the age of the granitic gneisses of the Klein Namaqualand Suite, most authors refer to these intrusives as syntectonic, as F_2 folds and fabrics are present (Joubert, 1971). However, it is possible that the poorly constrained Pb-Pb age of 1500 Ma (Barton, 1983) could represent an emplacement age, with isotopic resetting during high grade metamorphism giving Rb-Sr ages around 1200 Ma. It is important to note that late tectonic granites of the Spektakel Suite give similar ages (1200-1100 Ma) yet lack the regional flat-flying foliation and mineral lineation. Moore et al. (1990) show syn-tectonic granitoids intruding both Richtersveld and Bushmanland basement rocks. In the Buffels River area it can be demonstrated that the augen gneisses contain xenoliths of supracrustal rocks and are intruded by small mafic dykes. The mafic dykes show evidence of F_2 and F_3 deformation. Later granitic and ultramafic intrusions have a weak foliation (syn- to post-D_3). As re-foliation along steep D_3 zones is defined by the growth of granulite-facies mineral assemblages at Hytkoras it is proposed that high grade conditions outlasted all the major tectonic events in this region. However, it is apparent that the peak of metamorphism in the Aggeneys region occurred in conjunction with the earlier thrust dominated event (Joubert, 1971; Rozendaal, 1978; Moore et al., 1990). Further south in the Springbok area late D_2 re-foliation is associated with granulite-facies assemblages (Blignaut et al., 1983).

The time relations between late D_2 and early D_3 deformations are not known but it is thought that the intrusion of the Spektakel Suite granites occurred around this time. The mineral textures in the study area are consistent with a peak metamorphic event that was essentially a thermal annealing event. This was accompanied by local re-foliation along zones of high strain associated with shearing along the steep limbs of large-scale F_3 structures. The difference between the D_3 metamorphic imprint in the Buffels River area and the Aggeneys region is that the latter is at a lower temperature and a much higher water activity. In both cases fabric development is limited. Until detailed isotopic dating is carried out on individual minerals that can be related to distinct fabric forming events the true relationship between structural and metamorphic evolution cannot be fully resolved.

In reviewing the structural relationships of granulite-facies terranes Newton (1987) and Bohlen (1987) both commented upon the overprinting of early flat-lying deformation by the granulite-facies peak. Early tectonic events producing recumbent overfolds, thrusting, nappes and isoclinal folding are common in many granulite-facies terranes; including southern India (Drury et al., 1984), the Adirondacks (Weiner et al., 1983) and Broken Hill, Australia (Laing et al., 1976). Extensive crustal shortening must accompany sub-horizontal deformation typified by overfolding. Although horizontal fabrics are commonly associated with compressional tectonics, they may also be formed in extensional regimes (Sandiford, 1989).

The positions of isograds in central Namaqualand as indicated by Waters (1988) see Chapter 2, seem to suggest some form of structural control on the amphibolite-facies - granulite-facies transition. This study concludes that the area from Hytkoras in the south to Verdruk in the north underwent granulite-facies metamorphism under very similar P-T conditions. The more schistose nature of pelitic rocks and the presence of clinopyroxene-bearing amphibolites suggests that the northern areas experienced slightly lower temperatures, or higher water activities than the Buffels River area to the south. On the farm Kouberg in the far eastern part of the sampled area the rocks are sillimanite-biotite schists and quartzites. This represents the southern most extension of amphibolite facies rocks in central Namaqualand. Outcrop is very limited in this region and it is difficult to determine the relationship of the schist-quartzite succession with the underlying augen gneisses. Structural control of

this isograd boundary cannot be ruled out. It is not clear from the outcrop pattern whether the Kouberg occurrence is controlled by F_3 major folding or a later shearing.

An important feature of supracrustal sequences with prominent quartzite layers is the level of hydrous retrogression exhibited in the rocks underlying the quartzites. It is proposed that this is due to a multiple pass circulation of aqueous fluid trapped below the quartzites, which act as metamorphic aquicludes. The paucity of thick quartzites in the Buffels River area and further south may aid the escape of aqueous fluids released during prograde metamorphism. The change in structural style from flat-lying ductile structures to steep dipping zones may be important in providing pathways for fluid infiltration and escape during granulite-facies metamorphism.

The regional distribution of strain during F_3 deformation is important in the textural interpretation of fabric development accompanying granulite-facies metamorphism. In low strain areas it is possible that crystal growth may be mimetic upon the dominant anisotropy produced during earlier deformation. Likewise in areas of high strain early fabrics and mineral generations are unlikely to be well preserved. It was not intended to establish the absolute age and kinematics of deformation during the course of this study but as can be seen from the discussion above much work of this nature is required as existing tectonic models cannot explain many of the metamorphic phenomena observed in the study area.

11.4 PRESSURE AND TEMPERATURE OF METAMORPHISM

There are two important questions concerning the pressure and temperature conditions recorded in granulite-facies terranes: 1. are peak metamorphic conditions accurately preserved by mineralogical geothermobarometers and 2. are the calculated pressures and temperatures indicative of a particular tectonothermal environment?

One of the difficulties encountered in this was the lack of suitable geobarometers. The most useful barometers applied in other granulite terranes involve garnet-pyroxene-plagioclase-quartz (Newton & Perkins, 1982 and Bohlen et al., 1983) or garnet-rutile-ilmenite-sillimanite-quartz (GRAIL, Bohlen et al., 1983). The absence of garnet in mafic gneisses places the granulites of the Buffels River

area in the low pressure category of granulite-facies (Green & Ringwood, 1967; Newton 1983, Bohlen, 1987 and Harley, 1989) see fig. 11.1, but precludes more quantitative barometry. No assemblages could be found to enable the use of the GRAIL barometer. The only barometric estimates were thus limited to equilibria between garnet-plagioclase-sillimanite-quartz (Ghent, 1976; Newton & Haselton, 1981). The main problem concerning the use of this equilibria is the strong temperature dependance of the reaction and the low activity of the grossular component in garnets from pelitic gneisses. Pressure estimates derived from equilibria involving cordierite-garnet-sillimanite-quartz lack accuracy and precision as temperature and H_2O-CO_2 activity in the fluid phase and in cordierite are important parameters controlling compositions in the natural assemblage. Pressure estimates in this study range from 5.2 kb to 6.6 kb at 750°C depending on the calibration used, see Chapter 4. Waters (1989) gives a pressure estimate of 5.8 ± 0.4 kb at 770°C for the low temperature granulite-facies zone of central Namaqualand.

The main problem in the quantitative geothermometry of granulites is the relationship between the closure temperature of the thermometer reactions and the actual temperature experienced by the rocks. This problem is addressed in Chapter 6 for the Fe-Mg exchange equlibrium in garnet and biotite and for oxygen isotope exchange between coexisting minerals in Chapter 9. In slow cooled terranes subsequent exchange by diffusion will reset the thermometer to temperatures that are in the most part controlled by the closure temperature in the slowest diffusing phase (normally garnet). Consistent results can be generated by using the core composition of crystals and by selecting analyses from minerals which are armoured by non-exchanging matrix minerals. In this study much of the analytical work was carried out on isofacial samples, and was largely devoted to examining the extent of local equilibrium and retrograde zonation. From a kinetic point of view thermometers involving phases with slow diffusion rates are most likely to preserve peak metamorphic temperatures. Cation and anion exchange thermometry between garnet and pyroxene would be most suitable. Thus, it is likely that the calculated values represent minimum estimates. Based on the results in Chapter 4 and Chapter 9 the peak temperature experienced in the Buffels River area was probably between 750 and 800°C.

There is considerable debate whether or not the tempertures and

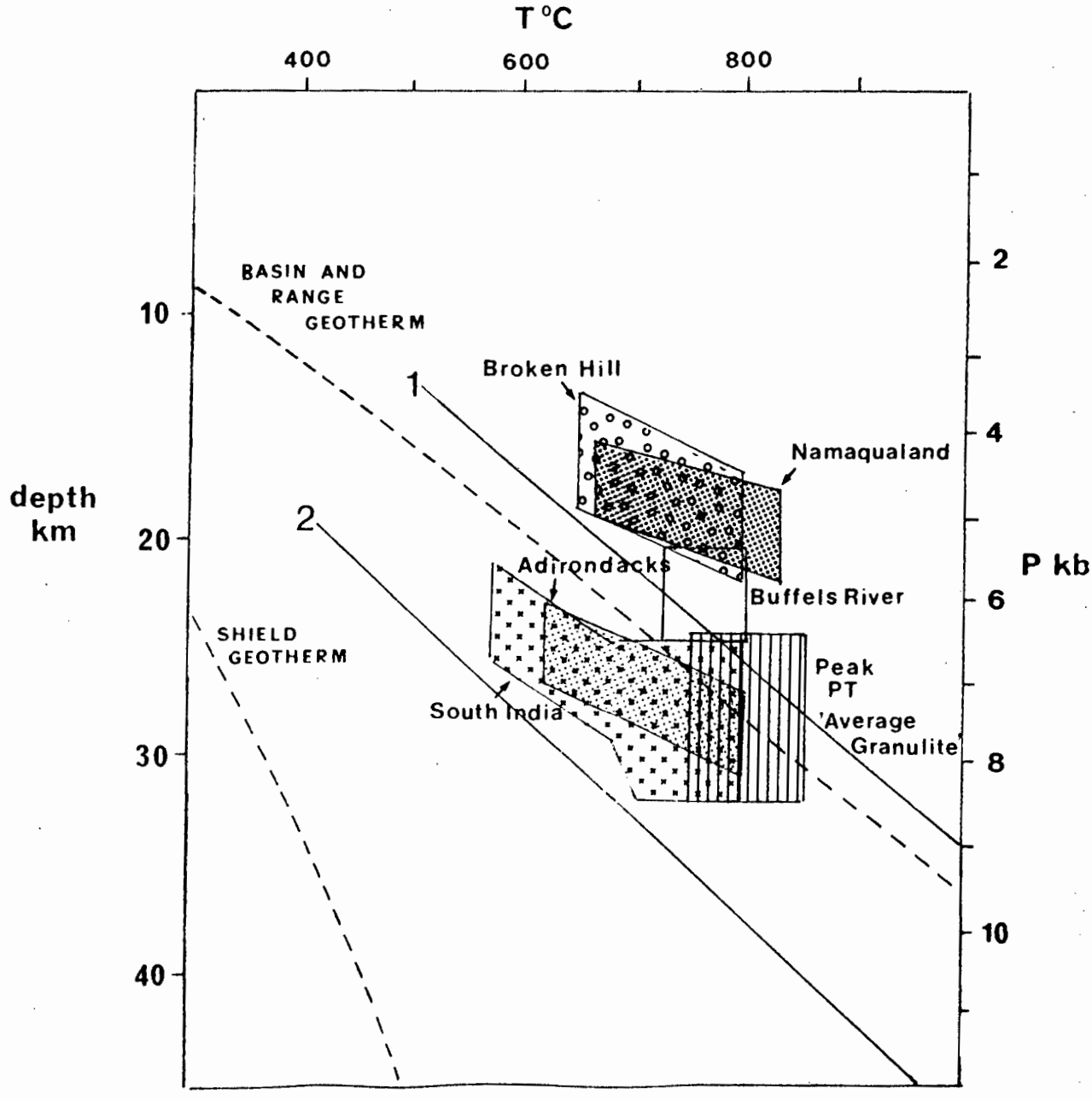

Fig. 11.1 P-T conditions of some granulite-facies terranes. Peak P-T of 'average granulite' from Bohlen (1987). Based on data listed in Newton (1983), Bohlen (1987), Harley (1989) and Waters (1989). Estimates from this study indicate slightly higher pressures for Namaqualand than listed in Waters (1989).

pressures estimated by using conventional geothermobarometry provide a true record of granulite-facies conditions. Frost & Chacko (1989) term this "the Granulite Uncertainity Principle", implying an inherent uncertainity in the application of ion-exchange thermometers caused by apparent closure temperatures being lower than granulite-facies temperatures. Frost & Chacko (1989) consider that it is unlikely that ion-exchange thermometers can preserve temperatures in excess of 800°C in slow cooled granulite-facies terranes. This is a feature of all compilations of granulite-facies terranes (see Bohlen, 1987 and Harley, 1989) yet there is considerable evidence of anhydrous mafic and felsic magmatism accompanying metamorphism in many terranes. Local temperatures may have been in excess of 1000°C. The only evidence of ultra-high temperature conditions comes from relict mineral assemblages. An example is the occurrence of the assemblage osumilite-sapphirine-quartz in the granulite of Enderby Land (Ellis et al., 1980; Grew, 1980; Harley, 1986).

Most geobarometers, including garnet-plagioclase-sillimanite-quartz, involve net-transfer reactions and have higher closure temperatures than the simple exchange reactions used in geothermometry. The garnet-plagioclase-sillimanite-quartz barometer does not involve Fe-Mg end-members and will not be affected by retrograde Fe-Mg exchange, thus the calculated pressure should reflect peak pressure conditions. However, it is unlikely that the pressure conditions experienced by the terrane during the retrograde part of the PT path can be recovered by using this equilibria on the composition of rims and mineral inclusions. Use of garnet core to rim compositions will indicate near-isobaric cooling, regardless of the actual PT path followed by the terrane.

At high temperatures diffusion rates are high and at temperatures around 800°C complete homogenisation of minerals such as garnet occurs within a few million years (Cygan & Lasaga, 1985). If decompression took place at higher temperatures the resultant zonation profile would be rapidly reset. The difficulty in estimating the nature of the peak PT conditions is best solved by qualitative observations of phase relations with reference to experimental data. The nature of the PT path experienced can only be solved by the interpretation of prograde and retrograde mineral textures.

11.5 P-T-t PATH

As there is a lack of tightly constrained radiometric data from individual minerals in the Buffels River area it is only possible to construct a generalised Pressure-Temperature-time path (P-T-t path) based on the data summarised by Clifford et al. (1990). The P-T path is constrained by mineral textures, mineral equilibria, mineral zonation profiles and fluid inclusion data, see fig. 11.2.

The P-T path for Namaqualand granulites is based on petrographic evidence from pelitic and magnesian gneisses described by Waters (1986 and 1989). Amphibolite-facies precursor assemblages are deduced from isolated relics and pseudomorphs in granulites. Garnet-, spinel- and sapphirine-forming reactions in pelitic and magnesian gneisses are consistent with an increase in pressure towards the metamorphic peak (Waters, 1986a, 1986b and 1989). The breakdown of cordierite to produce spinel in the high temperature granulite-facies zone has been modelled by Waters (1989) and suggests a pressure increase of 1.2 kb over a temperature range of 770° to 850°C. The retrograde path is constrained by retrograde reactions observed from pelitic gneisses from the high temperature granulite-facies zone. They include coronas of cordierite around spinel and replacement of spinel by garnet and sillimanite (Waters, 1989 and 1990). The P-T path constructed by Waters (1989) takes the form of an anticlockwise loop. In an earlier work, Waters (1986a) indicates increasing pressure during initial cooling. In the Buffels River area the P-T path is constrained by the absence of mineral textures indicative of isothermal decompression. In pelitic gneisses decompression results in the breakdown of garnet via the continuous reactions:

garnet + sillimanite + quartz = cordierite

and

garnet + quartz = orthopyroxene + cordierite

This is seen in a number of granulite-facies terranes and produces symplectitic coronas around resorbed garnets (Harley, 1989). Rinds of plagioclase between garnet and sillimanite are also considered to be indicative of decompression (Harley, 1989).

Isobaric cooling paths occur in various granulite-facies terranes ranging in pressure conditions from 10 kb to 4 kb (Harley, 1989). One

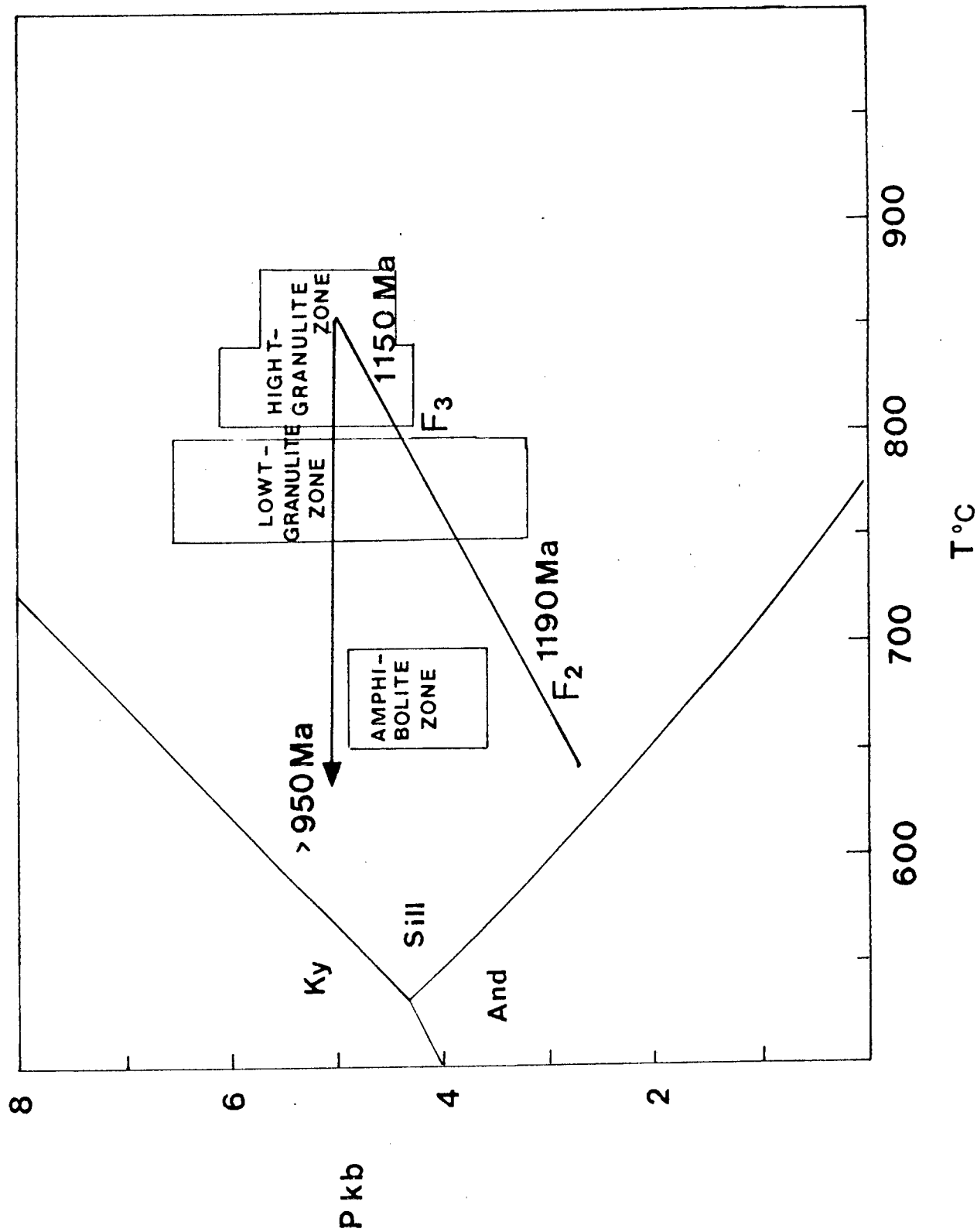

Fig. 11.2 P-T-t path envisaged for Namaqualand granulites, based on Waters (1989).

of the consequences of isobaric cooling would be the formation of kyanite in pelitic rocks during retrograde alteration. The absence of kyanite amongst pelitic rocks that have undergone amphibolite-facies retrogression puts an effective limit on the pressure reached during cooling. If isobaric cooling occurred then pressure conditions did not exceed 6 kb during cooling, see fig. 11.2.

11.6 TECTONOTHERMAL EVOLUTION

The granulites of central Namaqualand provide a classic example of regional, low pressure-high temperature metamorphism. Many tectonothermal models have been suggested for low pressure facies-series metamorphic belts, they are examined here and a possible model for the thermal evolution of central Namaqualand is proposed.

England & Thompson (1984) produced a series of one-dimensional, conductive heat transfer models of crustal thickening. These models are successful in accounting for P-T-t paths recorded from terranes showing Barrovian-type metamorphism. Andalusite-sillimanite P-T conditions can only be achieved by crustal thickening models if crustal radioactive heat production is high, together with high mantle heat flux, or low crustal thermal conductivity. However, in these models the prograde P-T path does not cross the andalusite-sillimanite phase boundary, and the modelled paths indicate retrograde conversion of sillimanite to andalusite. The presence of sillimanite as inclusions within poikiloblasts, as blocky prismatic crystals in the matrix, and in retrograde replacement rims after garnet or cordierite demonstrates that the formation of sillimanite occurred during both the prograde and retrograde parts of the P-T path. This suggests that a considerable period of time was spent within the sillimanite stability field. England & Thompson (1984) predict extensive partial melting of the lower crust in tectonothermal models producing andalusite-sillimanite conditions. In these cases a purely conductive heat transfer model may be inapplicable.

It seems that simple models involving crustal thickening via continental collision cannot generate the anti-clockwise P-T-t path suggested for Namaqualand Granulites by Waters (1989 and 1990) and in this study. Isobaric cooling paths require that peak metamorphism occurs in crust of near normal thickness or crust which is in

isostatic equilibrium. A number of models have been proposed, the key features that each model must account for are: the structural style of the terrane, which indicates shortening of the crust during prograde metamorphism; the prograde portion of the P-T path involved an increase in pressure (Waters, 1986 and 1989); the recorded P-T conditions of near 800°C for pressures around 5-6 kb for the granulite-facies zones indicate a geothermal gradient of 35-40°C/km; peak metamorphism post dates the F_2 penetrative deformation and is closely associated with steeply dipping shear zones; geophysical evidence that suggests a present crustal thickness of 42 km (Green & Durrheim, 1988), with the deepest 27 km above the Moho being composed of dense, probably basaltic rocks.

Models that predict low pressure granulite-facies metamorphism are of two-types: 1. Magmatic accretion models (Wells, 1980 and Bohlen, 1987) and 2. Extensional tectonic models (Sandiford & Powell, 1986). A third type of tectonothermal model combines elements of the above combined with an early stage of crustal thickening to explain the thrusting and folding recorded in most granulite terranes (Ellis, 1987; Etheridge et al., 1987 and Loosveld & Etheridge, 1990). Each of these types of model are discussed below.

11.6.1 Magmatic accretion models

Many granulite-facies terranes show evidence of abundant syn-tectonic magmatism e.g. Greenland (Wells, 1980 and Garde, 1990); the Adirondacks (Powers & Bohlen, 1985 and Bohlen, 1987) and the Lachlan fold belt, Australia (Sandiford & Powell, 1986 and Ellis, 1987). Namaqualand also shows an abundance of intrusive granitoids emplaced as sheet-like bodies along F_2 structures (Watkeys, 1986 and Moore et al., 1990). Crustal partial melts should dominate at shallow depths and should be accompanied by more mafic, mantle-derived melts at depth. The isotopic composition of such rocks should be devoid of any earlier crustal residence history (model ages should match metamorphic ages). The region must be underlain by lower crust of mafic composition as the basaltic underplate might be expected to have cooled into the granulite facies (Bohlen, 1987). The maximum temperature reached in the crust should be broadly similar over a range of crustal depths (Waters, 1986 and Harley, 1989) and the amphibolite-facies - granulite-facies transition should be marked by a lateral increase in temperature without changing pressure (Waters,

1986; Newton, 1987). The timescale of metamorphism is generally short-lived (<50 Ma) and could be episodic in nature (Harley, 1989). P-T-t paths for magmatic accretion in the context of the crustal structure o Namaqualand are shown in fig. 11.3.

The increase in pressure during prograde metamorphism proposed by Waters (1986 and 1988) could be achieved by placing a large amount of crust above the present erosion level in the form of giant, felsic sills and volcanics. Waters (1990) has modelled the thermal effect of emplacing basic sills towards the base of the crust and felsic sills at shallow crustal levels, see fig. 11.4. The temperature at 20 km depth, similar to todays present erosion surface, is controlled dominantly by the thickness of the basaltic underplate and the distance between the 20 km depth zone and the underplate, i.e. the crustal thickness, if the underplate is at the base of the crust. The thermal effects of individual sills are short-lived events compared to thermal effect of the underplate itself and local heat is easily dissipated by conduction. In order to produce a thermal anomaly capable of sustaining a granulite-facies event of 30 Ma duration, a 40 km thick underplate, placed 10 km beneath the 20 km crustal level is required. Thinner underplates produce shorter lived thermal events. The most important aspect of this model is that the temperature maximum experienced by the rocks is controlled strongly by the distance to the underplate. Waters (1990) suggests an underplate 30 km thick, emplaced 10 km below the present erosion surface with 10 km of additional felsic magma emplaced above this. As illustrated in fig. 11.3 the P-T-t paths generated by magmatic accretion vary depending on the original crustal depth prior to the accretion event. Anticlockwise paths are generated for rocks within and below the accretion zone, but not for rocks above it, as there would be an isostatic response for the newly thickened crust (Harley, 1989). Thermal modelling by Loosveld & Etheridge (1990) predict that even for unreasonably thick underplates of 75 km the temperatures in the middle crust would not rise sufficiently to stabilise sillimanite.

Problems with a purely magmatic accretion thermal model for the Namaqua metamorphism concern the shape of the predicted P-T-t path, the the timing of magmatism and the time span envisaged for metamorphism. Uplift is a consequence of crustal thickening by underplating. The thermal effect of the underplate is relatively short lived, thus it is unlikely that mineral assemblages could be

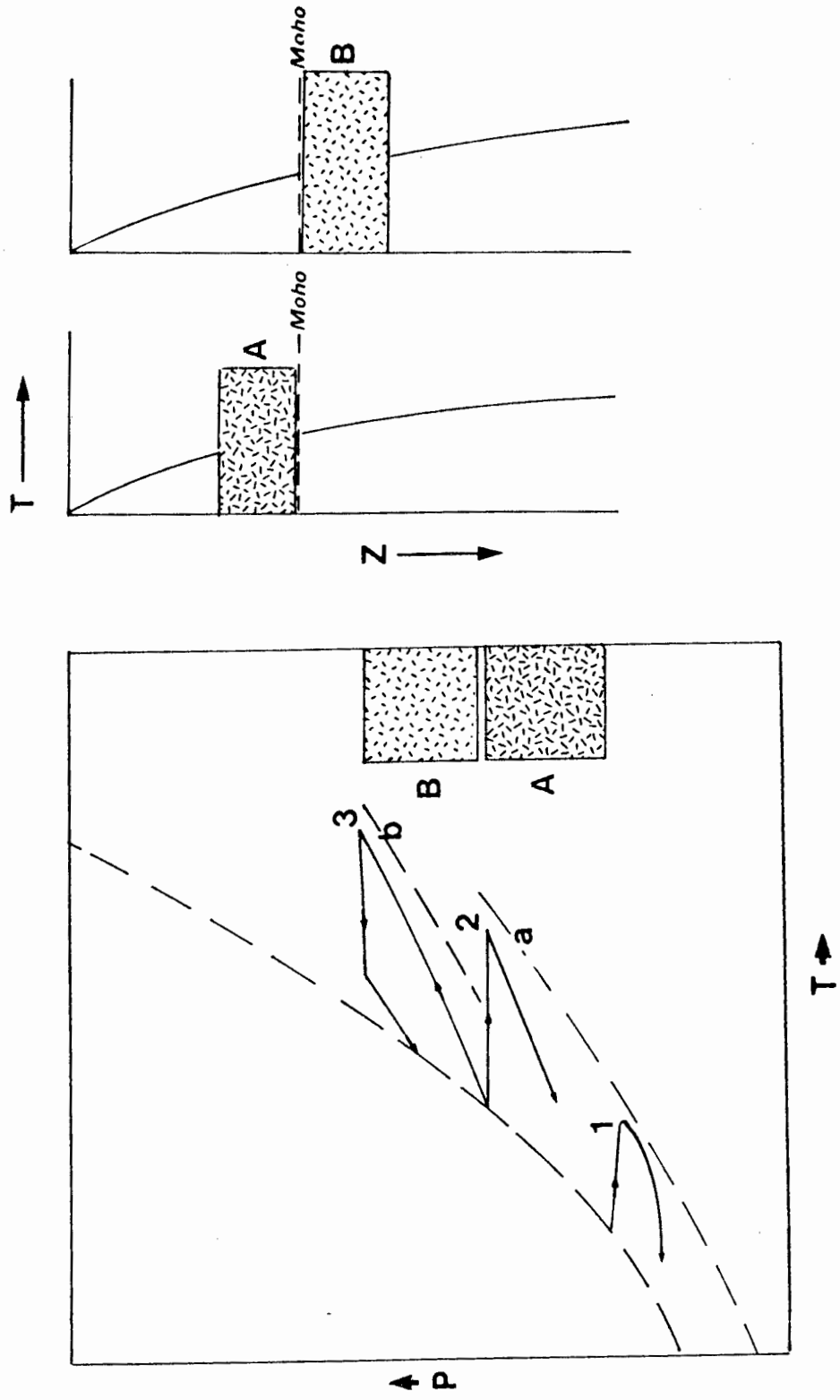

Fig. 11.3 P-T-t paths for magmatic accretion models of granulite formation. Curve 1: a clockwise path for rocks in the crust above the accretion zone. Curve 2: a clockwise path for rocks at the base of the crust. Curve 3: an anticlockwise path for rocks within or below the accretion zone. Curves a and b represent geotherms produced by magmatic accretion above and below the Moho respectively.

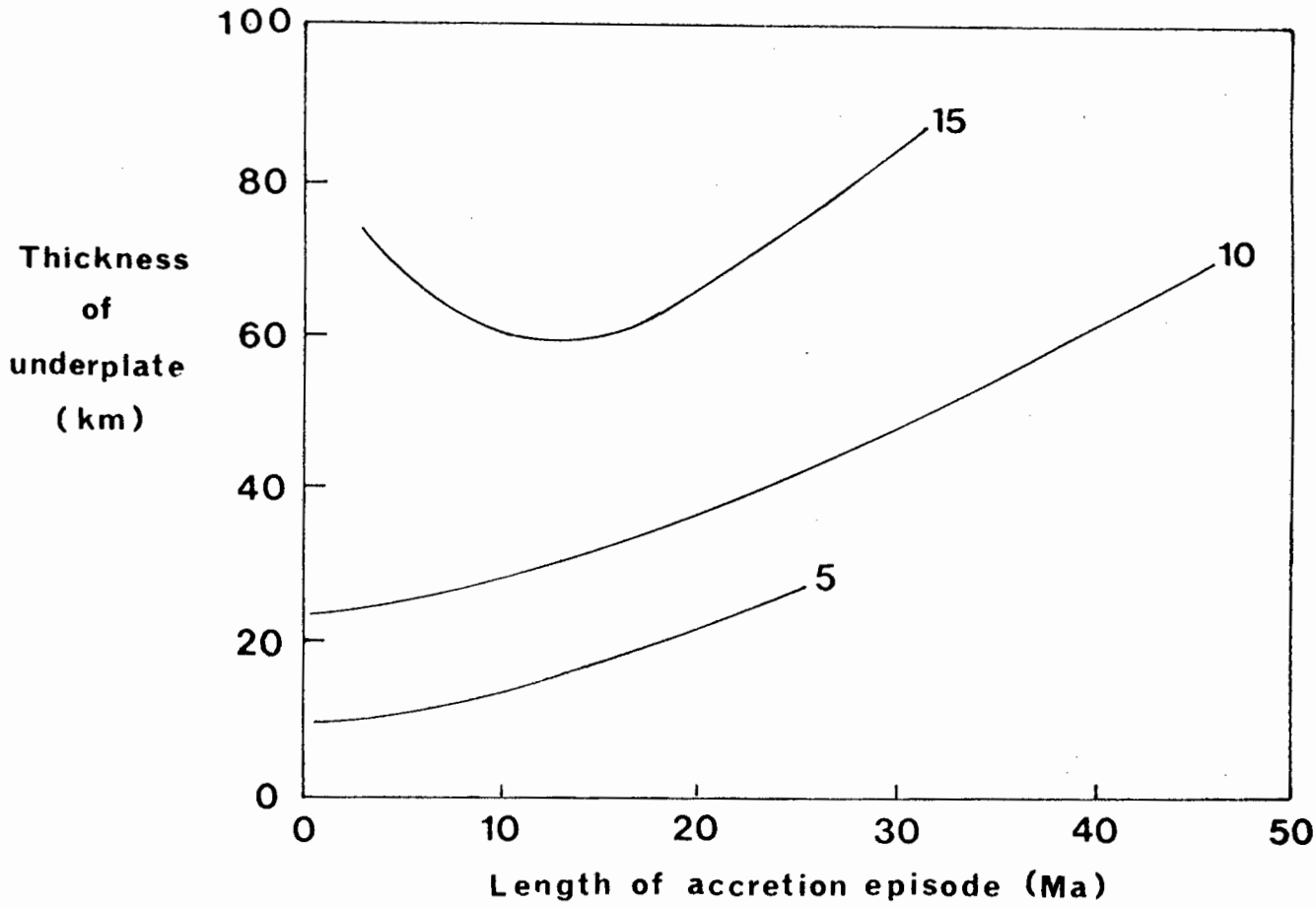

Fig. 11.4 The thermal effect of basaltic underplates of varying thickness over different lengths of time. Curves indicate vertical distance from the underplate in km. Long lived thermal events occur in the mid-crustal levels of crust with moderate thickness over areas with relatively thick underplating. After Waters (1990).

reset to mask all record of decompression, although much would depend on the landsurface elevation, the rise in topography and accompanying rates of erosion. This model requires the intrusion of large amounts of syn-tectonic magmas at various levels of the crust. It fails to explain the continued intrusion of crustal partial melts into hot country rocks long after the assumed metamorphic peak as evidenced from the intrusive Koperberg Suite. Cooling rates consistent with the thermal models of Waters (1990) for magmatic underplating would have to be between 10-20°C/My, this agrees with the maximum estimates derived from garnet zonation profiles (see Chapter 6) and reequlibration of oxygen isotopes (see Chapter 9). Although there are many outstanding problems with the time constraints of metamorphism in central Namaqualand, present radiometric data suggests that metamorphism took place over a time-span of at least 90 Ma, three times longer than the maximum predicted thermal anomaly would persist if magmatic underplating was the sole source of thermal energy required.

11.6.2 Extension of normal thickness crust

Areas of anomalous heat-flow in modern day continental crust are typified by extensional tectonics, e.g. the Basin and Range Province of western U.S.A. The calculated temperatures at the base of the crust in these areas are in excess of that required for granulite-facies metamorphism. Thinning of the crust is fundamentally linked to thinning of the continental lithosphere and hence a rise in the asthenosphere-lithosphere boundary, and consequently a steepening of the continental geotherm (McKenzie, 1978). Wickham & Oxburgh (1985) attributed the extremely high geotherm (>80°C/km) inferred for the Trois Seigneur Massif in the Pyrenees to continental extension. P-T-t paths for extensional models were developed by Sandiford & Powell (1986). Crustal extension P-T-t paths are characterised by heating into the granulite-facies at constant or decreasing pressure and cooling at constant or increasing pressure. A rifting model allows for high heat flux from the upwelling of hot asthenosphere and the intrusion of mantle-derived basalts into the crust. Large-scale crustal anatexis can occur at relatively shallow depths.

Thinning of the crust may be symmetrical or asymmetrical. In the symmetrical extension models, near-isobaric cooling will occur after an episode of decompression associated with the maximum extension.

For axially symmetrical models of extension, the steepest geotherms occur where the lithosphere is thinnest and the crust undergoes maximum extension. P-T-t paths are charaterised by decompression at maximum temperature (see fig. 11.5) if extension is accompanied by substantial magmatic accretion, then the P-T-t paths produced are similar to those in fig 11.3. Isobaric heating and cooling paths are predicted for asymmetrical extension models (Sandiford & Powell, 1986; Harley, 1989). The model outlined by Sandiford & Powell (1986) involves crustal extension accomodated by simple shear along detachment zones in the lithosphere accompanied by extension by pure-shear in the underlying asthenosphere (see fig. 11.6). The greatest thermal perturbation is produced where upwelling asthenosphere occurs underneath an area of near-normal crustal thickness. In these non-extended (little deformed) regions the resultant granulite-facies event will be seen as a thermal overprint on the lower crust (Harley, 1989). Extension may progress during metamorphism by migration or by collapse of the detachment zone into its footwall. Intense shearing will accompany granulite-facies metamorphism in the hanging wall (Harley, 1989). The precise form of the cooling path will be controlled by the position of the rocks relative to the detachment zone. In the areas where the geotherm is most perturbed, a small amount of thermal subsidence is predicted (Sandiford & Powell, 1986). Towards the zone of maximum crustal extension the thermal subsidence is greater due to the isostatic response of the thinned crust and may result in the formation of sedimentary basins (McKenzie, 1978), this could result in a slight increase in pressure during cooling.

A number of granulite terranes were considered as being possible examples of ancient extensional thermal regimes by Sandiford & Powell (1986), including Namaqualand and Broken Hill, Australia. However, the structural style in Namaqualand suggests compressional tectonics and emplacement of granitoid magmas along thrust zones (Watkeys, 1986 and Moore et al., 1990) during the prograde stage of metamorphism. It is not clear whether D_3 deformation as developed in the Buffels River area is consistent with continued crustal shortening. The abundant late tectonic shear zones in Namaqualand may reflect extensional strain in the lower crust. An asymmetrical extension model may preserve an earlier compressional history, but differences in structural style and metamorphic history would exist with the adjacent amphibolite-facies terrane. Surface expression of major lithospheric detachment zones would be expected, this is not apparent in Namaqualand. Loosveld & Etheridge (1990) discuss the limitations

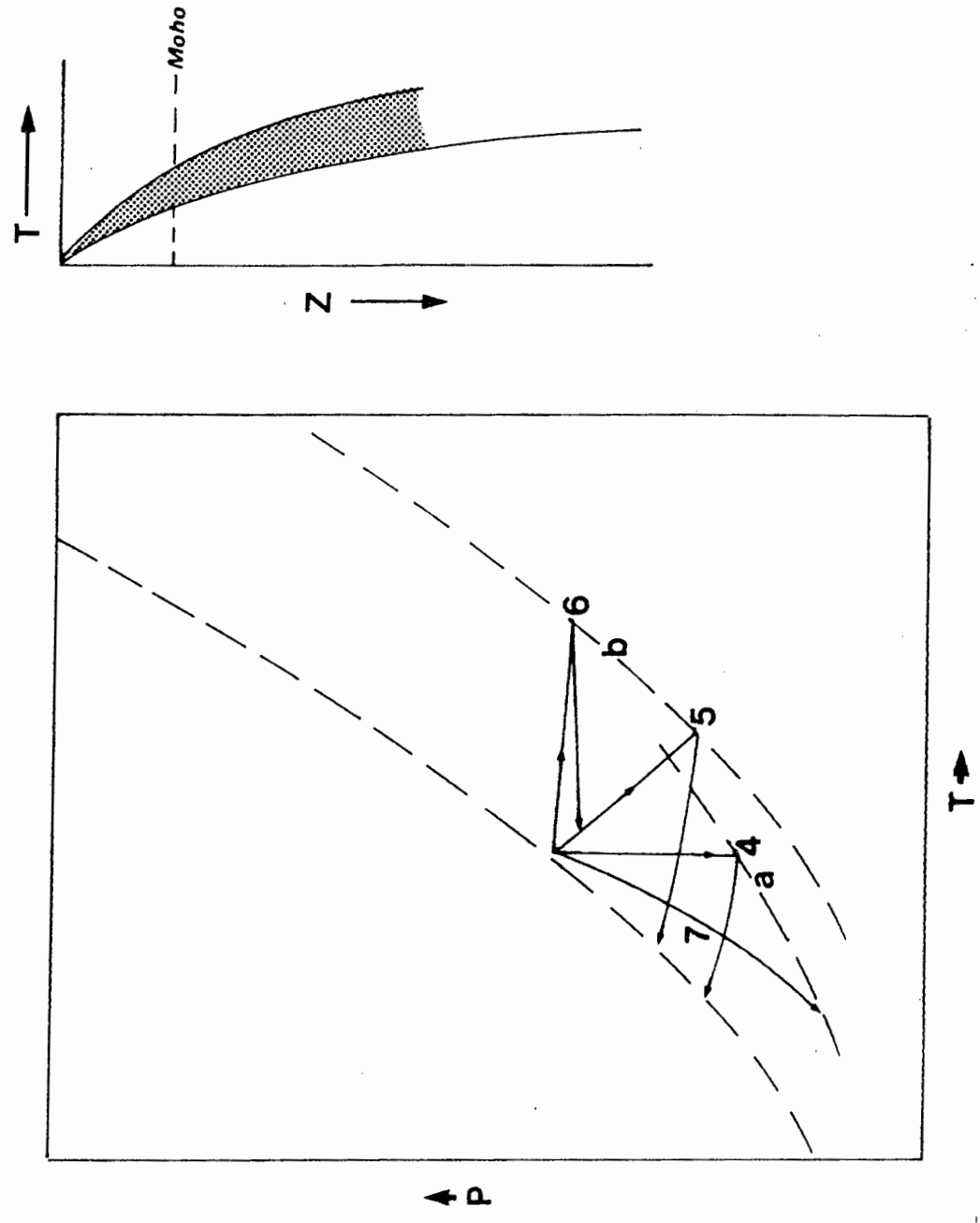

Fig. 11.5 P-T-t paths produced by extension of continental crust. Curve 4: for lower crustal rocks undergoing symmetrical extension. Curve 5: asymetrical extension in or below detachment zone near region of sub-crustal thinning. Curve 6: for rocks at the base of the crust in discrepant zones. Curve 7: lower crustal rocks in core complex sections. After Harley, 1989.

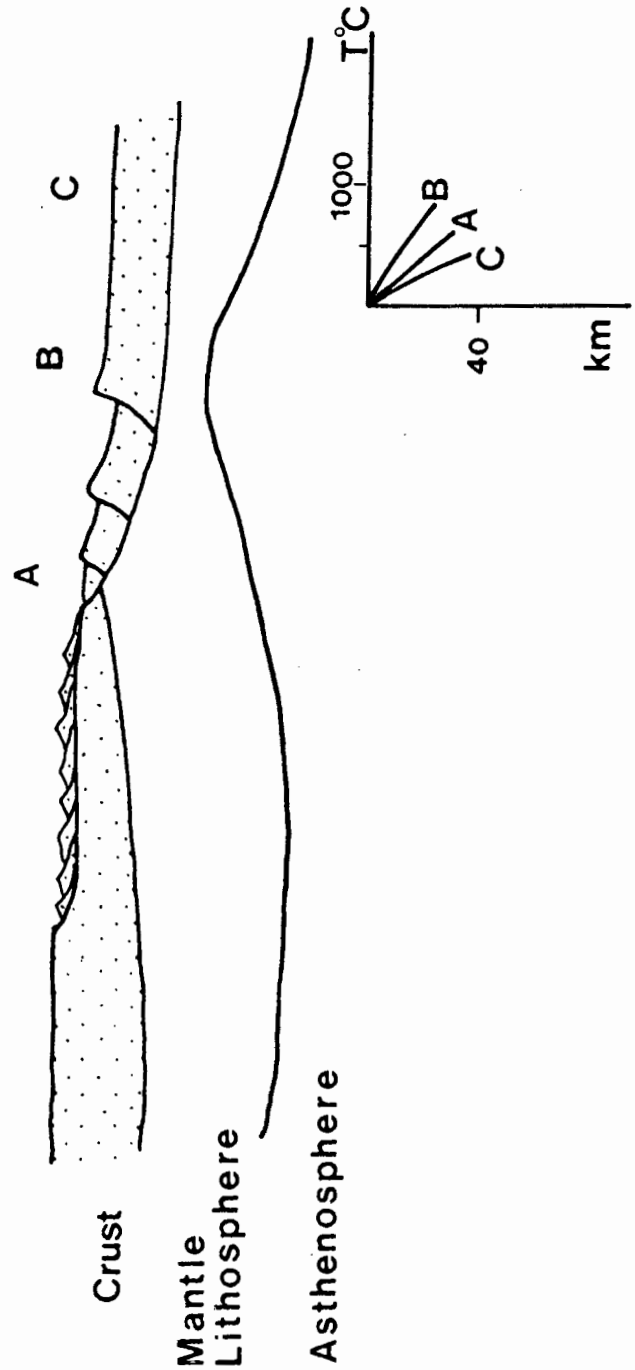

Fig. 11.6 The Sandiford & Powell (1986) model of asymmetric extension of mantle lithosphere. The greatest thermal effect, curve B, is seen where upwelling asthenosphere occurs underneath an area of near normal crustal thickness.

of the extensional model. The major constraints are the limited amount of heat added to the crust during and after extension. Loosveld & Etheridge (1990) calculate that the amount of symmetrical extension required for andalusite-sillimanite metamorphism is greater than 140%, unless a mantle plume produces abnormally high temperatures at the base of the lithosphere. Such large extensions are rare in intracontinental rifts. Asymmetrical extension could produce zones of high heat input at lower extension values. The other major problem with the extensional model is the relatively short time scale for thermal relaxation, especially if magmatic advection plays a large role in heat transfer. Substantial amounts of mantle and crustal derived melts are predicted for extensional models which involve thinning of the mantle lithosphere. An expected consequence of continental extension would be bimodal volcanism and an abundance of mafic dykes.

Thompson (1989) invokes moderate overthickening of previously thinned crust to explain low pressure-high temperature metamorphism in the Slave Province, Canada. The combination of thinning prior to thickening produces a crustal thickness of 47 km, not considerably greater than normal crustal thicknesses. In this way Thompson reconciles structural style indicative of crustal shortening with low degrees of post-metamorphic uplift and a slow cooling history (nearly 175 My, indicated by K-Ar ages for biotite). In the Slave province there is evidence of I-type pretectonic and syntectonic magmatism followed by syn- to post-tectonic S-type granite emplacement.

Evidence for extension in Namaqualand can be found in the pre-metamorphic history of the area. Moore et al. (1990) postulate that felsic magmatism is associated with shallow basin sediments and base metal sulphides in the Aggeneys area. In the Buffels River area the intrusion of mafic magmas into the supracrustal sequence may have occurred during an earlier extensional episode. An early history of extensional tectonics is also recorded in the Broken Hill area of Australia but as in the case of Namaqualand the metamorphic peak post-dates extension by well over 100 Ma.

11.6.3 Extension of thickened crust and non-extensional lithospheric thinning

Post-orogenic extension is a feature of many modern collisional belts, such as the Himalayas and the Andes (Molnar, 1986; Dewey, 1988 and Gaudemer et al., 1988). Widespread extension seems to reflect the thinning of previously thickened crust (Gaudemer et al., 1988). There is a general correlation between the width of modern orogenic belts and the occurence of anatectic granitoids and extensional structures. Gaudemer et al. (1988) model the thermal effects of crustal shortening, orogenic belt width and radioactive heat production. Crustal temperatures increase with belt width, especially where there is substantial crustal heat production. Extension can occur late in the history of wide orogenic belts, but never occur in thin belts, such as the Alps. Sonder et al. (1987) consider modern extensional belts such as the Basin and Range Province as being the end product of extension of overthickened crust. Anovitz & Chase (1990) attribute P-T-t paths recorded in Grenville Province terranes in Ontario as being the result of post-thrusting extension. P-T-t path produced by post-thickening extension should be characterised by decompression followed by isobaric cooling at depth. This may explain isobaric cooling paths experienced in medium pressure granulite-facies terranes (Bohlen, 1987 and Harley, 1989). As there is no obvious evidence of crustal extension following crustal thickening in central Namaqualand models involving thinning of the sub-crustal lithosphere without appreciable crustal extension may provide a plausible alternative.

Houseman et al. (1981) proposed that crustal thickening would be intially accompanied by thickening of the underlying lithospheric mantle. This would lead to the formation of a dense lithospheric "root". Houseman et al. (1981) argue that this "root" may become gravitationally unstable and cause the mantle lithosphere to detach from the overlying crust. Removal of the lithospheric mantle in such a fashion is the thermal equivalent of infinite extension of the lithosphere. Loosveld & Etheridge (1990) have modelled the thermal effects of thinning of the mantle lithosphere during progressive, homogeneous crustal thickening (see fig. 11.7).

In the models of Loosveld & Etheridge (1990) the trajectory of

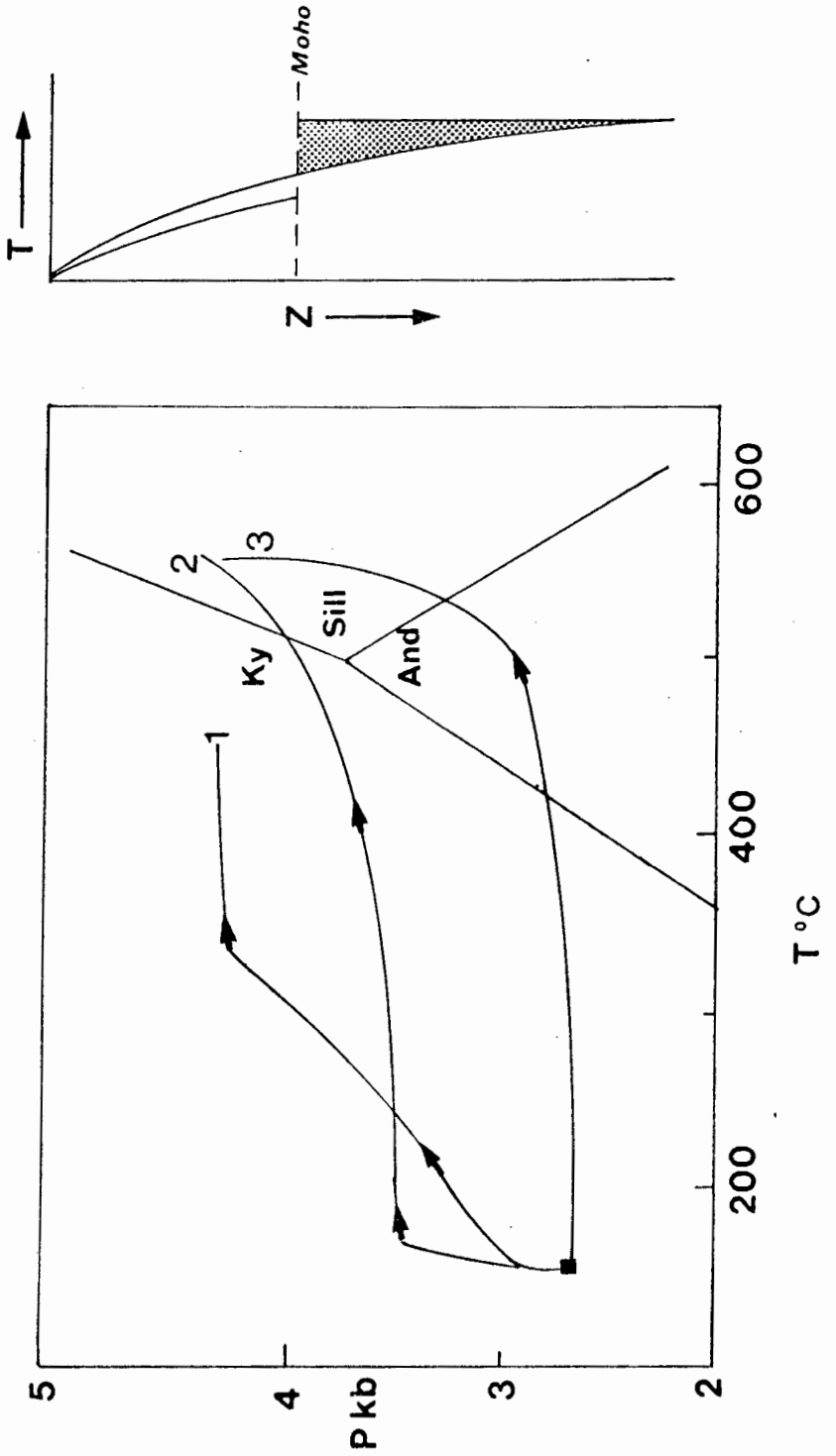

Fig. 11.7 The thermal effects of thinning the mantle lithosphere. Curve 1: 75 km underplate at 1300°C at the base of the crust. Curve 2: convective thinning of the Mantle lithosphere 15 Ma after crustal thickening. Total duration of crustal thickening = 30 Ma. Curve 3: slow deformation with constant asthenospheric temperature at the onset of crustal thickening. After Loosveld & Etheridge (1990) based on T at surface of 0 and 1350°C at a depth of 100 km. Initial crustal thickness = 25 km. Thermal diffusivity = 1.2 x 10^{-6} m^2/s. ρ = 2700 kg/m^3.

the P-T-t path is controlled by the vertical crustal strain rate, the duration of convection at the base of the crust and the overlap in time between thinning of the mantle lithosphere and thickening of the crust. In order for the P-T-t path to transect the andalusite-sillimanite stability field it is important that asthenospheric upwelling accompanies crustal thickening. Continuous convection in the asthenosphere keeps the temperature at the base of the crust around 1300°C throughout crustal thickening without the relatively rapid thermal relaxation associated with even very thick underplating. Constant asthenospheric temperatures and slow deformation rates produce P-T-t paths that transect the andalusite-sillimanite phase boundary during the prograde part of the path (Loosveld & Etheridge, 1990). When convection at the base of the crust stops, the mantle cools by conduction and thus behaves similar to an underplate emplaced at the base of the crust. This accounts for the relatively slow cooling histories experienced by low pressure granulites. If mantle convection stops at the end of crustal thickening, the post-thickening phase of the P-T-t path will be characterised by isobaric or near-isobaric cooling. If crustal thickening continues, the initial retrograde part of the P-T-t path will be characterised by increasing pressure during cooling. An important feature of the "Crustal Thickening/Convective Lithospheric Thinning" model of Loosveld & Etheridge (1990) is that it can explain peak metamorphic temperatures occuring during the later stages of, or post-dating crustal thickening. Another strength of this model is that the magmatic activity associated with low pressure-facies series metamorphism is a natural consequence of the model rather than the causative mechanism behind granulite-facies metamorphism.

Oxburgh (1990) outlines a thermal model for slowly cooled granulites based on lithospheric thinning without significant crustal extension, termed by Oxburgh "Non-Extensional Lithospheric Thinning". The Oxburgh (1990) model for Namaqualand granulites based on the data and the assumptions of Waters (1989) involves modelling the thinned lithosphere as a layer that has fixed temperatures at its upper and lower surfaces (10 and 1400°C respectively). The layer is allowed to thicken by conductive cooling to the thickness of the undisturbed adjacent lithosphere. It is assumed that granulite-facies metamorphism is synchronous with maximum thinning of the lithosphere. Oxburgh's model predicts that cooling rate depends on depth within the lithosphere. Oxburgh models temperature against non-dimensional time for points at different depths in thinned lithosphere, see fig.

11.8 The curves in fig. 11.8 correspond to different cooling histories at different depths of burial expressed as fractions of the final (equilibrium) lithospheric thickness. Fig. 11.9 shows the relationship between the cooling interval recorded in the rocks, the difference in maximum and minimum cooling (blocking) temperatures and the equilibrium lithospheric thickness. The values used by Oxburgh are summarised in Table 11.1.

The values for d converted to depth in km, bound the depth range within which the rocks could have cooled if the thermal model of Oxburgh is applicable to Namaqualand granulites. These values are decreased if crustal heating by radioactivity is increased. A more thorough testing of this model will be possible if new radiometric mineral data is produced and cooling history can be more accurately determined. Oxburgh considers that most granulites that show evidence of a slow-cooling history were formed in the lower part of a 30-40 km thick crust in a lithosphere that was about 100 km thick, similar to modern lithospheric thicknesses.

TABLE 11.1

DATA USED IN THE THERMAL MODEL OF OXBURGH (1990) FOR NAMAQUALAND

T = Temperature interval recorded from mineral blocking temperatures

= 800 - 500°C = 300°C

t = Time taken to cool through the temperature interval T, above

= 140 Ma

Depth recorded by rocks from geobarometry

= 5 kb = 17 km

Model values from the curves in figs. 11.8 and 11.9

t'	L, km	d	km
0.22	140	0.27	38
0.95	60	0.31	25

where t'= difference between the times

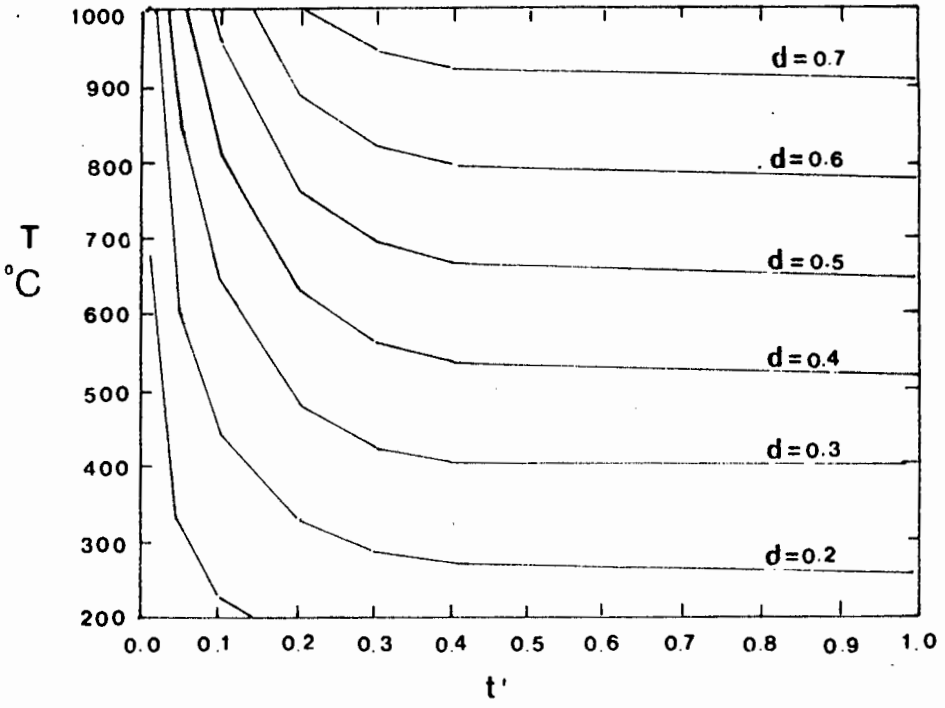

Fig. 11.8 Cooling history in °C for rocks at different depths in the crustal lithosphere. Position of the rocks is shown as a function of total lithospheric thickness, d. t′ represent non-dimensional time, i.e. 1 equals an infinite period. After Oxburgh (1990).

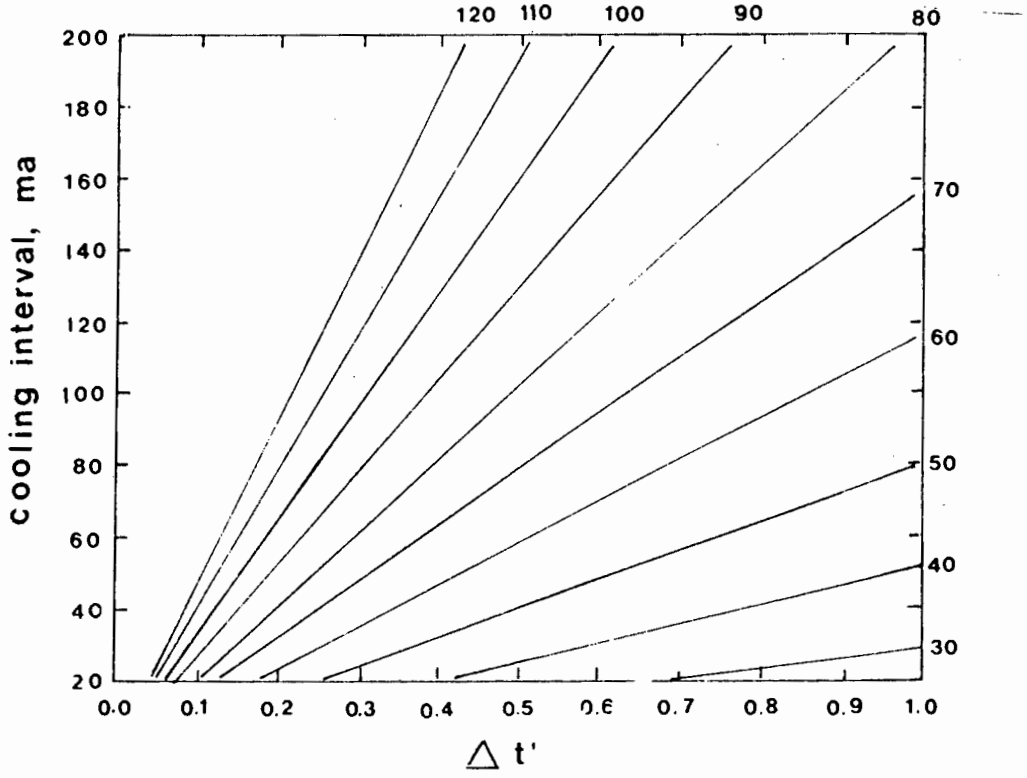

Fig. 11.9 Cooling history of rocks for different cooling intervals. $\Delta t'$ is the difference between the times at which the higher and the lower cooling temperatures were recorded. Assuming $t' = t\ k/L^2$, where t is the time, k is the thermal diffusivity (10^{-6} m^2/sec) and L is the thickness of the lithosphere. After Oxburgh (1990).

11.7 THE ROLE OF FLUIDS IN GRANULITE-FACIES METAMORPHISM

Over the last ten years there has been much discussion over the role of fluids in granulite formation. Low a_{H2O} values are necessary to stabilise anhydrous assemblages at temperatures below 800°C and prevent wholescale melting of crustal rocks. The discovery of abundant CO_2-rich fluid inclusions in granulites by Touret (1971) suggested that fluids may have had a causative role in granulite formation rather than granulites simply representing the dessicated portion of the lower crust. The formation of granulites is normally attributed to one of three principal mechanisms:

1. Partial Melting. H_2O is strongly partitioned into melt, thus insitu anatexis or the passage of silicate melts in the crust is likely to dessicate the surrounding rocks. Migmatites are an essential component of most granulite-terranes and syntectonic magmatism is normally recorded.

2. CO_2 flushing. In areas where there is less direct evidence of partial melting dilution of H_2O-rich fluid by a substantial flux of CO_2-rich fluid is preferred. Evidence for CO_2 involvement in granulite forming processes comes from the presence of CO_2-rich fluid inclusions and from the pattern of geochemical depletions recorded in some granulites which are inconsistent with partial melting.

3. Metamorphism of dry rocks. In some terranes the amount of fluid present during high grade metamorphism may have been neglible. This is thought to be the case in terranes dominantly comprised of orthogneisses and those which have a previous history of contact metamorphism.

These processes are not entirely mutually exclusive and a single terrane may show evidence of all three mechanisms. It is important to address the following questions when considering the role of fluids in granulite metamorphism:

1. Do the rocks equilibrate with a free-fluid phase during metamorphism or are they vapour-absent?

2. If fluid infiltration occurs during metamorphism, what is the composition of the fluid and is the movement of fluid pervasive or

channelised?

3. As most rocks evolve an H_2O-rich fluid during devolatilisation, how does this fluid escape?

Evidence from this study is summarised below and a model for fluid behaviour during granulite-facies metamorphism is proposed.

The nature of the fluid composition in equilibrium with granulite-facies assemblages can be estimated from mineral equlibria studies on simple dehydration reactions. In this study semi-quantitative modelling of water activity from various dehydration equilibria in isofacial samples was undertaken. The results are summarised in Table 11.2. Estimates of a_{H2O} represent minima if the assumed temperature is lower than the actual peak conditions. Comparison of a_{H2O} values from different rock types may be misleading as values are extremely model dependant. The same uncertainities caused by diffusion controlled exchange between phases during slow cooling that affect thermobarometry will affect a_{H2O} estimates.

TABLE 11.2

X_{H2O} estimates from dehydration equilibria in the Buffels River area.
Calculated at T = 750°C, P = 5 kb

Rock type	**Equilibria**	**X_{H2O}**
Mafic gneisses	$2hb = 2di + 3en + 2an + 2H_2O$	0.09 - 0.21 0.18 - 0.33*
Pelitic gneisses	$ann + sill + 2qtz = alm + Kfsp + H_2O$	0.22 - 0.31

* contains retrograde hornblende

X_{H2O} estimates vary on a small-scale and show good correlation with observed petrographic features. Mafic gneisses showing textural replacement of early anhydrous minerals with large crystals of retrograde hornblende give higher values of X_{H2O} compared to rocks with prograde hornblende. The values above suggest local control on water activity and argue against a pervasive influx of low a_{H2O} fluid. However, local scale infiltration of low a_{H2O} fluid is not

ruled out. The ubiquitous presence of thin, cm-scale anhydrous granulite margins around hornblende-bearing mafic gneisses provides evidence for the existence of fluid activity gradients between adjacent rock-types. The scale of such metamorphic banding in mafic gneisses is best explained by intercrystalline diffusion and does not require the presence of a fluid phase. The evidence of disequilibrium compositions recorded by plagioclase coexisting with hornblende and pyroxene in mafic gneisses suggests that the mechanism that controls the development of the granulite-margins occurs at rates faster than can be accomodated by internal diffusion within plagioclase. Thus, lowering of a_{H2O} in the adjacent rock must be relatively rapid and non-reversible. This could be achieved when major melt generating reactions are met or by passage of CO_2-rich fluid along the lithological contacts.

Fig. 11.10 shows the T-X_{H2O} relationships of the major dehydration and melting reactions in mafic gneisses, pelitic gneisses and biotite gneisses. On increasing temperature each rock type with a fluid buffering assemblage will define a unique water activity. Pelitic gneisses containing biotite or melt coexisting with garnet and/or cordierite will define much lower water activities than an adjacent layer of mafic gneiss. The imposition of a water activity gradient on the mafic gneiss results in local dehydration. This process is favoured when reactions are met which cause dramatic lowering a_{H2O}, or remove, or partition H_2O from the system. Partial melting appears to be the most viable mechanism. Evidence of local reaction control suggests that a fluid phase, if present, in equilibrium with the granulite-facies assemblage is non-pervasive, perhaps channelised and transitory in nature.

The presence of low variance assemblages in most rocks and the textural history of mineral growth during granulite-facies metamorphism in the Buffels River area are consistent with rock dominated metamorphism and internal buffering of fluid composition. Many of the rocks may have been vapour-absent. But, as the transition from amphibolite-facies to granulite-facies assemblages involves the loss of H_2O from the system a mechanism is necessary to extract and move that fluid. Under the highest temperature conditions experienced by the gneisses in the Buffels River area the rocks contained a diffuse network of water-undersaturated quartzo-feldspathic melts, water expelled on crystallisation of such melts is expected to stabilise amphibole or biotite in the surrounding gneiss. There is no

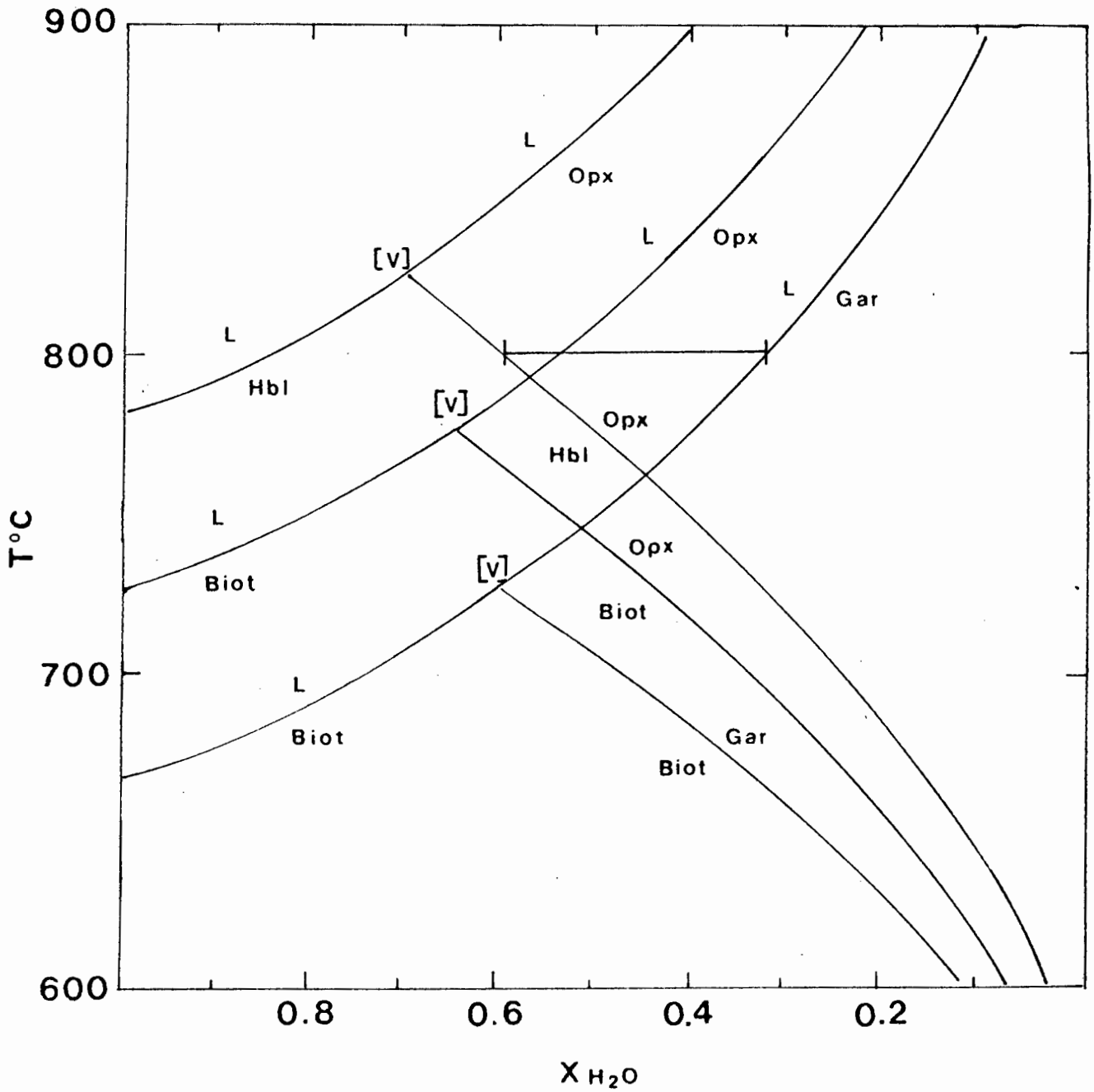

Fig. 11.10 Comparative T-X_{H_2O} relations for simple dehydration and melting curves in mafic, pelitic and biotite gneisses.

observable hydrous retrogression adjacent to any melt segregations. Net loss of water must have accompanied granulite metamorphism, yet in most cases migration of melts is extremely limited. Sharp cm-scale prograde facies transitions are preserved in individual rocks. Fluid inclusions are scarce and small, and consist of distinct CO_2-rich and H_2O-rich fluid populations, mostly secondary in origin.

The general behaviour of fluid during metamorphism has been discussed by Walther & Wood (1984) and Thompson (1987). Fluids released in the lower crust appear to be focused into high permeability channelways. Metamorphism in the absence of a pervasive fluid-phase results in incomplete reactions and other disequilibrium features. Fluid motion via convection is possible for permeabilities greater than about 10^{-17} m^2, if hydrostatic pressure conditions are maintained (Etheridge, 1983; England & Thompson, 1984). Collapse or compaction of pores will pressurise the fluid to lithospheric pressure and convection will cease. Isolated porous layers beneath an impermeable cap-rock can sustain convective fluid-flow as long as temperature and fluid density gradients exist (Etheridge, 1983; Thompson, 1987). Layers undergoing devolatilisation are likely to represent transient channelways for fluid movement until porosity and fluid pressure gradients are diminished. Ferry (1986) and Wood & Walther (1986) indicate that H_2O released from devolatilisation in pelites and amphibolites will rarely leave a diagnostic oxygen isotopic signature because the fluids are close to isotopic equilibrium with the reacting minerals.

Differences in style of fluid release and migration will have profound effects on the isotopic composition of rocks. Pervasive fluid flow requires fluid movement independant of structural controls, permeating all rocks equally. The result of pervasive fluid flow would be to cause isotopic reequilibration across lithological boundaries. Channelised fluid flow involves fluid movement along permeable zones, such as shear zones, veins, lithological contacts and permeable rock types. Channelised fluid flow allows the isotopic composition of some rocks to remain unaffected while others could be considerably reequilibrated. The extent of isotopic reequilibration in infiltrated rocks is a function of the fluid/rock ratio, the isotopic difference between the rock and the infiltrating fluid and the temperature. The approach adopted in this study was to compare the $\delta^{18}O$ values of minerals from closely associated gneisses. The oxygen isotopic fractionations of quartz-mineral pairs produces a

sequence of decreasing apparent temperatures, quartz-garnet > quartz-biotite > quartz-magnetite. This observed disequilibrium is difficult to explain in terms of open system processes as each of the phases within the same rock is isotopically distinct and isotopic difference between rocks are retained on a cm-scale. If the values recorded from mineral-pairs were the result of fluid infiltration then it would require a complex combination of one or more of the following conditions: the infiltrating fluids were of varying isotopic compositions; or the infiltration of fluid occurred at different temperatures; or the fluid/rock ratios varied on a local scale. Two closed-system processes could account for the observed oxygen isotope mineral data. If continued growth or recrystallisation occurred during cooling then the isotopic fractionations between minerals record the final temperature of crystallisation. Isotopic re-setting of minerals occurs by intercrystalline diffusional exchange of oxygen during cooling. The former is most likely in melt segregations where garnet may be a solid phase associated with a liquid which crystallises quartz and feldspar on cooling. Exchange of oxygen between solid phases and fluid can occur via three mechanisms: 1. by reaction with fluid to produce an alteration assemblage; 2. by solution and precipitation and 3. by volume diffusion. Isotopic exchange by volume diffusion is the dominant mechanism in anhydrous systems and has the slowest rate of isotopic exchange of the three mechanisms (Matthews et al., 1983; Cole et al., 1983). Volume diffusion is the favoured mechanism of exchange between minerals and small amounts of grain boundary fluid in these rocks as the mineral assemblages show no alteration and little textural evidence for recrystallisation. A solution and precipitation mechanism may be applicable to oxygen exchange in vein quartz and melt segregations.

Partial melting may play an important role in the oxygen isotope fractionation. Partitioning of water into the melt phase will reduce diffusional exchange rates in the host gneiss and may help preserve the oxygen isotope composition of minerals in the host. Fluids expelled by crystallising melts will aid intercrystalline diffusion amongst mineral phases.

Evidence from fluid inclusions is ambiguous. There are a group of high density CO_2-rich inclusions that may have been trapped close to the peak of metamorphism and may represent small quantities of residual grain boundary fluid. There is much textural evidence, in the form of necked, stretched and naturally decrepitated inclusions

indicating that post-entrapment modification of fluid density has occurred. Lack of definitive criteria makes correlation of high density inclusions with peak metamorphism at best tentative, or entirely speculative. However, the trapped fluid, probably a CO_2-rich mixture with H_2O would correlate well with calculated a_{H2O} and fO_2 conditions from mineral assemblages. Fluid equilibria studies predict H_2O-CO_2 fluids at high fO_2, H_2O-rich fluids at intermediate fO_2, and H_2O-CH_4 fluids at low fO_2 (Lamb et al., 1987). Studies on granulites from the Adirondacks (Lamb et al., 1987) showed that the presence of high density CO_2 fluid inclusions was incompatible with fluid activity calculations that predicted an evolving H_2O-rich fluid at low to moderate fO_2 at peak metamorphic temperatures. Hence the fluid inclusion were secondary in origin and had no direct or causative relationship with granulite-facies metamorphism.

Experimental work on the role of CO_2 in the melting of biotite and quartz by Peterson & Newton (1990) suggests that infiltration of CO_2-bearing fluids can produce partial melting in granitic rocks. Peterson & Newton (1990) record a substantial increase in the solubility of CO_2 in KMASH liquids above 3 kb. A granitic magma in the KMASH model system containing some CO_2, crystallising at a constant pressure of 6 kb, would form biotite by reaction of orthopyroxene with liquid at a temperature of about 745°C. Magmas with no CO_2 could crystallise under vapour-absent conditions to produce biotite-orthopyroxene-bearing charnockites at 810°C. In the presence of a mixed H_2O-CO_2 fluid at high temperatures crystallisation of orthopyroxene takes place and fluids in equilibrium with magmas would be very CO_2-rich. On cooling liquids tend towards granite compositions and coexisting vapour becomes progressively enriched in H_2O. If melting is triggered by infiltration of CO_2-rich fluids crystallisation of orthopyroxene is favoured. On cooling the vapour would tend towards more H_2O-rich compositions, fluids released during the early stages of crystallisation would be CO_2-rich. Evidence of a change from CO_2-rich to H_2O-rich fluids during the crystallisation of migmatites could provide an explanation for the presence of early CO_2-rich fluid inclusions followed by later H_2O-rich inclusion as recorded in a number of fluid inclusion studies (Touret & Dietvorst, 1983 and Olsen, 1987) including this work (see Chapter 10). Peterson & Newton (1990) regard the absence of hydrating back-reactions in leucosomes between orthopyroxene and vapour as being consistent with the evolution of a CO_2 fluid from liquids in equilibrium with

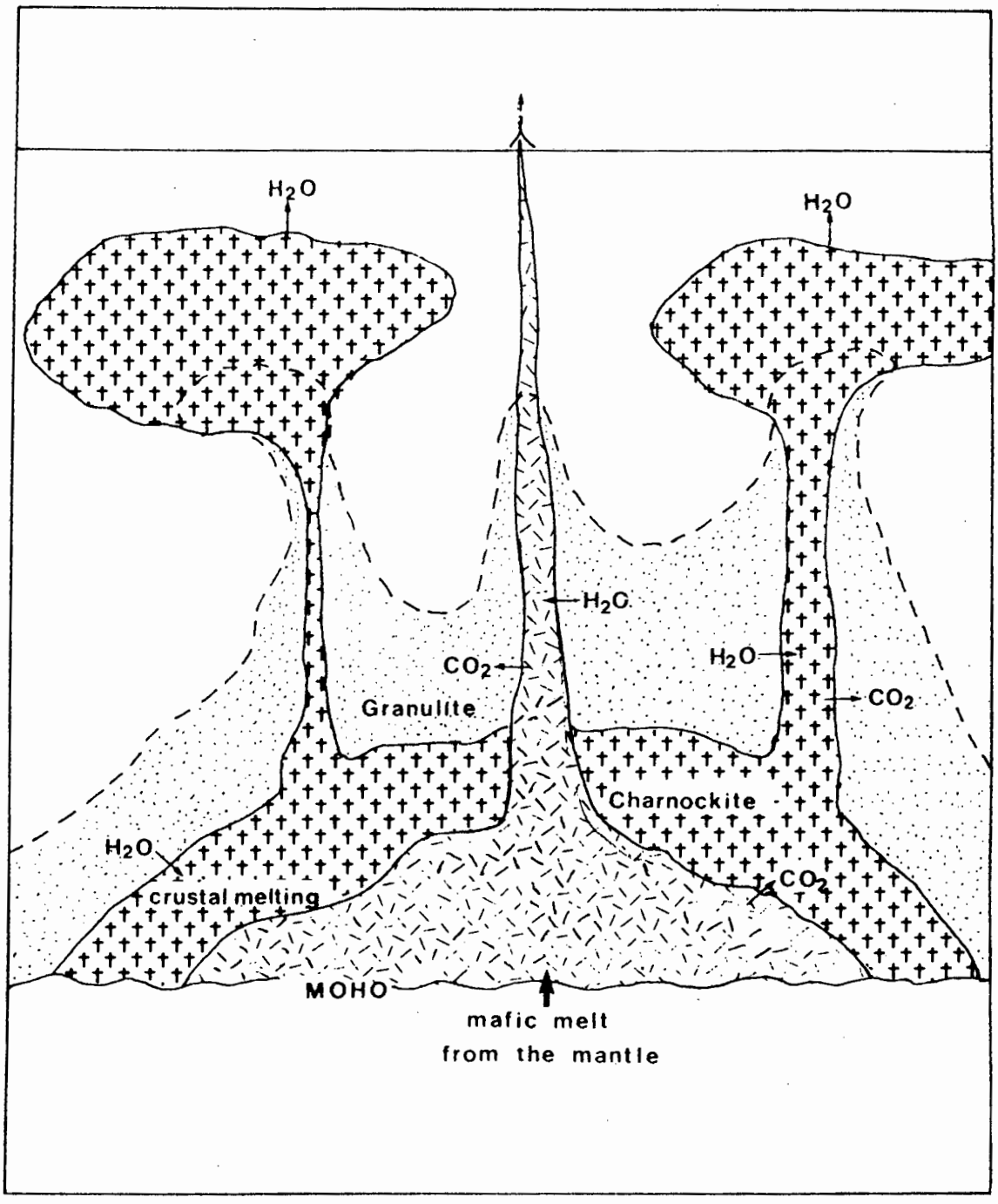

Fig. 11.11 The Frost & Frost (1987) model of granulite formation. Basaltic underplates give rise to partial melting of the crust and evolve CO_2 on crystallisation. H_2O is partitioned into silicate melts and migrates to higher levels of the crust.

orthopyroxene. Harley (examiners comments) contends that CO_2 infiltration is unlikely to trigger melting unless the temperature is very high. Furthermore CO_2 solubility in KMASH liquids has not been demonstrated in the absence of H_2O.

Frost & Frost (1987) present a model that includes aspects of the three often cited processes that may be responsible; that is CO_2-flushing, partial melting and recrystallisation of originally dry rocks. Frost & Frost (1987) argue that large volumes of CO_2 can migrate through the Earth's crust associated with melts. The Frost & Frost model involves magmatism in an area of high heat flow associated with the emplacement of a basaltic underplate (a rifting environment is indicated in their original model). The emplaced basalt may evolve a CO_2-rich fluid or cause partial melting in adjacent crustal rocks. The movement of vapour-undersaturated crustal melts not only aids heat transfer but lowers water activities by absorbing water in the surrounding rocks. This broad, multi-stage model implies that granulite-facies metamorphism is directly linked to large scale thermal events involving the earth's mantle. The main aspects of the Frost & Frost (1987) model are depicted in fig. 11.11.

11.8 SUMMARY AND CONCLUSIONS

1. The area studied at Hytkoras consists of a volcano-sedimentary sequence intruded by granitic orthogneisses. A basement-cover relationship cannot be demonstrated in this area.

2. The intrusion of granitic augen gneisses is syntectonic with a period of compressional deformation that imparts a near-horizontal fabric and shallow plunging mineral lineation on the supracrustal sequence (regional F_2). A thrusted contact between the supracrustal sequence and the orthogneisses has been postulated by Moore (1986). In this study the contact is interpreted as intrusive due the presence of supracrustal xenoliths in the augen gneisses. The contact between the supracrustal rocks and the augen gneisses is marked by dextral shearing. The Buffels River Shear Zone (or the Kameelboomberg Shear Zone, as it may become known) imparts a strong southward dipping foliation, which is developed as an axial planar fabric associated with upright, asymetrical folds (local F_3).

3. The metamorphic conditions accompanying the regional D_2 phase of deformation are difficult to quantify as growth of new minerals and near total recrystallisation of prexisting minerals during the thermal maximum obliterates much of the evidence. The L_2 lineation is commonly defined by prismatic sillimanite, in parts overgrown in mimetic fashion by later garnet poikiloblasts. It is suggested that the compressional D_2 phase of deformation took place under upper amphibolite-facies conditions.

4. The local D_3 shearing deformation occured at granulite-facies conditions, as demonstrated by the presence of foliated orthopyroxene in the sheared margins of boudinaged mafic gneisses. The thermal maximum outlasted the deformation event as numerous migmatitic veins and patches varying in scale from a few millimetres to several tens of metres cut across the S_3 fabric. Annealing and recrystallisation accompanied cooling resulting in most rocks showing well equilibrated granular textures. Secondary growth of hornblende in some mafic gneisses and the presence of kornerupine and gedrite in some magnesian gneisses (Waters & Moore, 1985) suggests an influx of water-rich fluids occurred at relatively high temperatures, probably not long after the thermal maximum. There is no evidence of a later pervasive retrogressive event in the Hytkoras area.

5. The pressure-temperature conditions of metamorphism were determined using cation exchange thermobarometers and oxygen isotope thermometry. Pyroxene thermometry (Lindsley, 1982) on 30 samples yields a mean temperature determination of 756°C ± 50°C. Garnet-biotite thermometry on 16 samples give mean temperature determinations, according to method and calibration, of 694°C (Perchuk & Lavrent'eva, 1983), 721°C (Holdaway & Lee, 1977), 763°C (Thompson, 1976) and 806°C (Ferry & Spear, 1978). Garnet-cordierite thermometry on 9 samples yielded lower temperatures estimates of 741°C (Bhattacharya et al., 1988) 726°C (Thompson, 1976), 699°C (Perchuk & Lavrent'eva, 1983) and 698°C (Holdaway & Lee, 1977). Geobarometry is limited to three samples using the assemblage garnet-plagioclase-sillimanite-quartz. Pressure determinations vary between 5.2-6.2 kb (Ghent, 1976), 5.6-6.3 kb (Powell & Holland, 1987) and 5.6-6.6 kb (Newton & Haselton, 1981). Apparent equilibration temperatures for oxygen isotope fractionation using the empirical calibrations of Bottinga & Javoy (1975) give mean values that vary from 806°C for quartz-garnet mineral pairs (5 samples), to 591°C quartz-biotite (13 samples) 576°C for quartz-magnetite (4 samples).

6. Mineral equilibria from a number of different lithologies have been used to model fluid activities. In hornblende-bearing mafic gneisses fluid composition is buffered by coexisting hornblende, orthopyroxene, clinopyroxene and plagioclase. X_{H2O} estimates calculated from the breakdown of hornblende using the thermodynamic data of Holland & Powell (1987) yield values for X_{H2O} of 0.09 to 0.20 for rocks containing prograde hornblende with temperature fixed at 750°C. Retrograde hornblende gives values of 0.31 to 0.33. Water activity in pelitic gneisses is modelled using equilibria between biotite, sillimanite, quartz, garnet and K-feldspar following the approach of Phillips (1980), using the thermodynamic data of Holland & Powell (1990). Values for X_{H2O} range from 0.25 to 0.31 in sillimanite-bearing assemblages and 0.31 to 0.40 in sillimanite-absent assemblages, with temperature fixed at 750°C. Other rocks without hydrous minerals in the assemblage obviously define water actvities of zero. Rocks coexisting with silicate melts define higher water activities. Although model and temperature dependant, the data above suggests that variations in fluid activity exist between different lithologies at peak metamorphic temperatures. Similar variations exist in oxygen fugacity between different rocks.

7. Field evidence and petrography from rocks in the Hytkoras area demonstrates a close spatial association between hydrous and anhydrous mineral assemblages. Mafic gneisses occur as boudinaged lenses in contact with a variety of quartz-bearing supracrustal and ortho- gneisses. In all cases the mafic units contain a cm-scale margin of pyroxene granulite mantling a hornblende-bearing interior. The surrounding rocks are poor in hydrous phases with biotite removed in dehydration reactions to form orthopyroxene in granitic compositions and garnet and/or cordierite in pelitic rocks. Many of the surrounding rock types are migmatitic in nature and suggest that the biotite-out reaction involved melting. The breakdown of biotite in the adjacent rocks imposes a water activity gradient upon the mafic gneiss unit. The dehydration of hornblende in the mafic gneiss is promoted by a lowering of water activity and possibly by the high silica activity in the adjacent rock. A short range infiltration-exfiltration process controlled by intergranular diffusion is aided by shearing and recrystallisation along the margins of the mafic lenses during F_3 deformation.

8. The above relationships suggest that local reaction control played

the dominant role in granulite-facies metamorphism in the Buffels River area. The extent of fluid infiltration can be investigated by assessing the variation in oxygen isotope values across a small area of interbanded gneisses. $\delta^{18}O$ values for minerals vary on a cm-scale, which suggests that different rocks were infiltrated by fluids of different isotopic compositions to varying extents, or more likely, that the rocks have retained their isotopic integrity through the granulilte-facies event. Quartz veins associated with veins of coarse-grained charnockitic gneiss have $\delta^{18}O$ values between 6.1 and 6.6 ‰ which are consistent with deposition from a water-rich fluid derived from the host gneisses at temperatures above 700°C. $\delta^{18}O$ values for quartz from all lithologies range between 7.7 to 10.2 ‰, the highest values are recorded in peltic gneisses and quartzites. These values are low compared to most granulite-facies terranes and may indicate derivation from ^{18}O depleted protoliths.

9. All rocks observed in the Hytkoras area contain coarse-grained discordant veins and segregations that consist of feldspar and quartz together with anhydrous phases such as garnet, cordierite, orthopyroxene and clinopyroxene. The veins and patches normally have an anhydrous halo of finer grained matrix minerals around them, and are hosted by gneisses of similar bulk composition which contain biotite or hornblende. The segregations are best interpreted as the solid and liquid products of vapour-absent partial melting reactions. Mass balance calculations suggest that H_2O and K_2O are the only major components that are lost during vapour-absent melting of hydrous silicates. Except in some pelitic compositions, there appears to be insufficient liquid generated to escape from the parent gneiss. Water must be lost on crystallisation of the liquid, either channelled into preferential zones and reacting to produce a late-metamorphic generation of hydrous minerals, or diffusing out of the segregation to rehydrate the rock matrix.

10. In most gneisses the matrix minerals (including quartz) are devoid of fluid inclusions. In contrast, quartz in veins and segregations shows numerous inclusion trails. Most inclusions are secondary in nature, others are more difficult to categorise and may represent samples of grain boundary fluid associated with granulite-facies conditions. CO_2-rich, H_2O-rich and N_2-rich inclusions are found in the early generation inclusion types. There is considerable variation in fluid types and fluid densities within individual samples and between samples. There is no obvious sign of a pervasive

fluid event accompanying granulite-facies metamorphism. Fluid compositions and densities were probably modified by leakage during cooling and decompression.

11. The evidence above from mineral textures, variation in fluid composition calculated from dehydration equilibria, abundant field evidence for local-scale partial melting, cm-scale variation in oxygen isotope compositions and fluid inclusion observations all point to granulite-facies metamorphism in a relatively closed system. There is evidence for cm-scale interactions between adjacent rock-types and their evolving fluids but no evidence of an outside fluid agent acting as a mechanism for generating granulite-facies assemblages.

12. The retrograde history of the Buffels River area can be determined from mineral textures and from the composition and zonation profiles of minerals pairs involved in retrograde reequilibration. Cation and oxygen isotope thermometry suffers from diffusional exchange during cooling between mineral pairs, and in the case of oxygen isotopes, between minerals and grain boundary fluid. By applying experimentally derived diffusion coefficents to Fe-Mg exhange between garnet and biotite and to the oxygen isotopic fractionation amongst mineral pairs rough qualitative modelling of cooling rates can be made. Diffusion models indicate that cooling was moderate to slow with a maximum value of 20°C/My.

13. There is an absence of mineral textures associated with a rapid isothermal uplift path. In particular, the absence of decompression haloes of cordierite around garnet favours an initial isobaric cooling path. The many generations of secondary fluid inclusions are best explained by successive periods of entrapment, leakage and reentrapment along an anticlockwise retrograde P-T-t path.

14. The anticlockwise trajectory of the uplift path together with the moderate to slow cooling rate experienced can be used to model the tectonothermal evolution of the terrane. Models that predict low pressure granulite-facies metamorphism involve either magmatic accretion and/or extensional tectonic regimes. If magmatic underplating was the sole source of the thermal anomaly the uplift path would have a clockwise trajectory due to the isostatic response to lithospheric thickening. The time span for high grade conditions in Namaqualand is three times greater than that predicted for

magmatic accretion models. The structural style in Namaqualand suggests compressional stress, with emplacement of granitoid magmas along thrust zones during high grade metamorphism. This is not consistent with a thermal anomaly due to extension of the continental lithosphere. The preferred model for central Namaqualand involves continental thickening with convective lithospheric thinning (Loosveld & Etheridge, 1990). This model provides a large and long-lived heat source as the convecting asthenosphere acts in the same fashion as an infinitely thick underplate. Crustal thickening can be accompanied by heating which outlasts the tectonic episode of crustal thickening. The duration of granulite facies metamorphism is thus governed by the duration of mantle convection. The magmatic activity associated with low pressure-facies series metamorphism is a natural consequence of the model.

REFERENCES

ABBOTT, R.N. & CLARKE, D.B. (1979) Hypothetical liquidus relationships in the subsystem Al_2O_3-FeO-MgO projected from quartz, alkali feldspar and plagioclase for $a(H_2O) \leq 1$. Can. Miner. 17, 549-560.

ALBAT, H.M. (1984) The Proterozoic granulite facies terrane around Kliprand. Namaqualand Metamorphic Complex. Chamber of Mines Precambrian Research Unit. University of Cape Town Bulletin., 33, 382p.

ALLEN, P., CONDIE, K.C. & NARAYANA, B.L. (1985) The geochemistry of prograde and retrograde charnockite-gneiss reactions in southern India. Geochim. Cosmochim. Acta, 49, 323-336.

ANDERSEN, T. (1986) Compositional variation of some rare earth minerals from the Fen Complex (Telemark, S.E. Norway): implications for the mobility of rare earths in a carbonatite system. Miner. Mag., 50, 503-509.

ANDREOLI, M.A.G. & HART, R.J. (1987) Explosive KREEP-norite from Namaqualand, South Africa, with implications for the Sudbury irruptive. Contrib. Int. Workshop on Cryptoexplosions and Catastrophes in the Geological Record, Parys, South Africa, A 1-9.

ANDREOLI, M.A.G., HART, R.J. & MOORE, J.M. (1988) The geology of the Steenkampskraal monazite mine in southern Namaqualand. Ext. Abstr. Symposium on Rare Eart Elements as a Future Resource, edited by D. Cornell, Univ. Stellenbosch, 6-7.

ANDREOLI, M.A.G., HART, R.J., MOORE, J.M., WELKE, J.H., SMITH, C., BRYNARD, H.J., ANDERSEN, N.J.B. & ASHWAL, L.D. (1990) The geology of the Vaalputs waste disposal site, with implications for granite-charnockite relationships and crustal evolution in western Namaqualand. Ext. Abstr. Geocongress '90, Geol. Soc. S. Afr., Cape Town. 16-19.

ANOVITZ, L.M. & CHASE, C.G. (1990) Implications of post-thrusting extension and underplating for P-T-t paths in granulite facies terranes: a Grenville example. Geology, 18, 466-469.

ARANOVICH, L.Ya. & PODLESSKII, K.K. (1983) The cordierite-garnet-sillimanite-quartz equilibrium : Experiments and applications. In Kinetics and Equilibrium in Mineral Reactions, edited by S.K. Saxena, pp 173-198, Springer-Verlag, New York.

ARMSTRONG, R.A., REID, D.L., WATKEYS, M.K., WELKE, H.J., LIPSON, R.D., COMPSTON, W. (1988) Zircon U-Pb ages from the Aggeneys area, central Bushmanland. Ext. Abstr., Geocongress 1988, Geol. Soc. S.A., Durban. 493-499.

ARZI, A.A. (1978) Critical phenomena in the rheology of partially melted rocks. Tectonophysics, 44, 173-184.

ASHWORTH, J.R. (1985) Introduction, in Migmatites, edited by J.R. Ashworth, pp 1-31, Blackie, Glasgow.

ASHWORTH, J.R. & MCLELLAN, E.L. (1985) Textures, in Migmatites, edited by J.R. Ashworth, pp 180-203, Blackie, Glasgow.

BAARS, F.J. (1986) Granulite facies production of orthopyroxene in a band of ortho- and paragneisses near Platbakkies, Namaqualand. Unpubl. Hons. Thesis, University of Cape Town.

BARBEY, P., BERTRAND, J-M., ANGOUA, S. & DAUTEL, D. (1989) Petrology and U/Pb geochronology of the Telohot migmatites, Aleksod, Central Hoggar, Algeria. Contrib. Mineral. Petrol., 101, 207-219.

BARD, J.P. (1970) Composition of hornblende formed during the Hercynian progressive metamorphism of the Aracena metamorphic belt (SW Spain). Contrib. Mineral. Petrol., 28, 117-134.

BARTON, E.S. (1983) Reconnaissance isotopic investigations in the Namaqua mobile belt and implcations for Proterozoic crustal evolution - Namaqualand geotraverse. In Namaqualand Metamorphic Complex, 173-192, edited B.J.V. Botha, Geol. Soc. S. Afr. Spec. Publ., 10, pp 198.

BARTON, E.S. & BURGER, A.J. (1983) Reconnaissance isotopic investigations in the Namaqua mobile belt and implications for Proterozoic crustal evolution - Upington geotraverse. 173-191. In Namaqualand Metamorphic Complex edited by B.J.V. Botha, Spec. Publ. Geol. Soc. S. Afr., 10. pp. 198.

BENCE, A.E. & ALBEE, A.L. (1968) Empirical correction factors for the electron microanalysis of silicates and oxides. Jour. Geology., 76, 382-394.

BHATTACHARYA, A. & SEN, S.K. (1986) Granulite metamorphism, fluid buffering, and dehydration melting in the Madras charnockites and metapelites. J. Petrol. 27, 1119-1141.

BHATTACHARYA, A., MAZUMDAR, A.L. & SEN, S.K. (1988) Fe-Mg mixing in cordierite: Constraints from natural data and inplications for cordierite-garnet geothermometry in granulites. Amer. Mineral., 73, 338-344.

BINNS, R.A. (1965) The mineralogy of metamorphosed basic rocks from the Willyama complex, Broken Hill district, New South Wales. Parts 1 and 2. Min. Mag., 35, 306-326 and 561-587.

BLACK, P.M. (1970) A note on the occurrence of allanite in hornfelses at Paritu, Coromandel County. N.Z. Jour. Geol. Geophys., 13, 343-345.

BLIGNAUT, H.J. (1977) Structural-metamorphic imprint on part of the Namaqua Mobile Belt in South West Africa. Bull. Precambr. Res. Unit, Univ. Cape Town, 23, 197p.

BLIGNAUT, H.J., MARAIS, J.A.H., VAN DER MERWE, S.W., VAN ASWEGEN, G. & MULLER, J.A. (1980) The Namaqualand Geotraverse. Annex to Spec. Publ. Geol. Soc. S. Afr., 10.

BLIGNAUT, H.J., VAN ASWEGEN, G., VAN DER MERWE, S.W. & COLLISTON, W.P. (1983) The Namaqualand geotraverse and environs: part of the Proterozoic Namaqua mobile belt. 1-29. In Namaqualand Metamorphic Complex edited by B.J.V. Botha, pp 198. Spec. Publ. Geol. Soc. S. Afr. 10.

BOHLEN, S.R. (1987) Pressure-temperature-time paths and a tectonic model for the evolution of granulites. Jour. Geology., 95, 617-632.

BOHLEN, S.R. & ESSENE, E.J. (1977) Feldspar and oxide thermometry of granulites in the Adirondacks Highlands. Contrib. Mineral. Petrol. 62, 153-169.

BOHLEN, S.R. & ESSENE, E.J. (1979) A critical evaluation of two-pyroxene thermometry in Adirondack granulites. Lithos, 12, 335-345.

BOHLEN, S.R., PEACOR, D.R. & ESSENE, E.J. (1980) Crystal chemistry of a metamorphic biotite and its significance in water barometry. Amer. Miner. 65, 55-62.

BOHLEN, S.R., WALL, V.J. & BOETTCHER, A.L. (1983a) Geobarometry in granulites, in Kinetics and Equilibrium in Mineral Reactions, edited by S.K. Saxena, pp 141-172, Springer-Verlag, New York.

BOHLEN, S.R., BOETTCHER, A.L., WALL, V.J. & CLEMENS, J.D. (1983b) Stability of phlogopite-quartz and sanidine-quartz: a model for melting in the lower crust. Contrib. Miner. Petrol. 83, 270-277.

BOHLEN, S.R., VALLEY, J.W. & ESSENE, E.J. (1985) Metamorphism in the Adirondacks. I. Petrology, pressure, and temperature. J. Petrol., 26, 971-992.

BOTTINGA, Y. & JAVOY, M. (1975) Oxygen isotope partitioning among the minerals in igneous and metamorphic rocks, Rev of Geophysics and Space Geophysics, 13, 401-408.

BOWERS, T.S. & HELGESON, H.C. (1983) Calculation of the thermodynamic and geochemical consequences of non-ideal mixing in the system H_2O-CO_2-NaCl on phase relations in the geological systems: Metamorphic equilibria at high pressures and temperatures. Amer. Miner., 68, 1059-1075.

BOYD, F.R. & SCHAIRER, J.F. (1964) The system $MgSiO_3$ - $CaMgSi_2O_6$. J. Petrol., 5, 275-309.

BUDDINGTON, A.F. & LINDSLEY, D.H. (1964) Iron-titanium oxide minerals and synthetic equivalents. J. Petrol. 5, 310-357.

BUDDINGTON, A.F., FAHEY, J. & VLISIDIS, A. (1963) Degree of oxidation of Adirondack iron-titanium minerals in relation to petrogeny. J. Petrol., 4, 138-146.

BURNHAM, C.W. (1979) Magmas and hydrothermal fluids. In Geochemistry of hydrothermal ore deposits, edited by H.L. Barnes, 2nd edition, Wiley, New York, 71-136.

BURNHAM, C.W., HOLLOWAY, J.R. & DAVIS, N.F. (1969) Thermodynamic properties of water to 1000°C and 10,000 bars. Geol. Soc. Am. Spec. Pap. 132.

BURRUSS, R.L. (1981) Analysis of fluid inclusions: phase equilibria at constant volume. Amer. J. Sci., 281, 1104-1126.

BURRUSS, R.L. (1981) Analysis of phase equilibria in COHS fluid inclusions. In Short Course in Fluid Inclusions: Applications to Petrology, edited by L.S. Hollister & M.L. Crawford. Min. Assoc. Canada, 6, 39-74..

CLEMENS, J.D. & VIELZEUF, D. (1987) Constaints on melting and magma production in the crust. Earth Planet. Sci. Lett. 86, 287-306.

CLEMENS, J.D. & WALL, V.J. (1981) Origin and crystallization of some peraluminous (S-type) granitic magmas. Can. Miner. 19, 111-131.

CLIFFORD, T.W., GRONOW, J., REX, D.C. & BURGER, A.J. (1975a) Geochronological and petrogenetic studies of high grade metamorphic rocks and intrusives in Namaqualand, South Africa. J. Petrol., 16, 154-188.

CLIFFORD, T.W., STUMPFL, E.F. & MCIVER, J.R. (1975b) A sapphirine-cordierite-bronzite-phlogopite paragenesis from Namaqualand, South Africa. Miner. Mag., 40, 347-356.

CLIFFORD, T.W., STUMPFL, E.F., BURGER, A.J., MCCARTHY, T.S. & REX, D.C. (1981) Mineral-chemical and isotopic studies of Namaqualand granulites, South Africa: a Grenville analogue. Contrib. Miner. Petrol., 77, 225-250.

CLIFFORD, T.N., BARTON, E.S., EDWARD, A., RETIEF, E.A. & REX, D.C. (1990) New isotope data from the Koperberg Suite and some associated rocks, Okiep district, Namaqualand, South Africa. Ext. Abstr. Geocongress '90, Geol. Soc. S. Afr., Cape Town. 96-99.

COLE, D.R., OHMOTO,H. & LASAGA, A.C. (1983) Isotopic exchange in mineral fluid systems, I. Theoretical evaluation of oxygen isotopic exchange accompanying surface reactions and diffusion. Geochim. Cosmochim. Acta, 47, 1681-1693.

COLE, D.R., & OHMOTO, H. (1986) Kinetics of isotopic exchange at elevated temperatures and pressures, in Reviews in Mineralogy, Vol. 16, edited by J.W. Valley, H.P. Taylor, & J.R. O'Neil, 41-90. Miner. Soc. of Amer., Washington, D.C.

COLLISTON, W.P., PRAEKELT, H.E., STRYDOM, D., VAN ASWEGEN, G., BLIGNAUT, H.J. & SCHOCH, A.E. (1984) The recognition of low angle thrusts in Central Bushmanland, Namaqua Mobile Belt. Ext. Abstr. Geocongress '84, Geol. Soc. S. Afr., Univ. Potchefstroom, 29-32.

COLLISTON, W.P. & PRAEKELT, H.E. (1988) The recognition of overthrust terranes in the Namaqua Mobile Belt. Ext. Absr. Geocongress '88, Geol. Soc. S. Afr. Durban, 113-116.

COLLISTON, W.P., PRAEKELT, H.E. & SCHOCH, A.E. (1989) A broad perspective (Haramoep) of geological relations established by sequence mapping in the Proterozoic Aggeneys terrane, Bushmanland, South Africa. S. Afr. J. Geol., 92, 42-48.

COLLISTON, W.P., PRAEKELT, H.E. & SCHOCH, A.E. (1991) A progressive ductile shear model for the Proterozoic Aggeneys Terrane, Namaqua mobile belt, South Africa. Precambr. Res., 49, 205-215.

CONDIE, K.C., ALLEN P., NARAYANA, B.L. (1982) Geochemistry of the Archean low- to high-grade transition zone, Southern India. Contrib. Miner. Petrol., 81, 157-167.

CONRADIE, J.A. & SCHOCH, A.E. (1986a) Iron-titanium oxide equilibria in copper-bearing diorites, Namaqualand. Trans. Geol. Soc. S. Afr., 89, 29-34.

CONRADIE, J.A. & SCHOCH, A.E. (1986b) Petrographical characteristics of the Koperberg Suite, South Africa: An analogy to massif-type anorthosites? Precambr. Res., 31, 157-188.

CORBETT, G.J. & PHILLIPS G.N. (1981) Regional retrograde metamorphism of a high grade terrain: the Willyama Complex, Broken Hill, Australia. Lithos, 14, 59-73.

CRANK, J. (1975) The Mathematics of Diffusion (2nd Ed.) Oxford, Clarendon Press, 414p.

CRAWFORD, M.L. & HOLLISTER, L.S. (1986) Metamorphic fluids: The evidence from fluid inclusions. In Fluid Interactions during Metamorphism, pp 1-35, edited by J.V. Walther & B.J. Wood, Springer Verlag, New York.

CRAWFORD, M.L., KRAUS, D.W. & HOLLISTER, L.S. (1979) Petrologic and fluid inclusion study of calc-silicate rocks, Prince Rupert, British Columbia. Amer. J. Sci., 279, 1135-1159.

CURRIE, K.L. (1971) The reaction 3 cordierite = 2 garnet + 4 sillimanite + 5 quartz as a geologic thermometer in the Opinicon Lake Region, Ontario, Contrib. Mineral. Petrol., 33, 215-226.

CYGAN, R.T. & LASAGA, A.C. (1985) Self diffusion of magnesium in garnet at 750°C to 950°C, Am. Jour. Sci., 285, 328-350.

DAVIS, B.T.C. & BOYD, F.R. (1966) The join $Mg_2Si_2O_6$ - $CaMgSi_2O_6$ at 30 kilobars pressure and its application to pyroxenes from kimberlites. J. Geophys. Res., 71, 3567-3576.

DE BEER, J.H. & MEYER, R. (1983) Geoelectrical and gravitational characteristics of the Namaqua-Natal mobile belt and its boundaries. Geol. Soc. S. Afr. Spec. Publ., 10, 91-100.

DEWEY, J.F. (1988) Extensional collapse of orogens. Tectonics, 7, 1123-1139.

DODSON, M.H. (1973) Closure temperature in cooling geochronological and petrological systems, Contrib. Mineral. Petrol., 40, 259-274.

DRAKE, M.J. & WEILL, D.F. (1972) New rare earth element standards for electron microprobe analysis. Chem. Geol., 10, 179-181.

DROOP, G (1987) A general equation for estimating Fe^{3+} concentrations in ferromagnesian silicates and oxides from microprobe analyses using stoichiometric criteria. Miner. Mag., 51, 431-435.

DRURY, S.A., HARRIS, N.B.W., HOLT, R.W., REEVES-SMITH, G.J. & WIGHTMAN R.T. (1984) Precambrian tectonics and crustal evolution in South India. Jour. Geology, 92, 3-20.

DUCKWORTH, S. & FREER, R. (1981) Cation diffusion studies in garnet-garnet and garnet-pyroxene couples at high temperatures and pressures, Fifth Progress Report of Research Supported by Natural Environment Research Council (1978-1980), 18, 36-39.

DUIT, W., JANSEN, J.B.H., VAN BREEMEN, A. & BOS, A. (1986) Ammonium micas in metamorphic rocks as exemplified by Dome L'Agout (France). Amer. J. Sci., 286, 702-732.

DYMEK, R.F. (1983) Titanium, Aluminium and interlayer cations substitutions in biotite from high grade gneisses, West Greenland. Amer. Mineral., 68, 880-899.

EGLINTON, B.M., HARMER, R.E. & KERR, A. (1989) Rb-Sr isotopic constraints on the ages of the Mgeni and Nqwadolo, Valley of a Thousand Hills, Natal. S. Afr. J. Geol., 92, 393-399.

ELLIS, D.J. (1987) Origin and evolution of granulites in normal and thickened crusts, Geology, 15, 167-170.

ELLIS, D.J., SHERATON, J.W., ENGLAND, R.N., DALLWITZ, W.B. (1980) Osumilite-sapphirine-quartz granulites from Enderby Land, Antarctica - mineral assemblages and reactions. Contrib. Mineral. Petrol., 72, 353-367.

ENGEL, A.E.J. & ENGEL, C.G. (1962) Hornblendes formed during progressive metamorphism of amphibolites, NW Adirondack Mountains, New York. Bull. Geol. Soc. Am., 73, 1499-1514.

ENGLAND, P.C. & THOMPSON, A.B. (1984) Pressure-temperature-time paths of regional metamorphism I. Heat transfer during the evolution of regions of thickened continental crust. J. Petrol., 24, 894-928.

ELPHICK, S.C., GANGULY, J. & LOOMIS, T.P. (1981) Experimental study of Fe-Mg interdiffusion in aluminosilicate garnet. Abstr. Am. Geophys. Union Trans., 62, 411.

ELPHICK, S.C., GANGULY, J. & LOOMIS, T.P. (1982) Experimental study of Fe-Mn interdiffusion in aluminosilicate garnet. Abstr. Geol. Soc. Am. 14, 483.

ELPHICK, S.C., GANGULY, J. & LOOMIS, T.P. (1985) Experimental determination of cation diffusivities in aluminosilicate garnets. I. Experimental methods and interdiffusion data. Contrib. Mineral. Petrol., 90, 36-44.

ERMAKOV, N.P. (1965) Research on the nature of mineral-forming solutions with special reference to data from fluid inclusions. Int. Ser. Monogr. Earth Sci., 22, Pergamon Press, Oxford.

ERNST, W.G. (1981) Petrogenesis of eclogites and peridotites from the Western and Ligurian Alps. Amer. Mineral., 66, 443-472.

ESKOLA, P. (1939) Die metamorphen Gesteine. In Die Entstehung der Gesteine, edited by T.J.W. Barth, C.W. Correns and P. Eskola, 263-407. Julius Springer, Berlin. Reprinted 1960 and 1970.

ESSENE, E.J. (1982) Geologic thermometry and barometry, in Reviews in Mineralogy, Vol. 10, edited by J.B.Ferry, 153-206. Miner. Soc. of Amer., Washington, D.C.

ETHERIDGE, M.A. (1983) Differential stress magnitudes during regional deformation and metamorphism. Upper bound imposed by tensile fracturing. Geology, 11, 231-234.

ETHERIDGE, M.A., RUTLAND, R.W.R. & WYBORN, L.A.I. (1987) Orogenesis and tectonic process in the early to middle Proterozoic of northern Australia. In Proterozoic Lithospheric Evolution, edited by A. Kröner, Am. Geophys. Union, Geodynamics Series, 17, 131-147.

EVANS, J.A. (1988) Gahnite and its formation in the context of regional metamorphism and mineralization in the Namaqualand Metamorphic Complex. Unpubl. M. Sc. thesis, University of Cape Town

EXLEY, R.A. (1980) Microprobe studies of REE-rich accessory minerals: Implications for Skye Granite petrogenesis and REE mobility in hydrothermal systems. Earth Planet. Sci. Lett., 48, 97-110.

FERRY, J.M. (1986) Reaction progress: a monitor of fluid-rock interaction during metamorphism. In Fluid-Rock Interactions during Metamorphism, edited by J.V. Walther & B.J. Wood, Springer-Verlag, New York, 60-88.

FERRY, J.B. & SPEAR, F.S. (1978) Experimental calibration of the partitioning Fe and Mg between biotite and garnet, Contrib. Mineral. Petrol. 66, 113-117.

FONAREV, V.I. & GRAPHICHIKOV, A.A. (1982) Experimental study of Fe-Mg and Ca distribution between coexisting ortho- and clinopyroxenes at P = 294 MPa, T = 750 and 800 C. Contrib. Mineral. Petrol., 79, 311-318.

FOURCADE, S. & JAVOY, M. (1973) Rapports $^{18}O/^{16}O$ dans les roches du vieux socle catazonal d'In Ouzzal (Sahar algérien), Contrib. Mineral. Petrol., 42, 235-244.

FREER, R. (1981) Diffusion in silicate minerals and glasses: a data digest and guide to the literature. Contr. Mineral. Petrol., 76, 440-454.

FREER, R. & DENNIS, P.F. (1982) Oxygen diffusion studies: I. A preliminary ion microprobe investigation of oxygen isotope in some rock-forming minerals, Mineral. Mag., 45, 179-192.

FRIEDMAN, I. & O'NEIL, J.R. (1977) Compilation of stable isotope fractionation factors of geochemical interest. In Data of Geochemistry, edited by M. Fleischer, U.S. Geol. Survey Prof. Paper 440-K, 108p.

FRIEND, C.R.L. (1983) The link between charnockite formation and granite production: evidence from Kabbaldurga, Karnataka, southern India. In Migmatites, Melting and Metamorphism, edited by M.P. Atherton and C.D. Gribble, 264-276, Shiva, Nantwich.

FRIEND, C.R.L. (1985) Evidence for fluid pathways through Archean crust and the generation of the Closepet Granite, Karnataka, South India. Precambr. Res. 27, 239-250.

FROESE, E. (1988) Metamorphic P-T conditions of the Kerala (South India) khondalite belt. A granulite-facies supracrustal terrain: A discussion. Jour. Geology, 96, 383-384.

FROST, B.R. & CHACKO, (1989) The granulite uncertainty principle: limitations on thermobarometry in granulites. Jour. Geology, 97, 435-450.

FROST, B.R. & FROST, C.D. (1987) CO_2, melts, and granulite metamorphism. Nature., 327, 503-506.

FYFE, W.S. (1973) The granulite facies, partial melting and the Archaean crust. Phil. Trans. Royal Soc. London., A273, 457-462.

GANGULY, J. & SAXENA, S.K. (1984) Mixing properties of aluminosilicate garnets: constaints from nature and experimental data, and applications to geothermobarometry. Amer. Mineral., 69, 88-97.

GARDE, A.A. (1990) Thermal granulite facies metamorphism with diffuse retrogression in Archaean orthogneisses, Fiskefjord, southern West Greenland. J. Metamorphic Geol., 8, 663-683.

GAUDEMER, Y., JAUPERT, C. & TAPPONNIER, P. (1988) Thermal control on post-orogenic extension in collision belts. Earth Planet. Sci. Lett., 89, 48-62.

GHENT, E.A. (1976) Plagioclase-garnet-Al_2SiO_5-quartz : A potential geothermometer-geobarometry, Amer. Mineral. 64, 710-714.

GHENT, E.A., ROBBINS, D.B. & STOUT, M.Z. (1979) Geothermometry, geobarometry and fluid compositions of metamorphosed calc-silicates and pelites, Mica Creek, British Columbia. Amer. Mineral., 64, 874-885.

GERINGER, G.J., (1979) The origin and tectonic setting of amphibolites in part of the Namaqua Metamorphic Belt, South Africa. Trans. Geol. Soc. S. Afr., 82, 287-303.

GILETTI, B.J. (1986) Diffusion effects on oxygen isotope temperatures of slowly cooled igneous and metamorphic rocks, Earth Planet. Sci. Lett., 77, 218-228.

GILETTI, B.J. & ANDERSON, T.F. (1977) Studies in diffusion: II. Oxygen in phlogopite mica, Earth Planet. Sci. Lett., 28, 225-233.

GILETTI, B.J. & HESS, K.C. (1988) Oxygen diffusion in magnetite, Earth Planet. Sci. Lett., 89, 115-122.

GILETTI, B.J. & YUND, R.A. (1984) Oxygen diffusion in quartz, Jour. Geophys. Res., 89, 4039-4046.

GILETTI, B.J., SEMET, M.P. & YUND, R.A. (1978) Studies in diffusion III Oxygen in feldspars: An ion microprobe determination. Geochim. Cosmochim. Acta., 42, 45-47.

GLASSLEY, W.E. (1983) The role of CO_2 in the chemical modification of deep continental crust. Geochim. Cosmochim. Acta. 47, 597-616.

GLASSLEY, W.E. & SORENSEN, K. (1980) Constant P_S-T amphibolite to granulite facies transition in Agto (West Greenland) metadolerites: implications and applications, J. Petrol., 21, 69-105.

GRANT, J.A. (1973) Phase equilibria in high grade metamorphism and partial melting of pelitic rocks. Amer. J. Sci. 273, 289-317.

GRANT, J.A. (1985) Phase equilibria in partial melting of pelitic rocks. In Migmatites, edited by J.R. Ashworth, pp 86-144, Blackie, Glasgow.

GRANT, J.A. (1986) The Isocon diagram - a simple solution to Gresens equation for metasomatic alteration. Econ. Geol., 81, 1976-1983.

GRANT, J.A. (1986) Quartz-phlogopite-liquid equilibria and origins of charnockites. Amer. Mineral. 71, 1071-1075.

GRANTHAM, G.H. (1988) Mineralogical and geochemical variations associated with charnockitisation in the Nicholson's Point Granite, South Coast Natal. Ext. Abstr. Geocongress '88, Geol. Soc. S. Afr., Durban, 199-202.

GREEN, D.H. & RINGWOOD, A.E. (1967) An experimental investigation of the gabbro to eclogite transformation and its petrological applications. Geochim. Cosmochim. Acta, 31, 767-833.

GREEN, R.W. & DURRHEIM, R.J. (1988) The seismic structure of the Namaqualand Metamorphic Complex. Ext. Abstr. Geocongress '88 Geol. Soc. S. Afr., Durban, 171-174.

GREENWOOD, H.J. (1975) The buffering of pore fluids by metamorphic reactions. Amer. J. Sci.,275, 573-593.

GREGORY, R.T. (1986) Oxygen isotope systematics of quartz-magnetite pairs from Precambrian Iron formations: evidence for fluid rock interaction during diagenesis and metamorphism. In Fluid Rock Interactions During Metamorphism, edited by J.V. Walther & B.J. Wood, pp 132-153, Springer-Verlag, New York.

GREGORY, R.T. & CRISS, R.E. (1986) Isotopic exchange in open and closed systems. In Reviews in Mineralogy, Stable Isotopes in High Temperature Geologic Processes. Am. Mineral. Soc., 16, 91-128.

GREW, E.S. (1980) Sapphirine + quartz association from Archaean rocks in Enderby Land, Antarctica. Amer. Mineral., 65, 762-787.

GROENEWALD, P.B., GRANTHAM, G.H. & MOYES, A.B. (1988) Kibaran and Pan African orogeny in Droning Maud Land, Antartica, Southeastern Africa: Relations in a Gondwana context. Ext. Abstr. Geocongress '88, Geol. Soc. S. Afr., Durban. 203-206.

GRUTTER, H. (1986) The Petrography and Petrology of Polymetamorphic Cordierite-Quartz Gneisses near Geselskapbank, Northeast of Springbok. Unpubl. B.Sc.(Hons.) thesis Univ. Cape Town, Cape Town, South Africa.

GUIDOTTI C.V. (1984) Micas in metamorphic rocks. Reviews in Mineralogy, Miner. Soc. Am., 13, 357-456.

HAGGERTY, S. (1976) Opaque minerals in terrestrial igneous rocks. Reviews in Mineralogy, Min. Soc. Am., 3, H101-H176.

HALL, D.L. & BODNAR, R.J. (1990) Methane in fluid inclusions from granulites: A product of hydrogen diffusion. Geochim. Cosmochim. Acta., 54, 641-651.

HANSEN, E.C., NEWTON, R.C. & JANARDHAN, A.S. (1984) Fluid inclusions in rocks from the amphibolite-facies gneiss to charnockite progression in southern Karnataka, India: direct evidence concerning the fluids of granulite metamorphism. J. Met. Geol. 2, 249-264.

HANSEN, E.C., JANARDHAN, A.S., NEWTON, R.C., PRAME, W.K.B.N. & RAVINDRA KUMAR, G.R. (1987) Arrested charnockite formation in southern India and Sri Lanka, Contrib. Mineral. Petrol., 96, 225-244.

HARDING, R.R., MERRIMAN, R.J. & NANCARROW, P.H.A. (1982) A note on the occurrence of chevkinite, allanite and zirkelite on St Kilda, Scotland. Miner. Mag., 46, 445-448.

HARLEY, S.L. (1984) An experimental study of the partitioning of Fe and Mg between Fe and Mg between garnet and orthopyroxene. Contrib. Mineral. Petrol., 86, 359-373.

HARLEY, S.L. (1986) A sapphirine-cordierite-garnet-sillimanite granulite from Enderby Land: Implications for FMAS petrogenetic grids in the granulite facies. Contrib. Mineral. Petrol., 94, 452-460.

HARLEY, S.L. (1989) The origins of granulites: a metamorphic perspective, Geol. Mag., 126, 215-247.

HARTNADY, C.J., STOWE, C., & JOUBERT, P. (1985) Proterozoic crustal evolution in southwestern Africa, Episodes, 8, 236-244.

HARRIS, R.W. (1988) Examination of dextral transpression as a model for the development of thrusts and late folds in eastern Namaqualand. S. Afr. J. Geol., 91, 329-336.

HENSEN, B.J. & GREEN D. (1973) Experimental study of the stability of cordierite and garnet in pelitic compositions at high pressure and temperatures. III. Synthesis of experimental data and geological applications. Contrib. Mineral. Petrol., 38, 151-66

HOERNES, S & HOFFER, E. (1985) Stable isotope evidence for fluid-present and fluid-absent metamorphism in metapelites from the Damara Orogen, Namibia. Contrib. Mineral. Petrol. 90, 322-330.

HOLDAWAY, M.J. & LEE, S.M. (1977) Mg-Fe cordierite stability in high grade pelitic rocks based on experimental, theoretical and natural observations, Contrib. Mineral. Petrol. 63, 175-198.

HOLLAND, T.J.B. & POWELL, R. (1985). An internally consistent thermodynamic dataset with uncertainties and correlations. 2. Data and results. J. Metamorphic. Geol., 3, 343-370.

HOLLAND, T.J.B., & POWELL, R. (1990) An enlarged and updated internally consistent thermodynamic dataset with uncertainties and correlations: the system K_2O-Na_2O-CaO-MgO-MnO-FeO-Fe_2O_3-Al_2O_3-TiO_2-SiO_2-C-H_2-O_2. J. Metamorphic Geol., 8, 89-124.

HOLLISTER, L.S. (1979) Metamorphism and crustal displacements: New Insights. Episodes, 3-7.

HOLLISTER, L.S. (1981) Information intrinsically avalable from fluid inclusions. In Short Course in Fluid Inclusions: Applications in Petrology. Min. Assoc. Canada. 6,

HOLLISTER, L.S. (1982) Metamorphic evidence for rapid (2mm/year) uplift of a portion of the Central Gneiss Complex, Coast Mountains, British Columbia. Can. Mineral., 20, 319-332.

HOLLISTER, L.S. (1988) On the origin of CO_2 in migmatites. J. Metamorphic Geol., 6, 467-474.

HOLLISTER, L.S. & BURRUSS, R.L. (1976) Phase equilibria in fluid inclusions from the Khtada Lake metamorphic complex. Geochim. Cosmochim. Acta. 40, 163-175.

HOLLISTER, L.S. & CRAWFORD, M.L. (1981) Short Course in Fluid Inclusions: Applications in Petrology. Min. Assoc. Canada. 6.

HOLLISTER, L.S., BURRUS, R.C., HENRY, D.L. & HENDEL, E.M. (1979) Physical conditions during uplift of metamorphic terranes as recorded by fluid inclusions. Bull. Mineral., 102, 562-568.

HOUSEMAN, G., MC KENZIE, D & MOLNAR, P. (1981) Convective instability of a thickened boundary layer and its relevance for the thermal evolution of continental convergence belts. Journal of Geophysical Research, 86, 6115-6132.

HUEBNER, M., KYSER, T.K. & NISBET, E.G. (1986) Stable isotope geochemistry of high-grade metapelites from the Central Zone of the Limpopo Belt, Am. Mineral., 71, 1343-1353.

HUMPHRIS, S.E. (1984) The mobility of the rare earth elements in the Crust. In Rare Earth Geochemistry, edited by P. Henderson, pp 317-342, Elsevier, Amsterdam.

INDARES, A & MARTIGNOLE, J. (1985) Biotite-garnet geothermometry in the granulite facies: the influence of Ti- and Al in biotite. Amer. Mineral., 70, 272-278.

JACK, A.M. (1980). The geology of western Namaqualand. Bull. Precambrian Res. Unit, Univ. Cape Town, 29, 173 pp.

JACKSON, D.H., MATTEY, D.P. & HARRIS, N.B.W. (1988) Carbon isotope composition of fluid inclusions in charnockites from southern India. Nature, 333, 167-170.

JACKSON, M.P.A. (1976) High grade metamorphism and migmatization of the Namaqua Metamorphic Complex around Aus in the southern Namib Desert, South West Africa. Bull. Precambrian Res. Unit, Univ. Cape Town., 18, 299 pp.

JACKSON, M.P.A. (1979) A major charnockite-granulite province in southwestern Africa. Geology, 7, 22-26.

JACKSON, M.P.A. & ZELT, G. (1984) Proterozoic crustal reworking and superposed deformation of metabasite dykes, layered intrusions and lavas in Namaqualand, South Africa. In: Precambrian Tectonics Illustrated, edited by A. Kroner & R. Greiling. E. Schweizerbart'sche Verslagsbuchhandlung, Stuttgart, 381-400.

JACOBS, G.K. & KERRICK, D.M. (1981) APL and FORTRAN programs for a new equation of state for the H_2O, CO_2, and their mixtures at supercritical conditions. Computers Geosci., 7, 131-143.

JANARDHAN, A.S. NEWTON, R.C. & SMITH, J.V. (1979) Ancient crustal metamorphism at low pH_2O; charnockite formation at Kabbaldurga, South India. Nature, 278, 511-514.

JANARDHAN, A.S., NEWTON, R.C. & HANSEN, E.C. (1982) The transition from amphibolite facies gneiss to charnockite in southern Karnataka and northern Tamil Nadu, India, Contrib. Mineral. Petrol. 79, 130-149.

JIANG, J., CLAYTON, R.N. & NEWTON, R.C. (1988) Fluids in granulite facies metamorphism: A comparative oxygen isotope study on the South India and Adirondack high-grade terrains, Jour. Geology, 96, 517-533.

JOHANNES, W. (1983) On the origin of layered migmatites. In Migmatites, Melting and Metamorphism, edited by M.P. Atherton & C.D. Gribble, Shiva, Nantwich, 234-248.

JOHANNES, W. (1985) The significance of experimental studies for the formation of migmatites. In Migmatites, edited by J.R. Ashworth, Blackie, Glasgow.

JOUBERT, P. (1971) The regional tectonism of the gneisses of part of Namaqualand. Bull. Precambrian Res. Unit, Univ. Cape Town., 10, 220 pp.

JOUBERT, P. (1972) Geological Survey of part of Namaqualand and Bushmanland. Ann. Rep. of the Precambrian Res. Unit, Univ. Cape Town. 4-11.

JOUBERT, P. (1974) Geological survey of Namaqualand and Bushmanland. Ann. Rep. Precambrian Res. Unit., Univ. Cape Town., 10-11, 24-30.

JOUBERT, P. (1981). The Namaqualand Metamorphic Complex, In Precambrian of the Southern Hemisphere., edited by D.R. Hunter pp 671-704, Elsevier, Amsterdam.

JOUBERT, P. (1984). The tectonic subdivisions of the Richtersveld and Bushmanland subprovinces and the evolution of the western Namaqua Province. Abstr. Int. Conf. Mid-Late Proterozoic Lithosphere Evolution. Precambrian Res. Unit. Univ. Cape Town, 33-34.

JOUBERT, P. (1986) Namaqualand - a model of Proterozoic accretion? Trans. Geol. Soc. S. Afr., 89, 79-96.

JUREWICZ, S.R. & WATSON, E.B. (1985) The distribution of partial melt in a granitic system: application of liquid phase sintering theory. Geochim. Cosmochim. Acta., 49, 1104-1121.

KEPPLER, H. (1989) The influence of the fluid phase composition on the solidus temperatures in the haplogranite system $NaAlSi_3O_8$-$KAlSi_3O_8$-SiO_2-H_2O-CO_2. Contri. Mineral. Petrol., 102, 321-327.

KERR, A, MILNE, G.C., EGLINTON, B.M. & HARMER, R.E. (1988) The Proterozoic rocks of the Valley of a Thousand Hills. Ext. Abstr. Geocongress '88, Geol. Soc. S. Afr., Durban. 321-324.

KERRICK, D.M. (1976) Some effects of tectonic recrystallisation on fluid inclusions in quartz. Contrib. Miner. Petrol., 59, 195-202.

KERRICK, D.M. & JACOBS, G.K. (1981) A modified Redlich-Kwong equation for H_2O, CO_2, and H_2O-CO_2 mixtures at elevated pressures and temperatures. Amer. J. Sci. 281, 735-767.

KRETZ, R. (1982) Transfer and exchange equilibria in a portion of the pyroxene quadrilateral as deuced from natural and experimental data. Geochim. Cosmochim. Acta, 46, 411-422.

KRETZ, R. (1990) Biotite and garnet compositional variation and mineral equilibria in Grenville gneisses of the Otter Lake area, Quebec. J. Metamorphic Geol., 8, 493-506.

KREULEN, R. (1980) CO_2-rich fluid fluids during regional metamorphism on Naxos, Greece: carbon isotopes and fluid inclusions. Amer. J. Sci., 280, 745-771.

KREULEN, R. & SCHUILING, R.D. (1982) N_2-CH_4-CO_2 fluids during formation of the Dome de L'Agout, France. Geochim. Cosmochim. Acta. 46, 193-203.

KRÖNER, A. & BLIGNAUT, H.J. (1976) Towards a definition of some tectonic and igneous provinces in western South Africa and southern South-West Africa. Trans. Geol. S. Afr., 79, 232-238.

LAING, W.P., MAJORIBANKS, R.W. & RUTLAND, R.W.R. (1976) Structure of the Broken Hill mine area and its significance for the genesis of ore bodies. Econ. Geol., 73, 1112-1136.

LAIRD, J. & ALBEE, A.L. (1981) Pressure, temperature and time indicators in mafic schist: their application to reconstructing the polymetamorphic history of Vermont. Am. J. Sci., 281, 127-175.

LAMB, R.G., SMALLEY, P.G. & FIELD, D. (1986) P-T conditions for the Arendal granulites, southern Norway: implications for the roles of P, T and CO_2 in deep crustal LILE depletion, J. Metamorphic Geol., 4, 143-160.

LAMB, W.B. & VALLEY, J.M. (1984) Metamorphism of reduced granulites in low-CO_2 vapor-free environment. Nature, 312, 56-58.

LAMB, W.B., VALLEY, J.M., & BROWN, P.E. (1987) Post-meatamorphic CO_2-rich fluid inclusions in granulites, Contrib. Mineral. Petrol., 96, 485-495.

LASAGA, A.C. (1983) Geospeedometry : An extension of geothermometry, in Kinetics and Equilibrium in Mineral Reactions, edited by S.K. Saxena, pp 81-114, Springer-Verlag, New York.

LASAGA, A.C., RICHARDSON, S.M. & HOLLAND, H.D. (1979) The mathematics of cation diffusion and exchange between silicate minerals during retrogression. In Energetics of Geological Processes, edited by S.K. Saxena & S.Bhattacharji, pp 353-388, Springer-Verlag, New York.

LEAKE, B.E. (1978) Nomenclature of amphiboles. Am. Mineral., 63, 1023-1052.

LINDSLEY, D.H. (1980) Phase equilibria of Ca-Mg-Fe pyroxenes at pressure greater than 1 atm. Rev. in Mineral., Miner. Soc. Amer., 7.

LINDSLEY, D.H. (1983) Pyroxene thermometry. Am. Mineral., 68, 477-493.

LINDSLEY, D.H. & ANDERSON (1983) A two pyroxene thermometer. Proceedings of the thirteenth Lunar and Planetary Science Conference. Part 2. J. Geophys. Res. 88, Supplement A 887-906.

LINDSLEY, D.H. & DIXON, S.S.(1976) Diopside - Enstatite equilibria at 850 - 1400°C, 5-35 kb. Amer. J. Sci, 276, 1285-1301.

LIOU, J.G. (1973) Synthesis and stability relations of epidote $Ca_2Al_2FeSi_3O_{12}(OH)$. J. Petrol., 14, 381-413.

LONKER, S.W. (1981) The P-T-X relations of the cordierite-garnet-sillimanite-quartz equilibrium, Amer. J. Sci. 281, 1056-1090.

LOOMIS, T.P. (1983) Compositional zoning of crystals : A record of growth and reaction history, in Kinetics and Equilibrium in Mineral Reactions, edited by S.K. Saxena, pp. 1-60, Springer-Verlag, New York.

LOOSVELD, R. & ETHERIDGE, M.A. (1990) A model for low-pressure facies metamorphism during crustal thickening. J. Metamorphic Geol., 8, 257-267.

MARTINGNOLE, J. & SISI, J.C. (1981) Cordierite-garnet-H_2O equilibrium : A geological thermometer, barometer and water fugacity indicator, Contrib. Mineral. Petrol. 77,38-46.

MATTHEWS, A., GOLDSMITH, J.R. & CLAYTON, R.N. (1983) Oxygen isotope fractionation involving pyroxenes: the calibration of mineral-pair geothermometers. Geochim. Cosmochim. Acta, 47, 631-644.

MCIVER, J.R., MCCARTHY, T.S. & PACKHAM, B.deV. (1983) The Copper-bearing basic rocks of Namaqualand, South Africa. Miner. Deposita, 18, 135-160.

MCKENZIE, D.P. (1978) Some remarks on the development of sedimentary basins. Earth Planet. Sci. Lett., 40, 25-32.

MCKENZIE, D.P. (1985) the extraction of magma from the crust and mantle. Earth. Planet. Sci. Lett., 74, 81-91.

MCLAREN, A.H. (1988) The geology of the area east of Pofadder with emphasis on shearing associated with the Pofadder Lineament, Nortwest Cape. Bull. Precambr. Res. Unit, Univ. Cape Town, 35, 123 pp.

MCLELLAND, J., HUNT, W.M. & HANSEN, E.C. (1988) The relationship between metamorphic charnockites and marble near Speculator, central Adirondack Mountains, New York. Jour. Geology, 96, 455-467.

MEHNERT, K.R. (1968) Migmatites and the Origin of Granitic Rocks. Elsevier, Amsterdam.

MIYASHIRO, A. (1973) Metamorphism and Metamorphic Belts. Wiley and Sons, New York. 492pp.

MOORE, J.M. (1977) The geology of Namiesberg, northern Cape. Bull. Precambr. Res. Unit, Univ. Cape Town, 20, 69p.

MOORE, J.M. (1980) A study of certain paragneissses associations and their metallogenic characteristics in Namaqualand and Bushmanland. Ann. Rep. Precambrian Res. Unit, Univ. Cape Town, 17, 65-73.

MOORE, J.M. (1986) A comparative study of supracrustal rocks from the western Namaqualand Metamorphic Complex. Unpublished Ph D, Univ. Cape Town., 370p.

MOORE, J.M. & REID, A.M. (1988) Implications of sphalerite inclusions in gahnite from the Namaqualand Metamorphic Complex, South Africa. Can. Mineral., 26, 293-300.

MOORE, J.M. & MCSTAY, J.H. (1990) The formation of allanite-(Ce) in calcic granofelses, Namaqualand, South Africa. Can. Mineral., 28, 77-86.

MOORE, J.M., WATKEYS, M.K. & REID, D.L. (1990) The regional setting of the Aggeneys/Gamsberg base metal deposits, Namaqualand, South Africa. In Regional Metamorphism of Ore Deposits. edited by Spry & Bryndzia. VSP. pp 77-95.

MORIMOTO, N., FABRIES J., FERGUSEN, A.K., GINZBURG, I.V, ROSS, M., SEIFERT, F.A., ZUSSMAN, J., AOKI, K. & GOTTARDI, G. (1988) Nomenclature of pyroxenes. Amer. Miner. 73, 1123-1133.

MORRISON, J. & VALLEY, J.W. (1988) Post- granulite facies fluid infiltration in the Adirondack Mountains. Geology, 16, 513-516.

MUEHLENBACHS, K. & KUSHIRO, I. (1974) Oxygen isotope exchange and equilibration of silicates with CO_2 or O_2, Carnegie Institution of Washington Year Book, 73, 232-236.

NAUMOV, V.B., BALISTKY, V.S. & KHETCHIKOV, L.N. (1966) Correlation of temperatures of formation, homogenisation and decrepitation of gas-fluid inclusions. Doklad. Acad. Sci., USSR, Earth Sci. Sect., 171, 146-148.

NEARY, C.R. & HIGHLEY, D.E. (1984) The economic importance of rare earth elements. In Rare Earth Element Geochemistry, edited by P. Henderson, Elsevier, Amsterdam, 423-466.

NESBITT, H.W. (1980) Genesis of the New Quebec and Adirondack granulites: evidence for their production by partial melting. Contrib. Miner. Petrol., 72, 303-310.

NEWTON, R.C. (1983) Geobarometry of high-grade metamorphic rocks. Amer. J. Sci., 283-A, 1-28.

NEWTON, R.C. (1985) Temperature, pressure, and metamorphic fluid regimes in the amphibolite facies to granulite facies transition zone. In The deep Proterozioc crust in the North Atlantic Province, edited by A.C. Tobi & J.L.R. Touret, D. Riedel Publ. Co., Dordrecht. 75-104.

NEWTON, R.C. (1986) Fluids of granulite facies metamorphism. In Fluid- Rock Interaction during Metamorphism. edited by J.V. Walther & B.J. Wood, pp 36-59, Springer-Verlag, New York.

NEWTON, R.C. (1987) Petrological aspects of Precambrian granulite facies terranes bearing on their origins. In Proterozoic Lithospheric Evolution, edited by A. Kroner, Am. Geophys. U. Geodynamics Series, 17, 11-26.

NEWTON, R.C., SMITH, J.V. & WINDLEY, B.F. (1980) Carbonic metamorphism, granulites and granulites and crustal growth, Nature. 288, 45-50.

NEWTON, R.C. & HASELTON, H.T. (1981) Thermodynamics of the garnet-plagioclase-Al_2SiO_5-quartz geobarometer, in Thermodynamics of Minerals and Melts, edited by R.C. Newton, A. Navrotsky, and B.J. Wood, pp. 129-149, Springer-Verlag, New York.

NEWTON, R.C. & PERKINS, D. III. (1982) Thermodynamic calibration of geobarometers for charnockites and basic granulites based on the assemblages garnet-plagioclase-orthopyroxene (clinopyroxene)-quartz with applications to high grade metamorphism, Amer. Mineral. 67, 203-222.

NICHOLLS, J. & CRAWFORD, M.L. (1985) FORTRAN programs for the calculation of fluid properties from microthermometric data on fluid inclusions. Computers Geosci., 11, 619-645.

OLSEN, S.N. (1985) Mass balance in migmatites. In Migmatites, edited by J.R. Ashworth, pp 145-179, Blackie, Glasgow.

OLSEN, S.N. (1987) The composition and role of the fluid in migmatites a fluid inclusion study of the Front Range Rocks. Contrib. Miner. Petrol., 96, 104-120.

OLSEN, S.N. (1988) High density CO_2 inclusions in the Colorado Front Range. Contrib. Miner. Petrol., 100, 226-235.

OXBURGH, E.R. (1990) Some thermal aspects of granulite history. In Petrology and Geochemistry of Granulites, edited by D. Vieulzeuf, P. Vidal, Kluwer, Amsterdam.

PARK, A.F. & DASH, B. (1984) Charnockite and related neosome development in the Eastern Ghats, Orissa, India: petrographic evidence. Trans. Royal Soc. Edinburgh: Earth Sci., 75, 341-352.

PAXTON, S.T. (1984) Occurrence and distribution of ammonium illite in the Pennslyvanian, USA coalfields and proposed relationship to thermal maturity. Geol. Soc. Am. Abstr. Progs., 16, 620.

PERCHUK, L.L. (1977) Thermodynamic control of metamorphic processes, in: Energetics of Geological Processes, edited by Saxena, S.K. & Battachacharji, S., pp. 285-352, Springer-Verlag, New York.

PERCHUK, L.L., MISKIN, M.A., KOTELNIKOV, A.R., LAVRENT'EVA, I.V., GIRNIS, A.V., PODLESSKII, K.K. & GERASIMOV, V.Yu. (1980) Thermodynamic conditions of metamorphism of rocks of the Hauhay formation, Far East. Contrib. Physico-Chem. Petrol., 9, 134-170. (in Russian).

PERCHUK, L.L. & LAVRENT'EVA, I.V. (1983) Experimental investigation of the exchange equilibrium in the system cordierite-garnet-biotite, in Kinetics and Equilibrium in Mineral Reactions, edited by Saxena S.K., pp. 199-240, Springer-Verlag, New York.

PETERSON, J.W. & NEWTON, R.C. (1989) Reversed experiments on biotite-quartz-feldspar melting in the system KMASH: implications for crustal anatexis. Jour. Geology, 97, 465-485.

PETERSON, J.W. & NEWTON, R.C. (1989) CO_2-enhanced melting of biotite-bearing rocks at deep crustal pressure and temperature conditions. Nature, 340, 378-380.

PHILLIPS, G.N. (1980) Water activity changes across an amphibolite-granulite facies transition. Broken Hill. Australia. Contrib. Miner. Petrol., 75, 377-386.

PICHAMUTHU, C.S. (1960) Charnockite in the making. Nature, 188, 135-136.

POUCHOU, J.L. & PICHOIR, F. (1984) A new model for quantitative X-ray microanalysis: 1. Application to the analysis of homogeneous samples. Rech. Aerosp., 3, 13-54.

POWELL, R. (1978) Equilibrium Thermodynamics in Petrology., Harper Row, London, pp284.

POWELL, R. (1983a) Fluids and melting under upper amphibolite-facies conditions. J. Geol. Soc. London., 140, 629-633.

POWELL, R. (1983b) Processes in granulite in granulite-facies metamorphism, in Migmatites, Melting and Metamorphism, edited by M.P. Atherton & C.D. Gribble, pp. 127-139. Shiva, Nantwich.

POWELL, R. & HOLLAND, T.J.B. (1985) An internally consistent thermodynamic dataset with uncertainities and and correlations. I. Methods and a worked example. J. Metamorphic Geol., 3, 327-342.

POWELL, R. & HOLLAND, T.J.B. (1988) An internally consistent thermodynamic dataset with uncertainities and correlations. 3. applications to geobarometry, worked examples and a computer program. J. Metamorphic Geol., 6, 173-204.

POWERS, R.E. & BOHLEN, S.R. (1985) The role of synmetamorphic igneous rocks in the metamorphism and partial melting of metasediments, N.W. Adirondacks. Contrib. Mineral. Petrol., 90, 401-409.

PRAEKELT, H.E., COLLISTON, W.P. & SCHOCH, A.E. (1983) The stratigraphic interpretation of a highly deformed Proterozoic region in central Bushmanland, South Africa: first correlation of structurally separated metasediments of the Aggeneys Subgroup. Precambr. Res., 23, 177-185.

RAASE, P. (1974) Aluminium and titanium contents of hornblende, indicators of pressure and temperature of regional metamorphism. Contrib. Miner. Petrol., 45, 231-236.

RAASE, P., RAITH, M., ACKERMAND, D. & LAL, R.K. (1986) Progressive metamorphism of mafic rocks from greenschist to granulite facies in the Dharwar craton of South India. Jour. Geology, 94, 261-282.

RAO, A.T., RAMAN, C.V. & APPA RAO, G. (1979) Fluorian allanite from calc-granulite and pegmatite contacts at Garividi, Andhra Pradesh, India. Miner. Mag., 43, 312.

REID, D.L. (1977) Geochemistry of Precambrian igneous rocks in the lower Orange River region. Bull. Precambrian Res. Unit, Univ. Cape Town, 22, 397 pp.

REID, D.L. (1979a) Age relationships within the Mid-Proterozoic Vioolsdrif batholith, lower Orange River region. Trans. geol. Soc. S. Afr., 82, 305-311.

REID, D.L. (1979b) Total rock Rb-Sr and U-Th-Pb isotopic study of the Precambrian metavolcanic rocks in the lower Orange River region, Southern Africa. Earth Planet. Sci. Lett., 42, 368-378.

REID, D.L. (1982) Age relationships within the Vioolsdrif batholith, lower Orange River region. II. A two stage emplacement history and the extent of Kibaran overprinting. Trans. geol. Soc. S. Afr., 10, 108-110.

REID, D.L. & BARTON, E.S. (1983) Geochemical characterization of granitoids in the Namaqualand geotraverse, in Namaqualand Metamorphic Complex, edited by B.J.V. Botha. Spec. Public. geol. Soc. S. Afr., 10, pp. 67-82.

REID, D.L., WELKE, H.J., ERLANK, A.J., & MOYES, A. (1987a) The Orange River Group: a major Proterozoic calcalkaline volcanic belt in the western Namaqua Province, southern Africa. In Geochemistry and Mineralization of Proterozoic Volcanic Suites., edited by T.C. Pharoah, R.D. Beckinsale and D. Rickard, Spec. Pub. Geol. Soc., 33, 327-346.

REID, D.L., WELKE, H.J., ERLANK, A.J. & BETTON, P.J. (1987b) Composition, age and tectonic setting of amphibolites in the central Bushmanland Group, western Namaqua Province, southern Africa. Precambr. Res., 36, 99-126.

RICE, J.M. & FERRY, J.B. (1982) Buffering, infiltration, and the control of intensive variables during metamorphism, in Reviews in Mineralogy, Vol 10, edited by J.B. Ferry, pp. 263-326, Miner. Soc. Amer., Washington, D.C.

RIDLEY, J.A. & KRAMERS, J. (1990) The evolution and tectonic consequences of a tonalitic magma layer within Archaean continents. Can. J. Earth Sci.

RITTER, U. (1980) The Precambrian evolution of the eastern Richtersveld. Bull. Precambrian Unit, Univ. Cape Town 26, pp. 276.

ROBINSON, P., SPEAR, F.S., SCHUMACHER, J.C., LAIRD, J., KLEIN, C., EVANS, B.W. & DOOLAN, B.L. (1982) Phase relations of metamorphic amphiboles: natural occurrence and theory. In Amphiboles: Petrology and Experimental Phase Relations, edited by D.R. Veblen & P.H. Ribbe, Reviews in Mineralogy, 9B, pp 1-228, Miner. Soc. Amer., Washington, D.C.

ROEDDER, E. (1971) Fluid inclusion studies on the porphyry-type ore deposits at Bingham (Utah), Butte (Montana), Climax (Colorado). Econ. Geol., 66, 98-120.

ROEDDER, E. (1984) Fluid inclusions. Reviews in Mineralogy, Vol 12, pp. 1-644, Miner. Soc. Amer., Washington, D.C.

ROZENDAAL, A. (1978) The Gamsberg zinc deposit, Namaqualand. In Mineralization in metamorphic terranes, edited W.J. Verwoerd, pp 235-265, Spec. Publ. Geol. Soc. S. Afr., 4.

RUDNICK, R.L., ASHWAL L.D. & HENRY, D.J. (1984) Fluid inclusions in high-grade gneisses of the Kapuskasing structural zone, Ontario: metamorphic fluids and uplift/erosion path. Contrib. Mineral. Petrol. 87, 399-406.

RUMBLE, D. III (1976) Oxide minerals in metamorphic rocks. Rev. Mineral., 3, edited by D. Rumble III, R1-R20.

RYAN, P.J., LAWRENCE, A.L., LIPSON, A.L., MOORE, J.M., PATERSON, A., STEDMAN, D.P. & VAN ZYL, D. (1986) The Aggeneys base metal sulphide deposits, Namaqualand District. In Mineral Deposits of Southern Africa, edited by C.R. Anhaeusser and S. Maske, Geol. Soc. S. Afr., II, 1447-1474.

SAXENA, S.K. (1981) The $MgO-Al_2O_3-SiO_2$ System: Free energy of pyrope and Al_2O_3 enstatite. Geochim. Cosmochim. Acta, 45, 821-827.

SAXENA, S.K. (1983) Exsolution and Fe^{2+}-Mg order-disorder in pyroxenes. In Kinematics and Equilibrium in Mineral Reactions, edited by S.K. Saxena, Springer Verlag, New York.

SANDIFORD, M.A. (1989) Horizontal structures in granulite terrains: a record of mountain building or mountain collapse? Geology, 17, 449-452.

SANDIFORD, M.A. & POWELL, R. (1986) Deep crustal metamorphism during continental extension: modern and ancient examples. Earth. Planet. Sci. Lett. 79, 151-158.

SANTOSH, M. (1985) Fluid evolution characteristics and piezothermic array of south Indian charnockites. Geology. 13, 361-363.

SANTOSH, M. (1987) Cordierite gneisses of southern Kerala, India: petrology, fluid inclusions and implications for crustal uplift history. Contrib. Mineral. Petrol., 96, 343-356.

SCHENK, V. (1984) Petrology of felsic granulites, metapelites, metabasites, ultramafics and metacarbonates fron southern Calabria (Italy): prograde metamorphism, uplift and cooling of a former lower crust. J. Petrol., 25, 255-298.

SCHREURS, J. (1984) The amphibolite-granulite facies transition in West Uusimaa, S.W. Finland. A fluid inclusion study. J. Metamorphic Geol. 2, 327-342.

SCHREURS, J. (1985a) Prograde metamorphism of metapelites, garnet-biotite thermometry and prograde changes of biotite chemistry in high grade rocks of West Uusimaa, southwest Finland. Lithos, 18, 69-80.

SELVERSTONE, J., SPEAR, F.S., FRANZ, G. & MORTEANI, G. (1984) High pressure metamorphism in the SW Tauern Window, Austria. P-T paths from hornblende-kyanite-staurolite schists. J. Petrol., 25, 501-531.

SEN, S.K. & RAY, S. (1971) Breakdown reactions for natural hornblendes in granulite facies. Neu. Jahrb. Mineral. Abh., 114, 301-319.

SHEPHERD, T.J., RANKIN, A.H. & ALDERTON, D.H. (1985) A practical guide to fluid inclusion studies. Blackie, Glasgow, pp239.

SHIEH, Y-N, & SCHWARCZ, H.P. (1974) Oxygen isotope studies of granite and migmatite. Grenville province of Ontario, Canada, Geochim. Cosmochim. Acta., 38, 21-45.

SISSON, V.B., CRAWFORD, M.L. & THOMPSON, P.H. (1981) CO_2-brine immiscibility at high tempertures, evidence from calcareous metasedimentary rocks. Contrib. Miner. Petrol., 78, 371-378.

SPEAR, F.S. (1980) Na Si Ca Al exchange equilibria between plagioclase and amphibole. Contrib. Miner. Petrol., 72, 33-41.

SPEAR, F.S. (1981) Amphibole-Plagioclase equilibria: an epirical mode for the relation Albite + Tremolite = Edenite + 4 Quartz. Contrib. Mineral. Petrol., 77, 355-364.

SPEAR, F.S. (1981) An experimental study of hornblende stability and compositional variability in amphibolite. Amer. J. Sci., 281, 697-734.

SPEAR, F. S. & SELVERSTONE, J. (1983) Quantitative PT paths from zoned minerals, theory and tectonic applications. Contrib. Mineral. Petrol., 83, 348-357.

SPENCER, K.J & LINDSLEY, D.H. (1981) A solution model for coexisting iron-titanium oxides. Amer. Mineral. 66, 1189-1201.

STAHLE, H.J., RAITH, M., HOERNES, S., DELFS, A. (1987) Element mobility during incipient granulite formation at Kabbuldurga, Southern India. J. Petrol., 28, 803-834.

STORMER, J.C. (1975) A practical two-feldspar geothermometer. Amer. Mineral., 60, 667-674.

STODDARD, E.F. (1985) Zoned plagioclase and the breakdown of hornblende in pyroxene amphibolites. Can. Mineral., 23, 195-204.

ST-ONGE, M.R. (1984) Geothermometry and geobarometry in pelitic rocks of the north-central Wopmay Orogen (early Proterozoic) North West Territories, Canada. Geol. Soc. Amer. Bull., 95, 196-208.

STOWE, C.W. (1983) The Upington geotraverse and its implications for craton margin tectonics, in Namaqualand Metamorphic Complex, edited by B.J.V. Botha, Spec. Publ. geol. Soc. S. Afr., 10, 14-171.

STOWE, C.W. (1984) The Lower-Middle Proterozoic tectonic framework of Southern Africa. Abstr. Int. Conf. Mid-Late Proterozoic. Lithosphere Evolution. Precambrian Res. Unit, Univ. Cape Town, 30-32.

STOWE, C.W. (1986) Synthesis and interpretation of structures along the north-eastern boundary of the Namaqua Tectonic Province, South Africa. Trans. geol. Soc. S. Afr., 88, 185-198.

STRYDOM, D. (1985) n' Struktureel-Stratigrafiese Studie van die Metasedimente en Ander Metamorfiete van Noordwestelike Boesmanland. Unpubl. Ph. D. thesis, Univ. Orange Free State, Bloemfontein.

STRYDOM, D. & VISSER, J.N.J. (1986) Nappe structures in the highly deformed Proterozoic metasedimentary Aggeneys-type sequence of western Bushmanland, South Africa. Precambr. Res., 33, 171-187.

SOUTH AFRICAN COMMITTEE FOR STRATIGRAPHY (SACS) (1980) Statigraphy of South Africa. Part 1 (Comp. L.E. Kent). Lithostratigraphy of the Republic of South Africa, Soth West Africa/Namibia and the Republics of Bophuthatswana, Transkei and Venda. Handbk. geol. Surv. S. Afr., 8, 690 pp.

SWANENBERG, H.E.C. (1980) Fluid inclusions in high grade metamorphic rocks from S.W. Norway. Geologica Ultraiectina, University of Utrecht, 25, 1-147.

TAIT, R.E. & HARLEY, S.L. (1988) Local processes involved in the generation of migmatites within mafic granulites. Trans. Royal Soc. Edinburgh, Earth Sci Sect., 79, 209-222.

TANKARD, A.J., JACKSON, M.P.A., ERIKSSON, K.A., HOBDAY, D.K., HUNTER, D.R. & MINTER, W.E.L. (1982). Crustal Evolution of Southern Africa: 3.8 Billion Years of Earth History. Springer-Verlag, New York.

TAYLOR, H.P., FRECHEN, J. & DEGENS, E.T. (1967) Oxygen and carbon isotope studies of carbonatites from the Laacher See District, West Germany and the Alnö District, Sweden. Geochim. Cosmochim. Acta , 31, 407-430.

THEART, H.F.J. (1980) The geology of the Precambrian terrane in parts of western Namaqualand. Bull. Precambr. Res. Unit, Univ. Cape Town, 30, 103p.

THOMPSON, A.B. (1976) Mineral reactions in pelitic rocks : II. Calculation of some P-T-X(Fe-Mg) phase relations, Amer. J. Sci. 276, 425-454.

THOMPSON, A.B. (1982) Dehydration melting of pelitic rocks and the generation of H_2O undersaturated granitic liquids. Am. J. Sci., 276, 1567-1595.

THOMPSON, A.B. (1983) Fluid absent metamorphism, Jour. Geol. Soc. London., 140, 533-547.

THOMPSON, A.B. (1987) Some aspects of fluid motion during metamorphism. Jour. Geol. Soc. London, 144, 309-322.

THOMPSON, A.B. & ENGLAND, P.C. (1984) Pressure-temperature-time paths of regional metamorphism II. Their influence and interpretation using mineral assemblages in metamorphic rocks. J. Petrol., 25, 929-955.

THOMPSON, P.H. (1989) Moderate overthickening of thinned sialic crust and the origin of granitic magmatism and regional metamorphism in low pressure-high temperature terranes. Geology, 17, 520-523.

TOOGOOD, D.J. (1976) Structural and metamorphic evolution of a gneiss terrain in the Namaqua Belt near Onseepkans, South West Africa. Bull. Precambr. Res. Unit, Univ. Cape Town, 19, 189p.

TOURET, J. (1971) Le facies granulite en Norvege meridionale. II. Les inclusions fluides. Lithos. 4, 423-436.

TOURET, J. (1986) Fluid inclusions in rocks from the lower continental crust. In The Nature of the Lower Continental Crust, edited by, J.B. Dawson, D.A. Carswell, J.Hall and K.D. Wedepohl, Geol. Soc. London Spec. Publ. no. 24, pp. 161-172.

TOURET, J. & DIETVORST, P. (1983) Fluid inclusions in high grade anatectic metamorphites. Jour. Geol. Soc. London, 140, 635-649.

TOURET, J. & OLSEN, S.N. (1985) Fluid inclusions in migmatites. In Migmatites, edited by J.R. Ashworth, pp 265-288, Blackie, Glasgow.

TRACY, R.J. & ROBINSON, P. (1983) Acadian migmatite types in pelitic rocks of central Massachusetts. In: Migmatites, Melting and Metamorphism, edited by M.P. Atherton & C.D. Gribble, pp 250-263, Shiva, Nantwich.

TRACY, R.J., ROBINSON, P. & THOMPSON, A.B. (1976) Garnet composition and zoning in the determination of temperature and pressure of metamorphism, central Massachusetts, Amer. Mineral. 61, 762-775.

VALLEY, J.W., MCLELLAND, J., ESSENE, E.J. & LAMB, W.M. (1983) Metamorphic fluids in the deep crust: evidence from the Adirondacks, Nature, 301, 226-228.

VALLEY, J.W. & O'NEIL, J.R. (1984) Fluid heterogeneity during granulite facies metamorphism in the Adirondacks: stable isotope evidence, Contrib. Mineral. Petrol., 85, 158-173.

VAN ASWEGEN, G. (1983) The Gladkop Suite - grey and pink gneisses of Steinkopf. In Namaqualand Metamorphic Complex, edited by B.J.V. Botha, Spec. Publ. Geol. Soc. S. Afr., 10, 31-44.

VAN ASWEGEN, G. (1988) The evolution of the Proterozoic gneisses and other metamorphites in the Namaqualand Geotraverse between Springbok and Vioolsdrif. Unpubl. Ph. D., Univ. Orange Free State, Bloemfontein.

VAN ASWEGEN, G., STRYDOM, D., COLLISTON, W.P., PRAEKELT, H.E., SCHOCH, A.E., BLIGNAUT H.J., BOTHA, B.J.V. & VAN DER MERWE, S.W. (1987) The structural-stratigraphic development of part of the Namaqua Metamorphic Complex, South Africa - an example of Proterozoic major thrust tectonics. In Proterozoic Lithospheric Evolution. Edited by A. Kröner, Geodynamics Series, 17, 207-216.

VAN DEN KERKOFF, (1990) Isochoric phase diagrams in the systems CO_2-CH_4 and CO_2-N_2: Application to fluid inclusions. Geochim. Cosmochim. Acta, 54, 621-629.

VAN DER MERWE, S.W., & BOTHA, B.J.V. (1989) The Groothoek thrust belt in western Namaqualand: an example of a mid-crustal structure. S. Afr. J. Geol., 92, 155-166.

VENNEMANN, T.W. (1989) A geochemical and stable isotope study of some rocks from the Bandelierkop formation, Southern Marginal Zone of the Limpopo belt, South Africa. Unpubl. PhD thesis, Univ. Cape Town.

VENNEMANN, T.W. & SMITH, H.S. (1990) The rate and temperture of reaction of ClF_3 with silicate minerals, and their relevance to oxygen isotpe analysis. Chem. Geol (Isotope Geosc. Sect.), 86, 83-88.

VRY, J.K. & BROWN, P.E. (1986) Fluid inclusions in Archaean granulites- Pikwitonei domain, Manitoba. J. Geol. Soc. Canada, 11, 140.

WALTHER, J.V. & ORVILLE, P.M. (1982) Volatile production and transpor in regional metamorphism, Contrib. Mineral. Petrol., 79, 252-257.

WALTHER, J.V. & WOOD, B.J. eds. (1984) Fluid-Rock Interactions during Metamorphism. Advances in Physical Geochemistry 5, Springer-Verlag, New York, 218 pp.

WARD, J.H.W. (1989) Discussion on 'A broad perspective (Haramoep) of geological relations established by sequence mapping in the Proterozoic Aggeneys terrane, Bushmanland, South Africa. S. Afr. J. Geol., 92, 456-458.

WATERS, D.J. (1986a) Metamorphic zonation and thermal history of pelitic gneisses from western Namaqualand, South Africa, Trans. geol. Soc. South Africa, 89, 97-102.

WATERS, D.J. (1986b) Metamorphic history of sapphirine-bearing and related magnesian gneisses from Namaqualand, South Africa, J. Petrol., 91, 541-565.

WATERS, D.J. (1988) Partial melting and the formation of granulite facies assemblages in Namaqualand, South Africa, J. Metamorphic Geol.,6,

WATERS, D.J. (1989) Metamorphic evidence for the heating and cooling path of Namaqualand granulites. In Evolution of Metamorphic Belts, edited by Daly, J.S., Cliff, R.A. & Yardley, B.W.D., Geol. Soc. Sp. Publ.

WATERS, D.J. (1990) Thermal history and tectonic setting of the Namaqualand Granulites, Southern Africa: Clues to Proterozoic crustal development. In Granulites and Crustal Differentiation, NATO ASI-Series , edited by D. Vielzeuf & Ph. Vidal.

WATERS, D.J., JOUBERT, P. & MOORE, J.M. (1983) A suggested re-interpretation of Namaqua basement rocks south and west of Bitterfontein. Trans. Geol. Soc. S. Afr., 86, 293-299.

WATERS, D.J. & MOORE, J.M. (1985) Kornerupine in Mg-Al-rich gneisses from Namaqualand, South Africa: mineralogy and evidence for late-metamorphic fluid activity, Contrib. Miner. Petrol., 91, 97-102.

WATERS, D.J. & WHALES, C.J. (1984) Dehydration melting and the granulite transition in metapelites from southern Namaqualand, S. Africa. Contrib. Miner. Petrol, 88, 269-275.

WATKEYS, M.K. (1986) The Achab Gneiss: a "floor" in Bushmanland or a flaw in Namaqualand? Trans. geol. Soc. S. Afr., 89, 103-116.

WATKEYS, M.K. (1988) A spectrum of thrust related structures in Bushmanland. Ext. Abstr., Geocongress '88, Geol. Soc. S. Afr., Durban, 729-732.

WATKEYS, M.K.; MOORE, J.M. & DUNCAN, A.R. (1988) The pink gneiss of Bushmanland: Mid-Proterozoic felsic pyroclastics. Ext. Abstr., Geocongress, Univ. Natal, Durban, 717-720.

WEAVER, B.L. & TARNEY, J. (1983) Elemental depletion in Archaean granulite-facies rocks, in Migmatites, Melting and Metamorphism, edited by M.P. Atherton & C.D. Gribble, pp. 250-263, Shiva, Nantwich.

WEINER, R.W., MC LELLAND, J.M., ISACHSEN, Y.M. & HALL, L.M. (1983) Stratigraphy and structural geology of the Adirondack Mountains, New York: review and synthesis. Geol. Soc. Amer. Spec. Paper, 194, 1-55.

WELKE, H.J. & SMITH, C.B. (1984) Lead isotope characterization of the Aggeneys-Gamsberg ore bodies in relation to possible source rocks, with implications for Bushmanland metallogenesis. Abstr., Mid-Late Proterozoic Crustal Evolution, Precambr. Res. Unit, Univ. Cape Town, 8-9.

WELLS, P.R.A., (1977) Pyroxene thermometry in simple and complex systems. Contrib. Mineral. Petrol., 62, 129-139.

WELLS, P.R.A., (1979) Chemical and thermal evolution of Archaean sialic crust, southern West Greenland. J. Petrol., 20, 187-226.

WELLS, P.R.A, (1980) Thermal models for the magmatic accretion and subsequent metamorphism of continental crust. Earth Planet. Sci. Lett.. 46, 253-265.

WENDLANDT, R.F. (1981) Influence of CO_2 on melting of model granulite facies assemblages: a model for the genesis of charnockites, Am. Miner., 66, 1164-1174.

WENDLANDT, R.F. & HARRISON, W.J. (1979) Rare earth partitioning between immiscible carbonarte and silicate liquids and CO_2 vapour: results and implications for the formation of light rare earth enriched rocks. Contrib. Mineral. Petrol., 69, 409-419.

WHITE, A.R. & CHAPPELL, B.W. (1977) Ultrametamorphism ang granitoid genesis. Tectonophysics, 43, 7-22.

WICKHAM, S.M. (1987) The segregation and emplacement of granitic magmas. J. Geol. Soc. London, 144, 281-297.

WICKHAM, S.M. & OXBURGH, E.R. (1985) Continental rifts as a setting for regional metamorphism. Nature, 318, 330-333.

WICKHAM, S.M. & OXBURGH, E.R. (1987) Low pressure regional metamorphism in the Pyrenees and its implications for the thermal evolution of rifted continental crust. Phil Trans. R. Soc. Lond. A 321, 1557, 219-242.

WILSON, A.F. & BAKSI, A.K. (1983) Widespread ^{18}O depletion in some Precambrian granulites of Australia. Precambr. Res., 23, 33-56.

WONES, D.R. (1989) Significance of the assemblage titanite + magnetite + quartz in granitic rocks. Amer. Mineral., 74, 744-749.

WOOD, B.J. & BANNO, S. (1973) Garnet-orthopyroxene and orthopyroxene -clinopyroxene relationships in simple and complex systems, Contrib. Mineral. Petrol. 42, 109-124.

YARDLEY, B.W.D., SHEPHERD, T.J. & BARBER, J.P. (1983) Fluid inclusion studies of high-grade rocks from Connemara, Ireland. In Migmatites, Melting and Metamorphism., edited by M.P Atherton & C.D. Gribble, pp 110-126, Shiva, Nantwich.

YOUNG, ED., ANDERSON, J.L., CLARKE, H.S. & THOMAS, W.M. (1989) Petrology of biotite-cordierite-garnet gneiss of the McCullough Range, Nevada. I Evidence for Proterozoic low pressure fluid-absent granulite grade metamorphism in the Southern Cordillera. J. Petrol., 30, 39-60.

ZELT, G.A.D. (1980) Granulite-facies metamorphism in Namaqualand, South Africa. Precambrian Res., 13, 253-274.

APPENDIX

A.1 SAMPLING

Samples in this study were collected at various stages of the project. Initially samples collected by J.M. Moore (see Moore, 1986) provided a basis for initial petrography and in a few of these samples mineral chemistry was investigated by electron microprobe. Reconnaissance work covering diverse areas of metamorphic grade from the Orange River south to the Kamiesberg Mountains provided additional material. Only samples pertaining to the area between Verdruk and Hytkoras are included in this thesis. The bulk of the samples were collected during subsequent field seasons, mainly in the Buffels River area, but also in the northern parts of the study strip. Additional material was supplied from the sampling of D.J. Waters in the areas above between 1982 and 1988. A considerable number of thin sections of rocks from various other parts of Namaqualand collected by the above workers and from the collections of Albat (1984) and Joubert (1971) were examined but are not discussed here. Sample localities for important and representative samples from the Buffels River area are indicated on the maps included in Chapter 3. Table A.1 list sample localities. The farm Hytkoras has several prominent outcrops of supracrustal rocks which were investigated in this study these localities are referred to as:1. River area, comprising rock pavements of the dry river bed of the Buffels River and adjacent outcrops in the south-west part of the farm; this area includes all the rocks sampled for stable isotope studies. 2. Draaihoek, a series of supracrustal rocks a few km north of 1. 3. East Hytkoras, outcrops in the ridges to the east of the Buffels River bordering the farm Dabeep, includes samples from Snake Gully and neighbouring ridges.

TABLE A.1

Sample localities

Sample	Rock Type	Locality
DWN129	mafic gneiss	East Hytkoras
DWN288	mafic gneiss	River, Hytkoras
DWN332	mafic gneiss	East Hytkoras
DWN347	mafic gneiss	Snake Gully, East Hytkoras
DWN348	mafic gneiss	-
DWN349	mafic gneiss	-
DWN353	mafic gneiss	-
DWN354	mafic gneiss	-
DWN380	mafic gneiss	River, Hytkoras
DWN381	mafic gneiss	-
DWN613	biotite gneiss	-
DWN614	qtz-fsp paragneiss	-
DWN615	mafic gneiss	-
DWN616	magnesian gneiss	-
DWN617	semi-pelitic gneiss	-
DWN618	magnesian gneiss	-
DWN619	magnesian gneiss	-
DWN620	pelitic gneiss	-
DWN621	leucogneiss	-
DWN622	magnesian-pelitic gneiss	-
DWN623	magnesian-pelitic gneiss	-
DWN624	pelitic gneiss	-
DWN625	mafic gneiss	-
DWN626	leucogneiss	-
DWN627	garnet-biotite gneiss	-
DWN628	biotite gneiss	-
DWN629	charnockite	-
DWN630	pegmatite	-
DWN631	quartz vein	-
DWN632	quartz vein	-
HY8	mafic gneiss	Hytkoras
HY23	mafic gneiss	-
SS3	calc-silicate	Smorgen Schaduwe
SS4	calc-silicate	-
SS18	calc-silicate	-
VD3	pelitic gneiss	Verdruk
VK7	mafic gneiss	Velskoen, Tweefontein
MCSBV08	mafic gneiss	Pedroskloof, Kamiesbergs
MCSBV09	mafic gneiss	Pedroskloof, Kamiesbergs
MCSGM01	biotite gneiss	Gamoep
MCSGM02	biotite gneiss	Gamoep
MCSH01	charnockite	South Hytkoras
MCSH02	peltic gneiss	-
MCSH04	metagabbro	-
MCSH05	metagabbro	-
MCSH08	charnockite	-
MCSR01	calc-silicate	Rietfontein
MCSR02	calc-silicate	-
MCSR03	calc-silicate	-
MCSR06	biotite gneiss	-
MCSS01	pelitic gneiss	Silverfontein
MCSS04	mafic gneiss	-
MCSS05	mafic gneiss	-

MCSS08	mafic gneiss	-
MCST02	mafic gneiss	Tweefontein
MCST03	mafic gneiss	-
MCS207	mafic gneiss	Goinoep
MCS212	pelitic gneiss	Kouberg
MCS216	calc-silicate	-
MCS217	mafic gneiss	-
MCS218	calc-silicate	-
MCS220	mafic gneiss	-
MCS221	mafic gneiss	-
MCS222	calc-silicate	-
MCS223	calc-silicate	Areb
MCS224	calc-silicate	-
MCS232	calc-silicate	-
MCS233	calc-silicate	-
MCS234	calc-silicate	-
MCS235	mafic gneiss	-
MCS236	calc-silicate	-
MCS272	orthogneiss	Verdruk
MCS273	pelitic gneiss	-
MCS281	orthogneiss	-
MCS282	orthogneiss	-
MCS283	orthogneiss	-
MCS300	mafic gneiss	East Hytkoras
MCS301	mafic gneiss	-
MCS302	mafic gneiss	-
MCS303	mafic gneiss	-
MCS304	mafic gneiss	-
MCS305	mafic gneiss	-
MCS306	mafic gneiss	-
MCS310	leucogneiss	Dabeep
MCS311	charnockite	-
MCS312	mafic gneiss	-
MCS313	mafic gneiss	-
MCS314	mafic gneiss	East Hytkoras
MCS315	mafic gneiss	-
MCS316	mafic gneiss	-
MCS317	mafic gneiss	Snake Gully, East Hytkoras
MCS318	mafic gneiss	-
MCS319	calc-silicate	East Hytkoras
MCS320	mafic gneiss	River, Hytkoras
MCS321	pelitic gneiss	-
MCS322	pelitic gneiss	-
MCS324	pelitic gneiss	-
MCS327	mafic gneiss	-
MCS329	pelitic gneiss	-
MCS330	pelitic gneiss	East Hytkoras
MCS331	pelitic gneiss	-
MCS332	pelitic gneiss	-
MCS335	mafic gneiss	-
MCS338	calc-silicate	-
MCS339	calc-silicate	-
MCS340	calc-silicate	Rietfontein
MCS341	calc-silicate	-
MCS342	calc-silicate	-
MCS343	pelitic gneiss	-
MCS344	charnockite	-
MCS345	charnockite	-
MCS346	calc-silicate	-

MCS347	calc-silicate	-
MCS348	calc-silicate	-
MCS349	calc-silicate	-
MCS350	calc-silicate	-
MCS351	calc-silicate	-
MCS352	calc-silicate	-
MCS353	mafic gneiss	Draaihoek
MCS354	mafic gneiss	-
MCS355	mafic gneiss	-
MCS357	biotite gneiss	-
MCS358	mafic gneiss	River, Hytkoras
MCS359	charnockite	-
MCS360	charnockite	-
MCS361	orthogneiss	Dabeep
MCS362	mafic gneiss	-
MCS363	mafic gneiss	-
MCS365	mafic gneiss	-
MCS367	calc-silicate	East Hytkoras
MCS368	mafic gneiss	-
MCS369	mafic gneiss	-
MCS371	calc-silicate	Rietfontein
MCS373	charnockite	-
MCS374	mafic gneiss	Draaihoek
MCS375	mafic gneiss	River Hytkoras
MCS377	charnockite	-
MCS378	calc-silicate	Dabeep
MCS379	mafic gneiss	-
MCS380	mafic gneiss	-
MCS381	calc-silicate	Rietfontein
MCS383	mafic gneiss	-
MCS384	mafic gneiss	River, Hytkoras
MCS385	mafic gneiss	-
MCS386	mafic gneiss	-
MCS387	pelitic gneiss	-
MCS389	pelitic gneiss	-
MCS390	pelitic gneiss	-
MCS391	pelitic gneiss	-
MCS392	quartzite	-
MCS393	pelitic gneiss	-
MCS394	pelitic gneiss	-
MCS395	pelitic gneiss	-
MCS396	mafic gneiss	-
MCS399	pelitic gneiss	-
MCS401	mafic gneiss	-
MCS402	calc-silicate	-
MCS403	pelitic gneiss	Draaihoek
MCS404	mafic gneiss	-
MCS405	mafic gneiss	Rietfontein
MCS407	calc-silicate	-
MCS408	calc-silicate	-

A.2 ELECTRON MICROPROBE ANALYSIS

Mineral compositions were determined using a 4-channel Cameca Camebax Microbeam electron microprobe in the Department of Geochemistry, University of Cape Town. All analyses were performed on graphite coated, glass-mounted polished rock-sections. For all minerals except K-feldspar a focussed beam (1-2 microns; 40 nA) with an accelerating voltage of 15 kV was used. For K-feldspar a defocussed beam (10-20 microns, 20 nA) was used. X-ray intensities were calibrated against a matrix of natural and synthetic mineral standards. Standards used, errors and detection limits are listed in Table A.2. Counting time on peaks of all elements analysed was 10 seconds, except for F and Cl in biotite and REE in allanite and titanite, where counting times of 100 seconds were used. The raw counts were corrected for dead time and background, with resulting nominal concentration being corrected using the ZAF procedure. Data for minerals with a high Fe content, such as garnet and orthopyroxene, was corrected using the procedure of Bence & Albee (1968). In the case of Fe-rich phases (> 20% FeO) the ZAF factors lead to high totals of over 101%, with anomalies in the SiO_2 and Al_2O_3 contents.

Microprobe analyses listed in the Appendix are representative analyses of the phases in various samples. For those minerals which show internal variation, normally core and rim values are quoted. If a mineral phase shows variation in composition within a rock section more than one analysis is given. A minimum of five analyses were conducted on each phase within a rock and multiple analyses were carried out on certain individual crystals in order to assess homogeneity and analytical variation.

CLINOPYROXENE

	Standard	Weight %	LLD	2σ
SiO_2	DIOP	51.70	0.043	0.268
TiO_2	RUT	0.23	0.041	0.035
Al_2O_3	K-P	2.03	0.032	0.057
FeO	K-P	10.90	0.084	0.274
MnO	RHOD	1.45	0.066	0.109
MgO	DIOP	12.22	0.026	0.126
CaO	DIOP	20.72	0.032	0.192
Na_2O	K-H	0.56	0.029	0.040

ZAF

CORDIERITE

	Standard	Weight %	LLD	2σ
SiO_2	DIOP	48.79	0.043	0.277
Al_2O_3	K-P	32.75	0.038	0.211
FeO	K-P	7.60	0.070	0.230
MgO	DIOP	8.85	0.023	0.103
Na_2O	K-H	0.10	0.024	0.021

ZAF

GARNET

	Standard	Weight %	LLD	2σ
SiO_2	K-P	36.83	0.043	0.238
Al_2O_3	K-P	21.36	0.037	0.180
FeO	K-P	36.87	0.083	0.489
MnO	RHOD	0.38	0.066	0.067
MgO	K-P	4.44	0.026	0.080
CaO	K-P	0.15	0.031	0.027

Bence & Albee (1968)

HORNBLENDE

	Standard	Weight %	LLD	2σ
SiO_2	K-H	43.36	0.044	0.244
TiO_2	RUT	1.59	0.042	0.063
Al_2O_3	K-H	10.86	0.035	0.123
Cr_2O_3	CHRO	0.01	0.047	0.032
FeO	K-H	14.39	0.075	0.323
MnO	RHOD	0.19	0.071	0.060
MgO	K-H	13.08	0.030	0.132
CaO	K-H	12.03	0.036	0.148
Na_2O	K-H	1.19	0.030	0.054
K_2O	K-H	1.40	0.024	0.051

ZAF

K-FELDSPAR

	Standard	Weight %	LLD	2σ
SiO_2	NUNI	65.36	0.063	0.406
Al_2O_3	NUNI	18.54	0.044	0.202
FeO	K-H	0.02	0.102	0.071
CaO	LACO	0.08	0.043	0.033
BaO	BASI	0.28	0.090	0.074
Na_2O	NUNI	0.84	0.033	0.057
K_2O	OR-1	15.20	0.030	0.222

ZAF

ORTHOPYROXENE

	Standard	Weight %	LLD	2σ
SiO_2	DIOP	52.16	0.045	0.281
TiO_2	RUT	0.09	0.041	0.030
Al_2O_3	K-P	1.38	0.034	0.052
Cr_2O_3	CHRO	0.01	0.047	0.031
FeO	K-P	23.15	0.086	0.402
MnO	RHOD	0.81	0.070	0.088
MgO	DIOP	21.58	0.031	0.174
CaO	DIOP	0.55	0.027	0.036
Na_2O	K-H	0.01	0.029	0.020

Bence & Albee (1968)

OXIDES

	Standard	Weight %	LLD	2σ
SiO_2	K-P	0.02	0.042	0.029
TiO_2	RUT	49.82	0.048	0.306
Al_2O_3	CHRO	0.01	0.035	0.024
Cr_2O_3	CHRO	0.00	0.000	0.000
FeO	ILMT	45.34	0.105	0.558
MnO	RHOD	4.44	0.083	0.186
MgO	CHRO	0.18	0.033	0.029
CaO	K-P	0.03	0.033	0.023

ZAF

PLAGIOCLASE

	Standard	Weight %	LLD	2σ
SiO_2	NUNI	59.09	0.053	0.358
Al_2O_3	NUNI	25.09	0.040	0.210
FeO	K-H	0.14	0.083	0.069
CaO	LACO	8.41	0.038	0.163
Na_2O	NUNI	0.66	0.038	0.152
K_2O	OR-1	0.44	0.027	0.042

ZAF

SCAPOLITE

	Standard	Weight %	LLD	2σ
SiO_2	K-H	45.39	0.063	0.347
Al_2O_3	K-H	27.88	0.049	0.258
FeO	K-H	0.22	0.098	0.084
MnO	RHOD	0.01	0.098	0.066
MgO	K-H	0.01	0.032	0.022
CaO	K-H	18.46	0.042	0.253
Na_2O	K-H	2.95	0.036	0.104
K_2O	K-H	0.29	0.029	0.036
F	FLUR	0.00	0.000	0.000
Cl	SCAP	0.18	0.032	0.035

ZAF

TITANITE

	Standard	Weight %	LLD	2σ
SiO_2	K-H	30.57	0.036	0.175
TiO_2	RUT	34.26	0.032	0.161
Al_2O_3	K-H	2.62	0.033	0.060
FeO	K-H	2.04	0.035	0.067
MnO	RHOD	0.28	0.037	0.035
MgO	K-H	0.02	0.025	0.018
CaO	K-H	26.51	0.019	0.138
La_2O_3	REE3	0.41	0.062	0.048
Ce_2O_3	REE3	1.43	0.124	0.144
Nd_2O_3	REE3	0.59	0.142	0.122
ThO_2	THO2	0.27	0.081	0.065

Pichoir & Poupon (1984)

A.3 WHOLE ROCK MAJOR ELEMENT ANALYSIS BY X-RAY FLUORESCENCE

Only two sets of samples were selected for XRF analysis. Both samples contained a transition in mineral assemblage and were prepare for analysis by cutting the samples on a slow diamond rock-saw. All weathered material was discarded and the fresh cut sections were crushed and finally powdered using a carbon-steel swingmill that had been precontaminated with a portion of the sample. All major elements contents were determined from analysis of lithium tetraborate fusion discs according to the method of Norrish & Hutton (1969). Powders for fusion discs were dried overnight at 110°C. The recorded weight loss being attributed to loss of adsorbed water. The powders were then ashed at 1000°C overnight, with the recorded weight loss reported as loss on ignition (LOI). Sodium was analysed from pressed powder brickettes. XRF analysis was carried in the Department of Geochemistry, University of Cape Town. Operating conditions are descibed in detail by Willis et al. (1971; 1972).

TABLE A.3

X-Ray Fluorescence Analysis - Average Absolute Errors and Detection Limits (LLD; 95% confidence limits).

	Average Abs. Error	Detection Limit
SiO_2	0.27	0.011
TiO_2	0.02	0.004
Al_2O_3	0.17	0.016
Fe_2O_3	0.10	0.015
MnO	0.24	0.030
MgO	0.15	0.105
CaO	0.06	0.004
Na_2O	0.12	0.020
K_2O	0.03	0.003
P_2O_5	0.01	0.006

A.4 A NOTE ON THE USE OF THE COMPUTER PROGRAM THERMOCALC

Most thermodynamic modelling of mineral reactions in this project was carried out using the program THERMOCALC of Powell & Holland (1985, 1988 and 1990). THERMOCALC has three modes of operation: Rock mode, which calculates average pressure and temperature from the activities of coexisting mineral phases. Phase diagram mode, which gives P-T slopes of reactions for pure end-members or for activities of end-member components within a pre-set P-T window for varying fluid compositions. Customised mode, is used to create a specific dataset for modelling. THERMOCALC uses the internally consistent database of Holland & Powell (1985, 1988 and 1990) which allows the determination of the reliability of thermodynamic calculations by performing error propogation calculations.

Low variance assemblages, such as those encountered in the Buffels River are ideal for the type of metamorphic characterisation that can be attempted using THERMOCALC. All applicable reactions can be used together to calculate the physical conditions of metamorphism. In this study the program was not used to calculate average pressures and temperatures as such. As the rocks chosen proved to be isofacial and good agreement was found amongst conventional exchange geothermometers. The phase diagram and rock mode options were used to assess the PT slopes of reactions for natural compositions assumed to be in equilibrium. Reactions which were metastable or had large uncertainties in pressure or temperature were discarded. In the case of the mafic gneisses from the Buffels River the natural assemblage was not in equilibrium. Model equilibrium activities were produced from independant reactions generated by THERMOCALC and compared to well equilibrated natural examples. Using THERMOCALC to calculate P-T conditions for a single well characterised reaction it was possible to fix temperature and pressure and allow fluid composition to vary independantly. Thus for any given hornblende-bearing, two-pyroxene granulite a unique water activity could be calculated at a fixed pressure and temperature.

The program RECALC was developed by Powell (Powell & Holland, 1988) and accompanies THERMOCALC. The program calculates thermodynamic mole fractions and activities from mineral analyses. Error propogation is calculated assuming 1% relative on weight %

oxides with a 'blow-up' factor at small weight %. Activity coefficients can be combined with the calculated mole fractions and used in the THERMOCALC program.

TABLE OF MINERAL ANALYSES

MAFIC GNEISSES

ORTHOPYROXENE

	$DWN129_A$	$DWN129_B$	$DWN332_1$	$DWN332_2$	$DWN332_3$	DWN347	DWN348	DWN349	DWN353	$DWN353_S$	$DWN354_1$
SiO_2	52.19	52.39	51.09	52.07	52.10	52.07	52.26	51.58	52.38	52.19	52.08
TiO_2	0.10	0.10	0.07	0.07	0.06	0.07	0.08	0.07	0.07	0.09	0.08
Al_2O_3	1.19	1.28	2.43	1.42	1.29	1.25	1.53	1.43	1.30	1.49	1.74
Cr_2O_3	----	----	----	----	----	----	----	----	----	----	----
FeO	22.92	21.91	23.34	23.25	23.26	21.56	21.50	22.49	23.14	22.76	23.43
MnO	0.44	0.44	1.37	0.93	0.97	0.82	0.81	0.94	0.90	0.80	0.68
MgO	22.52	23.24	21.56	21.82	21.87	23.68	23.48	22.91	22.24	22.27	22.11
CaO	0.52	0.54	0.23	0.53	0.54	0.47	0.55	0.60	0.51	0.61	0.43
Na_2O	----	----	----	----	----	----	----	----	----	----	----
Total	99.88	99.90	100.09	100.09	100.09	99.92	100.21	100.02	100.54	100.21	100.55

CATION PROPORTIONS BASED ON 6 OXYGENS

Si	1.953	1.950	1.920	1.952	1.953	1.940	1.940	1.932	1.952	1.947	1.941
Ti	0.003	0.003	0.002	0.002	0.002	0.002	0.002	0.002	0.002	0.003	0.002
Al	0.052	0.056	0.107	0.063	0.057	0.055	0.067	0.063	0.057	0.066	0.076
Cr	-----	-----	-----	-----	-----	-----	-----	-----	-----	-----	-----
Fe	0.719	0.682	0.733	0.729	0.729	0.672	0.667	0.704	0.721	0.710	0.730
Mn	0.014	0.014	0.044	0.030	0.031	0.026	0.025	0.030	0.028	0.025	0.022
Mg	1.255	1.289	1.207	1.218	1.222	1.315	1.299	1.279	1.235	1.238	1.228
Ca	0.021	0.022	0.010	0.021	0.022	0.019	0.022	0.024	0.020	0.024	0.017
Na	-----	-----	-----	-----	-----	-----	-----	-----	-----	-----	-----
Sum	4.017	4.016	4.023	4.015	4.016	4.029	4.022	4.034	4.015	4.013	4.016
X_{Mg}	0.636	0.654	0.622	0.626	0.626	0.618	0.661	0.645	0.632	0.636	0.627

MAFIC GNEISSES

ORTHOPYROXENE

	DWN354$_2$	DWN380	DWN381	DWN615	DWN625	HY8	HY23	MCSH04	MCSH05	MCSS04	MCSS05
SiO_2	52.04	51.46	51.42	51.92	52.23	51.91	51.45	52.50	53.94	51.08	51.25
TiO_2	0.07	0.08	0.08	0.08	0.09	0.09	0.09	0.03	0.07	0.10	0.07
Al_2O_3	1.74	1.34	1.37	1.27	1.42	1.37	1.33	1.22	1.37	1.34	1.04
Cr_2O_3	----	----	----	----	----	----	----	----	----	----	----
FeO	23.28	23.55	23.74	24.32	23.32	22.74	23.43	18.48	16.15	25.58	25.22
MnO	0.68	1.82	0.83	1.08	0.81	0.89	0.74	0.33	0.39	0.87	0.83
MgO	22.01	21.35	22.03	20.69	21.36	22.31	22.33	26.79	27.56	20.14	20.63
CaO	0.42	0.62	0.57	0.62	0.56	0.59	0.64	0.45	0.41	0.67	0.58
Na_2O	----	0.03	----	----	----	----	----	----	----	----	----
Total	100.24	100.22	100.04	99.98	99.79	99.90	100.01	99.77	99.89	99.78	99.62

CATION PROPORTIONS BASED ON 6 OXYGENS

Si	1.944	1.940	1.935	1.959	1.962	1.946	1.934	1.927	1.952	1.945	1.951
Ti	0.002	0.002	0.002	0.002	0.002	0.003	0.003	0.001	0.002	0.003	0.002
Al	0.077	0.060	0.061	0.057	0.063	0.061	0.059	0.054	0.058	0.060	0.047
Cr	-----	-----	-----	-----	-----	-----	-----	-----	-----	-----	-----
Fe	0.727	0.742	0.747	0.767	0.732	0.713	0.737	0.567	0.489	0.815	0.803
Mn	0.022	0.058	0.026	0.035	0.026	0.028	0.024	0.010	0.012	0.027	0.027
Mg	1.225	1.199	1.235	1.163	1.196	1.246	1.251	1.465	1.486	1.143	1.170
Ca	0.017	0.025	0.023	0.025	0.023	0.024	0.026	0.018	0.016	0.027	0.024
Na	-----	-----	-----	-----	-----	-----	-----	-----	-----	-----	------
Sum	4.014	4.026	4.029	4.008	4.004	4.021	4.034	4.041	4.015	4.020	4.024
X_{Mg}	0.628	0.618	0.623	0.603	0.620	0.636	0.629	0.721	0.753	0.584	0.593

MAFIC GNEISSES

ORTHOPYROXENE

	$MCS301_A$	$MCS301_C$	MCS302	MCS303	$MCS304_M$	$MCS304_I$	MCS305	MCS317	$MCS317_S$	$MCS327_T$	$MCS327_B$
SiO_2	51.78	51.93	51.60	51.79	51.44	52.08	52.66	52.38	52.70	51.74	51.55
TiO_2	0.06	0.08	0.06	0.06	0.05	0.09	0.08	0.09	0.06	0.08	0.09
Al_2O_3	1.27	1.23	1.23	1.33	1.41	1.50	1.30	1.38	1.29	1.43	1.46
Cr_2O_3	----	----	----	----	----	----	----	----	----	----	----
FeO	23.18	22.65	23.52	23.66	23.61	24.08	22.75	22.79	21.44	24.24	24.32
MnO	1.04	1.02	1.52	0.77	0.98	0.93	1.18	1.03	0.92	0.91	0.76
MgO	22.10	22.63	21.68	22.17	22.39	20.89	22.10	22.32	23.13	21.04	21.27
CaO	0.58	0.56	0.53	0.52	0.54	0.58	0.52	0.54	0.49	0.62	0.57
Na_2O	----	----	----	----	----	----	----	0.03	0.03	----	----
Total	100.01	100.10	100.14	100.30	100.42	100.15	100.59	100.53	100.03	100.06	100.02

CATION PROPORTIONS BASED ON 6 OXYGENS

Si	1.944	1.944	1.943	1.941	1.929	1.957	1.959	1.950	1.958	1.950	1.944
Ti	0.002	0.002	0.002	0.002	0.001	0.003	0.002	0.003	0.002	0.002	0.003
Al	0.056	0.054	0.054	0.059	0.062	0.066	0.057	0.060	0.057	0.063	0.065
Cr	-----	-----	-----	-----	-----	-----	-----	-----	-----	-----	-----
Fe	0.728	0.709	0.741	0.741	0.740	0.757	0.708	0.710	0.666	0.764	0.767
Mn	0.033	0.032	0.048	0.024	0.031	0.030	0.037	0.032	0.029	0.029	0.024
Mg	1.237	1.262	1.217	1.238	1.251	1.170	1.225	1.239	1.280	1.182	1.195
Ca	0.023	0.023	0.022	0.021	0.022	0.023	0.021	0.022	0.019	0.025	0.023
Na	-----	-----	-----	-----	-----	-----	-----	-----	-----	-----	-----
Sum	4.023	4.026	4.027	4.026	4.036	4.006	4.008	4.016	4.011	4.015	4.021
X_{Mg}	0.622	0.626	0.628	0.607	0.636	0.658	0.633	0.607	0.609	0.667	0.641

MAFIC GNEISSES

ORTHOPYROXENE

	$MCS358_M$	MCS383	MCS384	MCS385	MCS386	$MCS386_S$	MCS207
SiO_2	51.65	50.28	52.20	51.67	51.70	51.27	51.34
TiO_2	0.07	0.15	0.11	0.08	----	----	0.07
Al_2O_3	2.80	1.54	1.43	1.82	1.31	1.06	1.20
Cr_2O_3	----	----	----	0.12	----	----	----
FeO	20.62	26.92	22.62	22.89	23.96	24.97	25.59
MnO	1.22	1.19	0.73	0.67	1.00	0.87	0.87
MgO	23.20	19.10	22.62	22.91	21.67	21.52	20.41
CaO	0.22	0.57	0.62	0.41	0.46	0.34	0.55
Na_2O	----	----	----	----	----	----	----
Total	99.78	99.75	100.33	100.57	100.10	100.03	100.03

CATION PROPORTIONS BASED ON 6 OXYGENS

Si	1.919	1.933	1.945	1.924	1.948	1.944	1.949
Ti	0.002	0.004	0.003	0.002	-----	-----	0.002
Al	0.123	0.070	0.063	0.080	0.058	0.047	0.054
Cr	-----	-----	-----	0.003	-----	-----	-----
Fe	0.641	0.866	0.705	0.713	0.755	0.792	0.812
Mn	0.038	0.039	0.023	0.021	0.032	0.028	0.028
Mg	1.285	1.095	1.256	1.272	1.217	1.216	1.154
Ca	0.009	0.024	0.025	0.016	0.019	0.014	0.022
Na	-----	-----	-----	-----	-----	-----	-----
Sum	4.017	4.031	4.020	4.031	4.029	4.041	4.021
X_{Mg}	0.587	0.558	0.641	0.641	0.617	0.606	0.587

MAFIC GNEISSES

CLINOPYROXENE

	$DWN129_A$	$DWN129_B$	$DWN332_2$	$DWN332_3$	DWN347	DWN348	DWN349	$DWN349_S$	DWN353	$DWN353_S$	DWN380
SiO_2	51.44	51.52	51.41	51.48	51.63	51.79	51.55	51.05	51.80	51.28	51.58
TiO_2	0.29	0.31	0.22	0.24	0.26	0.26	0.25	0.21	0.23	0.25	0.26
Al_2O_3	2.17	2.33	2.46	2.26	2.47	2.57	2.47	2.26	2.34	2.52	2.46
Cr_2O_3	0.12	----	----	----	----	----	----	----	----	----	----
FeO	8.84	8.26	9.37	9.52	8.67	8.76	9.15	9.36	9.14	9.70	9.83
MnO	0.16	0.18	0.38	0.44	0.36	0.38	0.41	0.55	0.38	0.31	0.84
MgO	13.94	14.44	13.58	13.68	14.02	13.86	13.41	13.29	13.64	13.39	13.55
CaO	22.12	22.42	21.52	21.50	21.69	21.85	22.05	22.51	22.17	22.18	20.98
Na_2O	0.43	0.45	0.37	0.34	0.49	0.48	0.44	0.45	0.42	0.46	0.35
Total	99.51	99.91	99.31	99.46	99.57	99.95	99.73	99.68	100.12	100.09	99.85

CATION PROPORTIONS BASED ON 6 OXYGENS

Si	1.933	1.957	1.936	1.938	1.934	1.933	1.935	1.924	1.935	1.923	1.936
Ti	0.008	0.009	0.006	0.007	0.007	0.007	0.007	0.006	0.006	0.007	0.007
Al	0.097	0.102	0.109	0.100	0.109	0.113	0.109	0.100	0.103	0.111	0.109
Cr	0.003	-----	-----	-----	-----	-----	-----	-----	-----	-----	-----
Fe	0.278	0.262	0.295	0.299	0.271	0.273	0.287	0.295	0.286	0.304	0.309
Mn	0.005	0.006	0.012	0.015	0.012	0.012	0.013	0.017	0.012	0.010	0.027
Mg	0.781	0.817	0.762	0.767	0.783	0.784	0.750	0.747	0.760	0.749	0.758
Ca	0.891	0.912	0.868	0.867	0.870	0.874	0.886	0.909	0.887	0.891	0.844
Na	0.031	0.033	0.027	0.024	0.036	0.035	0.032	0.033	0.031	0.034	0.025
Sum	4.027	4.098	4.015	4.017	4.022	4.031	4.019	4.031	4.020	4.029	4.015
X_{Mg}	0.738	0.757	0.721	0.719	0.743	0.742	0.723	0.717	0.727	0.711	0.711

MAFIC GNEISSES

CLINOPYROXENE

	DWN381	DWN625	HY8	HY23	VK7	MCSH04	MCSH05	MCSS04	MCSS05	$MCS301_A$	$MCS301_B$
SiO_2	51.68	51.11	52.00	50.78	49.95	52.76	52.42	51.01	51.80	51.24	51.18
TiO_2	0.23	0.16	0.26	0.25	0.34	0.21	0.20	0.26	0.22	0.27	0.31
Al_2O_3	2.25	2.24	2.21	2.23	2.00	2.09	1.94	2.17	2.03	2.43	2.64
Cr_2O_3	----	----	----	----	----	0.16	0.14	----	----	----	----
FeO	9.23	9.63	9.25	9.40	13.69	6.55	5.54	9.80	9.84	9.04	9.46
MnO	0.34	0.37	0.38	0.34	0.37	0.18	0.17	0.32	0.35	0.50	0.52
MgO	13.94	13.45	14.15	14.10	11.70	15.24	15.58	13.29	13.35	13.57	13.31
CaO	21.80	22.23	22.04	22.17	21.32	22.91	22.82	22.24	22.18	22.31	21.73
Na_2O	0.34	0.42	0.45	0.40	0.41	0.44	0.39	0.36	0.42	0.46	0.48
Total	99.81	99.61	100.74	99.69	99.78	100.54	99.20	99.45	100.19	99.82	99.63

CATION PROPORTIONS BASED ON 6 OXYGENS

Si	1.935	1.928	1.942	1.914	1.916	1.942	1.948	1.928	1.941	1.924	1.926
Ti	0.007	0.004	0.007	0.007	0.010	0.006	0.006	0.008	0.006	0.008	0.009
Al	0.099	0.100	0.097	0.099	0.090	0.091	0.085	0.097	0.090	0.108	0.117
Cr	-----	-----	-----	-----	-----	0.005	0.002	-----	-----	-----	-----
Fe	0.289	0.304	0.287	0.296	0.439	0.202	0.172	0.310	0.308	0.284	0.297
Mn	0.011	0.012	0.012	0.011	0.012	0.006	0.005	0.010	0.011	0.016	0.017
Mg	0.778	0.756	0.783	0.792	0.671	0.836	0.748	0.745	0.808	0.759	0.746
Ca	0.874	0.899	0.877	0.895	0.876	0.903	0.909	0.900	0.890	0.897	0.876
Na	0.024	0.031	0.033	0.029	0.030	0.031	0.027	0.026	0.030	0.033	0.035
Sum	4.017	4.034	4.028	4.043	4.044	4.022	4.017	4.024	4.021	4.029	4.023
X_{Mg}	0.729	0.713	0.732	0.728	0.605	0.806	0.834	0.707	0.708	0.728	0.715

MAFIC GNEISSES

CLINOPYROXENE

	$MCS301_C$	MCS302	MCS303	$MCS304_M$	$MCS304_I$	MCS305	MCS317	$MCS327_T$	$MCS327_I$	$MCS327_B$	MCS380
SiO_2	50.56	51.88	51.21	51.69	52.38	51.49	51.61	51.86	51.63	51.15	51.74
TiO_2	0.26	0.22	0.19	0.21	0.19	0.25	0.25	0.25	0.21	0.27	0.19
Al_2O_3	2.56	2.35	2.05	2.44	2.18	2.55	2.53	2.35	2.12	2.39	1.89
Cr_2O_3	----	----	----	----	----	----	----	----	----	----	----
FeO	9.17	9.67	8.85	9.32	8.74	9.31	9.15	9.92	9.60	10.21	10.73
MnO	0.43	0.72	0.31	0.44	0.38	0.41	0.45	0.39	0.52	0.33	1.36
MgO	14.10	13.11	14.58	13.49	13.71	13.48	13.84	13.49	13.78	13.59	12.28
CaO	22.30	21.27	22.43	22.03	21.99	22.40	21.78	21.74	22.28	21.73	20.88
Na_2O	0.53	0.44	0.47	0.32	0.31	0.45	0.46	0.29	0.31	0.31	0.52
Total	99.91	99.66	100.01	99.94	99.88	100.36	100.07	100.29	100.45	99.98	99.59

CATION PROPORTIONS BASED ON 6 OXYGENS

Si	1.902	1.949	1.919	1.936	1.954	1.924	1.929	1.938	1.926	1.923	1.960
Ti	0.007	0.006	0.003	0.006	0.005	0.007	0.007	0.007	0.005	0.008	0.005
Al	0.114	0.104	0.091	0.108	0.096	0.112	0.112	0.104	0.093	0.106	0.084
Cr	-----	-----	-----	-----	-----	-----	-----	-----	-----	-----	-----
Fe	0.289	0.304	0.277	0.292	0.272	0.291	0.286	0.310	0.299	0.321	0.340
Mn	0.014	0.023	0.010	0.014	0.012	0.013	0.014	0.012	0.029	0.011	0.044
Mg	0.790	0.734	0.814	0.753	0.762	0.751	0.771	0.751	0.766	0.762	0.693
Ca	0.899	0.856	0.901	0.884	0.879	0.897	0.872	0.870	0.890	0.875	0.847
Na	0.039	0.032	0.034	0.023	0.023	0.083	0.033	0.021	0.011	0.023	0.018
Sum	4.054	4.008	4.049	4.016	4.003	4.028	4.024	4.013	4.019	4.029	3.991
X_{Mg}	0.733	0.707	0.746	0.721	0.737	0.721	0.730	0.708	0.719	0.704	0.671

MAFIC GNEISSES

CLINOPYROXENE

	MC384	MCS207	MCS220	MCS235
SiO_2	51.32	50.84	51.00	51.47
TiO_2	0.23	0.24	0.27	0.19
Al_2O_3	2.36	2.40	3.07	2.51
Cr_2O_3	----	----	----	0.11
FeO	9.06	10.49	8.15	7.31
MnO	0.28	0.37	1.06	1.93
MgO	13.88	13.13	13.36	13.71
CaO	22.22	21.72	21.94	21.99
Na_2O	0.36	0.23	0.52	0.48
Total	99.71	99.42	99.37	99.70

CATION PROPORTIONS BASED ON 6 OXYGENS

Si	1.926	1.925	1.917	1.930
Ti	0.006	0.007	0.008	0.005
Al	0.104	0.107	0.136	0.111
Cr	-----	-----	-----	0.003
Fe	0.284	0.332	0.256	0.229
Mn	0.009	0.012	0.034	0.061
Mg	0.776	0.741	0.749	0.766
Ca	0.893	0.881	0.884	0.883
Na	0.026	0.017	0.038	0.035
Sum	4.024	4.022	4.022	4.023
X_{Mg}	0.732	0.691	0.745	0.770

MAFIC GNEISSES

HORNBLENDE

	DWN129$_A$	DWN129$_B$	DWN288	DWN332$_2$	DWN332$_3$	DWN347	DWN348	DWN349	DWN353	DWN380	DWN381
SiO_2	42.92	43.38	43.10	43.76	42.77	43.44	43.36	43.69	43.58	44.03	44.42
TiO_2	2.17	2.16	1.67	1.62	1.74	1.93	1.94	1.70	2.04	1.40	1.40
Al_2O_3	11.37	11.16	10.85	11.27	11.42	11.18	10.98	10.60	10.87	10.89	10.14
Cr_2O_3	----	0.13	----	----	----	----	----	----	----	----	0.23
FeO	13.68	13.43	15.72	13.52	13.92	13.30	13.41	14.16	14.09	13.79	13.20
MnO	0.14	0.13	0.36	0.27	0.25	0.20	0.18	0.25	0.20	0.46	0.20
MgO	13.00	13.17	12.14	13.44	12.74	13.40	13.09	12.86	12.83	13.27	13.90
CaO	11.87	11.76	11.65	12.09	11.86	11.41	11.76	11.81	11.63	11.78	11.84
Na_2O	1.67	1.62	1.64	1.18	1.22	1.33	1.08	1.22	1.25	1.05	1.03
K_2O	0.94	0.84	1.05	1.26	1.41	1.36	1.43	1.13	1.33	1.26	1.31
Total	97.75	97.78	98.18	98.41	97.33	97.55	97.23	97.42	97.82	97.94	97.67

CATION PROPORTIONS BASED ON 23 OXYGENS

Si	6.559	6.413	6.430	6.434	6.388	6.434	6.450	6.502	6.462	6.510	6.566
Ti	0.192	0.240	0.187	0.179	0.196	0.214	0.217	0.190	0.228	0.155	0.155
Al	1.791	1.946	1.910	1.956	2.012	1.953	1.927	1.861	1.901	1.899	1.769
Cr	-----	0.015	-----	-----	-----	-----	-----	-----	-----	-----	0.028
Fe	1.650	1.660	1.961	1.662	1.738	1.647	1.668	1.762	1.747	1.705	1.631
Mn	0.010	0.017	0.046	0.033	0.031	0.025	0.023	0.031	0.025	0.058	0.025
Mg	3.031	2.901	2.699	2.945	2.835	2.957	2.902	2.851	2.834	2.923	3.062
Ca	1.844	1.863	1.861	1.905	1.898	1.811	1.875	1.883	1.847	1.865	1.875
Na	0.360	0.465	0.473	0.337	0.352	0.381	0.313	0.361	0.360	0.300	0.295
K	0.192	0.158	0.199	0.237	0.269	0.256	0.272	0.215	0.251	0.236	0.247
Sum	15.629	15.678	15.766	15.688	15.719	15.678	15.647	15.656	15.655	15.651	15.653
X_{Mg}	0.648	0.636	0.579	0.639	0.620	0.642	0.635	0.618	0.619	0.632	0.652

MAFIC GNEISSES

HORNBLENDE

	HY8	VK7	MCSH04	MCSH05	MCSS04	MCSS05	MCST02	MCST03	$MCS301_A$	$MCS301_C$	MCS302
SiO_2	43.04	40.52	45.13	45.09	42.03	42.25	41.29	41.74	43.30	43.39	43.72
TiO_2	2.14	3.01	1.90	1.69	2.54	2.30	2.43	2.24	1.56	1.74	1.53
Al_2O_3	10.64	11.62	11.05	10.89	11.98	11.49	13.45	12.90	11.02	10.96	11.21
Cr_2O_3	0.16	----	0.45	0.44	-----	-----	-----	-----	0.25	0.16	----
FeO	14.22	19.08	10.78	8.81	15.30	15.78	14.26	14.81	13.77	13.83	14.38
MnO	0.23	0.23	0.11	0.11	0.19	0.20	0.24	0.27	0.25	0.32	0.37
MgO	12.64	8.23	14.40	15.71	11.44	11.44	11.64	11.69	13.13	13.16	12.41
CaO	11.78	11.50	12.23	12.12	11.52	11.72	11.02	11.13	11.67	11.74	11.41
Na_2O	1.29	1.94	1.51	1.36	1.34	1.48	2.03	2.27	1.44	1.37	1.25
K_2O	1.39	1.35	1.23	0.98	1.51	1.67	0.94	0.89	1.26	1.31	1.23
Total	97.53	97.48	98.79	97.20	97.85	98.33	97.30	97.94	97.65	97.98	97.51

CATION PROPORTIONS BASED ON 23 OXYGENS

Si	6.429	6.227	6.532	6.563	6.295	6.318	6.171	6.217	6.437	6.431	6.502
Ti	0.240	0.348	0.207	0.185	0.286	0.258	0.273	0.251	0.174	0.194	0.172
Al	1.875	2.107	1.884	1.870	2.116	2.027	2.371	2.268	1.932	1.917	1.968
Cr	0.019	-----	0.052	0.045	-----	-----	-----	-----	0.029	0.019	-----
Fe	1.776	2.452	1.302	1.072	1.916	1.973	1.782	1.844	1.712	1.714	1.788
Mn	0.029	0.031	0.014	0.013	0.024	0.025	0.030	0.034	0.031	0.040	0.047
Mg	2.813	1.885	3.102	3.408	2.554	2.549	2.593	2.594	2.909	2.908	2.749
Ca	1.884	1.893	1.893	1.891	1.849	1.877	1.764	1.775	1.859	1.865	1.818
Na	0.373	0.578	0.424	0.383	0.389	0.428	0.589	0.655	0.414	0.392	0.361
K	0.264	0.264	0.226	0.182	0.234	0.318	0.178	0.168	0.239	0.248	0.234
Sum	15.702	15.785	15.636	15.612	15.669	15.773	15.751	15.806	15.736	15.728	15.639
X_{Mg}	0.613	0.435	0.704	0.761	0.571	0.564	0.583	0.584	0.630	0.629	0.606

MAFIC GNEISSES

HORNBLENDE

	MCS303	MCS304$_M$	MCS304$_I$	MCS305	MCS327$_T$	MCS327$_I$	MCS358$_I$	MCS380	MCS385	MCS220	MCS235
SiO_2	43.52	42.91	43.39	42.79	42.25	42.93	46.08	42.02	44.91	44.47	43.98
TiO_2	1.81	1.58	1.52	1.93	1.50	1.98	0.86	2.00	1.55	1.12	1.32
Al_2O_3	10.80	11.65	11.15	11.22	11.57	11.39	11.04	11.31	10.90	10.75	10.86
Cr_2O_3	-----	-----	-----	-----	-----	-----	-----	-----	0.21	0.30	0.18
FeO	14.19	14.17	14.04	14.75	14.70	14.36	12.23	16.84	11.92	11.65	12.11
MnO	0.17	0.22	0.22	0.21	0.23	0.30	0.54	0.84	0.21	1.10	0.69
MgO	12.90	13.07	13.34	12.60	12.82	12.78	14.72	10.68	14.20	14.35	13.92
CaO	11.71	12.05	12.16	11.84	11.86	11.84	10.96	11.13	11.68	11.85	11.75
Na_2O	1.42	1.20	1.27	1.30	1.22	1.26	1.22	1.43	1.23	1.45	1.27
K_2O	1.45	1.27	1.36	1.59	1.41	1.69	0.44	1.53	0.89	1.15	1.22
Total	97.97	98.12	98.45	98.23	97.56	98.53	98.09	97.78	97.70	98.19	97.30

CATION PROPORTIONS BASED ON 23 OXYGENS

Si	6.456	6.358	6.406	6.366	6.325	6.360	6.673	6.356	6.568	6.520	6.503
Ti	0.202	0.176	0.169	0.215	0.169	0.220	0.094	0.228	0.171	0.123	0.147
Al	1.891	2.034	1.941	1.969	2.043	1.990	1.884	2.019	1.879	1.859	1.893
Cr	-----	-----	-----	-----	-----	-----	-----	-----	0.024	0.034	0.021
Fe	1.761	1.756	1.733	1.835	1.841	1.779	1.481	2.130	1.457	1.428	1.499
Mn	0.021	0.028	0.028	0.026	0.030	0.038	0.067	0.106	0.026	0.137	0.086
Mg	2.853	2.887	2.937	2.793	2.860	2.821	3.177	2.407	3.094	3.136	3.071
Ca	1.862	1.913	1.923	1.887	1.901	1.878	1.700	1.804	1.831	1.861	1.863
Na	0.408	0.345	0.363	0.375	0.354	0.361	0.343	0.420	0.349	0.412	0.363
K	0.275	0.239	0.256	0.302	0.270	0.319	0.081	0.294	0.166	0.215	0.230
Sum	15.729	15.736	15.756	15.768	15.793	15.766	15.500	15.764	15.565	15.725	15.681
X_{Mg}	0.618	0.622	0.629	0.604	0.609	0.613	0.682	0.531	0.680	0.687	0.672

MAFIC GNEISSES

PLAGIOCLASE

	DWN129$_A$ core	DWN129$_A$ core	DWN129$_A$ rim	DWN129$_B$ core	DWN288 core	DWN332$_1$ core	DWN332$_1$ core	DWN332$_1$ rim	DWN332$_2$ core	DWN332$_3$ core
SiO_2	49.26	53.28	51.39	50.01	56.33	54.68	50.99	49.08	48.14	48.27
Al_2O_3	31.49	29.19	30.91	31.19	27.62	28.23	30.51	32.03	32.84	33.00
FeO	0.15	0.17	0.23	0.18	0.19	0.08	0.13	0.28	0.20	0.16
MgO	----	----	----	----	----	----	----	----	----	----
CaO	15.23	12.06	13.98	15.20	10.42	11.34	14.27	16.67	16.67	16.75
Na_2O	2.84	4.52	3.45	2.90	5.59	5.19	3.49	2.49	1.89	1.84
K_2O	0.08	0.15	0.09	0.14	0.19	0.12	0.09	0.07	0.07	0.07
Total	99.05	99.37	100.05	99.62	100.35	99.56	99.48	100.17	99.81	100.10

CATION PROPORTIONS BASED ON 8 OXYGENS

Si	2.272	2.426	2.335	2.293	2.526	2.478	2.334	2.245	2.210	2.209
Al	1.712	1.566	1.656	1.566	1.461	1.508	1.646	1.727	1.777	1.780
Fe	0.006	0.007	0.009	0.007	0.007	0.003	0.005	0.011	0.008	0.060
Mg	-----	-----	-----	-----	-----	-----	-----	-----	-----	0.001
Ca	0.753	0.588	0.681	0.746	0.500	0.551	0.700	0.795	0.820	0.821
Na	0.254	0.399	0.304	0.257	0.486	0.449	0.309	0.221	0.168	0.163
K	0.005	0.009	0.006	0.008	0.011	0.007	0.005	0.004	0.004	0.004
Sum	5.002	4.995	4.991	4.996	4.992	4.996	4.999	5.003	4.987	4.984
An	74.42	59.06	68.77	73.78	50.13	54.72	69.01	77.95	82.61	83.11
Ab	25.14	40.08	30.68	25.44	48.74	44.62	30.50	21.65	16.96	16.49
Or	0.44	0.86	0.55	0.78	1.13	0.66	0.49	0.40	0.40	0.40

MAFIC GNEISSES

PLAGIOCLASE

	DWN347		DWN348		DWN349				DWN353				
	core	rim	core	rim	core	rim	$core_S$	$core_S$	core	core	core	rim	$core_S$
SiO_2	53.53	51.40	52.69	54.97	51.22	49.62	52.96	50.89	55.87	55.30	52.82	49.68	55.26
Al_2O_3	29.27	30.71	30.28	28.55	30.60	31.71	29.28	31.42	28.09	28.62	30.54	32.42	28.17
FeO	0.20	0.26	0.10	0.15	0.25	0.24	0.15	0.16	0.12	0.18	0.16	0.26	0.18
MgO	----	----	----	----	----	----	----	----	----	----	----	----	----
CaO	12.12	13.59	12.96	11.46	13.73	14.93	12.06	14.40	10.39	11.24	13.25	15.33	10.97
Na_2O	4.39	3.69	3.61	4.50	3.73	3.09	4.59	3.47	5.49	4.78	3.69	2.50	4.88
K_2O	0.25	0.12	0.17	0.24	0.10	0.08	0.18	0.13	0.33	0.19	0.19	0.10	0.31
Total	99.78	99.77	99.80	99.85	99.63	99.67	99.23	100.67	100.28	99.64	99.67	99.22	100.47

CATION PROPORTIONS BASED ON 8 OXYGENS

Si	2.438	2.343	2.388	2.480	2.339	2.274	2.417	2.309	2.509	2.483	2.378	2.261	2.495
Al	1.565	1.650	1.618	1.518	1.647	1.713	1.575	1.680	1.486	1.514	1.621	1.738	1.499
Fe	0.008	0.010	0.004	0.006	0.010	0.009	0.006	0.006	0.005	0.007	0.006	0.010	0.007
Mg	-----	-----	-----	-----	-----	-----	-----	-----	-----	-----	-----	-----	-----
Ca	0.589	0.664	0.629	0.554	0.672	0.733	0.590	0.700	0.500	0.541	0.639	0.747	0.531
Na	0.386	0.326	0.317	0.394	0.330	0.275	0.406	0.305	0.478	0.416	0.322	0.220	0.428
K	0.015	0.007	0.010	0.014	0.006	0.005	0.011	0.007	0.019	0.011	0.011	0.006	0.018
Sum	4.990	4.999	4.966	4.964	5.005	5.009	5.004	5.007	4.997	4.973	4.978	4.982	4.978
An	59.51	66.56	65.82	57.65	66.65	72.41	58.58	69.15	50.18	55.89	65.73	76.79	54.35
Ab	39.02	32.73	33.18	40.94	32.76	27.13	40.38	30.14	47.92	42.97	33.16	22.62	43.80
Or	1.47	0.71	0.10	1.41	0.59	0.46	1.04	0.72	1.90	1.14	1.11	0.59	1.85

MAFIC GNEISSES

PLAGIOCLASE

	DWN354		DWN380	DWN381		DWN615	DWN625		HY8	VK7	MCSH04	MCSH05
	core	core	core	core	rim	core	core	rim	core	core	core	core
SiO_2	48.81	47.53	47.17	47.73	45.88	47.87	56.60	55.35	55.79	57.71	50.30	54.06
Al_2O_3	32.19	33.68	33.34	33.46	34.84	33.42	27.62	28.42	27.75	26.09	31.09	29.65
FeO	0.13	0.18	0.33	0.30	0.40	0.27	0.17	0.15	0.18	0.09	0.17	0.17
MgO	----	----	----	----	----	----	----	----	----	----	----	----
CaO	15.60	16.95	17.60	16.67	17.90	16.91	10.01	10.93	10.58	9.67	14.57	11.96
Na_2O	2.66	1.70	1.52	1.60	0.86	1.64	5.30	4.90	5.23	6.23	3.26	4.71
K_2O	0.47	0.06	0.05	0.06	0.04	0.07	0.27	0.23	0.29	0.21	0.11	0.20
Total	99.88	100.12	100.01	99.84	99.93	100.18	99.97	99.98	99.82	99.99	99.50	100.75

CATION PROPORTIONS BASED ON 8 OXYGENS

Si	2.241	2.177	2.170	2.190	2.112	2.190	2.541	2.492	2.515	2.591	2.313	2.426
Al	1.742	1.819	1.807	1.809	1.891	1.803	1.461	1.508	1.476	1.382	1.679	1.570
Fe	0.005	0.007	0.013	0.012	0.015	0.010	0.006	0.006	0.007	0.004	0.006	0.006
Mg	-----	-----	-----	-----	-----	-----	-----	-----	-----	-----	-----	-----
Ca	0.767	0.836	0.867	0.819	0.883	0.829	0.481	0.527	0.519	0.465	0.704	0.575
Na	0.237	0.151	0.137	0.142	0.076	0.146	0.462	0.427	0.464	0.542	0.285	0.409
K	0.028	0.004	0.003	0.003	0.002	0.004	0.015	0.013	0.017	0.012	0.006	0.012
Sum	5.020	4.994	4.997	4.977	4.980	4.983	4.966	4.973	4.997	4.996	4.994	4.998
An	74.40	84.33	86.14	84.96	91.80	84.70	50.22	54.46	51.86	45.63	70.71	57.72
Ab	22.95	15.29	13.58	14.73	7.94	14.86	48.17	44.16	46.43	53.20	28.66	41.08
Or	2.65	0.38	0.28	0.31	0.26	0.44	1.61	1.38	1.71	1.17	0.63	1.20

MAFIC GNEISSES

PLAGIOCLASE

	MCSS04		MCSS05		MCSS08	MCST02	MCS301$_A$			MCS301$_B$		MCS301$_C$	
	core	rim	core	core$_S$	core	core	core	core	rim	core	core	core	core
SiO_2	55.22	55.52	56.70	56.33	59.23	55.84	53.90	51.27	49.61	50.21	48.31	54.88	50.67
Al_2O_3	27.28	28.34	27.66	27.65	25.21	28.10	28.35	30.77	31.37	32.08	32.92	28.82	30.98
FeO	1.49	0.23	0.20	0.34	0.12	0.13	0.12	0.11	0.28	0.22	0.16	0.13	0.15
MgO	0.66	----	----	----	----	----	----	----	----	----	----	----	----
CaO	9.16	10.27	9.93	10.16	7.55	10.19	11.61	14.03	15.41	14.57	16.11	11.67	14.10
Na_2O	5.49	5.72	5.79	5.69	6.84	5.66	4.91	3.64	2.79	2.88	2.17	4.86	3.20
K_2O	0.19	0.21	0.31	0.29	0.30	0.12	0.20	0.16	0.11	0.14	0.09	0.17	0.08
Total	99.49	100.29	100.60	100.46	99.25	100.04	99.09	99.97	99.56	100.10	99.75	100.54	99.16

CATION PROPORTIONS BASED ON 8 OXYGENS

Si	2.508	2.495	2.535	2.526	2.661	2.510	2.459	2.335	2.278	2.285	2.216	2.464	2.323
Al	1.460	1.501	1.459	1.461	1.336	1.490	1.524	1.651	1.698	1.721	1.780	1.525	1.674
Fe	0.057	0.009	0.007	0.013	0.004	0.007	0.005	0.004	0.011	0.008	0.006	0.005	0.006
Mg	0.045	-----	-----	-----	-----	-----	-----	-----	-----	-----	-----	-----	-----
Ca	0.446	0.495	0.476	0.488	0.363	0.476	0.568	0.684	0.758	0.710	0.792	0.561	0.693
Na	0.484	0.498	0.502	0.495	0.595	0.502	0.434	0.310	0.248	0.254	0.193	0.423	0.285
K	0.011	0.012	0.018	0.016	0.017	0.018	0.011	0.009	0.006	0.008	0.005	0.010	0.005
Sum	5.011	5.010	4.997	4.999	4.976	4.996	5.001	5.005	5.000	4.986	4.992	4.989	4.984
An	47.39	49.23	47.79	48.83	37.23	47.79	56.02	67.45	74.86	71.95	80.03	56.45	70.54
Ab	51.43	49.59	50.43	49.51	58.07	50.43	42.85	31.63	24.53	27.24	19.47	42.56	28.98
Or	1.18	1.18	1.78	1.66	1.69	1.78	1.13	0.92	0.61	0.81	0.50	0.99	0.48

MAFIC GNEISSES

PLAGIOCLASE

	MCS302	MCS303			MCS304$_M$	MCS304$_I$		MCS305		MCS317		
	core	core	core	rim	core	core	rim	core	rim	core	rim	core$_S$
SiO_2	56.44	56.25	54.47	52.27	48.19	49.11	46.92	50.21	51.67	55.74	53.40	54.97
Al_2O_3	27.60	27.13	28.82	30.09	32.91	32.17	33.60	31.98	30.59	28.06	29.77	28.55
FeO	----	0.25	0.13	0.18	0.24	0.16	0.37	0.19	0.24	0.25	0.23	0.15
MgO	----	----	----	----	----	----	----	----	----	----	----	----
CaO	9.96	9.67	11.36	13.19	17.00	16.19	17.63	15.23	14.02	10.57	12.47	11.46
Na_2O	5.60	5.86	4.87	3.90	1.72	2.07	1.19	2.84	3.63	4.97	4.03	4.50
K_2O	0.17	0.25	0.24	0.19	----	0.04	----	0.11	0.13	0.34	0.24	0.24
Total	99.87	99.41	99.89	99.82	100.06	99.74	99.71	100.56	100.28	99.93	100.14	99.87

CATION PROPORTIONS BASED ON 8 OXYGENS

Si	2.547	2.544	2.461	2.377	2.207	2.250	2.162	2.278	2.345	2.510	2.413	2.480
Al	1.462	1.446	1.535	1.613	1.776	1.737	1.825	1.712	1.637	1.489	1.585	1.518
Fe	-----	0.010	0.005	0.007	0.009	0.006	0.014	0.008	0.009	0.009	0.009	0.006
Mg	-----	-----	-----	-----	-----	-----	-----	-----	-----	-----	-----	-----
Ca	0.480	0.468	0.550	0.643	0.834	0.795	0.870	0.741	0.681	0.510	0.604	0.554
Na	0.488	0.514	0.426	0.344	0.153	0.184	0.106	0.250	0.319	0.434	0.353	0.394
K	0.010	0.015	0.014	0.011	-----	0.002	-----	0.006	0.008	0.019	0.014	0.014
Sum	4.981	4.994	4.991	4.995	4.979	4.974	4.977	4.995	4.999	4.971	4.978	4.966
An	49.06	46.98	55.53	64.39	84.50	80.99	89.14	74.34	67.61	52.93	62.19	57.65
Ab	49.96	51.57	43.06	34.49	15.50	18.76	10.86	25.06	31.64	45.07	36.40	40.94
Or	0.98	1.42	1.41	1.12	-----	0.25	-----	0.60	0.75	2.00	1.41	1.41

MAFIC GNEISSES

PLAGIOCLASE

	$MCS327_T$ core	$MCS327_I$ core	$MCS327_B$ core	$MCS358_M$ core	$MCS358_M$ rim	$MCS358_I$ core	MCS380 core	MCS207 core
SiO_2	46.47	47.21	46.95	55.72	53.45	48.66	59.65	45.29
Al_2O_3	34.92	34.26	34.43	27.83	29.61	32.62	24.99	34.47
FeO	0.23	0.24	0.21	0.04	0.10	0.20	0.17	0.34
MgO	----	----	----	----	----	----	----	----
CaO	17.17	17.20	17.60	10.79	12.50	16.68	7.73	18.04
Na_2O	1.49	1.57	1.37	5.57	4.41	1.94	6.50	0.92
K_2O	0.04	0.06	0.04	0.06	0.04	----	0.26	----
Total	100.32	100.54	100.60	100.01	100.11	100.10	99.30	99.06

CATION PROPORTIONS BASED ON 8 OXYGENS

Si	2.127	2.152	2.144	2.508	2.414	2.225	2.675	2.106
Al	1.886	1.849	1.855	1.476	1.576	1.750	1.321	1.889
Fe	0.009	0.010	0.008	0.002	0.004	0.008	0.006	0.013
Mg	-----	-----	-----	-----	-----	-----	-----	-----
Ca	0.842	0.843	0.861	0.521	0.609	0.817	0.372	0.899
Na	0.132	0.139	0.121	0.486	0.386	0.172	0.565	0.083
K	0.001	0.003	0.002	0.003	0.003	-----	0.015	-----
Sum	4.997	4.996	4.991	4.996	4.992	4.972	4.954	4.990
An	86.35	85.55	87.46	51.54	61.05	82.61	39.05	91.55
Ab	13.54	14.11	12.31	48.13	38.70	17.39	59.41	8.45
Or	0.11	0.34	0.23	0.33	0.25	-----	1.54	----

MAFIC GNEISSES

BIOTITE

	DWN332$_1$	DWN332$_3$	DWN347	DWN348	DWN353	DWN354	DWN380	DWN381	DWN615	DWN625
SiO_2	37.21	37.60	36.65	36.30	36.78	36.26	37.71	37.63	37.10	37.45
TiO_2	4.16	4.02	5.27	5.50	5.36	5.18	4.60	4.30	5.15	4.60
Al_2O_3	15.63	14.74	14.92	14.57	15.19	16.42	14.42	14.31	15.39	15.07
Cr_2O_3	----	----	----	----	----	0.11	----	0.20	----	----
FeO	13.37	12.81	14.78	13.28	13.82	14.19	14.11	13.09	15.02	15.06
MnO	0.11	----	----	----	----	----	0.20	----	----	----
MgO	15.65	17.12	14.98	15.67	15.12	13.92	15.61	16.74	14.33	15.24
Na_2O	0.12	0.11	----	----	----	----	0.14	0.12	----	----
K_2O	9.07	9.13	8.91	9.49	8.91	8.93	9.15	9.31	9.56	9.30
F_2	0.89	0.91	n.d.	0.32	0.42	0.30	1.14	0.69	0.56	0.50
Total	96.21	96.48	95.67	95.28	95.72	95.36	97.08	96.39	97.11	97.22

CATION PROPORTIONS BASED ON 22 OXYGENS

Si	5.500	5.531	5.443	5.421	5.449	5.394	5.566	5.546	5.464	5.498
Ti	0.462	0.445	0.588	0.618	0.597	0.580	0.511	0.447	0.570	0.508
Al	2.726	2.559	2.615	2.567	2.656	2.882	2.511	2.488	2.672	2.607
Cr	-----	-----	-----	-----	-----	0.013	-----	0.023	-----	-----
Fe	1.652	1.576	1.835	1.656	1.712	1.766	1.741	1.613	1.850	1.849
Mn	0.014	-----	-----	-----	-----	-----	0.025	-----	-----	-----
Mg	3.447	3.752	3.314	3.487	3.338	3.084	3.433	3.676	3.147	3.334
Na	0.034	0.032	-----	-----	-----	-----	0.041	0.034	-----	-----
K	1.710	1.712	1.686	1.808	1.684	1.694	1.722	1.749	1.796	1.742
Sum	15.545	15.612	15.507	15.578	15.480	15.427	15.550	15.606	15.499	15.538
X_{Mg}	0.676	0.704	0.644	0.678	0.661	0.636	0.664	0.695	0.630	0.643

MAFIC GNEISSES

BIOTITE

	MCSH05	MCS301$_B$	MCS301$_C$	MCS302	MCS304$_M$	MCS304$_I$	MCS305	MCS317	MCS383	MCS385	MCS386
SiO_2	37.18	37.02	36.88	37.03	37.90	37.82	37.57	36.89	37.12	38.01	36.66
TiO_2	4.58	6.97	5.09	4.32	3.98	4.38	4.79	4.97	5.25	3.86	5.31
Al_2O_3	15.87	14.91	14.61	14.93	14.73	14.71	14.73	15.65	14.92	14.58	14.38
Cr_2O_3	0.50	0.10	0.14	----	----	----	----	----	----	0.41	----
FeO	11.28	13.08	14.19	13.77	13.15	14.77	13.74	12.39	16.08	10.90	14.44
MnO	----	0.15	0.12	0.13	----	0.11	----	0.10	----	----	0.17
MgO	17.51	14.28	15.58	15.63	13.15	15.82	15.99	13.62	17.67	14.52	14.52
Na_2O	0.15	----	----	----	0.14	----	0.10	----	0.11	0.28	----
K_2O	9.49	9.24	9.16	9.12	9.51	9.26	9.14	9.37	9.59	9.00	9.33
F^2	n.d.	0.27	0.34	0.41	1.12	1.10	0.60	n.d.	n.d.	1.50	n.d.
Total	96.61	96.09	96.14	95.40	97.16	96.87	96.66	95.26	97.16	96.31	94.81

CATION PROPORTIONS BASED ON 22 OXYGENS

Si	5.368	5.454	5.463	5.513	5.560	5.536	5.523	5.445	5.513	5.594	5.509
Ti	0.497	0.772	0.567	0.484	0.439	0.482	0.529	0.551	0.586	0.427	0.600
Al	2.704	2.591	2.553	2.622	2.546	2.538	2.555	2.725	2.612	2.530	2.546
Cr	0.121	0.012	0.017	-----	-----	-----	-----	-----	-----	0.048	-----
Fe	1.362	1.611	1.758	1.714	1.613	1.808	1.689	1.529	1.997	1.341	1.814
Mn	-----	0.019	0.014	0.016	-----	0.014	-----	0.012	-----	-----	0.022
Mg	3.769	3.136	3.439	3.467	3.636	3.452	3.503	3.473	3.016	3.876	3.252
Na	0.043	0.021	0.014	0.018	0.040	-----	0.028	-----	0.023	0.079	-----
K	1.748	1.736	1.732	1.731	1.780	1.729	1.713	1.764	1.839	1.690	1.789
Sum	15.618	15.352	15.558	15.565	15.586	15.569	15.540	15.530	15.586	15.585	15.813
X_{Mg}	0.735	0.661	0.662	0.669	0.693	0.656	0.675	0.694	0.602	0.743	0.642

PELITIC GNEISSES

BIOTITE

	DWN617			DWN618	DWN619	DWN620	DWN622			DWN623	
	Matrix	Rim	Inclusion	Matrix	Matrix	Matrix	Matrix	Skeletal	Rim	Matrix	Skeletal
SiO_2	37.37	37.32	37.21	36.62	37.60	36.30	37.26	38.05	37.24	38.17	38.93
TiO_2	5.65	4.65	5.57	1.29	1.26	4.51	4.17	3.32	3.35	2.96	2.36
Al_2O_3	16.98	17.36	17.06	18.64	19.12	16.92	16.60	16.53	16.27	16.69	16.85
Cr_2O_3	-----	-----	0.09	0.07	0.09	-----	-----	-----	-----	-----	-----
FeO	13.71	15.87	12.15	14.45	14.25	15.17	14.18	12.37	13.67	12.54	10.04
MnO	-----	-----	-----	-----	-----	-----	-----	-----	-----	-----	-----
MgO	14.06	12.81	14.75	15.63	15.35	13.46	14.57	16.63	16.39	17.04	19.20
Na_2O	0.22	0.08	0.12	0.26	0.21	0.09	0.18	0.24	0.18	0.32	0.41
K_2O	8.74	8.43	8.91	9.22	8.56	9.81	9.38	8.99	9.06	8.90	8.48
F	0.62	0.47	0.30	0.70	0.79	0.48	0.68	0.93	0.70	1.15	1.10
Total	97.35	96.99	96.80	97.58	97.23	97.22	97.02	97.06	97.64	97.77	97.37

CATION PROPORTIONS BASED ON 22 OXYGENS

Si	5.421	5.463	5.419	5.379	5.459	5.377	5.468	5.526	5.455	5.516	5.559
Ti	0.617	0.512	0.610	0.143	0.137	0.502	0.460	0.362	0.369	0.322	0.253
Al	2.903	2.995	2.928	3.227	3.271	2.954	2.871	2.829	2.809	2.843	2.835
Cr	-----	-----	0.011	-----	0.011	-----	-----	-----	-----	-----	-----
Fe	1.663	1.943	1.479	1.775	1.731	1.880	1.741	1.502	1.675	1.515	1.198
Mn	-----	-----	-----	-----	-----	-----	-----	-----	0.010	-----	-----
Mg	3.039	2.795	3.200	3.422	3.321	2.972	3.186	3.600	3.579	3.671	4.085
Na	0.061	0.022	0.034	0.073	0.060	0.027	0.052	0.067	0.051	0.089	0.113
K	1.618	1.574	1.655	1.728	1.585	1.855	1.757	1.665	1.693	1.640	1.545
Sum	15.322	15.304	15.336	15.767	15.575	15.567	15.535	15.551	15.641	15.596	15.588
F	0.284	0.218	0.300	0.323	0.363	0.225	0.318	0.428	0.323	0.527	0.496
X_{Mg}	0.646	0.590	0.684	0.658	0.657	0.613	0.647	0.706	0.681	0.708	0.773

PELITIC GNEISSES

BIOTITE

	DWN624 Rim [A]	DWN624 Matrix [B]	DWN627 Matrix	MCSHO2 Matrix	MCS321 Matrix	MCS322 Matrix	MCS331 Matrix	MCS332 Matrix	MCS343 Matrix	MCS343 Inclusion	MCS343 Rim
SiO_2	36.94	35.57	36.13	35.39	36.52	36.23	36.28	35.87	34.89	35.36	35.70
TiO_2	4.35	5.57	2.09	4.94	3.25	3.87	4.23	3.63	5.17	5.01	5.15
Al_2O_3	17.56	17.02	19.65	14.41	17.64	18.04	17.96	18.82	15.99	15.66	15.32
Cr_2O_3	0.09	0.11	-----	-----	-----	-----	0.05	-----	-----	-----	-----
FeO	15.03	17.80	15.76	21.11	16.15	16.73	17.22	16.19	18.92	16.67	15.95
MnO	-----	-----	-----	-----	0.11	-----	0.18	0.11	0.11	0.09	-----
MgO	13.66	11.01	12.90	9.65	13.17	12.62	12.25	12.37	10.58	13.26	13.57
Na_2O	0.12	0.08	0.22	0.12	0.22	0.16	0.19	0.16	0.13	0.16	0.10
K_2O	9.08	9.36	8.50	9.58	9.18	9.24	8.13	9.61	9.51	9.26	9.83
F	0.79	0.64	1.10		0.87	0.54	0.72				
Cl						0.20					
Total	97.62	97.16	96.35	95.20	97.11	97.63	97.16	96.81	95.30	95.47	95.62

CATION PROPORTIONS BASED ON 22 OXYGENS

Si	5.402	5.320	5.362	5.484	5.411	5.347	5.354	5.300	5.341	5.336	5.372
Ti	0.478	0.626	0.234	0.576	0.362	0.430	0.469	0.403	0.595	0.568	0.583
Al	3.026	3.000	3.436	2.632	3.081	3.136	3.124	3.277	2.884	2.785	2.717
Cr	0.011	0.013	-----	-----	-----	-----	-----	0.006	-----	-----	-----
Fe	1.838	2.227	1.956	2.736	2.001	2.065	2.126	2.000	2.422	2.104	2.007
Mn	-----	-----	-----	-----	0.014	-----	0.023	0.014	0.014	0.011	-----
Mg	2.978	2.456	2.853	2.229	2.909	2.775	2.696	2.724	2.413	2.984	3.043
Na	0.034	0.022	0.063	0.035	0.064	0.047	0.056	0.045	0.039	0.047	0.030
K	1.695	1.785	1.609	1.894	1.734	1.739	1.530	1.811	1.857	1.783	1.886
Sum	15.462	15.449	15.513	15.586	15.576	15.539	15.378	15.580	15.565	15.618	15.638
F	0.364	0.305	0.514		0.408	0.254	0.335				
Cl						0.049					
X_{Mg}	0.618	0.524	0.593	0.449	0.592	0.573	0.559	0.577	0.499	0.586	0.603

PELITIC GNEISSES

BIOTITE

	MCS393	MCS394	MCS395			MCS273		VD3	
	Matrix	Matrix	Matrix	Skeletal	Rim	Matrix	Rim	Matrix	Rim
SiO_2	36.43	35.70	36.14	37.45	36.09	36.80	37.63	35.89	35.53
TiO_2	3.58	4.41	3.95	3.62	3.53	3.74	3.22	4.47	4.43
Al_2O_3	18.80	17.47	18.33	18.97	18.61	17.84	18.48	18.44	18.15
Cr_2O_3	-----	-----	-----	-----	-----	-----	-----	-----	-----
FeO	15.46	17.42	17.66	14.34	14.04	16.10	12.04	19.02	18.74
MnO	-----	-----	-----	0.11	-----	-----	-----	-----	-----
MgO	13.06	11.94	11.58	12.72	14.04	12.92	16.28	9.97	11.48
Na_2O	0.14	0.11	0.17	0.23	0.13	0.22	0.30	0.15	0.16
K_2O	9.43	9.83	9.33	8.94	9.39	8.92	8.25	9.55	9.30
Total	96.90	96.88	97.16	96.38	95.83	96.59	96.20	97.49	97.79

CATION PROPORTIONS BASED ON 22 OXYGENS

Si	5.340	5.317	5.340	5.460	5.321	5.416	5.420	5.331	5.256
Ti	0.395	0.494	0.439	0.397	0.391	0.414	0.349	0.499	0.493
Al	3.248	3.067	3.192	3.260	3.234	3.097	3.137	3.229	3.165
Cr	-----	-----	-----	-----	-----	-----	-----	-----	-----
Fe	1.895	2.171	2.183	1.748	1.732	1.982	1.451	2.363	2.531
Mn	-----	-----	-----	0.014	-----	-----	-----	-----	-----
Mg	2.853	2.650	2.551	2.765	3.086	2.834	3.495	2.207	2.531
Na	0.040	0.033	0.049	0.065	0.038	0.064	0.083	0.042	0.045
K	1.763	1.868	1.758	1.663	1.766	1.675	1.517	1.809	1.755
Sum	15.534	15.600	15.512	15.372	15.568	15.489	15.461	15.480	15.563
X_{Mg}	0.601	0.550	0.461	0.613	0.641	0.588	0.707	0.483	0.500

PELITIC GNEISSES

CORDIERITE

	$DWN619_A$	$DWN619_B$	$DWN620_A$	$DWN620_B$	$DWN622_A$	$DWN622_B$	DWN623	DWN624
SiO_2	48.49	49.67	49.36	49.20	48.88	48.54	49.52	49.37
Al_2O_3	33.10	33.28	32.94	32.77	33.26	33.29	33.41	32.91
FeO	4.63	4.55	5.47	5.55	4.95	5.03	5.04	5.83
MnO	0.07	----	----	0.14	0.11	0.08	0.10	0.09
MgO	10.83	10.41	9.98	10.00	10.27	10.19	10.24	9.75
Na_2O	0.08	0.07	0.13	0.09	0.14	0.21	0.16	0.07
Total	97.20	97.98	97.88	97.75	97.61	97.34	98.47	98.02

CATION PROPORTIONS BASED ON 18 OXYGENS

Si	4.966	5.031	5.031	5.028	4.992	4.974	5.010	5.034
Al	3.996	3.975	3.957	3.948	4.002	4.020	3.984	3.957
Fe	0.398	0.387	0.465	0.474	0.423	0.432	0.426	0.498
Mn	0.006	-----	-----	0.012	0.009	0.006	0.009	0.009
Mg	1.653	1.572	1.515	1.503	1.563	1.557	1.545	1.482
Na	0.015	0.015	0.027	0.018	0.027	0.042	0.030	0.015
Sum	11.034	10.980	10.995	10.983	11.016	11.031	11.004	10.995
X_{Mg}	0.806	0.802	0.765	0.764	0.787	0.783	0.784	0.748

PELITIC GNEISSES

CORDIERITE

	MCS321	MCS331	MCS390	MCS393	MCS394 core	MCS394 rim	MCS395	MCS273	VD3
SiO_2	48.52	48.78	49.06	48.64	49.06	49.17	49.24	48.86	48.80
Al_2O_3	33.31	33.12	32.48	32.78	33.03	33.34	32.71	32.60	32.75
FeO	5.96	5.53	5.86	5.90	5.78	4.62	6.04	6.19	7.61
MnO	0.33	0.43	0.25	0.06	0.07	----	0.18	----	----
MgO	9.61	10.02	9.97	10.03	10.00	10.29	10.01	10.18	8.85
Na_2O	0.19	0.09	0.08	0.05	0.11	0.43	0.11	0.08	0.11
Total	97.92	97.97	97.70	97.46	98.08	97.75	98.29	97.91	98.12
	CATION PROPORTIONS BASED ON 18 OXYGENS								
Si	4.968	4.983	5.028	4.995	5.004	5.004	5.019	5.001	5.013
Al	4.020	3.990	3.924	3.969	3.969	3.987	3.930	3.933	3.966
Fe	0.510	0.471	0.501	0.507	0.492	0.393	0.516	0.531	0.654
Mn	0.027	0.036	0.021	0.006	0.006	-----	0.015	-----	-----
Mg	1.467	1.527	1.524	1.536	1.518	1.563	1.521	1.554	1.356
Na	0.036	0.018	0.018	0.012	0.021	0.084	0.024	0.015	0.021
Sum	11.028	11.025	11.016	11.025	11.010	11.031	11.025	11.034	11.010
X_{Mg}	0.742	0.764	0.753	0.770	0.755	0.799	0.747	0.745	0.675

PELITIC GNEISSES

ORTHOPYROXENE

	DWN619	DWN622A core	DWN622A rim	DWN623 core	DWN623 rim
SiO_2	47.49	47.07	50.26	49.29	49.64
TiO_2	0.05	0.11	0.08	0.05	0.06
Al_2O_3	7.22	7.53	7.11	5.31	6.28
FeO	23.59	24.38	22.33	25.77	22.59
MnO	0.45	0.49	0.79	0.64	1.03
MgO	20.39	19.50	19.68	19.32	20.61
CaO	0.11	0.09	0.07	0.07	0.07
Total	99.30	99.17	100.32	100.45	100.28
CATION PROPORTIONS BASED ON 6 OXYGENS					
Si	1.802	1.791	1.861	1.859	1.849
Ti	0.003	0.006	0.004	0.002	0.002
Al	0.313	0.338	0.310	0.236	0.276
Fe	0.749	0.776	0.692	0.813	0.704
Mn	0.014	0.016	0.025	0.021	0.032
Mg	1.154	1.106	1.086	1.087	1.144
Ca	0.004	0.004	0.003	0.003	0.003
Sum	4.039	4.037	3.981	4.021	4.010
X_{Mg}	0.606	0.588	0.611	0.572	0.619

PELITIC GNEISSES

K-FELDSPAR

	MCS321	MCS331	MCS332	MCS343	MCS387	MCS395
SiO_2	65.05	65.58	65.93	65.05	65.52	65.11
Al_2O_3	18.59	18.57	18.44	18.03	18.19	18.40
FeO	----	0.15	----	0.08	----	----
CaO	0.26	----	0.12	0.12	0.21	0.28
BaO	n.d.	n.d.	n.d.	n.d.	0.33	0.46
Na_2O	3.79	2.34	2.10	1.24	2.03	1.69
K_2O	11.52	13.02	13.35	14.86	13.53	13.83
Total	99.18	99.66	99.94	99.37	99.81	99.77

CATION PROPORTIONS BASED ON 8 OXYGENS

Si	2.985	3.002	3.011	3.011	3.009	2.999
Al	1.006	1.002	0.992	0.983	0.985	0.999
Fe	-----	0.006	-----	0.003	-----	-----
Ca	0.013	-----	0.006	0.006	0.010	0.014
Ba	-----	-----	-----	-----	0.006	0.008
Na	0.337	0.208	0.186	0.111	0.180	0.151
K	0.675	0.760	0.777	0.878	0.792	0.812
Sum	5.016	4.978	4.972	4.992	4.982	4.983
An	1.27	0.29	0.59	0.60	1.05	1.43
Ab	32.89	21.38	19.20	11.17	18.34	15.42
Or	65.84	78.33	80.21	88.23	80.61	83.15

PELITIC GNEISSES

PLAGIOCLASE

	DWN617	$DWN620_A$	$DWN620_B$	$DWN624_A$	$DWN624_B$	MCS322	MCS331	MCS343	MCS387	MCS393	MCS395
SiO_2	60.40	61.31	60.91	59.37	59.37	61.59	61.77	58.36	60.96	60.88	61.88
Al_2O_3	25.05	25.07	24.49	25.00	25.39	23.35	23.82	25.52	24.13	24.76	23.91
FeO	0.06	----	----	----	----	0.16	0.11	0.10	----	----	----
CaO	6.96	6.62	6.53	7.16	7.60	5.44	5.53	8.81	6.55	6.59	6.51
Na_2O	6.95	7.17	7.12	7.44	6.83	8.65	8.51	6.81	7.50	7.58	7.51
K_2O	0.47	0.31	0.42	0.30	0.27	0.14	0.16	0.23	0.21	0.21	0.29
Total	99.89	100.47	99.47	99.69	99.46	99.33	99.90	99.82	99.35	100.02	100.10

CATION PROPORTIONS BASED ON 8 OXYGENS

Si	2.690	2.707	2.717	2.674	2.659	2.754	2.744	2.621	2.723	2.704	2.742
Al	1.315	1.305	1.288	1.318	1.340	1.230	1.247	1.351	1.270	1.296	1.248
Fe	0.002	-----	-----	-----	-----	0.006	0.004	0.004	-----	-----	-----
Ca	0.332	0.313	0.312	0.343	0.365	0.261	0.263	0.424	0.314	0.314	0.309
Na	0.600	0.614	0.616	0.645	0.593	0.749	0.733	0.593	0.650	0.652	0.645
K	0.027	0.017	0.024	0.017	0.016	0.008	0.009	0.013	0.012	0.012	0.017
Sum	4.966	4.956	4.957	4.997	4.973	5.008	5.000	5.006	4.971	4.978	4.961
An	34.62	33.16	32.77	34.13	37.47	25.61	26.20	41.47	32.16	32.11	31.86
Ab	62.60	65.02	64.71	64.17	60.93	73.60	72.87	57.57	66.62	66.67	66.44
Or	2.78	1.82	2.52	1.70	1.60	0.79	0.92	1.26	1.22	1.22	1.70

PELITIC GNEISSES

GARNET

	DWN617			DWN618		DWN620		DWN622			DWN623	
	core	rim/biot	rim/qtz	core	rim/biot	core	rim/qtz	core	rim/qtz	rim/biot	core	rim/biot
SiO_2	38.47	37.64	38.26	38.75	37.60	39.33	38.82	38.42	38.25	37.11	38.33	37.67
TiO_2	-----	0.06	-----	-----	-----	0.04	-----	-----	-----	-----	-----	-----
Al_2O_3	21.77	21.50	21.70	22.33	21.72	22.08	22.32	22.25	22.09	21.45	22.19	21.80
FeO	29.60	33.50	29.96	22.33	21.72	27.46	27.22	29.79	30.22	33.27	30.12	33.24
MnO	1.11	1.37	1.26	1.25	2.03	1.19	1.04	1.49	1.42	2.26	1.71	2.36
MgO	7.91	5.24	7.21	10.13	6.18	9.60	9.49	7.80	7.64	4.96	7.64	5.03
CaO	1.26	1.44	1.37	0.79	0.70	1.10	1.13	0.71	0.84	0.68	0.90	1.05
Total	100.12	100.75	99.76	100.02	100.53	100.80	100.02	100.46	100.46	99.73	100.89	101.15

CATION PROPORTIONS BASED ON 12 OXYGENS

Si	2.991	2.971	2.995	2.973	2.966	3.001	2.983	2.979	2.974	2.967	2.969	2.967
Ti	-----	0.004	-----	-----	-----	0.002	-----	-----	-----	-----	-----	-----
Al	1.995	2.001	2.002	2.019	2.016	1.985	2.021	2.033	2.024	2.022	2.026	2.024
Fe	1.925	2.212	1.961	1.718	2.124	1.752	1.749	1.932	1.965	2.225	1.951	2.189
Mn	0.073	0.092	0.084	0.081	0.136	0.077	0.068	0.098	0.093	0.153	0.112	0.157
Mg	0.916	0.616	0.841	1.159	0.725	1.092	1.087	0.902	0.885	0.591	0.882	0.591
Ca	0.105	0.122	0.115	0.065	0.059	0.090	0.093	0.059	0.070	0.058	0.075	0.089
Sum	8.005	8.018	8.001	8.020	8.026	7.999	8.001	8.003	8.011	8.016	8.015	8.017
Gr	3.48	4.01	3.83	2.15	1.94	2.99	2.27	1.97	2.32	1.92	2.48	2.94
Py	30.34	20.25	28.02	38.34	23.82	36.27	36.27	30.16	29.37	19.52	29.21	19.53
Sp	2.42	3.02	2.80	2.68	4.47	2.56	2.27	3.28	3.09	5.05	3.71	5.19
Al	63.76	72.72	65.34	56.83	69.78	58.19	58.36	64.59	65.22	73.51	64.60	72.34

PELITIC GNEISSES

GARNET

	DWN624			DWN627		MCSH02		MCS322		MCS332	
	core	rim/biot	rim/qtz	core	rim/qtz	core	rim/biot	core	rim/qtz	core	rim/biot
SiO_2	38.38	37.42	38.18	38.00	37.78	37.66	37.55	37.36	37.32	37.89	36.53
TiO_2	-----	-----	-----	0.05	0.06	0.04	-----	-----	-----	-----	-----
Al_2O_3	22.28	21.68	22.13	22.06	22.33	19.76	19.26	21.93	21.84	21.99	22.05
FeO	28.49	32.59	29.09	29.33	28.96	35.28	36.74	32.13	31.69	28.82	32.15
MnO	1.03	1.34	0.80	1.87	1.78	0.87	0.93	0.68	0.65	3.94	4.83
MgO	8.71	5.65	8.34	7.86	8.24	4.86	3.96	6.92	6.85	6.30	3.91
CaO	1.17	1.22	1.16	0.85	0.76	1.55	1.51	1.42	1.16	0.98	0.94
Total	100.06	99.97	99.70	100.02	99.91	100.02	99.95	100.44	99.51	99.92	100.41

CATION PROPORTIONS BASED ON 12 OXYGENS

Si	2.969	2.966	2.970	2.964	2.944	3.023	3.041	2.933	2.950	2.980	2.924
Ti	-----	-----	-----	0.003	0.003	0.003	-----	-----	-----	-----	-----
Al	2.032	2.025	2.029	2.028	2.051	1.870	1.838	2.029	2.034	2.039	2.080
Fe	1.844	2.161	1.893	1.913	1.888	2.369	2.488	2.109	2.095	1.896	2.152
Mn	0.067	0.090	0.053	0.124	0.117	0.059	0.063	0.045	0.043	0.262	0.328
Mg	1.004	0.668	0.968	0.914	0.957	0.581	0.478	0.809	0.807	0.738	0.466
Ca	0.097	0.103	0.097	0.071	0.064	0.133	0.131	0.120	0.098	0.083	0.080
Sum	8.013	8.017	8.010	8.071	8.029	8.038	8.040	8.049	8.027	7.998	8.030
Gr	3.22	3.41	3.22	2.21	1.94	4.23	4.15	3.73	3.22	2.79	2.64
Py	33.33	22.11	32.15	30.26	31.64	18.49	15.13	26.25	26.52	24.77	15.40
Sp	2.22	2.98	1.76	4.09	3.88	1.88	1.99	1.46	1.41	8.79	10.84
Al	61.22	71.51	62.87	63.34	62.44	75.40	78.73	68.42	68.85	63.65	71.12

PELITIC GNEISSES

GARNET

	MCS343		MCS387		MCS393		MCS394		MCS395	
	core	rim/qtz	core	rim/qtz	core	rim/biot	core	rim/crd	core	rim/biot
SiO_2	37.31	37.22	37.23	37.19	35.75	36.90	38.03	37.31	37.54	37.41
TiO_2	-----	-----	-----	-----	-----	0.25	-----	-----	-----	-----
Al_2O_3	21.05	20.98	22.07	22.06	22.57	22.66	21.92	22.00	22.07	21.96
FeO	31.04	31.60	32.47	32.47	31.33	33.62	30.78	32.38	30.11	31.54
MnO	2.35	2.32	1.03	1.06	0.80	1.34	0.98	1.17	2.65	2.79
MgO	5.22	4.96	6.24	6.26	7.79	5.36	7.33	5.89	7.09	5.52
CaO	2.58	2.61	1.47	1.13	1.01	1.14	0.96	1.23	1.09	1.03
Total	99.55	99.69	100.51	100.17	99.25	101.27	100.00	99.98	100.55	100.25
Si	2.977	2.974	2.931	2.936	2.840	2.900	2.975	2.951	2.939	2.958
Ti	-----	-----	-----	-----	-----	0.015	-----	-----	-----	-----
Al	1.980	1.976	2.048	2.053	2.113	2.098	2.021	2.051	2.036	2.047
Fe	2.071	2.111	2.138	2.144	2.082	2.209	2.014	2.142	1.971	2.086
Mn	0.159	0.157	0.068	0.071	0.054	0.089	0.065	0.078	0.176	0.187
Mg	0.621	0.590	0.732	0.736	0.922	0.628	0.854	0.695	0.827	0.650
Ca	0.220	0.223	0.124	0.096	0.086	0.096	0.080	0.104	0.091	0.087
Sum	8.028	8.031	8.041	8.036	8.097	8.035	8.009	8.021	8.040	8.015
Gr	7.16	7.24	4.05	3.15	2.74	3.18	2.66	3.44	2.97	2.89
Py	20.22	19.15	23.91	24.15	29.33	20.78	28.34	23.02	26.98	21.59
Sp	5.18	5.10	2.22	2.33	1.72	2.95	2.16	2.58	5.74	6.21
Al	67.44	68.51	69.82	70.36	66.22	73.10	66.84	70.95	64.31	69.30

PELITIC GNEISSES

GARNET

	VD3		MCS212		MCS273	
	core	rim/biot	core	rim/qtz	core	rim/biot
SiO_2	37.11	36.58	38.06	38.13	36.84	36.58
TiO_2	0.04	-----	-----	-----	0.06	-----
Al_2O_3	22.07	21.06	21.28	20.79	22.07	21.06
FeO	34.20	37.62	32.86	32.35	32.77	37.62
MnO	0.22	0.33	1.24	1.21	0.66	0.33
MgO	6.58	4.02	5.11	5.28	7.20	4.02
CaO	0.17	0.15	1.70	1.72	0.41	0.15
Total	100.39	99.76	100.25	99.51	100.01	100.09
CATION PROPORTIONS BASED ON 12 OXYGENS						
Si	2.927	2.959	3.009	3.033	2.908	2.932
Ti	0.003	-----	-----	-----	0.003	-----
Al	2.052	2.007	1.982	1.949	2.054	2.066
Fe	2.256	2.545	2.173	2.152	2.164	2.354
Mn	0.015	0.022	0.083	0.082	0.044	0.053
Mg	0.773	0.485	0.602	0.625	0.847	0.580
Ca	0.014	0.013	0.144	0.147	0.035	0.039
Sum	8.040	8.031	7.993	7.993	8.055	8.024
Gr	0.22	0.42	4.80	4.89	1.13	1.29
Py	25.30	15.82	20.05	20.79	27.41	19.17
Sp	0.48	0.72	2.76	2.73	1.42	1.75
Al	73.80	83.03	72.39	71.59	70.03	77.79

CALC-SILICATE ROCKS

CLINOPYROXENE

	MCSR02	MCS350		MCS351		SS4		SS18
		core	rim	core	rim	core	rim	
SiO_2	48.17	44.79	45.06	44.55	46.26	46.54	47.56	48.13
TiO_2	0.30	0.34	0.26	0.37	0.28	0.21	0.17	0.14
Al_2O_3	3.04	4.69	3.72	4.65	3.41	4.01	3.24	3.17
Fe_2O_3	4.18	7.45	8.28	7.99	6.04	6.29	5.46	4.47
FeO	12.64	17.77	16.21	17.50	17.28	15.48	15.68	14.49
MnO	1.17	0.34	0.42	0.67	0.60	0.33	0.34	0.96
MgO	8.14	2.98	3.75	2.76	4.03	4.60	5.20	6.19
CaO	21.93	21.98	22.30	21.93	22.03	22.49	22.74	21.00
Na_2O	0.31	0.49	0.48	0.52	0.49	0.65	0.56	0.92
Total	99.88	100.84	100.48	100.94	100.46	100.60	100.95	99.49

CATION PROPORTIONS BASED ON 6 OXYGENS

Si	1.872	1.787	1.799	1.780	1.840	1.832	1.862	1.891
Ti	0.009	0.010	0.008	0.011	0.008	0.006	0.005	0.004
Al_{3+}	0.139	0.221	0.175	0.219	0.160	0.186	0.149	0.147
Fe_{2+}^{3+}	0.122	0.224	0.249	0.240	0.181	0.186	0.161	0.132
Fe^{2+}	0.411	0.593	0.541	0.584	0.575	0.510	0.513	0.476
Mn	0.039	0.011	0.014	0.023	0.020	0.011	0.011	0.032
Mg	0.471	0.177	0.223	0.164	0.239	0.270	0.303	0.363
Ca	0.913	0.939	0.954	0.939	0.939	0.949	0.954	0.884
Na	0.023	0.038	0.037	0.040	0.038	0.050	0.042	0.070
Sum	4.000	4.000	4.000	4.000	4.000	4.000	4.000	4.000
X_{Mg}	0.452	0.176	0.217	0.162	0.235	0.276	0.307	0.362

* Fe^{3+} calculated on the basis of stoichiometry

CALC-SILICATE ROCKS

GARNET

	MCS350		MCS351		SS4	
	core	rim	core	rim	core	rim
SiO_2	35.41	35.68	36.32	36.23	35.97	36.00
TiO_2	0.87	0.68	0.34	0.53	0.65	0.70
Al_2O_3	8.43	8.51	8.93	7.74	6.95	7.09
Fe_2O_3	19.07	18.98	18.56	20.23	20.97	21.35
FeO	7.01	6.67	6.57	4.62	3.62	3.17
MnO	0.96	1.00	1.79	1.68	0.51	0.53
MgO	0.06	0.09	0.10	0.08	0.11	0.11
CaO	28.38	28.43	27.91	28.85	31.55	31.36
Total	100.19	100.04	100.52	99.96	100.33	100.31
CATION PROPORTIONS BASED ON 12 OXYGENS						
Si	2.905	2.927	2.991	2.979	2.941	2.945
Ti	0.054	0.042	0.021	0.033	0.040	0.043
Al_{3+}	0.815	0.823	0.858	0.750	0.671	0.683
Fe_{2+}	1.177	1.172	1.138	1.252	1.290	1.315
Fe^{2+}	0.481	0.458	0.448	0.317	0.247	0.217
Mn	0.067	0.070	0.124	0.117	0.035	0.037
Mg	0.007	0.011	0.012	0.010	0.013	0.013
Ca	2.494	2.499	2.438	2.542	2.763	2.748
Sum	8.000	8.000	8.000	8.000	8.000	8.000

* Fe^{3+} calculated on the basis of stoichiometry

CALC-SILICATE ROCKS

	PLAGIOCLASE				SCAPOLITE
	MCS350	MCS351	SS44	SS18	SS4
SiO_2	47.66	48.87	49.96	60.78	45.39
Al_2O_3	33.07	31.84	31.76	24.70	28.13
FeO	0.44	0.31	0.36	0.20	0.26
CaO	17.30	17.07	15.31	7.20	18.26
Na_2O	1.43	2.28	2.52	6.70	2.93
K_2O	----	0.10	0.12	0.36	0.32
Total	99.90	100.41	100.03	99.94	95.47
	CATION PROPORTIONS BASED ON 8 OXYGENS				
Si	2.190	2.236	2.280	2.703	2.221
Al	1.791	1.717	1.708	1.295	1.623
Fe	0.017	0.012	0.014	0.008	0.011
Ca	0.852	0.837	0.749	0.343	0.964
Na	0.128	0.202	0.223	0.578	0.278
K	-----	0.006	0.007	0.020	0.020
Sum	4.978	5.010	4.981	4.947	5.117
An	86.92	80.10	76.51	36.45	
Ab	13.08	19.33	22.77	61.42	
Or	-----	0.57	0.72	2.13	

CALC-SILICATE ROCKS

ALLANITE-(Ce)

	SS18a		SS18b		SS18c	SS18c	SS4	MCS350	MCS351
	core	rim	core	rim		metamict			
SiO_2	32.82	33.32	32.22	33.10	31.80	32.29	33.29	32.89	32.75
TiO_2	0.35	0.28	0.51	0.31	0.57	0.64	0.24	0.56	0.50
Al_2O_3	15.98	17.15	13.66	15.84	13.15	12.92	17.81	17.04	16.73
Fe_2O_3	9.12	7.93	9.78	11.14	9.31	-----	8.89	10.64	8.95
FeO	7.99	8.32	8.12	5.74	8.06	15.39	7.51	6.89	8.21
MnO	0.33	0.29	0.37	0.34	0.40	0.42	----	----	0.15
MgO	0.53	0.47	0.68	0.51	0.93	0.85	0.28	0.08	0.14
CaO	13.36	14.31	13.17	15.35	12.27	9.97	15.09	14.68	14.05
ThO_2	-----	-----	-----	0.11	0.14	0.24	-----	-----	-----
La_2O_3	6.33	5.58	6.85	5.32	7.40	7.26	5.39	6.02	6.30
Ce_2O_3	10.62	9.31	11.67	9.23	12.71	12.20	8.84	9.04	9.77
Nd_2O_3	1.72	1.62	1.88	1.56	1.87	1.82	1.43	1.79	1.71
F	-----	-----	-----	-----	-----	-----	-----	-----	-----
Total	99.15	98.58	98.91	98.55	98.61	94.00	98.63	99.63	99.27

CATION PROPORTIONS 12.5 OXYGENS

Si	2.994	2.994	3.012	2.990	3.020	3.220	2.897	2.950	2.968
Ti	0.024	0.020	0.036	0.020	0.041	0.048	0.017	0.038	0.034
Al_{III}	1.719	1.817	1.505	1.686	1.448	1.519	1.875	1.801	1.786
Fe_{II}^{III}	0.625	0.622	0.663	0.758	0.666	-----	0.636	0.675	0.610
Fe^{II}	0.609	0.725	0.612	0.434	0.641	1.284	0.579	0.486	0.622
Mn	0.025	0.022	0.028	0.025	0.032	0.036	-----	-----	0.015
Mg	0.072	0.063	0.094	0.064	0.132	0.127	0.036	0.012	0.010
Ca	1.307	1.378	1.318	1.485	1.249	1.066	1.431	1.411	1.364
Th	-----	-----	-----	0.002	0.006	0.012	-----	-----	-----
La	0.214	0.185	0.237	0.177	0.254	0.267	0.177	0.198	0.211
Ce	0.355	0.307	0.400	0.305	0.442	0.446	0.288	0.297	0.325
Nd	0.056	0.052	0.063	0.050	0.064	0.065	0.046	0.058	0.055
F	-----	-----	-----	-----	-----	-----	-----	-----	-----
Sum	8.000	8.000	8.000	8.000	8.000	8.090	8.000	8.000	8.000

*Fe^{III} based on stoichiometry
ζAll Fe as FeO due to poor stoichiometry of metamict grains

CALC-SILICATE ROCKS

TITANITE

	MCSR01		MCSR02	SS18a	SS18b	SS18c		MCS350	MCS351
SiO_2	29.59	29.56	29.31	29.52	29.81	30.15	29.41	29.76	29.45
TiO_2	34.68	32.66	33.52	27.91	29.00	30.51	30.05	32.41	32.89
Al_2O_3	2.67	2.95	3.02	4.85	4.77	4.78	3.67	2.95	2.72
FeO	2.02	2.72	2.01	3.93	3.77	2.96	3.63	2.69	2.55
MnO	0.04	0.04	0.23	0.13	0.13	0.17	0.28	----	0.14
MgO	----	----	----	0.14	0.11	0.14	0.22	----	----
CaO	28.27	26.87	27.09	26.57	27.09	27.65	26.14	26.81	26.32
La_2O_3	----	0.28	0.22	0.20	0.17	----	0.43	0.26	0.42
Ce_2O_3	----	1.14	0.60	1.15	0.94	0.42	2.09	1.20	1.46
Nd_2O_3	----	0.60	0.33	0.76	0.60	0.30	1.13	0.77	0.80
ThO_2	----	----	0.11	----	----	----	----	----	----
Total	97.27	96.82	96.44	95.16	96.39	97.08	97.05	96.76	96.75

CATION PROPORTIONS BASED ON 5 OXYGENS

Si	0.999	1.015	1.004	1.033	1.028	1.022	1.020	1.033	1.033
Ti	0.880	0.843	0.864	0.735	0.752	0.778	0.784	0.830	0.852
Al	0.106	0.119	0.121	0.200	0.194	0.191	0.150	0.118	0.110
Fe	0.058	0.079	0.058	0.115	0.109	0.084	0.105	0.077	0.074
Mn	0.001	0.001	0.006	0.004	-----	0.004	0.005	0.008	0.006
Mg	-----	-----	-----	0.007	0.006	0.007	0.012	-----	-----
Ca	1.023	0.989	0.994	0.997	1.001	1.004	0.972	0.978	0.972
La	-----	0.004	0.008	0.003	0.002	-----	0.006	0.003	0.005
Ce	-----	0.014	0.004	0.015	0.012	0.005	0.027	0.015	0.018
Nd	-----	0.008	0.001	0.010	0.007	0.004	0.014	0.009	0.010
Sum	3.067	3.072	3.060	3.119	3.115	3.100	3.098	3.063	3.055

CALC-SILICATE ROCKS

TITANITE

	MCS338	MCS346				
		1	2		metamict	rim/mgt
SiO_2	30.52	30.56	30.54	31.18	30.58	30.15
TiO_2	31.56	33.14	31.24	32.94	34.27	32.95
Al_2O_3	3.70	3.05	3.98	3.53	2.62	2.77
FeO	2.21	1.98	2.35	2.13	2.05	2.49
MnO	0.09	0.09	0.10	0.14	0.28	0.39
MgO	0.07	0.06	0.07	0.07	----	0.05
CaO	25.52	26.89	25.82	27.10	26.52	25.09
La_2O_3	0.12	0.18	0.10	0.19	0.42	0.41
Ce_2O_3	0.56	0.66	0.41	0.62	1.42	1.85
Nd_2O_3	0.41	0.32	0.26	0.29	0.60	1.05
ThO_2	0.13	0.14	0.10	0.14	0.23	0.09
Total	94.89	97.07	94.88	98.33	99.06	97.29
	CATION PROPORTIONS BASED ON 5 OXYGENS					
Si	1.053	1.035	1.048	1.040	1.025	1.033
Ti	0.819	0.844	0.809	0.827	0.864	0.849
Al	0.150	0.122	0.162	0.139	0.104	0.112
Fe	0.064	0.056	0.068	0.059	0.057	0.071
Mn	0.003	0.003	0.003	0.004	0.008	0.011
Mg	0.004	0.003	0.003	0.004	-----	0.002
Ca	0.936	0.975	0.953	0.969	0.952	0.921
La	0.002	0.002	0.001	0.002	0.005	0.005
Ce	0.007	0.008	0.005	0.008	0.018	0.023
Nd	0.005	0.004	0.003	0.004	0.007	0.013
Th	0.001	0.001	0.001	0.001	0.002	0.001
Sum	3.044	3.053	3.056	3.057	3.042	3.041

BIOTITE GNEISSES

BIOTITE

	AUGEN ORTHOGNEISSES			LEUCOGNEISSES			
	DWN613	DWN628	DWN629$_A$	DWN614	DWN621		DWN626
SiO_2	35.25	35.89	35.90	35.57	35.77	36.60	36.41
TiO_2	3.94	5.19	5.84	3.90	4.34	3.53	4.46
Al_2O_3	17.95	13.76	13.36	18.04	18.19	18.58	17.57
FeO	20.52	23.18	24.17	20.17	17.52	14.67	17.51
MnO	0.37	0.23	0.25	0.42	0.10	0.10	0.33
MgO	9.52	8.72	7.86	9.38	11.09	13.84	11.26
Na_2O	0.20	0.13	0.10	0.12	0.21	0.16	0.16
K_2O	9.41	9.09	9.09	9.14	9.74	9.86	8.90
F	0.64	0.98	0.71	1.06	0.70	0.77	0.72
Total	97.80	97.17	97.28	97.80	97.61	98.16	97.32

CATION PROPORTIONS BASED ON 24 OXYGENS

Si	5.311	5.541	5.551	5.357	5.322	5.339	5.406
Ti	0.446	0.603	0.679	0.442	0.486	0.387	0.498
Al	3.188	2.503	2.435	3.202	3.189	3.194	3.076
Fe	2.585	2.993	3.125	2.541	2.180	1.789	2.174
Mn	0.047	0.030	0.033	0.053	0.012	0.012	0.041
Mg	2.138	2.007	1.812	2.107	2.459	3.008	2.492
Na	0.057	0.040	0.029	0.036	0.046	0.059	0.045
K	1.809	1.790	1.794	1.755	1.849	1.834	1.685
Total	15.581	15.527	15.558	15.493	15.543	15.662	15.417
X_{Mg}	0.453	0.401	0.367	0.453	0.530	0.627	0.534

BIOTITE GNEISSES

K-FELDSPAR

	AUGEN ORTHOGNEISSES				LEUCOGNEISSES		
	DWN613	DWN628	$DWN629_A$	$DWN629_B$	DWN614	DWN621	DWN626
SiO_2	64.84	65.76	65.23	65.50	65.24	65.12	65.40
Al_2O_3	18.65	18.28	18.59	18.38	18.77	18.18	18.23
CaO	0.18	0.23	0.22	0.10	0.19	0.09	0.20
BaO	0.27	0.28	0.25	0.36	0.25	0.75	0.15
Na_2O	1.38	1.65	1.73	1.01	1.50	1.60	1.45
K_2O	14.21	13.95	13.72	14.66	13.92	13.85	14.47
Total	99.53	100.15	99.74	100.01	99.87	99.57	99.90
	CATION PROPORTIONS BASED ON 8 OXYGENS						
Si	2.992	3.011	2.997	3.010	2.993	3.008	3.007
Al	1.014	0.989	1.007	0.995	1.015	0.990	0.988
Ca	0.009	0.011	0.011	0.005	0.010	0.004	0.010
Ba	0.005	0.005	0.004	0.006	0.005	0.014	0.003
Na	0.124	0.146	0.154	0.090	0.134	0.143	0.130
K	0.836	0.815	0.804	0.859	0.815	0.816	0.849
Sum	4.980	4.974	4.977	4.965	4.972	4.975	4.987
An	0.93	1.13	1.14	0.52	1.04	0.42	1.01
Ab	12.80	15.02	15.89	9.43	13.97	14.85	13.14
Or	86.27	83.85	82.97	90.05	84.98	84.74	85.85

PLAGIOCLASE

	AUGEN ORTHOGNEISSES					LEUCOGNEISSES		
	DWN613		DWN628	$DWN629_A$	$DWN629_B$	DWN614	DWN621	DWN626
	core	rim	core	core	core	core	core	core
SiO_2	59.95	63.72	60.95	61.28	61.01	61.14	61.14	61.96
Al_2O_3	24.68	22.67	24.57	24.15	24.84	24.53	24.40	23.58
FeO	-----	0.30	-----	-----	0.18	-----	-----	-----
CaO	6.66	2.76	6.50	6.21	6.44	6.49	6.30	5.43
Na_2O	8.15	9.27	8.09	7.85	7.13	8.01	8.00	8.54
K_2O	0.23	1.22	0.24	0.23	0.27	0.20	----	0.31
Total	99.67	99.94	100.35	99.72	99.87	100.37	100.06	99.82
	CATION PROPORTIONS BASED ON 8 OXYGENS							
Si	2.683	2.823	2.703	2.727	2.710	2.710	2.720	2.755
Al	1.301	1.184	1.284	1.267	1.300	1.281	1.271	1.235
Fe	-----	0.011	-----	-----	0.007	-----	-----	-----
Ca	0.320	0.131	0.309	0.296	0.306	0.308	0.306	0.259
Na	0.708	0.796	0.696	0.677	0.614	0.688	0.679	0.736
K	0.013	0.069	0.013	0.013	0.015	0.012	-----	0.017
Sum	5.025	5.014	5.005	4.980	4.952	4.999	4.985	5.002
An	30.72	13.14	30.34	30.04	32.77	30.59	31.07	25.57
Ab	68.04	79.92	68.34	68.66	65.62	68.27	68.93	72.71
Or	1.24	6.94	1.32	1.30	1.61	1.14	-----	1.72